

DUE DATE SLIP

GOVT. COLLEGE, LIBRARY

KOTA (Raj.)

Students can retain library books only for two weeks at the most.

**BORROWER'S
No.**

DUE DATE

SIGNATURE

Indian J Pure & Appl Phys, Vol 24 No 7 pp. 313-364

JULY 1986

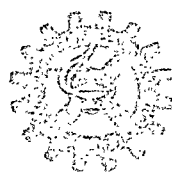
CODEN : IJOPAU ISSN : 0019-5396

24(7) 313-364 (1986)

11781
2

PR-109
Gr. -1 10/1

INDIAN JOURNAL OF PURE & APPLIED PHYSICS



Published by
PUBLICATIONS & INFORMATION DIRECTORATE, CSIR
NEW DELHI

in association with
THE INDIAN NATIONAL SCIENCE ACADEMY, NEW DELHI

THE WEALTH OF INDIA

An Encyclopaedia of Indian Raw Materials and Industrial Products, published in two series:

(i) Raw Materials, and (ii) Industrial Products.

RAW MATERIALS

The articles deal with Animal Products, Dyes & Tans, Essential Oils, Fats & Oils, Fibres & Pulps, Foods & Fodders, Drugs, Minerals, Spices & Flavourings, and Timbers and other Forest products. Names in Indian languages, and trade names are provided.

For important crops, their origin, distribution, evolution of cultivated types, and methods of cultivation, harvesting and storage are mentioned in detail. Data regarding area and yield and import and export are provided. Regarding minerals, their occurrence and distribution in the country and modes of exploitation and utilization are given. The articles are well illustrated. Adequate literature references are provided.

Eleven volumes of the series covering letters A – Z have been published.

Vol. I(A-B) Rs. 80.00; Vol. II (C) Rs. 95.00; Vol. III (D-E) Rs. 105.00; Vol. IV (F-G) Rs. 65.00; Vol. IV: Suppl. Fish & Fisheries Rs. 56.00; Vol. V (H-K) Rs. 114.00; Vol. VI (L-M) Rs. 90.00; Vol. VI: Suppl. Livestock Rs. 102.00; Vol. VII (N-P) Rs. 100.00; Vol. VII (Ph-Re) Rs. 86.00; Vol. IX (Rh-So) Rs. 104.00; Vol. X (Sp-W) Rs. 225.00; Vol. XI (X-Z) Rs. 115.00.

INDUSTRIAL PRODUCTS

Includes articles giving a comprehensive account of various large, medium and small scale industries. Some of the major industries included are: Acids, Carriages, Diesel Engines, Fertilizers, Insecticides & Pesticides, Iron & Steel, Paints & Varnishes, Petroleum Refining, Pharmaceuticals, Plastics, Ship & Boat-building, Rubber, Silk, etc.

The articles include an account of the raw materials and their availability, manufacturing processes, and uses of products, and industrial potentialities. Specifications of raw materials as well as finished products and statistical data regarding production, demand, exports, imports, prices, etc., are provided. The articles are suitably illustrated. References to the sources of information are provided.

Nine volumes of the series covering letters A – Z have been published.

Part I (A-B) Rs. 58.00; Part II (C) Rs. 74.00; Part III (D-E) Rs. 100.00; Part IV (F-H) Rs. 126.00; Part V (I-L) Rs. 90.00; Part VI (M-P) Rs. 28.00; Part VII (Pl-Sh) Rs. 60.00; Part VIII (Si-Ti) Rs. 66.00; Part IX (To-Z) Rs. 80.00.

HINDI EDITION: BHARAT KI SAMPADA—PRAKRITIK PADARTH

Vols. I to VII and two supplements of Wealth of India—Raw Materials series in Hindi already published.

Published Volumes:

Vol. I (अ-आ) Rs. 38; Vol. II (क) Rs. 36; Vol. III (ख-ख) Rs. 36; Vol. IV (घ) Rs. 83; Vol. V (च-चे) Rs. 60; Vol. VI (ज-झ) Rs. 80; Vol. VII (ट-ठ) Rs. 135

Supplements:

Fish & Fisheries (Matsya & Matsyakī) Rs. 49; Livestock (Pashudhan aur Kukkut Palan) Rs. 34.

Vols. VIII to XI under publication.

Please contact:

SALES AND DISTRIBUTION OFFICER
PUBLICATIONS & INFORMATION DIRECTORATE, CSIR
Hillside Road, New Delhi 110012

Indian Journal of Pure & Applied Physics

EDITORIAL BOARD

Prof. S. Chandrasekhar
Raman Research Institute
Bangalore

Prof. R V Gopala Rao
Jadavpur University
Calcutta

Prof. S K Joshi
Indian National Science Academy
New Delhi/Roorkee University
Roorkee

Prof. P Krishna
Indian National Science Academy,
New Delhi/Banaras Hindu University
Varanasi

Prof Kehar Singh
Indian Institute of Technology
New Delhi

Prof C L Mehta
Indian Institute of Technology
New Delhi

Prof. S P Pandya
Physical Research Laboratory
Ahmedabad

Dr K R Rao
Bhabha Atomic Research Centre
Bombay

Prof. D K Rai
Banaras Hindu University
Varanasi

Prof. B V Sreekantan
Tata Institute of Fundamental Research
Bombay

Prof. R Srinivasan
University of Madras
Madras

Prof. Suresh Chandra
Banaras Hindu University
Varanasi

Shri S P Ambasta, Editor-in-Chief (*Ex-officio*)

EDITORIAL STAFF

Editors

D S Sastry & K S Rangarajan

Assistant Editors

J B Dhawan, Tarun Banerjee & (Mrs) Poonam Bhatt

Published by the Publications & Information Directorate, CSIR, Hillside Road, New Delhi 110 012

Editor-in-Chief: S P Ambasta

The Indian Journal of Pure & Applied Physics is issued monthly. The Directorate assumes no responsibility for the statements and opinions advanced by contributors. The editorial staff in its work of examining papers received for publication is assisted, in an honorary capacity, by a large number of distinguished scientists, working in various parts of India.

Communications regarding contributions for publication in the journal should be addressed to the Editor, Indian Journal of Pure & Applied Physics, Publications & Information Directorate, Hillside Road, New Delhi 110012.

Correspondence regarding subscriptions and advertisements should be addressed to the Sales Distribution Officer, Publications & Information Directorate, Hillside Road, New Delhi 110012.

Annual Subscription

Rs. 180.00 £ 34.00 \$ 60.00

Single Copy

Rs. 18.00 £ 3.40 \$ 6.00

50% Discount is admissible to research workers and students and 25% discount to non-research individuals, on annual subscription. Payments in respect of subscriptions and advertisements may be sent by cheque, bank draft, money order or postal order marked payable *only* to **Publications & Information Directorate, New Delhi 110 012**. Claims for missing numbers of the journal will be allowed only if received within 3 months of the date of issue of the journal plus the time normally required for postal delivery of the journal and the claim.

Announcement

National Seminar on Crystallography

(Jammu 7-9 October 1986)

The 18th National Seminar on Crystallography is being organized by the Department of Physics, University of Jammu, Jammu, during 7-9 Oct 1986. The registration fee is Rs 25/- for research scholars and students, and Rs 50/- for others.

Abstracts neatly typed on bond papers (using a black ribbon) within a space of 12 × 16 cm should be submitted in duplicate to the secretaries and one more copy of the abstract should be sent direct to the concerned Programme Committee member.

Further details can be had from:

The Secretaries, XVIII National Seminar on Crystallography

Department of Physics, University of Jammu Canal Road, Jammu 180 001

CONTENTS

General Physics

- Profile of Vapour Layer on a Liquid Surface – Mathematical Model ... 344
J Ashok & C V N Vasantha Lakshmi

Nuclear Physics

- Annealing of Heavy Ion Tracks in Plastic Track Detectors ... 313
S M Farid
- Photon Attenuation Measurements in Soil Samples of Different Particle Sizes ... 346
G S Mudahar & H S Sahota*

Atomic & Molecular Physics

- Application of CNDO/S-RPA Method: Electronic Transition Energies & Oscillator Strengths 348
Rana Sen & Subir Nath Bhattacharyya*

Classical Areas of Phenomenology (Including Applications)

- A Stable Laser Interferometer for Recording Holographic Gratings ... 320
R P Shukla
- Ultrasonic Studies of Ternary System: Water + 2-Propanol + Nitromethane at Miscibility Point ... 353
T John Paulus, K Krishnamoorthy & P B Mathur*

Condensed Matter: Structure, Mechanical & Thermal Properties

- Mean Square Amplitudes of Vibration & Associated Debye Temperatures of Dysprosium, Gadolinium, Lutetium & Yttrium ... 324
N Gopi Krishna, D B Sirdeshmukh*, B Rama Rao, B J Beaudry & K A Gschneidner (Jr)
- Nearest Cation-Anion Distance in Fused Salts ... 327
Asim R Purkait & Dilip K Majumdar*
- Elastic Constants of Some Polycrystalline Antimony Alloys ... 331
N Swarnalata* & A R K L Padmini
- Akhieser Damping in KCN ... 336
S K Kor* & Raja Ram Yadav

Condensed Matter: Electronic Structure, Electrical, Magnetic & Optical Properties

- Indirect Tunnelling Current Density Based on a Rigorous Quantum Mechanical Treatment 339
D K Roy* & Amitabh Ghosh
- ESR Studies of Ternary Complexes of Copper(II) with Acetylacetone & Substituted 8-Hydroxyquinolines ... 355
Y Anjaneyulu*, V G K M Pisipati, N V S Rao, L N Murthy & R Prabhakara Rao

CONTENTS

ESR Hyperfine Line Width Studies of Some Aliphatic Polyamine Copper(II) Compounds V Muralikrishna, N V S Rao*, V G K M Pisipati	358
Drift Mobilities in Phenazine: A Candidate Material for Organic Photovoltaic Systems ... B Kumar	362
Surface Charge Density & Dielectric Constant of a Magneto-Electret of Carnauba Wax as a Function of Time K D Ray Chaudhuri, H De & S D Chatterjee*	364

The author for correspondence is indicated by () mark, in case of papers with more than one author.

Annealing of Heavy Ion Tracks in Plastic Track Detectors

S M FARID

Department of Physics, Rajshahi University, Rajshahi, Bangladesh

Received 30 August 1984; revised received 3 March 1986

Three samples of plastic track detectors, viz. CR-39, cellulose nitrate [CN(R)] and Makrofol-E polycarbonate (PC) have been irradiated with different ions from the cyclotron at the Joint Institute for Nuclear Research, Dubna, USSR, in order to study the thermal effects on the latent tracks of these ions. The bulk etch rates of CR-39 and CN(R) are found to increase with annealing temperature while that of PC does not change with annealing temperature. The track diameters of different ions in CN(R) and PC decrease with the increase in annealing time and temperature. The experimental results show that for heavier ions higher temperatures are needed for complete erasure of tracks. It is also observed that the track density and etchable range of different ions decrease by the application of heat. The oblique tracks are less stable than the vertical tracks. It is found that it will be possible in the case of PC detectors, to separate out tracks of different ions by a process of controlled annealing. The track diameters of ^{12}C ions in CR-39 are found to increase with annealing temperature. The sensitivity of CR-39 plastic detector is enhanced as a result of thermal annealing.

1 Introduction

Solid state nuclear track detectors (SSNTDs) have been extensively studied in recent years both with regard to their practical applications in diverse fields such as nuclear physics, earth and space physics, biology, dosimetry, etc. and as a tool for studies of basic phenomena¹. One of the important properties which should be properly taken into account during the applications of SSNTDs is the thermal fading of latent damages²⁻⁷. It may be required in some experiments to operate the detectors at a temperature higher than the normal room temperature. The subjection of SSNTD to high temperatures after irradiation but before etching, produces alterations in the damaged region which result in latent track shrinkage and an accompanying reduction of etching velocity along the track²⁻⁷. Thus, for accurate track analysis, proper temperature-dependent corrections to the efficiency factor must be applied. This paper reports the results of our study on the influence of different annealing conditions on the bulk etch rate, etch pit diameter, etchable track length and etching efficiency of plastic detectors.

2 Experimental Procedure

The investigations were performed on three types of plastics having different track registration sensitivities. The plastic materials used in the detectors were of Makrofol-E polycarbonate (PC), cellulose nitrate [CN(R)] obtained from Joint Institute for Nuclear Research (JINR), Dubna, USSR and CR-39 obtained from M/s Pershore Mouldings Ltd, England. The samples were exposed simultaneously under identical experimental conditions to different ions of different energies (Table 1) using cyclotron beams at JINR,

Dubna, USSR. The angles of exposure were 90°, 45° and 30° with respect to the surface of the detector.

The exposed samples were divided into a large number of lots and annealed in an oven (temperature range: from room temperature to 500°C and controlled within $\pm 3^\circ\text{C}$). The annealed samples of CR-39 and PC were etched in 6N NaOH at 70°C while CN(R) samples were etched in 6N NaOH at 60°C.

3 Results and Discussion

3.1 Effect of Annealing Temperature on the Bulk Etch Rate

Applying the etching conditions mentioned above, the bulk etching properties of the CN(R) and PC sheets were first studied. The results of these investigations are shown in Fig. 1 where the thickness of the layers removed from the individual sheets is shown as a function of etching time for plastics kept at various annealing temperatures. The data about the removed layers of the sheets were obtained through direct thickness measurements using a microthickness gauge having a least count $= 0.5\ \mu\text{m}$. The accuracy of

Table 1—Plastic Detectors and Ions Used in Annealing Experiments

Detector material	Ion and energy (in MeV/N)	Angle of exposure w.r.t. detector surface
Makrofol-E Polycarbonate (PC)	$^{133}_{54}\text{Xe}$, 1.1	90° and 45°
	$^{40}_{18}\text{Ar}$, 7.5	90° and 30°
	$^{16}_8\text{O}$, 9.10	90° and 30°
	^4_2He , 1.75	90°
CN(R)	$^{20}_{10}\text{Ne}$, 10.00	90° and 30°
CR-39	$^{16}_8\text{O}$, 8.75	30°
	$^{12}_6\text{C}$, 9.1	90°

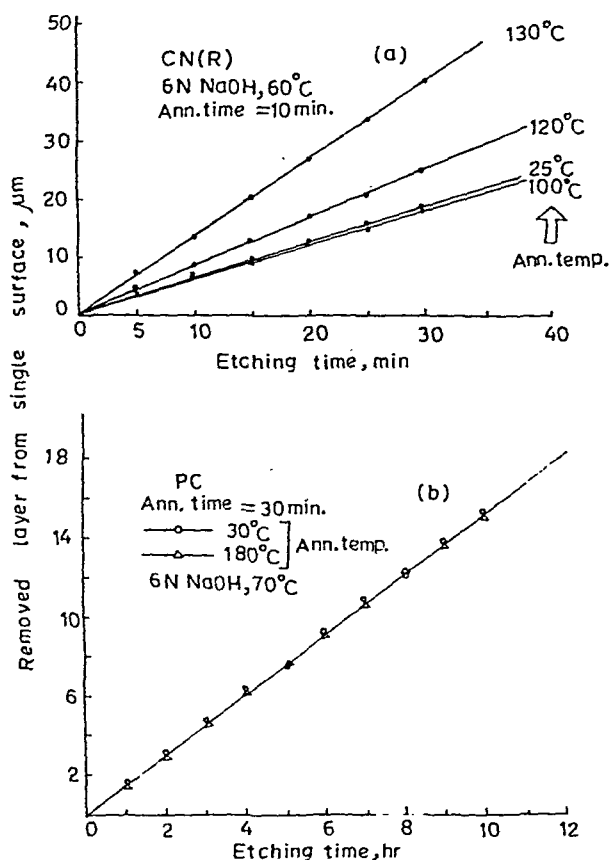


Fig. 1—Thickness of removed layer versus etching time curves for CN(R) and PC, annealed at various temperatures

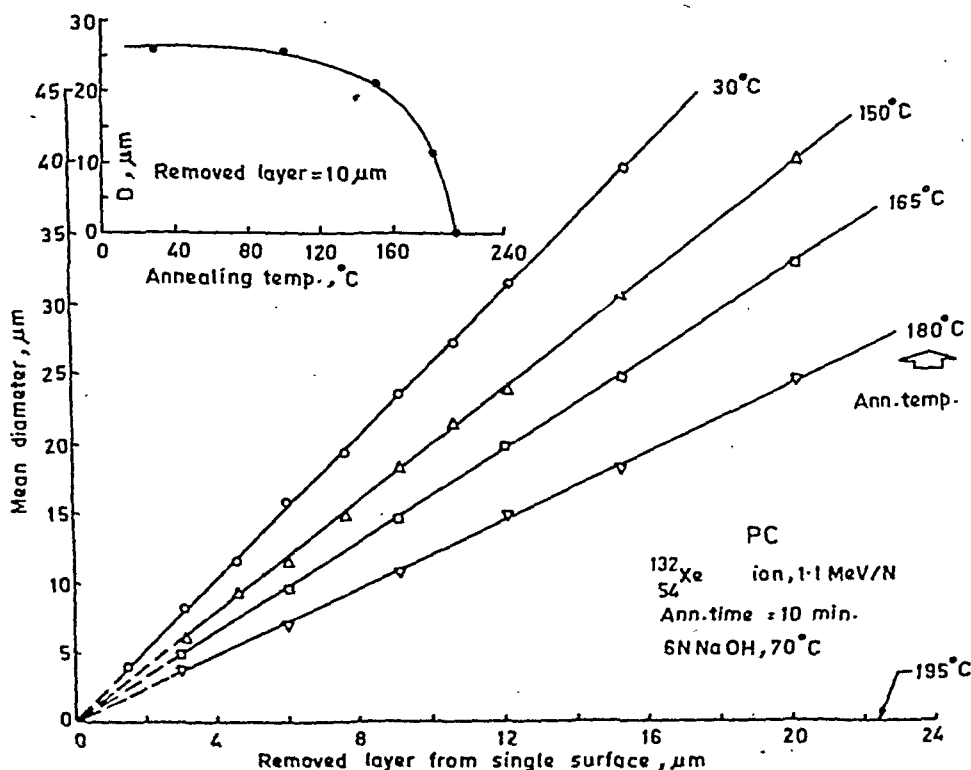


Fig. 2—Relationship between track diameter and thickness of removed layer for $^{132}_{54}\text{Xe}$ ion tracks in PC annealed for 10 min at different temperatures

measurements is quite high and hence there was no need to give error bars in the curves of Figs 1-14.

It can be observed that above 100°C the bulk etch rate of CN(R) sheet increases rapidly indicating the ever-growing degree of thermal degradation. Above 140°C, the mechanical properties strongly deteriorate, the sheet becomes glassy and brittle, and the measurement of the removed layer becomes unreliable.

With a PC sheet, no change is observed in the bulk etch rate even at 190°C and the sheets are satisfactorily elastic. However, lasting deformations are observed above 175°C.

3.2 Effect of Annealing Temperature on Track Diameter

Samples of PC exposed vertically to $^{132}_{54}\text{Xe}$ ions were annealed at various temperatures for 10 min. This value of annealing time has been recommended by Khan and Durrani² for a polycarbonate plastic detector. After annealing, the samples are etched in 6N NaOH at 70°C. The etchpit diameters were measured as a function of the removed layer. The results are shown in Fig. 2. The etchpit diameter decreases with increase in annealing temperature. Complete eradication of $^{132}_{54}\text{Xe}$ ion tracks in PC is achieved by annealing the samples at 195°C for 10 min.

Investigations similar to those relating to $^{132}_{54}\text{Xe}$ ion were made on ^4_2He , $^{16}_8\text{O}$ and $^{40}_{18}\text{Ar}$ ions also using PC

samples and a similar trend in diameter reduction with annealing temperature was observed. We conclude that complete thermal eradication of ^4He , ^{16}O and ^{40}Ar ion tracks in PC samples requires annealing at 165°C , 175°C and 190°C respectively for 10 min duration. CN(R) sheets exposed vertically to $^{20}_{10}\text{Ne}$ ions were annealed for 10 min at different temperatures. The effect of annealing temperature on $^{20}_{10}\text{Ne}$ ion tracks in CN(R) is shown in Fig. 3. For complete thermal eradication of $^{20}_{10}\text{Ne}$ ion tracks, an annealing period of 10 min had been applied at 130°C .

The relationships between track diameter and annealing temperature for $^{132}_{54}\text{Xe}$ -ion and $^{20}_{10}\text{Ne}$ ion are also shown in Figs 2 and 3 (insets). The track diameters were measured after removing a $10\text{ }\mu\text{m}$ thick surface layer from the individual detectors. Curves of track diameter vs annealing temperature plotted for PC samples showed a similar trend. It can be concluded

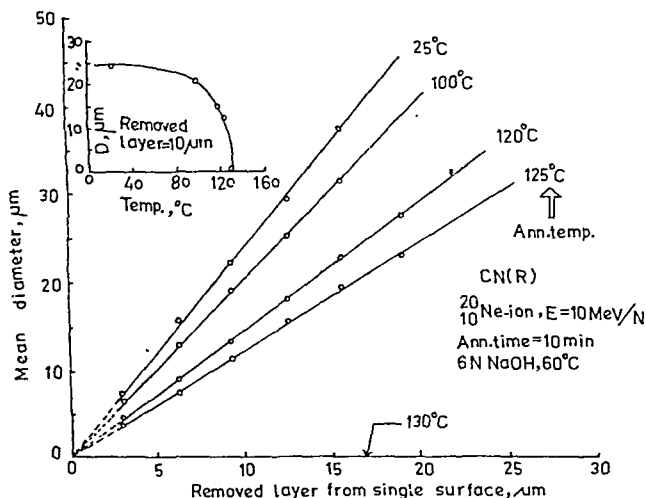


Fig. 3—Relationship between track diameter and thickness of removed layer for $^{20}_{10}\text{Ne}$ ion tracks in CN(R) annealed for 10 min at different temperatures

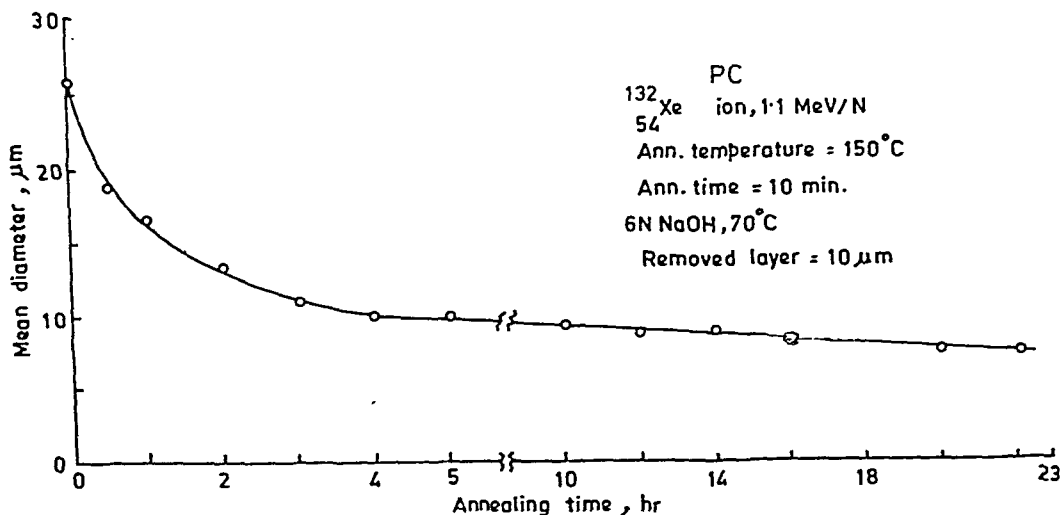


Fig. 4—Relationship between track diameter and annealing time for $^{132}_{54}\text{Xe}$ ions in PC annealed at 150°C

that for heavier ions higher temperatures of annealing are needed for their complete erasing. The heavier ions impart more energy on the samples and hence damage is more. As a result, higher temperature of annealing (i.e. higher thermal energy) is needed to cure the latent damage in the detectors.

3.3 Effect of Annealing Time on Track Diameter

Fig. 4 shows the effect of annealing time on the etchpit diameters of $^{132}_{54}\text{Xe}$ ions in PC samples entering at right angles. A $10\text{ }\mu\text{m}$ thick surface layer was removed from the individual detector before measurement. The annealing temperature was 150°C . The investigations were repeated using ^4He , ^{16}O and

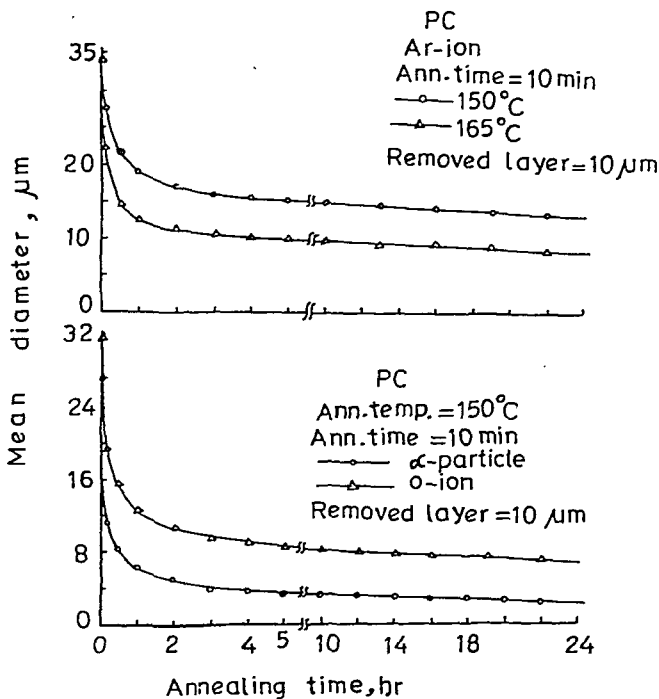


Fig. 5—Relationship between track diameter and annealing time for different ions in PC detector annealed at 150°C and 165°C

$^{40}_{18}\text{Ar}$ ions and the results are shown in Fig. 5. The effect of annealing time on track diameter of $^{20}_{10}\text{Ne}$ ion tracks in CN(R) is shown in Fig. 6. The annealing temperature was 120°C . The removed layer from each detector surface in this case was $15\text{ }\mu\text{m}$. It can be observed that all these curves consist of two regions, an initial region of steep fall followed by a long region of slow fall. It is apparent from Figs 4-6 that eradication of radiation tracks produced by different charged particles is done in two phases. In the first phase, a short annealing at a given temperature heals a major portion of the damage. In the second phase, healing is continued slowly at long durations of annealing time. Beyond a certain limit, no considerable change is brought about even by a significant extension of annealing time. At a higher temperature of annealing (165°C for $^{40}_{18}\text{Ar}$ ion in Fig. 5), the slowly falling component of the curve starts early. Measurements made at other annealing temperatures and by use of different ions revealed a similar trend for the plastics used.

3.4 Selective Thermal Track Eradication

From the measurements presented in Fig. 2 and from similar curves for different ions (not shown), we can establish the range of annealing temperature over which complete fading of tracks caused by feebly and highly ionizing nuclear particles takes place. If the width of this range is large enough, by following a procedure of controlled heat treatment, it will be possible to separate out tracks of different particles and identify them. To illustrate this, we have evaluated from the initial slopes S of the curves showing the increase of track diameters with thickness of removed layer (Fig. 2 and similar curves) and the ratio of track and bulk etch rates ($V = V_t/V_b$). The following relation⁷⁻¹⁰ is used to calculate V :

$$V = \frac{1 + 0.25S^2}{1 - 0.25S^2}$$

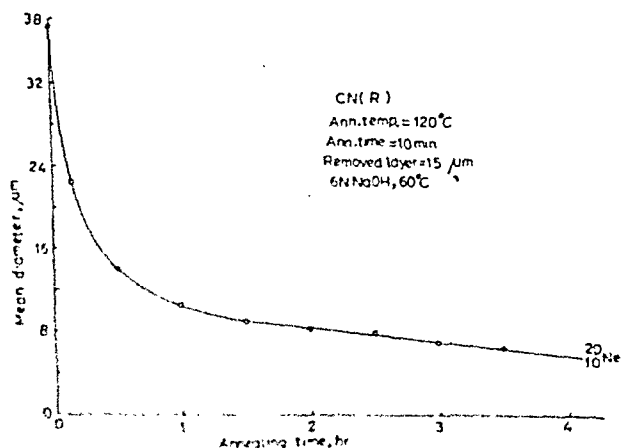


Fig. 6—Relationship between track diameter and annealing time for $^{20}_{10}\text{Ne}$ ion in CN(R) annealed at 120°C

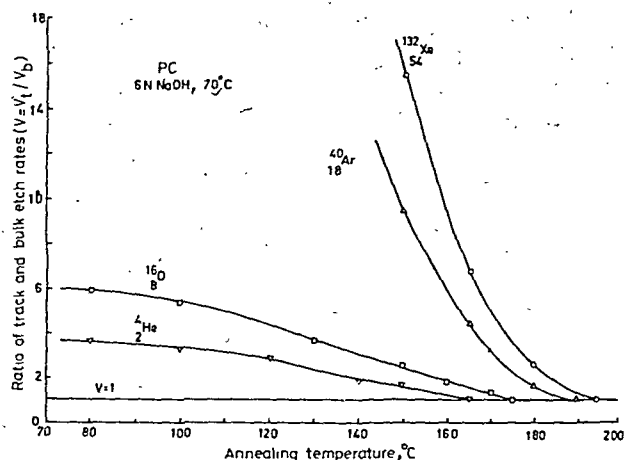


Fig. 7—Etch rate ratio ($V = V_t/V_b$) as a function of annealing temperature for different ions in PC detector

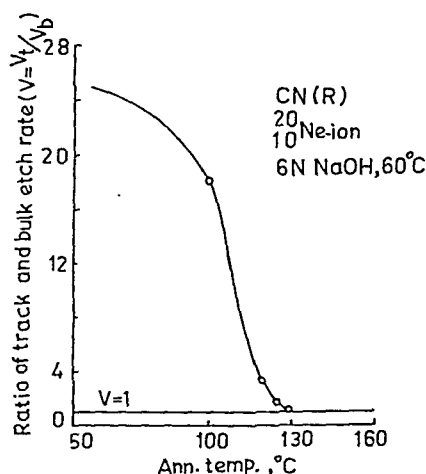


Fig. 8—Etch rate ratio ($V = V_t/V_b$) as a function of annealing temperature for $^{20}_{10}\text{Ne}$ ion in CN(R) detector

Then this etch rate ratio (V) is plotted against annealing temperature as shown in Fig. 7. A similar curve for $^{20}_{10}\text{Ne}$ ion in CN(R) is shown in Fig. 8. From Fig. 7 it is obvious that the range of annealing temperatures over which complete thermal eradication of ^4_2He and $^{132}_{54}\text{Xe}$ ion tracks in PC is possible, extends over 30°C . Thus it is evident that it will be possible to eradicate selectively ion tracks in PC by choosing an appropriate annealing temperature. The applications of selective thermal track eradication have been studied by Somogyi⁹ for different practical cases.

3.5 Effect of Temperature on Diameter Distribution

PC samples exposed vertically to $^{132}_{54}\text{Xe}$ ions were annealed for 10 min at 150°C . The areas of annealed and unannealed samples were determined precisely to obtain the track density. The annealed and unannealed samples were etched simultaneously in 6N NaOH at 70°C . Fig. 9 shows the diameter distributions of $^{132}_{54}\text{Xe}$ ion tracks in PC. Studies were made after removing a

12 μm thick layer from the surface of the individual detectors. The experiments reveal that as a result of annealing, etching velocity is lowered in the damage trail. Hence, one expects not only the track density to be reduced, but also the diameters of the etched $^{132}_{54}\text{Xe}$ ion tracks to be diminished. The annealing experiments conducted on the detectors exposed to different ions confirm the above deductions¹¹.

3.6 Effect of Temperature on Maximum Etchable Track Length

The detector sample exposed to a particular ion at an angle of 30° was cut into small pieces. They were then annealed for 10 min at different temperatures. The annealed samples were etched until the tips of the tracks became round. The maximum etched track lengths were determined following the procedure of Benton¹². The effect of annealing temperature on the maximum etchable lengths (i.e. range) of different ions in the plastic detectors is shown in Figs 10 and 11. From these curves it can be seen that the track lengths are, in general, decreased by the application of heat. Again, it is noted that the thermal stabilities of tracks of different ions are different. Thus, the process of discrimination of ion tracks by following different annealing procedures will help in particle identification and background eradication. From a comparison of the curves in Figs 10 and 11 with those in Figs 2 and 3 and similar curves (not shown) it is evident that oblique tracks are less stable than vertical tracks.

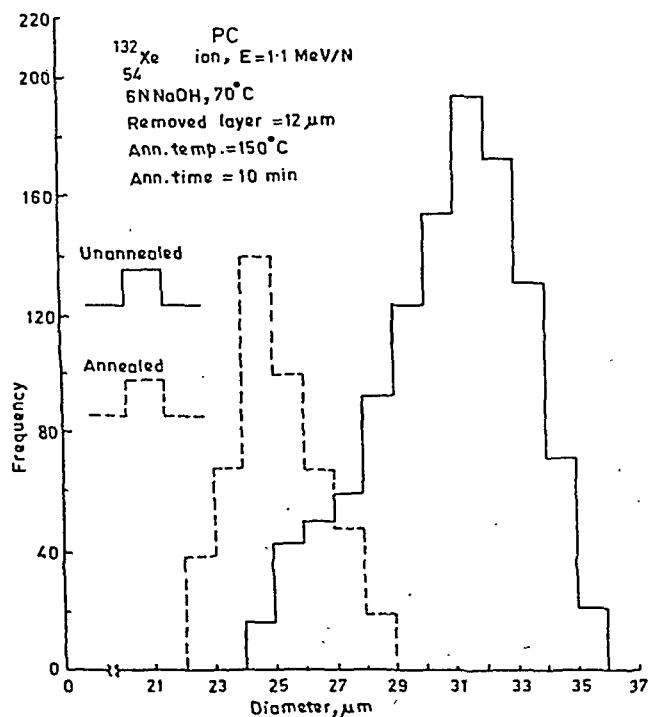


Fig. 9—Diameter distribution of unannealed and annealed $^{132}_{54}\text{Xe}$ ion tracks in PC detector

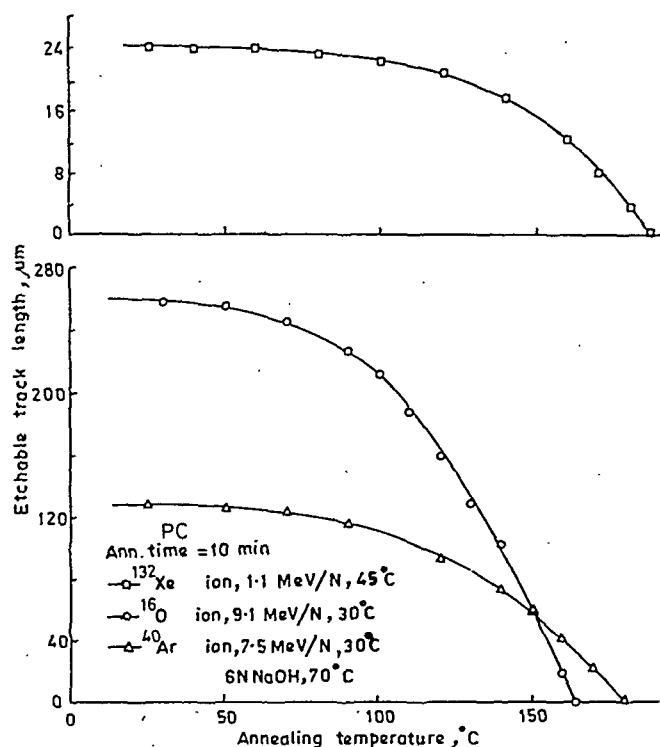


Fig. 10—Variation of maximum etchable track length (i.e. range) with annealing temperature for different ions in PC detector

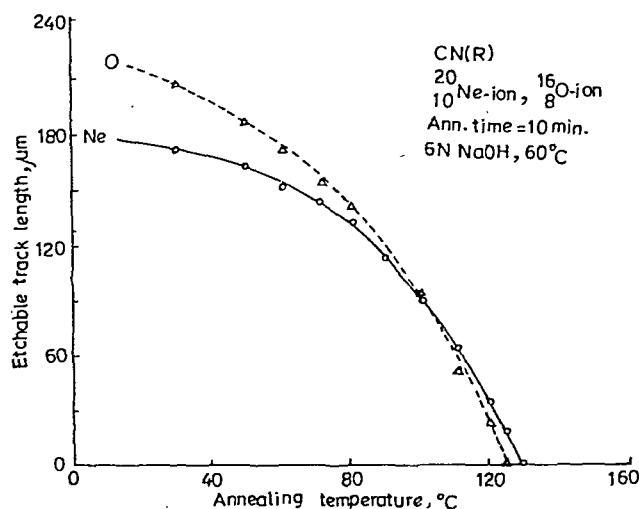


Fig. 11—Variation of maximum etchable track length of ^{20}Ne and ^{16}O ions in CN(R) with annealing temperature

3.7 Effect of Annealing Temperature on Bulk Etch Rate of CR-39

Unexposed samples of CR-39 detector were annealed at different temperatures for 10 min. The samples were then etched simultaneously in 6N NaOH at 70°C . The effect of heat treatment on bulk etch rate of CR-39 plastic is presented in Fig. 12 which shows the thickness of removed layer from a single surface of the detector as a function of etching time for the unannealed sample as well as for the samples annealed at 80, 100, 130 and 140°C . The samples annealed at 150°C and above, on etching for 1 hr, reveal that the plastic gets degraded to a large extent and shows a net-

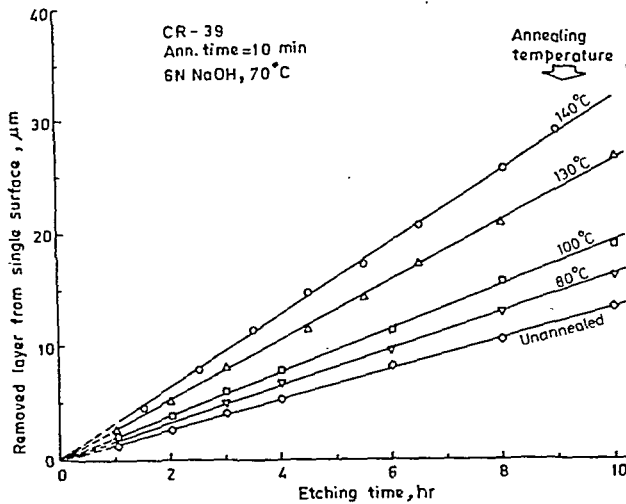


Fig. 12—Thickness of removed layer versus etching time curves for CR-39 annealed at different temperatures for 10 min

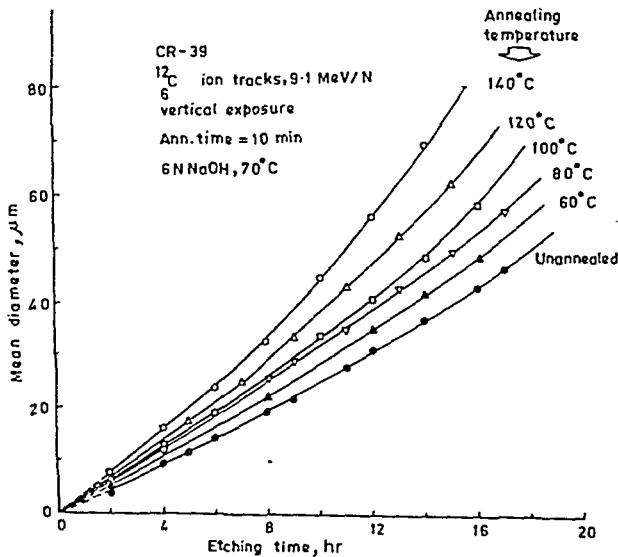


Fig. 13—Relationship between track diameter and etching time for ^{12}C ion tracks in CR-39 annealed for 10 min at different temperatures

like structure in its bulk, indicating that it has become useless from the point of view of track detection. It is observed from Fig. 12 that the bulk etch rate increases progressively with annealing temperature between 80°C and 140°C . This kind of effect may be due to evergrowing degree of thermal degradation of this thermoset plastic. In other words, we can say that the increased etchability of this plastic is due to the generation of free radicals and broken bonds in its bulk, resulting from heating (pyrolysis)¹³⁻¹⁵.

3.8 Effect of Temperature on Track Diameter

The effect of heat treatment on latent tracks of ^{12}C ions in CR-39 plastic is shown in Fig. 13 where the track diameter is plotted as a function of etching time. It is seen that the diameter of the annealed tracks is

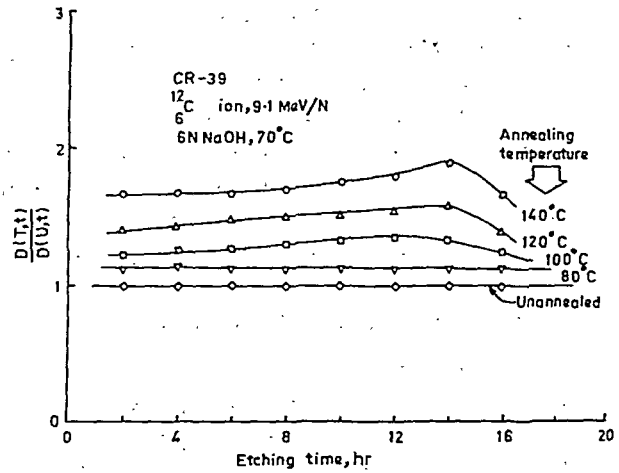


Fig. 14—Variation of the ratio of the diameters of ^{12}C ion tracks for the annealed and unannealed samples of CR-39 detector with etching time

greater than that of unannealed tracks. The ratio of the diameters for the annealed and unannealed tracks as a function of etching time is plotted in Fig. 14. This ratio increases gradually with annealing temperature and varies with etching time for samples annealed above 80°C .

3.9 Effect of Temperature on Etching Efficiency

The etching efficiency ($\eta_{2\pi}$) has been determined^{2,7,15} by counting the total number of tracks revealed in the annealed and unannealed samples which are irradiated in 2π -geometry with a ^{252}Cf source. The track etching efficiency of CR-39 plastic is observed to increase as a result of annealing and the maximum observable effect is seen at 140°C . At this temperature, there is an enhancement of 15% in the etching efficiency.

Thus, it appears to be established beyond doubt that the sensitivity of CR-39 plastic detector is enhanced as a result of thermal annealing. Since the heating of a polymer may generate free radicals and broken bonds¹²⁻¹⁴, which in fact are considered to be responsible for increased etchability of the latent track regions, it is plausible to attribute the enhanced sensitivity of heated CR-39 plastic to this basic phenomenon.

References

- 1 Fleischer R L, Price P B & Walker R M, *Nuclear tracks in solids* (University of California Press, Berkeley, USA), 1975.
- 2 Khan H A & Durrani S A, *Nucl Instrum & Methods (Netherlands)*, 113 (1974) 51.
- 3 Yadav J S, Gomber K L, Singh V P & Sharma A P, *Int J Appl Radiat Isot (GB)*, 31 (1980) 713.
- 4 Wong C F & Field D W, *Radiat Eff (GB)*, 81 (1984) 31.
- 5 Somogyi G, Toth-Szilagyi M, Hunyadi I & Hafez A F, 13th Int Conf on Solid State Nuclear Track Detector, *Nuclear Tracks (GB)*, 1985.

FARID: HEAVY ION TRACKS IN PLASTIC TRACK DETECTORS

- 6 Farid S M & Sharma A P, *Radiat Eff (GB)*, 80 (1984) 121.
- 7 Farid S M, *Study of radiation damage tracks in plastic and glass detectors*, Ph D thesis, Kurukshetra University, Kurukshetra, 1983.
- 8 Somogyi G & Szalay A S, *Nucl Instrum & Methods (Netherlands)*, 109 (1973) 211.
- 9 Somogyi G, *Radiat Eff (GB)*, 16 (1972) 245.
- 10 Schlenk B, Somogyi G & Valek A, *Radiat Eff (GB)*, 24 (1975) 247.
- 11 Luck H B, *Nucl Instrum & Methods (Netherlands)*, 114 (1974) 139.
- 12 Benton E V, *Study of radiation damage tracks in cellulose nitrate—A report* (U S Naval Radiological Defence Laboratory), 1968, TR-68-14.
- 13 Rentov O, *Theoretical principles of organic chemistry* (Translated from Russian by D Aclony (Mir Publications, Moscow) 1970.
- 14 Chand L, Tyagi R K & Srivastava D S, 'Track detection features and sensitivity enhancement of CR-39 plastic detector', Communicated to *Nuclear Tracks (GB)* (personal communication).
- 15 Farid S M, *Nucl Instrum Methods (Netherlands)*, 226 (1984) 501.

A Stable Laser Interferometer for Recording Holographic Gratings

R P SHUKLA

Spectroscopy Division, Bhabha Atomic Research Centre, Trombay, Bombay 400 085

Received 18 October 1985; revised received 14 April 1986

A stable laser interferometer is described for recording holographic gratings. The fringes in the interferometer are found to be very stable and, therefore, it is possible to tolerate longer exposure for recording the grating. It is not necessary to use specially designed massive vibration isolation table for setting up this interferometer. The interferometer may be considered as a modification of the Jamin interferometer which is well known for its stability. The set-up was used for recording the fringes of frequency 1200 lines/mm and 2160 lines/mm. The maximum efficiency of the gratings of frequency 1200 lines/mm recorded on Agfa 10-E-75 plates was achieved to be 25%.

1 Introduction

The conventional¹ set-up for recording holographic grating is shown in Fig. 1. Since the beam splitter, microscope objectives, lenses and plane mirrors are mounted separately, all of them must be mounted on a single massive vibrationless platform in order to keep the fringes free from vibration. Another optical arrangement was described by Yoshida *et al.*² to record the interference fringes. A simple method of producing a holographic grating using a single wedged plate was described by Murty and Shukla³ but it is not possible to obtain a fringe pattern of frequency greater than about 900 lines/mm in this set-up due to technical difficulty of mounting the photographic plate very close to the wedged plate. In the present paper we have described a method for producing a grating of high frequency which has the advantages that (i) the effect of vibration on the fringes is very much reduced, i.e. the fringes are found to be very stable and it is not necessary to use a specially designed massive vibration

isolation table for recording the fringes; and (ii) it is possible to tolerate longer exposure.

2 Interferometer and Experimental Details

A schematic arrangement for making a holographic grating using the method modified by us is shown in Fig. 2. Laser light is focussed on the focal point of a well-corrected lens by means of a microscope objective in order to obtain a collimated beam of light. A spatial filter is placed at the focus of the collimating lens. The collimation of the beam is checked by the Murty⁴ interferometer. The collimated beam of light is incident on a cube type of beam splitter at an angle of incidence of 45°. The partially reflected beam is made incident on a plane mirror at an angle of incidence of 45°. Consequently, the reflected beam from the plane mirror emerges parallel to the directly transmitted beam from the beam splitter. The beam splitter and plane mirror M_1 are held rigidly with respect to each other with a special spacer. The spacer⁵ is made from a glass tube of square cross-section. One end of the glass tube is cut at an angle of 45°. The other end is cut at angle of 90°. Both the ends are ground and the angles

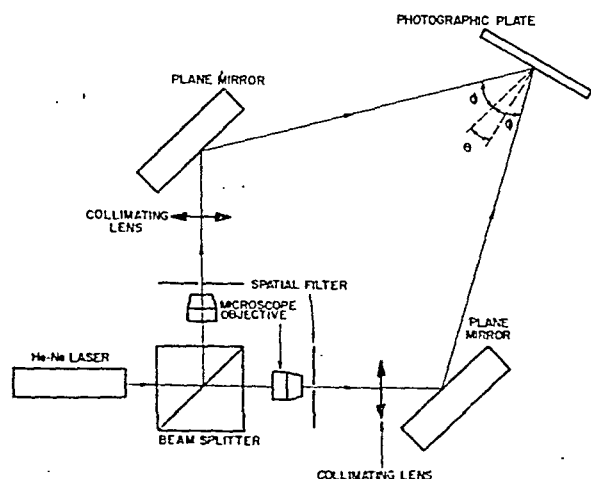


Fig. 1—Conventional set-up for obtaining interference fringes of high frequency

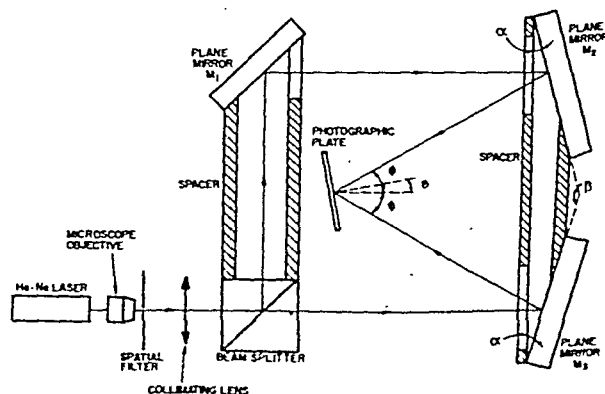


Fig. 2—Schematic diagram of a stable laser interferometer for obtaining interference fringes of high frequency

are corrected. The isometric view of a pair of beam splitter and plane mirror held with spacer is shown in Fig. 3. The system as a whole becomes equivalent to one thick Jamin plate whose front and rear surfaces are separated partly by air and partly by glass. The reflected and transmitted beams obtained by this assembly are superimposed on a photographic plate after reflections from the plane mirrors M_2 and M_3 . The interference fringes are recorded on the photographic plate and the fringe frequency (ν) is determined by the following relation:

$$\nu = \frac{2 \sin \varphi \cos \theta}{\lambda} \quad \dots (1)$$

where 2φ is the angle between the two interfering beams, θ the angle between the bisector of the beams and normal to the recording plate and λ the wavelength of light.

In order to make the fringes stable, the plane mirror M_2 and the plane mirror M_3 are held rigidly with respect to each other with a special spacer. This spacer is also made from a glass tube of rectangular cross-section. Both the ends of the tube are cut at an angle α and the angles are corrected by the grinding process. The isometric view of the two mirrors M_2 and M_3 held

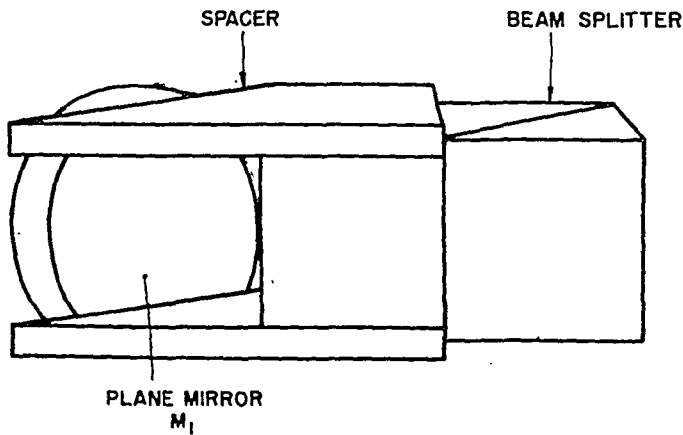


Fig. 3—Isometric view of the beam splitter and plane mirror held with a spacer

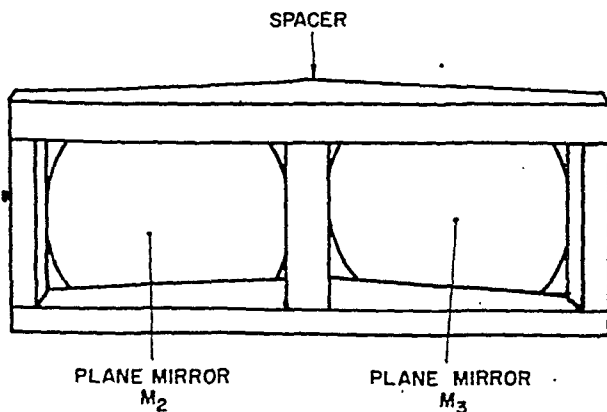


Fig. 4—Isometric view of the plane mirrors M_2 and M_3 held with a prism type of spacer

with spacer is shown in Fig. 4. The system as a whole becomes equivalent to an air prism whose angles are α , α and β . The relation between the prism angle (α) and the angle between the interfering beams (2φ) is given by $\varphi = 2\alpha$... (2)

Using Eq. (1) and Eq. (2) the prism angle can be calculated for the required frequency of the grating. Air prisms with the angle α being 11.157° and 21.555° were fabricated for making gratings of frequency 1200 lines/mm and 2160 lines/mm respectively. The interferometer was set up with such modified assemblies shown in Fig. 3 and Fig. 4.

In order to test the stability of the fringes, a low power He-Ne laser of power about 0.5 mW was used for making a grating. Exposure of the order of 5 min was given for recording the fringes on Agfa 10-E-75 plates. Another grating was made by using a He-Ne laser of power about 3 mW and giving an exposure of 1s. The maximum efficiency of the bleached^{6,7} holographic grating of frequency 1200 lines/mm was measured to be 10%. The efficiencies of the gratings made by the short and long exposures were compared. No change in the efficiency was noticed. This shows that the fringes remain stationary during the longer period of exposure. The stability of the fringes was also checked by observing the Moire fringes. These fringes were obtained by placing the grating of frequency 1200 lines/mm at the recording plane where the fringes of frequency 1200 lines/mm were formed due to the superposition of the two beams. The Moire fringes remained stationary during the period of observation. Hence, it is not necessary to set up the interferometer on a specially designed massive and expensive vibration isolation table. The efficiency of the gratings produced in this set-up can be increased by the use of a laser with a narrow band width and Kodak 120-02 plates as shown by Graube⁷. Because of non-availability of above mentioned materials with us we could not repeat Graube's experiments.

This set-up may be useful for recording the fringes of high frequency where the vibrations become much more important for recording the fringes. Longer exposures are required for recording the fringes on photoresist using Ar^+ laser due to low sensitivity of the photoresist. Hence the set-up may find application for making reflection gratings which are made on the photoresist⁸⁻¹⁰.

3 Alternative Optical Arrangements

However, Murty¹¹ pointed out that the set-up shown in Fig. 2 has an inherent large optical path difference built into it. Therefore, a laser with a narrow band width has to be used for recording. Due to the large path difference there may be a frequency-

dependent fringe shift at the recording plane. If the wavefronts are not truly plane, the path difference will cause a mismatch between their shapes at the recording plane. Then the fringes will not be straight. Hence it is better to arrange the scheme in such a way that the optical path difference is zero at the middle of the recording plate. Such an arrangement is shown schematically in Fig. 5. Additional plane mirrors M_4 and M_5 are introduced in the set-up of Fig. 2 in order to make the optical path difference zero at the recording plate. For achieving the stability of the fringes, the plane mirrors M_4 and M_5 are held rigidly with respect to a special spacer. The plane mirror assembly is then kept in contact with the beam splitter so that it becomes an integral part of it. The separation of the plane mirrors M_4 and M_5 can be calculated by knowing the distance of the recording plane from the beam splitting surface via the M_1 , M_2 path. The separation between the plane mirrors M_1 and the beam splitter is chosen according to the required separation of the interfering beams. The accuracy of the plane mirrors and the beam splitting surface needed for the set-up is very high.

Another optical arrangement for making holographic grating is shown schematically in Fig. 6. The positions of the plane mirrors M_1 and M_3 are chosen in such a way that the optical path difference is zero at the recording plate. The beam splitter and the plane mirror M_1 are held rigidly with respect to each other with a special spacer. Similarly, plane mirrors M_2 and M_3 are fixed rigidly on the ends of the spacer by a mechanical clamp in order to make a stable optical arrangement. This plane mirror assembly is then fixed at the exit face of the beam splitter. An interferometer based on the optical arrangement of Fig. 6 was set up for recording the grating of frequency 1200 lines/mm. The maximum efficiency of the gratings recorded in this set-up was measured to be 25% whereas the maximum efficiency of the gratings recorded in the set-up of Fig. 2 was 10%.

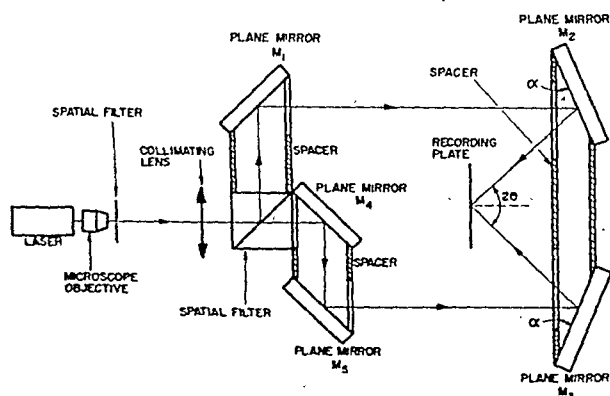


Fig. 5—Schematic optical arrangement for obtaining interference fringes of high frequency [The optical path difference between the two beams is nearly zero in this set-up.]

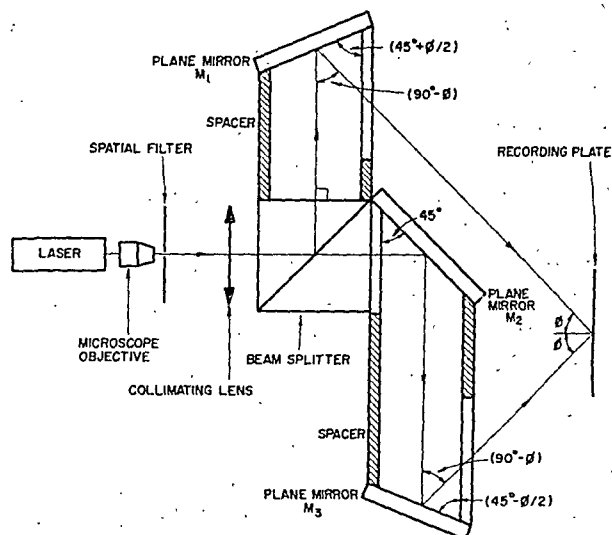


Fig. 6—Alternative optical arrangement for obtaining interference fringes of high frequency [The optical path difference between the two beams is nearly zero at the middle of the recording plate.]

This drop in efficiency may be due to large optical path difference which reduces the contrast of the fringes in the interferometer of Fig. 2. Hence the optical arrangement of Fig. 6 is superior to that of Fig. 2.

In Fig. 6, one of the beams becomes parallel to the plane mirror M_2 for the case $\varphi = 45^\circ$ and hence this beam will not be obstructed by the plane mirror M_2 before reaching the recording plate. Therefore, a limit can be set on the maximum value of φ which can be obtained in the set-up. Such a limit on φ is about 45° which corresponds to a fringe frequency of about 2900 lines/mm using a wavelength of 4880 \AA . The set-up shown in Fig. 6 is useful for making the gratings of frequency up to 2900 lines/mm. It should be kept in mind that only one frequency can be recorded for one set of spacers. It will be necessary to make a separate set of spacers for the gratings of a different frequency. This is a disadvantage of using spacers as compared to the conventional optical arrangement of Fig. 1 where gratings of any desired frequency can be obtained by changing the angular orientation of the mirrors. As far as the stability is concerned, the optical arrangements described above are superior to the conventional optical arrangement shown in Fig. 1.

Among the three optical arrangements shown in Fig. 2, Fig. 5 and Fig. 6, the arrangement of Fig. 6 is the best, as it requires the minimum number of optical components for setting up the interferometer, and also the optical path difference between the two beams can be made nearly zero at the middle of the recording plate.

Acknowledgements

The author is indebted to Dr S L N G Krishnamachari, Head, Spectroscopy Division for his

suggestions and encouragement throughout the course of this work. The author wishes to thank Dr M V R K Murty, Halo Technologies Inc, Costa Mesa, California (USA) for his suggestion during the course of this work.

References

- 1 Iwata F & Tsujiuchi J, *Appl Opt (USA)*, **13** (1974) 1327.
- 2 Yoshida M, Yoshihara K & Kamiya K, *Science of Light (Japan)*, **22** (1973) 146.
- 3 Murty M V R K & Shukla R P, *Indian J Pure & Appl Phys*, **14** (1976) 153.
- 4 Murty M V R K, *Appl Opt (USA)*, **3** (1964) 531.
- 5 Murty M V R K & Shukla R P, *Indian J Phys*, **50** (1976) 139.
- 6 Hariharan C P & Ramanathan C S, *Appl Opt (USA)*, **10** (1971) 2197.
- 7 Graube A, *Appl Opt (USA)*, **13** (1974) 2942.
- 8 Beesley M J & Castledine J G, *Appl Opt (USA)*, **9** (1970) 2720.
- 9 Bartolini R A, *Appl Opt (USA)*, **11** (1972) 1275.
- 10 Bartolini R A, *Appl Opt (USA)*, **13** (1974) 129.
- 11 Murty M V R K, private communication to the author, 1985.

Mean Square Amplitudes of Vibration & Associated Debye Temperatures of Dysprosium, Gadolinium, Lutetium & Yttrium*

N GOPI KRISHNA, D B SIRDESHMUKH

Physics Department, Kakatiya University, Warangal 506 009, India

and

B RAMA RAO

X-ray Division, Regional Research Laboratories, Hyderabad 500 009, India

and

B J BEAUDRY & K A GSCHNEIDNER(Jr)

Ames Laboratory, Iowa State University, Ames, Iowa 50011, USA

Received 3 February 1986; revised received 26 May 1986

The directional mean square amplitudes of vibration and associated Debye temperatures of hexagonal dysprosium, gadolinium, lutetium and yttrium have been obtained from X-ray intensities. The integrated intensities have been measured with a Philips PW 1051 powder diffractometer fitted with a proportional counter using CuK_α radiation at room temperature and have been corrected for thermal diffuse scattering. The experimental values of directional Debye temperature have been compared with corresponding values obtained from theoretical calculations. Values of energy of vacancy formation for the metals studied have been estimated using a relation connecting it with the Debye temperature given by HR Glyde [*J Phys & Chem Solids* (GB), 28 (1967) 2061].

1 Introduction

There is meagre work on the X-ray determination of Debye temperatures of rare earth metals. Holmium¹, erbium² and ytterbium³ appear to be the only rare earth metals to have been studied so far. Of these, holmium and erbium have the hcp structure. Recently Singh and Varshni⁴ made theoretical calculation of 'X-ray Debye temperatures' of hexagonal crystals including some rare earth metals using elastic constant data; average as well as directional Debye temperatures were calculated. They made a comparison of their calculated results with some available experimental results. In the case of rare earth metals, they could compare their theoretical results with experimental values only in the case of holmium as experimental results were not available for any other hcp rare earth metal. The results of an X-ray study of dysprosium, gadolinium, lutetium and yttrium are being reported here. Mean square amplitudes of vibration have been determined from the intensities. From these, average and directional Debye temperatures have been obtained and these are compared with values obtained from other methods.

2 Experimental Procedure

The metal samples used in this study were prepared at the Ames Laboratory, Iowa State University. These samples were prepared by the metallothermic

reduction of RF_3 (R=rare earth metal) with Ca followed by distillation. Chemical analysis given in Table I indicates that the metals were highly pure. The non-metallic impurities H, O and N were found to be present at a concentration (ppm atomic) of 800, 300, 3, respectively for dysprosium; 600, 350 and 45 for gadolinium; 1350, 1850 and 75 for lutetium and 700, 830 and 25 for yttrium. The metallic impurities found to be present with a concentration more than 5 ppm are reported in Table 1.

X-ray measurements were made with a Philips PW 1051 diffractometer fitted with a proportional counter using CuK_α radiation. The X-ray tube was operated at 36 kV and 15 mA. A 1° divergent slit was used for $2\theta < 80^\circ$ and 4° slit for $2\theta > 80^\circ$. All measurements were made at room temperature. The intensities were recorded on a strip-chart recorder. Integrated intensities were obtained from the area under a Bragg peak after subtracting the background.

The metal samples were available in the form of discs. Initially measurements were made on the discs in the as-received condition. A preliminary analysis of the intensity data revealed the presence of preferred orientation. As such, the data were discarded. Fine filings were obtained from the discs with the help of a jeweller's file. The filing was carried out slowly. In all cases, the first crop of filings from the surface of the discs was rejected and filings from the freshly revealed surface were employed. The filings were passed through a 325 mesh screen. Preferred orientation effects and extinction effects are minimised when the

*Project operated for the US Department of Energy by Iowa State University under contract No. W-7405-ENG-82. This work was supported by the office of Basic Energy Sciences.

filings are thus prepared⁵. The filing process, however, introduces two potential sources of error, which are discussed in Sec. 4.

The intensities have been corrected for thermal diffuse scattering using the method of Chipman and Paskin⁶. The absorption correction for a flat sample is angle independent⁵ and hence can be included in the scale factor. The 'porosity effect'⁷ can also be lumped with the scale factor. The surface roughness effect becomes significant only at $2\theta < 20^\circ$; the reflections used in these studies have $2\theta > 20^\circ$.

3 Analysis of Data

The integrated intensity of a Bragg reflection from a hexagonal crystal may be written as⁸⁻¹⁰:

$$I = C(LP)JF^2 \exp \{ -(4\pi \sin \theta / \lambda)^2 \} \times [\langle u_{\parallel}^2 \rangle \cos^2 \varphi + \langle u_{\perp}^2 \rangle \sin^2 \varphi] \quad \dots (1)$$

where I is the measured integrated intensity corrected as discussed, C the scale factor, (LP) the Lorentz-polarization factor, J the multiplicity factor and F the structure factor. θ and λ are the Bragg angle and wavelength. $\langle u_{\parallel}^2 \rangle$ and $\langle u_{\perp}^2 \rangle$ represent the components of the average mean square amplitude of vibration projected on the hexagonal axis and the basal plane respectively; φ is the angle between the diffraction vector and the hexagonal axis. The structure factors are calculated from the atomic scattering factors given by Cromder and Waber¹¹. These are corrected for anomalous dispersion¹². $\langle u_{\parallel}^2 \rangle$ and $\langle u_{\perp}^2 \rangle$ are obtained² from a least squares analysis of the logarithmic form of Eq. (1). From these, the average mean square amplitude $\langle u_{av}^2 \rangle$ can be obtained from the relation:

$$\langle u_{av}^2 \rangle = (1/3)(\langle u_{\parallel}^2 \rangle + 2\langle u_{\perp}^2 \rangle) \quad \dots (2)$$

The effective average Debye temperature (θ_{av}) and the directional Debye temperatures θ_{\parallel} and θ_{\perp} are obtained from $\langle u_{av}^2 \rangle$, $\langle u_{\parallel}^2 \rangle$ and $\langle u_{\perp}^2 \rangle$ by well-known procedures¹⁰.

4 Results

The values of the mean square amplitude of vibration and Debye temperatures are given in Table 2. Keeping the limits of error in view, it is seen that the

anisotropy in the value of the amplitude of vibration is slight. As a consequence, the directional Debye temperatures also exhibit only a slight anisotropy. The directional Debye temperatures are of the same order as those obtained by Singh and Varshni⁴. However, for all the four metals, the values obtained experimentally are lower than the values obtained theoretically. It is worth mentioning that Singh and Varshni⁴ have also concluded that, in general, the Debye temperatures obtained experimentally from X-rays are lower than those calculated theoretically. The average Debye temperature is also reported in Table 2. Values of the Debye temperature obtained from specific heat data (θ_D)¹³ are also given for comparison. The values of θ_D obtained using X-ray data agree well with those obtained using specific heat data, especially in the cases of Dy and Y. It may, however, be mentioned that exact agreement is not expected between the values of θ_D obtained by these two methods.

Since the materials examined in this study were prepared by filing, the filing process could have an effect on the measured θ_D . In the course of filing a metal, the material is cold-worked, hardening it. This stiffening of the lattice could cause an increase in θ_D over that of a fully annealed metal. At most, this would cause an increase in θ_D of 5 K. A potentially more serious problem is that during filing, the rare earth metals may pick up appreciable amounts of hydrogen¹⁴. As shown by Thome *et al.*¹⁵ small amounts of hydrogen, i.e. 5700 ppm atomic (28 ppm weight), can increase the θ_D value by more than 11% (20 K) in Lu metal. But since the measured X-ray θ_D values are only slightly larger for three of the four metals studied (Dy: 2K, Gd: 10K and Y: 5K) and considerably smaller (18 K) for the fourth than the heat-capacity derived θ_D values, it is doubtful that these two factors have much effect on the values reported here.

Imperfections in the crystal lattice play an important role in controlling many physical properties of metals. The concentration of vacancies in a metal at a given temperature depends upon the value of the energy of vacancy formation. Thus, an estimation of energy of vacancy formation is useful in understanding the

Table 1—Metallic Impurities in Dy, Gd, Lu and Y
(in ppm atomic)

Sample	Impurity												
	Fe	Nb	Na	Pb	Cu	Ho	Ta	Al	Ni	Cr	Si	Gd	Co
Dy	4	20	—	5	10	25	20	6	—	7	—	5	5
Gd	20	—	—	—	6	—	12	—	5	—	—	—	—
Lu	35	6	—	—	17	—	—	20	10	—	8	9	—
Y	6	—	7	—	—	—	42	—	—	—	—	—	—

Table 2—Mean Square Amplitudes of Vibration (in Å²), Directional and Average Debye Temperatures in (K) for Dy, Gd, Lu and Y.

Substance	$\langle u_{\parallel}^2 \rangle$	$\langle u_{\perp}^2 \rangle$	θ_{\parallel}	θ_{\perp}	θ_{av}	
					θ_{av} (X-ray)	θ_D^{13}
Dy	0.0113 ± 0.0009	0.0102 ± 0.0010	154 (185.0)	162 (181.3)	160	158
	0.0112 ± 0.0003	0.0101 ± 0.0002	157 (177.3)	166 (173.9)	165	155
Lu	0.0123 ± 0.0008	0.0109 ± 0.0008	142 (180.7)	151 (182.3)	148	166
	0.0101 ± 0.0004	0.0105 ± 0.0003	221 (252.6)	217 (249.4)	219	214

values of Debye temperatures in parentheses are those theoretically evaluated by Singh and Varshni⁴.

defect state of a metal. For many rare earth metals, this value is not known from experiment and it is desirable to obtain it from any other known physical quantity. An attempt is made here to obtain the information from Debye temperatures.

Glyde¹⁶ derived the following relation between the energy of vacancy formation (E_f) and the Debye temperature (θ) of a solid:

$$E_f = A(k/h)^2 M \theta^2 a^2 \quad \dots (3)$$

where a is the interatomic spacing, A a constant shown to be equal to 1.17. M the molecular weight and h and k are the Planck's and Boltzmann's constants respectively. Glyde¹⁶ had discussed the causes for the slight difference in Debye temperature values as obtained from specific heat data and from X-ray diffraction data and recommended the use of X-ray based values for use in Eq. (3). A rigorous derivation of Eq. (3) was given by Tewary¹⁷ who verified validity of Eq. (3) for a number of fcc, bcc and hcp metals.

Neither Glyde¹⁶ nor Tewary¹⁷ have included the rare earth metals in their studies. The values of θ_D based on X-ray data were used to calculate the vacancy formation energy for the rare earth metals using Eq. (3). The values estimated are 1.096 eV, 1.165 eV, 0.965 eV, and 1.154 eV for dysprosium, gadolinium, lutetium and yttrium respectively. The experimental values of E_f for dysprosium, gadolinium and lutetium are not available for comparison. However, the experimental value of 1.439 eV reported by Dariel¹⁸

for yttrium compares reasonably with the value calculated using Eq. (3).

References

- 1 Skelton E P, *J Appl Crystallogr (Denmark)*, 2 (1969) 106.
- 2 Gopi Krishna N & Sirdeshmukh D B, *Phys Status Solidi b (Germany)*, 116 (1983) K105.
- 3 Gopi Krishna N, Sirdeshmukh D B, Rama Rao B, Beaudry B J & Gschneidner K A (Jr), *Phys Status Solidi a (Germany)*, 89 (1985) K37.
- 4 Singh D & Varshni Y P, *Acta Crystallogr Sect A (Denmark)*, 38 (1982) 854.
- 5 Klug H P & Alexander L E, *X-ray diffraction procedures* (John Wiley & Sons, New York), 1974.
- 6 Chipman D R & Paskin A, *J Appl Phys (USA)*, 30 (1959) 1998.
- 7 Suortti P, *J Appl Crystallogr (Denmark)*, 5 (1972) 325.
- 8 Blackman M, *Acta Crystallogr (Denmark)*, 9 (1956) 734.
- 9 Lipson H, *International tables for X-ray crystallography*, Vol. 2 (Kynoch Press, Birmingham), 1959.
- 10 James R W, *The optical principles of the diffraction of X-rays* (Bell & Sons, London), 1967.
- 11 Cromder D T & Waber J T, *Acta Crystallogr (Denmark)*, 18 (1965) 104.
- 12 Cromder D T & Liberman D, *J Chem Phys (USA)*, 53 (1970) 1891.
- 13 Gschneidner K A (Jr), *Solid State Physics (USA)*, 16 (1964) 275.
- 14 Spedding F H & Beaudry B J, *J Less Common Metals (USA)*, 25 (1971) 61.
- 15 Thome D K, Gschneidner K A (Jr), Mowry G S & Smith J F, *Solid State Commun (USA)*, 25 (1978) 297.
- 16 Glyde H R, *J Phys & Chem Solids (GB)*, 28 (1967) 2061.
- 17 Tewary V K, *J Phys F (GB)*, 3 (1973) 704.
- 18 Dariel M P, *Handbook on the physics and chemistry of rare earths*, Editors K A Gschneidner (Jr) & L Eyring, Vol. 1 (North-Holland, Amsterdam), 1978, 847.

Nearest Cation-Anion Distance in Fused Salts

ASIM R PURKAIT & DILIP K MAJUMDAR

Department of Chemistry, University of Kalyani, Kalyani 741 235

Received 26 June 1985; revised received 12 May 1986

Based on an equation for α/β_c , the nearest cation-anion distances (σ) in fused salts have been evaluated within the hard-sphere approximation. The calculated values of σ for LiCl, LiBr, NaCl, NaBr, NaI, KCl, KBr, KI, CsCl and CsBr while decreasing with temperature, agree closely with the gas-phase bond length and increase in the order $\text{LiX} < \text{NaX} < \text{KX} < \text{CsX}$ at any temperature between 600-1000°C, X being Cl, Br or I. The hard-sphere approximation is justified by noting that the equation for α/β_c contains only second-order perturbation corrections which are usually small and the ratio α/β_c is thus predominantly determined by hard-sphere potential. Analysis of the computed values of nearest cation-anion distances reveal that melts of fused salts possess 'less structure' in the neighbourhood of melting points, while the hard-sphere approximation may not be valid for fused salts at temperatures far removed from the melting points.

1 Introduction

Information about cation-anion distance in alkali halide molecules is chiefly gathered from thermochemical studies on crystalline salts¹. The cation-anion separation obtained from such studies naturally refer to equilibrium values in crystalline state. Microwave absorption spectra of vapour yield very accurate data on interionic separation². These two sets of data, however, differ from each other. X-ray and neutron diffraction studies on fused salts may also be utilized to obtain mean ionic diameters of salts in the molten state³⁻⁶.

On the other hand, there have been several attempts at calculating cation-anion distance by the application of 'Scaled particle theory' to fused salts. This is based on the principle of 'corresponding state' idea, according to the properties of fused salts depend only on the value of parameter σ which represents the sum of the cation and anion radii, and not on their individual values.

By using experimental values of isothermal compressibility in an equation derived from the 'Scaled particle theory', Stillinger⁷ calculated the mean ionic diameter σ , which turned out to be smaller than the values determined following Pauling's theory in case of crystals, though they were usually higher than the gas-phase bond distances. Mayer⁸ based his calculation of σ on the 'Scaled particle theory' but using surface tension and compressibility data, while Reiss and Mayer⁹ used the gas-phase bond length to calculate the surface tension for fused salts. Values of surface tension calculated by Reiss and Mayer⁹ were in agreement with experimental values for all crystalline salts except partially covalent salts. All these studies indicate that the hard-sphere fluid concept is quite useful in obtaining and correlating properties of fused

salts using the hard-sphere diameter as the only parameter.

In the course of our studies on the theory of liquids, we had seen that the ratio of the expansion coefficient α to the isothermal compressibility β_c of liquids is determined predominantly by the hard-sphere potential. We have¹⁰

$$\alpha/\beta_c = \rho k [z_0 + y^2 \eta \{H(b_1 + 2b_2 \eta) + H' \eta (b_1 + b_2 \eta)\}] \quad \dots (1)$$

where ρ is the number density of molecules, k the Boltzmann's constant, b_1 and b_2 are second order perturbation correction constants and

$$y = \varepsilon_0/kT$$

$$H = (1 - \eta)^4/(1 + 2\eta)^2$$

$$H' = dH/d\eta \text{ and } \eta = \frac{\pi}{6} \rho \sigma^3$$

σ and ε_0 being the appropriate hard-sphere diameter and potential depth respectively. In Eq. (1), z_0 is the compressibility factor for hard-sphere fluid well described by Percus-Yevic equation^{11,12}

$$z_0 = (1 + \eta + \eta^2)/(1 - \eta)^3 \quad \dots (2)$$

Now, it has already been established for non-polar liquids, that the attractive potential does not have any significant contribution to the ratio α/β_c represented by Eq. (1). We may, therefore, neglect the second order correction in Eq. (1) and from Eqs (1) and (2), we have

$$\alpha/\beta_c = \rho k (1 + \eta + \eta^2)/(1 - \eta)^3 \quad \dots (3)$$

Eq. (3) has been employed for evaluation of effective hard-sphere molecular diameters of a variety of liquids at different temperatures¹⁰. The calculated values of σ are found to decrease with increasing temperature and

for aliphatic hydrocarbons, the value increases as one ascends the homologous series.

Eq. (3) is strictly valid for fluids having short-range interaction. For ionic liquids, such as molten alkali halides having long-range electrostatic interaction, it appears that contribution from attractive potential may not be negligible in determining the ratio α/β_c . Yet, there are evidences that the properties of molten salts may be adequately described within the hard-sphere approximation. The values of various properties such as compressibility^{13,14}, expansivity^{13,14}, heat capacity¹⁵, entropies of fusion¹⁵ and surface tension⁹ have been evaluated by employing equations based on hard-sphere equation of state and found to be in agreement with experimental values. These considerations led us to believe that a successful application of Eq. (3) can be made in case of molten salts as well.

2 Fused Salts: Calculation of Mean

Ionic Diameter

We restrict our discussion to 1-1 salts in the molten state. We further note that the salts are completely dissociated and the structural units are the ions, so that the number density ρ is:

$$\rho = \frac{N_+ + N_-}{V}$$

where N_+ and N_- are the number of positive and negative ions present in the volume V . If V is the molar volume and the salts are completely dissociated into ions, we have:

$$N_+ = N_- = N$$

where N is the Avogadro's number. Thus

$$\rho = 2N/V \quad \dots (4)$$

It is assumed that the only predominant interaction in an ionic melt is the nearest cation-anion contact, so that an ion, positive or negative may be regarded to possess an average diameter equal in magnitude to the cation-anion separation σ . Bearing in mind that for fused salts, σ in Eq. (3) represents the nearest cation-anion distance in molten salts, we have from Eqs (3) and (4)

$$\alpha/\beta_c = \frac{2R}{V} \cdot \frac{(1 + \eta + \eta^2)}{(1 - \eta)^3} \quad \dots (5)$$

Using in Eq. (5) the value of the molar gas constant R , we can solve for η , provided the values of expansion coefficient α , isothermal compressibility β_c , and molar volume V are known at that temperature. The mean cation-anion distance σ is then obtainable from Eq. (6)

$$\sigma = (3\eta V/\pi N)^{1/3} \quad \dots (6)$$

Bockris and Richards¹⁶ reported experimental values of isothermal compressibility β_c of a large number of molten salts at selected temperatures. We have utilized these values of β_c and wherever necessary interpolation was done to get the values of β_c at the required temperatures and these are shown in Table 1.

The values of density of the alkali halide melts at several temperatures, shown in Table 1 are taken from the International Critical Tables¹⁷ and from reports of Yaffe and Van Artsdahlen¹⁸. We have calculated the thermal expansion coefficient using the temperature variation of the density¹⁸ and these are given in Table 1.

With these values of α , β_c , and density from the literature¹⁶⁻¹⁸, values of σ have been calculated for 10 fused salts at several temperatures in the range 600-1000°C. These values of σ (Table 1) are comparable with the gas-phase bond distance^{2,19}.

3 Results and Discussion

It is seen (Table 1) that the mean ionic diameter decreases with increasing temperature for all the fused salts studied in this investigation. This is in agreement with the observation made by Stillinger²⁰. The values of σ increase in the order: $\text{LiX} < \text{NaX} < \text{KX} < \text{CsX}$, X being a halogen. The position of rubidium halides is not ascertained, since we could not evaluate the nearest cation-anion distance for these salts as the compressibility data are not available. Further, the values of σ computed by us is lower than those reported by Mayer⁸ and by Stillinger²⁰ but agree more closely with the gas-phase bond length for the salts in the vapour state as determined by Honig and coworkers². The values of σ based on Eq. (5) which utilizes the expansivity and compressibility of fused salts, decrease relatively slowly in comparison to those given by Stillinger.

It may be mentioned that large first-order perturbation correction over hard-sphere contribution enters into equations of expansion coefficient or of compressibility^{21,22}. This was seen to be true for several non-polar liquids¹⁰. It will, therefore, not be appropriate to ignore perturbation correction and employ the hard-sphere compressibility equation:

$$\beta_c = V(1 - \eta)^4/RT(1 + 2\eta)^2 \quad \dots (7)$$

or expansivity equation:

$$\alpha = (1 - \eta^3)/T(1 + 2\eta)^2 \quad \dots (8)$$

separately for the purpose of evaluating σ , even for molecular liquids. This criticism is, however, not relevant to the use of Eq. (5) in which the ratio α/β_c contains only second-order perturbation corrections,

Table 1—Calculated Values of Nearest Cation-Anion Distances (σ) in Fused Salts at Different Temperatures

Salt	Temperature °C	Density (g/cm ³)	Expansion coefficient* $\alpha \times 10^4 \text{ K}^{-1}$	compress- ibility $\beta_c \times 10^{12} \text{ cm}^2$ dyne (Ref. 16)	σ , Å	
					Present study	Litera- ture ²⁰
LiCl (2.0207)	700	1.4579	2.96	21.71	2.09	2.31
	800	1.4147	3.05	24.70	2.05	2.26
	900	1.3716	3.15	28.60	2.01	2.20
	1000	1.3284	3.25	33.00	1.96	2.14
LiBr (2.1704)	600	2.4966	2.61	22.70	2.22	2.53
	700	2.4314	2.68	25.80	2.18	2.49
	800	2.3661	2.76	29.40	2.14	2.43
	900	2.3009	2.84	33.60	2.08	2.38
	1000	2.2356	2.92	38.40	2.02	2.31
NaCl (2.3606)	800	1.5489	4.02	28.7	2.48	2.47
	900	1.4866	4.19	33.8	2.46	2.41
	1000	1.4243	4.37	40.0	2.44	2.34
NaBr (2.5020)	800	2.2983	3.55	33.6	2.55	2.63
	900	2.2166	3.69	38.6	2.53	2.58
	1000	2.1349	3.83	44.9	2.50	2.51
NaI (2.7115)	700	2.7039	3.51	40.0	2.76	2.88
	800	2.6090	3.64	47.3	2.71	2.82
	900	2.5141	3.78	55.6	2.67	2.74
	1000	2.4192	3.92	65.6	2.62	2.66
KCl (2.6666)	800	1.5080	4.02	38.4	2.70	2.70
	900	1.4474	4.19	45.7	2.66	2.63
	1000	1.3868	4.37	54.7	2.63	2.55
KBr (2.8207)	800	2.0732	4.00	43.8	2.84	2.85
	900	1.9903	4.17	52.1	2.81	2.78
	1000	1.9073	4.35	62.1	2.78	2.70
KI (3.0478)	700	2.4295	3.93	49.9	3.03	3.09
	800	2.3339	4.09	59.9	2.99	3.01
	900	2.2384	4.27	72.0	2.95	2.93
	1000	2.1428	4.46	87.3	2.89	2.82
CsCl (2.9062)	700	2.7327	3.90	42.9	2.96	3.01
	800	2.6262	4.06	51.2	2.93	2.93
	900	2.5197	4.23	62.7	2.87	2.84
	1000	2.4132	4.41	76.3	2.81	2.74
CsBr (3.0722)	700	3.0545	3.05	55.8	3.00	3.06
	800	2.9322	2.93	67.1	2.95	2.98
	900	2.8998	2.90	82.7	2.88	2.88
	1000	2.6875	2.69	103.1	2.78	2.75

*Based on density values at selected temperatures given in Refs 17 and 18
Values in parentheses indicate gas-phase bond distance in Å (Ref. 2)

which are usually negligibly small and, therefore, ignored.

It was stressed by Ubbelohde²³ that the bond length, in an isolated ion-pair is determined by the electrostatic polarization forces between the ions and correspond to the minimum in the potential energy curve. As a consequence of long-range order in crystals, the presence of neighbouring ions reduce the electrostatic polarization forces holding an ion-pair. This would result in an enhanced value for the bond length in a crystal compared to that in an isolated ion-pair or to gas-phase bond length. For melts, however, the long-range order is not fully destroyed as in

vapour. Consequently, the bond length or the nearest cation-anion distance in fused salts is expected to be larger than the gas-phase bond length but smaller than that in a crystal. This is clearly obeyed by the σ data computed in the present study (Column 6, Table 1) for fused salts at temperatures near the melting points. The exceptions are, however, KI and CsBr for which we notice that even at temperatures near melting points the value of σ is nearly the same or even less than the gas-phase bond length.

In general, this supports the prevalent idea that the fused salts possesses rudiments of a structure generated from the crystal by partial loss of long-range

order on melting. As the nearest cation-anion distance approximates closely to the gas-phase bond length, observations of the the present study indicate that a model with less long-range order, that is, with 'less structure' than would be expected from an analysis of σ reported by Stillinger, is preferable. The decrease of effective σ for fused salts with increase in temperature in the neighbourhood of melting points, is explainable as due to progressive loss of long-range order. However, the effective σ at around 1000°C falls below the gas-phase bond length. This implies that the hard-sphere approximation may not be valid for a fluid at temperatures far removed from the melting point.

References

- 1 Pauling L, *The nature of chemical bond* (Cornell University Press, Ithaca, New York), 3rd edn, 1960, 344.
- 2 Honig M A, Mandel M, Stich M L & Townes C H, *Phys Rev (USA)*, 96 (1954) 629.
- 3 Levy H A, Argon P A, Bredig M A & Danford M D, *Ann New York Acad Sci (USA)*, 79 (1960) 72.
- 4 Zarzycki J, *Phys Rad A (France)*, 18 (1957) 65; 19 (1958) 13.
- 5 Furukawa K, *Disc Faraday Soc (GB)*, 32 (1961) 53.
- 6 Bloom H, *Disc Faraday Soc (GB)*, 32 (1961) 7.
- 7 Stillinger F, *J Chem Phys (USA)*, 35 (1961) 1581.
- 8 Mayer S W, *J Chem Phys (USA)*, 40 (1964) 2429.
- 9 Reiss H & Mayer S W, *J Chem Phys (USA)*, 34 (1961) 2001.
- 10 Purkait A R & Majumdar D K, *Indian J Pure & Appl Phys*, 19 (1981) 973.
- 11 Thiele E, *J Chem Phys (USA)*, 39 (1963) 474.
- 12 Percus J K & Yevick G J, *Phys Rev (USA)*, 119 (1958) 1.
- 13 Bloom H & Snook J, in *Modern aspects of electrochemistry*, Editors B Conway & J O M Bockris (Plenum Press, New York) No. 9 (1974) 159.
- 14 Margulescu I G & Salageanu, *Rev Roumaine Chim (Rumania)*, 17 (1972) 603.
- 15 Yosim S J & Owen B B, *J Chem Phys (USA)*, 41 (1964) 2032.
- 16 Bockris J O M & Richards S E, *Proc R Soc A (London)*, 241 (1957) 44.
- 17 *International critical tables* (McGraw Hill Book Co, New York) Vol. 5, 1928.
- 18 Yaffe I S & Artsdahlen Van, *J Phys Chem (USA)*, 60 (1956) 1125.
- 19 Bauer S H & Rorter R F in *Molten salt chemistry*, Editor M Blander (Intersciences Publishers, Wiley & Sons, New York) 1964, 607.
- 20 Stillinger F H (Jr) in *Molten salt chemistry*, Editor M Blander (Interscience Publishers, Wiley & Sons, New York) 1964, 79.
- 21 Purkait A R & Majumdar D K, *Indian J Pure & Appl Phys*, 17 (1979) 222.
- 22 Purkait A R & Majumdar D K, *Indian J Pure & Appl Phys*, 19 (1981) 227.
- 23 Ubbelohde A R, *Melting and crystal structure* (Oxford University Press, Oxford) 1965, 135.

Elastic Constants of Some Polycrystalline Antimony Alloys

N SWARNALATA & A R K L PADMINI

Applied Physics Department, Faculty of Technology & Engineering, M S University of Baroda, Baroda 390 001

Received 5 August 1985; revised received 12 May 1986

Ultrasonic velocity and internal friction investigations have been carried out on antimony polycrystals containing Sn, Pb, Bi and Te impurities in the concentration range 0-1 at. % using the composite oscillator technique. A set of elastic constants have been estimated from velocity and density data. The results have been interpreted in the light of changes of lattice parameter, valency of the impurity, the electron: atom ratio, atomic size and Fermi energy.

1 Introduction

The semimetal antimony which crystalizes in a rhombohedral structure belongs to the V group of elements in the periodic table having 5 electrons in the outershell of the atom. In the semimetals Sb, Bi and As, five Brillouin zones are filled and the fifth band overlaps the sixth. A few electrons spill over into the conduction band creating an equal number of holes in the valence band. It is well established that there are 3 small electron pockets at the *L* band and 6 small hole pockets at the *H* band. The electron and hole concentrations are individually equal to $5.51 \pm 0.03 \times 10^{19} \text{ cm}^{-3}$. The physical properties of antimony are highly anisotropic and there are enormous differences in their values along the cleavage plane and perpendicular to it. This is demonstrated in the earliest investigations¹ on the solid solutions of Sb doped with Sn, Ge, Pb, and Te. Browne and Lane¹ have also evaluated the principal magnetic susceptibilities.

Galvanomagnetic studies have been made on antimony alloys with less than 0.8 at. % Sn by Epstein and Juretschke² and for concentrations between 2 and 8 at. % Sn by Saunders and Oktu³. The de Haas van Alphen (dHvA) measurements on a 0.1 at. % Sn alloy were undertaken by Ishizawa and Tanuma⁴ who indicated that the band shapes do not change greatly with alloying. The magneto-reflection studies on the band structure of antimony-bismuth alloys carried out by Apps and Huntley⁵ suggest that the band gap decreases with the addition of Bi to Sb. The work on band structure near the Sb Fermi level by doping it with small amounts of tin impurities was undertaken by Dunsworth and Datars⁶ to study the changes in the Fermi surface of an antimony-tin alloy. The data on ultrasonic velocities and elastic constants in Bi polycrystals containing Sb, Sn, Pb and Te impurities were due to Varkey *et al.*⁷ who observed a decrease in the above parameters on the addition of an impurity. Rashid *et al.*⁸ have computed the components of electron and hole mobility tensors, the carrier densities

and the tilt angles of the Fermi surface pockets in single crystals of antimony and its *p*-type alloys with Sn (up to 1.0 at. %) and Ge (up to 2.2 at. %) and found that each tin or germanium atom removes one electron from the states near the band edges.

Though considerable attention has been paid to the study of various properties of Bi, Sb and Bi-rich Bi-Sb alloys, comparatively very little work appears to have been done on antimony-rich alloys. In view of this, the present investigation of studying the ultrasonic velocities, elastic constants and internal friction in alloys of Sb doped with Te, Bi, Pb and Sn impurities is taken up by the authors to explore the effect of addition of impurities to Sb, on its ultrasonic velocities and elastic properties.

2 Experimental Details

The polycrystalline specimens used in the present investigation were prepared from 99.999% pure Sb, Bi, Sn and Te metals procured from the Nuclear Fuel Complex, India and Pb of 99.95% purity from Riedel, Germany. The method of preparation of the alloys was the same as described elsewhere⁹, which enabled us to get large polycrystalline specimens of homogeneous nature, from which two specimens were cut in mutually perpendicular directions. In order to test the isotropic nature of the specimens, they were etched in $\text{CH}_3\text{COOH}:\text{HNO}_3::5:1$ for 10s and observed in a Vicker's projection microscope. The method reported by Yim and Dismukes¹⁰ was employed for conducting the metallographic examinations on the alloys after electro-polishing them. The grains were equiaxed and the boundaries could be seen on all the faces of the samples, which suggested the polycrystalline nature of the samples.

The actual composition of the samples was estimated from the density measurements by Archimedeian method using a Metler microbalance to an accuracy of $10^{-4} \text{ g cm}^{-3}$. The density measure-

ments made on pieces which were cut from the end portions of the polycrystals exhibited no major variations in concentration, which confirmed the homogeneity in the specimens. All the specimens were annealed in vacuum at 150°C for a period of 48 hr.

The ultrasonic velocity and internal friction measurements were carried out using the composite oscillator technique, the details of which are already described elsewhere¹¹. An X-cut quartz crystal with resonant frequency of 110 kHz was used for longitudinal velocity and internal friction measurements and a Y-cut quartz crystal with resonant frequency of 120 kHz was used for shear wave velocity measurements. Each measurement was carried out in at least two or three specimens and the mean value is reported. The variation in the value from one specimen to another was found to be below 2%. The frequency was measured using an Aplab (type 1102) digital frequency counter to an accuracy of 1 in 10⁶. The velocity measurements are accurate to 0.1% and the modulus values to 0.2%.

3 Results and Discussion

From the ultrasonic velocities and densities of the specimens, the various constants such as Young's modulus (E), rigidity modulus (n), Poisson's ratio (σ),

bulk modulus (K), average sound velocity (V_m) and Debye temperature (θ_D) are estimated using the formulae:

$$E = \rho V_L^2 \quad n = \rho V_S^2$$

$$K = \frac{3E - 4n}{3} \quad \sigma = \frac{3K - 2n}{6K + 2n}$$

$$V_m = \frac{1}{3} \left(\frac{2}{V_S^3} + \frac{1}{V_L^3} \right)^{-1/3}$$

$$\theta_D = \frac{h}{K} \left(\frac{3N\rho}{4\pi m} \right)^{-1/3} V_m$$

The internal friction is calculated by the formula¹²

$$Q^{-1} = \frac{\Delta f}{f_r \sqrt{3}}$$

where f_r is the resonance frequency and Δf is the width of the resonance curve at half the maximum amplitude in the voltmeter reading. All the results are presented in Table 1 which exhibit a decrease in the ultrasonic velocities, elastic constants and internal friction with addition of Te, Bi, Pb and Sn impurities, the degree of decrease being different for different impurities. These results can be logically studied taking into consideration the factors which affect the elastic

Table 1—Ultrasonic Velocities and Elastic Constants of Antimony Polycrystals Containing Sn, Pb, Bi and Te Impurities

[All Measurements at room temperature (= 30°C)]

Atomic % in Sb	ρ g/cm ³	V_L m/s	V_S m/s	$E \times 10^{-11}$ dyn/cm ²	$n \times 10^{-11}$ dyn/cm ²	$Q^{-1} \times 10^4$	$K \times 10^{-11}$ dyn/cm ²	σ	V_m m/s	θ_D K
Dopant Sn										
0	6.7	2225	1273	3.317	1.086	16.63	1.869	0.257	1414	135.3
0.28	6.705	2125	1075	3.028	0.775	14.51	1.995	0.328	1205	91.9
0.49	6.708	2035	1065	2.778	0.761	12.22	1.763	0.311	1191	90.9
0.69	6.710	2000	1042	2.684	0.729	10.28	1.712	0.314	1166	88.9
1.00	6.715	1950	1000	2.553	0.672	8.00	1.657	0.321	1120	85.5
Dopant Pb										
0.29	6.713	2117	1120	3.009	0.842	14.93	1.886	0.306	1252	86.1
0.51	6.722	2035	1082	2.784	0.787	14.50	1.734	0.303	1209	83.2
0.68	6.729	2020	1055	2.746	0.749	13.44	1.747	0.312	1180	81.2
0.96	6.740	1985	1020	2.656	0.701	12.52	1.721	0.321	1142	78.6
Dopant Bi										
0.35	6.710	2075	1150	2.889	0.887	16.41	1.706	0.278	1281	87.9
0.49	6.713	2060	1112	2.849	0.830	16.02	1.742	0.294	1241	85.2
0.66	6.717	2045	1070	2.809	0.769	15.10	1.784	0.312	1197	82.2
0.96	6.725	2000	1030	2.690	0.714	14.20	1.739	0.320	1153	79.2
Dopant Te										
0.3	6.67	2160	1187	3.112	0.940	12.13	1.859	0.284	1323	99.3
0.5	6.65	2050	1125	2.715	0.842	9.08	1.672	0.284	1254	94.3
0.7	6.63	2035	1095	2.746	0.795	8.24	1.686	0.296	1223	91.8
1.0	6.60	2025	1050	2.706	0.728	7.15	1.735	0.316	1175	88.1

V_L = Longitudinal wave velocity
 E = Young's modulus
 σ = Poisson's ratio
 θ_D = Debye temperature

V_S = Shear wave velocity
 n = Rigidity modulus
 Q^{-1} = Internal friction

ρ = Density
 K = Bulk modulus
 V_m = Average sound velocity

constants of a metal or alloy crystals, viz. (i) the change in lattice parameter, (ii) the difference in atomic radii of the solute and solvent, (iii) the valency difference between solute and solvent, (iv) change in the electron atom ratio and (v) the Fermi energy. Of these, the Fermi energy is a major contributor to the binding energy of the crystal; the second derivative of the binding energy with respect to strain gives elastic constants.

3.1 Sb-Te Alloys

The longitudinal ultrasonic velocity presented in Table 1 shows an initial fast decrease on addition of Te followed by a slow decrease with increase in Te conc, while the shear velocity is found to exhibit a regular decrease. Data on lattice spacing changes when Sb is alloyed with Te, Sn and Pb are not available. Cucka and Barrett¹³ have observed that the lattice spacing of Bi is unchanged with the addition of Sn, Pb, Te in small concentrations. A similar behaviour can be expected with Sb which is analogous to Bi in all its physical, chemical, electrical and magnetic properties.

According to Zener¹⁴, the difference in atomic radii of the solute and solvent atoms lowers the elastic constants, which was experimentally verified by Köster and Rauscher¹⁵. The difference in atomic radii of Sb (0.141 nm) and Te (0.137 nm) in Sb-Te should decrease the elastic constant to a lesser extent as compared to that of Sb and Bi (Bi = 0.152 nm) in Sb-Bi and of Sb and Pb (Pb = 0.154 nm) in Sb-Pb alloys. Further, the valency difference between Sb and Te should lead to a reduction in the value of the elastic constants as, according to Smith¹⁶, the rate of decrease in elastic constant value $\left[-\frac{1}{E} \frac{dE}{dC} \right]$ increases with the valency of the solute. Presumably, with the addition of Te the elastic constants of Sb should decrease. Further, the addition of Te to Sb increases the electron: atom ratio and this in turn should produce an increase in the value of elastic constants as reported by Wazzan and Robinson¹⁷ based on their investigations on Mg-Li alloys. They found that as the electron: atom ratio is decreased in the alloy, the elastic constants show a decrease; inversely, if the electron: atom ratio is increased the elastic constants should increase.

Dunsworth and Datars⁶ have observed while studying the dHvA effect in Sb(Te) alloys, that the hole pockets in Sb disappear at 0.35 at. % Te. The increase in Fermi energy of Sb by 40 meV when it is doped with Te impurity of 0.29 at. % was estimated by Harte *et al.*¹⁸ The above investigations clearly establish that Fermi energy increases when Sb is doped with Te, which in turn, increases the binding energy of the crystal and hence the elastic constants.

Taking into account all these factors mentioned above and the effects they produce on the elastic constants, it can be concluded that the effect of factors (ii) and (iii) must be more than the effect of the factors (iv) and (v) and the net result is that the elastic constants of Sb-Te alloys decrease with increasing concentration of Te in the range 0-1 at. %. It is seen from Table 1 that the Young's modulus (E) shows an abrupt change at 0.3 at. % Te concentration. Rigidity modulus (n) exhibits change at 0.5 at. %, while Poisson's ratio, bulk modulus and Debye temperature exhibit changes at 0.3 at. %. These results clearly prove that the change in band structure of Sb, namely the disappearance of hole pockets around 0.35 at. % as predicted by Datars and Dunsworth⁶, is reflected by the abrupt change noticed in the values of E , K , σ , and θ_D .

3.2 Sb-Sn and Sb-Pb Alloys

The decrease in ultrasonic velocities V_L and V_S with addition of Sn and Pb to Sb presented in Table 1 shows that the extent of decrease in Sn alloys is more than in Pb alloys. The decrease in V_L and V_S for 1 at. % of Sn is 275 m/s and 273 m/s respectively while the corresponding values for 0.96 at. % of Pb are 240 m/s and 253 m/s. The E values decrease sharply up to 0.49 at. % Sn or 0.51 at. % Pb beyond which the decrease rate is low. The rigidity modulus shows a sharp decrease upto 0.28 at. % Sn or 0.29 at. % Pb beyond which the decrease is slow. The bulk modulus and Poisson's ratio show maxima at 0.28 at. % Sn and 0.29 at. % Pb. The mean velocities for Sb-Sn and Sb-Pb alloys are less than the velocities for Sb-Bi and Sb-Te alloys.

Analysis of the above results in light of the factor (i) mentioned above is not possible since data on lattice spacings of these alloys are not available. The atomic radii of the solute Sn (0.140 nm) and solvent Sb (0.141 nm) are nearly same and hence the effect on elastic constants may be zero. But in Sb-Pb alloys, the difference is comparable and this should lead to a decrease in the values of the elastic constants. The valency difference between Sb and Sn is the same as that between Sb and Pb; so this effect also leads to a decrease in the elastic constants. The number of electrons outside the closed shell for Sn and Pb is four; thus the addition of small quantities of Pb or Sn to Sb lowers the number of electrons per atom in the alloy. This factor should lead to a decrease in the elastic constant values.

As Sn or Pb is added, the band structure of Sb changes, the density of holes increases while the density of overlapped electrons decreases. Dunsworth and Datars⁶ have carried out investigations to explore the band structure of Sb near its Fermi level. By doping Sb with Sn up to 0.29 at. % they observed change in the

Fermi level and their results show that each Sn atom removes one carrier electron from Sb on alloy formation. This observation is in agreement with what one should expect on the basis of the valence difference between Sb and Sn. However, Epstein and Juretschke² have predicted that each Sn atom removes 0.3 carrier electrons per each Sn atom doped when the concentration of Sn reaches 2 at. %, and conduction in the alloy takes place by holes only. Harye *et al.*¹⁸ have found that the mean number of carrier electrons removed per Sn atom in Sb(Sn) containing 0.58 at. % Sn is 1 ± 0.01 . In the case of Sb(Te) alloy, the carrier electron added per Te atom is 0.89 at a Te concentration of 0.26 at. %. Their rigid band model predicts that in alloys with 0.8 to about 1.7 at. % Sn, conduction is only by holes at the H band and that for higher concentrations of Sn, the Fermi level will enter the valence band which is directly below the electron pocket at the L band.

The rigidity modulus (n) value has shown a decrease in the Sn concentration range of 0-0.28 at. % or Pb concentration of 0.29 at. %, indicating a removal of the overlapping electrons in Sb when Sn or Pb is added as the case may be. If all the overlapping electrons are removed, then there should occur a decrease in n as no contribution is made by the Fermi energy to the shear modulus unless the Fermi surface is in contact or intersects the Brillouin zone boundaries. Hence, the sharp decrease and variation in rigidity modulus can be attributed to (i) sharp decrease in the number of electrons, (ii) disappearance of the electron pockets in the L band and (iii) increase in the number of holes. The bulk modulus K and Poisson's ratio (σ) show an increase in the concentration range 0-0.28 at. %. σ reaches the highest value at Sn concentration of 0.28 at. % or Pb concentration of 0.29 at. %, beyond which the value of σ decreases. The maximum value of σ observed in Sb-Sn alloy is higher than that in the case of Sb-Pb alloys. It is seen that all the factors that affect the elastic constants tend to decrease the values of elastic constants of the alloys. Hence the observed decrease in ultrasonic velocity in Sb alloys with increase in concentration of dopant is explained.

A study of the variation of internal friction (Q^{-1}) in Sb-Sn and Sb-Pb alloys with increasing concentration of Sn or Pb indicates that Q^{-1} decreases in the concentration range 0-1 at. % of the dopant, though the extent of decrease is more in Sb-Sn alloys compared to Sb-Pb alloys. This might be due to the larger number of holes in Sb-Sn alloys. Further, the extent of decrease in Q^{-1} for Sb-Sn and Sb-Pb alloys is less compared to that in Sb-Te alloys. This manifestly indicates that the interaction between holes and ultrasonic waves is less than the interaction between ultrasonic waves and electrons.

3.3 Sb-Bi Alloys

It is evident from Table 1 that value of V_L decreases rapidly initially as Bi concentration increases from 0 to 0.35 at. %. After this, the decrease is moderate. On the other hand, the value of V_S gradually decreases. The values of E and n exhibit a variation similar to those of V_L and V_S respectively. The value of K exhibits minimum value at a Bi concentration of 0.35 at. % and then increases, to be followed by a decrease at higher concentrations of Bi. The value of σ exhibits a monotonous increase. The parameters V_m and Q^{-1} show an unvarying decrease in the concentration range studied.

The lattice parameter measurements in Sb-Bi alloys at concentrations of $\text{Sb}_{0.9}\text{Bi}_{0.1}$ and $\text{Sb}_{0.8}\text{Bi}_{0.2}$ are due to Kolobyagina *et al.*¹⁹ and they report that the lattice spacing increases with increasing concentration of Bi. Presumably, the effect of this factor on elastic constants is to enhance them on alloy formation. There is considerable difference in atomic sizes of the solvent ($\text{Sb} = 1.41 \text{ \AA}$) and the solute ($\text{Bi} = 1.52 \text{ \AA}$) atoms. The effect of this factor is to reduce the value of elastic constants. Further, as bismuth and antimony possess the same valency, the addition of bismuth to antimony

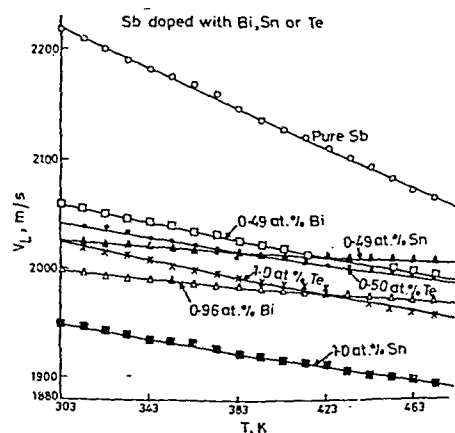


Fig. 1—Plot of V_L against temperature (T)

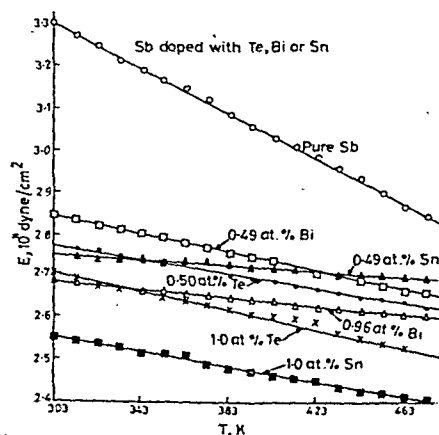


Fig. 2—Plot of E against temperature (T)

does not change the electron : atom ratio and hence the effect on elastic constants due to the factors (iii) and (iv) is negligible.

The addition of Bi in small quantities neither affects the electron: atom ratio nor the equality of electron-hole concentration, though it modifies the band structure. Gitsu *et al.*²⁰ established that in $\text{Sb}_{1-x}\text{Bi}_x$ alloys ($0 \leq x \leq 0.25$) the electron (n) and hole (p) concentrations decrease as x increases to 0.25 with $n = p$ in all alloys. The reduction in the electron and hole concentrations naturally reduces the Fermi energy and hence the elastic constants. It is interesting to note that the uniform decrease of elastic constants E and n and hence the uniform decrease of velocities V_L and V_S can be attributed partly to this effect. The decrease in the value of Q^{-1} in this Bi concentration range also manifests that as the electron-hole concentration is decreased, the interaction between ultrasonic is decreased, the interaction between ultrasonic waves and electrons and holes also gets decreased. It is interesting to note here that the value of Q^{-1} of Sb-Bi alloys is much less compared to that of Sb-Te, Sb-Sn, Sb-Pb alloys, which clearly shows that the electron-hole concentration is reduced in Sb-Bi alloys compared to the other alloys. An overall study of the variation of elastic constants reveals that the observed decrease in the values of elastic constants can be attributed to the combined effect of (i) the difference in atomic sizes of the solvent and solute atoms and (ii) the decrease in the Fermi energy. The increase in values of elastic constants caused by lattice parameter changes obviously appears to be negligible.

A comparative study of the variations of Q^{-1} with increase in concentration of dopant in Sb alloys indicates that the decrease in Q^{-1} is maximum for Te impurity, minimum for Bi impurity and intermediate for Sn and Pb impurities.

Figs 1 and 2 show the temperature dependence of V_L and E in Sb alloys at two different concentrations of the dopant and over the temperature range 303-463 K. The change in resonance frequency at various temperatures was noted. The values of E were calculated at each temperature using the equation E

$= \rho V_L^2$ where ρ is the density of the specimen. From Fig. 2 it is seen that values of E decrease linearly with temperature as is the characteristic of most of the metals and alloys. The above results indicate that investigations based on ultrasonic velocity and internal friction throw considerable light on the semiconducting properties and band structure of Sb alloys with Sn, Te and Bi as dopants.

Acknowledgement

The financial assistance by the CSIR, New Delhi, is gratefully acknowledged by one of the authors (NS).

References

- 1 Browne S H & Lane C T, *Phys Rev (USA)*, **60** (1941) 895.
- 2 Epstein S & Juretschke A J, *Phys Rev (USA)*, **129** (1963) 1148.
- 3 Saunders G A & Oktu O, *J Phys & Chem Solids (GB)*, **29** (1968) 1589.
- 4 Ishizawa Y & Tanuma S, *J Phys Soc Jpn (Japan)*, **20** (1965) 1279.
- 5 Apps M J & Huntley D A, *Solid State Commun (USA)*, **10** (1972) 1213.
- 6 Dunsworth A E & Datars W R, *Phys Rev B (USA)*, **7** (1973) 8.
- 7 Varkey P A, Pethe G V & Padmini A R K L, *Ultrasonics (USA)*, (1979) 27.
- 8 Rashid A A M, Ford P J, Miller A J & Saunders G A, *Philos Mag B (GB)*, **41** (1980) 21.
- 9 Gopinathan K K & Padmini A R K L, *J Phys D (GB)*, **7** (1974) 32.
- 10 Yim W M & Dismukes J P, *Proc Int Conf on Crystal Growth, Boston*, Ed. H. Steggen Peeser, **B27** (1966) 187.
- 11 Balamuth L, *Phys Rev (USA)*, **45** (1934) 715.
- 12 Postnikov V S, Tavazde F N & Gordienko L K, *Internal friction in metals and alloys* (Consultants Bureau, New York) 1967, 209.
- 13 Cucka P & Barrett C S, *Acta Crystallogr (Denmark)*, **15** (1962) 165.
- 14 Zener C, *Acta Crystallogr (Denmark)*, **2** (1949) 163.
- 15 Köster W & Rauscher W, *Z Metallkunde (Germany)*, **39** (1948) 110.
- 16 Smith A D N, *J Inst Metals (USA)*, **86** (1952) 477.
- 17 Wazzan A R & Robinson L B, *Phys Rev (USA)*, **155** (1967) 586.
- 18 Harte G A, Priestley M G, Vuillemin J J, *J Low Temp Phys (USA)*, **31** (1978).
- 19 Kolobyanina T N, Kabalkina S S, Vereschchagin L V, Michkov A Ya & Kachan M F, *Zh Eksp Teor Fiz (USSR)*, **59** (1970) 1146.
- 20 Gitsu D V, Muntyanu F K & Onu M I, *Sov J Low Temp Phys (USA)*, **3** (1977) 9.

Akhieser Damping in KCN

S K KOR & RAJA RAM YADAV

Department of Physics, University of Allahabad, Allahabad 211 002

Received 1 August 1985; accepted 26 May 1986

It is established that the phonon-viscosity mechanism and thermo-elastic phenomenon are the principal thermal causes of acoustic wave attenuation in solids at room temperature. In the present investigation, ultrasonic absorption due to phonon-viscosity mechanism in KCN has been discussed at 293 K, with reference to anomalous thermal elastic properties of the crystal.

1 Introduction

Potassium cyanide is known to be a deadly poison. Many of the structural and thermo-elastic properties have been studied earlier¹⁻⁶. At higher temperatures, KCN exhibits NaCl-type crystal structure. KCN undergoes anomalous thermo-elastic properties, the most characteristic feature of which is softening of the shear constant C_{44} as the transition temperature is approached. Attenuation of an ultrasonic wave propagating in a crystal depends upon crystal structure. Therefore, in the present investigation, study of ultrasonic attenuation in KCN along various propagation directions has been made.

It is established that phonon-viscosity mechanism and the thermo-elastic phenomenon are the principal thermal causes of acoustic wave attenuation in solids at room temperature^{7,8}. Akhieser⁸ postulated that the equilibrium distribution of thermal phonons in a solid may be disturbed by the propagation of acoustic phonon and the re-establishment of equilibrium is a relaxational phenomenon. This mechanism is known as three-phonon process. Due to these perturbed phonons at various temperatures T s above ambient, there will be an increase in entropy and, therefore, attenuation of energy from the propagating wave. The dominating factor of attenuation in dielectrics is the interaction of thermal phonons with acoustical phonons. Whenever the lifetime of the thermal phonon (thermal relaxation time) falls below the time period of the acoustic wave cycle, the interaction between individual phonon modes becomes insignificant and a macroscopic model of phonon gas comes into the picture.

In the present communication, we have discussed the attenuation of compressional and shear wave propagating along $\langle 100 \rangle$, $\langle 110 \rangle$, $\langle 111 \rangle$ and $\langle 11\bar{2} \rangle$ crystallographic directions in KCN at 293 K.

2 Theoretical Expressions Used for the Calculations

The attenuation due to the phonon-viscosity mechanism (α_p) and that due to the thermo-elastic

phenomenon (α_{th}) in the frequency range covered by the condition $\omega\tau_{th} \ll 1$, are given as follows:

$$\alpha_p = \omega^2 E_0 D \eta \tau_{th} / 6\rho V^3$$

$$\alpha_{th} = \omega^2 \langle \gamma_i^2 \rangle^2 kT / 2\rho V^5 \quad \dots (1)$$

Here, the Grüneisen number γ_i corresponding to the i -th phonon branch and deformation in the acoustic mode j , is given as a typical combination of second and third order elastic constants:

$$-\gamma_i^k = p_i p_k + l_p l_q (C_{jkpq} + p_i p_s C_{jkprqs}) / 2C_e$$

where \mathbf{T} is the unit vector in the direction of phonon propagation, \mathbf{p} is the displacement vector, C_{jkpq} and C_{jkprqs} represent the second and third order elastic constants (in tensor notation), the subscripts pqr s refer to thermal phonons, and C_e is the effective elastic modulus for phonons, ω is the angular frequency of acoustic waves and E_0 is the internal energy per unit volume. The value of η is equal to 1 for shear waves and 2 for longitudinal waves, τ_{th} is the thermal phonon relaxation time which can be obtained from the relation

$$\tau_{th} = (3^{1/3} \rho k / C_v) (C_{11}^{-3/2} + 2C_{44}^{-3/2})^{2/3} \quad \dots (3)$$

and C_v is the specific heat per unit gram. D , the non linearity constant can be expressed as is

$$D = 9 \langle (\gamma_i^2) \rangle - (3C_v T / E_0) \langle \gamma_i^2 \rangle^2 \quad \dots (4)$$

where $\langle \gamma_i^2 \rangle$ and $\langle (\gamma_i^2)^2 \rangle$ are the average Grüneisen numbers and their square averages over a particular number of pure modes according to the propagation direction. The value of D has been calculated with the help of second and third order elastic constants⁶ (used particularly in the calculation of $\langle \gamma_i^2 \rangle$) and other data used in Eq. (4) (Refs 9-11). Other symbols have their usual meanings¹². In recent years, many workers reviewed the work on ultrasonic attenuation and internal structure of solids¹³⁻²⁰.

3 Results and Discussion

All the primary physical constants for KCN required for the evaluation of phonon viscosity loss

and thermo-elastic loss are listed in Table 1. Evaluated values of the nonlinearity constants D and the Grüneisen numbers along all the directions are given in Table 2. The ultrasonic absorption coefficients for KCN in terms of (α/f^2) are presented in Table 3.

From the data of τ_{th} , one can check that the condition $\omega\tau_{th} \ll 1$ holds good in the entire ultrasonic frequency range. From Table 3 one infers that the values of α/f^2 along the various directions are unequal, as in other fluorite-structure crystals⁷, cesium halides¹² and semiconductors^{21,22}.

The observation that the attenuation due to the phonon-viscosity mechanism is much higher than that due to thermo-elastic relaxation reveals that the major part of ultrasonic energy loss is used in achieving the equilibrium among different phonon branches and directions at various temperatures. The value of α_{th} is found to be 0.01%-0.02% of α_{Akh} in KCN.

The low values of τ_{th} can be expected due to the very low values of thermal conductivity, as observed in other dielectric crystals²³.

As seen from Table 3, the acoustic attenuation for shear wave is greater than that for longitudinal wave

along all propagation directions. This is not true for NaCl along $\langle 100 \rangle$ direction though KCN becomes NaCl-type crystal at room temperature.

This discrepancy can be explained as follows:

$D(\text{long})$ is greater than $D(\text{shear})$ for both NaCl and KCN along $\langle 100 \rangle$ direction. Therefore, the discrepancy arises due to very low value of shear wave velocity in comparison to longitudinal wave velocity (Table 1). This greater difference between longitudinal and shear wave velocity in KCN in comparison to NaCl arises due to anomalous behaviour of C_{44} at higher temperatures.

Comparing the values of $(\alpha/f^2)_{Akh}$ of KCN along $\langle 110 \rangle$ direction with the experimental values for KCl (same crystalline structure)¹⁰, it is found that longitudinal attenuation in KCN is observed to be 0.6%, whereas in KCl it is found to be 3%. Here also, it should be noted that $D(\text{shear})$ is greater than $D(\text{long})$ for both crystals. The higher difference between longitudinal and shear wave attenuation in KCN along $\langle 110 \rangle$ in comparison to KCl may be understood as follows:

First, the longitudinal constant C_{111} is about five times smaller and the transverse constants C_{112} and C_{123} about eight times longer than those in KCl. Secondly, the difference between shear wave and longitudinal wave velocity due to anomalous behaviour of C_{44} is larger than that in KCl. It is interesting to note that the crystalline structure of KCN at room temperature affects the ultrasonic attenuation along various propagation directions of the wave.

It indicates that ultrasonic attenuation may be used as a versatile tool to know the internal structure of the crystal.

Table 1—Primary Physical Constants for KCN at 293 K

Constants	Symbol and unit	Value
Longitudinal wave velocity	$V_l (10^5 \text{ cm/s})$	3.549
Shear wave velocity	$V_s (10^5 \text{ cm/s})$	0.963
Debye average velocity	$V (10^5 \text{ cm/s})$	1.098
Specific heat per unit volume	$\rho C_v (10^7 \text{ ergs/cc-K})$	0.575
Internal energy density	$E_0 (10^7 \text{ ergs/cc})$	128.10
Thermal relaxation time	$\tau_{th} (10^{-12} \text{ s})$	21.620
Debye temperature	$\theta_D (\text{K})$	195
Thermal conductivity	$K (\text{Wcm}^{-1} \text{K}^{-1})$	0.05

Table 2—Values $\langle \gamma_i^2 \rangle$, $\langle (\gamma_j^2) \rangle$ and D for KCN along Various Directions

Parameter	$\langle 100 \rangle$ long	$\langle 100 \rangle$ shear	$\langle 110 \rangle$ Long	$\langle 110 \rangle$ Shear polarizing along $\langle 1\bar{1}0 \rangle$	$\langle 110 \rangle$ Shear polarizing along $\langle 001 \rangle$	$\langle 111 \rangle$ Long	$\langle 111 \rangle$ Shear polarizing along $\langle \bar{1}10 \rangle$	$\langle 11\bar{2} \rangle$ Long
$\langle \gamma_i^2 \rangle$	0.2988	—	0.2065	—	—	0.0668	—	—0.5679
$\langle (\gamma_j^2) \rangle$	7.6344	0.7116	3.7708	22.9520	1.2367	1.6900	17.13,4	11.3384
D	68.3574	6.39	33.769	206.568	11.1303	15.1924	154.2366	100.7734

Table 1—Absorption Coefficients (α/f^2) for KCN along Various Directions at 293 K

(α/f^2)	Long	$\langle 100 \rangle$ Shear	$\langle 100 \rangle$ Long	$\langle 110 \rangle$ Shear polarizing along $\langle 1\bar{1}0 \rangle$	$\langle 110 \rangle$ Shear polarizing along $\langle 001 \rangle$	$\langle 110 \rangle$ Long	$\langle 111 \rangle$ Shear polarizing along $\langle \bar{1}10 \rangle$	$\langle 11\bar{2} \rangle$ Long
$(\alpha/f^2)_{Akh}$ ($10^{-17} \text{ dBs}^2 \text{cm}^{-1}$)	317.9	743.6	157.0	24038.6	1295.2	71.9	17948.7	468.7
$(\alpha/f^2)_{th}$ ($10^{-18} \text{ dBs}^2 \text{cm}^{-1}$)	0.26	—	0.124	—	—	0.008	—	0.96

References

- 1 Lesar R & Gardon R G, *J Chem Phys (USA)*, **77** (1982) 3682.
- 2 Sahu D & Mahanti S D, *Phys Rev B*, **26** (1982) 2981.
- 3 Haüssuhl S. *Solid State Commun (USA)*, **13** (1973) 147.
- 4 Haüssuhl S. *Acta Crystallogr Sect A (Denmark)*, **33** (1977) 847.
- 5 Krasser W & Buchenav V, *Solid State Commun (USA)*, **18** (1976) 287.
- 6 Haüssuhl S & Michaelas W, *Acta crystallogr Sec A (Denmark)*, **35** (1979) 240.
- 7 Kor S K, Tandon U S & Rai G, *Phys Rev B(USA)*, **5** (1972) 4143.
- 8 Akhiezer A, *J Phys (USSR)*, **1** (1939) 227.
- 9 Bateman T B, *Physical acoustics: Vol. IIB*, edited by W P Mason (Academic Press, New York) 1965.
- 10 Merkulov L G, *Sov Phys Solid State (USSR)*, **11** (1970) 2241.
- 11 Schrioder U, *J Phys (France)*, **42** (1981) 247, C-6.
- 12 Kor S K, Tandon U S & Mishra P K, *J Appl Phys (USA)*, **45** (1974) 2336.
- 13 Seventh International Conference on Internal Friction and Ultrasonic Attenuation in Solids, *J Phys (Paris) Colloq (France)*, **42** C-5, 6-9 July 1981.
- 14 Bruesch P, *Phonons: Theory and Experiments: I*—Springer Series in Solid State Sciences, Vol. 34, 1982.
- 15 Bonnet J P, Boisser M, Vedel C & Vacher R, *J Phys & Chem Solids (GB)*, **44** (1983) 515.
- 16 Krautkramer J & Krautkramer H, *Ultrasonic study of materials* (Academic Press, New York), 3rd Edn, 1983.
- 17 Soma T & Kagaya H M, *Phys Status Solidi b (Germany)*, **126** (1984) 91.
- 18 Powell B E, *J Appl Phys (USA)*, **56** (1984) 1549.
- 19 Malrein J, Maynan D & Daubey J P, *Phys Rev B(USA)*, **30** (1984) 1817.
- 20 Anderson M S & Swenson C A, *Phys Rev B(USA)*, **31** (1985) 668.
- 21 Kor S K & Khare R P, *Acta Phys Pol A (Poland)*, **58** (1980) 725.
- 22 Kor S K, Tandon U S & Rai G, *Phys Rev B(USA)*, **6** (1972) 2165; **7** (1973) 4640.
- 23 Kor S K & Khare R P, *Acustica (Germany)*, **56** (1984) 280.

Indirect Tunnelling Current Density Based on a Rigorous Quantum Mechanical Treatment

D K ROY* & AMITABH GHOSH

Department of Physics, Indian Institute of Technology, New Delhi 110016

Received 8 July 1985; revised received 1 February 1986

Conventionally, the indirect electron tunnelling current density has been evaluated by applying Fermi's golden rule of the perturbation theory. But, its predictions of the latter have been found to be relatively smaller compared to the experimentally reported values by several orders of magnitude. A rigorous quantum mechanical account of the problem of indirect tunnelling is first presented and then an attempt has been made to obtain an expression for the indirect tunnelling current density based upon the current continuity equation. The current density obtained in this manner is considerably larger compared to the golden rule predictions mentioned earlier and is found to be closer to the reported experimental values.

1 Introduction

The direct tunnelling transitions across a potential barrier are initiated by large scale electron potential energy fluctuations¹⁻³. If, on the other hand, such transitions are caused by small time-dependent perturbations in the electron barrier Hamiltonian, the process has been termed as the indirect tunnelling. Such perturbations may either be induced by photons emitted or the vibrational modes of the lattice excited during tunnelling transitions of electrons between different energy levels on either side of the potential barrier. Such processes provide additional paths or channels to the flow of tunnelling current. If ν happens to be the frequency of the excitations generated by the tunnelling electron, one is expected to observe a kink or a discontinuity at an applied bias $V (= h\nu/q)$ in the I - V , (dI/dV) - V , or (d^2I/dV^2) - V characteristics of tunnel junctions at very low temperatures⁴. Thus, by employing this technique, one would easily be able to determine the detailed vibrational spectrum of molecular species present within the potential barrier. Its basic advantage or usefulness over conventional optical techniques, e.g. Raman or infrared spectroscopies, is its greater sensitivity. Several of its useful applications in recent years have led to the development of a new branch of investigation now known as the Inelastic Electron Tunnelling Spectroscopy (IETS) as a very sensitive probe to investigate the spectra of materials⁵.

But, in spite of such remarkable experimental achievements in this area, the indirect electron tunnelling is interpreted even now in terms of the Fermi's golden rule of the time-dependent perturbation theory. Also, the indirect tunnelling current

density obtained on the basis of the latter has been found to fall short by several orders of magnitude (typically 10^3) relative to experimentally reported values⁶. The expression of the former, on the other hand, represents the transition rate which dimensionally is also not equivalent to the current density. In this paper, we first present a rigorous quantum mechanical analysis of the phenomenon of indirect tunnelling and next attempt to obtain an expression for the indirect electron tunnelling current density based upon the current continuity equation. The current density computed on the basis of this model is found to be larger by several orders of magnitude relative to golden rule predictions and is closer to experimental predictions. This current density is however to be superimposed upon the direct current density expression reported earlier³, to arrive at the net result.

2 Theory

The electron potential energy during the indirect tunnelling process may be isolated as

$$V(x, t) = V_1(x) + V_3 \cos \omega_p t \quad \dots(1)$$

where $V_1(x)$ denotes the electron potential energy as given by the barrier shape whereas the second term represents the perturbation induced by external agents. The electron Hamiltonian in the barrier region may then be expressed as

$$H = \left\{ -\frac{\hbar^2}{2m} \frac{\partial^2}{\partial x^2} + V_1(x) \right\} + V_3 \cos \omega_p t \\ \doteq H_0 + H_1(t) \quad (\text{say}) \quad \dots(2)$$

The unperturbed wave equation for the electron however is

$$H_0 \psi_0(x, t) = i\hbar \frac{\partial}{\partial t} \psi_0(x, t) \quad \dots(3)$$

* Present address: AT & T Bell Laboratories 600 Mountain Avenue, Murray Hill, New Jersey 07974 USA

On assuming $\psi_0(x, t) = X(x)T(t)$, Eq. (3) further reduces to

$$-\frac{\hbar^2}{2m} \frac{1}{X(x)} \frac{d^2 X(x)}{dx^2} + V_1(x) = \frac{i\hbar}{T(t)} \frac{dT(t)}{dt} = E_1 \quad \dots(4)$$

where the separation constant E_1 measures the total electron energy before incidence of electrons upon the barrier. The solutions of space and time parts of Eq. (4) may then be expressed as

$$X_1(x) = \alpha F(x) \\ X_r(x) = \beta G(x) \quad \dots(5)$$

and

$$T(t) = \gamma \exp(-iE_1 t/\hbar) \quad \dots(6)$$

where α , β and γ are arbitrary constants.

Now, if we regard the electron Hamiltonian to be perturbed in accordance with Eq. (2), the barrier wavefunction may then be written on the basis of the time-dependent perturbation theory as

$$\psi(x, t) = b_1(t) X_1(x) \exp(-iE_1 t/\hbar) + b_r(t) X_r(x) \exp(-iE_r t/\hbar) \quad \dots(7)$$

where $b_1(t)$ and $b_r(t)$ are the appropriate time-dependent coefficients to be evaluated. E_1 and E_r respectively denote the energies of the two states on either side of the barrier between which the indirect tunnelling transition is presumed to be occurring. The wavefunction in Eq. (7) must now satisfy the perturbed wave equation, viz.

$$H\psi(x, t) = i\hbar \frac{\partial}{\partial t} \psi(x, t) \quad \dots(8)$$

Combining Eqs (7) and (8) and upon simplification, one gets,

$$i\hbar \dot{b}_1(t) X_1(x) + i\hbar \dot{b}_r(t) X_r(x) \exp(i\omega_{lr} t) = b_1(t) H_1 X_1(x) + b_r(t) H_1 X_r(x) \exp(i\omega_{lr} t) \quad \dots(9)$$

where

$$\omega_{lr} = \omega_l - \omega_r = (E_1 - E_r)/\hbar \quad \dots(10)$$

Next, on multiplying Eq. (9) successively by $X_1^* dx$ and $X_r^* dx$ and on integrating between barrier extremities x_l and x_r , one gets the following two equations

$$i\hbar \dot{b}_1(t) R_{11} + i\hbar \dot{b}_r(t) R_{1r} \exp(i\omega_{lr} t) = b_1(t) \cos \omega_p t \cdot S_{11} + b_r(t) \cos \omega_p t \cdot S_{1r} \exp(i\omega_{lr} t) \quad \dots(11)$$

and

$$i\hbar \dot{b}_1(t) R_{r1} + i\hbar \dot{b}_r(t) R_{rr} \exp(i\omega_{lr} t) = b_1(t) \cos \omega_p t \cdot S_{r1} + b_r(t) \cos \omega_p t \cdot S_{rr} \exp(i\omega_{lr} t) \quad \dots(12)$$

where

$$R_{\mu\nu} = \int_{x_l}^{x_r} X_\mu^* X_\nu dx \quad \dots(13)$$

and

$$S_{\mu\nu} = \int_{x_l}^{x_r} X_\mu^* V_3 X_\nu dx \quad \dots(14)$$

On combining Eqs (11) and (12), one finds

$$i\hbar \dot{b}_1(t) = M_{11} b_1(t) \cos \omega_p t + M_{12} b_r(t) \cos \omega_p t \exp(i\omega_{lr} t) \quad \dots(15)$$

and

$$i\hbar \dot{b}_r(t) = M_{21} b_1(t) \cos \omega_p t \exp(-i\omega_{lr} t) + M_{22} b_r(t) \cos \omega_p t \quad \dots(16)$$

where

$$M_{11} = \frac{S_{11} R_{rr} - S_{r1} R_{1r}}{R_{11} R_{rr} - R_{1r} R_{r1}} \\ M_{12} = \frac{S_{1r} R_{rr} - S_{rr} R_{1r}}{R_{11} R_{rr} - R_{1r} R_{r1}} \\ M_{21} = \frac{R_{11} S_{r1} - S_{11} R_{r1}}{R_{11} R_{rr} - R_{1r} R_{r1}} \\ M_{22} = \frac{R_{11} S_{rr} - S_{1r} R_{r1}}{R_{11} R_{rr} - R_{1r} R_{r1}} \quad \dots(17)$$

Eqs (15) and (16) may further be simplified and rewritten for convenience, as follows

$$b_1(t) = \frac{1}{2i\hbar} [M_{11} b_1(t) \{ \exp(i\omega_p t) + \exp(-i\omega_p t) \} + M_{12} b_r(t) \times \{ \exp[i(\omega_p + \omega_{lr})t] + \exp(i\Delta\omega t) \}] \quad \dots(18)$$

and

$$\dot{b}_r(t) = \frac{1}{2i\hbar} [M_{21} b_1(t) \{ \exp[-i\Delta\omega t] + \exp[-i(\omega_{lr} + \omega_p)t] \} + M_{22} b_r(t) \times \{ \exp(i\omega_p t) + \exp(-i\omega_p t) \}] \quad \dots(19)$$

where $\omega_{lr} - \omega_p = \Delta\omega$. Now, if we carefully examine Eqs (18) and (19) we find that $\dot{b}_1(t)$ and $\dot{b}_r(t)$ are rapidly changing harmonic functions of time unless $\Delta\omega \rightarrow 0$ (or $\omega_p = \omega_l - \omega_r$). Thus, any electronic transitions between levels is noticeable only under this resonant condition. Therefore, on ignoring contributions due to high frequency terms, which in any case would be insignificant, we may rewrite Eqs (18) and (19) as follows:

$$\dot{b}_1(t) = \frac{M_{12}}{2i\hbar} \{ \exp(i\Delta\omega t) \cdot b_r(t) \} \quad \dots(20)$$

and

$$\dot{b}_r(t) = \frac{M_{21}}{2i\hbar} \{ \exp(-i\Delta\omega t) \cdot b_1(t) \} \quad \dots(21)$$

On combining Eqs (20) and (21), we finally get,

$$\ddot{b}_l(t) - i\omega b_l(t) + (\Omega^2/4)b_l(t) = 0 \quad \dots(22)$$

and

$$\ddot{b}_r(t) + i\omega b_r(t) + (\Omega^2/4)b_r(t) = 0 \quad \dots(23)$$

where

$$\Omega^2 = M_{12} \cdot M_{21} / \hbar^2 \quad \dots(24)$$

Now, Eq. (22) and (23) are to be solved for $b_l(t)$ and $b_r(t)$. The initial conditions of the problem are $b_l(0) = 1$ and $b_r(0) = 0$. To solve for $b_r(t)$, we may presume a trial solution of the type

$$b_r(t) = \exp(i\beta t) \quad \dots(25)$$

On combining Eqs (23) and (25), one finds,

$$\beta = \frac{1}{2}(-\Delta\omega \pm R) \quad \dots(26)$$

where

$$R = (\Delta\omega^2 + \Omega^2)^{1/2} \quad \dots(27)$$

Thus β is seen to be a very small quantity as both $\Delta\omega$ and Ω happen to be small. Hence, the most general solution for $b_r(t)$ may be expressed as

$$b_r(t) = A_1 \{\exp(i\beta_1 t) + A_2 \exp(i\beta_2 t)\} \quad \dots(28)$$

But, as $b_r(0) = 0 = A_1 + A_2$, Eq. (28) simplifies to:

$$b_r(t) = A [\exp(-i\Delta\omega t/2) \cdot \sin(RT/2)] \quad \dots(29)$$

where $A = 2iA_1$. Similarly, we may presume

$$b_l(t) = \exp(i\theta t) \quad \dots(30)$$

On combining Eqs (30) and (22), we get

$$\theta = \frac{1}{2}(\Delta\omega \pm R) \quad \dots(31)$$

Hence

$$b_l(t) = B_1 \{\exp(i\theta_1 t) + B_2 \exp(i\theta_2 t)\} \quad \dots(32)$$

Since $b_l(0) = 1$, $B_1 = 1 - B_2$. Then, on combining Eqs (31) and (32), we get

$$b_l(t) = \exp(i\Delta\omega t/2) \times [\cos(RT/2) + B \sin(RT/2)] \quad \dots(33)$$

where $B = i(2B_1 - 1)$. Now, only the constants A and B involved in Eqs (29) and (33) remain to be evaluated. To determine B first, we combine Eqs (20) and (29) to get

$$\dot{b}_l(t) = \frac{A M_{12}}{2i\hbar} \exp(i\Delta\omega t/2) \times \sin(RT/2) \quad \dots(34)$$

Next, on differentiating Eq. (33) and comparing with Eq. (34), we get at $t = 0$

$$B = (-i\Delta\omega/R) \quad \dots(35)$$

Next, on substituting for B in Eq. (33), we get

$$b_l(t) = \exp(i\Delta\omega t/2) [\cos(RT/2) - (i\Delta\omega/R) \sin(RT/2)] \quad \dots(36)$$

From Eq. (36), we may readily obtain

$$|b_l(t)|^2 = \cos^2(RT/2) + (\Delta\omega)^2 / [(\Delta\omega)^2 + \Omega^2] \sin^2(RT/2) \quad \dots(37)$$

which expresses the electron intensity in the state E_l as a function of time. Next, in order to determine A , we combine Eqs (21) and (36) to get

$$\dot{b}_r(t) = M_{12}/2i\hbar \exp(-i\Delta\omega t/2) \times [\cos(RT/2) - (i\Delta\omega/R) \sin(RT/2)] \quad \dots(38)$$

On differentiating Eq. (29) and on equating to Eq. (38), we then get at $t = 0$

$$A = -\frac{iM_{21}}{\hbar R} \quad \dots(39)$$

Hence, from Eq. (29), one may write

$$b_r(t) = M_{21}/i\hbar R [\exp(-i\Delta\omega t/2) \times \sin(RT/2)] \quad \dots(40)$$

From Eq. (40), we may also derive,

$$|b_r(t)|^2 = \frac{\Omega^2}{(\Delta\omega)^2 + \Omega^2} \cdot \sin^2 \frac{RT}{2} \quad \dots(41)$$

which measures the electron intensity in the state E_r . On combining Eqs (37) and (41), it follows that

$$|b_l(t)|^2 + |b_r(t)|^2 = 1 \quad \dots(42)$$

at all times. We may note that $b_l(t) = 1$ and $b_r(t) = 0$ successively whenever $t = 2\pi n/R$ (where $n = 0, 1, 2, 3, \dots$). Thus, the electronic transitions between levels alternate with a characteristic frequency $R/2\pi$ which is quite small.

2.1 Probability Density

The electron probability density due to indirect tunnelling may now be expressed as follows:

$$\begin{aligned} P(x, t) &= \psi^*(x, t) \psi(x, t) \\ &= |b_l(t)|^2 \cdot |X_l(x)|^2 \\ &\quad + |b_r(t)|^2 \cdot |X_r(x)|^2 \\ &\quad + [b_l b_r^* X_l X_r^* \exp(-i\omega_{lr} t) \\ &\quad + b_l^* b_r X_l^* X_r \exp(i\omega_{lr} t)] \\ &= C + D + F \text{ (say)} \end{aligned} \quad \dots(43)$$

where

$$\begin{aligned} C &= |b_l(t)|^2 \cdot |X_l(x)|^2 \\ &= [\cos^2(RT/2) + (\Delta\omega/R)^2 \sin^2(RT/2)] \cdot |X_l(x)|^2 \\ &\simeq |X_l(x)|^2 \end{aligned} \quad \dots(44)$$

$$\begin{aligned} D &= |b_r(t)|^2 \cdot |X_r(x)|^2 \\ &= (M_{21}^2 / \hbar^2 R^2) \cdot \sin^2(RT/2) \cdot |X_r(x)|^2 \end{aligned} \quad \dots(45)$$

and

$$F = (M_{21} X_1^* X_r / \hbar R) \times [\sin RT \cdot \sin \omega_p t + (2\Delta\omega/R) \cdot \sin^2(RT/2) \cdot \cos \omega_p t] \quad \dots (46)$$

Since F involves high frequency terms (involving ω_p), its contribution to observable and finite probability density would once again be insignificant. Hence, observable $P(x, t)$ would only arise due to C and D .

2.2 Tunnelling Current Density

The indirect tunnelling current density may now be computed by using the equation of continuity as follows:

$$J = q \int_{x_1}^{x_r} \frac{\partial P(x, t)}{\partial t} dx \quad \dots (47)$$

where x_1 and x_r denote the classical turning points of the potential barrier. Therefore, on combining Eqs (43) and (47), we find

$$J_i = J_{oi} \frac{\sin R\tau_i}{R\tau_i} = J_{oi} \frac{\sin \varphi}{\varphi} \text{ (say)} \quad \dots (48)$$

where

$$J_{oi} = q |M_{21}|^2 R_{rr} \tau_i / 2\hbar^2 \quad \dots (49)$$

τ_i denotes the interaction time of the electron with the agency responsible for indirect tunnelling. Now, as the phase of the current density expression in Eq. (48) is totally uncertain owing to the randomness in the incidence of electrons, the net indirect tunnelling current density produced by a group of incident electrons of density $\rho_i(E) f_i(E) dE_i$ having random phase differences is then given by

$$dJ_i = J_{oi} \rho_i(E) f_i(E) dE_i \times \sum_{\varphi=-\infty}^{+\infty} (\sin \varphi / \varphi) \quad \dots (50)$$

where $\varphi = R\tau_i$. But, from Eq. (27) we notice that $R^2 = (\Delta\omega)^2 + \Omega^2 \simeq (\Delta\omega)^2$. That is $R = \Delta\omega = (\Delta E / \hbar)$ so that $d\varphi = \tau_i dR = \tau_i \varepsilon / \hbar$ where ε denotes the energy difference between consecutive energy levels at the transmitted end. We may now convert² the summation in Eq. (50) into a convenient integral by multiplying with $(\hbar / \varepsilon \tau_i) d\varphi (= 1)$ as given below:

$$dJ_i = J_{oi} \rho_i(E) f_i(E) dE_i \times \int_{-\infty}^{+\infty} \frac{\sin \varphi}{\varphi} \frac{\hbar}{\varepsilon \tau_i} d\varphi \quad \dots (51)$$

On integrating Eq. (51) and on substituting

$$\frac{1}{\varepsilon} = \rho_r(E_1 - \hbar\omega_p) \{1 - f_r(E_1 - \hbar\omega_p)\} \Omega_v$$

where Ω_v denotes the volume of the electrode on the far side to which tunnelling is occurring, we get³

$$dJ_i = (\pi \hbar \Omega_v / \tau_i) J_{oi} \rho_i(E) f_i(E) \times \rho_r(E_1 - \hbar\omega_p) \{1 - f_r(E_1 - \hbar\omega_p)\} dE_1 \quad \dots (52)$$

Thus on integrating Eq. (52) over appropriate limits of E_1 which would be bias dependent, one arrives at an expression for the indirect tunnelling current density corresponding to the participation of a quantum of energy $\hbar\omega_p$. This, however, is to be superimposed upon the direct current component to arrive at the net effect. It is worthwhile to compare Eq. (52) with the current density obtained on the golden rule of the perturbation theory which is being appended below:

$$dJ_{ig} = (2\pi q / R) |S_{ri}|^2 \rho_i(E) f_i(E) \times \rho_r(E_1 - \hbar\omega_p) \{1 - f_r(E_1 - \hbar\omega_p)\} dE_1 \quad \dots (53)$$

Eq. (53), in fact, represents the transition probability per unit time and does not possess the dimensions of current density. In order to compare the relative magnitudes of the two current densities, we divide Eq. (52) by Eq. (53) to get

$$\frac{dJ_i}{dJ_{ig}} = \frac{\Omega_v R_{rr} |M_{21}|^2}{4 |S_{ri}|^2} = \frac{\Omega_v \chi^3}{2k^2} \quad \dots (54)$$

for a rectangular potential barrier of height v_0 where $\chi^2 = (2m/\hbar^2)(v_0 - E)$ and $k^2 = (2mE/\hbar^2)$. It is easy to notice that the ratio of the two current densities is typically around 10^3 . The experimentally observed current density is also greater compared to the golden rule predictions by this order of magnitude. We would, therefore, expect that the predictions of Eq. (52) would be closer to experimental results.

We would next attempt to evaluate Eq. (52) for a rectangular type of a potential barrier. On presuming $f_i(E_i) = 1$ and $f_r(E_1 - \hbar\omega_p) = 0$ at the low temperature at which the indirect tunnelling experiments are performed, we obtain on substituting the appropriate values of physical quantities in Eq. (52)

$$J_i = C \int_{\hbar\omega_p}^{qV} E^{3/2} (E - \hbar\omega_p) dE \quad \dots (55)$$

where

$$C = \frac{2^{15} \pi^6 q m^4 \Omega_v V_3^2 \exp(-2\chi W)}{\chi^3 \hbar^9} \quad \dots (56)$$

On integrating Eq. (55), we get the closed form expression for the indirect tunnelling current density as given below:

$$J_i = C \{qV(qV - \hbar\omega_p)\}^{1/2} \left[\frac{(qV)^2}{3} - \frac{(qV)(\hbar\omega_p)}{12} - \frac{(\hbar\omega_p)^2}{8} \right] - \frac{(\hbar\omega_p)^3}{8} \times \ln \left[\frac{(qV - \hbar\omega_p)^{1/2} + (qV)^{1/2} - (\hbar\omega_p)^{1/2}}{(qV - \hbar\omega_p)^{1/2} - (qV)^{1/2} + (\hbar\omega_p)^{1/2}} \right] \dots (57)$$

The dependence of the indirect tunnelling current density produced by a quantum of energy $\hbar\omega_p$ as a function of the applied voltage V is thus expressed by Eq. (57). The barrier height and the width enter the expression through the constant C expressed in Eq.

(56). Its mathematical form, is however, the same as predicted by the golden rule of the perturbation theory.

References

- 1 Roy P N, Singh P N & Roy D K, *Phys Lett A (Netherlands)*, **63** (1977) 81.
- 2 Roy D K, Sai N S T & Rai K N, *Pramana (India)*, **19** (1982) 231.
- 3 Roy D K, *Pramana (India)*, **25** (1985) 431.
- 4 Adkins C J & Phillips W A, *J Phys C (GB)*, **18** (1985) 1313.
- 5 Hansma P K, *Phys Rep Phys Lett C (Netherlands)*, **30** (1977) 145.
- 6 Kleinmann L, Phonon-assisted tunnelling in *Tunnelling phenomena in solids*, edited by E Burstein and S Lundqvist (Plenum Press, New York) 1969, 181.

Profile of Vapour Layer on a Liquid Surface – Mathematical Model

J ASHOK & C V N VASANTA LAKSHMI

Department of Applied Physics, Andhra University, Waltair

Received 11 November 1985; revised received 17 February 1986

The study of the properties of the inhomogeneous vapour layer over a liquid surface is of interest in atmospheric optics. The optical properties of this variable refractive index boundary layer have been determined using an ellipsometer. Using these data, a mathematical model for the refractive index variation along the thickness dimension of the vapour layer has been computed.

The study of vapour layer over a liquid surface is of interest in atmospheric optics¹. The water-air interface consists of a boundary layer whose composition varies from the boundary near water to the boundary near air. This boundary layer is an inhomogeneous layer whose refractive index varies from that of water to air. The equivalent refractive index and thickness of this vapour layer can be determined using an ellipsometer. The interpretation of these values in terms of an equivalent multilayer and its refractive index profile are reported in this note.

A symmetrical multilayer is equivalent to a single homogeneous film with equivalent index of refraction N_E and equivalent thickness T_E . The usual way to compute N_E and T_E for homogeneous multilayers is to compute the multilayer matrix as a product of the matrices of the individual homogeneous layers².

An inhomogeneous film is equivalent to a multilayer in a similar way³. This multilayer is, however, asymmetric and is a pile of thin films in which each discrete film is homogeneous. Its refractive index is constant and can be represented by a matrix which is the characteristic matrix of the film⁴. This can be extended to a pile of thin homogeneous films and the resultant matrix is obtained by the product of these matrices taken in the correct order. This final matrix represents the characteristic matrix for the equivalent film which is given by

$$\begin{bmatrix} m_{11} & m_{12} \\ m_{21} & m_{22} \end{bmatrix}$$

where $m_{11} = m_{22} = 1$ for maximum thickness which is sufficiently small.

$$m_{12} = \sum_{j=1}^N \left[\frac{1}{p_j} \sin(k_0 n_j \delta z_j \cos \theta_j) \right]$$

$$m_{21} = \sum_{j=1}^N [p_j \sin(k_0 n_j \delta z_j \cos \theta_j)]$$

where N is the number of films in multilayer and $p = (\epsilon/\mu)^{1/2} \cos \theta$ for transverse electric (TE) wave. The same equations hold good for transverse magnetic (TM) wave with p replaced by $q = (\mu/\epsilon)^{1/2} \cos \theta$, where ϵ , μ , n , θ are dielectric constant, magnetic permeability, refractive index and angle of incidence respectively. The reflection and transmission coefficients in terms of the elements of the characteristic matrix are given by

$$r_s = \frac{(m_{11} + m_{12} p_1) p_1 - (m_{21} + m_{22} p_1)}{(m_{11} + m_{12} p_1) p_1 + (m_{21} + m_{22} p_1)}$$

for TE wave

$$r_p = \frac{(m'_{11} + m'_{12} q_1) q_1 - (m'_{21} + m'_{22} q_1)}{(m'_{11} + m'_{12} q_1) q_1 + (m'_{21} + m'_{22} q_1)}$$

for TM wave

from which ellipsometric parameters Δ , ψ can be obtained.

This concept of a multilayer equivalent of an inhomogeneous film is best explained by the respective refractive index profiles of a given system. A minimum of two parameters are required for a refractive index profile, namely, the refractive indices n_1 and n_2 , at the surfaces of the inhomogeneous layer.

In addition, we have an important parameter used in defining the profile. This parameter is the equivalent thickness T_E which is defined as the thickness of the equivalent film, from which we can derive experimental values using mathematical model. The equivalent index N_E is defined as the refractive index for the equivalent film of the inhomogeneous boundary layer.

At an angle of incidence 75° , with a source of light of 5893 \AA wavelength, the phase difference Δ and azimuth ψ of the water-water vapour-air layer have been determined by means of an ellipsometer designed for this purpose, in our laboratory, and were obtained as 5.4° and 34.07° respectively.

Using Vasicek's method⁵ the equivalent refractive index N_E and the corresponding thickness T_E are obtained as 1.23 and 1317.3 \AA respectively.

For the refractive index profile, we have the necessary parameters $T_E = 1317.3 \text{ \AA}$ (on X-axis) and $n_1 = 1$, $n_2 = 1.33$ (on Y-axis) in Fig. 1. Different profiles are drawn as shown in Fig. 1 and the characteristic matrix for each profile is computed, which finally gives values of the ellipsometric parameters. The exact profile which suits the experimental values is located by curve fitting technique as shown in Fig. 2. The point of intersection of the two curves: 1, n vs Δ and 2, n vs ψ , extrapolated at a particular thickness d from Fig. 1,

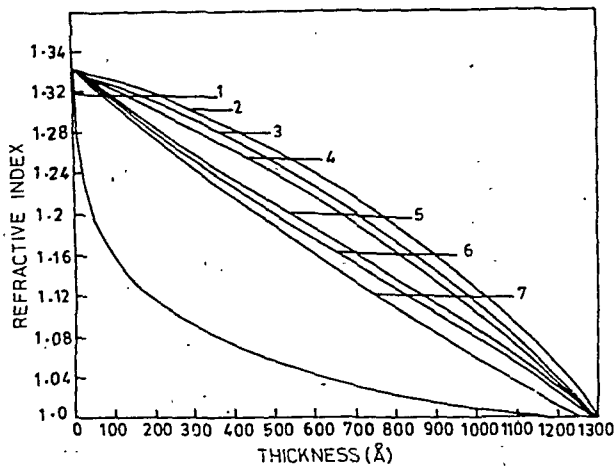


Fig. 1—Variation of refractive index with thickness. Curve 2 is the one which fits the experimental ellipsometric values

gives the n value. This variable (n, d) fixes the exact profile (curve 2) in Fig. 1.

This profile is taken as the suitable model for the given inhomogeneous water-water vapour-air layer. The characteristic matrix for this profile is obtained as

$$\begin{bmatrix} m_{11} & m_{12} \\ m_{21} & m_{22} \end{bmatrix} = \begin{bmatrix} 1 & 1.3821i \\ 0.7586i & 1 \end{bmatrix} \quad \text{for TE wave}$$

$$\begin{bmatrix} m'_{11} & m'_{12} \\ m'_{21} & m'_{22} \end{bmatrix} = \begin{bmatrix} 1 & 2.0542i \\ 0.4959i & 1 \end{bmatrix} \quad \text{for TM wave}$$

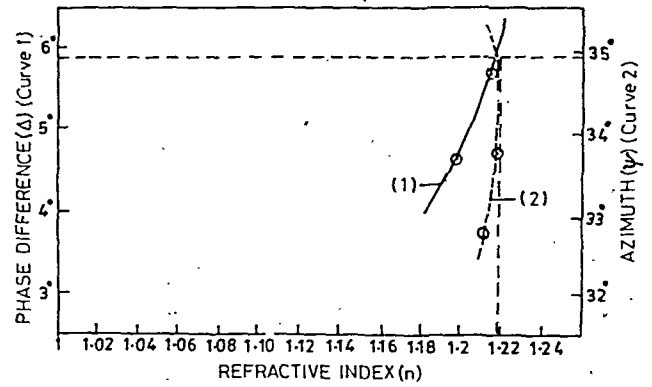


Fig. 2—Location of the exact profile which suits the experimental values. Curve 1, n vs Δ and curve 2, n vs ψ . The point of intersection gives (n, d).

After calculations for r_p and r_s in terms of $m_{11}, m_{12}, m_{21}, m_{22}$ and $m'_{11}, m'_{12}, m'_{21}, m'_{22}$ we get $\Delta = 5.43^\circ$, $\psi = 34.9^\circ$ which are nearer the experimental values.

On the day of the experiment, relative humidity and room temperature were observed to be 43% and 26°C respectively.

References

- 1 Carl A F, LaRue J C, Champagne F H, *et al.*, *J Opt Soc Am (USA)*, **65** (1985) 457.
- 2 Jacobson R, *Physics of thin films* (Academic Press, New York), **8** (1975) 51.
- 3 Southwell W H, *Appl Opt (USA)*, **24** (1985) 457.
- 4 Born M & Wolf G, *Principles of optics* (Pergamon, Oxford) 1970, 55.
- 5 Vasicek A, *J Opt Soc Am (USA)*, **37** (1947) 143.

Photon Attenuation Measurements in Soil Samples of Different Particle Sizes

G S MUDAHAR* & H S SAHOTA

Soil Science Laboratories, Department of Physics
Panjab University, Patiala 147 002

Received 13 May 1985; revised received 15 May 1986

The effect of grain size (d) on the linear (μ) and mass (μ_m) attenuation coefficients of uncompact soil samples has been tested in the energy range of 279 to 1250 keV. Values of μ and μ_m are found to decrease with increase in grain diameter of soil particles. The rate of change of μ or μ_m with d varies inversely with photon energy. The half-value layer ($t_{1/2}$) increases directly with d but the rate of change of $t_{1/2}$ with d is independent of photon energy in contrast with the results of El-Kamel *et al.*² [*Indian J Pure & Appl Phys*, 21 (1983) 457]

Gameel *et al.*¹ and El-Kamel *et al.*² suggested the use of compacted clay for shielding of radiations to safety levels. Both the groups studied the change in attenuation coefficients caused by the grain diameter of clay particles. El-Kamel *et al.*² reported that the linear attenuation coefficient (μ) decreases with increase in diameter of the particles (d) and that the rate of change of μ with d changes inversely with the photon energy (E), in the energy range 356-1250 keV. They also studied variation of half-value layer with d and E . Their results in graphical form indicate that the rate of change of half value layer ($t_{1/2}$) with d varies directly with E .

In our present study, the findings of El-Kamel *et al.*² have been tested in uncompact soil samples of different grain diameters. The effect of d on linear (μ) and mass (μ_m) attenuation coefficients was investigated using gamma rays from ²⁰³Hg (279 keV), ¹³³Ba (350 keV), ¹³⁷Cs (662 keV) and ⁶⁰Co (1250 keV). The study of $t_{1/2}$ was also undertaken. The sources were obtained from the Bhabha Atomic Research Centre, Bombay. Each source was housed in a lead container and properly shielded. A 3.81 × 3.81 cm² NaI(Tl) crystal scintillator optically coupled to RCA 6199 photomultiplier along with the assembly of amplifier, single channel analyser, scaler and recorder, was used for the spectroscopy of radiations. The gamma ray counting sequence and method of analysis suggested by Conner *et al.*³ were adopted for measurement of attenuation coefficients using narrow beam-collimated geometry (sample-detector solid angle $< 0.5 \times 10^{-4}$ sr). Samples were prepared by

sieving the oven-dried soil through a set of standard sieves: 0.308, 0.222, 0.160, 0.133 and 0.107 mm. The samples were filled in perspex boxes of 3 cm width under natural compaction. To calculate μ_m , the density values of soil samples were measured using mass/volume relation. The results are discussed in the following.

From a μ vs d plot (Fig. 1), it is clear that for all energies, μ decreases with increase of d . μ can be related

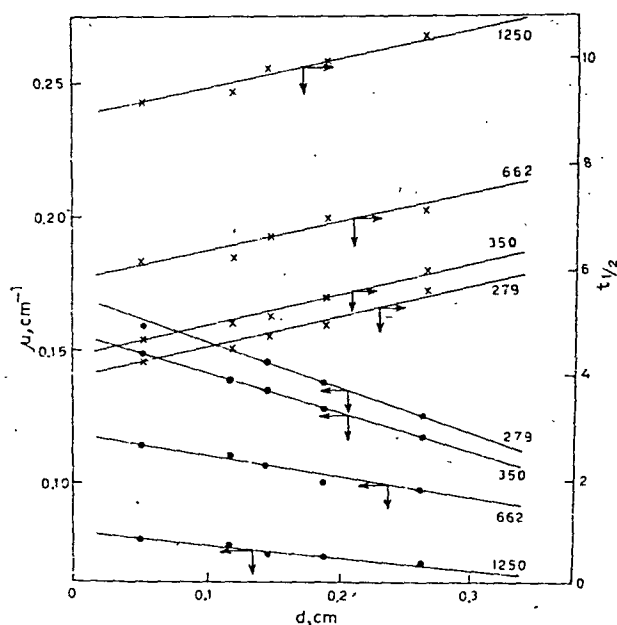


Fig. 1—Variations of linear attenuation coefficient (μ) and half value layer ($t_{1/2}$) with grain diameter (d)

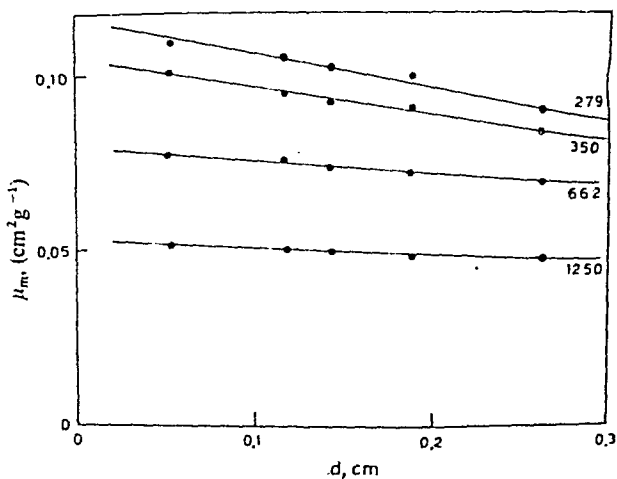


Fig. 2—Variation of mass attenuation coefficient (μ_m) with grain diameter (d)

* Present address: Department of Physics, Punjab Agricultural University, Ludhiana

to d according to the following empirical relation given by El-Kamel *et al.*²:

$$\mu = -ad + k \text{ for } 0.107 \leq d \leq 0.308$$

where a is the rate of change of μ with d (i.e. slope of μ - d curve). With the increase in photon energy E , slope a decreases. As E increases from 279 to 1250 keV, the slope decreases from 0.181 to 0.053. These results for uncompacted soil are similar in all respects to the results of El-Kamel *et al.*² who used targets of clay under 10 ton/cm² pressure.

Further, the value of μ_m has also been found to decrease linearly with increase in d (Fig. 2) and is related by

$$\mu_m = -bd + k \text{ for } 0.107 \leq d \leq 0.308$$

where b is the rate of change of μ_m with d . With the increase of photon energy, b decreases. As energy increases from 279 to 1250 keV, b decreases from 0.083 to 0.020. However, this change is small compared with the linear attenuation coefficient but significant and outside the limit of errors. As neither El-Kamel *et al.*²

nor anyone else has conducted this type of study, it is not possible to compare these results.

The values of $t_{1/2}$ were evaluated for all photon energies from the present data. It is found that $t_{1/2}$ increases linearly with increase of d (Fig. 1) and can be related as:

$$t_{1/2} = cd + k \text{ for } 0.107 \leq d \leq 0.308$$

where c is the rate of change of $t_{1/2}$ with d .

The value of the slope c was found constant in the energy range 279-1250 keV. This is in contradiction to the results of El-Kamel *et al.*² who showed in one of their plots that in the nearly same energy region, this slope increases linearly with the increase of photon energy.

References

- 1 Gameel Y H, Belal A & El-Kamel A H, *Indian J Pure & Appl Phys*, 16 (1978) 62.
- 2 El-Kamel A H, Saied M H & El-Attar A L, *Indian J Pure & Appl Phys*, 21 (1983) 457.
- 3 Conner A L, Atwater H F, Elizabeth H P & McCrary J H, *Phys Rev A*, 1 (1970) 539.

Applications of CNDO/S-RPA Method: Electronic Transition Energies & Oscillator Strengths

RANA SEN

Department of Chemistry, Scottish Church College, Calcutta
700 006
and

SUBIRNATH BHATTACHARYYA

Department of Pure Chemistry, University College of Science,
Calcutta 700 009

Received 3 December 1985; revised received 24 March 1986

The random phase approximation (RPA) has been employed within the semi-empirical CNDO/S framework to incorporate correlation effects in calculating transition energies and oscillator strengths of singlet \rightarrow singlet electronic transitions in some planar aromatic molecules with C_{2v} symmetry. The results are compared with those of the CNDO/S-CI and experimental data.

The calculation of dynamical properties of molecules like transition energy, oscillator strength, static and dynamic polarizability, etc. involves not just a 'good' (approximate) ground molecular state; a reasonable description of the excited manifold also becomes crucial in this context. Hence, one has to go beyond the independent particle (Hartree Fock, HF) model to incorporate electron correlation in the ground as well as excited electronic states of the molecule. The HF molecular orbitals can be generated by using any one of the several variants of the LCAO-MO-SCF schemes which have been developed with varying degrees of complexity and success^{1,2}. Insofar as actual computation within a semi-empirical framework is concerned, as is feasible or convenient in practice for large molecular systems, application of the CNDO/S-CI method of Del Bene and Jaffe³ has been found profitable⁴⁻¹⁸. In this scheme correlated excited states are generated by performing a limited CI composed entirely of singly-excited configurations, but the ground state is left uncorrelated (i.e., the HF function is employed). Stated in the equations of motion (EOM) language^{19,20}, this scheme amounts to working in the Tamm Dancoff approximation²¹ (TDA). Naturally, it is expected that results should improve if electron correlation effects are included in the ground state as well through the random phase approximation (RPA), for example.

In this note, transition energies and oscillator strengths of selected molecules calculated by the CNDO/S and RPA combination have been compared with experimental and other reported results⁵.

Computational scheme—The CNDO/S model Hamiltonian⁴ and parameters⁵ have been used to generate the ground state of the molecule which is assumed to have idealized geometry (see Ref. 22) for relevant bond angles and bond distances). The RPA transition energies (ω_i), appear as the eigenvalues of

$$\begin{pmatrix} A & B \\ -B & -A \end{pmatrix} \begin{pmatrix} X \\ Y \end{pmatrix} = \omega \begin{pmatrix} X \\ Y \end{pmatrix} \quad \dots(1)$$

A is the (NXN) hermitian, TDA matrix, B a (NXN) symmetric matrix and N the chosen number of one-hole one-particle pairs; explicit expressions for the matrix elements are given in reference 19.

In general, two approaches are in vogue for solving Eq. (1): (a) the $(2N \times 2N)$ non-hermitian, RPA matrix is diagonalized straightforwardly^{20,23} to obtain ω, X, Y , (b) the $(2N \times 2N)$ RPA matrix is first transformed to a $(N \times N)$ hermitian matrix and then diagonalized²⁴⁻²⁷. However, a transformation scheme different from that mentioned in (b) has been used in this work whereby ω, X, Y are all obtained by diagonalization of a $(N \times N)$ hermitian matrix via a *highly convergent* iterative pathway. The scheme has been outlined in the Appendix.

For a particular electronic transition, the oscillator strength (f), in the dipole length approximation, is given¹⁹ by:

$$f = \frac{2}{3} \omega |D|^2 \quad \dots(2)$$

where

$$D = \sqrt{2} \sum_{m\alpha} [X(m\alpha) + Y(m\alpha)] d_{m\alpha} \quad \dots(3)$$

$$\text{and } d_{m\alpha} = \langle m | \vec{r} | \alpha \rangle \quad \dots(4)$$

Results and discussion—The results of the CNDO/S-RPA calculation of transition energies and oscillator strengths for low-energy transitions are presented in Tables 1-4. Attention has been restricted to planar molecules with C_{2v} point group symmetry, containing not less than eight atoms and not more than forty atomic orbitals in the basis set. The symmetry assignment of the excited state associated with a transition has been emphasized in comparing theoretical results with experimental data.

In order to keep the RPA matrix dimension within workable limits, the following procedure has been adopted: (a) the one-hole one-particle pairs have been generated from the ten highest-occupied and ten lowest-unoccupied molecular orbitals resulting in a (200×200) unsymmetric RPA matrix, (b) this matrix

Table 1—Calculated & Experimental ${}^1\Psi_n \leftarrow {}^1\Psi_0$ Transition Energies (ω in eV) & Oscillator Strengths (f), for Pyridine, Pyridazine, Pyrimidine, Pyrazine, s-Triazine & s-Tetrazine

Method: Molecule	n	CNDO/S-RPA		Experimental		CNDO/S-CI	
		Symmetry	$\omega(f)$	Symmetry	$\omega^a(f)$	Symmetry	$\omega(f)$
Pyridine ^{b,c}	2	B ₁	4.22(0.006)	B ₁	4.27 ^S (0.003)	B ₁	4.2(0.00)
	3	B ₂	4.84(0.118)	B ₂	4.84 ^D (0.030)	B ₂	4.9(0.06)
	3	A ₁	5.77(0.111)	A ₁	6.17 ^D (0.200)	A ₁	6.0(0.22)
	3	A ₁	6.35(0.755)	A ₁	6.99 ^{VD} (1.30)	A ₁	6.8
	3	B ₂	6.45(0.749)	B ₂		B ₂	6.8(0.76)
Pyridazine ^{b,c}	2	B ₁	3.47(0.013)	B ₁	3.30 ^S (0.006)	B ₁	3.3(0.008)
	3	A ₁	4.66(0.099)	A ₁	4.90 ^D (0.020)	A ₁	6.1(0.11)
	3	B ₂	5.47(0.065)	B ₂	6.20 ^C (0.10)	B ₂	5.1(0.05)
	3	B ₂	6.04(0.713)				
	2	B ₁	6.36(0.002)	B ₁	6.39 ^S (0.01)	B ₁	6.2(0.005)
Pyrimidine ^{b,c}	3	B ₁	3.79(0.010)	B ₁	3.85 ^S (0.007)	B ₁	4.2(0.012)
	3	B ₂	4.80(0.119)	B ₂	5.00(0.052)	B ₂	5.1(0.07)
	3	B ₁	6.26(0.012)	B ₁	6.42 ^S (0.005)	B ₁	6.4(0.005)
	3	A ₁	5.36(0.047)	A ₁	6.49 ^D (0.160)	A ₁	6.1(0.11)
	3	A ₁	6.22(0.668)	A ₁ } B ₂ }	6.98(0.250)	A ₁	7.1(0.63)
Pyrazine ^{b,c}	3	B ₂	6.30(0.613)			B ₂	7.1(0.62)
	3	B ₁	3.17(0.007)	B ₁	3.83 ^S (0.010)	B ₁	3.2(0.006)
	3	B ₂	4.61(0.205)	B ₂	4.81 ^D (0.100)	B ₂	4.8(0.160)
	3	A ₁	5.92(0.177)	A ₁	6.31 ^D (0.145)	A ₁	6.3(0.12)
	3	A ₁	6.54(0.562)		6.69 ^S (—)	A ₁	7.2(0.48)
Symtriazine ^{b,d}	3	B ₂	6.91(0.559)	B ₂	6.84 ^S (0.250)	B ₂	7.5(0.97)
	3	B ₁	3.91(0.000)	B ₁	3.91(0.018)	B ₁	4.6(0.027)
	3	A ₂	3.94(—)	A ₂	4.03(—)	A ₂	4.5(—)
	3	A ₁	5.42(0.025)	A ₂	5.46(0.002)	A ₂	5.6(0.0)
	3	A ₂	6.59(—)	(—)	6.92(—)	B ₂	7.2(0.62)
s-Tetrazine ^{b,d}						A ₁	
	3	B ₁	2.59(0.017)	B ₁	2.25(0.004)	B ₁	2.6(0.018)
	3	B ₁	4.18(0.000)	B ₁	3.87(0.001)	B ₁	6.7(0.01)
	3	B ₂	4.18(0.214)	B ₂	4.40 ^{VD} (—)	B ₂	4.9(0.15)

^aDescription of spectra: S, sharp, D, diffuse, VD, very diffused, C, continuous. This convention applies to all the Tables.^bCNDO/S-CI results: Ellis *et al.*⁵^cExperimental results: Refs [28, 30]^dExperimental results: Refs [30, 31]Table 2—Calculated & Experimental ${}^1\Psi_n \leftarrow {}^1\Psi_0$ Transition Energies (ω eV) & Oscillator Strengths (f), for Pyrrole & Furan

Method: molecule	n	CNDO/S-RPA		Experimental		CNDO/S-CI	
		Symmetry	$\omega(f)$	Symmetry	$\omega(f)$	Symmetry	$\omega(f)$
Pyrrole ^a	3	B ₂	5.03(0.188)	B ₂	5.7(—)	B ₂	5.0(0.080)
	3	A ₁	5.68(0.014)	A ₁	6.5(—)	A ₁	5.4(0.006)
	3	B ₂	7.29(0.147)	B ₂	7.1(—)	B ₂	7.0(0.129)
Furan ^b		B ₂	4.26(0.238)	B ₂	5.58 to (0.12)	B ₂	5.2(0.078)
		B ₂	7.13(0.114)		6.42	B ₂	7.3(0.097)
		A ₁	5.37(0.178)	A ₁	6.42 to (0.078)	A ₁	5.8(0.009)
		A ₂	6.31(0.357)		7.18	A ₁	7.3(0.368)

^aCNDO/S-CI & experimental results: Del Bene & Jaffe⁵^bCNDO/S-CI results Del Bene & Jaffe⁵^cExperimental results: Ref. [29]

Table 3—Calculated and Experimental ${}^1\Psi_n \leftarrow {}^1\Psi_0$ Transition Energies (ω , in eV) and Oscillator Strengths (f) for Fluorobenzene, *o*-, *m*- and *p*-Difluorobenzenes

Method: Molecule	<i>n</i>	CNDO/S-RPA		Experimental		CNDO/S-CI	
		Symmetry	$\omega(f)$	Symmetry	$\omega(f)$	Symmetry	$\omega(f)$
Fluorobenzene ^a (FBZ)	3	B ₂	4.73(0.015)		4.84(0.003)	B ₁	4.8(0.002)
	3	A ₁	6.18(0.826)		6.19(0.150)	A ₁	6.0(0.24)
	3	A ₁	7.51(0.001)		7.00(1.433)	A ₁	6.7(0.863)
	3	B ₁	7.52(0.001)			B ₁	6.7(0.981)
ortho-diFBz ^a	3	A ₁	4.63(0.013)			B ₁	4.6(0.017)
	3	B ₂	5.45(0.074)			A ₁	5.7(0.065)
	3	B ₂	5.92(0.795)			B ₁	6.5(0.816)
	3	A ₁	5.93(0.938)			(-)	6.6(1.56)
meta-diFBz ^a	3	B ₂	4.65(0.021)		4.7(0.010)	B ₁	4.6(0.017)
	3	A ₁	5.50(0.040)		6.1(0.080)	A ₁	5.9(0.016)
	3	B ₂	5.99(0.947)			B ₁	6.7(1.125)
paradiFBz ^a	3	B ₂	4.59(0.067)		4.6(0.022)	B ₁	4.6(0.040)
	3	A ₁	5.42(0.097)		6.1(0.070)	A ₁	5.8(0.080)
	3	B ₂	5.91(0.767)			B ₁	6.7(0.793)
	3	A ₁	6.09(0.815)			A ₁	6.8(1.159)

^a CNDO/S-CI and experimental results: Kuehenlenz and Jaffe⁵Table 4—Calculated & Experimental ${}^1\Psi_n \leftarrow {}^1\Psi_0$ Transition Energies (ω in eV) & Oscillator Strengths (f) for Benzene, Aniline, Phenoxide Ion & *p*-Benzoquinone

Method: molecule	<i>n</i>	CNDO/S-RPA		Experimental		CNDO/S-CI	
		Symmetry	$\omega(f)$	Symmetry	$\omega(f)$	Symmetry	$\omega(f)$
Benzene ^a	3	B ₂	4.84(0.004)	B ₂	4.72 ^S (0.001)	B ₂	4.7(0.000)
	3	B ₂	6.45(1.150)	B ₂	6.07 ^D (0.010)	B ₁	5.2(0.000)
	2	B ₁	6.65(0.000)				
	2	B ₁	6.74(0.000)	B ₁	6.93 ^C (0.69)	B ₁	6.9(0.593)
Aniline ^b				B ₂		B ₂	
	3	B ₂	4.48(0.072)	B ₂	4.4(0.028)	B ₂	4.4(0.023)
	3	A ₁	5.23(0.261)	A ₁	5.4(0.144)	A ₁	4.7(0.041)
	3	A ₁	6.18(0.607)	A ₁	6.4(0.510)	A ₁	6.5(0.491)
Phenoxide ion ^b	3	B ₂	5.96(0.644)	B ₂	6.9(0.570)	B ₂	6.6(0.434)
	3	B ₂	3.92(0.116)	B ₂	4.3(-)	B ₂	3.8(0.048)
	3	A ₁	4.66(0.424)	A ₁	5.3(-)	A ₁	4.5(0.120)
	2	A ₂	2.31(-)		2.48	A ₂	2.31
para- Benzoquinone ^c	2	A ₂	2.36(-)	A ₂	2.49	A ₂	2.37
	3	B ₂	3.71(0.000)	A ₂	2.52	B ₂	3.78
	3	A ₁	4.86(0.788)		4.03	A ₁	4.99
	2	B ₁	5.36(0.000)		5.08	B ₁	5.38

^a CNDO/S-CI results: Del Bene & Jaffe; experimental data: Ref. [28]^b CNDO/S-CI and experimental results: Del Bene & Jaffe⁵^c Experimental data: H.P. Tromsdorff, *J Chem Phys (USA)*, 56 (1972) 5358. In absence of CNDO/S-CI results, CNDO/S-TDA results have been reported.

has been transformed (by the scheme outlined in the Appendix) to a hermitian matrix of half the dimension, (c) the symmetry of molecular orbitals has been so utilized that the matrix which has to be diagonalized in each iterative step has a maximum dimension of 30 only. The reduction of matrix dimension, in steps (b) and (c), helps to save computer storage space substantially. In addition, symmetrization of the matrix before diagonalization, in step (b), allows the use of very efficient, standard diagonalization

algorithms which reduces computational time effectively.

Lastly, in order to have a 'feel' of the rapidity of iterative convergence and hence the efficiency of the proposed scheme, the number of iterations (*n*) required to ensure a tolerance limit of 10^{-6} eV have also been included in Tables 1-4.

A study of Tables 1-4 reveals the following points: (i) the iterative diagonalization procedure proposed in this work is highly convergent in character; thus, in all

calculations performed so far, $n \leq 3$, (ii) the RPA transition energies are in close agreement with experimental results for the first few transitions and, in fact, the data in some cases agree better with experiments than those of the CNDO/S-CI. The maximum deviation from experimental data in RPA results is 1.1 eV (Table 1, pyrimidine, *fourth* transition) while in the CI results it is 2.8 eV (Table 1, s-tetrazine, *second* transition). (iii) Results of oscillator strengths for the first few transitions, only for which experimental values are available, are however, not quite encouraging. In fact, a similar conclusion also holds if the CNDO/S-CI scheme was employed; the work of Ellis *et al.*⁵ may be referred to for a discussion on the disparity between experimental and theoretical results. For high-energy transitions, it becomes difficult to correlate theory and experiment because the splitting of the near-degenerate levels through vibronic coupling and consequent 'intensity borrowing' may radically change oscillator strength values. In this work particularly, the truncation of the excitation manifold probably affects oscillator strength values adversely.

In calculating the singlet \rightarrow singlet transition energies, Jaffe *et al.* initially employed the Pariser charged sphere model to evaluate the two-centre repulsion integrals³; subsequently, however, they adopted the Mataga-Nishimoto (MN) approximation⁵. The MN approximation has been consistently used in this note for all molecules. This may sometimes lead to inconsistency in the RPA and CI results (in the case of benzene, Table 4, the RPA result for the first transition exceeds the CI value).

Summarizing, it may be said that the CNDO/S-RPA scheme offers itself as a promising alternative to other prescriptions for computing dynamical properties of molecules on the cost and labour basis; extension of this method to larger molecules can be immediate and worth while.

The authors are grateful to Dr K Bhattacharyya and Sri D Sinha for their valuable help in this work. Thanks are also due to the Department of Science and Technology, New Delhi, for computational grant and to the Regional Computer Centre, Calcutta, for providing computer facilities.

Appendix

In TDA one solves an eigenvalue equation $\mathbf{A}\mathbf{X}_0 = \omega_0\mathbf{X}_0$, which on diagonalization yields

$$\mathbf{X}_0^+ \mathbf{A} \mathbf{X}_0 = \omega_0 \quad \dots (A1)$$

where \mathbf{A} is a hermitian matrix, \mathbf{X}_0 is an ortho-normal matrix and ω_0 is a diagonal (TDA-energy) matrix. The RPA equation, Eq. (1), can be rewritten as

$$\mathbf{A}\mathbf{X} + \mathbf{B}\mathbf{Y} = \omega\mathbf{X} \quad \dots (A2)$$

$$-\mathbf{B}\mathbf{X} - \mathbf{A}\mathbf{Y} = \omega\mathbf{Y} \quad \dots (A3)$$

From Eq. (A3) one obtains

$$\mathbf{Y} = -(\mathbf{A} + \omega)^{-1} \mathbf{B}\mathbf{X} \quad \dots (A4)$$

which on similarity transformation by \mathbf{X}_0 yields:

$$\mathbf{Y} = -\mathbf{X}_0(\omega_0 + \omega)^{-1} \mathbf{X}_0^+ \mathbf{B}\mathbf{X} \quad \dots (A5)$$

Substituting Eq. (A5) in Eq. (A2) one obtains the eigenvalue equation for a hermitian matrix

$$[\mathbf{A} - (\mathbf{B}')^+(\omega_0 + \omega)^{-1} \mathbf{B}'] \mathbf{X} = \omega \mathbf{X} \quad \dots (A6)$$

where

$$\mathbf{B}' = \mathbf{X}_0^+ \mathbf{B} \quad \dots (A7)$$

Eq. (A6) can now be solved iteratively to obtain ω (RPA-energy matrix) and \mathbf{X} , with the initial value of ω being equated with ω_0 . The presence of a large denominator $(\omega_0 + \omega)$ ensures rapid convergence for this procedure; \mathbf{Y} is obtained from Eq. (A5). These \mathbf{X} and \mathbf{Y} are then *renormalized* in order that the following equation¹⁴ is satisfied:

$$\sum_{m\alpha} [X(m\alpha, \omega) X(m\alpha, \omega') - Y(m\alpha, \omega) Y(m\alpha, \omega')] = \delta_{\omega\omega'} \quad \dots (A8)$$

References

- 1 Pople J A & Beveridge D L, *Approximate molecular orbital theory* (McGraw-Hill, New York) 1970.
- 2 (a) Dunning T H & Hay P J, *Methods of electronic structure theory*, Vol. 4, edited by Schaefer H F III (Plenum Press, New York & London) 1977.
- 2 (b) Moskowitz J W & Snyder L C, *Methods of electronic structure theory*, Vol. 4, edited by H F Schaefer III (Plenum Press, New York & London) 1977.
- 3 Del Bene J & Jaffe H H, *J Chem Phys (USA)*, 48 (1968) 1807.
- 4 Ellis R L & Jaffe H H, *Semiempirical methods of electronic structure calculation, Part B*, edited by G A Segal (Plenum Press, New York & London) 1977.
- 5 Del Bene J & Jaffe H H, *J Chem Phys (USA)*, 49 (1968) 1221.
- 6 Ellis R L, Kuehenlenz G & Jaffe H H, *Theor Chim Acta (Germany)*, 26 (1972) 131.
- 7 Kuehenlenz G & Jaffe H H, *J Chem Phys (USA)*, 58 (1973) 2238.
- 8 Kuehenlenz G, Masmandis C A & Jaffe H H, *J Mol Struct (Netherlands)*, 15 (1973) 445.
- 9 Marchese F T & Jaffe H H, *Theor Chim Acta (Germany)*, 45 (1977) 241.
- 10 Del Bene J & Jaffe H H, *J Chem Phys (USA)*, 50 (1969) 563.
- 11 Singerman J A & Jaffe H H, *J Phys Chem (USA)*, 80 (1976) 1928.
- 12 Ellis R L, Jaffe H H & Masmandis C A, *J Am Chem Soc (USA)*, 96 (1974) 2623.
- 13 Freund H J & Bigelow W, *Chem Phys (Netherlands)*, 55 (1981) 407.
- 14 Chu N Y C & Weis K, *Chem Phys Lett (Netherlands)*, 27 (1974) 567.
- 15 Marconi G, Salvi P R & Quacquarelli R, *Chem Phys Lett (Netherlands)*, 107 (1984) 314.

- 16 Bigelow R W, Freund H J & Dick B, *Theor Chim Acta (Germany)*, **63** (1983) 177.
- 17 Bigelow R W, *J Chem Phys (USA)*, **73** (1980) 3864.
- 18 Guerra M, Jones D, Distefano G & Madelli A, *Chem Phys (Netherlands)*, **85** (1984) 389.
- 19 McCurdy C W, Rescigno T N, Yeager D L & McKoy V, *Methods of electronic structure theory*, Vol. 4, edited by H F Schaefer III, (Plenum Press, New York & London) 1977.
- 20 Rowe D J, *Rev Mod Phys (USA)*, **40** (1968) 53.
- 21 Dunning T H & McKoy V, *J Chem Phys (USA)*, **47** (1967) 1735.
- 22 Sutton L E, *Tables of interatomic distances* (The Chemical Society, London) 1958.
- 23 Shibuya T, Rose J & McKoy V, *J Chem Phys (USA)*, **58** (1973) 500.
- 24 Fukutome H, *Prog Theor Phys (Japan)*, **33** (1965) 380.
- 25 Tanaka M & Tanka J, *Theor Chim Acta (Germany)*, **30** (1973) 81.
- 26 Jorgensen P & Linderberg J, *Int J Quantum Chem (USA)*, **4** (1970) 587.
- 27 Bouman T D, Hansen A E, Voigt B & Rettrup S, *Int J Quantum Chem (USA)*, **23** (1983) 595.
- 28 Perkin J E & Innes K K, *J Mol Spectrosc (USA)*, **15** (1965) 407.
- 29 Pickett L W, Hoeflich N F & Liu T C, *J Am Chem Soc (USA)*, **73** (1951) 4862.
- 30 Goodman L, *J Mol Spectrosc (USA)*, **6** (1961) 109.
- 31 Innes K K, Byrene J P & Ross I G, *J Mol Spectrosc (USA)*, **22** (1967) 125 and references therein.

Ultrasonic Studies of Ternary System: Water + 2-Propanol + Nitromethane at Miscibility Point

T JOHN PAULUS*, K KRISHNAMOORTHY* & P B MATHUR

Central Electrochemical Research Institute, Karaikudi 623 006

Received 27 September 1985; revised received 10 February 1986

Ultrasonic velocity, density and viscosity of the ternary system consisting of water, 2-propanol and nitromethane are measured at 35°C for different proportions of the components. Adiabatic compressibility, molar sound velocity, free-volume and internal pressure are calculated. The observed increase in adiabatic compressibility and free-volume with increase in mole fraction of 2-propanol suggests polymerization of ternary pseudo molecules.

A third component added to a mixture of two immiscible components brings about the disappearance of the phase boundary resulting in a homogeneous mixture. This phenomenon in certain ternary systems has been studied earlier by observations on the distribution of molecules of one component between the other two components and by

looking for the formation of hitherto unknown compounds from a study of the change in adiabatic compressibility, the validity of additivity rule etc¹⁻³. The present study relates to the determination of the extent of the interaction of molecules in the ternary system: Water + 2-propanol + nitromethane, using ultrasonic method.

Mixtures of the three components mentioned above were prepared in different ratios and measurements were made. Ultrasonic velocity was measured using a single crystal ultrasonic interferometer working at a fixed frequency of 2 MHz. The cell of the interferometer was maintained at 35°C by circulating water from a thermostatic bath. The percentage of error in the measurement was 0.1%.

Densities of mixtures were measured using a specific gravity bottle. Percentage of error in density measurement was 0.135%. Ostwald's viscometer was used for the measurement of viscosity with a percentage error of 0.07%. For computation of parameters, the following formulae⁴⁻⁶ were used:

$$\beta_{ad} = \frac{1}{u^2 \rho} \quad \dots (1)$$

Table 1—Values of Measured and Calculated Parameters

Sl No. of system	Mole Fraction			Density (ρ) g cc	Viscosity (η) cP	Ultrasonic velocity (u) m s	Free-volume (V_f) ml.mol	Adiabatic compressibility (β_{ad}) cm ² dyn ⁻¹	Internal pressure atm
	Water (X_1)	2-Propanol (X_2)	N.M. (X_3)						
1	0.8598	0.06965	0.07065	0.9849	1.155	1530	0.02018	43.37×10^{-12}	22160
2	0.7720	0.1008	0.1269	0.9815	1.199	1410	0.02098	51.25×10^{-12}	19810
3	0.7104	0.1150	0.1751	0.9815	1.238	1373	0.02207	54.02×10^{-12}	18330
4	0.6159	0.1314	0.2530	0.9888	1.112	1315	0.02931	58.48×10^{-12}	15420
5	0.5775	0.1381	0.2846	0.9915	0.9317	1279	0.03933	61.65×10^{-12}	13550
6	0.5191	0.1390	0.3416	0.9972	0.8487	1275	0.05024	61.70×10^{-12}	12480

Table 2—Application of Additivity Rule in Case of β

Sl No. of system	Mole fraction			$\sum \beta_i X_i$	β_{123}
	Water (X_1)	N.M. (X_2)	2-Propanol (X_3)		
1	0.8598	0.07065	0.06965	42.55	43.37
2	0.7727	0.1269	0.1008	42.19	51.25
3	0.7104	0.1751	0.1150	42.30	54.02
4	0.6159	0.2530	0.1314	43.32	58.48
5	0.5775	0.2846	0.1381	42.88	61.65
6	0.5191	0.3416	0.1390	43.51	61.70

Table 3—Application of Additivity Rule in Case of R'

Sl No. of system	Mole fraction			$\sum R_i X_i$	R_{123}
	Water (X_1)	N.M. (X_2)	2-Propanol (X_3)		
1	0.8598	0.07065	0.06965	275.76	280
2	0.7727	0.1269	0.1008	316.18	316
3	0.7104	0.1751	0.1150	343.37	344
4	0.6159	0.2530	0.1314	383.30	378
5	0.5775	0.2846	0.1381	399.20	395
6	0.5191	0.3416	0.1390	422.4	419

* Department of Physics, Alagappa Chettiar College of Engineering & Technology, Karaikudi 623 004

$$R' = \frac{Mu^{1/3}}{\rho} \quad \dots(2)$$

$$V_f = \left(\frac{Mu}{K\eta} \right)^{3/2} \quad \dots(3)$$

$$\Pi_i = bRT \left(\frac{K\eta}{u} \right)^{1/2} \frac{\rho^{2/3}}{M^{7/6}} \quad \dots(4)$$

where β_{ad} is the adiabatic compressibility, u the ultrasonic velocity (in m/s), ρ the density of the liquid (in g/cc), R' the molar sound velocity (in m/s), M the effective molecular weight of the mixture, V_f the free-volume (in ml/mol), K a constant of value 4.28×10^9 , η viscosity in cP, Π_i the internal pressure (in atm), $b=2$ the packing factor for cubic system, R the gas constant and T the temperature in K.

Results and discussion—The measured and computed values of different parameters are given in Table 1. An examination of the data in columns 5 and 6 of Table 2 indicates that in this system, the additivity rule is not obeyed in respect of adiabatic

compressibility whereas it is obeyed in respect of molar sound velocity (Table 3). Values of adiabatic compressibility and free-volume are found to increase uniformly with increase in mole fraction of 2-propanol as is evident from columns 8 and 9 of Table 1. This may be due to the formation of ternary pseudo molecules which may be polymerizing in the liquid phase.

The authors thank Prof. K.I. Vasu, the Director for permission to carry out this study.

References

- 1 Krishnamoorthy K, Kuppusami J & Omayorupakam Pillai S, *Curr Sci (India)*, **44** (1975) 8.
- 2 Srivastava T N, & Sing R P, *Indian J Chem Sect A*, **23** (1984) 227.
- 3 Krishnamoorthy K, Omayorupakam Pillai S, Kuppusami J, *Indian J Pure & Appl Phys*, **11** (1973) 677.
- 4 Prakash O & Prakash S, *J Acoust Soc India*, **6** (1978) 11, 39.
- 5 Kocheshkov K A, Nad M M & Aleksandrov A P, *Chem Ber (Germany)*, **67** (1934) 1348.
- 6 Suryanarayana C V & Kuppusami J, *J Acoust Soc India*, **4** (1976) 75.

ESR Studies of Ternary Complexes of Copper(II) with Acetylacetone & Substituted 8-Hydroxyquinolines

Y ANJANEYULU, V G K M PISIPATI, N V S RAO,
L N MURTHY & R PRABHAKARA RAO

Faculty of Physical Sciences, Nagarjuna University, Nagarjuna
Nagar 522 510

Received 25 November 1985; revised received 17 March 1986

ESR studies are carried out on ternary complexes of copper(II) with acetylacetone (AA) and substituted 8-hydroxyquinolines (8-HQ) at room and liquid nitrogen temperatures in DMF solution. An unusual splitting of the parallel lines is observed for Cu(AA)(5,7-Br-OX) at liquid nitrogen temperature. No such splitting is observed for other complexes. The splitting is explained on the basis of either partial dissociation of 8-HQ ligand or the solution effect of DMF which solvates some copper chelate molecules. The molecular orbital coefficients are estimated and these indicate that in-plane π -bonding is weak compared to σ -bonding in all the complexes. The value of χ , which is proportional to hyperfine constants is found to be varying with substitution in the ligand 8-HQ.

The detailed study of magnetic parameters from the ESR spectra of transition metal complexes provides the information regarding the metal-ligand bond^{1,2}. It is found that these parameters representing the metal-ligand bonding exhibit analogous qualitative characteristics for a substance possessing similar type of environment around the paramagnetic copper(II) ion irrespective of the ligand chemical composition³⁻⁶ with few exceptions, depending upon electron withdrawing or donating characteristics of the substituent in the ligand and the solvent used for the ESR study⁷. Such studies are carried out on a number of binary and ternary copper(II) complexes for different type of environments such as [4O] (Ref. 2), [3O, N] (Ref. 8), [2O, 2N] (Refs 3 and 4), [O, 3N] (Ref. 9) and [4N] (Refs 5 and 6). From the analysis of the earlier studies it was inferred that the Abragam, Horowitz and Pryce parameter¹⁰ χ , proportional to the hyperfine interaction which is related to the hyperfine contact term K , is indeed constant for a particular type of environment around copper(II). However, for any particular environment, the studies of the relative dependence of magnitude on the chemical nature of the substituent in the ligand and on the solvent used, are meagre. Hence any information regarding the dependence of the χ parameter, on the chemical nature of the ligand and the substituent in the ligand, contributing an analogous environment around copper(II), provides an insight to understand the chemical effects^{7,11}. In this note, we present the

results of ESR studies of biologically important ternary complexes of copper(II) with acetylacetone and substituted 8-hydroxyquinolines. The complexes studied and their molecular structures are shown in Fig. 1.

Experimental details—The binary complex of copper(II) with acetylacetone was prepared following the procedure described earlier¹². The ternary copper(II) complexes were prepared by mixing 50 ml of each equimolar (0.02 M) ethanolic solutions of copper(II), acetylacetone and 8-hydroxyquinoline. The mixture after refluxing for 1 hr was concentrated to 10 ml. The solid complex was separated from the concentrate, then recrystallized from ethanol and dried in vacuum over anhydrous CaCl_2 . The purity of these complexes was established by elemental analysis. The first derivative tracings of the ESR signals in dimethylformamide (DMF) solutions of all the complexes (10^{-3} M) were recorded at room and liquid nitrogen temperatures using Varian E 4 X-Band ESR spectrometer. The optical absorption data were taken using Systronics digital spectrophotometer model 106, India.

Results and discussion—The spectra of all the complexes in solution (DMF) at room temperature (RT) showed four spin-dependent hyperfine lines as

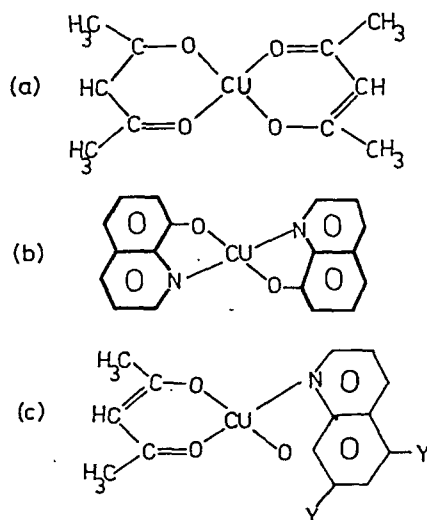


Fig. 1—Molecular structure of the complexes: (a) bis(acetylacetonato)-copper(II), Cu(AA)₂ (complex 1); (b) bis(8-hydroxyquinolinato)-copper(II), Cu(OX)₂ (complex 2); (c) Cu(AA)(OX), Y = H, (OX) = 8-hydroxyquinoline (complex 3), Cu(AA)(5,7-Cl-OX), Y = Cl, 5,7-Cl-OX = 5,7-dichloro-8-hydroxyquinoline (complex 4); Cu(AA)(5,7-Br-OX), Y = Br, 5,7-Br-OX = 5,7-dibromo-8-hydroxyquinoline (complex 5); Cu(AA)(5,7-I-OX), Y = I, 5,7-I-OX = 5,7-diiodo-8-hydroxyquinoline (complex 6); and Cu(AA)(5,7-NO₂-OX), Y = NO₂, 5,7-NO₂-OX = 5,7-dinitro-8-hydroxyquinoline (complex 7)

expected. The g_0 , A_0 and ΔE values are given in Table 1. At liquid nitrogen temperature (LNT) typical frozen solution (glassy) spectra are obtained giving rise to four well resolved hyperfine lines on g_{\parallel} with no resolution on the g_{\perp} line. No significant rhombic distortions were present which is in accordance with the results of Yokoi *et al.*¹³, who found that in frozen solution the effective symmetry of the ligand field tends to be higher than the symmetry of the ligand geometry. The g_{\parallel} , g_{\perp} and A_{\parallel} parameters are obtained from LNT spectra following the procedure described by Neiman and Kivelson¹⁴. The values of A_{\perp} are obtained from the equation $A_0 = (A_{\parallel} + 2A_{\perp})/3$. The g_{\parallel} , g_{\perp} , A_{\parallel} and A_{\perp} values are presented in Table 2. The ESR spectrum of Cu(AA) (5,7-Br-OX) at LNT exhibits an unusual splitting of the axial line, giving rise to a spectrum due to isolated ions of two species (Fig. 2). We believe that the species II of Cu(AA) (5,7-Br-OX) with $g_{\parallel} = 2.242$ and $A_{\parallel} = 159$ at LNT (Table 2) belongs to the ternary complex since these values are found to be similar to those of other ternary complexes. We could not definitely identify species I because of the discrepancy of A_{\parallel} value either with that of Cu(AA)₂ or Cu(AA) (5,7-Br-OX) even though the g_{\parallel} value is close to the value of Cu(AA)₂. The solvation effect observed in bromo substitution in complex 5 is due to the presence of two isolated species and is in accordance with the reported observations for ternary complexes of copper (II) (Ref. 8).

The binary complexes 1, Cu(AA)₂ and 2, Cu(OX)₂ possess [4O] and [2O, 2N] coordination respectively

 Table 1—Values of g_0 , A_0 and ΔE

Complex	g_0	$A_0 \times 10^4$ cm ⁻¹	ΔE cm ⁻¹
1. Cu(AA) ₂	2.129	64	16,129
2. Cu(OX) ₂	2.130	82	16,300
3. Cu(AA)(OX)	2.100	69	16,000
4. Cu(AA)(5,7-Cl-OX)	2.110	76	16,949
5. Cu(AA)(5,7-Br-OX)	2.105	78	16,129
6. Cu(AA)(5,7-I-OX)	2.106	77	16,000
7. Cu(AA)(5,7-NO ₂ -OX)	2.124	62	16,500

 Table 2—Values of Principal g and A

Complex	Room temperature			Liquid nitrogen temperature							
	Polycrystalline data			Polycrystalline data				Solution data			
	$g_1 = g_{\parallel}$	$g_2 = g_0$	$g_3 = g_{\perp}$	$g_1 = g_{\parallel}$	$g_2 = g_0$	$g_3 = g_{\perp}$	g_{\parallel}	g_{\perp}	A_{\parallel}	A_{\perp}	
1. Cu(AA) ₂		2.094					2.291	2.061	159	15	
2. Cu(OX) ₂	2.196		2.047				2.244	2.075	167	25	
3. Cu(AA)(OX)	2.225	2.060	2.040	2.223	2.054	2.034	2.242	2.042	144	32	
4. Cu(AA)(5,7-Cl-OX)		2.065			2.070		2.234	2.054	162	25	
5. Cu(AA)(5,7-Br-OX)		2.065			2.072		2.242	2.060	159	30	
6. Cu(AA)(5,7-I-OX)	2.191	2.040	2.189	2.040			2.242	2.054	162	27	
7. Cu(AA)(5,7-NO ₂ -OX)	2.199	2.052	2.052	2.184		2.054	2.238	2.059	177	14	

The accuracies in the values of g_{\parallel} , g_{\perp} , A_{\parallel} and A_{\perp} are ± 0.003 , ± 0.005 , $\pm 4 \times 10^{-4}$ cm⁻¹ and 6×10^{-4} cm⁻¹ respectively.

around copper(II) in their equatorial planes. The ternary complexes 3-7 possess [3O, N] coordination around copper(II) arising out of two oxygen atoms from the acetylacetonate, one oxygen and one nitrogen from the substituted oxines.

The g_{\parallel} and A_{\parallel} values are found to be different for different complexes. The magnetic parameters obtained for the ternary complexes are found to differ from the values of the ternary complexes formed with 8-hydroxyquinoline and substituted salicylic acids possessing analogous environment of [3O, N] (Ref. 8). The variation of these parameters was explained by using the interpretation given by Rockenbauer¹⁵, characteristic of copper complexes. The covalent character of the planar and axial bonds have opposite effects on the magnetic parameters, i.e. the g factor decreases when the planar bonds become more covalent and increases when the planar bond becomes less covalent or the axial bond becomes more covalent (donor solvents). The low g_{\parallel} values for these ternary complexes compared to the ternary complexes in Ref. 8 with analogous type of coordination, are probably

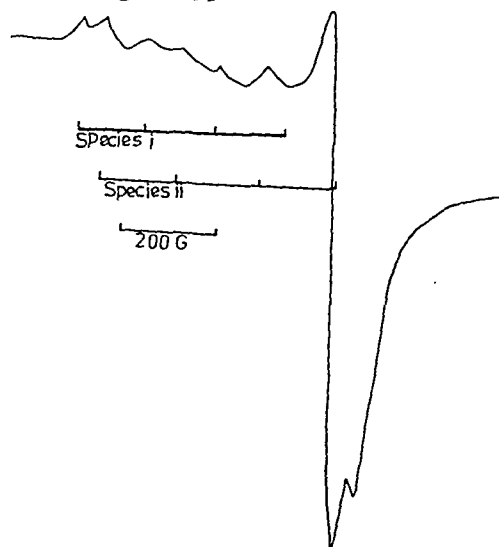


Fig. 2—ESR spectrum of Cu(AA)(5,7-Br-OX) in DMF at liquid nitrogen temperature

Table 3—Values of Z_{\parallel} , Z_{\perp} , Molecular Orbital Coefficients and χ

Complex	Z_{\parallel}	Z_{\perp}	α^2	α'^2	β^2	$-\chi$
1. Cu(AA) ₂	1.07	1.05	0.77	0.30	0.96	3.53
2. Cu(OX) ₂	1.12	1.06	0.75	0.34	0.82	3.92
3. Cu(AA)(OX)	1.10	1.07	0.66	0.43	0.93	3.43
4. Cu(AA)(5,7-Cl-OX)	1.10	1.06	0.72	0.36	0.87	3.67
5. Cu(AA)(5,7-Br-OX)	1.10	1.06	0.72	0.36	0.86	3.72
6. Cu(AA)(5,7-I-OX)	1.10	1.06	0.73	0.36	0.84	3.72
7. Cu(AA)(5,7-NO ₂ -OX)	1.09	1.05	0.80	0.28	0.82	3.41

due to the substituent ligand and the substituents in the ligand, i.e.: (a) electronic shielding or delocalization effect, (b) electron withdrawing groups in the complexes 3-7. The electron delocalization is high compared to Cu(AA)(SA) (Ref. 16) (SA = salicylic acid) complexes and it is indeed low when compared to Cu(OX)(SA) (Ref. 8). The observed g_{\parallel} values are found to be in agreement with the above observation¹¹. Similar observation in g_{\parallel} values (a change from 2.282 to 2.244) was also made in copper(II) complexes formed with a change in ligand^{7,11}, i.e. 2,2'-bipyridyl, N,N'-dimethylethylenediamine, and N,N,N',N'-tetramethylethylenediamine.

Molecular orbital coefficients and χ -parameter—The molecular orbital coefficients are evaluated using the iterative procedure following Gersmann and Swalen¹⁷. These values together with those of Z_{\parallel} , Z_{\perp} and χ parameters are presented in Table 3. The variation of covalency strength can be explained on the basis of interpretation given for the magnetic parameters. Even though the σ -bond strength in the two binary complexes is same, the in-plane π -bonding is very weak in complex 1 rather than in complex 2. The strength of the σ -bond in the ternary complexes 3 to 6 is stronger than the in-plane π -bonding, while the strength of π -bonding is as strong as that of σ -bonding in complex 7. The χ -value of complexes 3-7 showed anomalous behaviour (Table 3). The magnitude of χ varies from 3.41 to 3.72 and is relatively smaller than the average value (3.82) reported for analogous environment of [3O, N] around copper (II) in solution⁸. This significant deviation of χ values from the reported values can be explained as follows: (a), in solution the configuration may be different for the complexes possessing analogous environment of [3O, N] but dissimilar ligands providing the coordination of atoms; (b), the presence of atoms through solvation effect in the fifth and sixth positions of coordination will decrease the χ value due to the presence of 4s character in the ground state because it comes through the axial bond.

Conclusions—From a study of the molecular orbital coefficients and the parameter χ in the ternary complexes, the salient conclusions are: 1, the in-plane π -bonding is as strong as that of Cu(OX)₂ and is stronger than the π -bonding in Cu(AA)₂; 2, the characteristic χ value is found to be varying with substitution in the ligand 8-hydroxyquinoline in Cu(AA)(OX) while it is constant irrespective of substitution in the ligand salicylic acid in Cu(OX)(SA)⁸.

Financial assistance provided by the University Grants Commission, New Delhi, is gratefully acknowledged.

References

- 1 Toy A D, Chaston S H H, Pilbrow J R & Smith T D, *Inorg Chem (USA)*, **10** (1971) 2219.
- 2 Kuska H A, Rogers M T & Drullinger R E, *J Phys Chem (USA)*, **71** (1967) 109.
- 3 Allen H C (Jr) & Scullane M I, *J Coord Chem (GB)*, **8** (1978) 93.
- 4 Scullane M I & Allen H C (Jr), *J Coord Chem (GB)*, **7** (1978) 181; **9** (1979) 151.
- 5 Pisipati V G K M, Satyanandam G & Rao N V S, *Org Magn Reson (GB)*, **17** (1981) 235.
- 6 Lancione R L, Allen H C (Jr) & Buntaiane J R, *J Coord Chem (GB)*, **8** (1979) 201.
- 7 Pisipati V G K M, Rao N V S, Muralikrishna V, Murthy V S & Kesavan T, *Org Magn Reson (GB)*, **22** (1984) 629.
- 8 Anjaneyulu Y, Rao N V S, Swamy R Y, Rao R P & Pisipati V G K M, *Can J Chem (Canada)*, **61** (1983) 2154.
- 9 Kwik W L, Ang K P & Chen G, *J Inorg & Nucl Chem (GB)*, **42** (1980) 303.
- 10 Abragam A, Horowitz J & Pryce M H L, *Proc R Soc London Ser B (GB)*, **230** (1955) 169.
- 11 Rao N V S, Muralikrishna V & Pisipati V G K M, *Indian J Pure & Appl Phys*, **23** (1985) 617.
- 12 Faroni M F, Perry D C & Kuska H A, *Inorg Chem (USA)*, **7** (1968) 2415.
- 13 Yokoi H, Otagiri M & Isobe T, *Bull Chem Soc Jpn (Japan)*, **44** (1971) 2395.
- 14 Neiman R & Kivelson D, *J Chem Phys (USA)*, **35** (1961) 156.
- 15 Rockenbauer A, *J Magn Res (USA)*, **35** (1979) 429.
- 16 Anjaneyulu Y, Pisipati V G K M, Rao N V S & Rao R P (unpublished work).
- 17 Gersmann H R & Swalen J D, *J Chem Phys (USA)*, **36** (1962) 3221.

ESR Hyperfine Line Width Studies of Some Aliphatic Polyamine Copper(II) Compounds

V MURALIKRISHNA, N V S RAO & V G K M PISIPATI*

Faculty of Physical Sciences,
Nagarjuna University, Nagarjuna Nagar 522 510

Received 18 October 1985; revised received 17 March 1986

The ESR hyperfine line widths are analyzed in solution at room temperature in different solvents for a number of aliphatic polyamine copper(II) compounds, using the theory of R Wilson and D Kivelson [*J Chem Phys (USA)*, 44 (1966) 154, 4440, 4445]. The reasons for the difference between the calculated and experimental line widths, mainly in one of the extreme lines, are discussed.

Wilson and Kivelson¹ following the formulation of Kubo and Tomita², developed the theory of ESR line widths in solution. They carried out line widths analysis on vanadyl acetylacetonate and copper acetylacetonate assuming the solution to be very dilute so that the effect of the dipolar and exchange interactions can be neglected. They further considered only the effect of motional modulation of anisotropic g and A tensors and also reported the ESR line width variation with temperature and solvent.

Misra and Sharma³⁻⁵ carried out line width analysis on a number of amino acid copper(II) compounds and found out that the contribution of spin rotational mechanism is sufficiently large. Further, the agreement between the theory and experiment is not as good as that was found earlier¹.

This note presents the ESR line width analysis of ten copper(II) compounds formed with different aliphatic polyamines in methanol, ethanol and pyridine solvents following the formulation of Wilson and Kivelson.

Experimental Details—The compounds 1. Bis(N,N'-dimethylethylenediamine)copper(II) sulphate tetrahydrate., 2. Bis(N,N'-diethylethylenediamine)copper(II) nitrate., 3. Dithiocynato(N,N,N',N'-tetramethylethylenediamine)copper(II)., 4. Dichloro(2,2'-bipyridyl)-N-(2-hydroxyethylethylenediamine)copper(II)., 5. Dinitro-(2,2'-bipyridyl)-N-(2-hydroxyethylethylenediamine)copper(II)., 6. Diaquosulphato(N,N,N',N'-tetramethylthylenediamine)copper(II) hydrate., 7. Dinitro-(N,N,N',N'-tetramethylethylenediamine)copper(II)., 8. Dinitro(2,2'-bipyridyl)

copper(II)., 9. Dichloro(N,N'-dimethylethylenediamine)copper(II) and 10. Dichloro(N,N,N',N'-tetramethylethylenediamine)copper(II) were prepared using reported methods⁶⁻¹⁰. The spin-Hamiltonian parameters for these compounds are taken from our earlier papers^{11,12}. The ESR spectra of all the samples in different solvents with concentrations between 10^{-3} to 10^{-4} M are recorded. The representative spectra of some of the compounds are shown in Fig.1. The viscosity values for the solvents are taken from literature¹³.

Results and discussion—The ESR line widths calculations in solution are carried out using the procedure adopted in Refs 1,3,14,15. The ESR spectra at room temperature in solution show four spin-dependent lines ($I=3/2$ for copper II). The individual hyperfine lines are not completely symmetric having different intensities and of varying widths. The hyperfine lines can be represented by

$$\omega_0 = g_0\beta_e H/\hbar + A_0M + \frac{1/2(\hbar A_0^2)[K(I+1) - M^2]}{g_0\beta_e H} \dots (1)$$

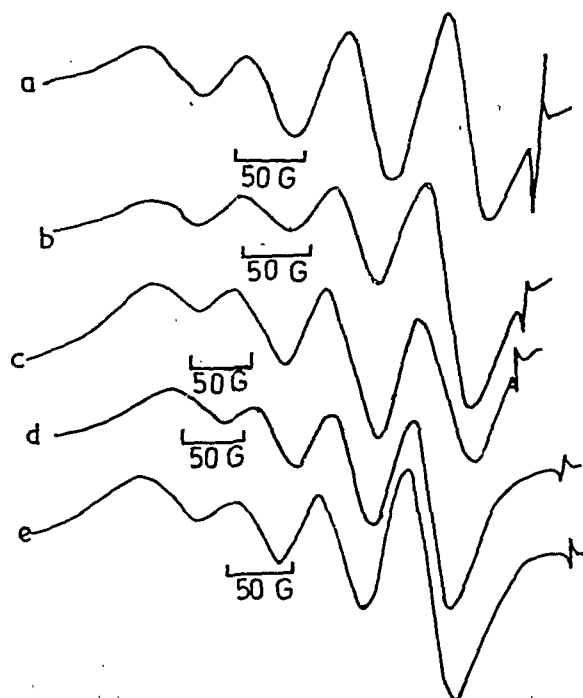


Fig.1—ESR spectra of copper(II) complexes at room temperature Bis(N,N'-diethylethylenediamine)copper(II): (a) in MeOH; (b) in Pyridine; (c) Dichloro(2,2'-bipyridyl)-N-(2-hydroxyethylethylenediamine)copper(II) in MeOH; (d) Diaquo sulphato(N,N,N',N'-tetramethylethylenediamine)-copper(II) hydrate in MeOH; (e) Dinitro(N,N,N',N'-tetramethylethylenediamine)copper(II) in MeOH.

*Present address: Department of Chemistry, G10 Baker Laboratory, Cornell University, Ithaca, New York 14853 USA.

NOTES

where ω_0 is the microwave frequency in radians per sec, g_0 the isotropic g factor, A_0 the isotropic hyperfine splitting constant in radians per sec, β_e the Bohr magneton, H the applied magnetic field and M the nuclear magnetic spin quantum number.

Eq.(1) indicates that the line at $M = -3/2$ is supposed to be at the lower field than the line at $M = 3/2$. A_0 should be negative. Then, the relative signs of all other parameters can be obtained. It was observed that the substitution of a positive value of A_0 was convenient for the calculations. This is because of the fact that the experimental value of the line widths parameter B is positive while its theoretical value can be either positive or negative depending upon the sign of A_0 .

The experimental peak-to-peak line widths for the solution spectrum of all the compounds are given in Table 1 and these line widths can be expressed in the following form

$$\Delta H = (A + A') + BM + CM^2 + DM^3 \quad \dots (2)$$

where M is the Z component of the nuclear spin. The parameters A , B , C , and D are related to the nuclear, electronic and anisotropic g -tensor interactions. A' is called the residual line width. The four line spectra are fitted in Eq. (2) for all the compounds in different solutions. The values of all these parameters are given in Table 2.

The same line width parameters A , B , C and D can be expressed as functions of spin-Hamiltonian parameters, g_0 , A_0 , g_{\parallel} , g_{\perp} , A_{\parallel} , A_{\perp} and Debye

Table 1—Experimental and Calculated Line Widths for the Solution Spectrum of All the Compounds and the Molecular Hydrodynamical Radius

Compd No.	Solvent	M	H_E	H_C	r Å	Compd No.	Solvent	M	H_E	H_C	r Å
1	MeOH	-3/2	52.4	43.4	2.20	5	MeOH	-3/2	61.0	56.0	2.35
		-1/2	45.4	45.5				-1/2	57.1	58.2	
		1/2	46.9	47.9				1/2	59.0	60.7	
		3/2	38.7	50.6				3/2	56.1	63.6	
2	MeH	-3/2	40.831.8		2.95	6	MeOH	-3/2	40.8	31.9	2.70
		-1/2	33.7	33.3				-1/2	34.6	34.3	
		1/2	35.2	35.3				1/2	36.7	37.7	
		3/2	38.7	38.0				3/2	35.7	40.3	
2	Py	-3/2	39.7	34.9	2.45	6	EtOH	-3/2	35.0	34.3	2.35
		-1/2	36.6	36.7				-1/2	37.5	38.2	
		1/2	38.6	38.9				1/2	41.0	42.5	
		3/2	40.7	42.4				3/2	37.5	47.3	
3	MeOH	-3/2	40.7	34.3	2.70	7	MeOH	-3/2	35.0	30.2	2.50
		-1/2	35.6	35.0				-1/2	32.5	32.3	
		1/2	38.0	37.9				1/2	34.5	34.8	
		3/2	45.8	42.3				3/2	37.0	37.6	
3	EtOH	-3/2	42.0	34.2	2.30	7	EtOH	-3/2	42.5	33.3	2.35
		-1/2	37.5	37.1				-1/2	35.0	34.7	
		1/2	40.5	40.7				1/2	38.5	38.7	
		3/2	45.0	45.0				3/2	45.5	45.6	
3	Py	-3/2	35.7	31.9	2.40	8	MeOH	-3/2	38.6	30.5	2.55
		-1/2	33.7	33.6				-1/2	33.5	33.1	
		1/2	35.7	35.9				1/2	36.0	36.0	
		3/2	38.8	38.9				3/2	41.5	39.3	
4	EtOH	-3/2	32.5	44.0	2.35	9	MeOH	-3/2	42.0	36.5	2.30
		-1/2	45.0	46.6				-1/2	38.9	38.6	
		1/2	48.0	49.9				1/2	41.1	41.0	
		3/2	42.5	54.2				3/2	46.1	43.8	
4	MeOH	-3/2	35.6	35.0	2.55	9	EtOH	-3/2	37.5	37.7	2.30
		-1/2	37.7	37.9				-1/2	40.5	41.4	
		1/2	39.9	40.4				1/2	43.5	45.4	
		3/2	42.7	43.4				3/2	32.5	50.6	
4	Py	-3/2	41.3	38.7	2.15	10	Py	-3/2	42.9	33.9	2.55
		-1/2	40.3	40.5				-1/2	36.8	36.5	
		1/2	41.8	42.5				1/2	39.5	39.9	
		3/2	39.3	44.8				3/2	40.9	44.1	

Table 2—Line Width Parameters Obtained from Experimental Spectra and Theory (in Gauss) along with the Values of T_R and α_{RS}

Compd No.	Solvent		α_{RS}					$T_R \times 10^{11}$	α_{RS}
			A	A'	B	C	D		
1	MeOH	Expt.	46.21		2.224	-0.285	-3.017	0.654	52.12
		Theo.	4.00	42.21	2.224	0.150	0.007		
2	MeOH	Expt.	33.94		1.829	2.592	-1.115	1.578	22.95
		Theo.	3.33	30.61	1.858	0.253	0.011		
2	Py	Expt.	37.30		2.242	1.275	-0.847	1.484	24.75
		Theo.	4.13	33.17	2.238	0.332	0.014		
3	MeOH	Expt.	35.99		2.487	3.22	-0.347	1.210	32.15
		Theo.	4.29	31.70	2.519	0.242	0.010		
3	EtOH	Expt.	38.43		3.250	2.250	-1.000	1.506	31.89
		Theo.	5.67	32.76	3.303	0.285	0.012		
3	Py.	Expt.	34.38		2.121	1.275	-0.483	1.395	37.77
		Theo.	3.86	30.51	2.137	0.300	0.011		
4	MeOH	Expt.	38.75		2.179	0.175	0.083	1.019	30.78
		Theo.	3.77	34.98	2.130	0.255	0.012		
4	EtOH	Expt.	47.62		2.988	-4.500	0.167	1.606	24.67
		Theo.	5.35	42.27	3.029	0.393	0.018		
4	Py.	Expt.	41.14		1.771	-0.375	-1.083	1.003	39.91
		Theo.	3.38	37.75	1.801	0.107	0.005		
5	MeOH	Expt.	58.03		2.307	0.243	-1.748	0.797	70.21
		Theo.	3.95	55.08	2.285	0.177	0.008		
6	MeOH	Expt.	35.33		2.575	1.300	-1.900	1.210	53.40
		Theo.	4.57	30.74	2.579	0.182	0.079		
6	EtOH	Expt.	39.62		3.833	-1.500	-1.333	1.606	44.94
		Theo.	8.00	31.62	3.936	0.209	0.088		
7	MeOH	Expt.	33.15		2.188	1.375	-0.750	0.960	53.90
		Theo.	3.95	29.20	2.246	0.160	0.071		
7	EtOH	Expt.	35.84		3.813	3.625	-1.250	1.606	41.78
		Theo.	6.80	29.04	3.737	1.255	0.109		
8	MeOH	Expt.	34.08		2.688	2.675	-0.750	1.099	57.84
		Theo.	4.93	29.14	2.675	0.163	0.068		
9	MeOH	Expt.	39.43		2.192	2.050	-0.367	0.748	69.04
		Theo.	3.85	35.58	2.194	0.153	0.007		
9	EtOH	Expt.	42.85		3.583	-3.500	-2.330	1.508	35.10
		Theo.	6.26	36.61	3.641	0.324	0.015		
10	Py.	Expt.	37.68		3.121	1.875	-1.683	1.674	47.07
		Theo.	5.33	32.34	3.384	0.015			

correlation time $T_R = (4\pi r^3 \eta / 3kT)$ where r is the molecular hydrodynamical radius of the equivalent rotating sphere and η the coefficient of viscosity. These line width parameters are calculated as a function of r^3 . The radius r , which is an adjustable parameter, is adjusted in all the compounds in order to give the best fit between theoretical and experimental values of B and C . The values of r obtained for all the compounds are presented in Table 1.

The general agreement between the theory and experiment is not as good as that was found in the case of vanadyl acetylacetonate¹. The theory holds good only for small values of $[b/\omega_0] [= 0.007]$ and $[\Delta\gamma/\gamma] [= 0.02]$ reported for vanadyl acetylacetonate, where $b = (A - A') (2/3)$ rad/s, ω_0 is the microwave frequency in rad/s, $\Delta\gamma = \beta_0 \Delta g / h$, $\Delta g = g - g$. For the compounds studied presently, the values of $[b/\omega_0] = 0.07$ and $[\Delta\gamma/\gamma] = 0.055$ to 0.11 are found to be higher

than the values reported for vanadyl acetylacetonate. However, the observed values of $[\Delta\gamma/\gamma]$ are in agreement with the reported values ($[\Delta\gamma/\gamma] = 0.10$) for copper acetylacetonate.

The theoretical value of A is then subtracted from the experimental values ($A + A'$) in order to obtain measured values of the residual line widths A' . These values of A' are given in Table 2.

The spin rotational peak-to-peak derivative line width is given by

$$\alpha_{RS} = \left(\frac{2h}{\sqrt{3} g_0 \beta_e} \right) \left(\frac{1}{12\pi r^3} \right) \left(\frac{\Delta g^2 + 2\Delta g^2}{\eta} \right) K T \quad \dots (3)$$

where $\Delta g = g - 2.0023$ and $\Delta g = g - 2.0023$.

The value of r obtained for a best fit between the experimental and theoretical values is used to calculate α_{RS} . The values of α_{RS} are given in Table 2. The

contribution to A' from spin-rotational relaxation mechanism (α_{RS}) is quite large and it is because of the fact that this mechanism is applicable to bigger molecules¹⁶ where anisotropic interactions with solvent molecules are large.

The value of the adjustable parameter r plays an important role in deciding the value of α_{RS} in view of its inverse proportionality relationship. Wilson and Kivelson¹ introduced λ , a dimensionless quantity related to r as

$$\lambda^{1/3} = \frac{r}{3.045} \hbar \quad \dots (4)$$

Using the Eq. (4), λ values are evaluated and found to be equal to 0.93 ± 0.05 in all the compounds, while the reported λ value tends to unity¹. λ shows no variation with the solvent in the present study.

The calculated line widths differ from the experimental results, in one of the extreme lines. The reason may be due to the fact that the theory does not give B and C of different signs. Both could be positive or negative depending upon the sign of A_0 . The value of r can be adjusted to the magnitude but not the ratios of these parameters.

The authors are grateful to Dr V S Murthy and Mr T Kesavan of the Indian Institute of Technology, Madras, for recording the ESR spectra. Financial

assistance to the study by the University Grants Commission, New Delhi, is gratefully acknowledged.

References

- 1 Wilson R & Kivelson D, *J Chem Phys (USA)*, **44** (1966) 154, 4440, 4445.
- 2 Kubo R & Tomita J, *J Phys Soc Jpn (Japan)*, **9** (1954) 888.
- 3 Misra B N & Sarma S D, *J Chem Phys (USA)*, **63** (1975) 5322.
- 4 Misra B N & Sarma S D, *J Mag Res (USA)*, **24** (1976) 1.
- 5 Misra B N & Sarma S D, *Indian J Pure & Appl Phys*, **15** (1977) 719.
- 6 Korveranta J, *Soum Kemistil (Finland) Vol B*, **46** (1973) 240.
- 7 Nasanen R & Lukkonen E, *Soum Kemistil (Finland) Vol B*, **41** (1968) 27.
- 8 NBalvich J, Fivizzami K P, Pavkovic S F & Brown J N, *Inorg Chem (USA)*, **15** (1976) 71.
- 9 Pavkovic S F, Miller D & Brown J N, *Acta Crystallogr (USA) Sect B*, **33** (1977) 2894.
- 10 Ester E D, Ester W E, Hatfield W E & Hodgson, *Inorg Chem (USA)*, **14** (1975) 106.
- 11 Pisipati V G K M, Rao N V S, Muralikrishna V, Murthy V S & Kesavan T, *Org Mag Res (UK)*, **22** (1984) 629.
- 12 Rao N V S, Muralikrishna V & Pisipati V G K M, *Indian J Pure & Appl Phys*, **23** (1985) 617.
- 13 *International critical tables* (McGraw Hill, New York), 1930.
- 14 Lewis W B, Alei M & Morgan L O, *J Chem Phys (USA)*, **44** (1966) 2409.
- 15 Prabhananda B S, *Indian J Chem Sect A*, **18** (1979) 290; *Indian J Pure & Appl Phys*, **18** (1980) 823.
- 16 Hubbard P S, *Phys Rev (USA)*, **13** (1963) 115.

Drift Mobilities in Phenazine: A Candidate Material for Organic Photovoltaic Systems

B KUMAR

Physics Department, Devi Ahilya Vishwavidyalaya, Indore 452 001

Received 13 January 1986

Excess hole and excess electron mobilities of phenazine have been calculated employing tight binding and constant relaxation time approximations. The results indicate that phenazine may be a candidate material for photovoltaic systems.

Ever since the discovery of semiconductor behaviour and weak *p-n* junctions in organic materials, there has been interest in the possibility of making low cost and easily fabricated devices including solar cells with organic materials. The organic materials can be readily and inexpensively fabricated in the form of large area thin films and photovoltage can be generated in response to radiation in ultraviolet and visible regions. Many organic compounds¹ have been investigated and found to have properties amenable to solar energy conversion. However, at the present state of art, the photovoltaic energy conversion efficiency is quite low because of several factors.

One of the main reasons for low efficiency is the high rate of carrier recombination which is expected to be low in materials showing large difference between hole and electron mobilities. We have, therefore, calculated theoretically excess electron and hole mobilities in a number of organic solids in order to select suitable materials. We report in this note such studies for phenazine which is a planar organic molecule with conjugated π -electron systems. It crystallizes² as a base centered monoclinic crystal with space group $P2_1/a \equiv C_{2h}^5$ having two molecules per unit cell. The numbering of atomic sites within the molecule is shown in Fig. 1.

The mobilities have been calculated using constant relaxation time approximation ($\tau_0 = \text{constant}$)

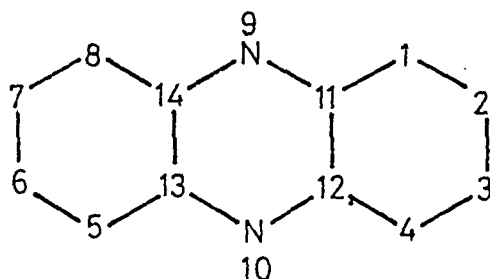


Fig. 1—Numbering of atomic sites

$$\mu_{ij} = \frac{e\tau_0}{kT} \langle V_i V_j \rangle$$

where V_i is the *i*th component of velocity vector $V(\mathbf{K})$.

The expression for $\langle V_i V_j \rangle$ for a crystal with two molecules per unit cell then becomes³

$$\langle V_i V_j \rangle = P/Q \quad \dots(1)$$

where

$$P = \int \left\{ \frac{\partial E}{\partial K_i} + \frac{\partial E_+}{\partial K_j} \exp[-\beta E_+(\mathbf{K})] + \frac{\partial E_-}{\partial K_i} \frac{\partial E_-}{\partial K_j} \exp[-\beta E_-(\mathbf{K})] \right\} d\mathbf{K}$$

and

$$Q = h^2 \int \left\{ \exp[-\beta E_+(\mathbf{K})] + \exp[-\beta E_-(\mathbf{K})] \right\} d\mathbf{K}$$

where $\beta = 1/kT$, E_s are intermolecular transfer integrals (IMTIs). The IMTIs have been calculated employing tight binding approximation⁴. The detailed calculations of IMTIs are given in our earlier papers^{5,6}.

Numerical computation involved in Eq. (1) has been carried out by dividing the integration range ($-\pi$ to π) along each axis into three equal intervals and then applying a four-point Gauss quadrature formula to each interval. The calculated values of velocity components along *a*, *b*, *c* ($c' = \frac{1}{2}a, b$) and *ac'* axes are given in Table 1.

From Table 1, we see that along axes *a* and *ac'* the mobilities for holes and electrons differ appreciably. This is consistent with the findings of our earlier paper⁷. We have pointed out⁷ that organic materials, which show large differences in the mobilities of holes and electrons, are expected to be potential candidates for photovoltaic devices. Thus, phenazine holds a great future promise and is worth exploring for photovoltaic devices.

Table 1—Velocity Components (in $10^{10} \text{ cm}^2/\text{s}^2$) along Different Axes

$\langle V_a^2 \rangle$	$\langle V_b^2 \rangle$	$\langle V_c^2 \rangle$	$\langle V_a V_c \rangle$
For holes			
445.72	702.89	486.10	-99.36
For electrons			
136.48	705.54	320.21	203.74

NOTES

The author thanks Prof. S C Mathur for many valuable discussions.

References

- 1 Hovel H J, *Semiconductor and semimetals*, Vol. 11, Edited by R W Wilardson & A C Bear (Academic Press, New York) 1975 211, 214.
- 2 Herbstem F H & Schmidt G M T, *Acta Crystallogr (Denmark)*, **8** (1955) 406.
- 3 Katz J L, Jortner J, Choi S I & Rice S A, *J Chem Phys (USA)*, **39** (1963) 1683.
- 4 Seitz F, *Modern theory of solids* (McGraw-Hill, New York), 1940.
- 5 Mathur S C & Kumar B, *Mol Cryst & Liq Cryst (GB)*, **23** (1973) 85.
- 6 Mathur S C, Kumar B & Roy Keya, *Mol Cryst & Liq Cryst (GB)*, **53** (1979) 271.
- 7 Kumar B, *Phys Status Solidi b (Germany)*, **133** (1986) 395.

Surface Charge Density & Dielectric Constant of a Magneto-Electret of Carnauba Wax as a Function of Time

K D RAY CHAUDHURI, H De & S D CHATTERJEE

Department of Physics, Jadavpur University, Calcutta 700032

Received 9 December 1985; revised received 19 May 1986

The surface charge density and dielectric constant of carnauba wax magneto-electret have been studied as a function of time. It is seen that both the parameters decay with time to reach steady values after about 8 days. The observation may be attributed to (i) orientational polarization and (ii) neutralization of surface charge due to migration of ions from the interior of the dielectric to the surface.

The surface charge and dielectric constant of a thermo-electret of carnauba wax have been measured as a function of time by Chatterjee *et al.*¹ In the present note, we report the time variation of these parameters for a magneto-electret. The magneto-electret was prepared in the usual way by the simultaneous application of magnetic field and heat as reported by Bhatnagar². The carnauba wax used was of prime yellow type having the following constituents by weight: C = 79.25%, H = 12.88%, and O = 7.87%.

The temperature of the dielectric was raised slightly above the melting point and the intensity of magnetic field was 4 kG. It is seen that no charge reversal takes place. The surface charge density dropped from the initial value of 0.48 esu/cm² to 0.13 esu/cm², while the dielectric constant decreased from 2.43 to 2.20 after a

lapse of about 8 days (Fig. 1). Subsequent measurements show that the values remain constant with further passage of time. It may be mentioned that our results do not agree completely with the work of Bhatnagar² who studied the formation and charge decay characteristics of carnauba wax magneto-electrets. This dissimilarity may be attributed to the fact that the temperature of the dielectric and the intensity of applied magnetic field were less than those used by Bhatnagar. It is pointed out in this connection that charge measurement was undertaken by us only on one surface.

To interpret the results, it is observed that a strong magnetic field applied during the formation of the magneto-electret orients the molecules of the dielectric so that magnetic and electric dipoles are aligned in the direction of the magnetic field. Evidence for dipolar orientation caused by a magnetic field has been obtained by both Chatterjee³ and McMohon⁴. The initial enhanced values of surface charge and dielectric constant of the treated sample may be attributed to the orientational polarization as in the case of a thermo-electret state. The finding of Chatterjee *et al.*⁵ that the magnetic anisotropy of a piece of the thermo-electret of carnauba wax remains unchanged for a period of five months also supports the hypothesis of permanency of orientational polarization. Nevertheless, due to the presence of a high electric field at the surface of the electret, the ions formed during the thermal treatment may migrate to the surface and neutralize some charge and diminish the dielectric constant.

One of the authors (H De) is indebted to the Asiatic Society, Calcutta, for granting him the Meghnad Saha research fellowship. Thanks are also due to the Biren Roy Trust, Behala, for financial support.

References

- 1 Chatterjee S D, De H, Roychaudhuri K D & Banerjee K, *J Franklin Inst (USA)*, 289 (1970) 473.
- 2 Bhatnagar C S, *Indian J Pure & Appl Phys*, 4 (1966) 355.
- 3 Chatterjee S D, *Indian J Phys*, 10 (1936) 399.
- 4 McMohon W, *J Amer Chem Soc (USA)*, 78 (1956) 3290.
- 5 Chatterjee S D, Banerjee K, Roychaudhuri K D & De H, *Phys Lett A (Netherlands)*, 29 (1969) 183.

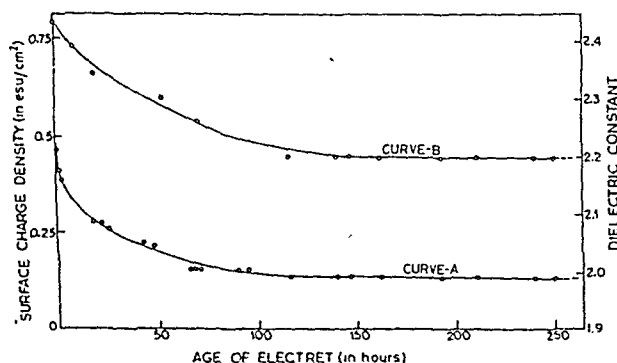


Fig. 1—Variation of surface charge density (curve A) and dielectric constant (curve B) of carnauba wax magneto-electret with time

Indian Journal of Pure & Applied Physics

INSTRUCTIONS TO AUTHORS

SCOPE

The journal welcomes, for publication, full papers and short notes, reporting significant new results of research, in all areas of physics except space physics. The applied fields covered are electronics, electrical engineering, instrumentation and applied mathematics. However, papers in applied mathematics with emphasis on only derivation and proofs and having no direct physical significance, will not be considered. Review articles are not published normally.

SUBMISSION OF MANUSCRIPT

Manuscripts for consideration should be submitted, *in duplicate*, to Editor, Indian Journal of Pure & Applied Physics, Publications & Information Directorate, Hillside Road, New Delhi 110012. They should neither have been already published nor be under consideration elsewhere.

Manuscripts should be in English and typewritten on only one side of good quality paper, in double space, with adequate margin on all four sides. One original and one carbon or photo-copy, each complete in all respects including abstract, illustrations, appendixes, etc. are to be submitted.

PREPARATION OF MANUSCRIPT

Authors may consult recent issues of the Journal to familiarize themselves with the general style and practices adopted in regard to the various elements of a paper.

General

Manuscript should be presented in as concise a form as possible. Good attention should be given to spelling and grammar. In giving names of chemical compounds and structures, abbreviations of units of measurements, symbols and notations, the style and practices recommended by the IUPAP and IUPAC, should be followed.

Frequently repeating combinations of words, e.g. electric field gradient (EFG), junction field effect transistor (JFET), stimulated Raman emission (SRE), should be abbreviated subsequently, indicating the abbreviated form in parenthesis, as shown, at the place of their first occurrence.

Pages should be numbered consecutively and arranged in the following order: Title, authors' names with their institutional affiliations and abstract, along with relevant footnotes whenever necessary (on a separate sheet); introduction; experimental details/theory/method/analysis; results; discussion; conclusion(s); acknowledgement; references and appendixes. Tables, captions for figures (with legends) and appendixes should be typed *on separate sheets* and attached at the end of the manuscript.

Title

The title should be neither too brief/general nor unnecessarily long. It should reflect the content of the paper so as to derive the maximum advantage in indexing. If a paper forms part of a general series, a specific subtitle, indicating the particular aspect of the work covered in the paper, should be provided.

A short running title for the paper, the broad PACS subject heading under which it should be classified in the contents page (authors may consult the January or July issue of the journal for this purpose), and the author's name and address for correspondence, should also be provided on the title page.

Abstract

highlighting the principal findings and conclusions. It should be in such a form that abstracting periodicals can use it without modification.

Introduction

Long and elaborate introduction should be avoided. It should be brief and state the exact scope of the study in relation to the present status of knowledge in the field. Literature review should be limited strictly to what is necessary to indicate the essential background and the justification for undertaking the study.

Materials, methods, apparatus, etc.

The sources of materials and their purity, methods of preparation, procedure for measurements and their accuracies, etc. should be clearly stated to enable any other worker to repeat the work if necessary. New methods, techniques, theories, etc. should be described in adequate detail; but if they are well known, a mere literature reference to them will do; differences from standard ones, improvements or innovations should, however, be clearly mentioned.

Results

Only such primary data as are essential for understanding the discussion and main conclusions emerging from the study should be included. All secondary data as are of interest to a specific category of readership *should not be included* in the paper. Such data should be retained by the authors for supply, on request, to any interested research worker. A footnote to this effect may be inserted at the relevant place in the paper.

The results must be presented in a coherent sequence in a unified logical structure, avoiding repetition or confusion. Limitations of the results should be clearly stated.

The same data should not be presented in both tabular and graphic forms. Only such tables and figures as are essential should be included. Simple linear plots that can easily be discussed in the text, should not be included. Infrared, ultraviolet, NMR and other spectra, DTA curves, etc. should be included only if they pertain to new compounds and/or are essential to the discussion; otherwise only significant numerical data should be given in the text or in a table.

Discussion

Long rambling discussion should be avoided. The discussion should deal with the interpretation of results without repeating information already presented under results. It should relate new findings to the known and include logical deductions. A separate section on 'conclusions' can be given only when they are well established and of outstanding significance. Mere observation of qualitative trends of results should be distinguished from firm conclusions. Also, limitations, if any, to the conclusions should be clearly pointed out.

Mathematical portions

Special attention should be given to the mathematical portions of the paper. Equations must be well separated from the text and written clearly with good separation between the successive lines. The usual norms of breaking long mathematical expressions should be adhered to. Equations should be numbered consecutively in Arabic numerals with the number in parenthesis near the right hand margin.

particularly of the same letter when both occur, as well as letters or symbols likely to be confused one for the other, should be clearly distinguished. Special characters (e.g. Greek, script, vector, tensor, etc.) required must be indicated by marginal notes. Letters and symbols which should appear in bold face must be clearly indicated. To simplify typesetting: (i) long and complicated mathematical expressions which are frequently repeated should be replaced with single letter/symbol, without clashing with the others used in the paper; (ii) the "exp" form of complex exponential functions should be used; and (iii) to simplify fractions, the solidus (/) is to be used and fractional exponents are to be used instead of root signs, e.g.

write $\exp\{-i\omega_0(t_1 - t_2)/2\}$ and not $e^{-i\omega_0(t_1 - t_2)/2}$

write $(4\omega_{pf} K_{3a}^2/\tilde{\omega} K_B^2)^{1/2}$ and not $\sqrt{\frac{4\omega_{pf} K_{3a}^2}{\tilde{\omega} K_B^2}}$

Tables

Tables should be numbered consecutively in Arabic numerals and should bear brief titles. Column headings should be brief. Units of measurement should be abbreviated and placed below the headings. Nil results should be indicated and distinguished clearly from absence of data. Inclusion of structural formulae inside the tables should be avoided as far as possible. Tables should be referred to in the text by numbers and not by terms like 'above', 'below', 'preceding' or 'following'. Results should not be presented to a greater accuracy than that of the method employed.

Illustrations

The number of illustrations should be kept to the minimum. Wherever possible, e.g. a number of individual analogous figures referring to different variables, substances, molecules, etc. may be combined into one composite figure. All illustrations should be numbered consecutively in Arabic numerals. Captions and legends to the figures should be self-explanatory. Line drawings should be made with Indian ink on white drawing paper/cellophane sheet/tracing cloth, and drawn to approximately twice the printed size.

The lettering should be uniform, preferably in stencil, so as to be not less than 1.5 mm after reduction widthwise to full page size (165 mm) or column size (80 mm). The size of geometrical shapes (used to distinguish different graphs), dots, lines, etc. should be sufficiently large to permit the necessary reduction without loss of detail. In the case of photographs, prints must be on glossy paper and contrasty. If an illustration is taken from another publication, reference to the source should be given and prior permission secured. Illustrations should be referred to in the text by numbers and not by terms like 'above', 'following' etc.

Acknowledgement

Acknowledgements should not be exuberant and must be made only to real assistance rendered in connection with the work reported in the paper.

References

References cited should be limited to the absolute minimum (particularly in the case of short notes) based on their essential relevance. In the text, references to literature should be numbered consecutively, in the order of their first occurrence, and should be indicated by superscript Arabic numbers at the relevant places; as far as possible the placement of references on numerals or other symbols should be avoided; in such cases the reference may be given in parenthesis in running text, e.g. "this yielded for n a value of 2.3 (Ref. 5)". Full bibliographic details for all the references mentioned in the text should be listed in serial order at the end of the paper.

In citing references to research papers, names and initials of authors should be followed, in order, by the title of the periodical in the abbreviated form (underlined), the volume number (two lines underneath), the year within circular brackets and the page number [e.g. Chandra B P & Shrivastava K K, *J Phys & Chem Solids (GB)*, 39 (1978) 939]. For names of periodicals, the abbreviations followed by the *Physics Abstracts* should be used. For periodicals not covered by *Physics Abstracts*, the title abbreviations should be according to the *Bibliographic Guide for Editors and Authors*, 1974, published by the American Chemical Society, Washington DC, USA; additionally the country from which the journal is published should be given in parenthesis immediately after the title abbreviation. If a paper has been accepted for publication, the names of the authors and the journal (with volume number and year, if known) should be given followed by the words "in press" [e.g. Wahi P K & Patel N D, *Can J Spectrosc (Canada)*, in press.].

In references containing up to four authors, the names of all the authors with their respective initials should be given. The abbreviations *et al.*, *idem* and *ibid* should be avoided. When there are more than four authors, only the names of the first three authors with their respective initials should be given, followed by the words 'et al.'

Reference to a book should include details in the following order: name and initials of authors, the title of the book (underlined), name of publisher and place of publication within circular brackets and year and page (s) [e.g. Clayton G B, *Operational amplifiers* (Newnes-Butterworths, London), 4th Edn, 1977, 26]. If the reference is to the work of an author published in a book by a different person, the fact that it is cited from the source book should be clearly indicated [e.g. Turnhout Van J, 'Thermally stimulated discharge of electrets' in *Topics in applied physics*: Vol. 33—*Elec. rts*, edited by C M Sessler (Springer Verlag, Berlin), 1980, 130].

Proceedings of conferences and symposia should be treated in the same manner as books. Reference to a paper presented at a conference, the proceedings of which are not published, should include, in the following order, names and initials of authors, title of the paper (underlined), name of the conference, and where and when it was held (e.g. Herczeg P, *Symmetry-violating kaon decays*, paper presented to the International Conference on High Energy Physics and Nuclear Structure, Vancouver, Canada, 13-17 August 1979).

Reference to a thesis should include the name of the author, title of the thesis (underlined), university or institution to which it was submitted and year of submission (e.g. Mehrotra S N, *Many-body techniques and their applications to interacting bosons*, Ph D thesis, Ranchi University, 1976).

Reference to a patent should include names of patentees, country of origin (underlined) and patent number, the organization to which the patent has been assigned (within circular brackets), date of acceptance of the patent and reference to an abstracting periodical where available [e.g. Labes M M, *US Pat.* 4,066,567 (to Temple University), 3 January 1978; *Chem. Abstr.*, 88 (No. 20) (1978), 138350 n].

PROOFS & REPRINTS

The edited manuscript will be sent to the author for his final approval before giving it to the press. No galley proofs will be sent to the authors for corrections, since the proofs will be checked at the editorial office. Authors are given 25 free reprints for each paper. Extra reprints can be ordered by the author while returning the edited manuscript. If the reprints order is not received, it will be presumed that no extra reprints are needed.

CSIR SCIENTIFIC PERIODICALS

JOURNAL OF SCIENTIFIC & INDUSTRIAL RESEARCH (Monthly)

With a fine record of over 45 years' service to the scientific community, this journal has grown into India's leading general science periodical. Intended to fulfil the responsibility of helping the research workers to keep themselves abreast of current developments in various fields of science and technology, the journal carries editorial features highlighting important scientific events in India and abroad, articles on science policy and management of science review articles on topics of current research interest, technical reports on international and national conferences, reviews of scientific and technical publications, and notes on major advances in various fields.

Annual subscription	Rs 120.00	\$ 40.00	£ 23.00
Single copy	12.00	4.00	2.30

INDIAN JOURNAL OF CHEMISTRY (Monthly)

Section A: Started in the year 1963, the journal is devoted to papers in Inorganic, Physical, Theoretical and Analytical Chemistry.

Annual subscription	Rs 160.00	\$ 53.00	£ 30.00
Single copy	16.00	5.30	3.00

Section B: This journal is devoted to papers in Organic Chemistry, including Medicinal Chemistry.

Annual subscription	Rs 160.00	\$ 53.00	£ 30.00
Single copy	16.00	5.30	3.00

INDIAN JOURNAL OF PURE & APPLIED PHYSICS (Monthly)

Started in the year 1963, this journal is devoted to original research communications (full papers and short communications) in all conventional branches of physics (except radio and space physics).

Annual subscription	Rs 180.00	\$ 60.00	£ 34.00
Single copy	18.00	6.00	3.40

INDIAN JOURNAL OF RADIO & SPACE PHYSICS (Bimonthly)

The journal, which is being published beginning from March 1972, is intended to serve as a medium for the publication of the growing research output in various areas of radio and space physics, such as ionospheric propagation, magnetosphere, radio and radar astronomy, physics and chemistry of the ionosphere; neutral atmosphere; airglow, winds and motion in the upper atmosphere; stratosphere-mesosphere coupling, ionosphere-magnetosphere coupling; solar-terrestrial relationship, etc.

Annual subscription	Rs 100.00	\$ 34.00	£ 19.00
Single copy	20.00	6.80	3.80

INDIAN JOURNAL OF TECHNOLOGY (INCLUDING ENGINEERING) (Monthly)

This journal publishes papers reporting results of original research of applied nature pertaining to unit operations, heat and mass transfer, products, processes, instruments and appliances, etc. The journal is of special interest to research workers in departments of applied sciences in universities, institutes of higher technology, commodity research laboratories, industrial cooperative research institutes, and industrial research laboratories.

Annual subscription	Rs 120.00	\$ 40.00	£ 23.00
Single copy	12.00	4.00	2.30

INDIAN JOURNAL OF EXPERIMENTAL BIOLOGY (Monthly)

This journal, devoted to the publication of research communications in the fields of experimental botany, zoology,

microbiology, pharmacology, endocrinology, nutrition, etc., is the only one in India with such a wide coverage and scope.

Annual subscription	Rs 180.00	\$ 68.00	£ 34.00
Single copy	18.00	6.80	3.40

INDIAN JOURNAL OF BIOCHEMISTRY & BIOPHYSICS (Bimonthly)

This journal, published in association with the Society of Biological Chemists (India), Bangalore, is the only research journal in India devoted exclusively to original research communications in biochemistry and biophysics.

Annual subscription	Rs 65.00	\$ 23.00	£ 12.00
Single copy	13.00	4.60	2.40

INDIAN JOURNAL OF MARINE SCIENCES (Quarterly)

Commencing publication from June 1972, this journal is devoted to research communications (full papers and short communications) pertaining to various facets of marine research, viz. biological, physical, geological and chemical oceanography.

Annual subscription	Rs 90.00	\$ 30.00	£ 17.00
Single copy	26.00	8.70	5.00

RESEARCH AND INDUSTRY (Quarterly)

Intended to serve as a link between science and industry, this journal is addressed primarily to technologists, engineers, executives and others in industry and trade. It publishes informative original articles containing practical details of processes and products devoted in India, which show promise of ready utilization, and technical digests on new processes, products, instruments and testing methods which are of interest to industry. Developments in Indian industry are regularly reported.

Annual subscription	Rs 70.00	\$ 23.00	£ 13.00
Single copy	22.00	7.00	4.00

INDIAN JOURNAL OF TEXTILE RESEARCH (Quarterly)

Commencing publication from March 1976, this journal is devoted to the publication of papers reporting results of fundamental and applied researches in the field of textiles.

Annual subscription	Rs 50.00	\$ 17.00	£ 10.00
Single copy	15.00	5.00	3.00

MEDICINAL & AROMATIC PLANTS ABSTRACTS (Bimonthly)

Carries informative abstracts of scientific papers published in important Indian and foreign journals relating to different aspects of medicinal and aromatic plants. Each issue contains about 350 abstracts with a subject index.

Annual subscription	Rs 120.00	\$ 40.00	£ 23.00
Single copy	24.00	8.00	4.60

CURRENT LITERATURE ON SCIENCE OF SCIENCE (Monthly)

Carries abstracts, digests, book reviews, news & notes and R&D statistics with emphasis on problems of S&T in developing countries. It also covers the areas of science policy, R&D planning and management, technology transfer, technology assessment and science and society.

Annual subscription	Rs 100.00	\$ 30.00	£ 12.00
---------------------	-----------	----------	---------

Please contact

Manager (Sales & Advertisement)
PUBLICATIONS & INFORMATION
DIRECTORATE, CSIR
Hillside Road, New Delhi-110012

CSIR PUBLICATIONS

WEALTH OF INDIA

An encyclopaedia of the economic products and industrial resources of India issued in two series

RAW MATERIALS SERIES—contains articles on plant, animal and mineral resources

	Rs	\$	£
Vol I (A-B)	80.00	30.00	13.00
Vol. II (C)	95.00	33.00	17.00
Vol. III (D-E)	105.00	32.00	20.00
Vol. IV (F-G)	65.00	27.00	12.00
Supplement (Fish & Fisheries)	56.00	16.00	10.50
Vol V (H-K)	114.00	34.00	21.00
Vol VI (L-M)	90.00	34.00	15.00
Supplement (Livestock)	102.00	34.00	19.50
Vol VII (N-Pc)	100.00	30.00	19.00
Vol. VIII (Ph-Re)	86.00	32.00	14.00
Vol IX (Rh-So)	104.00	35.00	19.00
Vol. X (Sp-W)	225.00	75.00	42.50
Vol. XI (X-Z)	115.00	38.50	22.00

INDUSTRIAL PRODUCTS SERIES—deals with major, small-scale and cottage industries

Part I (A-B)	58.00	20.00	11.00
Part II (C)	74.00	24.00	14.00
Part III (D-E)	100.00	33.50	19.50
Part IV (F-H)	126.00	42.00	24.00
Part V (I-L)	90.00	23.00	17.00
Part VI (M-Pi)	28.00	8.00	2.80
Part VII (Pi-Sh)	60.00	18.00	6.00
Part VIII (Si-Ti)	66.00	27.00	10.00
Part IX (To-Z)	80.00	34.00	12.00

BHARAT KI SAMPADA (Hindi Edition of Wealth of India, Raw Materials)

Vol. I (अ-ई)	38.00	16.00	6.50
Vol II (ऊ)	36.00	15.00	6.00
Vol III (ए-अ)	36.00	15.00	6.00
Vol IV (ब)	83.00	34.00	16.00
Vol V (क-के)	60.00	22.00	10.00
Vol VI (ख-ख)	80.00	27.00	13.00
Vol. VII (ग-ग)	135.00	40.00	25.00
Livestock (Kukkut Palan)	34.00	15.00	6.00
Fish & Fisheries (Matsya aur Matsyaki)	49.00	21.00	8.00
A Dictionary of Generic & Specific Names of Plants and Animals Useful to Man with their English and Latin pronunciation in Devanagari	30.00	11.00	5.00

OTHER PUBLICATIONS

Proceedings: seminar on primary communications in Science & Technology in India by Sh. R.N. Sharma & S. Seetharama	52.00	17.50	9.00
Flora of Delhi by J.K. Maheshwari	28.00	8.00	2.80
Indian Fossil Pteridophytes by K.R. Surange	66.00	22.00	12.50
Indian Thysanoptera by T.N. Ananthakrishnan	26.00	8.00	2.60
The Millipede Thyropygus by G. Krishnan	12.00	3.50	1.20
Drug Addiction with special reference to India by R.N. Chopra & I.C. Chopra	12.00	3.50	1.20
Glossary of Indian Medicinal Plants by R.N. Chopra & I.C. Chopra	35.00	13.00	6.00
Fluidization & Related Processes	12.00	4.00	1.20
Evolution of Life by M.S. Randhawa, A.K. Dey, Jagjit Singh & Vishnu Mitre	22.50	7.00	2.25
Collected Scientific Papers of Meghnad Saha	30.00	9.00	3.00
Proteaceae by C. Venkata Rao	72.00	24.00	13.50
Pinus by P. Maheshwari & R.N. Konar	30.00	11.00	5.00
Cellulose Research I	3.00	0.90	0.30
Cellulose Research II	6.00	1.75	0.60
Chemical Process Design	9.00	2.50	0.90
Low Temperature Carbonization of Non-coking Coals & Lignites & Briquetting Coal Fines: Vol. I & Vol. II (each volume)	17.50	5.50	1.75
Nucleic Acids	10.00	3.00	1.00
IGY Symposium: Vol. I	9.00	2.50	0.90
IGY Symposium: Vol. II	9.00	2.50	0.90
CNS Drugs	16.50	5.00	1.65
Kinetics of Electrode Processes & Null Points of Metals	2.50	0.75	0.25
Indian Sardines by R.V. Nair	22.00	7.00	2.20
Termite Problems in India	9.00	3.00	0.90
Loranthaceae by B.M. Johri & S.P. Bhatnagar	55.00	18.50	10.50
Abies and Picea by K.A. Chowdhury	14.00	6.00	2.10
Gnetum by P. Maheshwari and Vimla Vasil	20.00	6.00	2.00
Aquatic Angiosperms by K. Subramanyam	20.00	6.00	2.00
Supplement to Glossary of Indian Medicinal Plants by R.N. Chopra, I.C. Chopra & B.S. Varma	18.00	7.00	3.00
Herbaceous Flora of Dehra Dun by C.R. Babu	144.00	60.00	22.00
Diosgenin and Other Steroid Drug Precursors by Y.R. Chadha & Miss L.V. Asolkar	36.00	13.00	6.00
Research & Development Management by Inder Dev	25.00	10.00	—
Rural Development and Technology—A Status Report-cum Bibliography by P.R. Bose & V.N. Vashist	100.00	38.00	17.00
Cholera Bacteriophages by Sachimohan Mukherjee	30.00	10.00	6.00

Packing and Postage extra

Please contact:

SALES AND DISTRIBUTION OFFICER
PUBLICATIONS & INFORMATION DIRECTORATE, CSIR
Hillside Road, New Delhi 110012

Printed & Published by D.S. Sastry, Editor, Publications & Information Directorate (PID)
Hillside Road, New Delhi 110012, at PID Photocomposition Unit

Indian J Pure & Appl Phys. Vol 24 No 8 pp. 365-414

AUGUST 1986

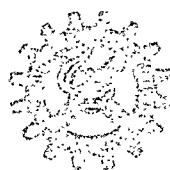
CODEN: IJOPAU ISSN: 0019-5396

24(8) 365-414 (1986)

PR-109
G-1

CDR

INDIAN JOURNAL OF PURE & APPLIED PHYSICS



Published by
PUBLICATIONS & INFORMATION DIRECTORATE, CSIR
NEW DELHI

in association with
THE INDIAN NATIONAL SCIENCE ACADEMY, NEW DELHI

THE WEALTH OF INDIA

An Encyclopaedia of Indian Raw Materials and Industrial Products, published in two series:
(i) Raw Materials, and (ii) Industrial Products.

RAW MATERIALS

The articles deal with Animal Products, Dyes & Tans, Essential Oils, Fats & Oils, Fibres & Pulps, Foods & Fodders, Drugs, Minerals, Spices & Flavourings, and Timbers and other Forest products. Names in Indian languages, and trade names are provided.

For important crops, their origin, distribution, evolution of cultivated types, and methods of cultivation, harvesting and storage are mentioned in detail. Data regarding area and yield and import and export are provided. Regarding minerals, their occurrence and distribution in the country and modes of exploitation and utilization are given. The articles are well illustrated. Adequate literature references are provided.

Eleven volumes of the series covering letters A—Z have been published.

Vol. I(A-B) Rs. 80.00; Vol. II (C) Rs. 95.00; Vol. III (D-E) Rs. 105.00; Vol. IV (F-G) Rs. 65.00; Vol. IV: Suppl. Fish & Fisheries Rs. 56.00; Vol. V (H-K) Rs. 114.00; Vol. VI (L-M) Rs. 90.00; Vol. VI: Suppl. Livestock Rs. 102.00; Vol. VII (N-P) Rs. 100.00; Vol. VII (Ph-Re) Rs. 86.00; Vol. IX (Rh-So) Rs. 104.00; Vol. X (Sp-W) Rs. 225.00; Vol. XI (X-Z) Rs. 115.00.

INDUSTRIAL PRODUCTS

Includes articles giving a comprehensive account of various large, medium and small scale industries. Some of the major industries included are: Acids, Carriages, Diesel Engines, Fertilizers, Insecticides & Pesticides, Iron & Steel, Paints & Varnishes, Petroleum Refining, Pharmaceuticals, Plastics, Ship & Boat-building, Rubber, Silk, etc.

The articles include an account of the raw materials and their availability, manufacturing processes, and uses of products, and industrial potentialities. Specifications of raw materials as well as finished products and statistical data regarding production, demand, exports, imports, prices, etc., are provided. The articles are suitably illustrated. References to the sources of information are provided.

Nine volumes of the series covering letters A—Z have been published.

Part I (A-B) Rs. 58.00; Part II (C) Rs. 74.00; Part III (D-E) Rs. 100.00; Part IV (F-H) Rs. 126.00; Part V (I-L) Rs. 90.00; Part VI (M-P) Rs. 28.00; Part VII (Pi-Sh) Rs. 60.00; Part VIII (Si-Ti) Rs. 66.00; Part IX (To-Z) Rs. 80.00.

HINDI EDITION: BHARAT KI SAMPADA—PRAKRITIK PADARTH

Vols. I to VII and two supplements of Wealth of India—Raw Materials series in Hindi already published.

Published Volumes:

Vol. I (अ-क) Rs. 38; Vol. II (क) Rs. 36; Vol. III (क-न) Rs. 36; Vol. IV (प) Rs. 83; Vol. V (क-मेरे) Rs. 60; Vol. VI (मेरे) Rs. 80; Vol. VII (रे-सा) Rs. 135

Supplements:

Fish & Fisheries (Matsya & Matsyaki) Rs. 49; Liverstock (Pashudhan aur Kukkut Palan) Rs. 34.

Vols. VIII to XI under publication.

Please contact:

SALES AND DISTRIBUTION OFFICER
PUBLICATIONS & INFORMATION DIRECTORATE, CSIR
Hillside Road, New Delhi 110012

Indian Journal of Pure & Applied Physics

EDITORIAL BOARD

Prof. S. Chandrasekhar
Raman Research Institute
Bangalore

Prof. S P Pandya
Physical Research Laboratory
Ahmedabad

Prof. R V Gopala Rao
Jadavpur University
Calcutta

Dr K R Rao
Bhabha Atomic Research Centre
Bombay

Prof. S K Joshi
Indian National Science Academy
New Delhi/Roorkee University
Roorkee

Prof. D K Rai
Banaras Hindu University
Varanasi

Prof. P Krishna
Indian National Science Academy,
New Delhi/Banaras Hindu University
Varanasi

Prof. B V Sreekantan
Tata Institute of Fundamental Research
Bombay

Prof Kehar Singh
Indian Institute of Technology
New Delhi

Prof. R Srinivasan
University of Madras
Madras

Prof C L Mehta
Indian Institute of Technology
New Delhi

Prof. Suresh Chandra
Banaras Hindu University
Varanasi

Shri S P Ambasta, Editor-in-Chief (*Ex-officio*)

EDITORIAL STAFF

Editors

D S Sastry & K S Rangarajan

Assistant Editors

J B Dhawan, Tarun Banerjee & (Mrs) Poonam Bhatt

Published by the Publications & Information Directorate, CSIR, Hillside Road, New Delhi 110012

Editor-in-Chief: S P Ambasta

The Indian Journal of Pure & Applied Physics is issued monthly. The Directorate assumes no responsibility for the statements and opinions advanced by contributors. The editorial staff in its work of examining papers received for publication is assisted, in an honorary capacity, by a large number of distinguished scientists, working in various parts of India.

Communications regarding contributions for publication in the journal should be addressed to the Editor, Indian Journal of Pure & Applied Physics, Publications & Information Directorate, Hillside Road, New Delhi 110012.

Correspondence regarding subscriptions and advertisements should be addressed to the Sales Distribution Officer, Publications & Information Directorate, Hillside Road, New Delhi 110012.

Annual Subscription

Rs. 180.00 £ 34.00 \$ 60.00

Single Copy

Rs. 18.00 £ 3.40 \$ 6.00

50% Discount is admissible to research workers and students and 25% discount to non-research individuals, on annual subscription. Payments in respect of subscriptions and advertisements may be sent by cheque, bank draft, money order or postal order marked payable *only* to Publications & Information Directorate, New Delhi 110012. Claims for missing numbers of the journal will be allowed only if received within 3 months of the date of issue of the journal plus the time normally required for postal delivery of the journal and the claim.

Announcements

National Symposium on Vacuum Technology & Analytical Instruments

(16-18 December 1986)

The above symposium to be organised by the Indian Vacuum Society (IVS) at the Central Scientific Instruments Organization, Chandigarh, during 16-18 December 1986, will have following sessions:

1. Vacuum Science & Technology
2. Vacuum Systems for Microelectronics
3. Electron Microscopy
4. Surface Analytical Instrumentation
5. Spectroscopy
6. Materials and Their Characterization

All papers accepted for presentation are proposed to be published in the Symposium proceedings Manuscripts (in triplicate) neatly typed in 1½ space on A4 size papers should reach the Convener by 20 Nov. 1986. The registration fee is Rs. 100/- for IVS members and Rs. 150/- for others. Further information can be had from:

Mr. A.K. Dimri,
Convener IVS National Symposium 1986
CSIO, Sector 30,
Chandigarh 160 020

National Seminar on Frontiers of Astronomy and Astrophysics

(17-19 February 1987)

The Indian Physical Society is organizing a National Seminar on "Frontiers of Astronomy and Astrophysics" from 17 to 19 February 1987. The venue of the seminar will be the Indian Association for the Cultivation of Science in Calcutta. The objective of the seminar is to offer a suitable forum for scientists and working groups to exchange ideas through mutual discussions. The seminar will also highlight the present status of research in these disciplines in India and the necessary future planning.

The seminar will have sessions on Optical Astronomy, Solar Astronomy, Radio Astronomy, Solar Radio and X-ray Astronomy, X-ray Astronomy, Millimetre-wave Astronomy, Cosmic Rays, High Energy Astrophysics, Cosmology, and Observatories in India.

The registration fee for participation in the seminar is Rs 100.

Scientists and research fellows working in these areas in different laboratories and observatories may contribute papers to be presented at the seminar. Abstracts of papers may be sent to the convener of the seminar latest by 30 November 1986 to the following address:

Prof. M.K. Dasgupta
Institute of Radiophysics and Electronics,
University of Calcutta,
92, Acharya Prafulla Chandra Road,
Calcutta 700 009

Announcement

III National Seminar on Crystal Growth

(Madras, 16-19 February 1987)

The above seminar sponsored by the Anna University, Madras, will be held during 16-19 February 1987. The topics to be covered will be as follows: 1. Theoretical aspects of crystal growth, 2. Experimental aspects of crystal growth, 3. Heat and mass transport, 4. Industrial crystallization, 5. Rapid solidification and casting, 6. Biological and molecular crystals, 7. Special crystals, new techniques and instrumentation, and 8. Crystal characterisation and applications.

It is also planned to have a panel discussion on the 'Present status of crystal growth in India'. Abstracts (in duplicate) of papers intended to be presented at the seminar should reach the convener before 15 Nov. 1986. The registration fee is Rs. 50/- and further details can be had from:

Prof. P. Ramasamy
Convener, III National Seminar on Crystal Growth,
Crystal Growth Centre, Anna University,
Madras 600 025

Errata

Note entitled, "Universal Input Signal Processing Technique in Control Engineering",
Vol. 23 April (1985) pp. 234-236

<i>Position</i>	<i>Function as printed</i>	<i>To be corrected as</i>
p. 235 Eq (8), I Line } p. 235 line below } Eq. (8)	$R_{i-1}(t)$	$R_{i-1}(t - t_r)$
p. 235 Eq. (10)	$\frac{d^i R_i(t)}{dt^i}$	$\frac{d^i R_i(t - t'_r)}{dt^i}$
p. 235 R H Col line 39 } p. 236 L H Col 2nd } line from bottom }	$\frac{dR_s(t)}{dt}$	$\frac{dR_s(t - t'_r)}{dt}$
p. 236 L H Col 2nd line from bottom	$u(t - t_r)$	$u(t - t'_r)$
p. 234 R H Col Eq. (7)	$C_{i-1}(t)$	$C_{i-1}(t - t_r)$
p. 235 R H Col line 20	$R_0(t)$	$R_0(t - t_r)$
p. 235 L H Col Eq. (9)	$\left(\frac{p_1}{p_{i-1} \omega_n} \right)$	$\left(\frac{1}{\omega_n} \right)$
p. 235 R H Col Eq. (11)	$\left(\frac{p_1}{p_0 \omega_n^i} \right)$	$\left(\frac{1}{\omega_n^i} \right)$
p. 236 R H Col line 9	negicast technique ² .	negicast or posicast technique ² .
p. 235 Eq. (2) 2nd line	$\frac{dR_i(t)}{dt}$	$\frac{dR_i(t - t_r)}{dt}$

CONTENTS

Nuclear Physics

- Fast Neutron Albedo Calculations for a Concrete Shield with Different Curvatures ... 365
F M Sayed Ahmed* & M Salama

Atomic & Molecular Physics

- Spectral Study of Nd^{3+} Ternary Complex of Amino Acid in Different Solvents 404
Kirty Mathur, M P Bhutra & S P Tandon*

Classical Areas of Phenomenology (Including Applications)

- Ultrasonic & Rheological Study of Binary & Ternary Mixtures 369
M S Khanwalkar

- Physics of Musical Scale and Ragas: Part I—Harmonic Progression Law Governing Natural
Scale of Musical Octave 373
P B Mathur

- Physics of Musical Scale and Ragas: Part II—Harmonic Laws Governing Evolution of Ragas
(the Scales of Melodies) 376
P B Mathur

Fluids, Plasmas & Electric Discharges

- Influence of Diffusion of H-Ions & of Gyro-Radius Effect on Diffusion Coefficient of H-Ions
across a Plasma with an Axial Magnetic Field 383
F F Elakshar

Condensed Matter: Structure, Mechanical & Thermal Properties

- Diffraction Intensities from Curved Crystallites with Layer Shift by $\varphi/3$ 388
A K Datta, B K Roy & S Bhattacharjee*

- Internal Pressure in Relation to the Structure of Polymers 406
C V Suryanarayana* & P Pugazhendhi

Condensed Matter: Electronic Structure, Electrical, Magnetic & Optical Properties

- Resolution Function of CMA Systems Used for Auger Signal Measurements 399
N C Jain

- Proton Magnetic Resonance Studies on $\text{Cu}(\text{3-AMI})_2\text{Br}_2$ and $\text{Co}(\text{3-AMI})_2\text{Cl}_2$ 408
K V R Chary, K V G Reddy, M N Chary, B A Sastry*,
G Ponticelli & M Massaccesi

- ^{57}Fe Mössbauer Analysis of the Cubic Spinel CoAlFeO_4 411
F M Mostafa* & J Suwalski

CONTENTS

Investigations of the Effect of Diode Geometry on the Reverse Recovery Experiments on Solar Cells	397
S K Agarwal & Harsh*	
Electrical & Optical Properties of Flash Evaporated CuInSe ₂ Thin Films	392
D Sridevi & K V Reddy*	
Cross-Disciplinary Physics & Related Areas of Science & Technology	
Determination of Surface Temperature of Microbead using Infrared, Thermocouple & Resistance Thermometric Techniques	401
R J Jaiswal* & S C Srivastava	
Book Reviews	
Thin Film Science & Technology 6: Coatings on Glass by H K Pulker	414
V V Shah	

The author for correspondence is indicated by () mark,
in case of papers with more than one author.

Fast Neutron Albedo Calculations for a Concrete Shield with Different Curvatures

F M SAYED AHMED & M SALAMA
Atomic Energy Authority, Cairo, Egypt

Received 14 October 1985; revised received 24 March 1986

The 05R Monte Carlo neutron transport code has been used to calculate the neutron albedo for plane and curved concrete shields. The aim of the present calculations is to characterize the fast-neutron albedo for a curved concrete shield, and to compare it with that for a flat surface. The calculations are performed for neutron source energies of 1, 5 and 15 MeV, neutron incident angles of 5°, 30°, 45°, 60° and 90° and for surfaces with different curvatures (flat, 100, 50, 20 and 5 cm radii). The results obtained reveal that there would be a significant error, if one uses flat wall albedo for calculating the streaming through cylindrical ducts. The error would arise due to neglecting the curvature and due to the improper choice of the neutron incident angle.

1 Introduction

It is well known that the shielding design for research and power reactors involves a number of problems due to the radiation propagation in heterogeneous media, particularly in media containing voids of various sizes and shapes¹⁻³. One of the most frequently encountered problems is that of the streaming along a cylindrical duct.

It was noticed that the analytical methods in this area were limited to some particular cases of isolated voids of simple shape (cylindrical holes, two-dimensional slits, etc.) or of lattices of voids for which it was possible to homogenize and employ bulk shield methods using either suitable calculated constants or experimentally derived ones.

The albedo concept has long been in use in shielding analysis⁴⁻⁹. In this concept, it is assumed that the emergent flux is either isotropic or cosine distributed about the normal to the wall. The albedo defined in this way is an integral quantity. It gives the total reflected flux. The reflected neutrons will have also an energy distribution and this energy degradation is assumed to be built into the albedo value in a way suitable to the problem to be solved. This necessitates definition of different albedos depending upon whether the desired result is a number flux, energy flux or dose. Zotokhin¹⁰ has reported a number of expressions for the different albedo forms of incident angle and neutron energy.

Experiments and calculations have shown that gamma rays produced by neutron absorptions in a concrete shield surrounding a duct make a significant contribution to the total dose in the duct and analysis of this component requires a knowledge of the distribution of low energy neutrons throughout the duct and the shield. These distributions can be

determined exactly using Monte Carlo calculations. Monte Carlo method seems to have a very wide field of application in neutron albedo calculations¹¹⁻¹³.

The aim of the present study is to carry out a series of albedo calculations using the Monte Carlo transport code 05R¹³ with emphasis on comparative study of albedo from curved and flat surfaces.

The calculations were performed at three selected neutron energy values and at five incident angles, as well as for five radii of curvature.

2 Description of the Problem

The present albedo calculations were performed for an ordinary concrete shield. The composition of the concrete assumed in our calculations is as follows:

Element	10^{21} Atoms/cm ³
H	8.66
O	41.49
Si	11.73
Ca	8.22

The density of concrete was 2.174 g/cm³ and the following three cases were considered: (i) slab shield, (ii) slab with a cylindrical depression and (iii) curved surface.

Fig. 1 shows sections representing the above cases. A monoenergetic as well as monodirectional neutron source was assumed in the present calculations; however, separate calculations were done for the source energies 1, 5 and 15 MeV as for the initial directions 5°, 10°, 30°, 45°, 60° and 90° relative to the shield surface. It was assumed that the initial neutron direction can be divided into directional components,

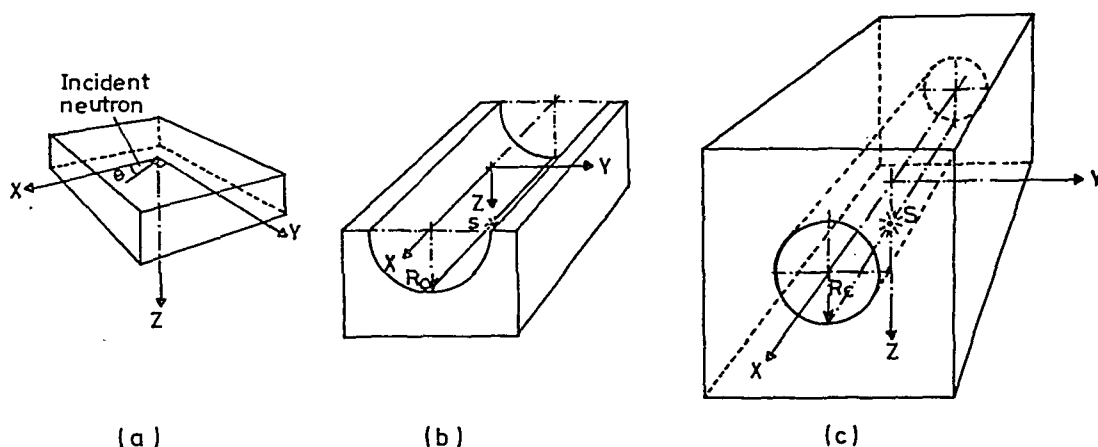


Fig. 1—Sections representing reflection from (a) semi infinite slab shield; (b) slab with cylindrical depression, (c) curved surface

so that one component is parallel to the duct axis while the other is normal to the shield surface.

The calculations have been performed using the Monte Carlo neutron transport code 05R, and the related cross-section handling code XSECT. The XSECT code is used to prepare group cross-sections for the elements and energy range to be used in the specific problem. Also using the XSECT code, a tape called phitape containing group data for calculation of the scattering angle distribution is prepared. A special concept of supergroups and subgroups is used in 05R. There are 40 supergroups, and these have fixed energy boundaries. Each supergroup may then be divided into a chosen number of subgroups; but the number must be a power of two and should not exceed 512 per supergroup. This group structure has been chosen to minimize tape handling time.

5×10^3 Neutron histories were considered in each calculation. A neutron is followed from collision to collision through its entire history. At each collision point, the energy degradation and change in direction are calculated. The life history is terminated when the neutron is absorbed or when it leaves the system. The absorption does not take place in the traditional way, but happens gradually. At each collision, the probability of absorption by the element and at the energy in question is calculated, and the neutron is allowed to survive with its statistical weight suitably reduced. Eventually the weight may become less than some limit specified in 05R input. At that time, Russian roulette is played to decide whether the neutron history should continue with its weight upgraded to unity or be terminated.

The neutrons are started in batches each containing a number of particles chosen. Each neutron is followed through its entire life history, and information like particle energy, position, direction, collision type, etc. is stored on the collision tape at each collision or

boundary crossing or other types of events. Any parameter out of a possible total of 34 may be written into the tape. The parameters desired are specified in 05R input.

The code follows all neutrons in one batch simultaneously. The first neutron in the batch is followed until it leaves the supergroup in which it was born, and then the search is continued for the second neutron in the batch and so on until all neutrons in the batch have been followed through the first supergroup. Then the search is continued for the first neutron in the second supergroup, etc. In this way, only a limited amount of cross-section data is needed at any instant of time.

The statistical error associated with the reported results on albedo is about $\pm 3\%$.

It is interesting to see what is the average displacement of the point of emergence of the neutron from the point of incidence. The neutrons are started with the initial direction in the x-z plane, where z is normal to the surface and the x-coordinates of the point of emergence of all emerging neutrons are collected and the average calculated. This represents the displacement. The displacement for normal incidence was found to be close to zero, as expected. However, the displacement was found to increase with decreasing angle of incidence and reaches a maximum of approximately 3 cm. Fig. 2 shows the dependence of the average x-coordinate of non-thermal reflected neutrons on the incident angle for source energy of 1 MeV.

Six, nine and ten energy bands were used respectively for neutron source energies of 1 MeV, 5 MeV and 15 MeV, respectively to encompass the ranges 0.018-1 MeV, 0.018-5 MeV and 0.018-15 MeV respectively. There were 36, 54 and 60 separate problems run in case of neutron source energies of 1, 5 and 15 MeV respectively.

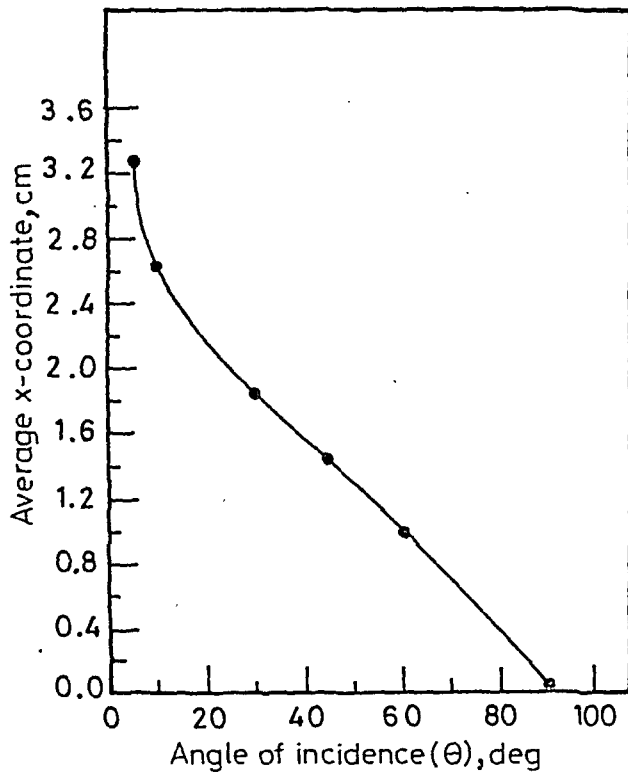


Fig. 2—Dependence of the average x-coordinate of nonthermal reflected neutrons on the incident angle (source energy 1 MeV)

3 Results and Discussion

Fig. 3 shows the reflected neutron energy per incident neutron as a function of duct curvature for different neutron incident angles and energies. These results reveal that the reflected energy per incident neutron, decreases with the increase of the incident angle; however, it increases with increase of both the radius of curvature and the neutron source energy. The ratio $A(R)/A_\infty$ which represents the ratio between the integral flux energy albedo of a curved wall $A(R)$ and the integral flux energy albedo for a flat wall A_∞ is graphically represented in Fig. 4 as a function of the radius of curvature at different neutron incident angles and for 15 MeV neutron source energy. Fig. 4 shows that the ratio $A(R)/A_\infty$ increases as a function of the radius of curvature. Moreover, for incident angles of 45° and 90° , the values of $A(R)/A_\infty$ are close to each other for all values of R_c .

The calculations have shown the expected wall curvature effects and provided quantitative values for the albedo under various conditions for a concrete shield with a simplified elemental composition.

Moreover, the results obtained have proved that the albedo for a surface with curvature radii larger than about 50 cm does not show much difference from the albedo for a flat wall at 1 MeV neutron source energy and it begins to show a pronounced difference only at high neutron source energies of 5 and 15 MeV. Moreover, for a surface with a small radius of

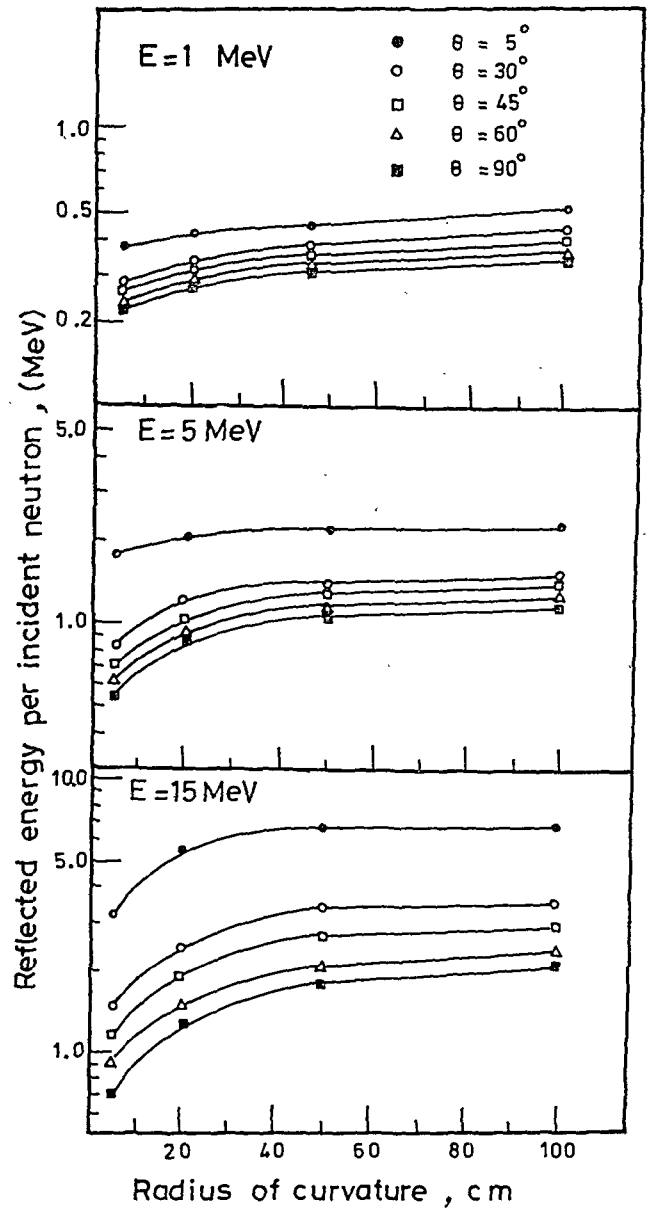


Fig. 3—Reflected neutron energy per incident neutron as a function of duct curvature for different neutron incident angles and for neutron source energies 1, 5 and 15 MeV

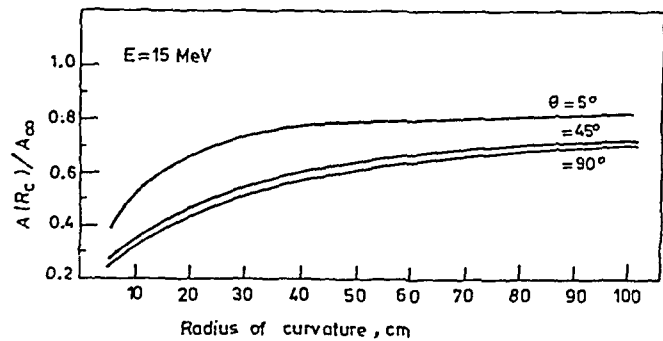


Fig. 4—Ratio $A(R)/A_\infty$ as a function of the radius of curvature for different incident angles and for 15 MeV neutron source energy

curvature, it is seen that the albedo tends to decrease as the radius of curvature decreases and these effects are more pronounced for high neutron source energies and at large incident angles.

In the present analysis, one has to point out that the thermal neutron absorption term was not represented in the 05R calculational model¹³, since the reduction in the statistical weight corresponding to the absorption term takes it below the limit set in the 05R input. It was surmised that the per cent of reflected neutrons would be very small compared to the high energy neutrons, and hence their treatment in the present calculations is not of much importance.

Acknowledgement

The assistance of Dr G Sabek, the computer programmer at the Nuclear Regulatory and Safety Centre, Atomic Energy Authority, Cairo, in adapting the 05R Monte Carlo code to the present computer facility, is acknowledged and highly appreciated.

References

- 1 Chase D M, Ducts and voids in shields, chapter 12 in *Reactor Handbook*, Part B, Vol III (Interscience Publishers, New York) 1962.
- 2 *Reactor shielding design manual* (McGraw-Hill Book Co, New York) 1965.
- 3 Price B T, Horton C C & Spinney K T, *Radiation shielding* (Pergamon Press, New York) 1957, 207.
- 4 Simon A & Clifford C E, *Nucl Sci & Engng (USA)*, 1 (1966) 156.
- 5 Meyer W, Leighty J W & Thiesing J W, *Nucl Sci & Engng (USA)*, 60 (1976) 405.
- 6 De Beer G P, *Nucl Eng & Design (USA)*, 33 (1975) 422.
- 7 Maerker R E, Nuckonthaler F J & Stevens P N, *Nucl Sci & Engng (USA)*, 27 (1967) 411.
- 8 Leimdorfer M, *Trans Chalmers Univ Technology (Gothenburg, Sweden)*, No 288 1964.
- 9 Selph W E & Clairborne H C, *Methods for calculating effects of ducts, access ways and holes in radiation shields*, Report ORNL-RSCIC (USA), 20 (1969).
- 10 Zotokhin V G, *Radiation transmission through inhomogeneities in shields* (translated from Russian by Israel Program for Scientific Translation, Jerusalem) 1971.
- 11 Devillers C, Laffore P & Lannore J M, *The physics problems of reactor shielding*, Centre d'Etude Nucleaires de Fontenay aux Roses.Commissariat A l'Energie Atomique, Paris 26-29 Sept, 1967.
- 12 Kawai M, Yamamuchi M, Kadatoni H & Suzuki I, *Proc 5th international conf reactor Shielding* (Science press, Princeton), 1977.
- 13 Irving D C, Freestone R M & Kam F B, 05R: *A general purpose Monte Carlo neutron transport Code*, Report ORNL-3622 USA, Feb. 1965.

Ultrasonic & Rheological Study of Binary & Ternary Mixtures

M S KHANWALKAR

Department of Physics, Indian Institute of Technology, Bombay 400 076

Received 1 November 1985

Excess volumes of mixing (V_{123}^E), excess isentropic compressibilities (β_{123}^E) and excess free-energies of activation of flow (G_{123}^E) for the ternary system: cyclohexane + CCl_4 + ethyl acetate and the constituent binary systems have been determined at 30°C over a wide composition range. Analysis of the results using the procedure suggested by R P Rastogi, J Nath & S S Das [*J Chem & Engng Data (USA)*, **22** (1977) 249] for V_{123}^E indicates that all the excess values can be fitted to the same analytical expression.

1 Introduction

Considerable interest has been stimulated by the ultrasonic and rheological investigations on binary and ternary liquid mixtures. The deviations from the law of additivity in the values of various parameters indicate the existence of specific interaction between unlike molecules. The present study deals with the evaluation of excess volumes of mixing (V^E), excess isentropic compressibilities (β^E) and excess free-energies of activation of flow (G^E) for binary systems and the ternary system made up of (1) cyclohexane, (2)

carbon tetrachloride and (3) ethyl acetate, using a single experimental set-up. The ternary contribution in V_{123}^E , β_{123}^E and G_{123}^E have been computed using binary and ternary data and the experimental values of V_{123}^E , β_{123}^E and G_{123}^E have been fitted to an equation proposed by Rastogi *et al.*¹ for fitting V_{123}^E values only.

2 Experimental Details

Components used were of 'Pure' grade and used as purchased. Densities, viscosities and ultrasonic velocities of the 'pure' components were measured and a comparison of these with literature values (Table 1) shows no evidence for existence of impurities.

Densities (d) were measured using a Lipkin pycnometer and sound velocity (u) at 8.5 MHz using a solid state pulsed sing-around system which is a modified version of the sing-around system developed by Soitkar *et al.*² The ultrasonic cell incorporated a pair of 15 mm diameter and 0.34 mm thick X-cut quartz

transducers mounted parallel to each other at a fixed distance of 4.212 cm. The cell was thermostated along with the Lipkin pycnometer to $30 \pm 0.02^\circ\text{C}$. The densities were reproducible to 1 part in 10^4 and the sound velocities to 5 parts in 10^4 .

Kinematic viscosities (ν) were measured at $30 \pm 0.02^\circ\text{C}$ by means of an Ubbelohde viscometer using the relation $\nu = at - (b/t)$ where t represents the time of flow in s and a and b are constants of the viscometer. The viscosities, $\eta = \nu d$, are accurate to ± 0.001 cP.

3 Results and Discussion

Experimental $V_{1...n}^E$ values for the binary and ternary systems were computed using relation (1):

$$V_{1...n}^E = V_{1...n} - \sum_{i=1}^n X_i V_i \quad \dots (1)$$

where X_i and V_i denote mole fraction and molar volume of component i . Isentropic compressibility $\beta_{1...n}$ and the deviation in isentropic compressibility $\beta_{1...n}^E$ for the binary and ternary systems were obtained using the equations:

$$\beta_{1...n} = [1/u_{1...n}^2 d_{1...n}] \quad \dots (2)$$

and

$$\beta_{1...n}^E = \beta_{1...n} - \sum_{i=1}^n \Phi_i \beta_i \quad \dots (3)$$

where Φ_i denotes the volume fraction of component i .

Table 1—Values of density (d), Viscosity (η) and Ultrasonic Velocity (u) for the Pure Liquids at 30°C

Liquid No.	d , g/ml		Ref. No.	η , cP		Ref. No.	u , m/s		Ref. No.
	Exptl	Litt		Exptl	Litt		Exptl	Litt	
(1)	0.7690	0.7692	3,5	0.8214	0.820	3	1232.4	1231.3	4
(2)	1.5751	1.5748	3,5	0.8427	0.843	3	907.2	908.0	5
(3)	0.8878	0.8883	3	0.4013	0.401	3	1120.1	1123.0	6,7

The excess free-energy of activation of flow, $G_{1...n}^E$ was obtained using the relation:

$$G_{1...n}^E = RT \left[\ln(\eta_{1...n} V_{1...n}) - \sum_{i=1}^n X_i \ln \eta_i V_i \right] \quad \dots (4)$$

The excess properties (A_{ij}^E) for the binary systems were fitted to the equation:

$$A_{ij}^E = x_i x_j [a_0 + a_1(x_i - x_j) + a_2(x_i - x_j)^2] \quad \dots (5)$$

where x_i and x_j represent the (binary) mole fractions wrt V_{ij}^E and G_{ij}^E and (binary) volume fractions wrt β_{ij}^E . The values of the constants a_0 , a_1 and a_2 (obtained by least squares analysis) along with the standard deviation (σ) defined by:

$$\sigma^2 = \sum_{k=1}^m [(A_{ij}^E)_{k, \text{exptl}} - (A_{ij}^E)_{k, \text{calc}}]^2 / (m - 3) \quad \dots (6)$$

where m is the total number of measurements, are given in Table 2. The last column of Table 2 compares the values of the excess functions for $x_i = x_j = 0.5$ obtained in the present study, with the values in the literature, wherever the latter are available.

Rastogi *et al.*¹ proposed Eqs (7) and (8) to calculate the ternary contributions ΔA^E :

$$\Delta A^E = A_{123}^E - A_{123}^E(a) \quad \dots (7)$$

and

$$A_{123}^E(a) = \frac{1}{2} [(X_1 + X_2) A_{12}^E + (X_2 + X_3) A_{23}^E + (X_3 + X_1) A_{31}^E] \quad \dots (8)$$

In Eqs (7) and (8), A_{123}^E is the excess property of a ternary mixture having mole fractions (in case of V_{123}^E and G_{123}^E) or volume fractions (in case of β_{123}^E) of the components 1, 2 and 3 equal to X_1 , X_2 and X_3 respectively. A_{ij}^E is the excess property of a binary mixture in which the mole fraction (or volume fraction) of component i is $X_i/(X_i + X_j)$ and of component j is $X_j/(X_i + X_j)$. Thus, for example, from Table 2,

$$V_{12}^E = \left(\frac{X_1}{X_1 + X_2} \right) \left(\frac{X_2}{X_1 + X_2} \right) \times \left[0.641 - 0.014 \left(\frac{X_1 - X_2}{X_1 + X_2} \right) + 0.079 \left(\frac{X_1 - X_2}{X_1 + X_2} \right)^2 \right]$$

The experimental values of the excess volume of mixing per mole (V_{123}^E), excess isentropic compressibility (β_{123}^E) and excess free-energies of activation of flow per mole (G_{123}^E), for the ternary system are reported in Tables 3-5. The ternary contribution ΔV^E , $\Delta \beta^E$ and ΔG^E calculated from Eqs (7) and (8) are also given in these Tables. We see that V_{123}^E , ΔV^E , β_{123}^E and $\Delta \beta^E$ are all positive and G_{123}^E and ΔG^E are negative over the entire composition range.

The experimental results of V_{123}^E , β_{123}^E and G_{123}^E for the ternary system have been fitted by the method of least squares to Eq. (9) proposed by Rastogi *et al.*¹ for fitting V_{123}^E . Thus,

$$A_{123}^E = A_{12}^{E*} + A_{23}^{E*} + A_{31}^{E*} + X_1 X_2 X_3 \times [A_0 + A_1 X_1 (X_2 - X_3) + A_2 X_1^2 (X_2 - X_3)^2] \quad \dots (9)$$

Table 2—Least Square Parameters and Standard Deviation for Binary Systems at 30°C

Function (A_{ij}^E)	a_0	a_1	a_2	Std. dev. σ	(A_{ij}^E) at $x_i = x_j = 0.5^*$		
					Exptl	Litt	Ref.
System (1) + (2)							
V_{12}^E ml/mol	0.641	-0.014	0.079	0.004	0.160	0.160	2
$10^6 \beta_{12}^E$ bar $^{-1}$	3.609	-0.079	-0.080	0.02	0.90	1.22 ^a	5
G_{12}^E cal/mol	-107.2	-4.1	12.7	0.8	-26.8	-25.1 ^b	8
System (2) + (3)							
V_{23}^E ml/mol	0.274	0.034	-0.023	0.004	0.069	0.043	9
$10^6 \beta_{23}^E$ bar $^{-1}$	0.946	0.165	0.507	0.03	0.24	—	—
G_{23}^E cal/mol	-88.2	-53.0	9.8	1.7	-22.1	-23.2	10
System (3) + (1)							
V_{31}^E ml/mol	4.966	-0.609	0.293	0.006	1.242	0.812 ^c	11
$10^6 \beta_{31}^E$ bar $^{-1}$	25.234	-2.398	1.025	0.04	6.31	—	—
G_{31}^E cal/mol	-467.6	147.1	-83.4	1.0	-116.9	-116.0	10

* x_i & x_j represent mole fractions wrt V_{ij}^E & G_{ij}^E and volume fractions wrt β_{ij}^E

^a From least square analysis of reference data wrt volume fractions

^b Value at 25°C (calculated from reference data)

^c Value at 20°C (calculated from reference data)

Table 3—Density (d_{123}) and Experimental Excess Volume (V_{123}^E) for the Ternary System 30°C

Mole fractions		d_{123} g/ml	V_{123}^E ml/mol	$V_{123}^E(a)$ ml/mol	ΔV^E ml/mol	$V_{123}^E(b)$ ml/mol	ΔV^{E*} ml/mol	δV ml/mol
X_1	X_2							
0.3956	0.1112	0.9017	0.984	0.578	0.406	1.000	-0.016	0.006
0.3985	0.2005	0.9604	0.832	0.556	0.276	0.866	-0.034	-0.006
0.3955	0.2940	1.0229	0.686	0.513	0.173	0.716	-0.030	-0.004
0.4020	0.3994	1.0925	0.509	0.429	0.080	0.532	-0.023	-0.005
0.4006	0.4994	1.1600	0.345	0.301	0.044	0.350	-0.005	0.003
0.1001	0.3996	1.1404	0.310	0.253	0.057	0.319	-0.009	0.006
0.1982	0.3966	1.1216	0.459	0.390	0.069	0.485	-0.026	-0.003
0.2997	0.3990	1.1071	0.532	0.452	0.80	0.559	-0.027	-0.003
0.4980	0.3990	1.0795	0.397	0.317	0.80	0.408	-0.011	-0.002
0.0997	0.5010	1.2096	0.267	0.247	0.20	0.280	-0.013	0.001
0.3001	0.3000	1.0405	0.659	0.490	0.169	0.679	-0.020	0.008
0.5001	0.1002	0.8813	1.022	0.598	0.424	1.048	-0.026	-0.006

Table 4—Density (d_{123}) Velocity (u_{123}) and Experimental Excess Isentropic Compressibility ($10^6 \beta_{123}^E$) for the Ternary System at 30°C

Vol fractions		d_{123} g/ml	u_{123} m/s	$10^6 \beta_{123}^E$ bar ⁻¹	$10^6 \beta_{123}^E(a)$ bar ⁻¹	$10^6 \Delta \beta^E$ bar ⁻¹	$10^6 \beta_{123}^E(b)$ bar ⁻¹	$10^6 \Delta \beta^{E*}$ bar ⁻¹	$10^6 \delta \beta$ bar ⁻¹
Φ_1	Φ_2								
0.4199	0.1054	0.9017	1099.3	5.07	2.99	2.08	5.21	-0.14	0.02
0.4235	0.1901	0.9604	1076.4	4.25	2.85	1.40	4.50	-0.25	-0.02
0.4210	0.2792	1.0229	1054.6	3.40	2.62	0.78	3.73	-0.33	-0.04
0.4283	0.3798	1.0925	1033.5	2.50	2.17	0.33	2.78	-0.28	0.04
0.4276	0.4757	1.1600	1015.5	1.61	1.53	0.08	1.87	-0.26	0.01
0.1100	0.3916	1.1404	1010.7	1.47	1.35	0.12	1.68	-0.21	-0.04
0.2155	0.3849	1.1216	1016.1	2.34	2.07	0.27	2.58	-0.24	0.03
0.3226	0.3833	1.1071	1023.7	2.60	2.35	0.25	2.96	-0.36	-0.04
0.5256	0.3758	1.0795	1045.8	1.86	1.58	0.28	2.12	-0.26	-0.02
0.1097	0.4919	1.2096	989.4	1.34	1.31	0.03	1.46	-0.12	0.06
0.3226	0.2877	1.0405	1044.5	3.29	2.56	0.73	3.59	-0.30	-0.02
0.5254	0.0939	0.8813	1113.1	5.17	3.01	2.16	5.33	-0.16	-0.01

Table 5—Viscosity (η_{123}) and Excess Free-Energy of Activation of Flow (G_{123}^E) for the Ternary System at 30°C

Mole fractions		η_{123} cP	G_{123}^E cal/mol	$G_{123}^E(a)$ cal/mol	ΔG^E cal/mol	$G_{123}^E(b)$ cal/mol	ΔG^{E*} cal/mol	δG cal/mol
X_1	X_2							
0.3956	0.112	0.4848	-100.1	-56.5	-43.6	-97.0	-3.1	-0.8
0.3985	0.2005	0.5253	-93.7	-58.5	-35.2	-89.5	-4.2	-0.7
0.3955	0.2940	0.5733	-82.3	-57.9	-24.4	-79.5	-2.8	1.6
0.4020	0.3994	0.6351	-71.6	-52.7	-18.9	-65.0	-6.6	-1.9
0.4006	0.4994	0.7102	-49.2	-40.3	-8.9	-47.5	-1.7	2.0
0.1001	0.3996	0.5374	-43.6	-30.1	-13.5	-41.9	-1.7	0.7
0.1982	0.3966	0.5584	-60.4	-44.1	-16.3	-57.8	-2.6	1.3
0.2997	0.3990	0.5908	-70.5	-52.4	-18.1	-66.2	-4.3	0.4
0.4980	0.3990	0.6956	-58.6	-42.3	-16.3	-53.2	-5.4	-1.8
0.0997	0.5010	0.5789	-44.2	-30.9	-13.3	-41.0	-3.2	-0.7
0.3001	0.3000	0.5410	-79.0	-53.4	-25.6	-74.0	-5.0	-0.8
0.5001	0.1002	0.5128	-106.2	-60.4	-45.8	-104.8	-1.4	0.1

In Eq. (9) X_1, X_2, X_3 are the mole fractions (in case of V_{123}^E and G_{123}^E) or volume fractions (in case of β_{123}^E) of components 1, 2 and 3 respectively in the ternary mixture and A_0, A_1 and A_2 are constants of the ternary system. The quantities A_{ij}^{E*} are:

$$A_{ij}^{E*} = X_i X_j [a_0 + a_1(X_i - X_j) + a_2(X_i - X_j)^2]$$

where X_i and X_j are the mole (or volume) fractions in the ternary mixture and a_0, a_1 and a_2 are taken from the data on excess properties for the binaries (Table 2). Thus, for example,

$$\beta_{23}^{E*} = \Phi_2 \Phi_3 [0.946 + 0.165(\Phi_2 - \Phi_3) + 0.507(\Phi_2 - \Phi_3)^2] \quad \dots (10)$$

Table 6—Least Square Parameters and Standard Deviation of V_{123}^E , β_{123}^E & G_{123}^E for the Ternary System at 30°C

Function	A_0	A_1	A_2	σ
V_{123}^E , ml/mol	-0.720	1.969	-0.196	0.006
$10^6 \beta_{123}^E$, bar ⁻¹	-8.300	-16.496	-87.524	0.04
G_{123}^E , cal/mol	-122.8	-240.8	-830.5	1.4

Φ_i being the volume fraction of component i in the ternary mixture.

The values of ($A_{12}^E + A_{23}^E + A_{31}^E$) for the ternary system are represented as A_{123}^E in Tables 3-5. Accordingly, the deviations $\Delta A^E = A_{123}^E - A_{123}^E(b)$ of the experimental values of A_{123}^E from the sum ($A_{12}^E + A_{23}^E + A_{31}^E$) are also reported in Tables 3-5. The values of the constants A_0 , A_1 and A_2 along with the standard deviations (σ) in the experimental values of A_{123}^E from these calculated from Eq. (9) are given in Table 6. The last columns of Tables 3, 4 and 5 show the deviation δA given by:

$$\delta A = A_{123}^E(\text{experimental}) - A_{123}^E[\text{from Eq. (9)}]$$

Our results indicate that Eq. (9) proposed by Rastogi *et al.*¹ for V_{123}^E fits the values for β_{123}^E and G_{123}^E as well.

Acknowledgement

The author expresses his grateful thanks to Prof J S Murty (Department of Physics, Indian Institute of Technology, Bombay), Prof D D Deshpande (Department of Chemistry, IIT, Bombay) and Prof G N Navaneeth (Department of Physics, Nagpur University, Nagpur) for their encouragement and guidance during the progress of this study.

References

- 1 Rastogi RP, Nath J & Das SS, *J Chem & Engng Data (USA)*, **22** (1977) 249.
- 2 Soitkar VS, Sunnapwar KP & Navaneeth GN, *Indian J Pure & Appl Phys*, **19** (1981) 555.
- 3 Timmermans J, *Physicochemical constants of pure organic compounds* (Elsevier, London), 1950.
- 4 Wilhelm E, Schaono R, Becker G *et al.*, *Trans Faraday Soc (GB)*, **65** (1969) 1443.
- 5 Reddy KC, Subrahmanyam SV & Bimasenachar J, *J Phys Soc Jpn (Japan)*, **19** (1964) 559.
- 6 Reddy KC, Sbrahmanyam SV & Bimasenachar J, *Trans Faraday Soc (GB)*, **58** (1962) 2352.
- 7 Rao KS & Rao BR, *J Acoust Soc Am (USA)*, **31** (1959) 439.
- 8 Katti P K, Chaudri MM & Prakash O, *J Chem & Engng Data (USA)*, **11** (1966) 593.
- 9 Oswal SL & Rathnam MV, *J Indian Chem Soc*, **61** (1984) 269.
- 10 Oswal SL & Rathnam MV, *Can J Chem (Canada)*, **62** (1984) 2851.
- 11 Aminabhavi T M, Patel RC, Bridger K *et al.*, *J Chem & Engng Data (USA)*, **27** (1982) 125.

Physics of Musical Scale and Ragas: Part I—Harmonic Progression Law Governing Natural Scale of Musical Octave

P B MATHUR

Central Electrochemical Research Institute, Karaikudi 623006

Received 18 March 1985; accepted 18 June 1986

So far, no single mathematical progression series is known from which all the twelve tones of a musical scale can be derived. In this communication is presented a harmonic progression series which appears to be the origin of the musical scale, as all the 12 tones of the scale could precisely be obtained from this series. This series thus unveils the harmonic unity existing within the apparent large diversity in the inter-tonic relationships of the scale.

1 Introduction

A number of basic scales¹⁻⁴ as well as temperament scales^{5,6} of music were advanced in ancient India, Greece, Egypt, China and Europe. Their merits and demerits have been discussed in literature. The frequency intervals between the fundamental and subsequent notes and also between the successive notes of a musical octave are apparently very incoherent. This random symmetry of tone frequencies led Ellis^{7,8} to view that the musical scale was not one, not natural and even founded necessarily on laws of constitution of musical sound, but very diverse, very artificial and very capricious. Parry⁹ and Lloyd¹⁰ expressed similar views on the disordered relationship among the notes of musical scales.

The objective of this communication is to derive the natural scale of music from a single mathematical law or series and thus to establish that the natural scale of music derived experimentally is not a random jumbling of tones of sound, but it follows rigorously certain harmonic progression laws of musical acoustics.

2 Postulations

Auditory nerve system of human ear is capable of resolving a complex tone into its partial components (Ohm's law). When this resolution is perfect, the complex tone does not produce any irritation or harsh effect on the ear; whenever the resolution of the composite tone into distinct components is not perfect, the effect is contrary and the sound appears as unpleasant noise to the ear. A wave frequency at one moment stimulates auditory nerve and at the subsequent moment allows the stimulated nerve to recover. Before this recovery is complete, if the nerve is stimulated again by a 'sound flicker' or say 'unpleasant beats' as observed by Helmholtz, it can cause a continuous sensation without permitting recovery from the

stimulation. Such a frequency would cause fatigue to the ear.

Hence, for getting a feeling of melody of tones, generation of fast beat or flicker of sound beyond the limits of the resolution capability of the auditory nerve system of the ear has to be avoided, and for this, certain frequency separation among the tones is necessary. This condition can be met with only when the tones produced bear certain simple relationships with one another and also with the key note of the scale. Consonant and dissonant combinations of tones thus form the basis of musical acoustics.

Let us consider a system which vibrates at the fundamental frequency of n and at its first octave frequency of $2n$. The frequencies of the next two partials within the octavian interval of n and $2n$ of this vibrator can be supposed to be as follows:

$$\text{First partial} = n + \frac{2n - n}{2} = 1.5n$$

$$\text{Second partial} = n + \frac{2n - n}{4} = 1.25n$$

The notes corresponding to the frequencies 1, 2, 1.5 and 1.25 are known to be C, c, G and E respectively.

Let us postulate that the other tones of the scale are the functions of the frequencies of the three notes 2, 1.5 and 1.25.

If this assumption is correct, we can do the exercise of deriving other notes of the scale by manipulating with frequencies of these three notes. It is interesting to note that simply by dividing the "even" number 2 (higher octave frequency), by the odd figures of 1.5 and 1.25 (lower partial harmonics), or by multiplying the two odd figures and dividing them by the even number 2, we get the additional eight tones of the scale as indicated in the following:

$$2/1.5 = 1.333; 2/1.25 = 1.6$$

$$2^2/(1.5)^2 = 1.777; 2/1.5 \times 1.25 = 1.0666$$

$$1.5 \times 1.25/2^0 = 1.875; (1.5)^3/2 = 1.68$$

$$1.5 \times 1.25/2 = 1.406; (1.5)^2/2 = 1.125$$

We can also express the frequencies of the earlier mentioned four notes in terms of ratios of frequencies 2, 1.5 and 1.25 as follows:

$$1 = 2/2; 1.25 = 1.25/2^0; 1.5 = 1.5/2^0 \text{ and } 2 = 2/1$$

We thus get all the 12 tones of the octavian scale by the same principle. It may be noted that in all the above derived quantities, the even number 2 is either in numerator or in the denominator, and the odd figures of 1.5 and 1.25 are always dividing 2 in the numerator or in denominator. In no case an odd figure is divided by another odd figure. The above relations can be generalized in the form of a single integrated law or a mathematical expression or a series, as follows:

$$\psi_{1-2} = \left[\frac{2^x}{(1.5)^y (1.25)^z} \right]^a \quad \dots (1)$$

where ψ_{1-2} represents tones obtained from the equation; $a = \pm 1$, and x, y and z are such smallest integers which can give tones of frequencies within the limits of 1 and 2.

3 Derivation of Notes of Musical Scale

3.1 Flat Tone Series

If $a = +1$ in Eq. (1), we get the following two series A and B which ultimately give five flat tones,
(A) $2^x/(1.5)^y$, where (x, y) are (1, 1), (2, 2) and (2, 3).
(B) $2^x/(1.5)^y (1.25)^z$, where (x, y, z) are (1, 0, 1) and (1, 1, 1).

The above two series give the following 3 and 2 flat tones respectively which correspond to the notes indicated in lines below the frequency values in each case:

(a)	$2/(1.5)$ 1.333 F	$2^2(1.5)^2$ 1.777 b	$2^2/(1.5)^3$ 1.185 E
(b)	$2/(1.5)^0(1.25)$ 1.6 a	$2/(1.5)(1.25)$ 1.0666 D	

3.2 Sharp Tone Series

If $a = -1$ in Eq. (1), we get the following series (C and D) which give six sharp tones,

(C) $(1.5)^y/2^x$, where (x, y) are (0, 1), (1, 2) and (1, 3)
(D) $(1.5)^y(1.25)^z/2^x$, where (x, y, z) are (0, 0, 1), (0, 1, 1) and (1, 2, 1).

The series C and D give the following 3 and 3 tones respectively,

(c)	$(1.5)/2^0$ 1.5 G	$(1.5)^2/2$ 1.125 D	$(1.5)^3/2$ 1.687 a
(d)	$(1.25)(1.5)^0/2^0$ 1.25 E	$(1.25)(1.5)/2^0$ 1.875 b	$(1.25)(1.5)^2/2$ 1.40625 F

It may be noted that z is either zero as in series (A) and (C) or unity as in series (B) and (D). Values of x higher than 2 are neglected as all the harmonics between 1 and 1.5, and between 1.5 and 2 are obtained with values 0, 1 and 2 only. Selection of the values of y depends on the value of x .

It may also be observed here that the division of 2 by fractional harmonics 1.5 or 1.25 gives rise to the flat tones, while division of fractional harmonic figures by 2, the first octave harmonic, gives sharp tones, that is 'tivra swara' (also known as "sudha swara", with the exception that F alone is termed as tivra and E as sudha, not komal. From this, it appears that the terminology of komal and tivra is more appropriate than calling a few tones as sudha.

In the above tabulations, sharp (tivra) tones are represented by the usual symbols of the notes of musical scale, viz. C, D, E, F and b whereas flat tones (komal) are represented for the sake of simplicity by an 'underline' notation placed below the symbols of these notes and symbolized as D, E, E, a and b.

The above four series of frequencies if combined together and are written in ascending order, we get the eleven tones of the musical scale, as depicted in Table 1.

Coupling series (A) with (C) constitutes Kafi rag whereas series (C) with (D) gives rise to Yaman rag—the two being basic of the musical scale.

All the sharp tones obtained by substituting

Table 1—Natural Octavian Scale of Music

Notes	C	<u>D</u>	<u>D</u>	E	<u>E</u>	F	F
Frequency	1	1.0666	1.125	1.185	1.25	1.333	1.40625
Frequency ratio	1	16/15	9/8	32/27	5/4	4/3	45/32
Notes		G	a	a	b	b	
Frequency		1.5	1.60	1.687	1.777	1.875	
Frequency ratio		3/2	8/5	27/16	16/9	15/8	

Table 2—Derivation of Tones (Sharp) when $a = -1$

Sl No.	x	y	z	Interval between note and fundamental		Corresponding note	Interval between successive degrees	
				As frequency	As ratio		Tone	Ratio
1	1	2	0	1.125	9/8	D	C-D	9/8
2	0	0	1	1.25	5/4	E	D-E	10/9
3	1	2	1	1.40625	45/32	F	E-F	9/8
4	0	1	0	1.5	3/2	G	F-G	16/15
5	1	3	0	1.687	27/16	a	G-a	9/8
6	0	1	1	1.875	15/8	b	a-b	10/9
							b-c	16/15

Table 3—Derivation of Tones (Flat) when $a = +1$

Sl No.	x	y	z	Interval between note and fundamental		Corresponding note	Interval between successive degrees	
				As frequency	As ratio		Tone	Ratio
1	1	1	1	1.0666	16/15	<u>D</u>	C- <u>D</u>	16/15
2	2	3	0	1.185	32/27	<u>E</u>	<u>D</u> - <u>E</u>	10/9
3	1	1	0	1.333	4/3	<u>F</u>	<u>E</u> - <u>F</u>	9/8
							<u>F</u> -G	9/8
4	1	0	1	1.60	8/5	<u>a</u>	G- <u>a</u>	16/15
5	2	2	0	1.777	16/9	<u>b</u>	<u>a</u> - <u>b</u>	10/9
6	2	0	0	2	2	<u>c</u>	<u>b</u> - <u>c</u>	9/8

$a = -1$ in Eq. (1) are tabulated in Table 2 and flat tones obtained by putting $a = +1$ in Eq. (1) are listed in Table 3.

It may be seen that the natural scale of music originates from the above mentioned single mathematical series (or law), where $a = \pm 1$ and x, y and z are simple integers. While Table 2 gives six sharp tones (including G), Table 3 gives five flat tones.

It may be noted that the frequency ratio of 5/3 which is present as the major sixth in certain other octavian scale² does not find a place in the 'natural harmonic scale of music' referred to above.

The derivation of the entire musical scale of 12 tones from a single mathematical progression series, points to the existence of an integral relationship among various notes of the natural scale of music and lays down the scientific basis for the natural scale of musical octave.

In a separate paper, Part II of this general title, the

author presents the science of ragas, and their characteristic wave patterns.

References

- 1 Lobo, A, *Three monographs on music* (Indian Musicological Society, Baroda, India), 1980, 1-24.
- 2 Ranade G H, *Hindustani music—Its physics and aesthetics* (Popular Prakashan, Bombay), 3rd Edn, 1971, 38-51.
- 3 Levy M, *Intonation in north Indian music* (Bibilia Impex Pvt Ltd, New Delhi), 1982, 5-25.
- 4 Bharata-Muni, *Natyasastra*, translated by MM Ghosh, Bibliotheca Indica Series, Issue Nos. 1559 and 1581, work No. 272 (The Asiatic Society, Calcutta) 1950 & 1967.
- 5 Rayleigh J W S, *The theory of sound*, Vol. 1 (Macmillan & Co., USA) 2nd Edn., 1945, 4.
- 6 *Encyclopedia Britannica*, Vol. 12, 15th Edn., 1981, 746-749.
- 7 Ellis, A J, *Proc R Soc London (GB)*, 37 (1884) 368.
- 8 Ellis A J, *J Soc Art*, 33 (1885) 485.
- 9 Parry H, *The art of music* (Kegan Paul, Trubner & Co., London), 1917, 15.
- 10 Lloyd L S, *The musical ear* (Oxford University Press, London) 1940, 54, 72.

Physics of Musical Scale and Ragas: Part II—Harmonic Laws Governing Evolution of Ragas (the Scales of Melodies)

P B MATHUR

Central Electrochemical Research Institute, Karaikudi 623 006

Received 29 October 1985

The importance of intertonal intervals, namely sruties in the constitution of ragas has been discussed. A series of 22 sruties are shown to exist. It is shown that only 14 sruties out of 22 are consonant in nature and which alone, when present in a scale, can constitute ragas. It is further enunciated that only such sequences of sruties which can produce similar-shaped wave patterns in the two lower and upper chords of a scale, constitute ragas. On the basis of these laws, various scales are analyzed. In the series of 32 heptatonic scales, only 15 scales exhibit harmonic waves and these scales can constitute ragas. Incidentally, 13 of these are also coinciding with the 13 known Hindustani heptatonic ragas.

1 Introduction

From the discussion in Part I¹ of this common title, it may be noted that the natural basic scale of music is constituted of seven notes (swara), five of which (D, E, F, a and b) are having two tones each, one a flat (komal) and the other a sharp (tivra); the basic scale thus consists of 12 tones, whose frequencies are defined in relation to the fundamental note C (Gram Sa) of the scale, and which are numerically simple ratios of the frequencies of particular notes to that of fundamental note C. These intervals between the fundamental and the tones fix the frequency points of consonant upper partial tones, in a continuum of noises produced from one pitch to higher ones, within an octave; their location, however, is governed by the Harmonic Law of Musical Scale expressed by Eq. (1) of Part I.

When a number of tones are played in sequence, the melody of compounded tone depends not only on their frequency positions in the octavian scale which are determined in relation to one single note C, the fundamental or the 'Gram' (in Hindi), but also on intertonal intervals which should also be consonant in nature. These intertonal intervals can be determined as the ratios of the frequency of one tone to that of the preceding lower tone. Each preceding tone becomes the fundamental or Gram for the succeeding tone. Hence, these intertonal intervals cannot constitute a scale as each interval has different reference level or say key note, or fundamental or Gram. But they are important in the constitution of ragas, as may be seen henceforth.

For the formulation of scales of melody, viz. ragas, it is not only necessary that the interval between each tone (degree) and the key note of the scale should be consonant as per derivation from Eq. (1) of Part I, but should also have a consonant intertonal interval among degrees.

The total number of frequency intervals which can arise from playing in sequences any two tones out of 12 tones of the basic scale, will be $\sum_{i=1}^{12} n = 78$, where n is taken as 1 to 12. All these successive pairs of semitones and their frequency intervals were listed. Although the total number of possible pairs of semitones are 78, many of these frequency intervals are repeated. The data listed in Table 1 are therefore organized in ascending order of intervals and the pairs of tones belonging to particular intervals are grouped together. Table 1 thus indicates the possible number of pairs of tones as 78 and the total number of different intervals as 31.

But all these 31 intervals may not be consonant. Dissonant intervals present in 31 will not constitute scales of melody. Formulation of ragas thus depends on the *exclusion* of all such dissonant intertonal intervals of the series of 31 of Table 1. The author proposes the following 'exclusion principles' for the identification and elimination of the dissonant pairs of intertonal intervals and thus to lay down the basis of formulation of ragas—the scales of melodies.

For the sake of simplicity, the author shall adopt in subsequent tables and paragraphs Indian notations of musical scale for the 7 notes or 11 tones in place of usual notations C, D etc. as indicated in the following lines

C	D	D	E	E	F	F	G	a	a	b	b
Sa	Re	Re	Ga	Ga	Ma	Ma	Pa	Dha	Dha	Ni	Ni

2 Microtonal Intervals—SRUTIES and Exclusion Principles for Formulation of Scales of Melodies

1. 12 note octavian scale which includes both lower and upper fundamental notes C and c respectively can be considered to be constituted of two

Table 1—Intertonal Intervals between Any Two Degrees in 12 Tonal Scale

Sl. No.	Intertonal ratio	Interval	Pair of notes forming identical intervals		Pair of notes of dissonant pair of intervals
			In lower chord	In upper chord	
1.	1/1	1	Sa		Key note
2.	256/243	1.0535	<u>Ga</u> /Re	Ni/Dha	—
3.	135/128	1.0547	Re/ <u>Re</u> , Ga/ <u>Ga</u> , Ma/ <u>Ma</u>	Dha/ <u>Dha</u> , Ni/ <u>Ni</u>	Yes
4.	16/15	1.0666	Re/Sa, <u>Ma</u> /Ga	Pa/Ma, <u>Dha</u> /Pa, Sa/Ni	—
5.	10/9	1.1111	<u>Ga</u> /Re, Ga/Re	Ni/ <u>Dha</u> , Ni/Dha	—
6.	9/8	1.1250	Re/Sa, <u>Ma</u> / <u>Ga</u> , Ma/Ga	Pa/ <u>Ma</u> , Dha/Pa, Sa/ <u>Ni</u>	—
7.	256/225	1.1378		<u>Dha</u> /Ma	—
8.	75/64	1.1718	Ga/Re	Ni/ <u>Dha</u>	—
9.	32/27	1.1850	<u>Ga</u> /Sa	Sa/Dha	—
10.	1215/1024	1.1865	Ma/ <u>Ga</u>		—
11.	6/5	1.200	Pa/Ga	<u>Dha</u> / <u>Ma</u> , Dha/Ma	—
12.	5/4	1.250	Ga/Sa, <u>Ma</u> / <u>Re</u> , Ma/Re	Ni/Pa, Sa/ <u>Dha</u>	—
13.	512/405	1.264	Ni/Ma		—
14.	81/64	1.266		Dha/ <u>Ma</u> , Pa/ <u>Ga</u>	—
15.	32/25	1.28		<u>Dha</u> /Ga	Yes
16.	675/512	1.318	Ma/ <u>Re</u>		—
17.	4/3	1.333	<u>Ma</u> /Sa, Pa/Re	Ni/ <u>Ma</u> , Ni/Ma, Sa/Pa	—
18.	27/20	1.35	<u>Dha</u> /Ga		Yes
19.	45/32	1.406	Pa/ <u>Re</u> , Ma/Sa	Ni/ <u>Ma</u>	Yes
20.	64/45	1.422	Dha/ <u>Re</u> , Ni/ <u>Ga</u>	Sa/Ma	Yes
21.	729/512	1.424	Dha/ <u>Ga</u> , Ni/ <u>Ga</u>		Yes
22.	3/2	1.5	Pa/Sa, Dha/ <u>Re</u>	Ni/Ga, Sa/ <u>Ma</u>	Yes
23.	128/81	1.580	<u>Ni</u> /Re, Ni/ <u>Ga</u>		Yes
24.	405/256	1.582	Dha/Re, Ni/Ga		Yes
25.	8/5	1.60	<u>Dha</u> /Sa, Sa/Ga		Yes
26.	5/3	1.666	<u>Ni</u> /Re, Ni/Re		Yes
27.	27/16	1.687	Dha/Sa, Sa/ <u>Ga</u>		Yes
28.	225/128	1.758	Ni/ <u>Re</u>		Yes
29.	16/9	1.777	<u>Ni</u> /Sa, Sa/Re		Yes
30.	15/8	1.875	Ni/Sa, Sa/ <u>Re</u>		Yes
31.	2	2.000	Sa		Scale's key note

Note: Second note (swara) of any pair of notes listed in columns 4 and 5 is always representing the lower frequency to the frequency of first note of the pair.

chords 'lower' and 'upper' of intertonal frequency lengths as indicated in the following:

Lower chord length		Upper chord length	
Tone gap	Frequency index	Tone gap	Frequency index
C – G	1.5	G – c	1.33
C – <u>F</u>	1.33	<u>F</u> – c	1.5

Here, the underlined note represents flat tone. When C – G is taken as lower chord, the upper chord will be G – c and when C – F is the lower chord, the upper chord will be F – c.

2. In order to produce at least one harmonic of a tone within the octavian length, an intertonal interval cannot be larger than a chord length.

(a) Intertonal intervals equal to the chord length of 1.5 and lesser index numbers are listed under Sl. Nos. 1 to 22 in Table 1. These intervals alone are significant intervals in the constitution of the scales and so they are designated here as 'Microtonal Intervals' or 'Sruties'. All the remaining intervals of Sl. Nos. 23 to 31 are therefore excluded as they cannot produce a harmonic in the octavian scale.

(b) Since the lengths of the two chords of an octave are unequal as indicated under item 1 above, the maximum length of intertonal interval which can produce a harmonic in the complementary chord cannot be larger than 1.33, the length of smaller chord. On this basis, another five microtonal intervals of Sl. Nos. 18 to 22 will be dissonant and so they are excluded.

3. Such microtonal intervals which partially overlap both of the two chords—lower and upper—can-

not produce a harmonic in the residual portions of any one of the two chords. Hence, these sruties are also excluded from the remaining 17. Sruti of Sl. No. 15 in Table 1 overlaps the two chords and so this dissonant sruti is excluded. We are thus left with 16 sruties 1 to 14, 16 and 17, from which we have to identify dissonant sruties, if existing any more.

4. Sruti of Sl. No. 3 and of index number 135/128 represents an interval which exists in between the sharp and flat tones of each of the five notes, D, E, F, a and b of the basis scale. Since this interval is too small in magnitude and falls in between the other two smallest microtones of index numbers 256/243 and 16/15, this sruti will produce dissonant sound in a scale. Hence, this sruti is excluded from the remaining. So we are left with 15 sruties.

5. Since the sruti of Sl. No. 1 corresponds to the interval of zero, this shruti should also be ignored for all practical purposes.

We are thus left with 14 consonant sruties of Sl. Nos. 2, 4 to 14, 16 and 17. The remaining sruties out of 1 to 22 of Table 1 are dissonant. Six consonant sruties of Sl. Nos. 2, 4, 5, 6, 8 and 10 out of 14, which do not involve a note gap in between any pair of tones constituting them, are listed in Table 2. Six consonant sruties of Sl. Nos. 7, 9, 11, 12, 14 and 16 having one note gap in between a pair of tones are listed below in the same Table 2, and the two consonant sruties of Sl. Nos. 13 and 17 having a gap of two notes are listed further below in the same Table 2.

From the exclusion of sruti 135/128 as mentioned in item 4 above, conclusion can be drawn that

(a) A scale of melody (Raga) cannot simultaneously incorporate both 'flat' and 'sharp' tones of one and the same note.

(b) Hence, a musical scale of melody cannot have more than seven notes (swara). The scales of melodies—Ragas, can be thus constituted with a maximum of seven notes only.

3 Characteristics of Sruties

Before proceeding further with the formulation of ragas, let us precisely characterize sruties. Sruties represent inter-tonal intervals between two successive tones and so they are not based on a single key note or a gram as does the basic scale of music. Key note for each sruti is different and is always the preceding note of each pair of tones which constitute sruties. Hence, sruties cannot and do not form a scale, a fact not understood earlier²⁻⁶ since the time of Bharat⁷ who wrote ten lines about sruties in *Natya Shastra*, around 2400 B.C. or even earlier. Sruties, are, however, the foundation stones of ragas—the scales of melodies, and so they are as important as the basic scale of music.

4 Formulation of Ragas—the Scales of Melodies

Eleven tones of basic scale can mathematically give rise to a very large figure of $11!$ combinations of tones. Even 7 notes can give rise to $7! = 5040$ combinations which is also a large number. Further, two fixed notes C and G and five variable notes D, E, F, a and b having each a pair of flat and sharp tones, can produce $2^5 = 32$ heptatonic scales. All such mathematical combinations of tones do not necessarily constitute ragas.

A scale of music has two chords C – G designated as lower chord and G – C as upper chord. The presence of orderly sequences of sruties in the two chords of a scale which can generate rhythmic wave pattern, constitutes scales of ragas.

In order to evolve rules of formation of raga scales, two diagrams, viz. Figs 1 and 2, named as 'Raga Jaties', or tonal horoscope for heptatonic ragas and penta- and hexatonic ragas respectively, will be helpful.

The sequence of sruties in a scale can easily be followed with the help of these two diagrams. As indicated earlier, 32 numbers of heptatonic scales are possible. Out of these, 16 scales will be formed with flat Ma and remaining 16 scales with sharp Ma. Sixteen scales with flat Ma are listed in Table 3 and the remaining 16 scales formed with sharp Ma, are listed in Table 4.

Table 2—Sruties with Different Note Gaps

a. Sruties without any note gap			
Sl. No.	Interval	Index No.	Consecutive notes of
			Lower chord Upper chord
1	1.0535	256/243	<u>Ga</u> /Re <u>Ni</u> /Dha
2	1.066	16/15	<u>Re</u> /Sa, <u>Ma</u> /Ga <u>Dha</u> /Pa, Sa/ <u>Ni</u>
			Pa/Ma
	1.111	10/9	Ga/Re, Ga/Re <u>Ni</u> /Dha, Ni/Dha
4	1.125	9/8	Re/Sa, <u>Ma</u> /Ga Dha/Pa, Sa/ <u>Ni</u>
			Ma/Ga, Pa/ <u>Ma</u>
5	1.1718	75/64	Ga/ <u>Re</u> Ni/ <u>Dha</u>
6	1.186	1215/1024	Ma/ <u>Ga</u>
b. Sruties with one note gap			
7	1.1378	256/225	Dha/Ma
8	1.185	32/27	Ga/Sa Sa/Dha
9	1.20	6/5	Pa/Ga <u>Dha</u> / <u>Ma</u> , Dha/Ma
10	1.25	5/4	Ga/Sa, <u>Ma</u> / <u>Re</u> Ni/Pa, Sa/ <u>Dha</u>
			Re/Ma
11	1.266	21/64	Pa/ <u>Ga</u> Dha/ <u>Ma</u>
12	1.318	675/512	Ma/ <u>Re</u>
c. Sruties with two notes gap			
13	1.264	512/405	<u>Ni</u> /Ma <u>Ni</u> /Ra
14	1.333	4/3	<u>Ma</u> /Sa, Pa/Re Sa/Pa, <u>Ni</u> / <u>Ma</u> , Ni/Ma

Note: Heptatonic ragas of 7 notes can be constituted with six sruties only which are listed in (a) whereas hexatonic and pentatonic ragas can be constructed with 14 sruties, 6 of (a) and the remaining 6 of (b) and 2 of (c).

Table 3—First Set of Heptatonal Scales with Flat Ma

Sl No.	HEPTATONAL SCALES WITH FLAT 'Ma' AND INTERTONAL INTERVALS	WAVE PATTERNS	C = CONSONANT D = DISSONANT	HINDUSTANI RAGAS
1	Sa <u>Re</u> Ga <u>Ma</u> Pa Dha Ni Sa 1.066 1.171 1.066 1.125 1.125 1.111 1.066		D	BHAIRAVI
2	Sa <u>Re</u> <u>Ga</u> <u>Ma</u> Pa Dha Ni Sa 1.066 1.111 1.125 1.125 1.125 1.111 1.066		D	
3	Sa <u>Re</u> <u>Ga</u> <u>Ma</u> Pa <u>Dha</u> Ni Sa 1.066 1.111 1.125 1.125 1.066 1.171 1.066		D	
4	Sa <u>Re</u> <u>Ga</u> <u>Ma</u> Pa <u>Dha</u> <u>Ni</u> Sa 1.066 1.111 1.125 1.125 1.066 1.111 1.125		C	
5	Sa Re <u>Ga</u> <u>Ma</u> Pa <u>Dha</u> <u>Ni</u> Sa 1.125 1.053 1.125 1.125 1.066 1.111 1.125		C	ASAWARI
6	Sa Re Ga <u>Ma</u> Pa <u>Dha</u> <u>Ni</u> Sa 1.125 1.111 1.066 1.125 1.066 1.111 1.125		D	KHAMMAJ
7	Sa Re Ga <u>Ma</u> Pa Dha <u>Ni</u> Sa 1.125 1.111 1.066 1.125 1.125 1.053 1.125		C	
8	Sa Re <u>Ga</u> <u>Ma</u> Pa <u>Dha</u> Ni Sa 1.125 1.053 1.125 1.125 1.066 1.171 1.066		D	
9	Sa Re <u>Ga</u> <u>Ma</u> Pa Dha <u>Ni</u> Sa 1.125 1.053 1.125 1.125 1.125 1.053 1.125		C	
10	Sa <u>Re</u> Ga <u>Ma</u> Pa Dha <u>Ni</u> Sa 1.066 1.171 1.066 1.125 1.125 1.053 1.125		D	BHAIRAV
11	Sa <u>Re</u> Ga <u>Ma</u> Pa <u>Dha</u> Ni Sa 1.066 1.171 1.066 1.125 1.066 1.171 1.066		C	
12	Sa <u>Re</u> Ga <u>Ma</u> Pa <u>Dha</u> <u>Ni</u> Sa 1.066 1.171 1.066 1.125 1.066 1.111 1.125		C	
13	Sa <u>Re</u> <u>Ga</u> <u>Ma</u> Pa Dha <u>Ni</u> Sa 1.066 1.111 1.125 1.125 1.125 1.111 1.066		D	
14	Sa Re <u>Ga</u> <u>Ma</u> Pa Dha Ni Sa 1.125 1.053 1.125 1.125 1.125 1.111 1.066		D	JOGIYA
15	Sa Re Ga <u>Ma</u> Pa <u>Dha</u> Ni Sa 1.125 1.111 1.066 1.125 1.066 1.171 1.066		D	
16	Sa Re Ga <u>Ma</u> Pa Dha Ni Sa 1.125 1.111 1.066 1.125 1.125 1.111 1.066		C	

Shapes of the wave patterns of two chords of each scale, are presented in column 3 of Tables 3 and 4. The shape pattern of the chord waves governs the acoustical character of the scales.

5 Rules for Formulation of Orderly Wave Patterns for Evolving Ragas

1. Presence of orderly sequences of sruties in the two chords of a scale which give rise to identical or closely rhythmic wave patterns in the two chords, constitute scales of ragas.

2. The pattern of waves and their modal amplitudes are governed by the magnitudes of sruties which constitute them.

3. Rhythmic wave patterns which constitute scales of melodies can have the following three shapes:

- Unidirectional shape where the magnitude of sruties of the waves increases in the same direction in the two chords, either in the right or left direction; as indicated by the symbol $\rightarrow \rightarrow$ or $\leftarrow \leftarrow$ in Tables 3 and 4.

Table 4—Second Set of Heptatonal Scales with Sharp Ma

Sl No.	HEPTATONAL SCALES WITH SHARP 'Ma' AND INTERTONAL INTERVALS	WAVE PATTERNS	C = CONSONANT D = DISSONANT	HINDUSTANI RAGAS
1	Sa <u>Re</u> Ga Ma Pa Dha Ni Sa 1.066 1.171 1.125 1.066 1.125 1.111 1.066		C	MARVA
2	Sa <u>Re</u> Ga Ma Pa Dha Ni Sa 1.066 1.111 1.066 1.066 1.125 1.111 1.066			
3	Sa <u>Re</u> Ga Ma Pa Dha Ni Sa 1.066 1.111 1.186 1.066 1.066 1.171 1.066		C	TODI
4	Sa <u>Re</u> Ga Ma Pa Dha Ni Sa 1.066 1.111 1.186 1.066 1.066 1.111 1.125		C	BAHADURI TODI
5	Sa Re <u>Ga</u> Ma Pa Dha Ni Sa 1.125 1.053 1.186 1.066 1.066 1.111 1.125		D	
6	Sa Re Ga Ma Pa Dha Ni Sa 1.125 1.111 1.125 1.066 1.066 1.111 1.125		D	
7	Sa Re Ga Ma Pa Dha Ni Sa 1.125 1.111 1.125 1.066 1.125 1.053 1.125		C	HARSRINGAR
8	Sa Re <u>Ga</u> Ma Pa Dha Ni Sa 1.125 1.053 1.186 1.066 1.066 1.171 1.066		C	
9	Sa Re <u>Ga</u> Ma Pa Dha Ni Sa 1.125 1.053 1.186 1.066 1.125 1.053 1.125		C	
10	Sa <u>Re</u> Ga Ma Pa Dha Ni Sa 1.066 1.171 1.125 1.066 1.125 1.053 1.125		D	
11	Sa <u>Re</u> Ga Ma Pa Dha Ni Sa 1.066 1.171 1.125 1.066 1.066 1.171 1.066		C	SREE
12	Sa <u>Re</u> Ga Ma Pa Dha Ni Sa 1.066 1.171 1.125 1.066 1.066 1.111 1.125		D	
13	Sa <u>Re</u> <u>Ga</u> Ma Pa Dha Ni Sa 1.066 1.111 1.186 1.066 1.125 1.053 1.125		D	
14	Sa Re <u>Ga</u> Ma Pa Dha Ni Sa 1.125 1.053 1.186 1.066 1.125 1.111 1.066		D	
15	Sa Re Ga Ma Pa Dha Ni Sa 1.125 1.111 1.125 1.066 1.066 1.171 1.066		D	
16	Sa Re Ga Ma Pa Dha Ni Sa 1.125 1.111 1.125 1.066 1.125 1.111 1.066		C	YAMAN

(b) Central peak shape, where the central sruties of the two chords are larger in magnitude than those of the two adjacent sruties as indicated by the symbol in Tables 3 and 4.

(c) Central trough shape when the central sruties of the two chords are smaller in magnitude than those of the two adjacent sruties, as indicated by the symbol in Tables 3 and 4.

6 Application of Laws of Rhythmic Wave Chords to Heptatonic Scales

Table 3 consists of 16 scales all with flat Ma. It may be noted that only seven scales of Sl Nos 4, 5, 7, 9, 11, 12 and 16 out of sixteen scales of this table, obey the laws of symmetrical wave pattern of the two chords. This is evident from the shapes of wave curves given in column 3 of Table 3. Hence, only these seven scales out of sixteen constitute ragas.

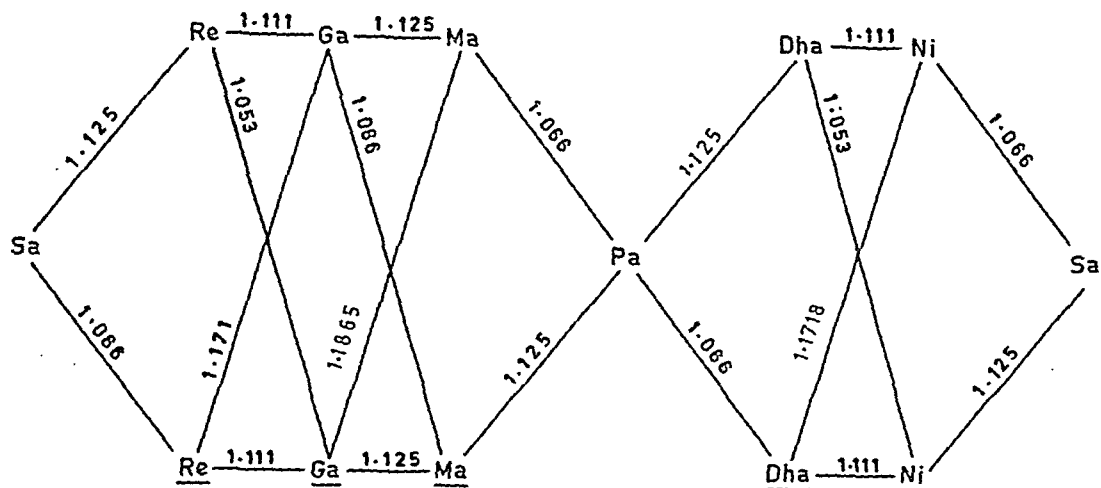


Fig. 1—Raga Jatica for heptatonal ragas

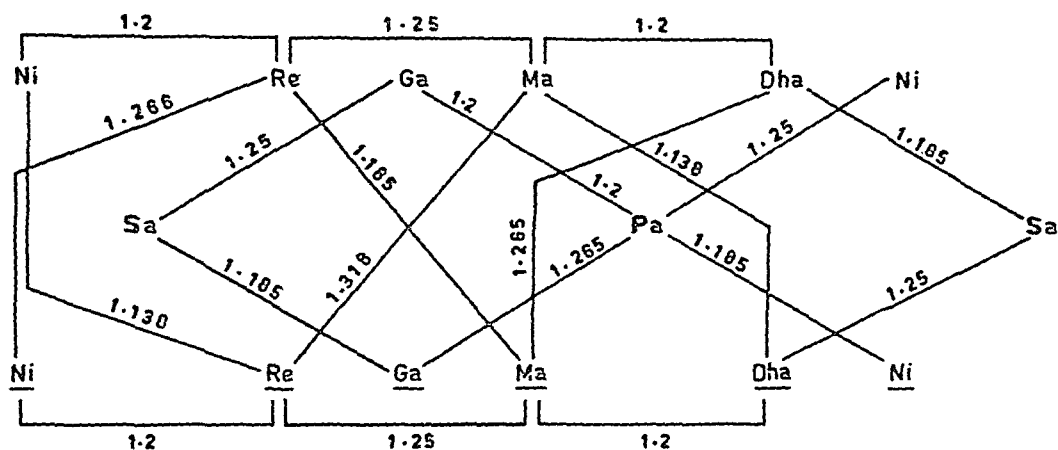


Fig. 2—Raga Jatica for penta- and hexa-tonal ragas

In Hindustani music, these scales are known as, Bhairavi (SI No.4), Asawari (SI No. 5), Khammaj (SI No 7), Kafi (SI No. 9), Bhairav (SI No. 11), Jogiya (SI No. 12) and Bilaval (SI. No. 16).

Scales corresponding to SI Nos 2, 6 and 13 show two opposite waves in the two chords, which produce incoherency. So these three scales cannot constitute Ragas. Wave patterns of the remaining scales of SI Nos 1, 3, 8, 10, 14 and 15 do not exhibit the presence of conjugal wave patterns in their two chords and so none of them can make a raga.

Table 4 consists of 16 scales all with sharp Mā. It may be seen that only eight scales of SI Nos 1, 3, 4, 7, 8, 9, 11 and 16 follow the law of construction of ragas. In Hindustani music system, six of them are known as Marva (SI No. 1), Todi (SI No. 3), Bahaduri todi (SI. No.4), Harsringar (SI, No. 7), Purvi or Sree (SI No. 11) and Yaman (SI No. 16).

Other scales of SI Nos 8 and 9 of Table 4 show some orderliness. The corresponding raga names of these scales in Hindustani music could not be identified by the author. It may, therefore, be noted that only 15 out of the 32 possible heptatonal scales listed in Tables 3 and 4, follow the laws of rhythmic patterns in their two chords and so they alone constitute ragas.

7 Conclusion

In this paper, the author has enunciated the laws of evolution of sruties and ragas and concluded with the derivation of 15 scales of melodies 13 of which incidentally are also the heptatonal scales of ragas of Hindustani music, from the mathematically possible 32 heptatonal scales. Derivation of the remaining series of scales of ragas of heptatonal intercombinations, hexatonal and pentatonal will be discussed in the third part of this series of papers on the physics of music.

The author compiled a large number of facts, figures and data, particularly on Indian music and processed the data in multitudes of ways and analyzed them in the light of the principles of modern physics, in search of finding hidden correlations, links and orderliness among the known melodies, and thus ended up with the advancement of acoustical laws and rules governing the basic scale of music and the origin of ragas—the scales of melodies, which are of universal nature and belong to the entire world as a piece of scientific truth, although they were discovered in the east in times immemorial. The author's contribution is only a part of the same stream of great heritage of India, flowing from vedic times to eternity.

Acknowledgement

The author wishes to express his gratitude to his wife, Mrs Sarojini Mathur for providing practical demonstrations of many ragas and raganies as and when the author wanted to observe their construction closely and also for her constant support in this work.

References

- 1 Mathur P B, *Indian J Pure & Appl Phys*, **24** (1986) 373.
- 2 Levy M, *Intonation in north Indian music* (Biblia Impex Pvt Ltd, New Delhi), 1902, 25-80.
- 3 Ranade G H, *Hindustani music—Its physics and Aesthetics* (Popular Prakashan, Bombay), 3rd Edn, 1971, 38-51.
- 4 Chaitanya Deva B, *The music of India: A scientific study* (Munshiram Manoharlal Publishers Pvt Ltd, New Delhi), 1981, 94-104.
- 5 Jairazboy N A, *J Indian Musicolog Soc*, **44** (1973) 5-18.
- 6 Sambamurthy P, *South Indian music*, Vol. V (The Indian Music Publishing House, Madras), 1972, 72.
- 7 Bharata-Muni, *Natyasastra*, translated by M M Ghosh, *Bibliotheca Indica Series*, Issue Nos. 1559 and 1581, Work No. 272 (The Asiatic Society, Calcutta), 1950 & 1967.

Influence of Diffusion of H-Ions & of Gyro-Radius Effect on Diffusion Coefficient of H-Ions across a Plasma with an Axial Magnetic Field

F F ELAKSHAR*

Physics Department, Faculty of Science, Mansoura University, Mansoura, Egypt

Received 24 September 1985

Measurements of cross-field diffusion coefficient were made in an axial magnetic field. The e-folding length of the plasma density (q_s) in the radial direction was measured in two pressure ranges: (i) low pressures where the plasma length (L) is smaller than the ion mean free-path (λ_i) and (ii) high pressures at which (L) is larger than (λ_i). The diffusion coefficient $D_{i\perp}(q_s)$ was calculated and compared with the estimated $D_{i\perp}(\tau_i)$, where τ_i is the ion collision time. Diffusion is found to be more effective in the determination of the ion density distribution compared to the ion gyro-radius, particularly at high pressures.

1 Introduction

Measurements of the diffusion coefficient of plasma for different plasma devices are described in the literature. However, most of them are made in multipole magnetic fields^{1,2}. We studied plasma diffusion across an axial magnetic field. The transverse diffusion coefficient ($D_{e\perp}$) can be estimated (i) from measurements of the radial distribution of the plasma density or (ii) from the ratio of electron-to-ion currents (I_e/I_i) collected by a single Langmuir probe which is directed perpendicular to the magnetic field B . These two methods are based on the application of the classical theory of Bohm³. The e-folding length of plasma density (q) in the radial direction is given by:

$$q = (LD_{e\perp}/\gamma)^{1/2} \quad \dots (1)$$

where L is the plasma length, D_e the transverse diffusion coefficient of the electrons and γ a quantity equal to the ion velocity v_i .

Value of $D_{e\perp}$ was calculated following Eq. (1) and it was found that this value was larger than the value theoretically estimated from the collision time of electrons with neutral particles by two orders of magnitude. Therefore, an alternative formula has to be used. Simon⁴ and more recently Okuda and Dawson⁵ have shown that the actual diffusion rate is faster than that predicted by the classical collision theory. The enhanced diffusion value is generally believed to be caused by 'fluctuation levels' which are excited, thus increasing the diffusion rate above the thermal level. The physical origin of the enhanced diffusion is due to convective cells which are thermally excited. It is found that the diffusion coefficient value changes with

the magnetic field at different rates depending on the magnetic field strength. At sufficiently weak magnetic fields, D is proportional to B^{-2} . At moderate magnetic fields, where the cyclotron frequency ω_{ce} is nearly equal to the plasma frequency ω_{pe} , the diffusion coefficient of electrons (D_e) is enhanced to that of ions (D_i) and is almost independent of B , and finally at large magnetic fields, where the ionic cyclotron frequency (ω_{ci}) is higher than the corresponding plasma frequency ω_{pi} , the value of D_e is proportional to B^{-1} (Bohm region). In our studies, we applied a magnetic field of about 500-1000 G which can be considered as a weak magnetic field.

Simon⁴ used the transverse diffusion coefficient of ions instead of that of electrons and thus Eq. (1) was modified to:

$$q = (LD_{i\perp}/v_i)^{1/2} \quad \dots (2)$$

The possibility of a short-circuiting mechanism was considered in the modified theory of Simon⁴. The influence of the radial electric field on the diffusion rate may be nullified by electrons diffusing along the magnetic field lines towards the end of the plasma device walls. The rate of diffusion along the radial direction thus may not any more be ambipolar. It will be determined only by the diffusion coefficient of the ions and not by the much smaller diffusion coefficient of the electrons perpendicular to the magnetic field. The influence of the radial electric field E_r on diffusion rate can be neglected compared to that of the axial electric field E_z if $E_r/(\omega_{ci}\tau_i)^2 \ll E_z$, where τ_i is the collision time of ions. When $L \gg \lambda_i$, the diffusion coefficient of the ions $D_{i\perp}$ is given by:

$$D_{i\perp} = \pi^2 q_s^2 D_2^0 / L^2 \quad \dots (3)$$

where D_2^0 is the ambipolar diffusion coefficient in the

*Present address: Al-Ahsa T T College, P.O. Box 2313, Hufuf, Saudia Arabia

direction of the magnetic field as given by Zharinov⁶, and Tonks⁷:

$$D_2^0 = 2D_1^0 = 2/3 \lambda_i v_{is}, \quad \text{for } T_e = T_i \quad \dots (4)$$

and

$$D_2^0 = D_1^0 T_e / T_i, \quad \text{for } T_e \gg T_i \quad \dots (5)$$

The e-folding length is given by:

$$q_s = 0.25 L / \lambda_i r_{ci} \quad \dots (6)$$

where r_{ci} is the ion Larmor radius, i.e. ion gyro-radius.

According to formulae (3)-(6), the e-folding length is expected to be of the same order of magnitude as that of the ion gyro-radius. In the following sections, these formulae are used to evaluate the diffusion coefficient of ions across an axial magnetic field in (i) high pressure ($L > \lambda_i$) and (ii) low pressure ($L < \lambda_i$) ranges. The effects of the ion gyro-radius and diffusion on the plasma density profile are also discussed.

2 Apparatus

The apparatus (Fig. 1) consists of an evacuated cylindrical glass vessel (1 m length and 15 cm diam), surrounded by water-cooled coils fed with electric current to produce magnetic fields of up to 1500 G. On top of the glass vessel is set a duoplasmatron as the plasma source, which releases ions and electrons into the vessel. The plasma flow is kept continuous and enters the vessel through the anode aperture of 2 mm diameter to enter an axial magnetic field, stretching over a length 50 cm of the vessel, starting at one end at 5 cm from the anode aperture. The magnetic field along the axis of the plasma device can be raised up to 1500 G. The vacuum vessel was connected to diffusion pumps and finally to rotary pumps. The final vacuum produced was better than 10^{-6} Torr, while

the running gas pressure was between 10^{-5} - 10^{-4} Torr. Measurements were made mainly with hydrogen gas. The pressure in the plasma source was between 0.01 and 0.1 Torr. The arc current inside the source was about 5 A for hydrogen gas.

The length of the plasma beam L was about 50 cm. The measurements of plasma characteristics were made using a single Langmuir probe and compared with those obtained from spectroscopic data. The electron temperature (T_e) was between 10 and 6 eV, the ion temperature (T_i) between 1 and 0.5 eV. The plasma density ranged between 10^{10} and 10^9 cm^{-3} when the pressure ranged between 10^{-5} and 10^{-4} Torr. The mean free-path in hydrogen plasma at the lowest pressure was about 5 m for electrons and 2 m for ions, as estimated from the collisions with neutral particles. This suggests that the particles leave the plasma source and do not collide with charged particles. By increasing the arc current, the plasma density in the centre of the glass vessel can be raised by a factor of 1.2. The plasma beam was hardly visible at high pressures; only a weak glow was observed. At the lowest pressure, a luminous plasma column appeared, its diameter decreasing with increase in applied magnetic field.

3 Results and Discussion

Investigations on the electron energies were made by an analysis of the I - V characteristics of a single probe following the method of Elakshar and Nossair⁸. The electrons leave the duoplasmatron with an electron temperature of about 10 eV, superposed with a group of fast electrons of about 20-30 eV, at the low pressure (10^{-5} Torr). Collisions of these fast electrons with the neutral gas molecules cause an additional ionization, so that the plasma density increased from a value of about 10^9 cm^{-3} at 10^{-4} Torr to densities as high as 10^{10} cm^{-3} at 10^{-5} Torr.

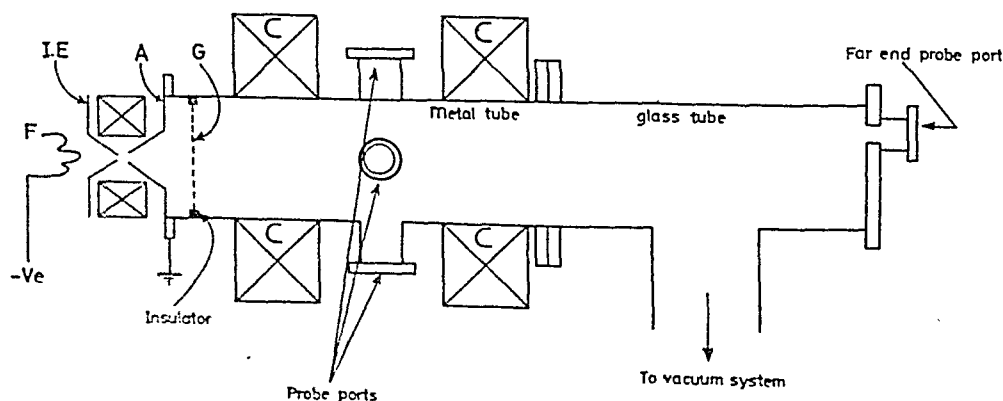


Fig. 1—Experimental arrangement [F: filament, I.E.: intermediate electrode, A: anode, G: grid and C: coils]

A mesh grid of 18 lines/inch was fixed just in front of the anode aperture. Plasma instability was observed when the grid was biased by a potential positive relative to the anode. Using a 1 mm single plane probe, which was set at 15 cm from the grid, frequencies in the range of 30-60 kHz were detected (Fig. 2). The frequency detector consisted of a band-pass filter, a calibrated spectrum analyzer and either an X-Y plotter or an oscilloscope. The instability may be attributed to drift waves which exist in the presence of a diamagnetic current⁹; full details of this observation will be published separately.

Since perturbation of the plasma by probes was anticipated, a plane probe (1 mm diam) was chosen to minimize the probe effect and also enable detection of short-range variations in plasma density. However, the probe measurements were calibrated by comparison with spectroscopic observations. The ratio of intensities of emission lines of helium was measured and compared with the results of theoretical calculation reported by Sovie¹⁰. This check revealed that the calibrations made with the probe are 90% reliable.

The diffusion coefficient of ions across the axial magnetic field was determined indirectly from the radial distribution of the plasma density, i.e. by measuring q_s and using Eq. (3). The plasma density distribution was measured using the planar single probe which sampled ions in proportion to their local density. Three different theories were applied to calculate the density; those of (a) Kagan and Perel¹¹, (b) Fujita and Akazaki¹², and (c) Langmuir and Blodgett¹³. The plots of plasma density as a function of r ac-

cording to the theories are shown in Fig. 3. The uncertainty in calculating the density as a function of the distance (r), when the Langmuir theory was used, was minimized by giving the probe a fixed potential equal to the space potential instead of biasing it by a relative variable negative voltage with respect to plasma potential. The plasma density was also measured using a double probe instead of the single probe and the results are shown in curve d in Fig. 3. The double probe theory suggested by Polman¹⁴ and modified by Swift and Schwar¹⁵ was used for plotting the curve. It is seen that curves (a)-(d) in Fig. 3 are reasonably close.

The e-folding length (q_s) was estimated from the slope of the straight portion of the plot of density in log scale (or the ion saturation current collected by the probe) versus radial distance r . According to Simon's theory⁴, the plot of inverse of q_s versus B should yield a straight line and it is found to be so from the inset of Fig. 3.

At a pressure of 5×10^{-4} Torr and a magnetic field of 500 G, the estimated value of q_s in metres was about $0.6 \pm 10\%$. The comparison of the experimental and theoretical values of q_s is difficult because of the uncertainty in the determination of the parameters T_i (and hence v_i) and λ_i . Values of T_i were measured using an ion-sensitive probe (Katsumata and Okaza¹⁶) and also compared with results using a multi-electrode probe. Typical ion temperature was estimated to be $1-0.5 \text{ eV} \pm 10\%$. Consequently, the error in the calculated ion Larmor radius $r_{ci} (= mv_i/eB)$ would not be more than 3%. For a value of B about 500 G, the ion Larmor radius was $2 \text{ mm} \pm 3\%$.

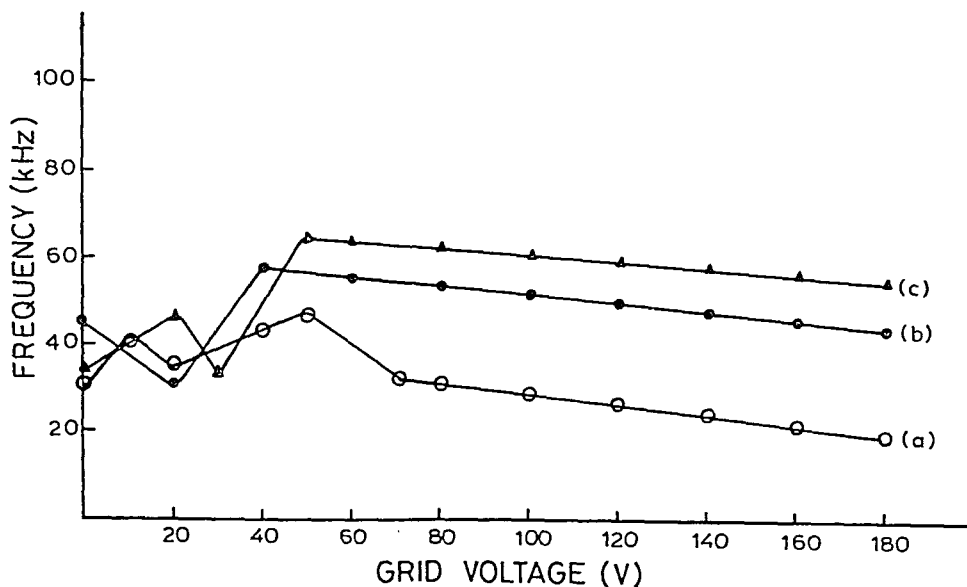


Fig. 2—Frequency of the observed plasma fluctuations at a gas pressure of 10^{-5} Torr [(a) at 300 G, (b) at 500 G, and (c) at 800 G]

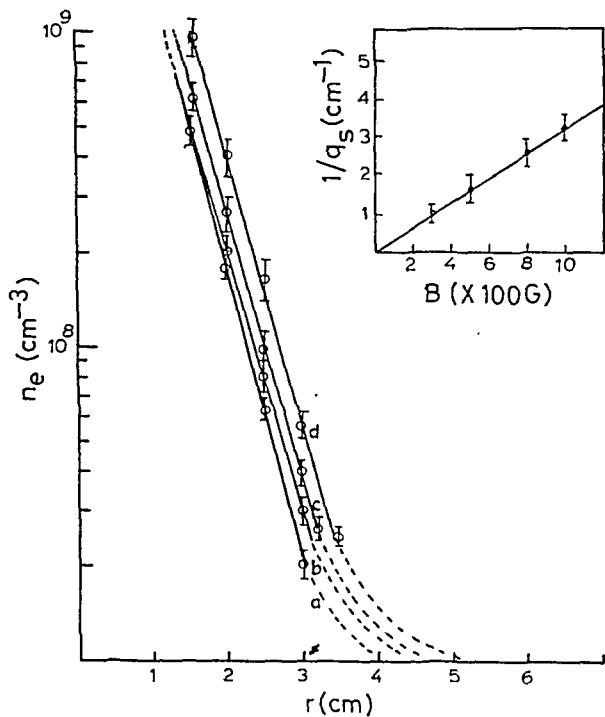


Fig. 3—Plots of the linear portions of log plasma density versus radial distance (r) at a pressure of 5×10^{-4} Torr. [Curves a, b, c, and d represent the probe theories: Kagan and Perel¹¹, Fujita and Akazaki¹², Langmuir and Blodgett¹³ and Polman¹⁴, respectively. Inset represents the relation between $1/q_s$ and B .]

The correct estimation of the ion mean free-path (λ_i) is influenced by the accuracy of determination of such parameters as: the gas pressure (p), the gas temperature (T_{gas}) and the ion-neutral particle collision cross-section (Q_{i-n}). The value of p was measured using a calibrated ionization gauge and a correction factor for hydrogen gas ($= 2.11$) was used. Still an experimental error in the value of p must be 8-10%. T_{gas} was assumed equal to room temperature (300 K), since the ratio of densities of ions and neutrals was only 1:1000. Values of Q_{i-n} was taken from different sources (e.g. Rapp and Francis¹⁷ and Drawin¹⁸). This value may have a 10% error. A total of 23% error must be allowed for q_s . Since the coefficient $D_{i\perp}$ depends upon the values of v_i^3 , λ_i , T_e and T_i , a total of about 50% error has to be allowed for the value estimated.

Assuming that the vacuum vessel contains mainly hydrogen ions ($T_i = 1-0.5$ eV), which were responsible for the density distribution, the e-folding length (q_s) of the hydrogen ions is calculated from Eq. (6). Substituting $\lambda_i = 5$ cm $\pm 20\%$, $p = 5 \times 10^{-4}$ Torr, $N_n = 5 \times 10^{13}$ cm $^{-3}$, $Q_{i-n} = 40 \times 10^{-16}$, value of q_s is found to be $2.5 r_{ci} \pm 23\%$, which value is in fair agreement with the experimental determination.

Since T_e/T_i in the present work is about 5, the rate of diffusion in the radial direction of the axial magnetic field was calculated using Eqs (3) and (5) and reported in Table 1.

Table 1—Comparison of Values of Diffusion Coefficient (D_i), Calculated Using Eqs (3) and (5)

[Gas Pressure = 5×10^{-4} Torr, $\lambda_i = 5$ cm and $v_i = 10^6$ cm/s]

B G	q_s cm	ω_{ci} s $^{-1}$	$D_{i\perp}$ (in cm 2 /s) calculated from	
			Eq. (3)	Eq. (8)
500	0.5	5×10^6	$8216 \pm 50\%$	2666
1000	0.3	1×10^7	$2957 \pm 50\%$	666

The diffusion coefficient can also be calculated theoretically from the estimated collision time (τ_i), using the equation¹⁹:

$$D_{i\perp}(\tau_i) = D_i^0/1 + \omega_{ci}^2 \tau_i^2 \quad \dots (7)$$

$$= D_i^0/\omega_{ci}^2 \tau_i^2 \quad \dots (8)$$

However, values of $D_{i\perp}(\tau_i)$ depend upon the collision time of the ions with neutral particles (τ_i). This quantity may not be determined better than a factor of 3. Hence the difference between the experimental [$D_{i\perp}(q_s)$] and theoretical [$D_{i\perp}(\tau_i)$] values of the diffusion coefficient may be expected to be one order of magnitude. Table 1 shows that the value of $D_{i\perp}(\tau_i)$ is lower than $D_{i\perp}(q_s)$ by a factor of 3 at low magnetic field. This difference rises to factor of 4, at a magnetic field of 100 G.

The agreement of the plots of N_e versus r from experimental observations with those based on Simon's theory, indicated that diffusion is mainly responsible for forming the density profile. Since the ratio L/λ_i observed during the present experiment to be 10 is larger compared to the value 3 found from calculations based on Simon's theory, it is evident that the ion gyro-radius effect should be less dominating compared to diffusion. According to Simon's theory, the value of L/λ_i should be chosen as high as possible in order that the plasma may come out of the region where the ion gyro-radius effect dominates. However, value of L/λ_i must be limited to such values at which the short-circuiting mechanism is still operative.

The measurements were repeated at the low pressure range (10^{-5} Torr), where λ_i is determined by ion-neutral particles collisions. In this pressure range, λ_i was about 2 m and thus $L < \lambda_i$. Simon's theory is modified in this case and the e-folding length is given by:

$$q_s = 0.5(L/\lambda_i)^{1/2} r_{ci} \quad \dots (9)$$

The e-folding length q_s is thus much smaller than r_{ci} so that the diffusion distribution is certainly lost in a density distribution given by the ion gyro-radius effect. Using the experimental curves of density as a function of radial distance (Fig. 4) q_s was determined at different magnetic fields. At B equal 500 G, q_s was

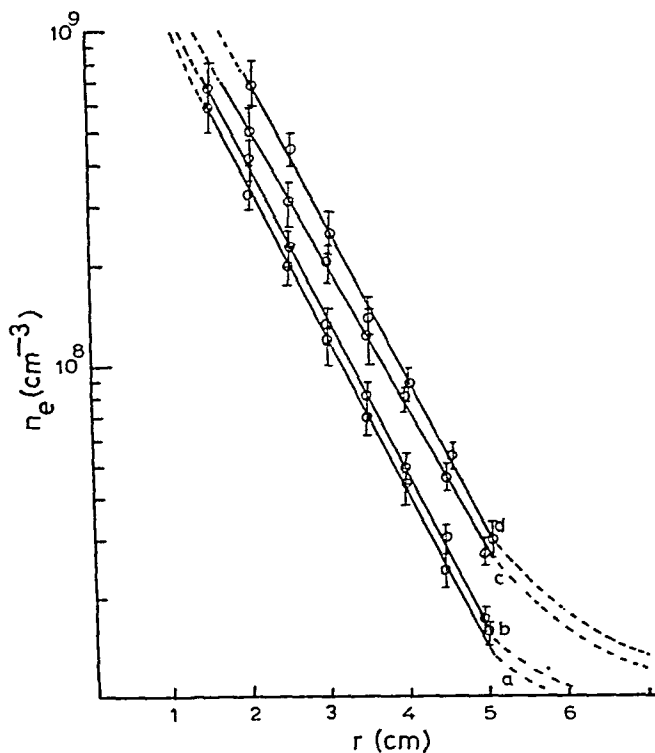


Fig. 4—Plots of linear portions of log plasma density versus radial distance (r) at a pressure of 10^{-5} Torr.

Table 2—Comparison of Values of Diffusion Coefficient (D_i) Calculated Using Eqs (3) and (8)

[Gas pressure = 10^{-5} Torr, $\lambda_i = 200$ cm, $v_i = 1.4 \times 10^6$ cm/s]

B G	q_s cm	ω_{ci} s^{-1}	$D_{i\perp}$ (in cm^2/s) calculated from	
			Eq. (3)	Eq. (8)
500	0.9	5×10^6	149×10^4	182
1000	0.5	1×10^7	46×10^4	45

about 0.9 cm which is about four times the gyro-radius r_{ci} . This is more than one order of magnitude higher than the theoretical calculation using Simon's theory [Eq. (9)]. The disagreement between the values of q_s experimentally determined and theoretically evaluated using Simon's formula shows that it is the ion gyro-radius effect which determines the radial density distribution at low pressures, i.e. when the ion mean free-path λ_i is much longer than the plasma beam length L . The measurements were also made at a higher magnetic field B (1000 G) and the same conclusion was arrived at. Values of D_i at the low pressure range for magnetic fields of 500 and 1000 G were also calculated. A comparison of the experimental $D_{i\perp}(q_s)$ and theoretical $D_{i\perp}(\tau_i)$ values is made in Table 2. The results show the considerable deviation between these two values when $\lambda_i > L$.

4 Conclusion

The ion density distribution in the radial direction is determined more by diffusion than by the ion gyro-radius effect, provided that the plasma length L is larger than the ion mean free-path λ_i so that a collisional, diffusion-determined model is set up. At low pressures, this is not the case since λ_i would be larger than L and, therefore, the density profile is probably determined by the ion gyro-radius effect.

Acknowledgement

The author thanks Prof. M G Rusbridge and Dr K Phillips, of the Institute of Science and Technology, University of Manchester (UMIST), for their interest and helpful discussions and also for providing experimental facilities. Thanks are also due to the British Council and to the Plasma Group at UMIST, for facilities provided.

Diffraction Intensities from Curved Crystallites with Layer Shift by $\varphi/3$

A K DATTA, B K ROY & S BHATTACHERJEE

Department of Physics, Indian Institute of Technology, Kharagpur 721 302

Received 26 July 1985; revised received 5 May 1986

Expressions for diffracted intensities from an aggregate of cylindrically curved crystallites according to the model proposed by G B Mitra and S Bhattacharjee [*Acta Crystallogr Sect B (Denmark)*, 31 (1975) 2851] have been derived assuming two different types of layer disorders as described by S Bhattacharjee *et al.* [*Indian J Pure & Appl Phys*, 18 (1980) 1]. Numerical computations have been carried out to study the effect of variation of the parameters on the diffracted intensities and the significant deviations from the intensities corresponding to ordered crystallites, are pointed out.

1 Introduction

In a recent publication, the present authors¹ derived expressions for the diffracted intensities of X-rays from an aggregate of cylindrically curved crystallites with different types of layer disorders. One of the disorders considered consists of a cylindrical layer displaced parallel to itself about the common axis by an angular distance $\varphi/2$ with respect to its adjacent layer. The other type of disorder is characterized by variability of interlayer spacings in layer lattices. The starting model and mathematical treatment were primarily based on the work of Mitra and Bhattacharjee². Following a similar approach, the intensity of X-rays diffracted by a conglomeration of disordered cylindrical crystallites with layer shift of the above type by an amount $\varphi/3$, analogous to $b/3$ shift in planar layer lattice, and with different extents of variability of interlayer spacings, has been worked out. All the symbols used in this work carry the same meaning as defined by Bhattacharjee *et al.*³

2 Derivation of Expression for Diffraction Intensity

Let the disordered cylindrical fragment consist of three different types of layers A, B and C. The crystallite starts with layer A which is taken as reference layer. B and C are shifted layers displaced by $\frac{1}{3}\varphi_m$ and $\frac{2}{3}\varphi_m$ respectively with respect to the reference layer where the subscript m denotes the position of the layer (Fig. 1). Let α_s be the probability of a mistake occurring to each added layer such that the sequence changes from AAA...BBB... or CCC... Assuming α_s to be the same for both types of mistakes and following Wilson⁴, it may be written as:

$$A_m + B_m + C_m = 1 \quad \dots (1)$$

where A_m , B_m and C_m are the probabilities of the m th layer being A, B or C respectively as defined by

Wilson⁴. According to Mitra and Bhattacharjee², the position vector \vec{r}_{nmt} of any lattice point occupying n th site in the m th arc or layer on the t th stack is described by the cylindrical coordinates $(R + mb)$, $n\varphi_m$ and t_c respectively. Due to layer shift as discussed above, the angular coordinate $n\varphi_m$ will be modified. Using Eq. (1), the average angular position of the lattice point can be written as $(n + B_m)\varphi_m$, since according to Wilson⁴ $B_m = C_m$. In the present model, only the azimuthal coordinate $n\varphi_m$ is to be replaced by $(n + B_m)\varphi_m$ for intensity calculation. The position vector \vec{r}_{nmt} can now be written as:

$$\vec{r}_{nmt} = \hat{i}_x(R + mb)\sin(n + B_m)\varphi_m + \hat{i}_y(R + mb)\cos(n + B_m)\varphi_m + \hat{i}_zt_c \quad \dots (2)$$

Using this value of \vec{r}_{nmt} and proceeding exactly in the same manner as that of Mitra and Bhattacharjee², the diffracted intensity, $I(h')$ from a conglomeration of identical cylindrical crystallites with layer shift can be shown to be given by:

$$I(h') = F'(h') \sum_{l_0} \frac{\sin^2(\pi T l_0)}{\sin^2(\pi l_0)}$$

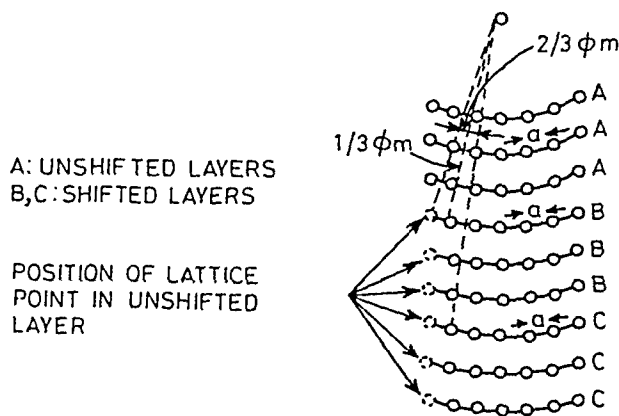


Fig. 1—Model of faulted cylindrical lattice with layer shift

$$\times \sum_{n,n',m,m'} J_0 \left(QNh' \left(1 - \frac{l_0^2}{r_1^2 h'^2} \right)^{1/2} \right) \times \left[(1 + mr_2 \varphi_0)^2 + (1 + m'r_2 \varphi_0)^2 - 2(1 + mr_2 \varphi_0)(1 + m'r_2 \varphi_0) \times \cos \frac{2\pi}{QN} \left\{ \frac{(n + B_m)}{(1 + mr_2 \varphi_0)} - \frac{(n' + B_{m'})}{(1 + m'r_2 \varphi_0)} \right\} \right]^{1/2} \quad \dots (3)$$

The common symbols have the same meanings as defined by Mitra and Bhattacharjee². If there is no slip, $B_m = B_{m'} = 0$ and Eq. (3) reduces exactly to Eq. (13) of Mitra and Bhattacharjee², as expected.

The second type of stacking fault is characterized by variability of interlayer spacings and consists of b being variable to the extent that b due to faulting is $b + gb$, where $|g|$ is a small fraction assumed to be constant. Following arguments similar to those of Wilson⁴, the average radial position of the m th layer has been worked out by Bhattacharjee *et al.*³ and is equal to $R + mb(1 + \alpha_c g)$, where α_c is the probability of a layer being so faulted. So to obtain intensity expression when both the faults are coexistent, we simply replace b by $b(1 + \alpha_c g)$ or r_2 (which is equal to b/a) by Ar_2 where $A = 1 + \alpha_c g$ in Eq. (3). The final expression for intensity from such a system is:

$$I(h') = F^2(h') \sum_{l_0} \frac{\sin^2(\pi T l_0)}{\sin^2(\pi l_0)}$$

$$\times \sum_{n,n',m,m'} J_0 \left(QNh' \left(1 - \frac{l_0^2}{r_1^2 h'^2} \right)^{1/2} \right) \times \left[(1 + mAr_2 \varphi_0)^2 + (1 + m'Ar_2 \varphi_0)^2 - 2(1 + mAr_2 \varphi_0)(1 + m'Ar_2 \varphi_0) \times \cos \frac{2\pi}{QN} \left\{ \frac{(n + B_m)}{(1 + mAr_2 \varphi_0)} - \frac{(n' + B_{m'})}{(1 + m'Ar_2 \varphi_0)} \right\} \right]^{1/2} \quad \dots (4)$$

Eq. (4) is the general expression for the diffracted intensity from an aggregate of disordered cylindrical crystallites with both the stacking faults as discussed. For crystallites without any defects $B_m = B_{m'} = 0$, $g = 0$ and Eq. (4) reduces again to Eq. (13) of Mitra and Bhattacharjee² as expected.

3 Results and Discussion

Numerical computations for typical cases have been carried out based on Eqs (3) and (4). The results of the calculations are shown in Figs 2-4.

Fig. 2 shows the variational patterns of intensities from crystallites with layer shift and with variability. The patterns follow more or less the same form as that for ordered crystallites having maxima nearly at identical positions. As expected, the heights and sharpness of the principal maxima decrease with defect—the effect being more apparent in case of variability. The secondary peaks are in general, broad

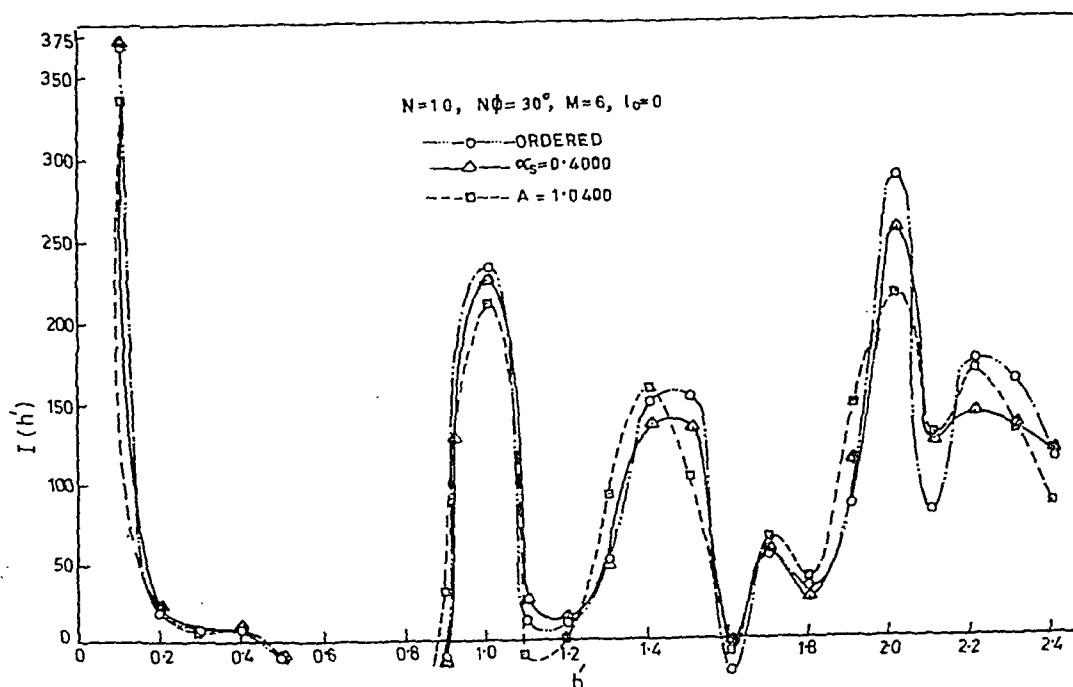


Fig. 2—Diffracted intensities from an axially parallel aggregate of cylindrical crystallites with ordered arrangement, with layer shift (α_s) and with variability (A)

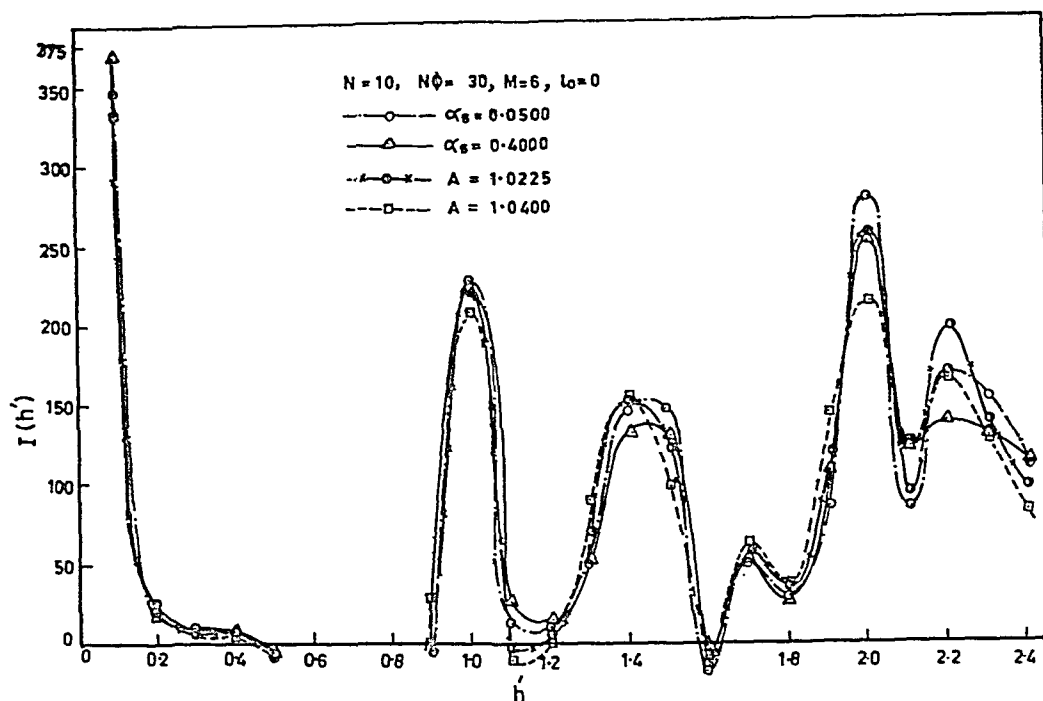


Fig. 3—Diffracted intensities from an axially parallel aggregate of cylindrical crystallites with different values of layer shift (α_s) and with different values of variability (A)

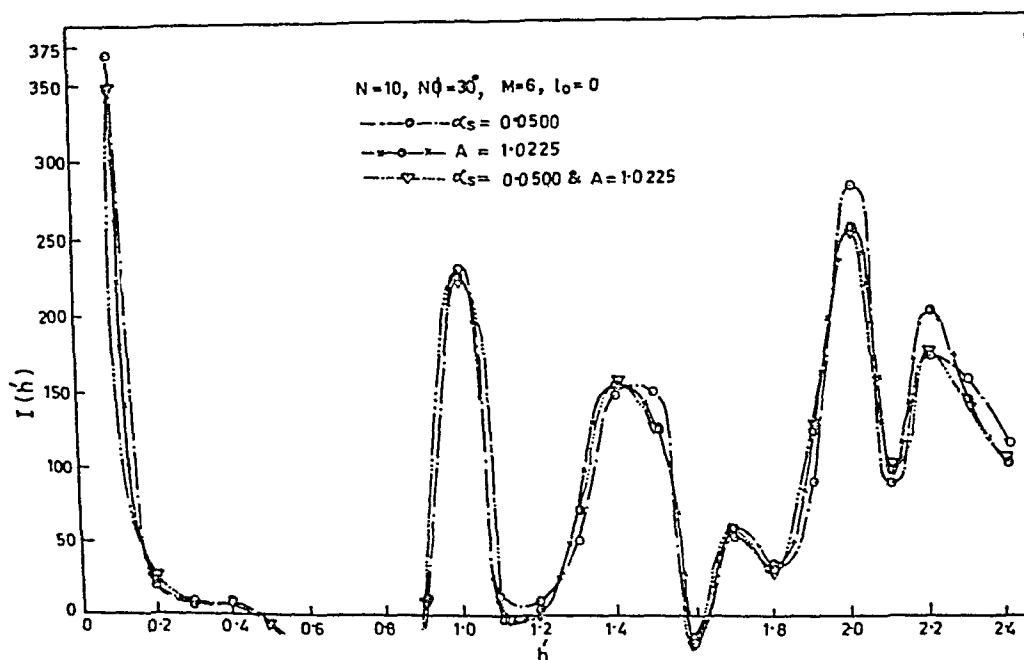


Fig. 4—Diffracted intensities from an axially parallel aggregate of cylindrical crystallites with layer shift (α_s), or variability (A) and with both the defects simultaneously present

with a tendency to shift towards the higher angle side. However, for these peaks the broadening is found to be more due to layer shift defect. It is observed that the peak around $h' = 1.4$ shifts towards the lower angle side due to variability defect as compared to peaks due to ordered crystallites and crystallites with layer shift. Unlike the principal maxima, the secondary ones appear to be affected more by the layer shift defect.

Fig. 3 reveals more or less the same features. A close examination, however, reveals that the effect of increasing α_s , in general, is to decrease the heights and increase the broadening of the peaks. Increase of variability has also similar effects. Comparison of these results with those reported by the authors³ for $\varphi/2$ shift shows that the changes of the corresponding features of the pattern are greater in case of $\varphi/3$ shift.

These observations are similar to those reported by Roy *et al.*⁵ for the model of crystallites developed by Mitra and Bhattacharjee⁶. Fig. 4 reveals one very interesting feature of the diffraction pattern from crystallite configuration where both the defects coexist. At the principal maxima (at $h' = 1$ and 2), the effect of combined defects is to reduce the peak heights compared to that for the individual defect, whereas at the other points the effect is not so noticeable. It is also observed that the diffraction intensities from crystallites with both the defects are almost identical with those from crystallites with variability having the same A value. This observation leads us to conclude that when both the defects are present, it is the variability which will affect the intensity more than the layer shift. On the other hand, independently, the effect of layer shift is more pronounced. Thus we can conclude that the effect of the defects, is general, is a diminution of peak heights accompanied by broadening and slight shift of peak positions. The secondary peaks are affected more by layer shift whereas the primary ones are more affected by variability.

4 Concluding Remarks

Several minerals such as chrysotile and halloysite are found to have cylindrical lattices. Assuming the

model to be similar to the one described by Mitra and Bhattacharjee² and considered in the present work, attempts have been made by Toman and Frueh⁷, and Mitra and Bhattacharjee² to solve the structures of chrysotile and halloysite respectively with appropriate diffraction theories developed by them. However, their theoretical predictions agreed only partially with experimental observations. This partial agreement may be attributed to the fact that none of these authors considered in their analyses the types of defects discussed here which are quite likely to be present in natural mineral samples. Hence, the results of the present calculations may find useful applications in solving such practical problems more convincingly.

References

- 1 Datta A K, Roy B K & Bhattacharjee S, *Z Kristallog (Germany)*, **172** (1985) 71.
- 2 Mitra G B & Bhattacharjee S, *Acta Crystallogr Sect B (Denmark)*, **31** (1975) 2851.
- 3 Bhattacharjee S, De A K & Roy B K, *Indian J Pure & Appl Phys*, **18** (1980) 1.
- 4 Wilson A J C, *X-ray optics* (Methuen, London), 1962.
- 5 Roy B K, De A K & Bhattacharjee S, *Acta Crystallogr Sect A (Denmark)*, **36** (1980) 153.
- 6 Mitra G B & Bhattacharjee S, *Acta Crystallogr Sect A*, **27** (1971) 22.
- 7 Toman K & Frueh A J (Jr), *Acta Crystallogr Sect A*, **24** (1968) 364.

Electrical & Optical Properties of Flash Evaporated CuInSe₂ Thin Films

D SRIDEVI & K V REDDY

Department of Physics, Indian Institute of Technology, Madras 600 036

Received 24 July 1985; revised received 6 February 1986

Finely powdered, pre-reacted, polycrystalline CuInSe₂ was flash evaporated onto glass substrates. The thin films obtained in this manner were characterized by Transmission Electron Microscopy (TEM). The optical absorption of the films was studied in the spectral range 700-1300 nm and analyzed. The effect of the background absorption on the absorption spectrum is discussed. From this analysis, the band-gap of CuInSe₂ is found to be 1.02 ± 0.01 eV. All films deposited were of *p*-type. The electrical conductivity of the films was measured in the temperature range 77-550 K by four-probe technique with indium pressure contacts. The activation energy of 100 meV obtained at high temperature is attributed to acceptor copper vacancies.

1 Introduction

The I-III-VI₂ ternary semiconductors crystallize in the chalcopyrite structure, which belongs to the space-group *I-4 2d*. They are the ternary analogues of the binary II-VI compounds (ZnS, ZnSe, CdS, etc.). This class of semiconductors covers a wide band-gap range (1.0-2.5 eV) and all of them have a very small lattice-mismatch with CdS, a wide band-gap semiconductor used in heterojunction solar cells as an *n*-type window. Moreover, most of them can be made either *n*- or *p*-type conducting. Hence, the chalcopyrites are very important in the field of photovoltaics. In fact, a 12% efficient single crystal solar-cell of *p*-CuInSe₂/CdS has been reported by Shay *et al.*¹ The space-group *I-4 2d* is an anisotropic, non-centrosymmetric crystal structure and permits non-linear optical properties and birefringence and is suitable for phase-matched parametric optical mixing. An excellent review of the ternary chalcopyrites is found in the book by Shay and Wernick².

The valence-band structure of the ternary chalcopyrites has been investigated by many research workers by utilizing the technique of electroreflectance³⁻⁵. The three-fold degeneracy of the *p*-like Γ_{15} level in the zinc-blende compounds is completely lifted by the combined influences of the spin-orbit interaction and the non-cubic crystalline field. The direct band-gaps of the I-III-VI₂ compounds are low relative to their binary analogues due to a partial cancellation of the positive spin-orbit parameters for *p*-levels and negative ones for *d*-levels. The presence of the *d*-levels has been directly observed in the electroreflectance spectra³. The technique of optical absorption in thin films has also been used by various workers⁶⁻⁸ to identify the three basic energy-gaps *A*, *B* and *C* which correspond to the forbidden band-gap, the crystal field split and the spin-orbit split levels respectively.

In the present study, the optical absorption and electrical conductivity of flash evaporated thin films of CuInSe₂ have been studied. The effect of the background absorption (BA) on the optical absorption spectrum has been investigated. Loferski⁹ has reviewed the performance of CuInSe₂/CdS thin film solar cells prepared by various techniques and it has been concluded that the flash evaporated and sputtered films were more nearly stoichiometric and of more reproducible compositions. Hence, the flash evaporation technique has been used for thin film preparation in our study. The compound CuInSe₂ has been studied by various research workers by different techniques. Shay *et al.*⁵ reported a band-gap of 1.04 eV by the electroreflectance technique, whereas, from the slope of the intrinsic region of electrical conductivity¹⁰, the intrinsic band-gap was found to be 1.07 eV. At least two donor and one acceptor levels were identified for CuInSe₂ by electrical conductivity and photoconductivity techniques¹¹. From electrical transport measurements on thin films¹², hole mobilities in the range 1-8 cm²/Vs were reported. From the photoconductivity of vacuum-deposited films¹³, decay times of the order of 1 ms for *p*- and *n*-type films were observed¹².

The optical absorption in flash evaporated CuInSe₂ thin films was studied by Horig *et al.*⁸ and the fundamental band-gap found to be 1.02 eV. An analysis of the spectrum enabled them to calculate the energy level *B* to be 1.03 eV. Neumann *et al.*⁷ have also studied the optical absorption of thin films of CuInSe₂ and reported the band-gap as 1.01 eV and the energy level *C* to be 1.25 eV. The three energy levels *A*, *B* and *C* were found to be 1.04, 1.04 and 1.27 eV respectively by electroreflectance measurements⁴.

2 Experimental Details

Preparation of CuInSe₂—Polycrystalline bulk of

CuInSe_2 was prepared by fusing together, stoichiometric quantities of 99.999% pure Cu, In and Se in evacuated quartz ampoules at 1150°C . The formation of good single phase chalcopyrite was verified by X-ray powder diffraction technique. The composition analysis of the bulk was done by Electron Probe Micro Analysis (EPMA) using pure copper and indium antimonide as standards and Se was estimated by the difference of atomic per cent. Point analysis at various regions of the ingot showed that the entire ingot was homogeneous and stoichiometric. The polycrystalline charge thus obtained was finely powdered and used for flash evaporation.

Thin film coating—A simple flash deposition technique developed in our laboratory was employed for coating CuInSe_2 thin films. A calling-bell type plunger was used as the vibrator, the amplitude of which was varied with the help of a variac. The hopper was filled with the finely powdered CuInSe_2 and vibrated with the help of the vibrator. The powder fell on to a tantalum boat at 1300°C and evaporated instantaneously. The evaporation was carried out in a Hind Highvac coating unit under a vacuum of 10^{-5} Torr. Thin films of thickness in the range $0.1\text{--}0.5\ \mu\text{m}$ were coated on glass substrates. The substrate temperature was 300 K in all the cases.

Transmission electron microscopy (TEM)—The films with minimum thickness were used for TEM. From the selected area diffractogram (SAD), it was clearly seen that the films are polycrystalline. From the diameter of the rings obtained, the lattice parameters of CuInSe_2 were calculated as $a = 5.85 \pm 0.03\ \text{\AA}$ and $c = 11.76 \pm 0.03\ \text{\AA}$ which are in good agreement with the bulk values reported earlier¹³.

Optical absorption—The optical absorption of as-deposited films was recorded in the spectral region 700–1300 nm using CARY 2300 spectrophotometer and the spectrum is shown in Fig. 1.

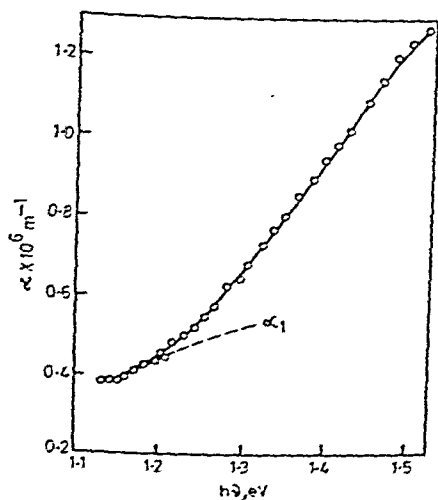


Fig. 1—Optical absorption spectrum of flash evaporated CuInSe_2 thin films before background correction

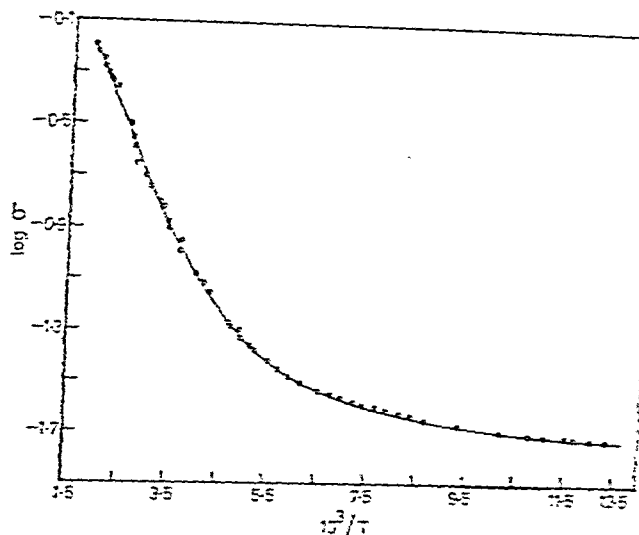


Fig. 2—Arrhenius plot of conductivity of CuInSe_2 thin films

Electrical conductivity—The electrical conductivity of the films was measured by the four-probe technique in the temperature range 77–550 K. The conductivity type of the film was separately tested by applying a lateral temperature gradient across the film and noting the direction of the developed thermo-emf. All films were found to be of *p*-type. The films used for these studies were evaporated through a specially designed contact mask, made photolithographically which gives films with four specific contact geometries. Steady-state measurements were made using indium pressure contacts which showed good ohmic nature. Fig. 2 shows the Arrhenius plot of conductivity of CuInSe_2 films.

3 Absorption Spectral Studies

3.1 Analysis of the Absorption Spectrum

Usually, the absorption is very weak for semiconductor films below the fundamental absorption edge (FAE) and the absorption coefficient (α) oscillates due to interference effects in the film and in the substrates. These interference effects can be neglected for films deposited on thick non-absorbing substrates near the FAE¹⁴. The relations for the spectral dependence of the transmittance (*T*) were given by Heavens¹⁵. These expressions have been modified by Neumann *et al.*⁶ for this case, and are adopted in the present work. A binary search procedure was adopted to solve the transmission expressions for the absorption index and then calculate α . In order to do this, the refractive index of the chalcopyrite was assumed to be a constant⁸ ($n = 3.1$).

An analysis of the absorption spectrum shows that the initial rise of α , for $h\nu \leq 1.20\ \text{eV}$ corresponds to a direct allowed transition of the form

$$\alpha = \frac{A}{h\nu} (h\nu - E_{g1})^{1/2} \quad \dots(1)$$

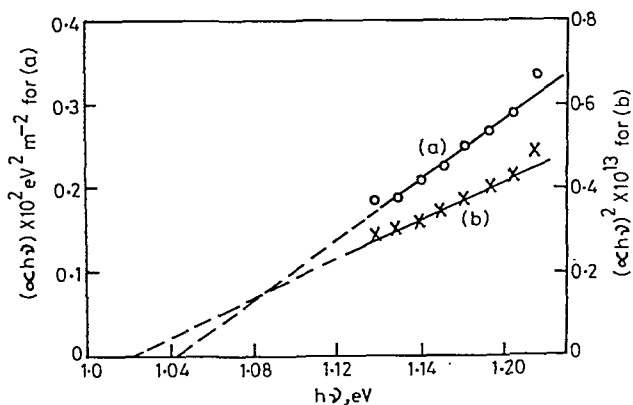


Fig. 3—Plot of $(\alpha h\nu)^2$ vs $h\nu$ showing $E_{g1} = 1.04$ eV for (a) and $E_{g1} = 1.02$ eV for (b)

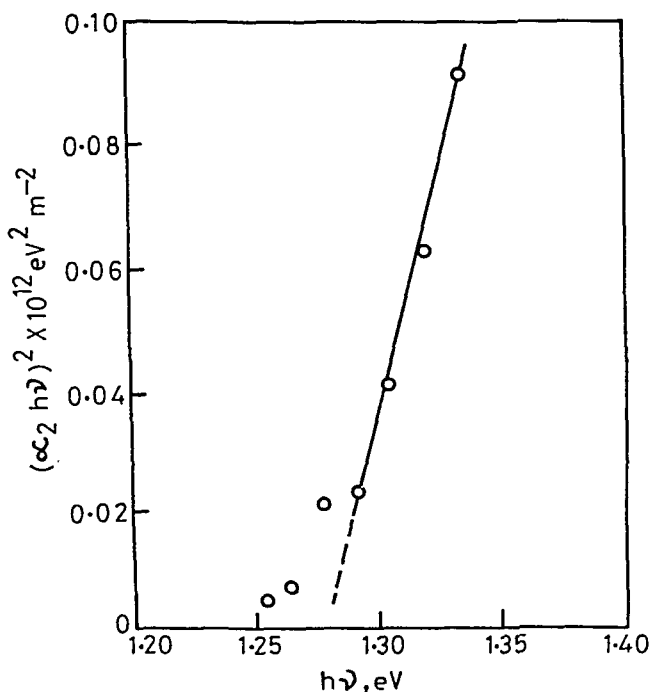


Fig. 4—Plot of $(\alpha_2 h\nu)^2$ vs $h\nu$ showing $E_{g2} = 1.28$ eV

with $E_{g1} = 1.04 \pm 0.01$ eV. A plot of $(\alpha h\nu)^2$ vs $h\nu$ is shown in Fig. 3. For energies greater than 1.20 eV, the observed optical absorption is always greater than the values α_1 , given by Eq. 1. This is due to the onset of additional absorption process. An analysis of the additional absorption coefficient $\alpha_2 = \alpha - \alpha_1$ shows that α_2 can again be described by a direct allowed transition given by Eq (1) with $E_{g2} = 1.28 \pm 0.01$ eV. Fig. 4 shows a plot of $(\alpha_2 h\nu)^2$ vs $h\nu$ for $h\nu > 1.20$ eV.

3.2 Effect of BA on Optical Absorption

In the above analysis, a perfectly smooth film on a perfectly smooth substrate has been assumed. The effect of surface imperfections (due to surface roughness) and the volume imperfections (due to grain boundaries, inclusions, stoichiometry deviations, etc.)

has been completely ignored. A model has been proposed by Pawlikowski¹⁶ for the analysis of α which takes into account the surface and volume imperfections. Within this model, for highly absorbing semiconductor films supported on thick non-absorbing substrates, the 'real' absorption coefficient of the film (α_2) due to valence band-conduction band transitions is given by

$$\alpha_2 d_2 + \alpha_2^i d_2 + \alpha_3 d_3 + A_s'' =$$

$$\ln \left[\frac{(1 - R_{12}^0)(1 - R_{23}^0)(1 - R_{34}^0)}{T} \right] \quad \dots(2)$$

where, the subscripts 1, 2, 3 and 4 refer to air, film, glass and air respectively and d_2 and d_3 are the respective thicknesses of the film and substrate. The term α_2^i is the absorption coefficient due to volume imperfections both physical (caused by the changes in the dielectric constant due to stoichiometry deviations, compositional changes due to adsorbing/doping, band-bending at the surface, differential thermal expansion at the interfaces, etc.) and geometrical imperfections (due to surface roughness, grain boundaries, etc.); α_3 is the absorption in the third medium, i.e. glass substrate. A_s'' characterizes the optical losses on the surface imperfections due to multiple reflections. The terms in RHS of Eq. 2 R_{lm}^0 (l, m are 12, 23, 34 etc.) refer to the reflectivity of the interfaces l and m and T is the experimental transmission ratio. The sum $(\alpha_2 d_2 + \alpha_3 d_3 + A_s'')$ represents the background absorption. The detailed procedure for the estimation of BA is already described in Ref. 16.

The BA of CuInSe₂ films was calculated¹⁶ using $\chi_2 = 0.1$, δ as 10% of the film thickness, $n_4 = n_1 = 1$, $n_3 = 1.5$, and the energy dependence on n_2 , the refractive index of CuInSe₂, was taken from Horig *et al.*¹⁷ A plot of the estimated BA is shown in Fig. 5, along with the individual contributions A_s'' and $\alpha_2^i d_2$. The reflectivity R_{12}^0 was calculated using $n_2 = 3.1$ and assumed

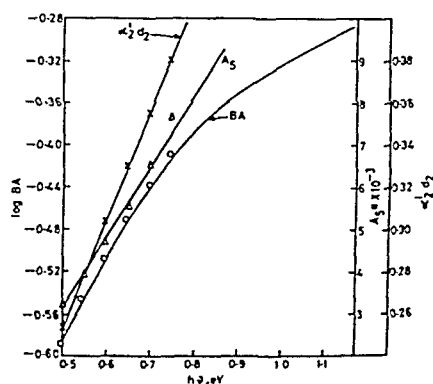


Fig. 5—Background absorption for CuInSe₂ thin films

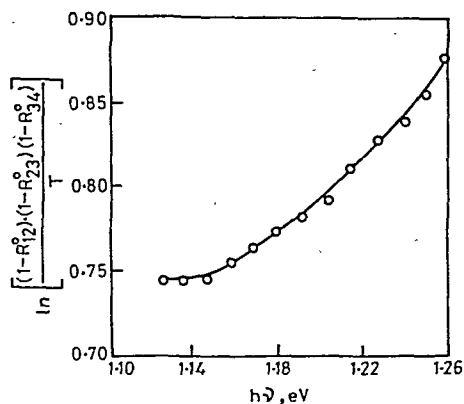
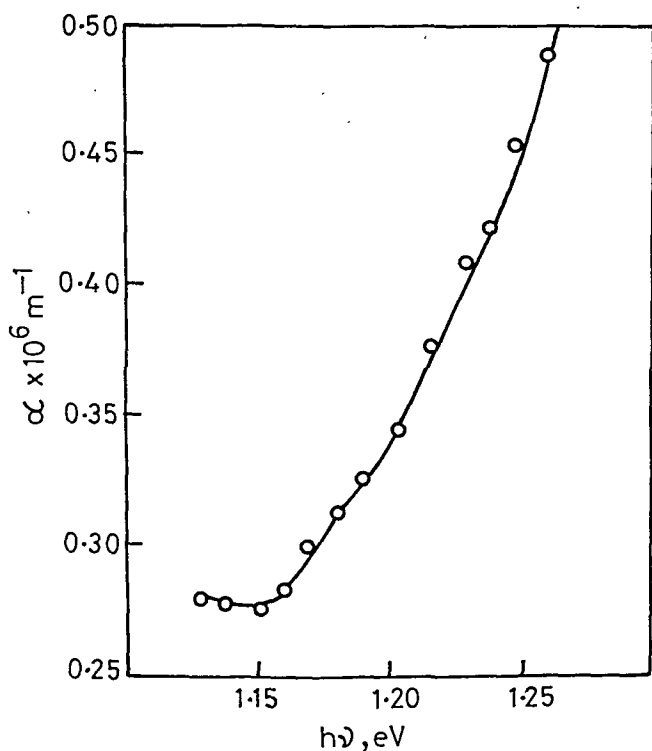


Fig. 6—Plot of RHS of Eq. (2)


 Fig. 7—Optical absorption of CuInSe₂ thin films corrected for the background absorption

constant throughout. The energy dependence of the RHS of Eq. (2) is shown in Fig. 6. The absorption coefficient α_2 of CuInSe₂ was corrected for BA and plotted in Fig. 7. Although the numerical values of α in Fig. 1 and Fig. 7 are not much different, the absorption edge sharpens quite a bit due to the elimination of most of the tail-states caused by surface adsorption of moisture and ambients.

Analysis of this absorption coefficient shows that the initial portion of the absorption spectrum is once again described by direct allowed transition [Eq. (1)] with a band gap of 1.02 ± 0.01 eV.

4 Discussion

4.1 Electrical Conductivity

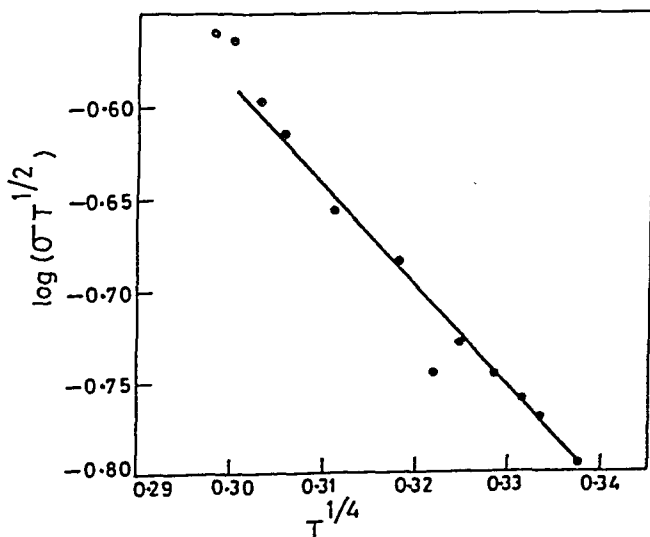
The Arrhenius plot of conductivity of CuInSe₂ films in the temperature range 500-77 K is shown in Fig. 2.

From the plot, we can see two distinct regions of conductivity. In the low temperature range from 110-77 K, the conductivity has an activation energy of 3×10^{-3} eV, and in the range 500-300 K, the activation energy is about 80 meV. Sobotta *et al.*¹¹ have discussed the influence of impurities and free carriers on the properties of CuInSe₂ and concluded that at least two donor states and one acceptor state are simultaneously present in the crystals. Various workers^{18,19,20} give three acceptor states $E_{A1}=20-40$ meV, $E_{A2}=85-100$ meV and $E_{A3}=400$ meV. All the films studied here were of *p*-type. Considering the vapour pressure data²¹ of In₂Se and Se₂, it may be seen that the vapour pressure of Se₂ is higher than that of In₂Se near the melting temperatures. Hence, selenium vacancies are the most probable defects for the bulk and Cu vacancies for thin films. If we consider CuInSe₂ in the covalent model, copper vacancies are acceptors. Hence, it is reasonable that all the films coated here are of *p*-type.

The low activation energy on the low temperature side may be due to variable range hopping conduction. Indeed, plots of $\log(\sigma T^{1/2})$ vs $T^{-1/4}$ (Fig. 8a) are linear in this temperature range indicating the validity of this conduction mechanism. In the temperature region above 150 K, a plot $\log(\sigma T^{1/2})$ vs $10^3/T$ was made, so as to include the grain-boundary effects taking into account the polycrystalline nature of the films (Fig. 8b). This plot shows two linear portions, viz. (i) 100-250 K with activation energy of 100 meV and (ii) 250-150 K with activation energy of 25 meV.

The shallow acceptor ionization energy was estimated from the hydrogenic model to be 114 meV using

$$E_a = 13.6 \left\{ \frac{m_p/m_o}{\epsilon_s^2} \right\} \quad \dots(3)$$


 Fig. 8a—Plot of $\log(\sigma T^{1/2})$ versus $T^{-1/4}$ showing hopping conduction in CuInSe₂ thin films below 120 K

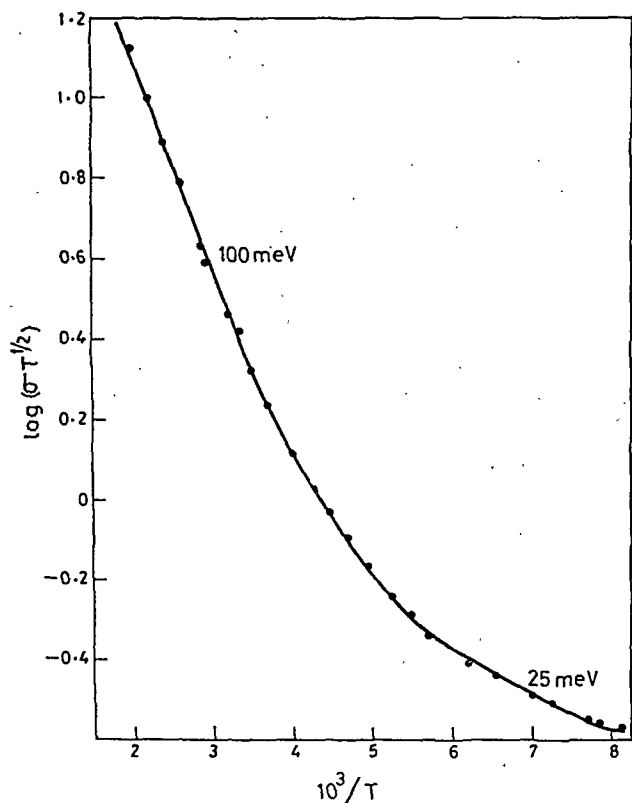


Fig. 8b—Plot of $\log(\sigma T^{1/2})$ versus $10^3/T$ showing grain boundary and impurity in CuInSe_2 thin films

with $(m_p/m_o)=0.73$ and $\epsilon_s=9.3$ (Ref. 22). This value is in good agreement with the activation energy obtained from Fig. 8b in the temperature range 500-250 K. The activation energy of 25 meV obtained in the range 250-150 K, is due to grain-boundaries.

4.2 Optical Properties

The energy band-gaps A and C found in our study, using the method reported in Sec 3.1, are 1.04 eV and 1.28 eV respectively. From these values, the spin-orbit splitting Δ_{so} is calculated to be 0.24 eV, which is in very good agreement with those reported by electro-reflectance and optical absorption studies. Subtracting the effect of BA makes the absorption edge rather sharp, but does not make much difference in the value of the fundamental band-gap.

Horig *et al.*⁸ have performed an analysis similar to that discussed in Sec. 3.1 in the present work. They have studied flash-evaporated CuInSe_2 thin films. From their analysis, they obtained the energy-gaps A and B to be 1.02 and 1.03 eV respectively but no report of the energy-gap C has been made so far from the optical studies for flash-evaporated thin films.

In the method proposed by Pawlikowski¹⁶, the effects of BA, the tail-states, etc., have been removed and so the value of the band-gap is more reliable. Since this method is applicable only in the vicinity of FAE, in the case of the chalcopyrites, this method cannot be used as it is to get the energies B and C , whereas, the method proposed by Neumann *et al.*⁷ yields these values readily.

References

- 1 Shay J L, Wagner S & Kasper H M, *Appl Phys Lett (USA)*, **27** (1975) 89.
- 2 Shay J L & Wernick J H, *Ternary chalcopyrite semi-conductors: growth, electronic properties and applications* (Pergamon Press, London) 1st Edn, 1975.
- 3 Tell B, Shay J L & Kasper H M, *Phys Rev B(USA)*, **4**(1971) 2463.
- 4 Thwaites M J, Tomlinson R D & Hampshire M J, *Solid-State Commun (USA)*, **23** (1977) 905.
- 5 Shay J L, Tell B, Kasper J M & Schiavone L M, *Phys Rev B (USA)*, **7** (1973) 4485.
- 6 Neumann H, Horig W, Reccius E *et al.*, *Thin Solid Films (Switzerland)*, **61** (1979) 13.
- 7 Neumann H, Perl T, Abdul Hussein N A K, *et al.*, *Crystal Res & Technol (Germany)*, **17** (1982) 469.
- 8 Horig W, Neumann H, Sobotta H *et al.*, *Thin Solid Films (Switzerland)*, **48** (1978) 67.
- 9 Loforski J J, *Thin film heterojunction solar cells based on n-CdS and p-Cu ternary alloys*, paper presented to the International Workshop on Physics of Semi-conductor Devices, New Delhi, India, 23-28 November 1981.
- 10 Zhuze V P, Sergeeva V M & Sutrum E L, *Sov Phys-Tech Phys (USA)*, **3** (1958) 1925.
- 11 Sobotta H, Neumann H, Riede V, *et al.*, *Phys Status Solidi a (Germany)*, **60** (1980) 531.
- 12 Kazmerski L L, Ayyagari M S, White F R & Sanborn G A, *J Vac Sci & Technol (USA)*, **13** (1976) 139.
- 13 Sridevi D & Reddy K V, *Mater Res Bull (USA)*, **20** (1985) 929.
- 14 Vaidhyanathan R, *Electrical and optical properties of ternary chalcopyrite semi-conductors AgInSe₂ and AgInTe₂*, Ph.D thesis, Indian Institute of Technology, Madras, 1984.
- 15 Heavens O S, *Optical properties of thin solid films* (Dover Publications, New York) 1965.
- 16 Pawlikowski J M, *Determination of absorption coefficient of a real semi-conductor film: Application to ZnSe*, paper presented to 6th International Conference on Thin films, Stockholm, Sweden, August 1984.
- 17 Horig W, Neumann H, Savlev V & Lagzdonis J, *Phys Lett A (Netherlands)*, **78** (1980) 189.
- 18 Rincon C, Gonzalez J & Perez G S, *J Appl Phys(USA)*, **54**(1983) 6634.
- 19 Schumann B, Georgi C, Tempel A, *et al.*, *Thin Solid Films (Switzerland)*, **52** (1978) 45.
- 20 Horig W, Kuhn G, Moller W *et al.*, *Krist & Tech (Germany)*, **14** (1979) 229.
- 21 Neumann H, *Crystal Res & Technol (Germany)*, **18** (1983) 483.
- 22 Irie T, Endo S & Kimura S, *Jpn J Appl Phys (Japan)*, **18** (1979) 1303.

Investigations of the Effect of Diode Geometry on the Reverse Recovery Experiments on Solar Cells

S K AGARWAL & HARSH

Solid State Physics Laboratory, Lucknow Road, Delhi 110007

Received 4 October 1985; revised received 3 June 1986

The storage time (t_s) of solar cells is measured as a function of I_F/I_R (I_F and I_R being the forward and reverse currents respectively), keeping I_F constant. It is observed that values of t_s obtained at any fixed value of I_F/I_R ratio are different and depend upon the value of I_F and the geometry, i.e. W/L ratio of the diode (W being the thickness of the diode and L the minority carrier diffusion length). Also the slope of the linear plots of t_s versus $\ln(1 + I_F/I_R)$ depends upon the value of I_F and not upon the I_F/I_R ratio. The analysis of the data obtained reveals that the value of minority carrier lifetime calculated using H J Kuno's formula [*IEEE Trans Electron Devices (USA)*, 11 (1964) 8] is nothing more than a time constant. The minority carrier lifetime in the base of a diode is a function of the injection level and can be obtained only on the application of a correction for the diode geometry to the time constant obtained from Kuno's formula.

1 Introduction

Minority carrier lifetime measurement and its control in semiconductor device fabrication has been of great interest from the beginning of semiconductor technology. Gossick¹ and Lederhandler and Giacolitto² gave the first method commonly known as open circuit voltage decay (OCVD) to measure the minority carrier lifetime in the $p-n$ junction devices. Kingston³ and Lax and Neustadten⁴ studied the switching behaviour of $p-n$ junction diodes and derived the switching time equations. Based on the switching behaviour of the $p-n$ junction diodes, Kingston³, Kuno⁵ and Dean and Nuese⁶ gave a relation connecting the minority carrier lifetime and the storage time of the injected carriers. This storage time is measured following the reverse current transient method commonly known as the reverse recovery (RR) method.

2 Experimental Details

The storage times (t_s) of a number of silicon solar cells and indium-alloyed Ge diodes of different thicknesses were measured as a function of the ratio of forward-to-reverse current (I_F/I_R), keeping I_F constant where I_F and I_R are the forward and reverse currents respectively. The observations were made on typical Si solar cells for five values of I_F . It was observed that the values of t_s obtained at a fixed value of I_F/I_R ratio were different for different I_F values.

Sample Fabrication—The solar cell studied was n^+p silicon solar cell fabricated in our Laboratory. The diode was fabricated using 270 μm thick p -type silicon wafer of 10 ohm-cm resistivity obtained from M/s Wacker Chemitronic Co, Germany. The POCl_3 technique was used to diffuse phosphorus to a depth of

$\sim 0.6 \mu\text{m}$. The surface concentration of the diffused layer was $\sim 2 \times 10^{19}/\text{cm}^3$. The diode area was $4 \times 10^{-2} \text{ cm}^2$.

3 Results and Discussion

Storage time of the diode was measured as a function of I_R keeping I_F constant at five different values of I_F which corresponded to the injected carrier concentrations of 2×10^{14} , 4×10^{14} , 1.6×10^{15} , 2.4×10^{15} and 4×10^{15} atoms per cm^3 respectively. Plots of storage time t_s versus $\ln(1 + I_F/I_R)$ are found to be linear for all the five sets of values of I_F as shown in Fig. 1. As suggested by Kuno⁵, the slope of these plots should give the minority carrier lifetime of the base of

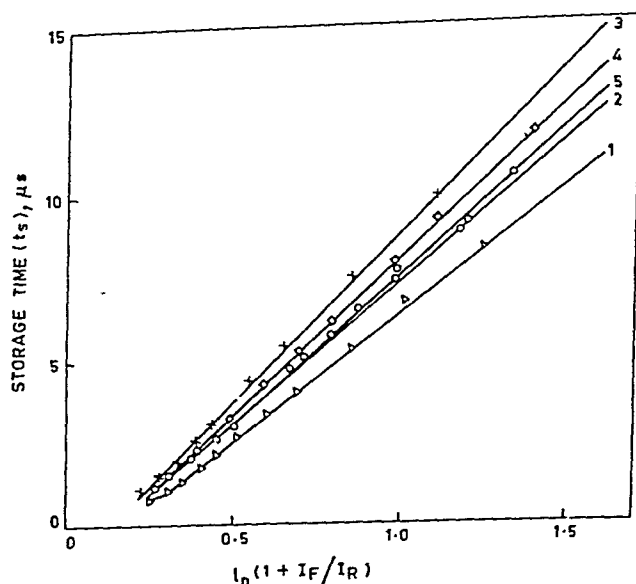


Fig. 1—Storage time (t_s) as a function of $\ln(1 + I_F/I_R)$ for silicon solar cells [Curves 1, 2, 3, 4 and 5 correspond to I_F values of 2, 4, 16, 24 and 40 mA respectively.]

the diode and accordingly the value of t_s should be the same for same I_F/I_R ratio at all the values of I_F . It is observed from Fig. 1 that the storage time values measured for different I_F values are different at the same value of I_F/I_R ratio. It can also be seen from Fig. 1 that the slope of these curves which is a measure of minority carrier lifetime⁵ (τ), first increases with increasing values of I_F and then starts decreasing at larger values of I_F . Fig. 2 shows the variation of t_s with $\ln(1 + I_F/I_R)$ keeping I_R constant.

We have earlier reported^{7,8} that the minority carrier lifetime increases monotonically with the injection level. Therefore, the apparent variation in slope of the plots in Fig. 1 can be explained in the following manner. Kuno's formula to calculate minority carrier lifetime τ from the slope of t_s versus $\ln(1 + I_F/I_R)$ plot is only valid under the low injection condition and in the case of infinitely thick-base diodes, i.e. for $W/L \gg 1$, where W is the thickness of the base and L the minority carrier diffusion length in the base. In this case at low injection, we obtain the value of τ to be $8 \mu\text{s}$ from the slope of the curve 1 in Fig. 1. The value of diffusion coefficient (D), at low injection is $32 \text{ cm}^2/\text{s}$ (Ref. 9). Calculation of minority carrier diffusion length $L = \sqrt{D\tau}$ at low injection gives $L \sim 160 \mu\text{m}$ which shows

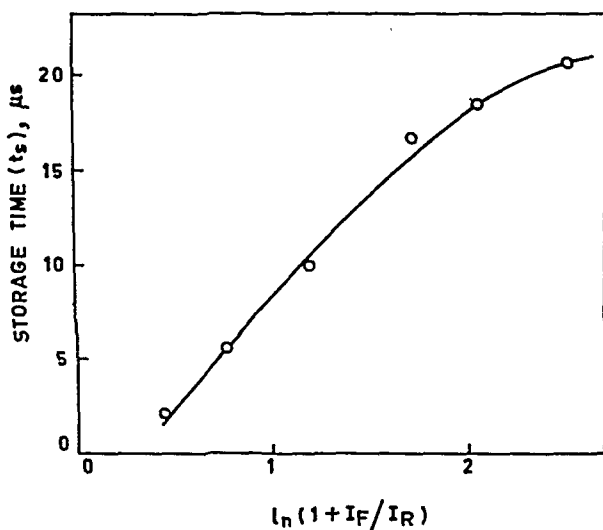


Fig. 2—Storage time (t_s) as a function of $\ln(1 + I_F/I_R)$, keeping $I_R = 3.5 \text{ mA}$, for silicon solar cells

that for such a diode the W/L ratio is not very much larger than unity. As reported earlier^{7,8}, the minority carrier lifetime increases with injection, and therefore, the minority carrier diffusion length L , given by $L = \sqrt{D\tau}$ also increases with injection level. The increase in L with increase in injection level decreases the W/L ratio. Thus the back contact recombinations which were not very significant at low level of injection become increasingly significant in removing the stored carrier at high level of injection due to increase in L at higher I_F values. This increase in back recombination causes a reduction in the measured values of t_s and thus indicates an apparent decrease in the slope of the plots. We, therefore, conclude that the value of t_s depends upon the absolute value of I_F as shown in Fig. 2 and not upon I_F/I_R ratio as suggested by Kuno. Also the slope of the plots will not give the minority carrier lifetime in the base for a practical diode but gives some time-constant which, when corrected for the diode geometry, i.e. W/L ratio and injection level I_F , will give the minority carrier lifetime in the base.

The results have been further verified on a set of germanium diodes with thick and very thin base and results are found to be in agreement with the above observations⁷.

Acknowledgement

The authors are thankful to Prof. S C Jain for many helpful discussions during the course of the study and also to the Director for permission to publish this paper.

References

- 1 Gossick B R, *Phys Rev (USA)*, **91** (1953) 1012.
- 2 Lederhandler S R & Giacoletto L J, *Proc IRE (USA)*, **43** (1955) 477.
- 3 Kingston R H, *Proc IRE (USA)*, **42** (1954) 829.
- 4 Lax B & Neustadter S F, *J Appl Phys (USA)*, **25** (1954) 2148.
- 5 Kuno H J, *IEEE Trans Electron Devices (USA)*, **11** (1964) 8.
- 6 Dean R H & Nuese C J, *IEEE Trans Electron Devices (USA)*, **18** (1971) 151.
- 7 Agarwal S K, Jain S C & Harsh, *Electron Lett (GB)*, **18** (1982) 298.
- 8 Jain S C, Agarwal S K & Harsh, *J Appl Phys (USA)*, **54** (1983) 3618.
- 9 Wolf H P, *Silicon semiconductor data* (Pergamon Press, Oxford), 1969.

Table 1—Values Obtained for the Characteristic Function $g(E_e)$ as a Function of E_e

E_e	$g(E_e)$	E_e	$g(E_e)$	E_e	$g(E_e)$
-20	0.222	-6	4.818	8	3.170
-18	0.447	-4	8.217	10	2.426
-16	0.731	-2	9.322	12	1.655
-14	1.019	0	9.888	14	1.030
-12	1.427	2	10.17	16	0.477
-10	1.908	4	10.21	18	0.000
-8	2.694	6	5.826	20	0.000

$$R(E_e) = \frac{-1}{2\pi e_0} \int_{-e_0}^{e_0} g(E - E') \frac{E'}{(e_0^2 - E'^2)^{1/2}} dE' \quad \dots (7)$$

where $R(E_e)$ is the resolution function for the system and it contains the complete instrument response.

3 Results and Discussion

ND500 computer was used to calculate the characteristic signal $g(E_e)$, instrument response function T_1 and the resolution function $R(E_e)$ for the system developed at the Bhabha Atomic Research Centre. Table 1 gives the values obtained for the characteristic signal for various values of E_e . The general feature of this function is a slow rise on the low energy side as compared to a fall on the higher energy side. This is responsible for a longer excursion⁶ seen in the peak-to-peak amplitude on the higher energy side in the resolution function. Fig. 1 shows a resolution function calculated for a modulation voltage of 1 V. A shift⁷ in the peak position due to modulation is also observed in Fig. 1. An additional feature of the resolution function is that the positive peak height is about 65% of the negative peak height which is consistent with the published spectra. It is, therefore, argued that a detailed analysis of the Auger profiles needs the inclusion of such features of the resolution function.

Acknowledgement

The author is thankful to Drs S S Kapoor and V C

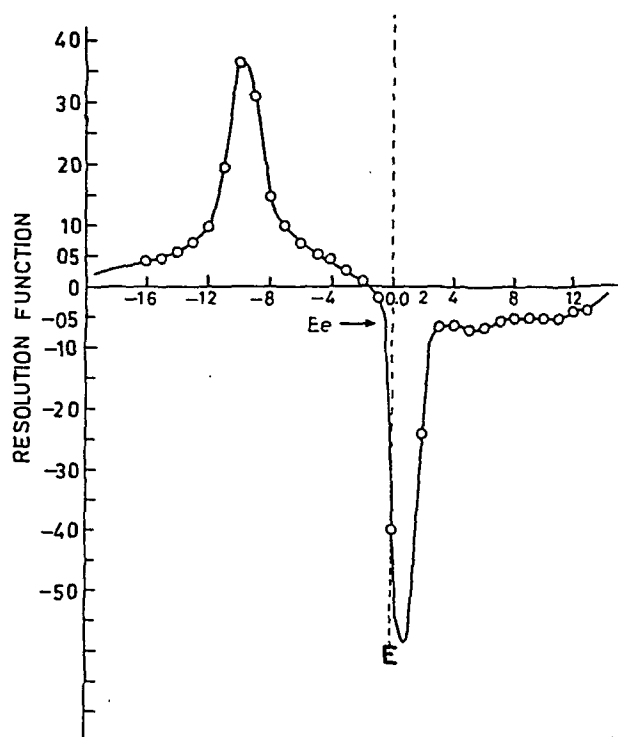


Fig. 1—Resolution function due to sinusoidal modulation of 1 Volt peak-to-peak at electron energy E

Sahni for their keen interest in the work. He is also thankful to Dr B A Dasannacharya for critical comments.

References

- 1 Sar-el H Z, *Rev Scient Instrum (USA)*, **38** (1967) 1210.
- 2 Sickafus E N & Holloway D M, *Surf Sci (Netherlands)*, **51** (1975) 131.
- 3 Bishop H E, Coad J P & Rivieure M, *J Electron Spectrosc & Related Phenomena (Netherlands)*, **1** (1973) 389.
- 4 Sahni V C, *Proc Indian Natl Sci Acad Sec A*, **51** (1985) 286.
- 5 Houston J E & Park R L, *Rev Scient Instrum (USA)*, **43** (1972) 1437.
- 6 Springer R W & Pocker D J, *Rev Scient Instrum (USA)*, **48** (1977) 74.
- 7 Anthony M T & Seah M P, *J Electron Spectrosc & Related Phenomena (Netherlands)*, **32** (1983) 73.
- 8 Palmberg P W, Riach G E, Weber R E & McDonald N C, *Handbook of Auger electron spectroscopy* (Physical Electronics, Edina Minnesota, USA), 1972.

Determination of Surface Temperature of Microbead using Infrared, Thermocouple & Resistance Thermometric Techniques

R J JAISWAL & S C SRIVASTAVA

Instrumentation Division, Central Mining Research Station, Dhanbad 826 001

Received 8 August 1985; revised received 14 March 1986

Three techniques for determination of surface temperature of catalytic microbeads have been developed using (i) infrared, (ii) resistance thermometric and (iii) thermocouple sensors. Method of fabrication alumina-supported microbeads for detection of exact surface temperature is indicated. The plots of measured temperature versus the methane content (which releases heat energy by oxidation in the beads) are linear and agree closely for the three techniques.

1 Introduction

In the fabrication of semiconductor/catalytic sensors for the measurement of concentration of highly inflammable or toxic gases, it is essential to use techniques to measure the surface temperature of the catalytic microbead sensors. Correct measurement of surface temperature of beads is an essential requisite in the investigation of such factors as suitable crystal structure formation on the support as well as on the catalyst, effect of input voltages on surface temperature of sensors, temperature of reduction of catalyst, temperature of formation of α -phase alumina, oxidation temperature of gases, and in kinetic studies.

Many workers¹⁻⁶ have investigated the above factors by employing either resistance thermometric or thermocouple techniques. But the temperatures so determined have not been compared with values determined by any supplementary method. In resistance thermometric technique, the change in resistance with temperature is correlated with concentration of methane. In the formula used for calculating change in resistance of bead, only the temperature coefficient of the resistance wire is included, but the temperature coefficient of the materials used for bead preparation is not included. So far as the thermocouple method is concerned, the earlier workers deposited the support and catalyst on the junction of thermocouple. This process may not give an exact estimate of surface temperature of microbeads.

Hence in the present study, the authors have given due consideration to the above factors and developed three different techniques based on (i) thermocouple (ii) resistance thermometric and (iii) IR methods for determining the surface temperature of the beads.

2 Thermocouple Technique

A platinum coil was prepared in the manner described earlier^{7,8}. Alumina support was deposited using a saturated solution of aluminium nitrate to ensure

complete covering of the platinum coil. The junction of a 10 % Rh-Pt/Pt thermocouple having wire diameter 40 swg, was carefully placed onto the surface of the support and further deposition of alumina support was made using subsequent drops of $\text{Al}(\text{NO}_3)_3$ solution. In this way, one junction of the thermocouple is rigidly fixed onto the surface of the support on which further deposition of catalyst was made. The sketch of the system is shown in Fig. 1. Finally a catalytic bead so fabricated was placed in a combustion chamber. The leads from the thermocouple were connected to a bridge circuit. Temperature measurements were made using a potentiometer and a deflection galvanometer, keeping the reference junction of the thermocouple in ice.

3 Resistance Thermometric Technique

The well known equation connecting temperature, resistance and temperature coefficient is given by:

$$R_1 T = R_0 (1 + \alpha t) \quad \dots (1)$$

where R_1 is the resistance at temperature T , R_0 the resistance at 0°C and α the temperature coefficient of

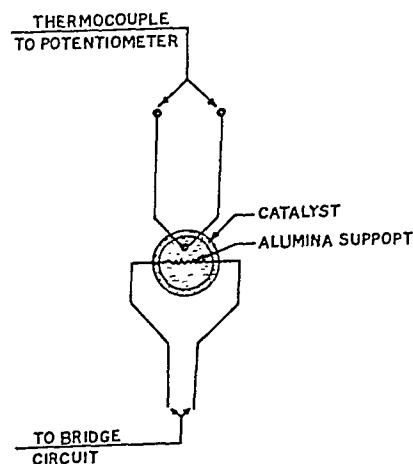


Fig. 1—Sketch of the thermocouple set-up for measurement of surface temperature of microbeads

the material. If due to change of temperature ΔT , the resistance $R_1 T$ changes to $\Delta R_1 T$, then Eq. (1) is modified to:

$$(R_1 T + \Delta R_1 T) = R_0(1 + \alpha t_1) \quad \dots (2)$$

where t_1 is the increase in temperature from $R_1 T$.

In earlier studies, the value of α used was that of the platinum metal. Since the value of α of the sensor used in the catalytic bead differs from α of platinum, we used the modified value of α for determination of temperature. The bridge circuit arrangement shown in Fig. 2 was used for determining $R_1 T$.

From Fig. 2 it is seen that

$$I = I_1 + I_2 \quad \dots (3)$$

$$I_2 = I - I_1$$

and

$$I' = I'_1 + I'_2$$

$$\text{or} \quad \dots (4)$$

$$I'_2 = I' - I'_1$$

where I and I' represent respectively current at balance and at unbalanced stages in different paths of the bridge when the bridge is balanced, we have

$$\frac{R_1 T}{R_2 T} = \frac{R_3 + R_m}{R_4} \quad \dots (5)$$

or

$$R_1 T = R_2 T \frac{(R_3 + R_m)}{R_4} \quad \dots (6)$$

$$\text{Again } R_1 T + R_2 T = V / I_2$$

$$\text{or } R_2 T = V / I_2 - R_1 T \quad \dots (7)$$

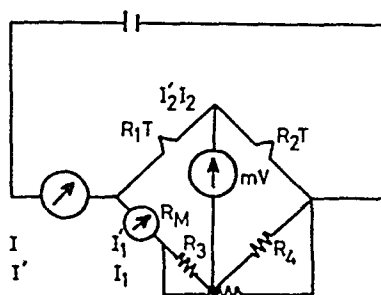


Fig. 2—Bridge circuit for measurement of change in resistance of microbead

Substituting the value of $R_2 T$ in Eq. (6) we have

$$R_1 T = \left(\frac{V}{I_2} \right) \left(\frac{R_3 + R_m}{R_4 + R_3 + R_m} \right) \quad \dots (8)$$

Values of R_3 , R_m , R_4 , V and I_2 are known and hence of $R_1 T$.

Again we have from the bridge circuit

$$I'_2 (R_1 T + \Delta R_1 T) - mV = I'_1 (R_m + R_3)$$

Substituting the value of I'_2 from Eq. (4)

$$R_1 T = \frac{I'_1 (R_m + R_3) + mV - (I' - I'_1) \Delta R_1 T}{I' - I'_1} \quad \dots (9)$$

Thus value of $R_1 T$ can be determined from Eq. (8) as well as Eq. (9) and temperature evaluated using Eq. (2).

4 Infrared Technique

Infrared radiations from the hot surface of a catalytic bead, will give an idea of the temperature of the catalytic surface. Hence the spatial temperature distribution over a catalytic surface may be determined without making contact with the surface by using an infrared sensor.

The set-up essentially consists of an IR sensor, a combustion chamber (Fig. 3) and circuit for IR sensor. The construction details of the combustion chamber have already been reported by the author⁹. The IR sensor (diameter 16 mm) is placed at 1 cm from the catalytic bead completely sealing the window facing the bead heads. The leads measuring circuit are as indicated in Fig. 3. The change in current in the sensor circuit is calibrated in terms of temperature actually measured with the help of a 10% Rh-Pt/Pt thermocouple.

A close agreement has been found (Fig. 4) between the values of temperature measured following the three different methods. The results also indicate that the temperature coefficient of a platinum coil changes as a result of deposition of the support and the catalyt-

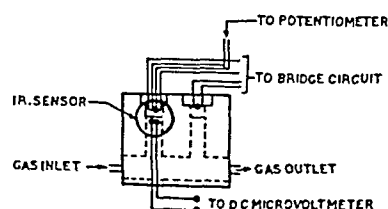


Fig. 3—Set-up for IR technique for measurement of surface temperature of microbeads

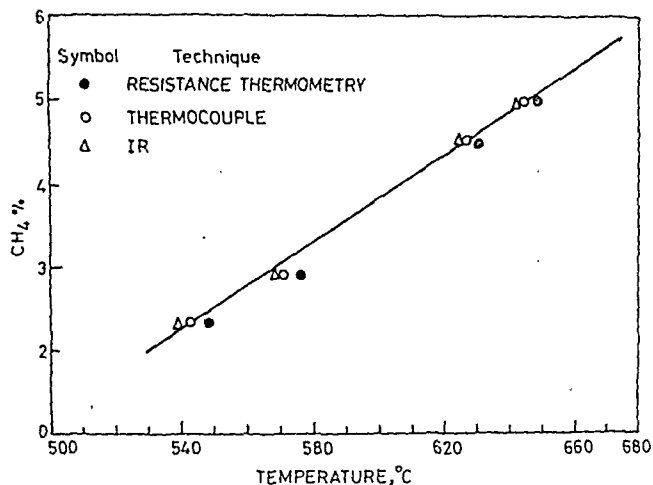


Fig. 4—Comparison of plots of surface temperature of microbeads versus CH₄ concentration for the three techniques

ic/semiconducting material. The techniques discussed will be helpful in the development of semiconductor/catalytic transducers, consequently in the development of instruments for the measurement of concentration of gases. These techniques will also be

helpful in the investigation of characteristics of a heterogeneous gas reaction, using microbeads.

Acknowledgement

The authors are grateful to Dr B Singh, Director, Central Mining Research Station, Dhanbad, for his interest, valuable suggestion and for permission to publish this paper. The authors are also thankful to Sri R N Das and I Sinha, for their assistance in preparing the paper and in the study.

References

- 1 Firth J C, *Trans Faraday Soc (GB)*, **62** (1966) 2566.
- 2 Firth J G, Jones A & Jones T A, *Ann Occup Hyg (GB)*, **115** (1972) 321-326.
- 3 Firth J G & Holland H B, *Nature (GB)*, **212** (1966) 1036.
- 4 Firth J G & Holland H B, *Nature (GB)*, **217** (1968) 1252.
- 5 Firth J G & Holland H B, *Trans Faraday Soc (GB)*, **65** (1969) 1121.
- 6 Anderson R B & Stein K C, *Ind Engng Chem (USA)*, **53** (1961) 809.
- 7 Srivastava S C & Jaiswal R J, *Indian J Technol*, **15** (1977) 1.
- 8 Baker A R & Firth J G, *Min Engr (USA)*, **128** (1969) 237.
- 9 Srivastava S C & Jaiswal R J, *Urja (India)*, **14** (No 4) (1983) 303.

Spectral Study of Nd^{3+} Ternary Complex of Amino Acid in Different Solvents

KIRTY MATHUR, M P BHUTRA & S P TANDON

Department of Physics, University of Jodhpur, Jodhpur 342 001

Received 19 September 1985; revised received 26 May 1986

The absorption spectra of the complex in different solvents has been studied in the visible region, and the values of Slater-Condon (F_k), Racah (E^k) and Lande (ξ_{4f}) parameters and Judd-Ofelt intensity parameter (T_λ) have been computed. The reasonable agreement between the calculated and experimental values of oscillator strengths shows that the theories proposed by B R Judd [*Phys Rev (USA)*, **127** (1962) 750] and G S Ofelt [*J Chem Phys (USA)*, **37** (1962) 511] are applicable for this system.

Lanthanide ions in different environments are well known laser materials¹. In the last two decades results of studies on energy states and their intensities have been reported²⁻⁸ for a number of lanthanide complexes from this laboratory. These complexes have many potential applications as structural probes⁹ in biological and model systems. Fluorescence enhancement, circular dichroism, relaxation enhancement and chemical shift studies are some of the techniques which have been used for probing the structures of many important biological molecules⁹. The information obtained using these techniques can be further confirmed and more information can be obtained about the structures of biological molecules by studying their absorption spectra in solution state¹⁰.

The present note reports the absorption spectra of the complex under study in the visible region in different solvents. From these, the values of Slater-

Condon (F_k), Racah (E^k) and Lande (ξ_{4f}) parameters and Judd-Ofelt intensity parameter (T_λ) have been computed.

Experimental details—The complexes have been synthesized by the standard method described by Crossby *et al.*¹¹ Chemicals of AR grade and triply distilled water were used. The absorption spectra in the region 360-1000 nm were recorded on Carl-Zeiss Jena VSU-2 spectrophotometer. For the computation of parameters, references may be made to our earlier work²⁻⁶. The least count of the spectrometer is 1 nm.

Results and discussion—The observed and computed values of energy levels for the complex in different solvents are given in Table 1. The rms deviations between the theoretical and experimental values support the validity of the theory used. The red shift of the energy levels of Nd^{3+} radical from those of Nd^{3+} ion in different solvents indicates complexation.

The hypersensitive transition $^4G_{5/2} \leftarrow ^4I_{9/2}$ shows a decreasing red shift as the solvents are changed in the order: DMSO, DMF and water. This may be attributed to some crossings of O_2 atomic orbitals of solvents with those of the metal at different distances in solution. The oscillator strengths for this hypersensitive transition increase as the solvents are changed in the order: water, DMF and DMSO, indicating that the coordinating affinity of Nd^{3+} is largest for DMSO and smallest for water in conformity with earlier results⁸.

The values of spectroscopic parameters F_k ($k = 2, 4, 6$), E^k and ξ_{4f} , as well as of the nephelauxetic ratio

Table 1—Energy Values (in cm^{-1}) of Bands of Nd^{3+} Ternary Complex in Different Solvents

Level	Water		DMF		DMSO	
	E_{Exptl}	$E_{\text{Calc.}}$	E_{Exptl}	E_{Calc}	E_{Exptl}	E_{Calc}
$^4I_{9/2}$	0	0	0	0	0	0
$^2P_{1/2}$	23310	23287	23310	23289	23256	23233
$^4G_{11/2}$	21739	21487	21552	21394	21505	21349
$^4G_{9/2}$	21322	21273	21322	21282	21277	21247
$^2G_{9/2}$	19569	19593	19569	19539	19531	19511
$^4G_{7/2}$	19194	19298	19157	19263	19157	19243
$^4G_{5/2}$	17361	17301	17241	17217	17241	17212
$^4F_{9/2}$	14599	14726	14577	14689	14535	14651
$^4F_{7/2}$	13298	13275	13280	13214	13263	13190
$^4F_{5/2}$	12422	12460	12346	12399	12346	12382
$^4F_{3/2}$	11468	11478	11426	11425	11390	11418
rms deviation		99		76		74

Table 2—Computed Values of Interaction Parameters (in cm^{-1}) of Nd^{3+} Complex in Different Solvents

Parameter	Free ion	Water	DMF	DMSO
F_2	331.16	329.85	328.58	328.04
F_4	50.71	53.33	53.96	54.10
F_6	5.15	5.32	5.37	5.29
ξ_{4f}	884.00	843.42	839.65	825.84
β	—	0.99	0.99	0.99
$b^{1/2}$	—	0.05	0.06	0.07
E^1	5024.00	5118.37	5135.68	5116.04
E^2	23.90	23.01	22.70	22.53
E^3	497.00	494.96	492.60	494.54

(β) and bonding parameter ($b^{1/2}$) are reported in Table 2. Values of β and $b^{1/2}$ were calculated from F_k and ξ_{4f} values. The degree of covalency indicated by $b^{1/2}$ decreased in the order of solvents: DMSO > DMF > water.

From the oscillator strengths of the observed bands P_{Exptl} (Table 3), Judd-Ofelt intensity parameters T_λ ($\lambda = 2, 4, 6$) were computed following the method of Carnall *et al.*¹² The relatively large difference between the calculated and observed values of the bands at ${}^4G_{9/2}$, ${}^2G_{9/2}$, ${}^4F_{9/2}$ and ${}^4F_{3/2}$ may be attributed to the mixing of the adjoining bands (Table 3). Values of T_λ are given in Table 4. The rms deviation between the observed and calculated values of P for the bands under study ranges over 7.9×10^{-7} – 8.8×10^{-7} for different solvents used. This indicates the applicability of the theories proposed by Judd¹³ and Ofelt¹⁴ to the present case. It is interesting to note that the T_2 parameter shows an appreciable change in different solvents in the order: DMSO > DMF > water.

The authors are grateful to Prof. A N Nigam, for providing the necessary facilities and Dr S S L Surana for valuable discussions. One of them (MPB) thanks the University Grants Commission, New Delhi, for financial assistance.

References

- 1 Surana S S L, Mathur R C & Tandon S P, *J Phys C (GB)*, **8** (1975) 2323.
- 2 Tandon S P & Mehta P C, *J Chem Phys (USA)*, **52** (1970) 4341, 4896, 5417.

Table 3—Oscillator Strength (P) of Nd^{3+} Ternary Complex in Different Solvents

Level	$P \times 10^6$ in Water		$P \times 10^6$ in DMF		$P \times 10^6$ in DMSO	
	Calc.	Exptl	Calc.	Exptl	Calc.	Exptl
${}^2P_{1/2}$	0.55	0.57	0.56	0.91	0.67	0.54
${}^4G_{11/2}$	0.28	0.34	0.34	0.14	0.38	0.10
${}^4G_{9/2}$	1.88	0.18	2.28	0.23	2.57	0.5
${}^2G_{9/2}$	0.50	0.95	0.62	1.45	0.69	1.04
${}^4G_{7/2}$	3.62	2.93	4.60	4.39	4.69	3.89
${}^4G_{5/2}$	13.75	13.67	21.07	20.43	23.29	22.51
${}^4F_{9/2}$	0.75	0.45	0.98	0.37	1.06	0.53
${}^4F_{7/2}$	6.97	6.19	9.25	8.27	9.98	8.96
${}^4F_{5/2}$	7.61	6.54	9.56	9.7	10.55	10.46
${}^4F_{3/2}$	2.37	1.47	2.63	3.56	3.05	2.35
rms deviation	0.79×10^{-6}		0.88×10^{-6}		0.87×10^{-6}	

Table 4—Computed Values of Intensity Parameters (T_λ)

Solvent	$T_\lambda \times 10^9, \text{cm}^{-1}$		
	T_2	T_4	T_6
Water	0.5537	0.6216	1.1707
DMF	1.0144	0.6263	1.5753
DMSO	1.0914	0.7617	1.6954

- 3 Mehta P C & Tandon S P, *J Chem Phys (USA)*, **53** (1970) 414.
- 4 Tandon S P & Govil R C, *J Chem Phys (USA)*, **57** (1972) 4097.
- 5 Mathur R C, Surana S S L & Tandon S P, *Can J Spectrosc (Canada)*, **20** (1975) 81.
- 6 Tandon S P & Vaishnava P P, *Can J Spectrosc (Canada)*, **22** (1977) 17.
- 7 Tandon S P, Vaishnava P P & Tandon K, *Phys Status Solidi a (Germany)*, **54** (1979) K117.
- 8 Tandon S P, Bhutra M P & Gupta A K, *Rev Tech Ing Univ Zulia (Germany)*, **7** (1984) 19.
- 9 Nieober E, *Struct & Bonding (Germany)*, **22** (1975) 1.
- 10 Gupta A K, *Spectral study of some ternary complexes of rare earth metals*, Ph D thesis, Jodhpur University, Jodhpur, 1983.
- 11 Crossby C A, Whan R E & Alire B M, *J Chem Phys (USA)*, **34** (1961) 743.
- 12 Carnall W T, Fields P R & Rajnak K, *J Chem Phys (USA)*, **49** (1968) 4412, 4424, 4443, 4447, 4450.
- 13 Judd B R, *Phys Rev (USA)*, **127** (1962) 750.
- 14 Ofelt G S, *J Chem Phys (USA)*, **37** (1962) 511.

Internal Pressure in Relation to the Structure of Polymers

C V SURYANARAYANA & P PUGAZHENDHI

Department of Chemical Engineering, Alagappa College of Technology, Anna University, Madras 600 025

Received 10 February 1986; revised received 12 May 1986

Dependence of internal pressure on molecular weights of three kinds of polymeric materials has been examined. It has been found that though there is a correlation between molecular weight and internal pressure, it is contextual and, as it should be, is dependent on the strength of intermolecular forces and, in turn, on the structure of the polymeric material.

Weissler *et al.*¹ and Lagemann *et al.*² reported data on ultrasonic velocities, densities and viscosities of some poly di-ols at 30°C and chlorotrifluoroethylene at 60°C respectively. With these data, internal pressure values have been computed and their variations are correlated with molecular weights. Computation of internal pressure (π_i) is made using the equation given by Suryanarayana³:

$$\pi_i = bRT \left[\frac{K\eta}{u} \right]^{1/2} \frac{\rho^{2/3}}{M_{\text{eff}}^{1/6}}$$

where b is the packing factor assumed as 1.78 for fcc or hcp structures in liquid systems, R the gas constant in ergs, T the temperature in K, η the viscosity in poises, u the ultrasonic velocity in cm/s, ρ the density in g/cm³, K a constant (4.28×10^9) independent of temperature and M_{eff} the (effective) molecular weight.

Data—A polymer of a particular group is characterized by the molecular weight of the monomer unit and for the present study the following three groups of polymers are considered:

1. Polyethylene glycol
2. Chlorotrifluoroethylene, and
3. A set of substituted cyclohexanes and a substituted heptane.

In Table 1, molecular weight, internal pressure and the relevant parameters of polymers of group 1, starting from ethylene glycol to polyethylene glycol are given under sections A and B. Similar data for chlorotrifluoroethylenes of varying molecular weights are given in the same table under section C while data for substituted cyclohexanes are given with their molecular weights under sections D and E.

Discussion—It is seen from Table 1(A), that as the molecular weight increases from that of ethylene glycol

to pentaethylene glycol, a gradual fall in the internal pressure is observed. A similar trend is seen in section B for polyethylene glycol. In contrast, it is seen from Table 1(C) that with a progressive increase in molecular weight, there is an increase of internal pressure for chlorotrifluoroethylenes. An explanation for such opposite trends will have to be based on the constitutional differences in the two polymers of the sets (B) and (C). In (C), because of highly electronegative fluorine atoms, there will be localization of δ^+ centres on the carbon atoms and δ^- centres on the electronegative atoms. This results in the positive centres of one monomer group interacting strongly with the negative centres of another monomer group producing a strong cohesion and a resultant high internal pressure. This explanation is supported by the evidence reported by Doler⁴ on polystyrene sulphonates. According to Doler, the polymeric chain of this group consists of long fully extended segments and there exists between the segments belonging to the same or to a neighbouring polyion, a considerable volume where the electric field intensity is close to zero. Naturally, between the locations of highly positive δ^+ and highly negative δ^- centres of chlorotrifluoroethylenes there should be a volume of zero electric field intensity. In ethylene glycols, there are no strong positive and negative centres, and therefore, a mere increase in the molecular weight results in a progressive decrease of internal pressure, particularly because of the absence of strong interactions. Irrespective of whether the increase in the molecular weight is due to the glycol units in the bound state or as separate units, there is a decrease in internal pressure with increase in molecular weight. Comparison of changes in values of η with increase in molecular weight shows that the rate of increase in η with increase in the molecular weight is smaller in the case of polyethylene glycols as compared to chlorotrifluoroethylenes.

Data for four kinds of polymer units given under section E of Table 1 show that the internal pressure has no relation with the molecular weight in these cases. However, under section E of Table 1 data given on fluoroluble oil polymers show systematically a progressive increase in internal pressure with the corresponding increase in molecular weight. Explanation for this trend is the same as for chlorotrifluoroethylenes.

From the above discussion, it is clear that the degree of cohesion quantified by internal pressure in a polymer is sensitive to the structure of the polymer.

Table 1—Values of Molecular Weight, Internal Pressure and Relevant Parameters for Polymers Studied

	Molecular weight M	u m/s	ρ g/cm ³	$\eta \times 10^2$ P	Π atm
Section A: Ethylene glycols ($t=30^\circ\text{C}$)					
Ethylene glycol $\text{CH}_2\text{OH}.\text{CH}_2\text{OH}$	62.1	1643	1.107	13.95	23419
Diethylene glycol $(\text{HOC}_2\text{H}_4)_2\text{O}$	106.1	1568	1.109	22.55	16335
Triethylene glycol $(\text{HOC}_2\text{H}_4)\text{OC}_2\text{H}_4\text{O}(\text{C}_2\text{H}_4\text{OH})$	150.1	1593	1.116	29.96	12515
Tetraethylene glycol $(\text{HOC}_2\text{H}_4)\text{OC}_2\text{H}_4\text{OC}_2\text{H}_4\text{O}(\text{C}_2\text{H}_4\text{OH})$	194.2	1580	1.116	35.16	10080
Pentaethylene glycol $(\text{HOC}_2\text{H}_4)\text{OC}_2\text{H}_4\text{OC}_2\text{H}_4(\text{C}_2\text{H}_4\text{OH})$	238.2	1580	1.117	42.37	8725
Section B: Polyethylene glycols					
Polyethylene glycol	200	1592	1.117	39.71	10318
$\left(\begin{array}{c} \text{H} \quad \text{H} \\ \quad \\ \text{---C---C---O---} \\ \quad \\ \text{H} \quad \text{H} \end{array} \right)_n$	300	1578	1.118	59.02	7877
	400	1576	1.118	74.70	6339
	600	1570	1.118	104.62	4684
Section C: Chlorotrifluoroethylenes ($t=60^\circ\text{C}$)					
	525	731	1.815	3.5937	2257
	563	747	1.831	5.1817	2485
	577	753	1.838	5.7713	2545
	664	785	1.869	15.0450	3455
	686	794	1.877	21.4541	3861
	713	804	1.885	30.9894	4535
	727	803	1.887	35.2114	4731
	789	811	1.901	68.7592	5998
	846	823	1.909	107.8394	6906
	886	831	1.914	154.3067	7804
	894	830	1.920	214.7904	9135
	911	836	1.919	225.4825	9120
	948	839	1.926	325.5325	10467
Section D: Four selected polymers (substituted cyclohexanes) ($t=60^\circ\text{C}$)					
(Trifluoromethyl)-unde- cafluorocyclohexane	350	477.8	1.78751	1.5900	2949
Hexadecafluoroheptane	388	444	1.62027	0.3290	1156
Bis(trifluoromethyl)- decafluorocyclohexane	400	513.1	1.74636	0.5600	1423
Bis(trifluoromethyl)chloronano- fluorocyclohexane	416	582.3	1.79126	1.3757	2035
Section E: Fluoroluble oil (polymers)					
	860	659.4	1.95467	30.6883	3994
	1016	710.4	1.96990	137.9130	6932
	1099	709.4	1.97817	212.6532	7882

Thus, internal pressure is also sensitive to attractive and repulsive forces in a given system.

The authors thank CSIR, New Delhi, for the award of a Emeritus Scientist Scheme to one of them (CVS) and a JRF to the other (PP). The authors place on record their thanks to Prof. V C Kulandaiswamy, Vice-Chancellor, Anna University, and Prof. B Jagannadhaswamy, Director, Alagappa College of Technology, for the encouragement given.

References

- 1 Weissler A, Fitzgerald J & Resnick I, *J Appl Phys (USA)*, 18 (1947) 434.
- 2 Lagemann R T, Woolf W E, Evans J S & Underwood N, *J Am Chem Soc (USA)*, 70 (1948) 2994.
- 3 Suryanarayana C V, *J Acoust Soc (India)*, 7 (1979) 131.
- 4 Doler D, Thermodynamic properties of polyelectrolyte solutions, in *Charged and reactive polymers: Vol. I—Polyelectrolytes*, edited by Eric Selegny and co-edited by Michael Mandel and Ulrich P Strains (D Reidel Publishing Co, Dordrecht, Holland), 1972, 97.

Proton Magnetic Resonance Studies on $\text{Cu}(\text{3-AMI})_2\text{Br}_2$ and $\text{Co}(\text{3-AMI})_2\text{Cl}_2$

K V R CHARY*, K V G REDDY,
M N CHARY & B A SASTRY

Solid State & Molecular Physics Laboratory, Department of
Physics, Osmania University, Hyderabad 500007, India
and

G PONTICELLI & M MASSACESSI

Istituto Di Chimica Generale, Inorganica Ed Analitica
Universita Di Cagliari, Via Ospedale 72
09100 Cagliari, Italy

Received 2 March 1984; accepted 25 April 1986

Proton magnetic resonance studies have been carried out on the title complexes to verify the hydrogen atom positions and also to detect the molecular motions. The low values of the second moments (S_2) even at 77 K indicate the CH_3 reorientations about C_3 axis. The second moment falls at high temperatures for both $\text{Cu}(\text{3-AMI})_2\text{Br}_2$ and $\text{Co}(\text{3-AMI})_2\text{Cl}_2$ are associated with the activation energies of 47.0 and 25.0 kJ/mol respectively.

Aminoisoxazole ligands are known for their coordinating ability with a number of metal ions¹⁻⁹. An interesting feature of these ligands is that the functional groups, viz. NH_2 and CH_3 , can undergo reorientations at favourable temperatures. These reorientations can only be detected by PMR spectroscopy and hence these studies will be useful to get information about the structure and rigidity of the molecule. In order to study the above aspects the authors have taken up PMR studies on $\text{Cu}(\text{3-AMI})_2\text{Br}_2$ and $\text{Co}(\text{3-AMI})_2\text{Cl}_2$ (3-AMI = 3-amino, 5-methyl isoxazole).

Experimental procedure—The two complexes under investigation were prepared using literature methods⁹. PMR studies on these complexes were carried out on home-made wide-line nmr spectrometer whose details were given elsewhere¹⁰. The first derivative PMR signals were recorded in the temperature range 77-350 K and their second moments (S_2) were estimated using the standard procedure¹¹. The experimental error in S_2 is about $\pm 1 \text{ G}^2$.

Results and discussion—The variation of S_2 values with the temperature for both $\text{Cu}(\text{3-AMI})_2\text{Br}_2$ and $\text{Co}(\text{3-AMI})_2\text{Cl}_2$ is shown in Fig. 1. The S_2 values in the case of $\text{Cu}(\text{3-AMI})_2\text{Br}_2$ were found to decrease slowly from $11.3 \pm 1 \text{ G}^2$ to $10.0 \pm 1 \text{ G}^2$ in the temperature range 77-340 K and a rapid fall in S_2 from the latter value to $5.6 \pm 1 \text{ G}^2$ is noticed between 340 K and 350

K. Beyond 350 K the compound was found to change its colour. In the case of $\text{Co}(\text{3-AMI})_2\text{Cl}_2$, S_2 is found to be constant at $12 \pm 1 \text{ G}^2$ in the temperature range 77-300 K and a rapid fall in S_2 from the above value to $3 \pm 1 \text{ G}^2$ is noticed in the temperature range 300-345 K. Above 345 K, similar to the copper complex, even this compound is found to change its colour.

In order to find the temperature below which the lattices of the two complexes were rigid, the theoretical value of S_2 i.e. $S_{2, \text{rig}}$ (Refs 12-15), calculated from the known hydrogen atom positions should be compared with the experimental S_2 values at different temperatures. Since the crystal structure of these two complexes is not solved so far, to get an approximate idea about the theoretical S_2 , the intramolecular contribution to the rigid lattice S_2 is calculated from the known hydrogen atom positions of $\text{Ni}(\text{3-AMI})_4(\text{NCS})_2$ (Ref. 9). The S_2 value obtained from the above calculations (91 G^2) is found to be very large compared to the experimental S_2 values of either of the compounds under investigation. To understand about this large discrepancy in theoretical and experimental S_2 values, an insight into the interatomic distances calculated from the known crystal structure of $\text{Ni}(\text{3-AMI})_4(\text{NCS})_2$ revealed that the H-H distances in CH_3 group are 1.27, 1.48 and 1.64 Å and in NH_2 group it is 1.54 Å, these values are small compared to the values (1.79 and 1.68 Å) given in the *Tables of interatomic distances*¹⁶. Evidently the small value of H-H distances is responsible for larger rigid lattice second moment ($S'_{2, \text{rig}}$) from the theoretical calculations. It is also found that the contribution to the $S'_{2, \text{rig}}$ from the other pairs of hydrogen atoms is small due to larger H-H distances of the order of 3 Å and above. Therefore, the $S_{2, \text{rig}}$ is calculated once again taking the H-H distances of the CH_3 and NH_2 groups as 1.79 and 1.68 Å, respectively, without changing the other H-H distances due to the fact

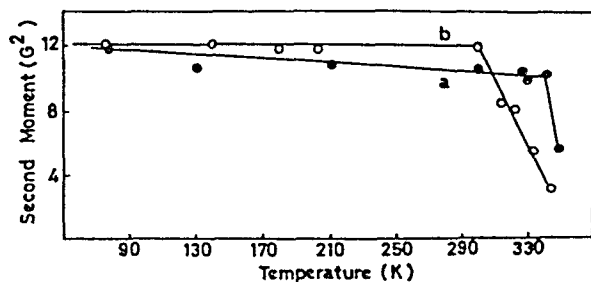


Fig. 1—Variation of the second moment with the temperature for: (a) $\text{Cu}(\text{3-AMI})_2\text{Br}_2$ and (b) $\text{Co}(\text{3-AMI})_2\text{Cl}_2$

*Present address: FT-NMR Centre, Tata Institute of Fundamental Research, Homi Bhabha Road, Bombay 400 005

mentioned above. From these calculations $S'_{2, \text{rig}}$ is coming out to be 17.4 G^2 . When this is added to the theoretical intermolecular contribution (S'_2), if the crystal structure is available, the value of $S_{2, \text{rig}}$ ($S_2 + S'_2$) will be still larger. Hence it is evident, from the above discrepancy, that the systems are not rigid even at 77 K . So the second moment observed at 77 K should correspond to some kind of intramolecular or molecular motions. The most probable motion to produce such low value of S_2 is the reorientation of the methyl group about C_3 axis. Similar kind of reorientation at 77 K is observed in the case of xylenes¹⁷. In most of the cases amine group reorientation¹⁸⁻²⁰ is not observed at 77 K . Thus it appears that the CH_3 reorientation may be the reason for getting low S_2 values at 77 K in both the samples.

The S_2 transition observed for $\text{Cu}(\text{3-AMI})_2\text{Br}_2$ in the temperature range $340\text{--}350 \text{ K}$ may be either due to the reorientation of NH_2 group or molecular reorientation about one or more than one axes or due to general molecular reorientation. The second moment for the general molecular reorientation is entirely intermolecular in nature, the intramolecular contribution being averaged to zero. The contribution from this can be calculated using the modified second moment formula²¹⁻²³ of Van Vleck¹⁵ and is given as

$$S_{\text{reor}} = 358.1 N_0 C_1 a^{-6}$$

where N_0 is the number of protons per molecule, C_1 is lattice factor and a is lattice constant. In many cases²⁴⁻²⁶ S_{reor} is found to have a value in the range $0.91\text{--}1.4 \text{ G}^2$. Therefore, in the present case the general molecular reorientation is ruled out. But here the fall is 6.2 G^2 ($11.8\text{--}5.6 \text{ G}^2$), which can be ascribed to the reorientation of NH_2 group along $\text{C} - \text{N}$ axis for the reason that the fall expected for NH_2 reorientation is 5.2 G^2 (taking $\text{H} - \text{H}$ distances from *Tables of interatomic distances*).

In case of $\text{Co}(\text{3-AMI})_2\text{Cl}_2$, the S_2 value is seen to fall from 12.0 ± 1 to $3.0 \pm 1 \text{ G}^2$ in the temperature range $300\text{--}345 \text{ K}$. Since this fall is more than that theoretically expected for NH_2 reorientation (5.2 G^2) the fall cannot be due to NH_2 reorientation; also, it cannot be due to the general molecular reorientation for the reason mentioned above. Therefore the fall may arise due to the molecular reorientation about one or more than one symmetry axes. As pointed out earlier, lack of crystal structure data prevents unambiguous interpretation about molecular motion.

The correlation frequencies associated with the S_2 transitions of the $\text{Cu}(\text{3-AMI})_2\text{Br}_2$ and $\text{Co}(\text{3-AMI})_2\text{Cl}_2$ are calculated from the modified equation of Bloembergen *et al.*²⁷⁻²⁹. These reorientation frequencies are assumed to fit in Arrhenius equation $\nu_c = \nu_0 \exp(-E_a/RT)$. Therefore, a plot of $\ln \nu_c$ vs

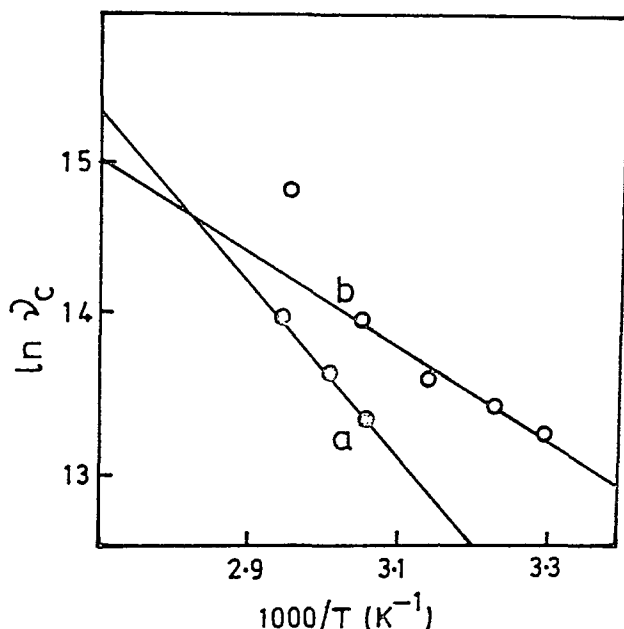


Fig. 2—Plot of $\ln \nu_c$ vs $1000/T$ for: (a) $\text{Cu}(\text{3-AMI})_2\text{Br}_2$ and (b) $\text{Co}(\text{3-AMI})_2\text{Cl}_2$

$1000/T$ yields a straight line as shown in Fig. 2, from which activation energies are calculated. In the present case, these values come out to be 47.0 kJ/mol for $\text{Cu}(\text{3-AMI})_2\text{Br}_2$ and 25.0 kJ/mol for $\text{Co}(\text{3-AMI})_2\text{Cl}_2$.

We thank the Head, Department of Physics, Osmania University, Hyderabad, for his cooperation in the present investigation. We express our gratitude to Prof. K Venkata Ramiah for his constant encouragement. We are also grateful to the University Grants Commission and CSIR, New Delhi, for providing financial assistance to carry out this work.

References

- Devoto G, Massaccesi M, Pinna R & Ponticelli G, *Transition Metal Chem (GB)*, 2 (1977) 236.
- Biddau M, Devoto G, Massaccesi M & Ponticelli G, *Transition Metal Chem (GB)*, 1 (1976) 295.
- Biddau M, Devoto G, Massaccesi M & Ponticelli G, *Transition Metal Chem (GB)*, 1 (1976) 99.
- Biddau M, Massaccesi M, Pinna R & Ponticelli G, *Transition Metal Chem (GB)*, 3 (1978) 153.
- Pinna R, Ponticelli G, Preti C & Tosi G, *Transition Metal Chem (GB)*, 1 (1976) 173.
- Ponticelli G, *J Inorg & Nucl Chem (GB)*, 39 (1977) 45.
- Sastry B A, Asadullah S Md, Ponticelli G & Pinna R, *J Mol Struct (GB)*, 73 (1981) 195.
- Sastry B A, Asadullah S Md, Ponticelli G & Massaccesi M, *J Inorg & Nucl Chem (GB)*, 43 (1981) 1531.
- Pelizzi G, *Transition Metal Chem (GB)*, 4 (1979) 199.
- Reddy K V G, Chary K V R & Sastry B A, *Aust J Chem (Australia)*, 35 (1982) 2367.
- Andrew E R, *Phys Rev (USA)*, 91 (1953) 425.
- Smith G W, *Phys Rev (USA)*, 36 (1962) 3081.
- Smith G W, *Phys Rev (USA)*, 42 (1965) 4229.
- Smith G W, *Phys Rev (USA)*, 43 (1968) 4368.
- Van Vleck J H, *Phys Rev (USA)*, 74 (1948) 1168.
- Tables of interatomic distances and configurations in molecules and ions* (The Chemical Society, London) 1958.

- 17 Gupta R C, *J F Prekt Chemie (Germany)*, **316** (1974) 185.
- 18 Sjoblom R & Tegenfeldt J, *Acta Chem Scand (Denmark)*, **26** (1972) 3068.
- 19 Gutowsky M S & Pake G E, *J Chem Phys (USA)*, **18** (1950) 167.
- 20 Kisore N, Agarwal P & Gupta R C, *Indian J Phys*, **48** (1974) 1007.
- 21 Jones J E & Ingham A E, *Proc R Soc, London, Ser A (GB)*, **107** (1925) 636.
- 22 Torrey H C, *Phys Rev (USA)*, **96** (1954) 690.
- 23 Gutowsky H S & McGarvey B R, *J Chem Phys (USA)*, **20** (1952) 1472.
- 24 Smith G W, *J Chem Phys (USA)*, **42** (1965) 4229.
- 25 Smith G W, *J Chem Phys (USA)*, **43** (1965) 4325.
- 26 Usha Pande & Gupta R C, *Indian J Pure & Appl Phys*, **15** (1977) 777.
- 27 Bloembergen N, Purcell E M & Pound R V, *Phys Rev (USA)*, **74** (1948) 1184.
- 28 Abragam A, *Principles of nuclear magnetism* (Oxford University Press, Oxford) 1961, 456.
- 29 O'Reilly D E & Tsang T, *J Chem Phys (USA)*, **46** (1967) 1298.

⁵⁷Fe Mössbauer Analysis of the Cubic Spinel CoAlFeO₄

F M MOSTAFA

Reactor & Neutron Physics Department, Nuclear Research Center,
Atomic Energy Post, Cairo, Egypt

&

J SUWALSKI

Solid State Laboratory, Institute of Atomic Energy
05-400 Otwock/Swierk, Warsaw, Poland

Received 7 October 1985; accepted 6 June 1986

Some physical properties of the spinel CoAlFeO₄, prepared using a slowly cooled ceramic method, have been investigated by means of Mössbauer spectroscopy. Mössbauer spectrum taken at liquid nitrogen temperature demonstrated the existence of two hyperfine fields, one due to the Fe³⁺ tetrahedral ions and the other due to the Fe³⁺ octahedral ions. The isomer shifts, quadrupole interactions, and nuclear magnetic fields of ⁵⁷Fe nuclei in both tetrahedral and octahedral sites, have been determined. Influence of the heat treatment on the Mössbauer parameters, has been discussed.

The spinel CoAlFeO₄ showed remarkable variation of its magnetic properties depending on the heat treatment during the preparation of the sample. The cation distribution, oxygen parameter, transition temperature, and magnetic structure of this spinel were determined using X-ray, magnetic susceptibility, and neutron diffraction techniques¹⁻³.

Mössbauer measurements carried out on a polycrystalline CoAlFeO₄, prepared using a quenching ceramic method, showed that: The isomer shifts of ⁵⁷Fe nuclei in both octahedral and tetrahedral sites were equal to each other, and the quadrupole splittings of these nuclei in the sites mentioned were also the same at 549 K (Ref. 4). The average of the hyperfine magnetic field of ⁵⁷Fe nuclei was 507 kOe at 80 K (Ref. 4).

The present Mössbauer studies on a powder sample of CoAlFeO₄, prepared using a slowly cooled ceramic method, were undertaken in the temperature range 78-450 K in order to determine the magnetic transition temperature, isomer shifts, quadrupole splittings, and the internal magnetic fields of ⁵⁷Fe ions, as well as to investigate the influence of heat treatment on the interaction parameters of ⁵⁷Fe nuclei.

Experimental details—Polycrystalline CoAlFeO₄, was prepared using a slowly cooled ceramic method. The method of preparation is given in reference 3. The X-ray powder pattern exhibited a pure cubic spinel phase. The lattice constant, *a*, was determined to be (8.2432 ± 0.0016) Å. Mössbauer spectra were obtained

using a linear Mössbauer spectrometer SM-4 at Swierk, Poland. The measurements were performed at different temperatures between the liquid nitrogen temperature and 450 K. The error in the temperature measurements was less than ±0.5 K. The thickness of the powdered CoAlFeO₄ absorber was 0.2 mg/cm² of ⁵⁷Fe nuclei. As a source of γ-radiation the ⁵⁷Co diffused in Cr matrix was applied. The Mössbauer spectra were stored in a conventional multichannel analyzer. The spectrometer was operating in a constant acceleration mode technique. We used a standard iron metal (ARMCO) at room temperature for calibration.

Results and discussion—The thermal dependence of the shape of the ⁵⁷Fe Mössbauer spectra was used to determine the magnetic-paramagnetic transition temperature of our sample. This was done using the temperature interval in which the transition takes place. Mössbauer absorption spectra taken at temperatures between 400 and 345 K were used for this purpose. Fig. 1 shows a relation between the sample temperature (*T*) and the halfwidth (Γ/2) of the absorption lines. The transition temperature was found to be (360 ± 2) K. This value is lower than the (405 ± 5) K obtained by measuring the disappearance of the magnetic contributions of the neutron diffraction pattern³. However the transition temperature determined by Mössbauer spectroscopy is usually lower than that determined by neutron diffraction. This is due to the time of γ photon-nucleus interaction (10⁻⁸ s) being longer than that of neutron-nucleus interaction (10⁻¹² s). The transition temperature

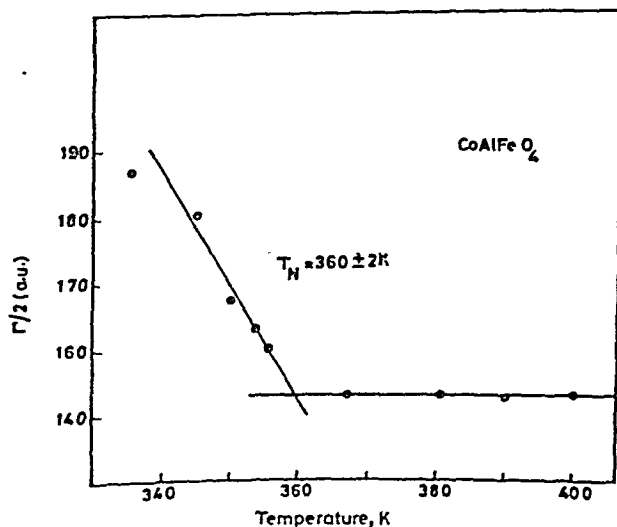
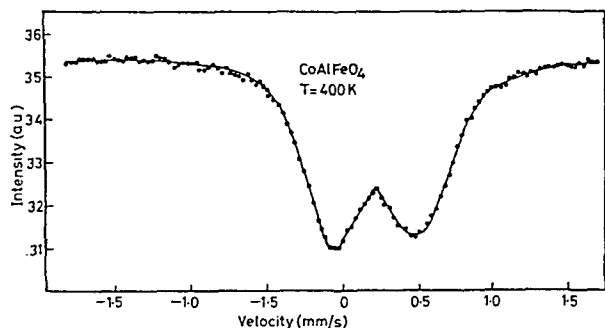
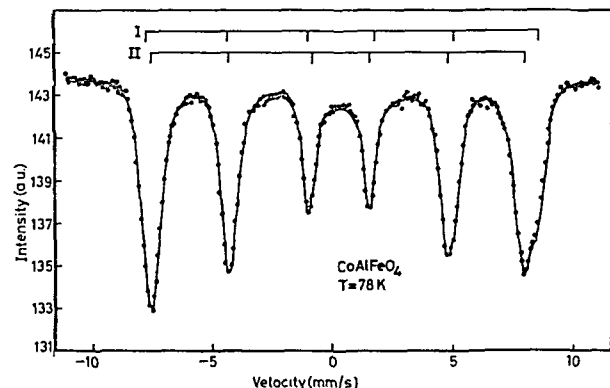


Fig. 1—The relation between the temperature (*T*) and the halfwidth of the absorption lines (Γ/2) of CoAlFeO₄


 Fig. 2—Mössbauer spectrum of CoAlFeO₄ at 400 K

 Fig. 3—Mössbauer spectrum of CoAlFeO₄ at 78 K

determined in this study is also considerably lower than the 500 K of a similar sample, CoAlFeO₄, but prepared using a quenching ceramic method⁴. This indicates that the magnetic-paramagnetic transition temperatures of the spinel ferrites are strongly affected by the heat treatment during the sample preparation. Therefore, the cation distributions and consequently the spontaneous magnetization of these ferrites are influenced by the heat treatment.

The paramagnetic Mössbauer spectrum of CoAlFeO₄ (Fig. 2) shows two overlapping doublets coming from ⁵⁷Fe³⁺ of tetrahedral (A) and octahedral (B) sites of the spinel. In Table 1 are listed the Mössbauer parameters obtained from this spectrum together with the earlier reported results.

The large overlapping of the absorption lines of Mössbauer spectra taken at 295, 345, 350, 353, 356, 367, 380, 390 and 400 K indicates that these lines are not accurate enough to distinguish the Fe³⁺ cations of A and B-sites. The line splitting observed in the well-resolved magnetic Mössbauer spectrum at liquid nitrogen temperature (Fig. 3) suggests that the spectrum is a superposition of two six-line patterns appearing due to the ferric ions being on two non-equivalent sites in the crystal structure. The two patterns are denoted by I and II.

The following observations are worth noting:

(i) The ratio of the Fe³⁺ tetrahedral to the Fe³⁺ octahedral of CoAlFeO₄ as determined by neutron

diffraction (1 to 1.63)³ is nearly equal to the corresponding ratio of the cubic spinel CuFe₂O₄ (1 to 1.41) as determined by Mössbauer spectroscopy⁵.

(ii) The magnetic Mössbauer spectrum of CoAlFeO₄ at liquid nitrogen temperature (Fig. 3) is very similar to the magnetic spectrum of the cubic spinel CuFe₂O₄ at liquid helium temperature⁵.

Based on (i) and (ii) above, we conclude that: Pattern I of the CoAlFeO₄ hyperfine spectrum at 78 K (Fig. 3) belongs to the Fe³⁺ ions located at B-sites and pattern II belongs to the Fe³⁺ ions located at A-sites. The separation of the two patterns was sufficient to determine the isomer shifts (IS), the quadrupole splittings (QS), and the effective hyperfine magnetic fields (H_{eff}) of the ⁵⁷Fe nuclei of both sites. Table 2 presents the calculated hyperfine parameters at 78 K together with the reported earlier results. The results listed in Tables 1 and 2 indicate that the paramagnetic and magnetic Mössbauer parameters of the spinel CoAlFeO₄ are affected by the heat treatment during sample preparation.

The values of hyperfine parameters given in Table 2, are consistent with the general facts that for the ferro-spinels, the values of IS and H_{eff} are lower for the A-site ions than for the B-site ions. Analysis of the non-equality between the cation radius, r , of Fe³⁺ ($r = 0.67 \text{ \AA}$) and the vacancy radii⁶ r_A and r_B of A and B-

 Table 1—Parameters of the Paramagnetic Mössbauer Spectra of CoAlFeO₄

Heat treatment	T^* [K]	QS [mm/s]	IS [mm/s]
Slowly cooled (present work)	400	0.55 ± 0.05	$0.24 \pm 0.02^\dagger$
Quenched ²	549	0.59	-0.09^\ddagger

*Temperature of measurements

[†]With respect to Fe metal

[‡]With respect to stainless steel

 Table 2—Interaction Parameters for ⁵⁷Fe Nuclei of CoAlFeO₄ Obtained at Liquid Nitrogen Temperature

Heat treatment	T^* [K]	Sub-spectrum	IS [†] [mm/s]	$H_{\text{eff}}^{\text{Fe}^{3+}}$ [kOe]	$\langle H_{\text{eff}}^{\text{Fe}^{3+}} \rangle$ [kOe]
Slowly cooled	78	Fe ³⁺ (A)	0.38 ± 0.01	475 ± 5	491
		Fe ³⁺ (B)	0.45 ± 0.01	508 ± 5	
Quenched ²	80	Fe ³⁺ (A)	—	—	507
		Fe ³⁺ (B)	—	—	

*Temperature of measurements

[†]With respect to Fe metal

sites [$r_A < 0.58$, $r_B < 0.72$ Å (Ref. 6)] suggests a considerable covalency of chemical bonds in spinels.

The smaller dimension of tetra-vacancy explains the bigger covalency of Fe^{3+} (A) and, in turn, the smaller IS and H_{eff} . The overlapping of the Fe^{3+} and O^{2-} shells eliminates the pure $3d^5$ configuration and makes the mixed $3d^5-4s$ configuration more favourable. The addition of $4s$ electron produces on the nucleus another magnetic contact field, which has an opposite sign with respect to the Fermi contact field. This arises from $s-d^5$ polarization effects. In this way, H_{eff} is more reduced on the tetrahedral than on the octahedral sites, because the covalency $4s$ of A-site is bigger than that for B-site.

We would like to thank Mrs. Z. Kucharski and M. Łukasiak for cooperation in the experimental

measurements and helpful discussions. The technical assistance of Mr. J. Ozimkowski is gratefully acknowledged. One of us (F.M. Mostafa) is pleased to thank IAEA in Vienna and IEA in Swierk for the award of a fellowship in Poland.

References

- 1 Popescu M & Ghizdeanu C, *Phys Status Solidi a (Germany)*, **52** (1979) K-169.
- 2 Blasse G, *Philips Res Rep (Netherlands)*, **18** (1963) 383.
- 3 Mostafa F, Ptasiwicz-Bak H & Ligenza S, *Phys Status Solidi a (Germany)*, **90** (1985), in press.
- 4 Aragon J, Fert A, Ferrer N, Schmidt M, Tejada J & Font-Altaba M, *Phys Chem Miner (Germany)*, **8** (1982) 206.
- 5 Janicki J, Pietrazak J, Porebska A & Suwalski J, *Phys Status Solidi a (Germany)*, **72** (1982) 95.
- 6 Bunget I, *Phys Status Solidi (Germany)*, **28** (1968) K-29.

BOOK REVIEWS

Thin Film Science & Technology 6: Coatings on Glass

by H K Pulker

Elsevier Science Publishers, Amsterdam, 1985 pp. xviii + 484, Hard Cover, Price Dfl 245.00 ISSN 0-444-41903-9; ISBN 0-444-42360-5

In the last three decades a good deal of literature has been published in the field of thin film technology covering a wide spectrum of subject matter including preparation, characterization and application of thin films. However, only in exceptional cases one finds comprehensive treatment of the subject covering relevant topics. Though the last few years have witnessed phenomenal growth in the field of thin film technology, a gap was felt in the available literature in that it could not provide, in a concise form, information on new and emerging techniques of film formation, characterization and applications. The book under review fulfils this requirement.

The first chapter gives a brief history of the various stages in the development of glasses and coatings including anti-reflection coatings, mirror coatings and interference coatings. In chapters 2 and 3, the author has discussed in depth the composition, structure, and physical properties of various types of glasses (both inorganic and organic glasses) as also the nature of the glass surface which includes chemical composition of the surface, structure of the surface, energy of the surface, etc., followed by methods of producing desired glass surfaces. The subject of clean glass surface and its implications are best known to a person working in the field of thin film technology. Half the battle in thin film coatings is won if the technique of cleaning the substrate surface is optimized. This topic is very well treated by the author in chapter 4 wherein clean surfaces are classified into two categories, viz. atomically clean surface and technologically clean surfaces. The various techniques of cleaning the surface are classified as those applicable in atmosphere and those that are applicable in vacuum. The subject of adhesion of films with glass surface is treated in chapter 5. Here the author gives the detailed mechanism of the phenomenon of adhesion and methods of quantitative measurement of the same.

The subject of thin film fabrication technique is of paramount importance in achieving a variety of

application-oriented goals. However, firms engaged in the production of thin film coatings opt for certain methods, which are not only proprietary but treated as 'trade secrets' and are not available in the published literature. This subject is, extensively covered in chapter 6 where one can see the 'experimental experience'. The various techniques of film deposition are classified under chemical film formation process and physical vapour deposition process (evaporation, sputtering and ion plating). This is the largest chapter covering 192 pages with an exhaustive list of 473 references. Chapter 7 deals with film thickness measurement and *in situ* monitor and control. In particular, quartz crystal film thickness monitor has been discussed in detail. The various physical properties of thin films, their structure, chemical composition, hardness, chemical and environmental stability, porosity, density, etc. are discussed in chapter 8. The last chapter deals with applications of thin films and is mostly confined to optical thin films. It also discusses, in brief, present status and trend which perhaps is a misnomer, since the discussion is limited to only integrated optics. However, a brief description of the scientific applications of thin films is very interesting and points to the potential applications of thin films in fields which were not thought of earlier. For example, thin film chromatography (TFC) which could achieve detection sensitivity in the nanogram region is much superior to the conventional thin layer chromatography (TLC). Similarly, the unconventional use of interference filters in determining thickness of ultrathin films (0.3 nm) observing crystallographic phenomena such as spiral growth of organic compounds *in situ*, gas kinetic studies, etc., are some of the expositions which perhaps were not known to many workers earlier.

The literature concerning the coatings on glass is vast but scattered and the attempt by H K Pulker, to put the useful material in a systematic and comprehensive form deserves appreciation. All the topics have been covered in detail backed by exhaustive list of references. Although rigorous mathematical treatment is avoided, useful hints and relevant references are always mentioned. In the opinion of the reviewer this book is equally useful to those involved in research, development and production of thin film devices.

V V Shah

National Physical Laboratory, New Delhi-12

Indian Journal of Pure & Applied Physics

INSTRUCTIONS TO AUTHORS

SCOPE

The journal welcomes, for publication, full papers and short notes, reporting significant new results of research, in all areas of physics except space physics. The applied fields covered are electronics, electrical engineering, instrumentation and applied mathematics. However, papers in applied mathematics with emphasis on only derivation and proofs and having no direct physical significance, will not be considered. Review articles are not published normally.

SUBMISSION OF MANUSCRIPT

Manuscripts for consideration should be submitted, *in duplicate*, to Editor, Indian Journal of Pure & Applied Physics, Publications & Information Directorate, Hillside Road, New Delhi 110012. They should neither have been already published nor be under consideration elsewhere.

Manuscripts should be in English and typewritten on only one side of good quality paper, in double space, with adequate margin on all four sides. One original and one carbon or photo-copy, each complete in all respects including abstract, illustrations, appendixes, etc. are to be submitted.

PREPARATION OF MANUSCRIPT

Authors may consult recent issues of the Journal to familiarize themselves with the general style and practices adopted in regard to the various elements of a paper.

General

Manuscript should be presented in as concise a form as possible. Good attention should be given to spelling and grammar. In giving names of chemical compounds and structures, abbreviations of units of measurements, symbols and notations, the style and practices recommended by the IUPAP and IUPAC, should be followed.

Frequently repeating combinations of words, e.g. electric field gradient (EFG), junction field effect transistor (JFET), stimulated Raman emission (SRE), should be abbreviated subsequently, indicating the abbreviated form in parenthesis, as shown, at the place of their first occurrence.

Pages should be numbered consecutively and arranged in the following order: Title, authors' names with their institutional affiliations and abstract, along with relevant footnotes whenever necessary (on a separate sheet); introduction; experimental details/theory/method/analysis; results; discussion; conclusion(s); acknowledgement; references and appendixes. Tables, captions for figures (with legends) and appendixes should be typed on *separate sheets* and attached at the end of the manuscript.

Title

The title should be neither too brief/general nor unnecessarily long. It should reflect the content of the paper so as to derive the maximum advantage in indexing. If a paper forms part of a general series, a specific subtitle, indicating the particular aspect of the work covered in the paper, should be provided.

A short running title for the paper, the broad PACS subject heading under which it should be classified in the contents page (authors may consult the January or July issue of the journal for this purpose), and the author's name and address for correspondence, should also be provided on the title page.

Abstract

The abstract, usually not exceeding 200 words, should indicate the scope and significant content of the paper.

highlighting the principal findings and conclusions. It should be in such a form that abstracting periodicals can use it without modification.

Introduction

Long and elaborate introduction should be avoided. It should be brief and state the exact scope of the study in relation to the present status of knowledge in the field. Literature review should be limited strictly to what is necessary to indicate the essential background and the justification for undertaking the study.

Materials, methods, apparatus, etc.

The sources of materials and their purity, methods of preparation, procedure for measurements and their accuracies, etc. should be clearly stated to enable any other worker to repeat the work if necessary. New methods, techniques, theories, etc. should be described in adequate detail; but if they are well known, a mere literature reference to them will do; differences from standard ones, improvements or innovations should, however, be clearly mentioned.

Results

Only such primary data as are essential for understanding the discussion and main conclusions emerging from the study should be included. All secondary data as are of interest to a specific category of readership *should not be included* in the paper. Such data should be retained by the authors for supply, on request, to any interested research worker. A footnote to this effect may be inserted at the relevant place in the paper.

The results must be presented in a coherent sequence in a unified logical structure, avoiding repetition or confusion. Limitations of the results should be clearly stated.

The same data should not be presented in both tabular and graphic forms. Only such tables and figures as are essential should be included. Simple linear plots that can easily be discussed in the text, should not be included. Infrared, ultraviolet, NMR and other spectra, DTA curves, etc. should be included only if they pertain to new compounds and/or are essential to the discussion; otherwise only significant numerical data should be given in the text or in a table.

Discussion

Long rambling discussion should be avoided. The discussion should deal with the interpretation of results without repeating information already presented under results. It should relate new findings to the known and include logical deductions. A separate section on 'conclusions' can be given only when they are well established and of outstanding significance. Mere observation of qualitative trends of results should be distinguished from firm conclusions. Also, limitations, if any, to the conclusions should be clearly pointed out.

Mathematical portions

Special attention should be given to the mathematical portions of the paper. Equations must be well separated from the text and written clearly with good separation between the successive lines. The usual norms of breaking long mathematical expressions should be adhered to. Equations should be numbered consecutively in Arabic numerals with the number in parenthesis near the right hand margin. Superscripts and subscripts should be clearly indicated in pencil by V and \wedge sign respectively. Capital and small letters,

particularly of the same letter when both occur, as well as letters or symbols likely to be confused one for the other, should be clearly distinguished. Special characters (e.g. Greek, script, vector, tensor, etc.) required must be indicated by marginal notes. Letters and symbols which should appear in bold face must be clearly indicated. To simplify typesetting: (i) long and complicated mathematical expressions which are frequently repeated should be replaced with single letter/symbol, without clashing with the others used in the paper; (ii) the "exp" form of complex exponential functions should be used; and (iii) to simplify fractions, the solidus (/) is to be used and fractional exponents are to be used instead of root signs, e.g.

write $\exp\{-i\omega_0(t_1 - t_2)/2\}$ and not $e^{-i\omega_0(t_1 - t_2)/2}$

write $(4\omega_{pl} K_{3\lambda}^2 / \tilde{\omega} K_D^2)^{1/2}$ and not $\sqrt{\frac{4\omega_{pl} K_{3\lambda}^2}{\tilde{\omega} K_D^2}}$

Tables

Tables should be numbered consecutively in Arabic numerals and should bear brief titles. Column headings should be brief. Units of measurement should be abbreviated and placed below the headings. Nil results should be indicated and distinguished clearly from absence of data. Inclusion of structural formulae inside the tables should be avoided as far as possible. Tables should be referred to in the text by numbers and not by terms like 'above', 'below', 'preceding' or 'following'. Results should not be presented to a greater accuracy than that of the method employed.

Illustrations

The number of illustrations should be kept to the minimum. Wherever possible, e.g. a number of individual analogous figures referring to different variables, substances, molecules, etc. may be combined into one composite figure. All illustrations should be numbered consecutively in Arabic numerals. Captions and legends to the figures should be self-explanatory. Line drawings should be made with Indian ink on white drawing paper/cellophane sheet/tracing cloth, and drawn to approximately twice the printed size.

The lettering should be uniform, preferably in stencil, so as to be not less than 1.5 mm after reduction widthwise to full page size (165 mm) or column size (80 mm). The size of geometrical shapes (used to distinguish different graphs), dots, lines, etc. should be sufficiently large to permit the necessary reduction without loss of detail. In the case of photographs, prints must be on glossy paper and contrasty. If an illustration is taken from another publication, reference to the source should be given and prior permission secured. Illustrations should be referred to in the text by numbers and not by terms like 'above', 'following' etc.

Acknowledgement

Acknowledgements should not be exuberant and must be made only to real assistance rendered in connection with the work reported in the paper.

References

References cited should be limited to the absolute minimum (particularly in the case of short notes) based on their essential relevance. In the text, references to literature should be numbered consecutively, in the order of their first occurrence, and should be indicated by superscript Arabic numbers at the relevant places; as far as possible the placement of references on numerals or other symbols should be avoided; in such cases the reference may be given in parenthesis in running text, e.g. "this yielded for n a value of 2.3 (Ref. 5)". Full bibliographic details for all the references mentioned in the text should be listed in serial order at the end of the paper.

In citing references to research papers, names and initials of authors should be followed, in order, by the title of the periodical in the abbreviated form (underlined), the volume number (two lines underneath), the year within circular brackets and the page number [e.g. Chandra B P & Shrivastava K K, *J Phys & Chem Solids (GB)*, 39 (1978) 939]. For names of periodicals, the abbreviations followed by the *Physics Abstracts* should be used. For periodicals not covered by *Physics Abstracts*, the title abbreviations should be according to the *Bibliographic Guide for Editors and Authors*, 1974, published by the American Chemical Society, Washington DC, USA; additionally the country from which the journal is published should be given in parenthesis immediately after the title abbreviation. If a paper has been accepted for publication, the names of the authors and the journal (with volume number and year, if known) should be given followed by the words "in press" [e.g. Wahi P K & Patel N D, *Can J Spectrosc (Canada)*, in press.].

In references containing up to four authors, the names of all the authors with their respective initials should be given. The abbreviations *et al.*, *idem* and *ibid* should be avoided. When there are more than four authors, only the names of the first three authors with their respective initials should be given, followed by the words 'et al.'

Reference to a book should include details in the following order: name and initials of authors, the title of the book (underlined), name of publisher and place of publication within circular brackets and year and page (s) [e.g. Clayton G B, *Operational amplifiers* (Newnes-Butterworths, London), 4th Edn, 1977, 26]. If the reference is to the work of an author published in a book by a different person, the fact that it is cited from the source book should be clearly indicated [e.g. Turnhout Van J, 'Thermally stimulated discharge of electrets' in *Topics in applied physics: Vol. 33—Electrets*, edited by C M Sessler (Springer Verlag, Berlin), 1980, 130].

Proceedings of conferences and symposia should be treated in the same manner as books. Reference to a paper presented at a conference, the proceedings of which are not published, should include, in the following order, names and initials of authors, title of the paper (underlined), name of the conference, and where and when it was held (e.g. Herczeg P, *Symmetry-violating kaon decays*, paper presented to the International Conference on High Energy Physics and Nuclear Structure, Vancouver, Canada, 13-17 August 1979).

Reference to a thesis should include the name of the author, title of the thesis (underlined), university or institution to which it was submitted and year of submission (e.g. Mehrotra S N, *Many-body techniques and their applications to interacting bosons*, Ph D thesis, Ranchi University, 1976).

Reference to a patent should include names of patentees, country of origin (underlined) and patent number, organization to which the patent has been assigned (within circular brackets), date of acceptance of the patent and reference to an abstracting periodical where available [e.g. Labes M M, *US Pat.* 4,066,567 (to Temple University), 3 January 1978; *Chem. Abstr.*, 88 (No. 20) (1978), 138350 n].

PROOFS & REPRINTS

The edited manuscript will be sent to the author for his final approval before giving it to the press. No galley proofs will be sent to the authors for corrections, since the proofs will be checked at the editorial office. Authors are given 25 free reprints for each paper. Extra reprints can be ordered by the author while returning the edited manuscript. If the reprints order is not received, it will be presumed that no extra reprints are needed.

CSIR SCIENTIFIC PERIODICALS

JOURNAL OF SCIENTIFIC & INDUSTRIAL RESEARCH (Monthly)

With a fine record of over 45 years' service to the scientific community, this journal has grown into India's leading general science periodical. Intended to fulfil the responsibility of helping the research workers to keep themselves abreast of current developments in various fields of science and technology, the journal carries editorial features highlighting important scientific events in India and abroad, articles on science policy and management of science review articles on topics of current research interest, technical reports on international and national conferences, reviews of scientific and technical publications, and notes on major advances in various fields.

Annual subscription	Rs 120.00	\$ 40.00	£ 23.00
Single copy	12.00	4.00	2.30

INDIAN JOURNAL OF CHEMISTRY (Monthly)

Section A: Started in the year 1963, the journal is devoted to papers in Inorganic, Physical, Theoretical and Analytical Chemistry.

Annual subscription	Rs 160.00	\$ 53.00	£ 30.00
Single copy	16.00	5.30	3.00

Section B: This journal is devoted to papers in Organic Chemistry, including Medicinal Chemistry.

Annual subscription	Rs 160.00	\$ 53.00	£ 30.00
Single copy	16.00	5.30	3.00

INDIAN JOURNAL OF PURE & APPLIED PHYSICS (Monthly)

Started in the year 1963, this journal is devoted to original research communications (full papers and short communications) in all conventional branches of physics (except radio and space physics).

Annual subscription	Rs 180.00	\$ 60.00	£ 34.00
Single copy	18.00	6.00	3.40

INDIAN JOURNAL OF RADIO & SPACE PHYSICS (Bimonthly)

The journal, which is being published beginning from March 1972, is intended to serve as a medium for the publication of the growing research output in various areas of radio and space physics, such as ionospheric propagation, magnetosphere, radio and radar astronomy, physics and chemistry of the ionosphere, neutral atmosphere, airglow, winds and motion in the upper atmosphere, stratosphere-mesosphere coupling, ionosphere-magnetosphere coupling, solar-terrestrial relationship, etc.

Annual subscription	Rs 100.00	\$ 34.00	£ 19.00
Single copy	20.00	6.80	3.80

INDIAN JOURNAL OF TECHNOLOGY (INCLUDING ENGINEERING) (Monthly)

This journal publishes papers reporting results of original research of applied nature pertaining to unit operations, heat and mass transfer, products, processes, instruments and appliances, etc. The journal is of special interest to research workers in departments of applied sciences in universities, institutes of higher technology, commodity research laboratories, industrial cooperative research institutes, and industrial research laboratories.

Annual subscription	Rs 120.00	\$ 40.00	£ 23.00
Single copy	12.00	4.00	2.30

INDIAN JOURNAL OF EXPERIMENTAL BIOLOGY (Monthly)

This journal, devoted to the publication of research communications in the fields of experimental botany, zoology,

microbiology, pharmacology, endocrinology, nutrition, etc., is the only one in India with such a wide coverage and scope.

Annual subscription	Rs 180.00	\$ 68.00	£ 34.00
Single copy	18.00	6.80	3.40

INDIAN JOURNAL OF BIOCHEMISTRY & BIOPHYSICS (Bimonthly)

This journal, published in association with the Society of Biological Chemists (India), Bangalore, is the only research journal in India devoted exclusively to original research communications in biochemistry and biophysics.

Annual subscription	Rs 65.00	\$ 23.00	£ 12.00
Single copy	13.00	4.60	2.40

INDIAN JOURNAL OF MARINE SCIENCES (Quarterly)

Commencing publication from June 1972, this journal is devoted to research communications (full papers and short communications) pertaining to various facets of marine research, viz. biological, physical, geological and chemical oceanography.

Annual subscription	Rs 90.00	\$ 30.00	£ 17.00
Single copy	26.00	8.70	5.00

RESEARCH AND INDUSTRY (Quarterly)

Intended to serve as a link between science and industry, this journal is addressed primarily to technologists, engineers, executives and others in industry and trade. It publishes informative original articles containing practical details of processes and products devoted in India, which show promise of ready utilization, and technical digests on new processes, products, instruments and testing methods which are of interest to industry. Developments in Indian industry are regularly reported.

Annual subscription	Rs 70.00	\$ 23.00	£ 13.00
Single copy	22.00	7.00	4.00

INDIAN JOURNAL OF TEXTILE RESEARCH (Quarterly)

Commencing publication from March 1976, this journal is devoted to the publication of papers reporting results of fundamental and applied researches in the field of textiles.

Annual subscription	Rs 50.00	\$ 17.00	£ 10.00
Single copy	15.00	5.00	3.00

MEDICINAL & AROMATIC PLANTS ABSTRACTS (Bimonthly)

Carries informative abstracts of scientific papers published in important Indian and foreign journals relating to different aspects of medicinal and aromatic plants. Each issue contains about 350 abstracts with a subject index.

Annual subscription	Rs 120.00	\$ 40.00	£ 23.00
Single copy	24.00	8.00	4.60

CURRENT LITERATURE ON SCIENCE OF SCIENCE (Monthly)

Carries abstracts, digests, book reviews, news & notes and R&D statistics with emphasis on problems of S&T in developing countries, it also covers the areas of science policy, R&D planning and management, technology transfer, technology assessment and science and society.

Annual subscription	Rs 100.00	\$ 30.00	£ 12.00
---------------------	-----------	----------	---------

Please contact

**SALES AND DISTRIBUTION OFFICER
PUBLICATIONS & INFORMATION
DIRECTORATE, CSIR
Hillside Road, New Delhi-110012**

CSIR PUBLICATIONS

WEALTH OF INDIA

An encyclopaedia of the economic products and industrial resources of India issued in two series

RAW MATERIALS SERIES—contains articles on plant, animal and mineral resources

	Rs	\$	£
Vol. I (A-B)	80.00	30.00	13.00
Vol. II (C)	95.00	33.00	17.00
Vol. III (D-E)	105.00	32.00	20.00
Vol. IV (F-G)	65.00	27.00	12.00
Supplement (Fish & Fisheries)	56.00	16.00	10.50
Vol. V (H-K)	114.00	34.00	21.00
Vol. VI (L-M)	90.00	34.00	15.00
Supplement (Livestock)	102.00	34.00	19.50
Vol. VII (N-Pe)	100.00	30.00	19.00
Vol. VIII (Ph-Re)	86.00	32.00	14.00
Vol. IX (Rh-So)	104.00	35.00	19.00
Vol. X (Sp-W)	225.00	75.00	42.50
Vol. XI (X-Z)	115.00	38.50	22.00

INDUSTRIAL PRODUCTS SERIES—deals with major small-scale and cottage industries

Part I (A-B)	58.00	20.00	11.00
Part II (C)	74.00	24.00	14.00
Part III (D-E)	100.00	33.50	19.50
Part IV (F-H)	126.00	42.00	24.00
Part V (I-L)	90.00	23.00	17.00
Part VI (M-Pi)	28.00	8.00	2.80
Part VII (Pi-Sh)	60.00	18.00	6.00
Part VIII (Si-Ti)	66.00	27.00	10.00
Part IX (To-Z)	80.00	34.00	12.00

BHARAT KI SAMPADA (Hindi Edition of Wealth of India. Raw Materials)

Vol. I (अ-क)	38.00	16.00	6.50
Vol. II (ख)	36.00	15.00	6.00
Vol. III (ग-घ)	36.00	15.00	6.00
Vol. IV (च)	83.00	34.00	16.00
Vol. V (झ-ञ)	60.00	22.00	10.00
Vol. VI (ट-ठ)	80.00	27.00	13.00
Vol. VII (ड-ढ)	135.00	40.00	25.00
Livestock (Kukkut Patan)	34.00	15.00	6.00
Fish & Fisheries (Matsya aur Matsyaki)	49.00	21.00	8.00
A Dictionary of Generic & Specific Names of Plants and Animals Useful to Man			
with their English and Latin pronunciation in Devanagari	30.00	11.00	5.00

OTHER PUBLICATIONS

Proceedings: seminar on primary communications in Science & Technology in India by Sh. R.N. Sharma & S. Seetharama	52.00	17.50	9.00
Flora of Delhi by J.K. Maheshwari	28.00	8.00	2.80
Indian Fossil Pteridophytes by K.R. Surange	66.00	22.00	12.50
Indian Thysanoptera by T.N. Ananthakrishnan	26.00	8.00	2.60
The Millipede Thyropygus by G. Krishnan	12.00	3.50	1.20
Drug Addiction with special reference to India by R.N. Chopra & I.C. Chopra	12.00	3.50	1.20
Glossary of Indian Medicinal Plants by R.N. Chopra & I.C. Chopra	35.00	13.00	6.00
Fluidization & Related Processes	12.00	4.00	1.20
Evolution of Life by M.S. Randhawa, A.K. Dey, Jagjit Singh & Vishnu Mitre	22.50	7.00	2.25
Collected Scientific Papers of Meghnad Saha	30.00	9.00	3.00
Proteaceae by C. Venkata Rao	72.00	24.00	13.50
Pinus by P. Maheshwari & R.N. Konar	30.00	11.00	5.00
Cellulose Research I	3.00	0.90	0.30
Cellulose Research II	6.00	1.75	0.60
Chemical Process Design	9.00	2.50	0.90
Low Temperature Carbonization of Non-coking Coals & Lignites & Briquetting Coal Fines:			
Vol. I & Vol. II (each volume)	17.50	5.50	1.75
Nucleic Acids	10.00	3.00	1.00
IGY Symposium: Vol. I	9.00	2.50	0.90
IGY Symposium: Vol. II	9.00	2.50	0.90
CNS Drugs	16.50	5.00	1.65
Kinetics of Electrode Processes & Null Points of Metals	2.50	0.75	0.25
Indian Sardines by R.V. Nair	22.00	7.00	2.20
Termite Problems in India	9.00	3.00	0.90
Loranthaceae by B.M. Johri & S.P. Bhatnagar	55.00	18.50	10.50
Abies and Picea by K.A. Chowdhury	14.00	6.00	2.10
Gnetum by P. Maheshwari and Vimla Vasil	20.00	6.00	2.00
Aquatic Angiosperms by K. Subramanyam	20.00	6.00	2.00
Supplement to Glossary of Indian Medicinal Plants by R.N. Chopra, I.C. Chopra & B.S. Varma	18.00	7.00	3.00
Herbaceous Flora of Dehra Dun by C.R. Babu	144.00	60.00	22.00
Diosgenin and Other Steroid Drug Precursors by Y.R. Chadha & Miss L.V. Asolkar	36.00	13.00	6.00
Research & Development Management by Inder Dev	25.00	10.00	—
Rural Development and Technology—A Status Report-cum Bibliography by P.R. Bose & V.N. Vashist	100.00	38.00	17.00
Cholera Bacteriophages by Sachinmohan Mukherjee	30.00	10.00	6.00

Packing and Postage extra.

Please contact:

SALES AND DISTRIBUTION OFFICER
PUBLICATIONS & INFORMATION DIRECTORATE, CSIR
Hillside Road, New Delhi 110012

Indian J Pure & Appl Phys, Vol 24 No 9 pp. 415-464

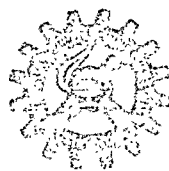
SEPTEMBER 1986

CODEN : IJOPAU ISSN : 0019-5596

24(9) 415-464 (1986)

PR-109
57-1

INDIAN JOURNAL OF PURE & APPLIED PHYSICS



Published by
PUBLICATIONS & INFORMATION DIRECTORATE, CSIR
NEW DELHI

in association with
THE INDIAN NATIONAL SCIENCE ACADEMY, NEW DELHI

Announcing

The Wealth of India

Raw Materials: Volume-I:A

(Revised Edition)

Contains 204 entries: 198 on plant genera and 6 on minerals

This volume is the first of the revised and enlarged edition of this encyclopaedic classic on Indian Raw Materials, brought out with updated information. It covers economically important raw materials of plants and minerals contained in the alphabet A. Each plant entry gives the correct nomenclature of the genus and species dealt with, their distribution in India, and a short description of the economically important parts.

The articles on crop plants, medicinal and timber yielding plants etc. give in considerable detail the methods of cultivation, silvicultural practices, agricultural inputs, harvesting and storage etc. besides mentioning diseases and pests and their control measures. Chemical composition and utilization of raw materials are covered in detail for important economic crops and products; statistical data concerning area, production, export, import etc. are given. In the case of minerals, their occurrence and distribution in the country, methods of mining, extraction, chemical composition and utilization are given.

Adequate references to the sources of information are provided at appropriate places. The articles are illustrated with half-tones, line drawings, charts and colour plates. The Index covers botanical and zoological names, and names of chemical compounds, besides common English, regional and trade names.

The revised edition provides useful updated information to research workers, students, industrialists, planners, and others interested in the raw material resources of India.

Pages: *Text*, 513 + *Index*, 54

Price: Rs. 200.00 \$ 47.00 £ 37.00

Kindly send your orders to:

The Sales & Distribution Officer
Publications & Information Directorate, CSIR
Hillside Road, New Delhi 110 012

Indian Journal of Pure & Applied Physics

EDITORIAL BOARD

Prof. S. Chandrasekhar
Raman Research Institute
Bangalore

Prof. R V Gopala Rao
Jadavpur University
Calcutta

Prof. S K Joshi
Indian National Science Academy
New Delhi/Roorkee University
Roorkee

Prof. P Krishna
Indian National Science Academy,
New Delhi/Banaras Hindu University
Varanasi

Prof Kehar Singh
Indian Institute of Technology
New Delhi

Prof C L Mehta
Indian Institute of Technology
New Delhi

Prof. S P Pandya
Physical Research Laboratory
Ahmedabad

Dr K R Rao
Bhabha Atomic Research Centre
Bombay

Prof. D K Rai
Banaras Hindu University
Varanasi

Prof. B V Sreekantan
Tata Institute of Fundamental Research
Bombay

Prof. R Srinivasan
University of Madras
Madras

Prof. Suresh Chandra
Banaras Hindu University
Varanasi

Shri S P Ambasta, Editor-in-Chief (*Ex-officio*)

EDITORIAL STAFF

Editors

D S Sastry & K S Rangarajan

Assistant Editors

J B Dhawan, Tarun Banerjee & (Mrs) Poonam Bhatt

Published by the Publications & Information Directorate, CSIR, Hillside Road, New Delhi 110012

Editor-in-Chief: S P Ambasta

The Indian Journal of Pure & Applied Physics is issued monthly. The Directorate assumes no responsibility for the statements and opinions advanced by contributors. The editorial staff in its work of examining papers received for publication is assisted, in an honorary capacity, by a large number of distinguished scientists, working in various parts of India.

Communications regarding contributions for publication in the journal should be addressed to the Editor, Indian Journal of Pure & Applied Physics, Publications & Information Directorate, Hillside Road, New Delhi 110012.

Correspondence regarding subscriptions and advertisements should be addressed to the Sales Distribution Officer, Publications & Information Directorate, Hillside Road, New Delhi 110012.

Annual Subscription
Rs. 180.00 £ 34.00 S 60.00

Single Copy
Rs. 18.00 £ 3.40 S 6.00

50% Discount is admissible to research workers and students and 25% discount to non-research individuals, on annual subscription. Payments in respect of subscriptions and advertisements may be sent by cheque, bank draft, money order or postal order marked payable *only* to Publications & Information Directorate, New Delhi 110012. Claims for missing numbers of the journal will be allowed only if received within 3 months of the date of issue of the journal plus the time normally required for postal delivery of the journal and the claim.

Ministry of Science & Technology

Department of Science & Technology

Science & Engineering Research Council

New Guidelines for R&D Programmes

Based on a review of the existing schemes, it has been decided by the Department of Science & Technology that the Science & Engineering Research Council (SERC) will provide an integrated and cohesive approach for supporting R&D programmes in the country. Accordingly, all R&D proposals will henceforth be reviewed by the SERC whose objectives will be:

- (i) To promote research in newly emerging and frontline areas of science and engineering including multidisciplinary fields;
- (ii) To selectively promote the general research capability in relevant areas of science and engineering taking into account existing research capabilities of the host institutions; and
- (iii) To encourage young scientists to take up challenging research and development activities.

Research proposals from scientific institutions/research laboratories under various Scientific Agencies/Departments which are in line with their normal research activities may not be considered for support under SERC. Only research proposals outside the normal activities of such institutions (e.g. National R&D Programmes, Programmes in newly emerging and frontline areas, etc.) will be considered. Further, proposals which involve purely survey-oriented work and routine studies will not be normally considered.

Past experience has revealed that some of the proposals received by the Department do not indicate specific research objectives and consist of generalities and involve large funding in terms of equipment, manpower, etc. In fact, the well-defined objectives of the proposals should be such that they are achievable in the framework of a time-bound project, using as far as possible, existing infrastructures in the host institution. The scientific community should, therefore, ensure that research proposals being written up involve, new and innovative ideas which can be pursued in a planned manner within the duration of the project and projecting only the very essential requirement of funds.

It is hoped that the scientific community will take up the challenge and undertake specific R&D programmes involving first rate science and possible application with optimal requirements of funds to achieve the above specific objectives of SERC.

It has also been decided that, in future, research proposals from the scientific community will be entertained only twice during a year. Proposals in the prescribed format obtainable from DST should reach during 1st to 30th April and 1st to 31st October of each calendar year. Through this approach, all efforts will be made to communicate a decision within six to nine months.

For further details, please contact:

Secretary
Department of Science & Technology
Technology Bhavan, New Delhi 110016

Indian Journal of Pure & Applied Physics

VOLUME 24

NUMBER 9

SEPTEMBER 1986

CONTENTS

General Physics

- Investigations on Focussing Property of Three-Element Electrostatic Lens 415
Hussein Mahmoud Saad* & Hassan Abd Elhamed

Physics of Elementary Particles & Fields

- Production of Tachyons in Extended Manifolds of General Relativity 421
A P Trofimenko* & V S Gurin

Nuclear Physics

- Differential Gamma Dose Rate for Neutral Beam Injection-ducted Concrete Shield . . 426
F M Sayedahmed* & A Abboud

- Compound-Nucleus Effects in Inelastic Deuteron Scattering from ^{24}Mg at
 $E_d = 10\text{-}15\text{ MeV}$ 452
S R Verma* & R Prasad

Atomic & Molecular Physics

- Influence of Correlation Function on Evaluation of the Correlation Energy 454
M A Kamel*, A Y Ghaly & M K Abdel-Hady

- Vibrational Spectrum of Isopropylammonium Dihydrogenoctamolybdate Dihydrate . . 456
V Ramakrishnan, G Aruldas* & M Kanakavel

Classical Areas of Phenomenology (Including Applications)

- Performance of Partial Circular Polarizers under Partially Polarized Light 430
S D Gupta* & A K Musla

Condensed Matter: Electronic Structure, Electrical, Magnetic & Optical Properties

- Microwave Absorption, Curie Temperature & Ultrasonic Attenuation in Ferroelectric
Solids 440
G N Baluni & U C Naithani*

- Temperature & Thickness Dependence of Electrical Conductivity of Polypropylene . . 444
H P Singh* & D Gupta

- Rhombic Symmetry Crystalline Field & Ground State Wavefunctions of Vanadyl Ion
Complexes 458
A Yadav, R S Bansal & V P Seth*

- ESR Studies on Some Copper(II) Complexes of Pyrazole 460
B A Sastry*, B Balaiah, K V G Reddy, B Madhu, G Ponticelli,
M Massaccesi & G Puggioni

- Towards a Thermal Conductivity Minimum – Thermoelectric Applications 463
C M Bhandari* & D M Rowe

Cross-Disciplinary Physics and Related Areas of Science & Technology

- An Ultrasonic A-Scan Ophthalmoscope for Diagnosis of Eye Abnormalities 448
V N Bindal* , V R Singh & Reeta Gupta

The author for correspondence is indicated by () mark, in case of papers with more than one author.

Investigations on Focussing Property of Three-Element Electrostatic Lens

HUSSEIN MAHMOUD SAAD & HASSAN ABD ELHAMED

National Center for Radiation Research & Technology, Madinet Nasr, POB 29, Egypt

Received 6 September 1985; accepted 8 August 1986

The properties of both physically symmetric and asymmetric three-element electric lens have been investigated experimentally for voltage-asymmetric and einzel lenses. Then, the dimensions of the intermediate electrode were varied with respect to the other electrodes. The einzel lens with equi-dimensions and electrode width to aperture diameter = 0.6, gave an appreciable agreement with theoretical expectation when the mid-focal length was measured against the intermediate electrode potential. Further measurements showed that while the mid-focal length increased with thickness and electrode separation, it decreased with aperture diameter. On the other hand, the asymmetric single lens exhibited almost the same results. In the voltage asymmetric mode, the beam was always focussed at the same point by readjusting the potential V_3 on the third electrode for different intermediate electrode potentials V_2 , at fixed V_1 . Again, when V_2 was varied with respect to V_1 at two fixed values of V_3 , the properties of the lens were nearly the same as that of the symmetric single lens but with shorter and finite focal length.

1 Introduction

The application of low energy electron beam in the study of surface irradiation and impact processes, in our laboratory, has stimulated the necessity to utilize a well collimating element, among our transport system, to control the beam subject to the requirement of beam spot-size and working distance. Comprehensive studies have been done so far to cover the various types of the electrostatic lens geometries and voltage. Double-element lenses are discussed by Cross *et al.*¹ and in the texts of Grivet² and Paszkowski³. Their focussing properties are functions of a variable parameter (V_2/V_1), V_1 , and V_2 being the accelerating (or retarding) potentials. Triple-element lenses are necessary when a beam is to be focussed without changing its energy. The beam energy may be higher or lower at the centre of the lens than at its entrance or exit, but the condition of higher energy at the centre results in lower aberrations of the image. They can also be operated in asymmetric modes, and in such a case they offer considerable advantages over the two-element lenses. The two variable parameters of a three-element lens (V_3/V_1 and V_2/V_1) can allow one property to be kept constant while the other properties are varied, thus forming the zoom lenses that would produce a beam of variable energy and magnification with fixed working distance. A three-electrode lens requires the specification of seven geometric parameters (three electrode thicknesses, two spacings and two aperture sizes as a ratio of the third), where upon the production of universal curves for the lens is impractical. This, in general, presents difficulties for the lens designer. Nevertheless, the calculation of the properties of mathematical models approximating the practical lens is made by solving Laplace's equation to find the potential dis-

tribution along the axis, whereon the focal properties can be simply calculated by numerical integration. However, the increasing availability of digital computers has made it possible to find the axial potential distribution more accurately, and hence achieving a large compilation of lens data. Read and others⁴⁻⁹ have calculated the focal lengths of a wide variety of lenses with thin electrodes. More recently, El-Kareh¹⁰ has published enough data that are much useful for the lens designer. Kuroda¹¹⁻¹³ has analyzed a voltage-asymmetric lens while Riddle¹⁴ computed the properties of a number of three-element single lenses.

However, in order to obtain an accurate lens design to give satisfactory performance, it is necessary to supplement theoretical information with a good deal of empirical data obtained from experimental studies. Therefore, in the light of the early theoretical works, we proposed certain versions of the lens that are considered to be adaptable with our next work, to investigate experimentally their characteristics. They are composed of coaxial, symmetric and asymmetric apertured disks held at different potentials with respect to that of the source.

2 Calculation of Lens Properties

There are no simple formulae that represent the performance of a given lens as its constants depend on the nature of the potential distribution along the axis. This distribution is a complicated function of the potential and geometry of the lens elements. The first stage is, then, of obtaining the potential distribution $V(r, z)$, within the lens; then the distribution in axially symmetrical system is determined from the potential along the axis $V(z)$ by Laplace's equation. Expanding the potential in power series about the axis, and neg-

lecting the higher terms for an electron path very close to the axis, we get:

$$V(r, z) = V - \frac{1}{4} V'' r^2 \quad \dots (1)$$

V'' is the second order derivative of the axial potential with respect to Z . Using this equation with the electron equation of motion:

$$\ddot{r} - \frac{e}{m} \frac{\partial V}{\partial r} = 0 \quad \dots (2)$$

we obtain the paraxial ray equation :

$$r'' + \frac{V'}{2V} r' + \frac{V''}{4V} r = 0 \quad \dots (3)$$

In most real lens fields, V'' changes sign at one or more points that makes the integration of the equation (to evaluate the focal length) rather difficult. It is, then, more convenient to introduce the variable :

$$R(z) = r V^{1/4}$$

in conjunction with Eq. (3) to obtain Pichet equation :

$$R'' + \frac{3}{16} \left(\frac{V'}{V} \right) R = 0 \quad \dots (4)$$

Taking the ratio of the slope to the radial distance leads to the focal length :

$$\frac{1}{f} = - \frac{\left(\frac{dr}{dz} \right)_{z_2}}{r(z)} = - \left(\frac{V_1}{V_2} \right)^{1/4} \frac{\left(\frac{dR}{dz} \right)_{z_2}}{R(z)}$$

where the subscripts 1 and 2 represent the parameters in the object and image space respectively. In contrast to thick lenses, within a thin lens, $r(z) \approx \text{constant}$ for the path of the electron, as both principal planes coincide with the mid-plane. Rearranging Eq (4) and evaluating the integration, the focal length f , and the mid-focal length F (defined in Fig. 1) can be obtained once the axial potential $V(z)$ is known. Hence, the formula for a two-element thin lens as derived by Sturrock¹⁵ and applied by Felici¹⁶ is

$$\frac{1}{f} = \frac{3}{16} \left(\frac{V_1}{V_2} \right)^{1/4} \int_{-\infty}^{\infty} \left(\frac{V'}{V} \right)^2 dz \quad \dots (5)$$

Three-element lens belongs to the same class if the potential of the intermediate electrode V_2 ranges between or is adjusted outside that of the outer electrodes. They may be realized by three-diaphragm or

three-tube systems. If $V_1 = V_3$ then, the lens has equal focal lengths on both sides, so that it is often called an einzel or single lens. It has been analytically found¹⁷ that the focal length f and the distance L of the principal plane to the left of the mid-plane of a thick single lens consisting of three thin plates with equal apertures, located distances a in between, are:

$$\frac{1}{f} = \frac{3}{8a} \left(\frac{V_2}{V_1} - 1 \right) \left[4 - \left(\frac{V_2}{V_1} \right)^{1/2} - 3 \left(\frac{V_1}{V_2} \right)^{1/2} \right] \quad \dots (6)$$

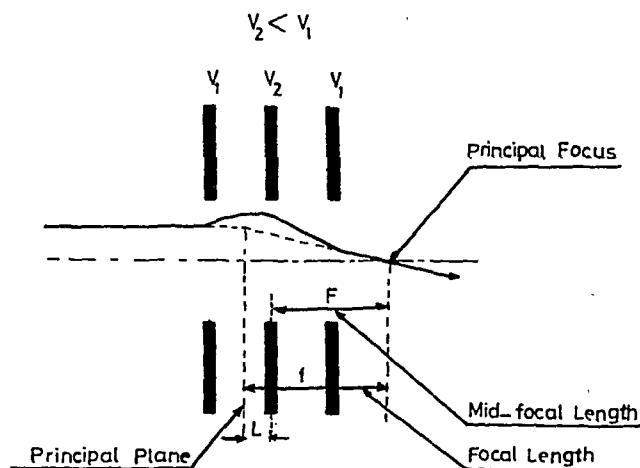


Fig. 1—Representation of focal and mid-focal lengths of a three-aperture symmetric single lens

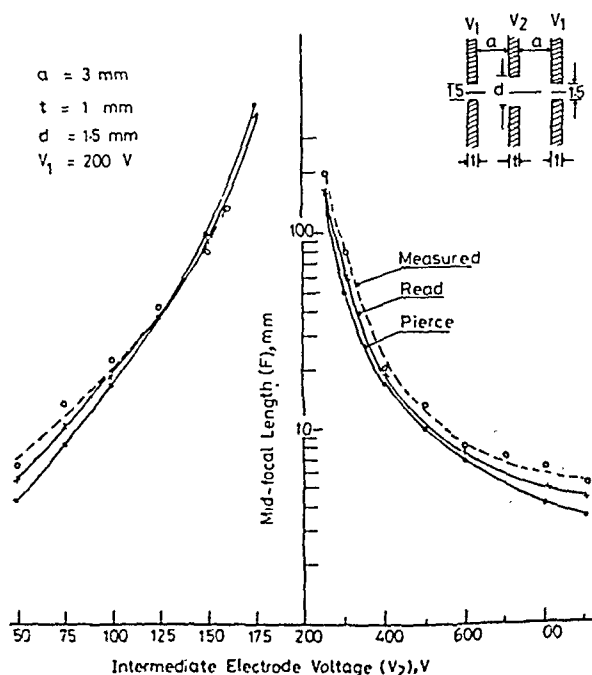


Fig. 2—Comparison of the results calculated by Pierce and Read with those experimentally measured for the mid-focal length, as a function of intermediate electrode voltage of a symmetric single lens

$$L = \frac{4a}{\left[3 - \left(\frac{V_2}{V_1} \right)^{1/2} \right] \left[\left(\frac{V_2}{V_1} \right)^{1/2} + 1 \right]} - a \quad \dots (7)$$

They are plotted in Fig. 2, where the mid-focal length ($f - L$) is considered. As there is a probability of fields on both sides of the lens, electrons may follow curved paths and will not cross the axis at the focus. Thus, Eq (6) represents an approximation to the thin electrodes single lens. However, for more accuracy various techniques have been derived to solve for the potential distributions. The early determination was made experimentally by analogue methods such as electrolytic plotting tank or the resistor network. The former is a perfect physical analogy between the propagation of electric currents through electrolytes and the spreading of the lines of force through an electrostatic field¹⁸. The accuracy is limited by electrolytic polarization and by the surface tension of the liquid producing a meniscus. In the latter, the electrolytic tank is replaced by a network of discrete resistance units connecting a square array of studs. The electrodes of the electron-optical system are simulated by short-circuiting corresponding studs^{19,20}. On the other hand, Glaser²¹ approximated the potential distribution of the single lens by a bell-shaped distribution. This approach has been elaborated by Kanaya *et al.*²² to give all optical data for the single lenses of three thin electrodes with apertures. The alternative methods, giving a more accurate solution for the complicated fields of actual lenses, involved integration of Laplace's equation by computational or numerical methods. The accuracy of these methods depends on the size of integration interval Δz for which $V(z)$ is considered constant. Therefore, more accurate data for the same lens type have been obtained by Read⁶ by numerical integration of

the ray equation using potential distribution calculated by a least square collocation method predicting a convergence of the iterative scheme. The focal length was deduced from the asymptotic behaviour of paraxial rays in the field-free regions. For comparison, his results are represented in Fig. 2. Nevertheless, the method most widely used recently, that does not differ much in accuracy, has been the finite difference method²³ (and its derivatives), in which the region under investigation is divided into a network of grids; each lattice point i is assigned a potential V_i , and Laplace's equation is then approximated by a set of linear equations connecting V_i with the potential V_j at the neighbouring lattice points j . The assumptions made are that the potential varies linearly between any two adjacent lattice points, and that the potential at any lattice point is affected only by the four surrounding points. Lattice points lying on boundary surfaces (that is on the lens elements) have fixed potentials, and potentials of the non-boundary lattice points are determined by solving the connected linear equations iteratively, using a relaxation technique. The accuracy of the solution clearly depends on the number of lattice points. One advantage of this method is that only the least estimate of the potential at each point need be stored. Coefficients of the potential terms are recalculated each time they are required.

3 Measurements and Discussion

For producing a possible parallel electron beam to the lens a simple form of Pierce gun, that has been discussed previously²⁴, was used and assembled 10 mm apart from the three-element lens. The electrodes of the lens were made of stainless steel with 1.5 mm aperture and 1 mm thickness for the outer two, while the dimensions of the intermediate electrode were subject to investigation requirements. The insulators were

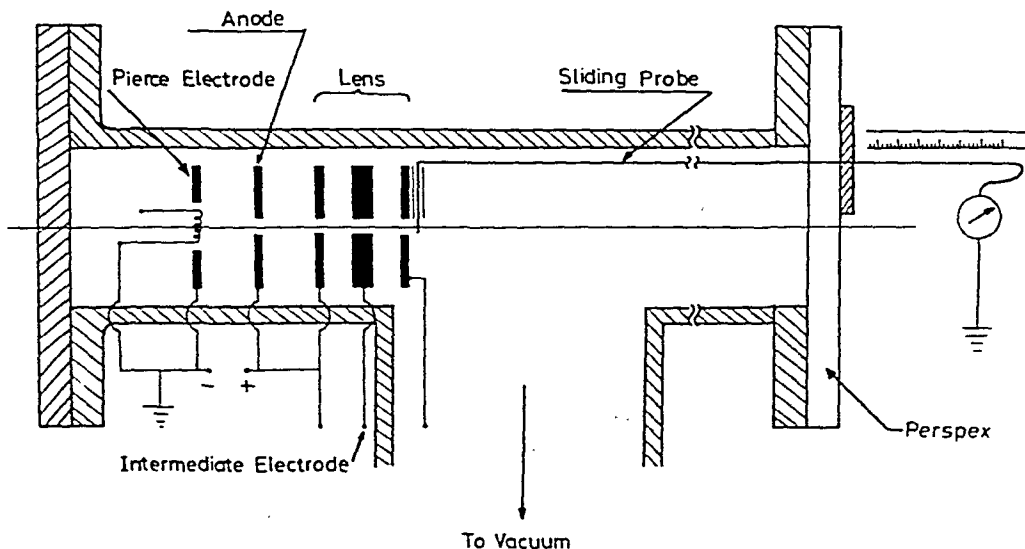


Fig. 3—A schematic drawing of the geometry of the system

kept away from the beam trace in order to avoid charging up and the build-up of contaminating layers on surfaces. The measurements were taken by a movable cylindrical probe 1 mm in diameter and 1 mm in length, made of tungsten. The vacuum chamber was made of iron coated with a thin layer of chromium to avoid stray fields. The system is schematically depicted in Fig. 3.

The studies were carried out with a vacuum of $\sim 10^{-6}$ mm Hg. The first experiment aimed to find out the extent of accuracy of the work. A symmetric single lens was prepared, with a ratio of electrode width (t) to aperture diameter (d), i.e. $t/d = 0.6$, while the theoretical plots of Fig. 2 were done for a lens of $t/d = 0.5$; it has been noticed that this difference makes no serious departure in the result²². The gun was then adjusted to give an electron beam of intensity $\sim 10 \mu\text{A}$, when the anode potential was fixed at 200 V with respect to the earthed cathode. For each voltage ratio (V_2/V_1), the probe was axially moved along the beam up to the position where the meter gives the maximum current. This was taken as the focus since the beam at the object side was nearly parallel. At the foci the readings were almost the same with a value of $\sim 3 \times 10^{-7}$ A, within the cases of higher voltages, then the foci became no longer definite. The results are shown in Fig. 2 too. It shows that for voltage ratio V_2/V_1 greater than unity the experimental values are a little higher than the corresponding calculated ones. This is thought to be due to errors in the extent of parallelism of the object beam and spherical aberration, as it makes the position inconsistent with the exact focus. However, the discrepancy is quite finite, since besides being comparable they behave in the same manner with voltage V_2 . Therefore, we could reliably proceed to investigate the dependence of the lens performance on the various parameters. Hence, next an experiment was done to find out how far the collimating effect depends on the thickness t . Fig. 4 represents the relation between V_2 and the mid-focal length F for different values of t . It shows that at $t = 8$ mm the focus could not be obtained unless V_2 was relatively increased. Then, at such higher voltage, the focal length showed to be longer for higher thicknesses. On the other hand, with thin electrode, as the voltage V_2 decreased from 1000 V, the mid-focal length was slightly increased, and when the voltage ratio V_2/V_1 became less than 2, it rapidly increased to infinity. Here, it is worth noticing that the focal length increases with thickness.

In the light of this result, we could conclude that the choice of both thickness and voltage are subject to the target location. However, it was noticed that with decreasing voltage, for longer focal lengths, the currents at the corresponding foci were gradually decreasing. Hence, it is appropriate to utilize cylindrical elements

rather than apertured disks for getting longer focal lengths. Three complementary experiments were performed. In Figs 5 and 6 the dependence of the mid-focal length on the voltage is demonstrated for different values of d and a respectively. It may be seen that with wider aperture the mid-focal length was more shortened and controlled at still lower voltage ratios. Here, we did not apply wider aperture; otherwise the system might suffer spherical aberration. Besides, it indicated appreciable increase when the spacing (a) increased, as shown in Fig. 6. In this case, precautions were taken to avoid spurious fields that affect electron paths within the spacings.

It must be noted that when the experiment was done to find out the difference between symmetric and its corresponding asymmetric lens, the results were nearly the same. The spacings were varied from $a = 3$ and 3 to 7 and 2 mm respectively, for a lens with 1 mm thickness and 1.5 mm intermediate electrode diameter.

Again, with an equi-dimensions symmetric lens having 6 mm spacing in between each two electrodes, other two experiments were performed to find out the behaviour of the lens for the voltage-asymmetric case. The first was done to produce a focussed beam with continuous voltage variability while keeping the probe at 1.5 cm from the lens, that is zoom mode. With V_1

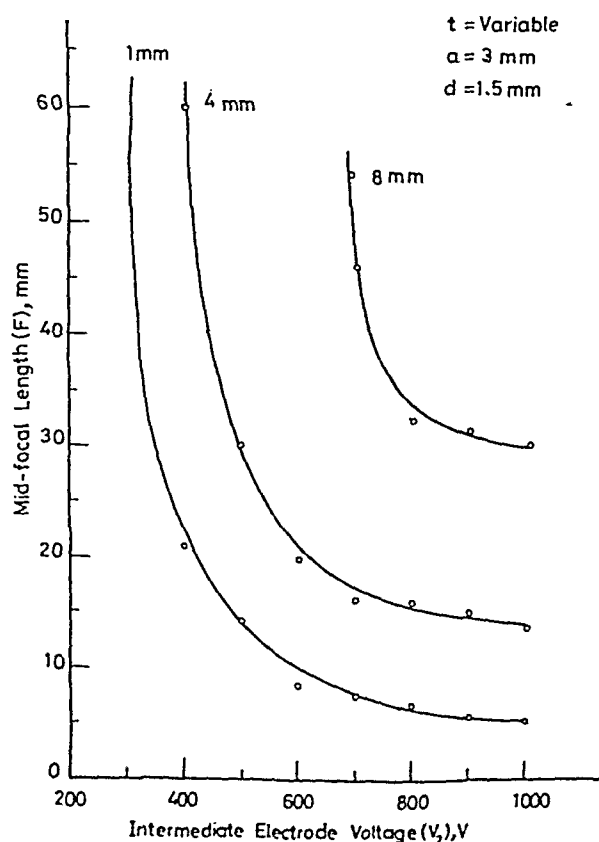


Fig. 4—Characteristic of symmetric single lens with intermediate electrode thickness as a parameter

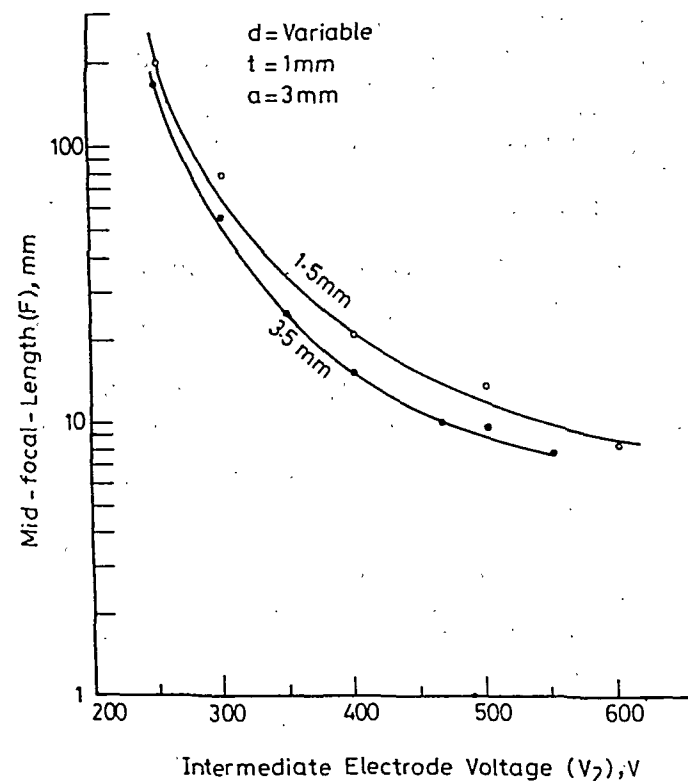
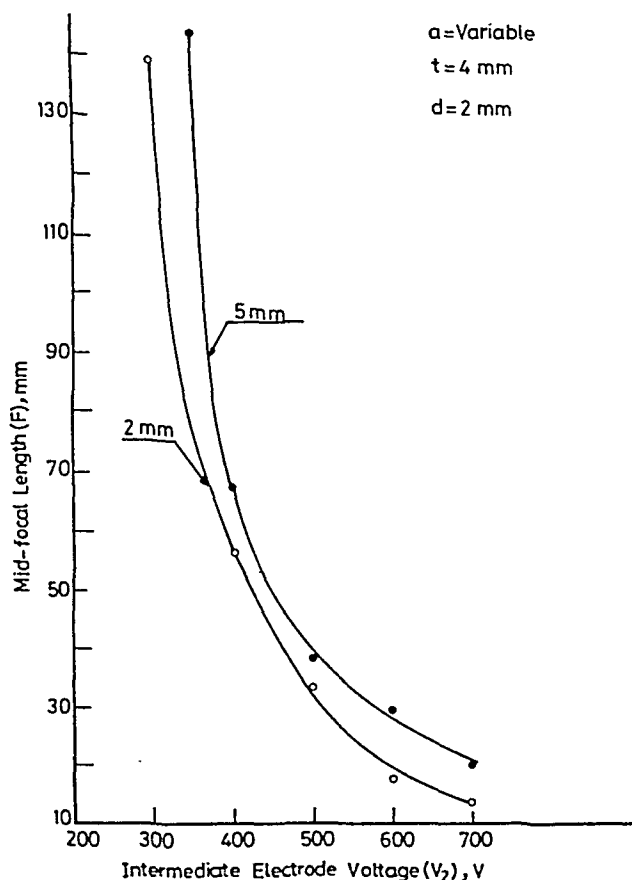
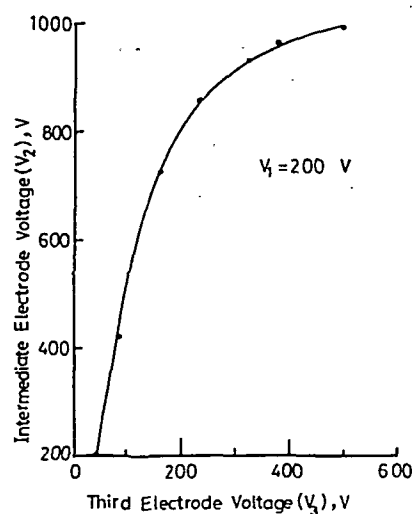
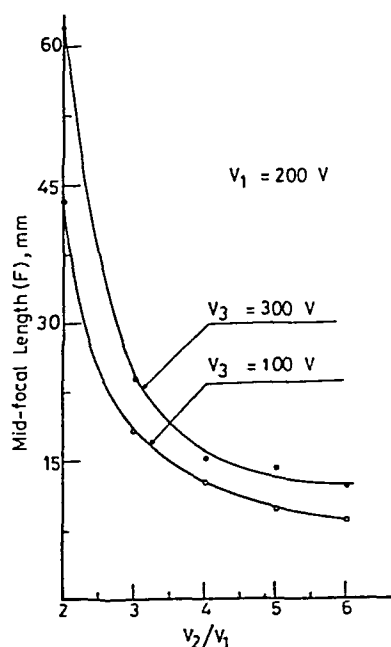


Fig. 5—Characteristic of symmetric single lens for two intermediate electrode apertures


 Fig. 6—Characteristic of symmetric single lens for two spacings (a) in between the electrodes

fixed at 200 V, V_3 was readjusted for the different values of V_2 , in order to obtain the maximum possible current ($V_2 \geq V_1$). It may be pointed out that the current measured by the probe was not the same for the different values of V_2 . This is due to the variation in spot magnification. However, we did not try to measure the magnification as it needs to replace the probe by a glass plate coated with phosphorus followed by a glass window joined with a travelling microscope. The variation we obtained is shown in Fig. 7. It is clear that V_3 linearly increases up to $V_2 = 730 \text{ V}$, then rapidly increases.

The next experiment was done to find how the mid-focal length varied when V_2 was varied with respect to


 Fig. 7—The plot of zoom lens, showing the relation between V_2 and V_3 for a constant value of V_1 of a symmetric lens with spacing $a = 6 \text{ mm}$

 Fig. 8—Mid-focal length as a function of V_2 for two values of V_3 when V_1 is fixed at 200 V

V_1 , for $V_3 = 100$ and 300 V respectively. The result is shown in Fig. 8. In general, the behaviour was like that of the single lens but with shorter mid-focal lengths. On the other hand, the mid-focal length was finite. This is because the control electrode V_2 caused the lens to act like two immersion lenses in series, one of which can be made with a voltage ratio other than unity. For an immersion lens, the mid-focal length becomes infinite when $V_2 = V_1$.

4 Conclusion

This it is clear that though, according to theory, the mid-focal length depends only on the potential gradient, it shows dependence on the lens dimensions as well, when studied experimentally. Hence, it is important to supplement theory with empirical data. Besides, it is adverse to compromise between target location and lens dimension on one hand; on the other hand, it is advantageous to use voltage-asymmetric lens since the mid-focal length can be made finite as V_3 is varied by making V_2 any value other than V_1 . It is worth clarifying that the latter strategy can be adopted at the expense of the number of the power supplies used. However, the ultimate choice depends on the role the lens is designed for.

References

- 1 Cross J D, Read F H & Riddle E A, *J Sci Instrum (GB)*, **44** (1967) 993.
- 2 Grivet P, *Electron optics* (Pergamon, New York), 1965.
- 3 Paszkowski B, *Electron optics* (Illife Books, London), 1968.
- 4 Imhof R E & Read F H, *J Sci Instrum (GB)*, **1** (1968) 859.
- 5 Read F H, *J Sci Instrum (GB)*, **2** (1969) 165.
- 6 Read F H, *J Sci Instrum (GB)*, **3** (1969) 679.
- 7 Read F H, *J Sci Instrum (GB)*, **3** (1970) 127.
- 8 Read F H, Adams A & Soto-Montiel J R, *J Sci Instrum (GB)*, **4** (1971) 625.
- 9 Harting E & Read F H, *Electrostatic lenses* (Elsevier, Amsterdam), 1976.
- 10 El-Kareh A B & El-Kareh J C J, *Electron beam, lenses and Optics* (Academic Press, London), 1970.
- 11 Kuroda K, Suzuki T, *J Appl Phys (USA)*, **45** (1974) 1436.
- 12 Kuroda K, Ebisui H & Suzuki T, *J Appl Phys (USA)*, **45** (1974) 2336.
- 13 Kuroda K & Suzuki T, *Appl Phys Lett (USA)*, **25** (1974) 23.
- 14 Riddle G H N, *J Vac Sci & Technol (USA)*, **15** (1978) 857.
- 15 Sturrock P A, *Proc London Conf on Electron Microscopy* (Royal Microscopical Society, London), 1954.
- 16 Felici N J, *J Phys Rad (France)*, **20** (1959) 97.
- 17 Pierce J R, *Theory and design of electron beams* (D. Van Nostrand, New York), 1954, 98.
- 18 Karplus J W, *Analog simulation* (New York), 1958.
- 19 Liebmann G, *Br J Appl Phys (GB)*, **1** (1950) 92.
- 20 Weber C, *Philips Res Rep (Netherlands)*, **6** (Suppl) (1967).
- 21 Glaser W, *Handb Phys (Germany)*, **33** (1956) 123-395.
- 22 Kanaya K, Kawakatsu H, Yamasaki H & Sibata S, *J Sci Instrum (GB)*, **43** (1966) 416.
- 23 Natali S, Dichio D, Uva E & Kuyatt C E, *Rev Sci Instrum (USA)*, **43** (1972) 80.
- 24 Saad H M & Abd-Elhamed H, *Arab J Nucl Sci & Appl (Egypt)*, (1986).

Production of Tachyons in Extended Manifolds of General Relativity

A P TROFIMENKO & V S GURIN

Astronomical Section of Minsk Department of Astronomical-Geodesical Society of the USSR,
Abonent Box 7, Minsk-12.2200 12, USSR

Received 11 June 1985; revised received 28 May 1986

The extended space-time manifold of a uniformly accelerating (decelerating) reference frame is considered. An analogy between the light barrier and a black hole event horizon in the theory of relativity, is shown. It is stated that there is a possibility for bradyon-tachyon transitions in the proper reference frame by a constant acceleration, i.e. for the light barrier penetration.

1 Introduction

In most results of special relativity (SR) and general relativity (GR), there exist similar peculiarities: the light barrier and an event horizon, occurrence of which is associated with the principle of short-range interaction being common for both the theories. The expressions which connect proper and coordinate times and distances are the following for uniform motion and the Schwarzschild gravitational field, respectively¹:

$$t = t_0(1 - V^2/c^2)^{-1/2}, \quad l = l_0(1 - V^2/c^2)^{1/2} \quad \dots (1)$$

$$t = t_0(1 - 2GM/rc^2)^{1/2}, \quad l = l_0(1 - 2GM/rc^2)^{-1/2} \quad \dots (2)$$

where t_0 and l_0 are the proper time and the proper distance respectively. The first pair of the expressions for $V = c$ and the second pair for $r = r_g = 2GM/c^2$ (G being gravitational constant and c the light speed) become singular. For $V > c$ and $r < r_g$, all the left-hand values become imaginary. If we pass over to the non-relativistic limit, $c \rightarrow \infty$, the singularities will disappear together with the division of the space-time into subluminal and superluminal regions as well as into regions over a horizon and under it. Thus, non-Euclidean topology of space-time (pseudospherical surfaces, the higher dimensionality, etc.) is conditioned by finiteness of the fundamental speed². It should be noted that non-Euclidean topology may be not only a theoretical construction of GR, but also it can develop in global structure of the universe by realizing such astronomical phenomena as quasars, gamma-bursts, voids in the large-scale structure, etc.²

Superluminal objects are obtained in relativity through the generalization of the usual Lorentz transformations to $V > c$ by means of both real^{3,4} and complex (imaginary)⁵⁻⁷ transformations. It is important

for further consideration that both types of superluminal transformations (SPL transformations) conserve some common principles of superluminal physics. Specifically, there is the reciprocity^{3,4,8} (or duality⁵⁻⁷) principle on symmetry of bradyonic and tachyonic worlds, which maps the bradyonic 4-space to the tachyonic one. Also, in similarity to the horizon crossing in black hole extended manifolds, under SPL transformations the roles of time and space coordinate are interchanged^{6,8}.

We would like to emphasize that analogies between features of black hole extended manifolds and superluminal physics are not accidental. They are linked with the extension of relativity principles to superluminal phenomena which consists of transformations of the Minkowski metric tensor to a more general form, i.e.

$$\gamma_{\mu\theta} = \begin{pmatrix} \pm 1 & & & \\ & \pm 1 & & \\ & & \pm 1 & \\ & & & \pm 1 \end{pmatrix} \quad \dots (3)$$

This is true both for complex and real SPL transformations. Such a metric tensor is, in essence, a particular case of a GR-metric (diagonal) when the metric tensor is in a general case, the arbitrary function of space-time coordinates. So, for example, in the spherical polar coordinates we have instead, the tensor (3)

$$\gamma_{\mu\theta} = \begin{pmatrix} \pm 1 & & & \\ & \pm 1 & & \\ & & \pm r^2 & \\ & & & \pm r^2 \sin^2 \theta \end{pmatrix} \quad \dots (4)$$

while in the Schwarzschild case

$$g_{\mu\nu} = \begin{pmatrix} (1 - 2GM/rc^2) & & & \\ & -(1 - 2GM/rc^2)^{-1} & & \\ & & -r^2 & \\ & & & -r^2 \sin^2 \theta \end{pmatrix} \dots (5)$$

Thus, the transformation from $\gamma_{\mu\alpha}$ (Minkowski) to some other form (3) corresponds to the transformation from $r > r_g$ region to $r < r_g$ one in (5).

According to the duality principle, tachyons behave as bradyons and bradyons do as tachyons in a SPL reference frame. Within the framework of SPL extensions of SR, tachyons and bradyons remain separate. It is impossible to transit between tachyonic and bradyonic objects. However, within the framework of GR, the situation is principally changed.

In this paper, we consider the extended manifold construction procedure in the reference frame of a uniformly accelerating observer. The possibility of transition from bradyons to tachyons through motion in the proper reference frame with intersection of metric pseudo-singularities, is shown. Such transitions are possible in black hole extended manifolds, for example, in the Kerr black hole.

2 Extended Manifold of a Uniformly Accelerating Observer

Let us consider the geometry of the reference frame for an observer moving with a constant acceleration A (> 0) or deceleration A (< 0)^{9,10}, which is described by the metric

$$ds^2 = (1 + Ar \cos \theta)^{-2} [(1 - A^2 r^2) dt^2 - (1 - A^2 r^2)^{-1} dr^2 - r^2 (d\theta^2 + \sin^2 \theta d\phi^2)] \dots (6)$$

where r is the distance from the observer to the accelerating object. We use here the geometrized units, where $c = G = 1$.

We shall consider the conformal structure of the space-time, when character of pseudosingularities in the metric (6) takes an importance. This metric is very similar to the well-known de Sitter metric with constant curvature¹¹. It takes the de Sitter form in the equatorial plane $\theta = \pi/2$ and in the renotation of the constant $A^2 = \Lambda/3$, where Λ is the cosmological constant. In such a space-time manifold, the surfaces $r = \pm A^{-1}$ are horizons but not singularities. The extension of the de Sitter metric beyond the horizon was performed in some studies¹²⁻¹⁴. We shall apply the analysis of the de Sitter metric for an investigation of the conformal structure of the uniformly accelerating metric (6). We shall demonstrate the possibility of motion across the horizon surfaces $r = \pm A^{-1}$.

In order to remove the pseudosingularities at horizons in the metric (6), we adopt the following new coordinates¹²

$$u = 2C \exp(\gamma r^*) \cosh(\gamma t), \quad v = 2C \exp(\gamma r^*) \sinh(\gamma t) \dots (7)$$

with the ranges $-\infty < u < +\infty$, $-\infty < v < +\infty$, where $C = \text{constant}$, $\gamma = \text{constant}$. Then the metric gets the form:

$$ds^2 = (1 + Ar \cos \theta)^{-2} [f^2(u, v) (dv^2 - du^2) - r^2 (d\theta^2 + \sin^2 \theta d\phi^2)] \dots (8)$$

We define here

$$f^2(u, v) = \frac{1}{4} C^{-2} \gamma^2 (1 - A^2 r^2) \exp(-2\gamma r^*) \dots (9)$$

$$r^* = \int (1 - A^2 r^2) dr = \frac{1}{2} \log[(1 + Ar)(1 - Ar)] \dots (10)$$

We can easily obtain

$$f^2(u, v) = \frac{1}{4} C^{-2} \gamma^{-2} (1 + Ar)^{1-\gamma} (1 - Ar)^{1+\gamma} \dots (11)$$

The metric of a uniformly accelerating observer (6), will not be singular at the horizons $r = \pm A^{-1}$ if the parameters are constrained within certain conditions. We choose $\gamma = \pm 1$ for $A \leq 0$, respectively, and C is an arbitrary constant. Then,

$$\begin{aligned} f^2 &= (1 + Ar)^2 / 4C^2 \text{ for } A > 0 \text{ (} \cos \theta > 0 \text{)} \\ f^2 &= (1 - Ar)^2 / 4C^2 \text{ for } A < 0 \text{ (} \cos \theta < 0 \text{)} \end{aligned} \dots (12)$$

Therefore, the new non-singular space-time coordinates are connected with (t, r) -coordinates by the following formulae

$$\begin{aligned} u &= C[(1 \mp Ar)(1 \pm Ar)]^{1/2} \cosh(\mp At) \text{ for } A \geq 0 \\ v &= C[(1 \mp Ar)(1 \pm Ar)]^{1/2} \sinh(\mp At) \text{ for } A \geq 0 \end{aligned} \dots (13)$$

The inverse transformations are:

$$r = \pm (1/A) (C^2 - u^2 + v^2) / (C^2 + u^2 - v^2)^{-1} \dots (14)$$

$$t = \mp (1/A) \coth^{-1}(u/v) \dots (15)$$

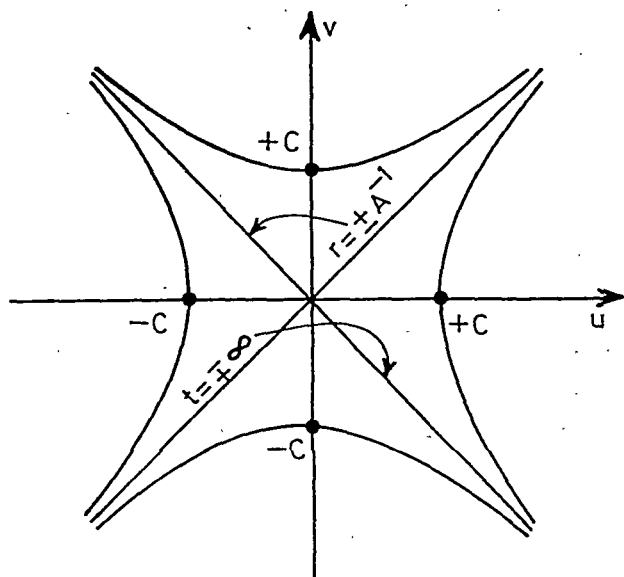


Fig. 1—Kruskal-like diagram for the extended space-time manifold of a uniformly accelerating reference frame

With the help of the set of correlations, the space-time manifold can be represented as the Kruskal-like diagram in the (u, v) -coordinates. The space-times for both $A > 0$ (acceleration) and $A < 0$ (deceleration) cases can be drawn on the same diagram since they have the same conformal structure (Fig. 1).

The compactified representation of the conformal structure for the space-time under investigation can be done¹ with the help of transformations which are used to construct Penrose-like diagrams, i.e. by transforming (u, v) -coordinates to (p, q) -ones according to the formulae

$$u = \tan p, \quad v = \tan q \quad \dots (16)$$

with the ranges $-\pi/2 \leq q \leq +\pi/2$ and $-\pi/2 \leq p \leq +\pi/2$. In Fig. 2, two cases of the uniformly accelerating (or decelerating) space-times are shown in (p, q) -coordinates.

One can see four regions on these diagrams which are divided by the future horizon $r = A^{-1}, t = +\infty$ or $r = -A^{-1}, t = +\infty$ and the past horizon $r = A^{-1}, t = -\infty$ or $r = -A^{-1}, t = -\infty$ for acceleration or deceleration, respectively. They are bounded by the origin and the spatial infinity $r = \infty$, which are not singularities but emerge as physical boundaries of the space-time.

It can be remarked¹ that some similarities exist between this representation of the space-time of a uniformly accelerating observer and the analogous representation for the Schwarzschild space-time manifold. For example, the asymptotically flat Schwarzschild region corresponds to $r = 0$ region here; the Schwarzschild singularity at $r = 0$ conforms to $r = \infty$ in Fig. 2 and the Schwarzschild past and fu-

ture horizons at $r = 2M, t = \mp \infty$ show analogous properties with $r = \pm A^{-1}$ surfaces.

The above facts do not restrict the possible similarities of the space-time structure between the Schwarzschild manifold and the manifold of a uniformly accelerating (decelerating) observer. One can investigate the behaviour of geodesics in the geometry (6) and show that the coordinate and proper time intervals are very much analogous to those in the Schwarzschild geometry: the geodesics in the proper time will be finite at the horizons. This fact indicates again a possibility to pass the horizons from the region $r < \pm A^{-1}$ to the region $r > \pm A^{-1}$, i.e. from the subluminal (SBL) region to the SPL one. This process corresponds to the passage from the region over an event horizon to the one under it¹⁵⁻¹⁷. Moreover, we must emphasize on the basis of the earlier studies¹⁵⁻²⁰ that regions under an event horizon are nothing but SPL ones; hence every horizon divides a space-time into SBL and SPL regions forming a space-time manifold with non-trivial topology. In other words, taking into account the six-dimensional interpretation of SPL phenomena^{6, 21}; and phenomena under black hole event horizons^{2, 18-20}, we can conclude that a

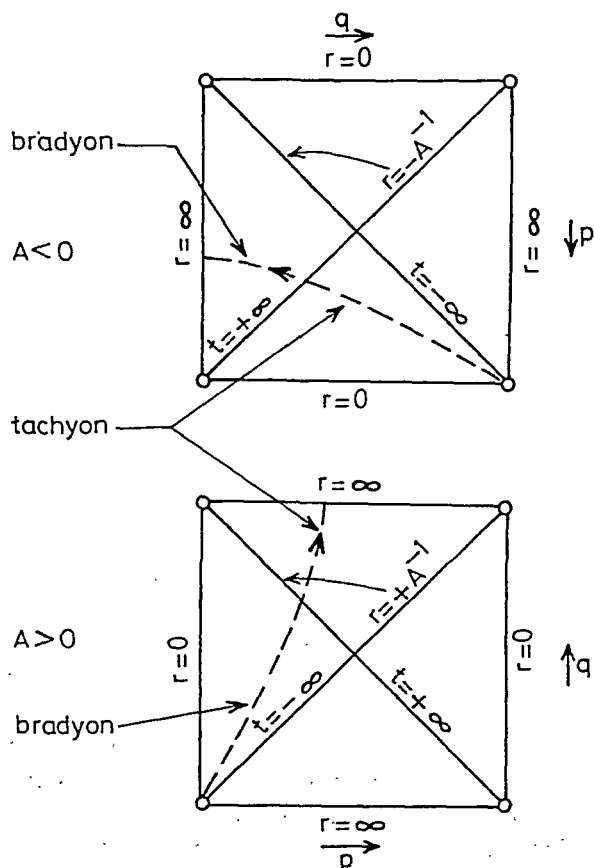


Fig. 2—Representation of the extended manifold of uniformly accelerating and decelerating frames by means of Penrose diagrams. [It is obtained from Fig. 1 through compactifying conformal transformations. The dashed line shows motion with transitions: bradyon \rightarrow tachyon and vice versa.]

horizon and the light barrier divided $R^4 \equiv (\mathbf{r}, t)$ and $T^4 \equiv (\mathbf{t}, r)$ subspaces in the global $D^6 \equiv (\mathbf{r}, \mathbf{t})$ space.

We would like to point out here that the above mentioned six-dimensional consideration of SPL phenomena is not an alternative to the complex ones which are developed in earlier studies^{2, 19, 24}. The six-dimensional consideration can be interpreted as an intermediate step of complex representation of extended manifolds in GR.

Let us consider qualitatively the motion a body pictured by the dashed line in the Fig. 2. When an object is approximating to the horizon with a constant acceleration, it will gradually disappear becoming asymptotic to the $r = A^{-1}$ surface with regard to the observer at rest in some point (such a situation is analogous to some object 'disappearing' when it falls on a black hole). But in the reference frame of an observer at rest, the object will never pass across the surface $r = A^{-1}$. In the proper reference frame of an accelerating body, this surface is not peculiar at all, and passing across it the object goes to the SPL region, i.e. it becomes a tachyon. A similar consideration can be given for a decelerating body from SPL region to SBL one, when it crosses the surface $r = -A^{-1}$. In this case, a tachyon is transforming into a bradyon with respect to the original reference frame (see Fig. 2). We notice that the above conclusion regarding the horizon crossing in the proper reference frame of a uniformly accelerating (decelerating) body is valid only in this frame, and for a rest frame the crossing through the horizon is not observable.

Thus, space-time manifolds of uniformly accelerating and decelerating observers have a chance to produce tachyons from bradyons and bradyons from tachyons, respectively, in principle.

3 Discussion

In many studies on SPL extension of SR, SPL speeds of inertial motion are considered on equal footing with SBL ones, but the value of the light speed remains limited for both tachyons and bradyons. In other words, the light barrier penetration is impossible: bradyons remain always bradyons and tachyons are always tachyons with respect to an inertial frame. This thesis is unquestionably true for an inertial motion and in the absence of gravitational fields.

The conclusions of the present paper show the possibility to transform continuously from one class of objects to other one. It can be realized due to non-inertial motion. However, the light barrier penetration is possible only in a proper uniformly accelerating or decelerating reference frame without any violation of the principles of relativity. This deduction is contradicting the relativity-violating analogous conclusions^{22, 23}. Although our results might seem a little un-

expected, they can be easily understood within the framework of GR. They are the consequence of the fundamental principle of equivalence and do not contradict SR because while analyzing accelerating motion, we leave its realm and pass over to GR, where, as we have shown, the light barrier penetration is quite possible.

We should note that while discussing accelerating motion, evidences are found in literature (see, for example, Refs 25, 26) indicating possibility of infinitely long motion with a constant accelerating, i.e. possibility to penetrate the light barrier. However, no conclusions are reported on the possibility of passage to the superluminal region even in extended manifolds of GR.

Continuing the analogy between space-time structures with horizons for the uniformly accelerating frame and gravitational fields²⁷, we can propose the possibility of tachyon-bradyon transitions in space-time manifolds of a black hole. Further details of this problem will be reported by the author in future. However, we point out that tachyon production from the Schwarzschild black hole was recently investigated by Srivastava¹⁸.

Let us perform some estimations concerning the proposed possibility of the light barrier penetration. Consider an object from the point of view of its own reference frame which travels with a constant acceleration A (value of A being equal to that of the free fall acceleration in the Earth's field, g). Such an object can travel for an unlimited time without any restrictions (in the proper reference frame!). In such an accelerating frame, there will be observed local effects analogous to those occurring in the earth's gravitational field. The distance to the accelerating horizon can be estimated to be²: $r = c^2 g^{-1} \approx 10^{18}$ cm \approx a light year, i.e. a distance of about the size of the solar system.

In conclusion, we draw attention to the fact that within the framework of SPL extension of relativity and electrodynamics, the behaviour of an electric charge as a magnet has been studied^{3, 4, 28, 29}. Hence, our deduction on the possibility of tachyon production by an accelerating motion suggests a possibility of production of particles having properties of magnetic monopoles.

Acknowledgement

The authors thank the referee for useful remarks and suggestions. They express their thanks to Professors G M Idlis and Y P Terletsky for their interest and discussions, and also to the participants of various seminars arranged by the Astronomical Section of the Minsk Department of the Astronomical-Geodesical Society of the USSR, for valuable comments.

References

- 1 Misner Ch W, Thorne K S & Wheeler J A, *Gravitation* (Freeman & Co, San Francisco), 1973, Ch. 30, 31.
- 2 Trofimenko A P, *Genesis and contemporary problems of Oton astrophysics* (in Russian), Deposited in INION of the Academy of Science of the USSR, 1984, No. 16810.
- 3 Antippa A F, *Phys Rev D (USA)*, **11** (1975) 724.
- 4 Negi O P S & Rajput B S, *Phys Lett B (Netherlands)*, **113** (1982) 183; *Indian J Pure & Appl Phys*, **21** (1983) 232.
- 5 Recami E & Mignani R, *Riv Nuovo Cimento (Italy)*, **4** (1974) 209.
- 6 Pavišič M & Recami E, *Lett Nuovo Cimento (Italy)*, **19** (1977) 273.
- 7 Recami E & Rodrigues W A, *Found Phys (USA)*, **12** (1982) 709.
- 8 Rajput B S, Purohit K D & Negi O P S, *Indian J Pure & Appl Phys*, **19** (1981) 1081, **20** (1982) 22.
- 9 Gibbons G W & Perry M J, *Phys Rev D (USA)*, **22** (1980) 319.
- 10 Kinnersley W & Walker M, *Phys Rev D (USA)*, **2** (1970) 1359.
- 11 Tolman R S, *Relativity, thermodynamics, and cosmology* (Clarendon Press, Oxford), 1969, 144.
- 12 Graves J C & Brill D R, *Phys Rev (USA)*, **120** (1960) 1507.
- 13 Geyer K H, *Astron Nachricht (Germany)*, **301** (1980) 135.
- 14 Gautreau R, *Phys Rev D (USA)*, **27** (1983) 764.
- 15 Goldoni R, *Acta Physica Austriaca (Austria)*, **41** (1975) 75, 133; *Lett Nuovo Cimento (Italy)*, **21** (1980) 333.
- 16 Narlikar J V & Dhurandhar S V, *Lett Nuovo Cimento (Italy)*, **23** (1978) 513.
- 17 DeSabbata V, Pavišič M & Recami E, *Lett Nuovo Cimento (Italy)*, **19** (1977) 341.
- 18 Srivastava S K, *J Math Phys (USA)*, **24** (1983) 1317.
- 19 Gurin V S, *Fizika (Yugoslavia)*, **16** (1984) 87.
- 20 Gurin V S, *Pramana (India)*, **24** (1985) 817; *Nuovo Cimento A (Italy)*, **88** (1985) 253.
- 21 Chandola H C & Rajput B S, *J Math Phys (USA)*, **26** (1985) 208; *Lett Nuovo Cimento (Italy)*, **40** (1984) 277; *Indian J Pure & Appl Phys*, **21** (1983) 651.
- 22 Everett A, *Phys Rev D (USA)*, **13** (1976) 785.
- 23 Froning H D (Jr), *J Brit Interplanet Soc (GB)*, **36** (1983) 227.
- 24 Trofimenko A P & Gurin V S, *Oton systematics*, Deposited in INION of the Academy of Sciences of the USSR, 1985, No. 21353; *Fizika (Yugoslavia)*, **17** (1985) 101.
- 25 Bondi H, *Relativity and common sense* (Anchor Books Doubleday & Co, New York) 1964.
- 26 Morgan J W, *Spaceflight (GB)*, **32** (1973) 252.
- 27 Rindler W, *Am J Phys (USA)*, **34** (1966) 1174.
- 28 Mignani R & Recami E, *Lett Nuovo Cimento (Italy)*, **9** (1974) 367; *Nuovo Cimento A (Italy)*, **30** (1975) 533.
- 29 Gunawant R, Negi O P S & Rajput B S, *Lett Nuovo Cimento (Italy)*, **41** (1984) 21, 505.

Differential Gamma Dose Rate for Neutral Beam Injection-ducted Concrete Shield

F M SAYEDAHMED & A ABOUD

Reactor & Neutron Physics Department, Nuclear Research Centre, Atomic Energy Authority Cairo, Egypt

Received 22 October 1985; revised received 7 April 1986

The shielding problems that arise due to the irregular penetrations, such as neutral beam injection ducts (NBID), should be treated carefully to aid in the shield design. The effects due to radiation streaming through NBID on the angular distribution of the total gamma ray doses at the outer surface of an ilmenite concrete shield ($\rho = 4.6 \text{ g/cm}^3$) are discussed. The shield was pierced with NBID of different diameters and lengths and the measurements were made using a collimated beam of both gamma rays and neutrons and ^7LiF teflon thermoluminescent dosimeters. The total dose is highest at the centreline of NBID and tends to decrease with the increase of scattered angle. The experimental data obtained have good agreement with the ones calculated using an empirical expression connecting differential dose rate with scattering angle.

1 Introduction

As previously reported by Selph and Claiborne¹, most of the shields designed for nuclear reactors contain air-filled holes. These irregularities represent serious problems for shield designers.

The most effective method available for reducing the amount of gamma rays and neutrons that travel through such holes is to design the ducts or the pathways so that these radiations do not penetrate straight forward through shields. Bend ducts, and neutral beam injector ducts are typical examples of bad designs for this purpose. In these cases, the radiation transmitted through the holes may constitute a major fraction of the dose penetrating through the shield. A shield designer has to take into account the effect of various types of holes on leakage of gamma rays and neutrons under given set of conditions in the duct construction for effecting maximum economy.

Raso^{2,3} had calculated differential back-scattered dose rate from a semi-infinite medium of a concrete shield using the Monte Carlo technique. Experiments for measuring the differential dose albedo for thick slabs of concrete and several other materials have been previously performed by Clifford⁴ using ^{137}Cs source and by Barrett and Wadmann⁵ using ^{60}Co source. In their studies, the gamma radiation incident on the material slabs was collimated while uncollimated isotropic detectors were used for detection. The radiation streaming through the neutral beam injector (NBI) has been studied by several others^{6,7}.

In the present study, the gamma ray angular dependence is discussed and an empirical expression has been derived for the differential dose rates of the back-scattered gamma rays from the neutral beam injector duct.

2 Experimental Details

The angular gamma ray dose distributions through the NBID ilmenite concrete shield blocks were measured using sets of three large concrete samples in the form of rectangular blocks each of dimension $120 \times 120 \times 40 \text{ cm}^3$. Each block contained a cylindrical hole. For each set of 3 blocks, the first two blocks had holes with 10 cm diameter. The diameter of the hole of the 3rd block ranged from 2.9 to 10 cm. This type of construction enabled us to design a neutral beam of diameter 10 cm and length 80 cm connected with an injector duct of length 40 cm, but having diameters 2.9, 5.8 or 10 cm. The NBID ilmenite concrete shield blocks were arranged in front of one of the horizontal channels of the Egyptian Research Reactor-1 (ET-RR-1). A schematic diagram of the experimental layout is shown in Fig. 1.

Special care was taken to see that the ducted axis coincides with the beam axis, in order to minimize the effect of scattering from the front face of the concrete blocks. The chemical composition of the ilmenite concrete has been reported previously by Megahed *et al.*⁸ A perspex sample holder with special openings was arranged to place the detectors at different distances in two perpendicular directions (R , x directions) with respect to the duct centre-line at the end surface of the ducted shield. The ratio of the distance perpendicular to the duct axis to the length of the neutral beam injector duct helps to evaluate the scattering angle θ , of the scattered gamma rays. Measurements were performed using a collimated beam of gamma rays and neutrons emitted from one of the horizontal channels of the ET-RR-1 reactor.

The gamma doses were measured using small discs of ^7LiF teflon thermoluminescent dosimeters each of

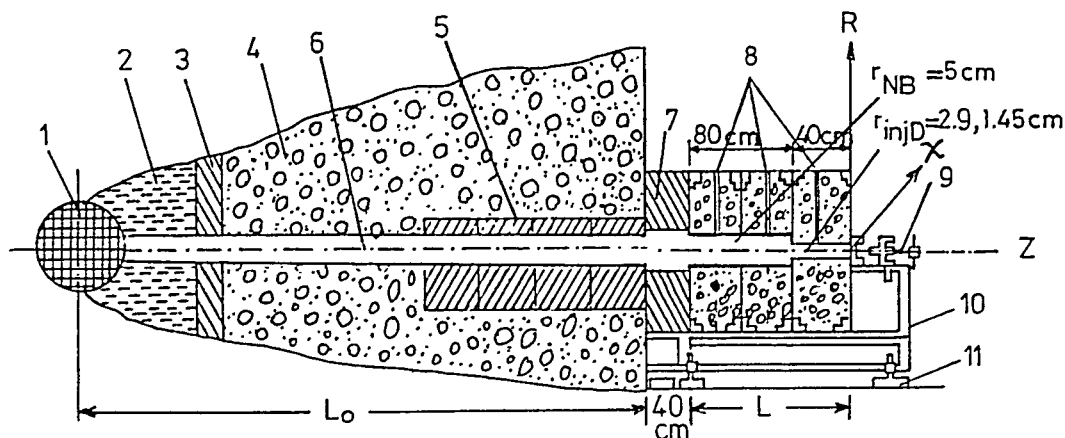


Fig. 1—Schematic diagram of the experiments layout

12.7 mm diameter and 0.4 mm thickness. The isotopic abundance of ^7Li in such a dosimeter is 99.99% and that of ^6Li is 0.01%. ^7LiF dosimeter was chosen for such measurements because it has a low or negligible response to neutrons of different energies, so it serves as a detector suitable for gamma rays in mixed fields of radiations coming from a nuclear reactor^{9,10}. In addition, it has the advantage of accumulating the incident doses during any irradiation time, and therefore, can be used for measurements of very low intensity gamma doses.

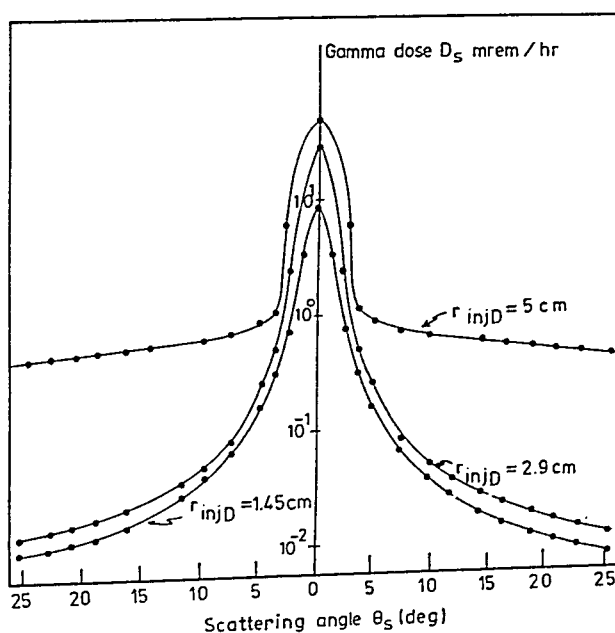
The ^7LiF dosimeters were first calibrated against gamma doses using a ^{137}Cs standard gamma source and the calibration coefficients obtained were used to transform the responses of ^7LiF dosimeters to absolute gamma doses.

The ^7LiF dosimeters were annealed before each measurement in a pre-heated oven maintained at 300°C for 4 hr, and then transferred to another pre-heated oven at 80°C for 24 hr and then left to cool gradually. The annealing time and procedure were systematically repeated every time. The response of the dosimeters was measured using a TLD read-out instrument model Teledyne Isotopes-7300. Before each measurement, the system was calibrated using ^{14}C standard source.

Each measurement was repeated at least twice to reduce statistical uncertainties and to guard against the fluctuation of the reactor power. The accuracy of the measurements was within $\pm 11\%$.

3 Results and Discussion

In the present investigation, the differential dose rate ratio was taken as the ratio between the scattered dose rate D_s at the front face of the neutral beam injector duct at its centre position. Fig. 2 shows the variation of both D_s and the duct radius r as a function of scattering angle θ_s (in degrees), along the


 Fig. 2—Angular gamma dose rate distribution as a function of scattering angle θ_s

perpendicular direction of the NBID axis in the form of isodose curves.

Fig. 2 reveals that the total dose intensity has a pronounced maximum when $\theta_s = 0$. The isodose curves also show that the doses decrease with the increase of the scattering angle θ_s . This decrease is faster for injector ducts of diameters 5.8 and 2.9 cm compared to that with a diameter of 10 cm. This may be attributed to the fact that in the last case, the neutral beam injector duct behaves as a straight duct of diameter 10 cm.

From Fig. 2 one can see also that the total dose at any angle has higher values at larger injector diameters. It is well known that the total dose consists mainly of components of unscattered dose streaming directly as well as the albedo dose scattered and reflected, at the duct walls and inside the shield.

Consequently, one could expect that the value of dose albedo would increase with the decrease of the injector diameter which, in turn, affects the total dose value at the end of the concrete shield.

Raso^{2,3} and Haggmark *et al.*¹¹ have calculated the differential dose of the back-scattered rays, using a semi-infinite medium of concrete. They used the following formula in their calculations:

$$A_d(\vec{\Omega}) = \frac{D_s}{\Omega_c D_0} \quad \dots(1)$$

where $A_d(\vec{\Omega})$ is the differential dose rate ratio; Ω_c the effective detection solid angle; D_0 the incident dose rate at the centre of the slab, and D_s the detected dose rate.

Eq. (1) can be transformed to:

$$A_d(\vec{\Omega}) \Omega_c = \frac{D_s}{D_0} \quad \dots(2)$$

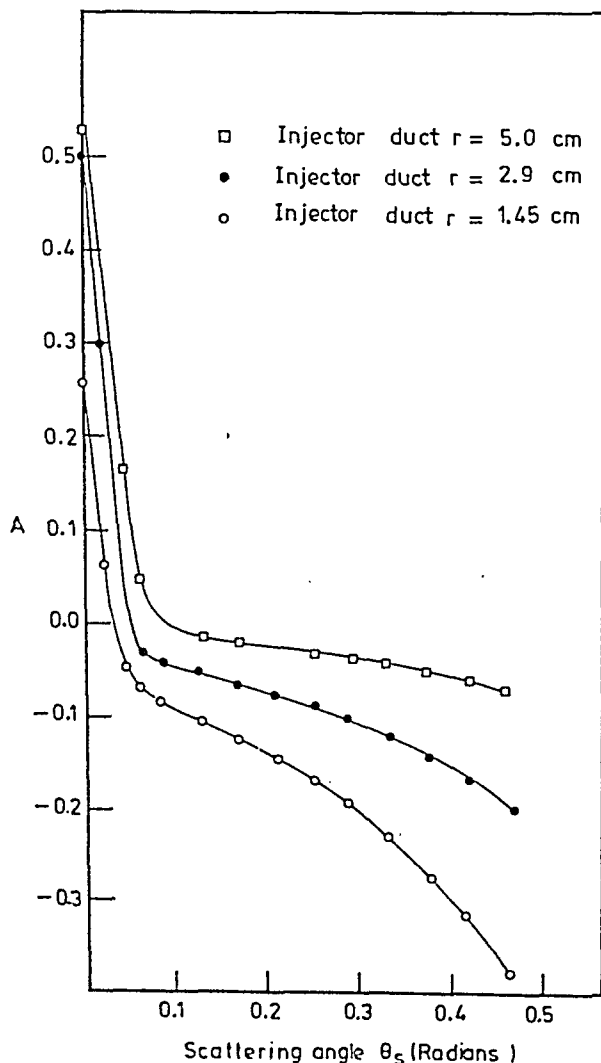


Fig. 3—Variation of parameter A as a function of scattering angle

Raso^{2,3} as well as Haggmark *et al.*¹¹ tried to find a relation between $A_d(\vec{\Omega})$ and the scattering angle θ_s . They found that all the data points for both the same source energy and incident angle (θ_0) could be fitted in a single smooth curve so that an empirical formula in the following form could be derived:

$$A_d(\vec{\Omega}) = A \exp(-m\theta_s) + b \quad \dots(3)$$

where c, m, b are constants to be evaluated for each set of the data.

In the present study, it was found that formula (3) was not able to reproduce the experimental data. This may be attributed to the differences in the geometrical factors (source, geometry, type of shield) applied in the present study. The best fit for the experimental data for the geometry used in the present study was obtained with the following modified formula:

$$A_d(\vec{\Omega}) \Omega_c = G A \exp(-m\theta_s) + b \quad \dots(4)$$

$$G = \left(\frac{L_0}{L_0 + L} \right)^2 \frac{r_{inj}}{r_{NB}} \quad \dots(5)$$

where L_0 = the channel length = 375 cm, L = the neutral beam length + the injector duct length = 80 + 40 = 120 cm, r_{inj} = the injector duct radius = 5, 2.9 or 1.45 cm, r_{NB} = the neutral beam radius = 5 cm, A

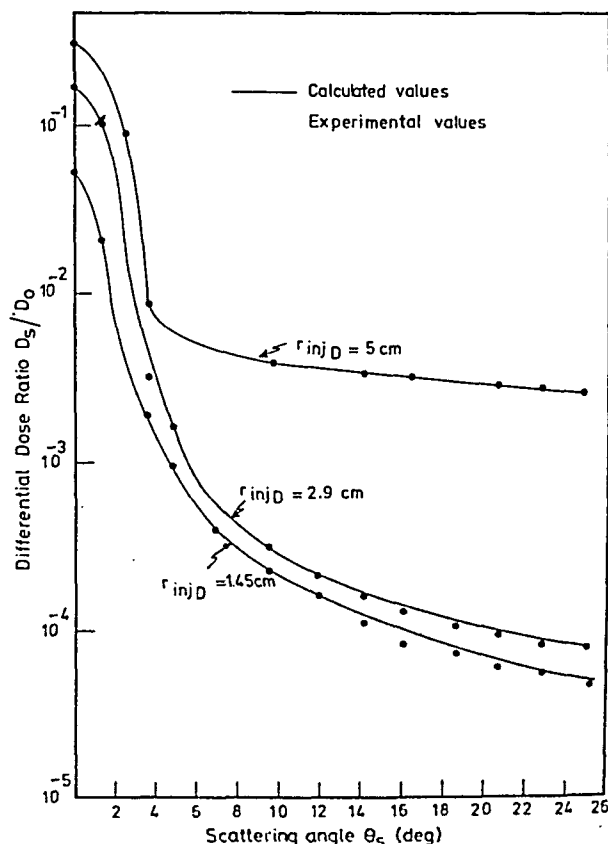


Fig. 4—Comparison of experimental and calculated differential gamma-dose ratios (D_s/D_0)

= the function of scattering angle and duct radius as seen in Fig. 3; $m = \pi$ (according to Ref. 11), and b a function of source energy E , incident angle and the type of shielding material.

The parameters L_0 , L , r_{NB} and m were kept as constants throughout the calculations. The value of r_{inj} was 145, 2.9 or 5 cm depending on the duct used. Attempts were made to obtain the best value of the parameter b which fits the present experimental data. For the case, $r_{NB} = r_{inj}$ (straight duct)

$$b = 6.471 \times 10^{-3} \theta_s + 8.333 \times 10^{-3} \quad \dots (6)$$

For the case $r_{inj} < r_{NB}$

$$b = \left(7.927 \times 10^{-3} + 1.101 \times 10^{-3} \frac{r_{inj}}{r_{NB}} \right) \theta_s + \left(1.08 \times 10^{-2} - 5.1035 \times 10^{-4} \frac{r_{inj}}{r_{NB}} \right) \quad \dots (7)$$

By substituting the values of the relevant parameters in formula (4), a good agreement was obtained between the experimental and calculated differential gamma dose ratio as shown in Fig. 4.

Acknowledgement

The authors express their thanks to Dr A S Makarious for his cooperation and assistance during the experimental work.

References

- 1 Selph W E & Claiborne H C, *Methods for calculating effects of ducts, access ways and holes in radiation shields*, Report (ORNL-RSIC, USA) 20, 1963.
- 2 Raso D J, *Monte Carlo calculations on the reflection and transmission of scattered gamma radiation* (Technical Operations, Inc, New York) Report B 61-39 USA (Revised), 1961.
- 3 Raso D J, *Nucl Sci & Engng (USA)*, 17 (1963) 411.
- 4 Clifford C E, *Differential dose albedo measurements for 0.66 MeV's incident on concrete, iron and lead (U)*, *Def Res Chem Lab Rep* 412 Ottawa, Canada 1963; and *Can J Phys (Canada)*, 42 (1964) 957.
- 5 Barrett M J & Wadmann J, *Experimental gamma ray back-scattering by various materials* (Technical Operations Inc, New York) Research Report No. TO-P 64-68, USA, 1964.
- 6 Ide T, Seki & Iida H, *Second Topical Meeting: Technology of controlled nuclear fusion conference* 760935 USA P2 1976, 395.
- 7 Santore R T, Lillie R A, Alsmiller R G & Barnes J M, *Two- and three-dimensional neutronics calculations for the TFTR neutral beam injectors*, Report ORNL ITM USA (Oak Ridge National Lab), 1978, 6354.
- 8 Megahed R M, Makarious A S & El-Kolaly M A, *Egypt J Phys*, 12 (1981) (No. 1) 1.
- 9 Eid A M, Gomaa M A & Morsy S M, *Nucl Instruments & Methods (Netherlands)*, 160 (1979) 371.
- 10 Eid A M & Delafield H J, *The neutron response of a ^7LiF thermoluminescent dosimeter incorporated in OKAMA criticality dosimeters*, Harwell, AERE M-2803, 1976.
- 11 Haggmerk L G, Jones T H, Scofield N E & Gurne W J, *Nucl Sci & Engng (USA)*, 23 (1965) 138.

Performance of Partial Circular Polarizers under Partially Polarized Light

S D GUPTA & AK MUSLA

Instruments Research & Development Establishment, Dehradun 248 008

Received 1 October 1984; accepted 15 May 1986

The performance of an optical system employing different combinations of right and left partial circular polarizers in the two zones of the optical system illuminated with partially polarized light, has been investigated by making use of coherency matrix approach. The effects of the degree of polarization, polarization form of the incident illuminating beam and relative size of the two zones on the performance of the optical system, have also been taken into account.

1 Introduction

In the previous paper¹, the effect of using linear polarization masks placed at different orientations on different zones of the optical system has been investigated. It has been shown that by suitably choosing the state of polarization of the incident beam and the orientation of the polarization masks, the performance of the optical system can be effectively modified for desired roles. In the present investigation, we study the effect of using circular polarization masks in two zones of the optical system, illustrated in Fig. 1. By employing partial circular polarizers P_1 and P_2 , having relative attenuation ratios α_1 and α_2 , in the two zones of the optical system, it becomes possible to have relatively different pupil transmissions in the two zones and hence modification in the imaging characteristics can be achieved. Further, we consider analyzer also of partial circular type having attenuation ratio α for further modifying the imaging characteristics.

We study in this paper the image intensity distributions of an optical system having two partial circular polarizers in terms of propagation of partially polarized light through non-depolarizing optical system using coherency matrix formation. We have considered three different combinations of partial circular polarizers, i.e. right circular, left circular and also right and left circular combinations. Besides image intensity distributions, the degree of polarization P_0 , and polarization form θ_0 (azimuth angle) and ϵ_0 (ellipticity angle) of the output beam in the image plane, have also been worked out. The effect of degree of polarization P' and polarization form θ' and ϵ' of the incident beam which characterizes a beam of partially polarized light, relative size of the two zones ϵ and relative attenuation of the analyzer α on the image intensity distributions, have been taken into consideration.

2 Theory

In this section we give the derivation of the results of the point image intensity distribution of the optical system masked by two circular polarizers P_1 and P_2 in the central and outer zones when the incident beam is partially polarized. Consider this optical system divided into two zones in which radius (R) of the full circular aperture is unity and radius of the central zone is $R_1 = \epsilon$. The general layout of the optical system divided into two zones and various coordinate axes used are shown in Fig. 1 and are the same as in our earlier paper¹.

To deal with the propagation of partially polarized light through polarizing optical system, coherency matrix formulation has been employed with the state of polarization represented by coherency matrix J^i

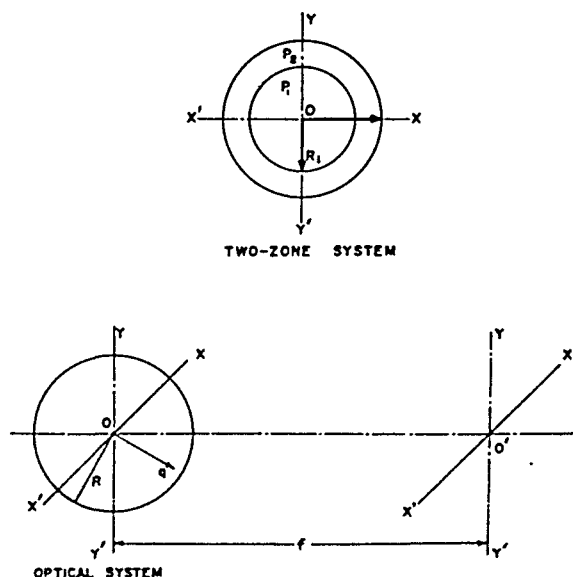


Fig. 1—Schematic diagram of two-zones system and optical coordinatessystem

and optical system by its Jones matrix P . The coherency matrix J^o of the emergent beam is obtained by matrix multiplication

$$J^o = PJ^iP^\dagger \quad \dots(1)$$

where J^i represents the coherency matrix of the incident beam. The coherency matrix J^i is defined as.

$$\begin{aligned} J^i &= \langle E \times E^\dagger \rangle \\ &= \begin{bmatrix} \langle E_x E_x^\dagger \rangle & \langle E_x E_y^\dagger \rangle \\ \langle E_y E_x^\dagger \rangle & \langle E_y E_y^\dagger \rangle \end{bmatrix} \\ &= \begin{bmatrix} J_{xx} & J_{xy} \\ J_{yx} & J_{yy} \end{bmatrix} \end{aligned} \quad \dots(2)$$

where E^\dagger is the Hermetian conjugate of E and is the row matrix. The angle brackets denote statistical averaging. The coherency matrix of partially polarized incident beam having intensity unity, azimuth θ' and ellipticity ϵ' and degree of polarization P' may be expressed as²

$$J^i = \frac{1}{2} \begin{bmatrix} (1 + P' \cos 2\theta' \cos 2\epsilon') & P'(\sin 2\theta' \cos 2\epsilon' - i \sin 2\epsilon') \\ P'(\sin 2\theta' \sin 2\epsilon' + i \sin 2\epsilon') & (1 - P' \cos 2\theta' \cos 2\epsilon') \end{bmatrix} \quad \dots(3)$$

Now we derive the results of the image intensity distributions for the three combinations one by one.

2.1 Right Circular Combination (RCP)

The polarizers P_1 and P_2 of the right circular type having relative attenuation ratios α_1 and α_2 are placed in the central and outer zones. The Jones matrix of the right circular type is expressed as²

$$P = \begin{bmatrix} \cosh \frac{\alpha}{2} & -i \sinh \frac{\alpha}{2} \\ +i \sinh \frac{\alpha}{2} & \cosh \frac{\alpha}{2} \end{bmatrix} \quad \dots(4)$$

where α represents the relative attenuation of the partial polarizer.

The incident beam on falling upon the optical system is differently modified in the two zones and let the corresponding Jones vectors be represented by E_1^p and E_2^p in the central and outer zones. Eq. (4) represents the corresponding Jones matrices for P_1 and P_2 when α is replaced by α_1 and α_2 respectively. Now the expressions for E_1^p and E_2^p can be expressed as:

$$E_1^p = P_1 E = \begin{bmatrix} \cosh \frac{\alpha_1}{2} & -i \sinh \frac{\alpha_1}{2} \\ i \sinh \frac{\alpha_1}{2} & \cosh \frac{\alpha_1}{2} \end{bmatrix} \times \begin{bmatrix} E_x \\ E_y \end{bmatrix}$$

$$= \begin{bmatrix} \cosh \frac{\alpha_1}{2} E_x & -i \sinh \frac{\alpha_1}{2} E_y \\ i \sinh \frac{\alpha_1}{2} E_x & + \cosh \frac{\alpha_1}{2} E_y \end{bmatrix}$$

and

$$E_2^p = P_2 E = \begin{bmatrix} \cosh \frac{\alpha_2}{2} E_x & -i \sinh \frac{\alpha_2}{2} E_y \\ i \sinh \frac{\alpha_2}{2} E_x & + \cosh \frac{\alpha_2}{2} E_y \end{bmatrix} \quad \dots(5)$$

Now we find out the Jones vector contributions E_1^d and E_2^d in the Fraunhofer diffraction plane. These are related in the following way³:

$$E_1^d = \epsilon \frac{J_1(v)}{v} E_1^p$$

and

$$E_2^d = \left[\frac{J_1(v)}{v} - \epsilon \frac{J_1(v\epsilon)}{v} \right] E_2^p \quad \dots(6)$$

where v is defined as $(2\pi/\lambda)(r/f)$ with $r = (x^2 + y^2)^{1/2}$, f being the focal length of the system and $R_1 = \epsilon$ is the radius of the central zone. $J_1(v)$ and $J_1(v\epsilon)$ represent Bessel functions of the first order.

The expressions for total coherency matrix J^d in the Fraunhofer diffraction plane may be expressed as

$$\begin{aligned} J^d &= \langle (E_1^d + E_2^d) \times (E_1^d + E_2^d)^\dagger \rangle \\ &= J_{11}^d + J_{22}^d + J_{12}^d + J_{21}^d \end{aligned}$$

where

$$J_{mn}^d = \langle E_m^d \times E_n^{d\dagger} \rangle \quad \dots(7)$$

If analyzer is also placed in the image plane. the coherency matrix is given by⁴

$$J^a = PJ^dP^\dagger \quad \dots(8)$$

where P represents the Jones matrix of the analyzer of the right circular type represented by Eq. (4). Now we work out the expressions for J_{11}^d , J_{22}^d , J_{12}^d and J_{21}^d . J_{11}^d can be expressed as

$$\begin{aligned} J_{11}^d &= \langle E_1^d \times E_1^{d\dagger} \rangle \\ &= \langle E_1^p \times E_1^{p\dagger} \rangle + \epsilon^2 \frac{J_1^2(v\epsilon)}{v^2} \end{aligned} \quad \dots(9)$$

After substituting the values of E_1^p from Eq. (5) into Eq. (9), we get

$$J_{11}^d = \begin{vmatrix} J_{xx} \left(\cosh^2 \frac{\alpha_1}{2} \right) & J_{xx} \left(-\sinh \frac{\alpha_1}{2} \cosh \frac{\alpha_1}{2} \right) \\ + J_{yy} \left(\sinh^2 \frac{\alpha_1}{2} \right) & + J_{yy} \left(-\sinh \frac{\alpha_1}{2} \cosh \frac{\alpha_1}{2} \right) \\ + J_{xy} \left(\sinh \frac{\alpha_1}{2} \cosh \frac{\alpha_1}{2} \right) & + J_{xy} \left(\cosh^2 \frac{\alpha_1}{2} \right) \\ + J_{yx} \left(-\sinh \frac{\alpha_1}{2} \cosh \frac{\alpha_1}{2} \right) & + J_{yx} \left(-\sinh^2 \frac{\alpha_1}{2} \right) \\ J_{xx} \left(-\sinh \frac{\alpha_1}{2} \cosh \frac{\alpha_1}{2} \right) & J_{xx} \left(\sinh^2 \frac{\alpha_1}{2} \right) \\ + J_{yy} \left(-\sinh \frac{\alpha_1}{2} \cosh \frac{\alpha_1}{2} \right) & + J_{yy} \left(\cosh^2 \frac{\alpha_1}{2} \right) \\ + J_{xy} \left(-\sinh^2 \frac{\alpha_1}{2} \right) & + J_{xy} \left(\sinh \frac{\alpha_1}{2} \cosh \frac{\alpha_1}{2} \right) \\ + J_{yx} \left(\cosh^2 \frac{\alpha_1}{2} \right) & + J_{yx} \left(-\sinh \frac{\alpha_1}{2} \cosh \frac{\alpha_1}{2} \right) \end{vmatrix} \times \varepsilon^2 \frac{J_{1(v\epsilon)}^2}{v^2} \dots (9a)$$

Similarly, we can obtain the values of J_{12}^d , J_{22}^d and J_{21}^d by substituting the values of E_1^p and E_2^p into Eqs (6) and (7). Now we work out the expressions for J_{11}^a , J_{12}^a , J_{21}^a and J_{22}^a . By substituting the values of sub-coherency matrices of J^d into Eq. (8) we get, after simplification:

$$J_{11}^a = \begin{vmatrix} J_{xx} \left[\cosh^2 \frac{(\alpha + \alpha_1)}{2} \right] & J_{xx} \left[-\sinh \frac{(\alpha + \alpha_1)}{2} \cosh \frac{(\alpha + \alpha_1)}{2} \right] \\ + J_{yy} \left[\sinh^2 \frac{(\alpha + \alpha_1)}{2} \right] & + J_{yy} \left[-\sinh \frac{(\alpha + \alpha_1)}{2} \cosh \frac{(\alpha + \alpha_1)}{2} \right] \\ + J_{xy} \left[\sinh \frac{(\alpha + \alpha_1)}{2} \cosh \frac{(\alpha + \alpha_1)}{2} \right] & + J_{xy} \left[\cosh^2 \frac{(\alpha + \alpha_1)}{2} \right] \\ + J_{yx} \left[-\sinh \frac{(\alpha + \alpha_1)}{2} \cosh \frac{(\alpha + \alpha_1)}{2} \right] & + J_{yx} \left[-\sinh^2 \frac{(\alpha + \alpha_1)}{2} \right] \end{vmatrix}$$

—Contd.

$$J_{11}^a = \left| \begin{array}{cc} J_{xx} \left[\operatorname{isinh} \frac{(\alpha + \alpha_1)}{2} \cosh \frac{(\alpha + \alpha_1)}{2} \right] & J_{xx} \left[\sinh^2 \frac{(\alpha + \alpha_1)}{2} \right] \\ + J_{yy} \left[\operatorname{isinh} \frac{(\alpha + \alpha_1)}{2} \cosh \frac{(\alpha + \alpha_1)}{2} \right] & + J_{yy} \left[\cosh^2 \frac{(\alpha + \alpha_1)}{2} \right] \\ + J_{xy} \left[-\sinh^2 \frac{(\alpha + \alpha_1)}{2} \right] & + J_{xy} \left[\operatorname{isinh} \frac{(\alpha + \alpha_1)}{2} \cosh \frac{(\alpha + \alpha_1)}{2} \right] \\ + J_{yx} \left[\cosh^2 \frac{(\alpha + \alpha_1)}{2} \right] & + J_{yx} \left[-\operatorname{isinh} \frac{(\alpha + \alpha_1)}{2} \cosh \frac{(\alpha + \alpha_1)}{2} \right] \end{array} \right| \times \varepsilon^2 \left[\frac{J_1(v\varepsilon)}{v} \right]^2 \quad \dots(10)$$

and

$$J_{12}^a = \left| \begin{array}{cc} J_{xx} \left[\cosh \frac{(\alpha + \alpha_1)}{2} \cosh \frac{(\alpha + \alpha_2)}{2} \right] & J_{xx} \left[\operatorname{icosh} \frac{(\alpha + \alpha_1)}{2} \sinh \frac{(\alpha + \alpha_2)}{2} \right] \\ + J_{yy} \left[\sinh \frac{(\alpha + \alpha_1)}{2} \sinh \frac{(\alpha + \alpha_2)}{2} \right] & + J_{yy} \left[\operatorname{isinh} \frac{(\alpha + \alpha_1)}{2} \cosh \frac{(\alpha + \alpha_2)}{2} \right] \\ + J_{xy} \left[\operatorname{icosh} \frac{(\alpha + \alpha_1)}{2} \sinh \frac{(\alpha + \alpha_2)}{2} \right] & + J_{xy} \left[\cosh \frac{(\alpha + \alpha_1)}{2} \cosh \frac{(\alpha + \alpha_2)}{2} \right] \\ + J_{yx} \left[-\sinh \frac{(\alpha + \alpha_1)}{2} \cosh \frac{(\alpha + \alpha_2)}{2} \right] & + J_{yx} \left[-\sinh \frac{(\alpha + \alpha_1)}{2} \sinh \frac{(\alpha + \alpha_2)}{2} \right] \end{array} \right|$$

$$\begin{array}{l} J_{xx} \left[\operatorname{isinh} \frac{(\alpha + \alpha_1)}{2} \cosh \frac{(\alpha + \alpha_2)}{2} \right] \\ + J_{yy} \left[\operatorname{icosh} \frac{(\alpha + \alpha_1)}{2} \sinh \frac{(\alpha + \alpha_2)}{2} \right] \\ + J_{xy} \left[-\sinh \frac{(\alpha + \alpha_1)}{2} \sinh \frac{(\alpha + \alpha_2)}{2} \right] \\ + J_{yx} \left[\cosh \frac{(\alpha + \alpha_1)}{2} \cosh \frac{(\alpha + \alpha_2)}{2} \right] \end{array} \left| \begin{array}{l} J_{xx} \left[\sinh \frac{(\alpha + \alpha_1)}{2} \sinh \frac{(\alpha + \alpha_2)}{2} \right] \\ + J_{yy} \left[\cosh \frac{(\alpha + \alpha_1)}{2} \cosh \frac{(\alpha + \alpha_2)}{2} \right] \\ + J_{xy} \left[\operatorname{isinh} \frac{(\alpha + \alpha_1)}{2} \cosh \frac{(\alpha + \alpha_2)}{2} \right] \\ + J_{yx} \left[-\operatorname{icosh} \frac{(\alpha + \alpha_1)}{2} \sinh \frac{(\alpha + \alpha_2)}{2} \right] \end{array} \right|$$

$$\times \varepsilon \left[\times \varepsilon \frac{J_1(v\varepsilon)}{v} \left\{ \frac{J_1(v)}{v} - \varepsilon \frac{J_1(v\varepsilon)}{v} \right\} \right] \quad \dots(11)$$

The expressions for J_{21}^a can be obtained from J_{12}^a by interchanging α_1 and α_2 in Eq. (11). Further, the expressions for J_{22}^a can be written as:

$$J_{22}^a = \begin{vmatrix} J_{xx} \left[\cosh^2 \frac{(\alpha + \alpha_2)}{2} \right] & J_{xx} \left[-\sinh \frac{(\alpha + \alpha_2)}{2} \cosh \frac{(\alpha + \alpha_2)}{2} \right] \\ + J_{yy} \left[\sinh^2 \frac{(\alpha + \alpha_2)}{2} \right] & + J_{yy} \left[-\sinh \frac{(\alpha + \alpha_2)}{2} \cosh \frac{(\alpha + \alpha_2)}{2} \right] \\ + J_{xy} \left[\sinh \frac{(\alpha + \alpha_2)}{2} \cosh \frac{(\alpha + \alpha_2)}{2} \right] & + J_{xy} \left[\cosh^2 \frac{(\alpha + \alpha_2)}{2} \right] \\ + J_{yx} \left[-\sinh \frac{(\alpha + \alpha_2)}{2} \cosh \frac{(\alpha + \alpha_2)}{2} \right] & + J_{yx} \left[-\sinh^2 \frac{(\alpha + \alpha_2)}{2} \right] \\ J_{xx} \left[\sinh \frac{(\alpha + \alpha_2)}{2} \cosh \frac{(\alpha + \alpha_2)}{2} \right] & J_{xx} \left[\sinh^2 \frac{(\alpha + \alpha_2)}{2} \right] \\ + J_{yy} \left[\sinh \frac{(\alpha + \alpha_2)}{2} \cosh \frac{(\alpha + \alpha_2)}{2} \right] & + J_{yy} \left[\cosh^2 \frac{(\alpha + \alpha_2)}{2} \right] \\ + J_{xy} \left[-\sinh^2 \frac{(\alpha + \alpha_2)}{2} \right] & + J_{xy} \left[\sinh \frac{(\alpha + \alpha_2)}{2} \cosh \frac{(\alpha + \alpha_2)}{2} \right] \\ + J_{yx} \left[\cosh^2 \frac{(\alpha + \alpha_2)}{2} \right] & + J_{yx} \left[-\sinh \frac{(\alpha + \alpha_2)}{2} \cosh \frac{(\alpha + \alpha_2)}{2} \right] \end{vmatrix} \times \left[\frac{J_1(v)}{v} - \varepsilon \frac{J_1(v\varepsilon)}{v} \right]^2 \quad \dots (12)$$

The expression for the intensity distribution can be obtained by taking the trace of the matrix J^a . After substituting the values of J_{xx} , J_{yy} , J_{xy} and J_{yx} from Eq. (3) we get:

$$B(v, \theta) = \left\{ \cosh(\alpha + \alpha_1) + P' \sin 2\varepsilon' \sinh(\alpha + \alpha_1) \right\} \varepsilon^2 \frac{J_1^2(v\varepsilon)}{v^2} \\ + \left\{ \cosh(\alpha + \alpha_2) + P' \sin 2\varepsilon' \sinh(\alpha + \alpha_2) \right\} \times \left[\frac{J_1(v)}{v} - \varepsilon \frac{J_1(v\varepsilon)}{v} \right]^2 \\ + 2 \left\{ \cosh \left(\alpha + \frac{\alpha_1 + \alpha_2}{2} \right) + P' \sin 2\varepsilon' \sinh \left(\alpha + \frac{\alpha_1 + \alpha_2}{2} \right) \right\} \\ \times \left\{ \left(\varepsilon \frac{J_1(v\varepsilon)}{v} \right) \times \left(\frac{J_1(v)}{v} - \varepsilon \frac{J_1(v\varepsilon)}{v} \right) \right\} \quad \dots (13)$$

The expressions for θ_0 , P_0 and ε'_0 of the output beam in terms of coherency matrix elements J_{11}^a , J_{22}^a , J_{12}^a and J_{21}^a may be expressed as²

$$\begin{aligned}\theta_0 &= \frac{1}{2} \tan^{-1} \left(\frac{J_{12}^a + J_{21}^a}{J_{11}^a - J_{22}^a} \right) \\ P_0 &= \left[1 - \frac{4 \det J^a}{(\text{Tr } J^a)^2} \right]^{1/2} \\ \text{and} \\ \varepsilon'_0 &= \frac{1}{2} \sin^{-1} \left[\frac{i(J_{12}^a - J_{21}^a)}{(J_{11}^a + J_{22}^a)P_0} \right] \quad \dots (14)\end{aligned}$$

After substituting the values of J_{11}^a , J_{21}^a , J_{22}^a and J_{12}^a into Eq. (14) for azimuth angle θ_0 , we get

$$\begin{aligned}\theta_0 &= \frac{1}{2} \tan^{-1} \left[\frac{\sin 2\theta' \cos 2\varepsilon'}{\cos 2\theta' \cos 2\varepsilon'} \right] \\ &= \frac{1}{2} \tan^{-1} [\tan 2\theta'] = \theta' \quad \dots (15)\end{aligned}$$

i.e. azimuth of the output beam is unchanged.

Next we work out the expression for P_0 . In order to evaluate P_0 we have to work out the value of $\det. J^a$. After simplification, the value of $\det. J^a$ comes out to be:

$$\begin{aligned}\det. J^a &= \frac{1}{4} (1 - P'^2) \left[\left\{ \frac{J_1^2(v)}{v^2} + 2\varepsilon^2 \frac{J_1^2(v\varepsilon)}{v^2} \right\} \right. \\ &\quad \times \left\{ \frac{J_1^2(v)}{v^2} + 2\varepsilon^2 \frac{J_1^2(v\varepsilon)}{v^2} \right. \\ &\quad \left. \left. + 4\varepsilon \frac{J_1(v)}{v} \times \frac{J_1(v\varepsilon)}{v} \right\} \right. \\ &\quad \left. + 4\varepsilon^2 \frac{J_1^2(v)}{v^2} \times \frac{J_1^2(v\varepsilon)}{v^2} \right] \quad \dots (16)\end{aligned}$$

Knowing the values of $\det. J^a$ and $\text{Tr } J^a$, the value of P_0 can be worked out. After putting the values of $(J_{12}^a - J_{21}^a)$ and $(J_{11}^a + J_{22}^a)$ in Eq. (14) for ε'_0 , we can find out its value.

2.2 Left Circular Combination (LCP)

In this case, two polarizers P_1 and P_2 of left circular type are placed in the central and outer zones. The left circular polarizer in the form of Jones matrix can be expressed as²

$$P = \begin{bmatrix} \cosh \frac{\alpha}{2} & +i \sinh \frac{\alpha}{2} \\ -i \sinh \frac{\alpha}{2} & \cosh \frac{\alpha}{2} \end{bmatrix} \quad \dots (17)$$

For polarizers P_1 and P_2 , we have $\alpha = \alpha_1$ and $\alpha = \alpha_2$. Proceeding on similar lines as in Sec. 2.1, we get expressions for E_1^p and E_2^p in the following form:

$$\begin{aligned}E_1^p &= P_1 E = \begin{bmatrix} \cosh \frac{\alpha_1}{2} E_x + i \sinh \frac{\alpha_1}{2} E_y \\ -i \sinh \frac{\alpha_1}{2} E_x + \cosh \frac{\alpha_1}{2} E_y \end{bmatrix} \\ E_2^p &= P_2 E = \begin{bmatrix} \cosh \frac{\alpha_2}{2} E_x + i \sinh \frac{\alpha_2}{2} E_y \\ -i \sinh \frac{\alpha_2}{2} E_x + \cosh \frac{\alpha_2}{2} E_y \end{bmatrix} \quad \dots (18)\end{aligned}$$

On comparing Eqs (5) and (18), we observe that i has been replaced by $-i$. By proceeding on similar lines, the values of coherency matrix elements J_{11}^d , J_{22}^d , J_{12}^d and J_{21}^d remain the same except that i has been replaced by $-i$ as compared to RCP combination [Eq. (9a)].

If analyzer of left circular type is employed in the image plane, the resulting coherency matrix is given by Eq. (8), as

$$J^a = P J^d P^\dagger$$

where P now represents the Jones matrix of the analyzer of left circular type represented by Eq. (17). By proceeding on similar lines as in Sec 2.1, we work out the expressions for J_{11}^a , J_{22}^a , J_{12}^a and J_{21}^a .

By taking the trace of the matrix J^a , we get the expression for image intensity distribution in the following simplified form:

$$\begin{aligned}B(v, \theta) &= \left\{ \cosh (\alpha + \alpha_1) - P' \sin 2\varepsilon' \sinh (\alpha + \alpha_1) \right. \\ &\quad \times \varepsilon^2 \frac{J_1^2(v\varepsilon)}{v^2} + \left\{ \cosh (\alpha + \alpha_2) \right. \\ &\quad \left. - P' \sin 2\varepsilon' \sinh (\alpha + \alpha_2) \right\} \\ &\quad \times \left\{ \frac{J_1(v)}{v} - \varepsilon \frac{J_1(v\varepsilon)}{v} \right\}^2 \\ &\quad \left. + 2 \left\{ \cosh \left(\alpha + \frac{\alpha_1 + \alpha_2}{2} \right) \right\} \right\}\end{aligned}$$

$$-P' \sin 2\epsilon' \sinh \left(\alpha + \frac{\alpha_1 + \alpha_2}{2} \right) \left\{ \epsilon \frac{J_1(v\epsilon)}{v} \left(\frac{J_1(v)}{v} - \epsilon \frac{J_1(v\epsilon)}{v} \right) \right\} \quad \dots (19)$$

The expressions for P'_0 , θ'_0 and ϵ' are worked out on similar lines as in the case of the RCP combination.

2.3 Right and Left Circular Combination (RLCP)

The two polarizers P_1 and P_2 placed in the central and outer zone can be represented as:

$$P_1 = \begin{bmatrix} \cosh \frac{\alpha_1}{2} & -i \sinh \frac{\alpha_1}{2} \\ i \sinh \frac{\alpha_1}{2} & \cosh \frac{\alpha_1}{2} \end{bmatrix}$$

and

$$P_2 = \begin{bmatrix} \cosh \frac{\alpha_2}{2} & +i \sinh \frac{\alpha_2}{2} \\ -i \sinh \frac{\alpha_2}{2} & \cosh \frac{\alpha_2}{2} \end{bmatrix} \quad \dots (20)$$

We get the following expressions for E_1^P and E_2^P :

$$E_1^P = \begin{bmatrix} \cosh \frac{\alpha_1}{2} E_x & -i \sinh \frac{\alpha_1}{2} E_y \\ i \sinh \frac{\alpha_1}{2} E_x & + \cosh \frac{\alpha_1}{2} E_y \end{bmatrix}$$

and

$$E_2^P = \begin{bmatrix} \cosh \frac{\alpha_2}{2} E_x & +i \sinh \frac{\alpha_2}{2} E_y \\ -i \sinh \frac{\alpha_2}{2} E_x & + \cosh \frac{\alpha_2}{2} E_y \end{bmatrix} \quad \dots (21)$$

By proceeding on similar lines as in sections 2.1 and 2.2, the expressions for J_{11}^d , J_{22}^d , J_{12}^d and J_{21}^d are worked out. If analyzer of the right circular type 'P' is also placed in the image plane, the new coherency matrix is given by Eq. (8).

Making use of Eq. (8) and expressions for J_{11}^d , J_{22}^d , J_{12}^d and J_{21}^d , we work out the expressions for the sub-coherency matrices J_{11}^a , J_{22}^a , J_{12}^a and J_{21}^a .

The intensity distribution in the image plane has been obtained by taking trace of coherency matrix J^a and after simplification we get:

$$\begin{aligned} \{B(v, \theta)\} = & \left\{ \cosh(\alpha + \alpha_1) + P' \sin 2\epsilon' \sinh(\alpha + \alpha_1) \right\}^2 \\ & \times \epsilon^2 \frac{J_1^2(v\epsilon)}{v^2} + \left\{ \frac{J_1(v)}{v} - \epsilon \frac{J_1(v\epsilon)}{v} \right\}^2 \\ & \times \{ \cosh(\alpha + \alpha_2) - P' \sin 2\epsilon' \sinh(\alpha + \alpha_2) \} \\ & + 2 \left\{ \cosh \left(\alpha + \frac{\alpha_1 - \alpha_2}{2} \right) \right. \\ & \left. + P' \sin 2\epsilon' \sinh \left(\alpha + \frac{\alpha_1 - \alpha_2}{2} \right) \right\} \\ & \times \left\{ \epsilon \frac{J_1(v\epsilon)}{v} \left(\frac{J_1(v)}{v} - \epsilon \frac{J_1(v\epsilon)}{v} \right) \right\} \quad \dots (22) \end{aligned}$$

After substituting the values of J_{11}^a , J_{12}^a , J_{22}^a and J_{21}^a into Eq. (14) for azimuth angle θ_0 , we get:

$$\begin{aligned} \theta_0 &= \frac{1}{2} \tan^{-1} \left[\frac{\sin 2\theta' \cos 2\epsilon'}{\cos 2\theta' \cos 2\epsilon'} \right] \\ &= \frac{1}{2} \tan^{-1} [\tan 2\theta'] = \theta' \end{aligned}$$

i.e. azimuth angle in the image plane is unchanged. Knowing the values of $\det J^a$ and $\text{Tr} J^a$, the value of P_0 has been worked out. Putting the value of P_0 and $(J_{12}^a - J_{21}^a)$, $(J_{11}^a + J_{22}^a)$ in Eq. (14) we can work out the value of ϵ_0 .

Proceeding on similar lines, we have derived the results of the optical system masked by P_1 of left circular type and P_2 of right circular type placed into central and outer zone respectively.

3 Results and Discussion

We have computed the image intensity distributions of an optical system masked by two polarizers P_1 and P_2 of circular type. A circular polarizer may consist of combination of a linear polarizer whose transmission axis is at some azimuth θ , and a 90 linear retarder whose transmission axis is at azimuth $\theta \pm 45^\circ$. Such a combination produces circularly polarized light and may be of either handedness depending on whether the retarder is oriented at $\theta + 45^\circ$ or $\theta - 45^\circ$ (Ref. 4). The common type of circular polarizer is the CP-HN-35 polarizer, which consists of a sheet of HN-35 and a sheet of stretched polyvinyl alcohol⁵.

In case of linear polarizers, by changing the orientations of the masks we get different contributions to the diffraction pattern. However, there is no similar parameter in the case of ideal circular polarizer. Therefore, for the apodization role we have to resort to partial circular polarizers. These have orthogonal

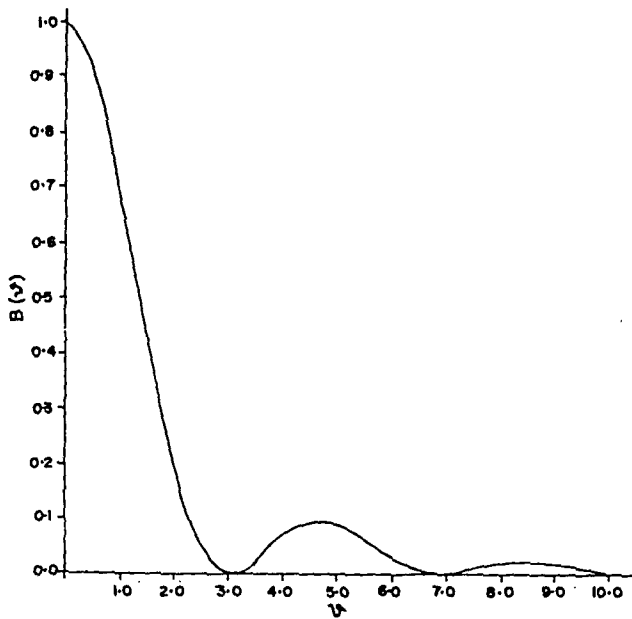


Fig. 2—Plot of image intensity distribution for right circular polarizer (RCP) combination at $\alpha = 5$, $\alpha_1 = 10$ and $\alpha_2 = 15$ and for different values of P' and ϵ'

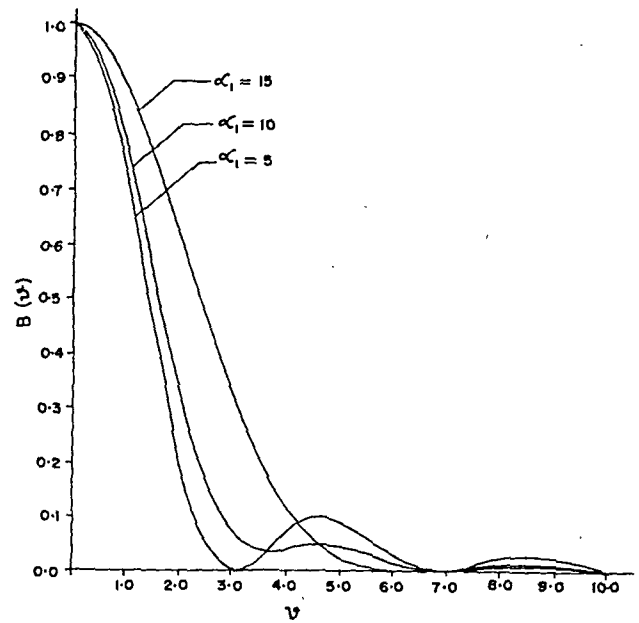


Fig. 3—Plot of image intensity distribution for RCP combination at $P' = 0.5$, $\epsilon' = \pi/12$, $\epsilon = 0.6$, $\alpha = 5$, $\alpha_2 = 10$ and for different values of α_1 .

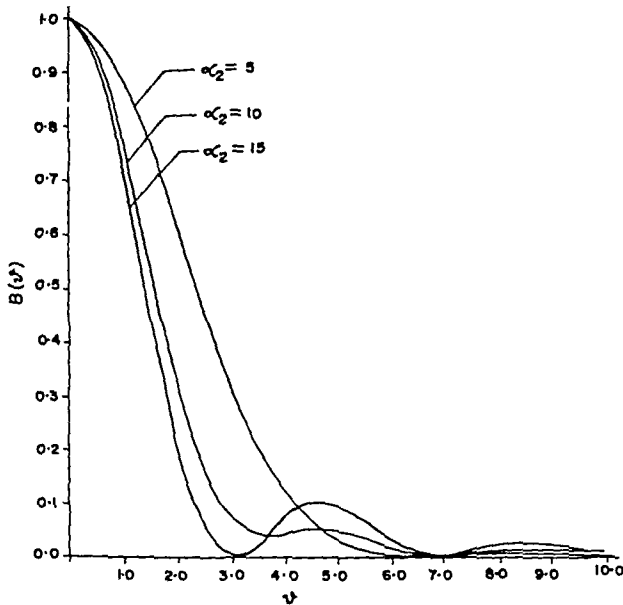


Fig. 4—Image intensity distribution for RCP combination at $P' = 0.5$, $\epsilon' = \pi/12$, $\epsilon = 0.6$, $\alpha = 5$, $\alpha_1 = 10$ and for different values of α_2

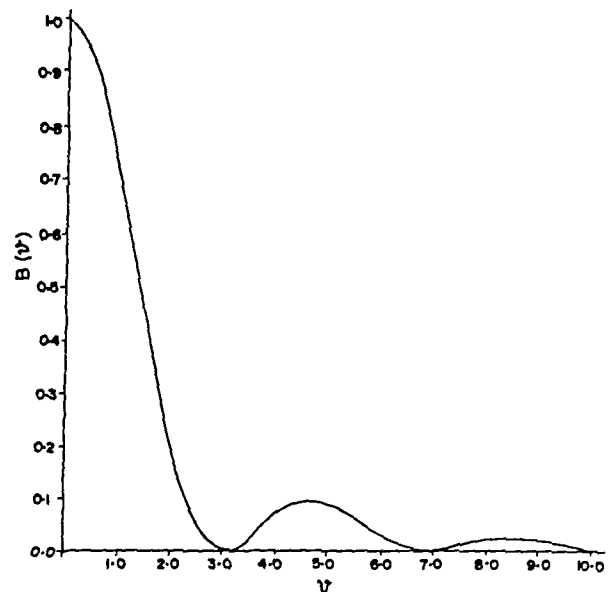


Fig. 5—Plot of image intensity distribution for RCP combination at $\alpha = 5$, $\alpha_1 = 10$, $\alpha_2 = 15$, $P' = 0.50$, $\epsilon' = \pi/12$ and for different values of α

circular eigen-polarizations χ_l , χ_h with associated eigen-values $V_l = e^{(1/2)\alpha}$ and $V_h = e^{-(1/2)\alpha}$ that are real and positive. The subscripts l and h refer to low and high absorption eigen-polarizations respectively and α defines the relative attenuation of the partial polarizer.

Three different combinations of right, right; left, left; and right and left circular types have been considered. The computations have been made for different attenuation ratios α_1 and α_2 of two polarizers P_1 and P_2 , and relative sizes of the two zones. The effect of varying the attenuation ratio α of the analyzer has also been studied.

3.1 RCP Combination

Figs 2-6 represent the results obtained in case of right circular polarizer (RCP) combination. Fig. 2 shows the plot of image intensity distribution for different values of ellipticity angle ϵ' and degree of polarization P' . It is to be noticed that normalized image intensity distributions remain the same with variation of ϵ' and P' . From the computed results it is observed that for fixed values of P' , there is change in the absolute intensity distribution and it is maximum for circularly polarized light illumination ($\epsilon' = \pi/4$) as expected.

Fig. 3 shows the image intensity distribution for

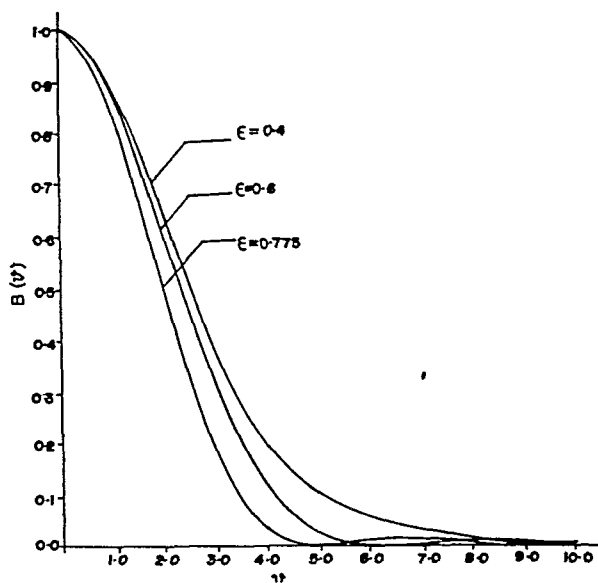


Fig. 6—Plot of image intensity distribution for RCP combination at $P' = 0.5$, $\epsilon' = \pi/12$, $\alpha = 5$, $\alpha_1 = 10$, $\alpha_2 = 5$ for different values of ϵ

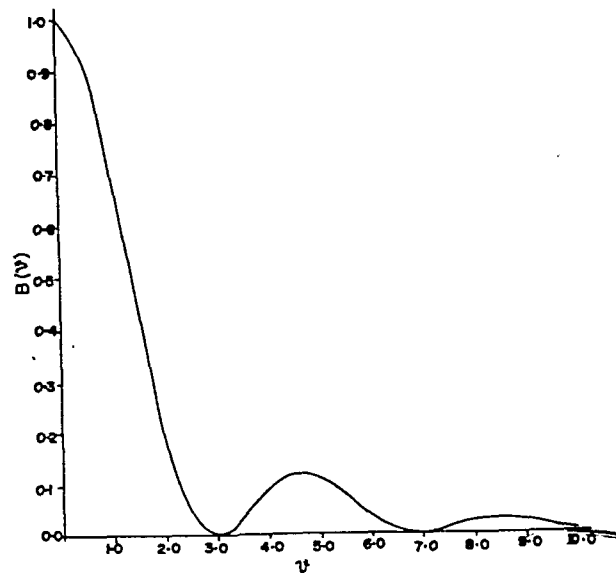


Fig. 7—Plot of images for right and left circular polarizer combination (RLCP) at $\alpha = 5$, $\alpha_1 = 10$, $\alpha_2 = 15$, $\epsilon' = 0.6$ for different values of P' and ϵ'

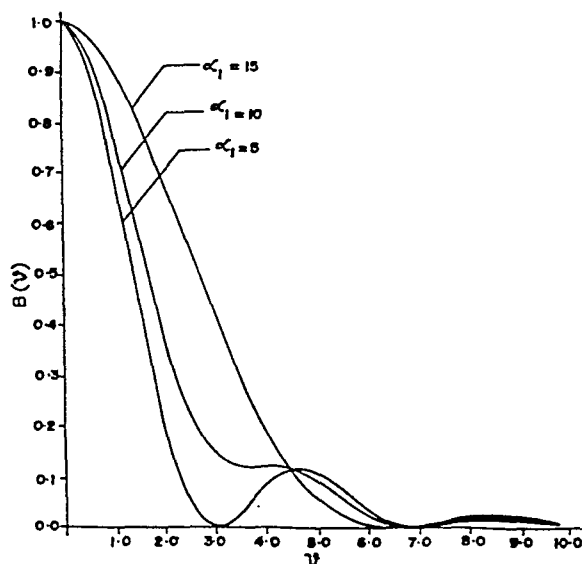


Fig. 8—Plot of image intensity distribution of RLCP combination at $P' = 0.50$, $\epsilon' = \pi/12$, $\epsilon = 0.60$, $\alpha_2 = 10$, $\alpha = 5$ for different values of α_1

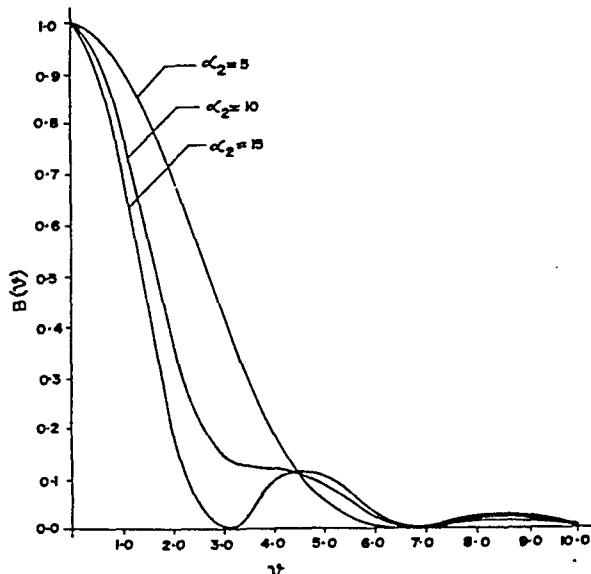


Fig. 9—Plot of image intensity distribution for RLCP combination at $P' = 0.50$, $\epsilon' = \pi/12$, $\epsilon = 0.60$, $\alpha_1 = 10$, $\alpha = 5$ for different values of α_2

different values of attenuation ratio α_1 of polarizer P_1 . It is observed that as the value of α_1 increases, the central maximum is broadened and secondary maxima become less prominent as compared to an ordinary optical system. We can, therefore, say that higher values of α_1 are preferable for increasing the contrast in the resolved details. Fig. 4 shows the image intensity distribution plot with variation of α_2 of polarizer P_2 in the second zone. It is observed that higher values of α_2 are favourable for increasing the two-point resolution as compared to an ordinary optical system. Fig. 5 rep-

resents the plot similar to those in Figs 2-4 with variation of analyzer attenuation ratio α . From the computed results it is noticed that with variation of α , the normalized intensity distribution remains the same; however, the absolute intensity increases with α .

The plots of image intensity distribution with change in relative size of the two zones are presented in Fig. 6. It is observed that as the radius of the central zone ϵ is increased from 0.40 to 0.60 and 0.60 to 0.775, the central maximum is sharpened with slight increase in energy into the secondary maxima. Thus,

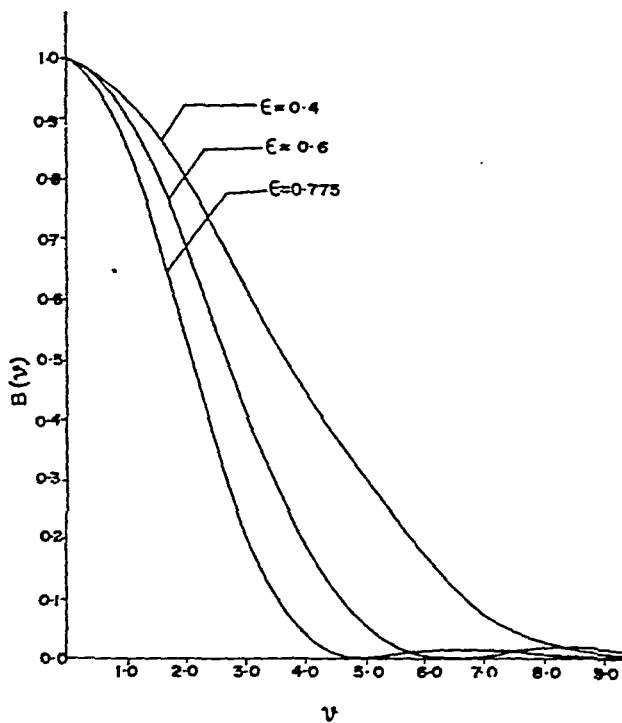


Fig. 10—Plot of image intensity distribution of RLCP combination at $P' = 0.5$, $\epsilon' = \pi/12$, $\alpha = 5$, $\alpha_1 = 10$, $\alpha_2 = 5$ for different values of ϵ

there is an increase in two-point resolution with slight decrease in contrast in the images as compared to unobstructed optical system ($\epsilon = 0.0$). Besides the image intensity distributions, P and θ_0 and ϵ_0 have also been worked out. P_0 approaches unity when large values of α_1 , α_2 and α are used. Further, the value of ϵ_0 comes out to be $\pi/4$ which means right circularly polarized light as expected. The value of azimuth angle θ_0 is not dependent on any of the factors under consideration.

3.2 LCP Combination

Now we discuss the results obtained when left circular polarizer (LCP) combination is employed. The normalized intensity distribution comes out exactly the same as obtained in the case of RCP combination. Therefore, the same results are valid here also. Further, the absolute intensity distribution is also the same if incident illumination is left elliptically polarized as compared to the case of RCP combination when the incident illumination is right elliptically polarized.

3.3 RLCP Combination

In this subsection, we discuss the results obtained in

the case of right and left circular polarizer (RLCP) combination. Fig. 7 shows the plot with variation of P' and ϵ' . It is found that normalized image intensity distribution does not change with variation of P' as well as ϵ' . Fig. 8 represents the plot with variation of attenuation ratio α_1 of the polarizer P_1 . With an increase in the value of α_1 , central maximum is broadened and secondary maximum is sharpened. Fig. 9 represents the variation with α_2 . It is observed that as the value of α_2 is increased, the central maximum is sharpened and energy is shifted into secondary maxima. The plot of the results with variation of ϵ is shown in Fig. 10. The trend of the results observed is the same as noticed in Fig. 6.

4 Conclusions

From the results of the image intensity distribution obtained for three different combinations of polarizers, it may be concluded that the performance of the polarizing optical system can be modified by changing the attenuation ratios α_1 , α_2 and α . The performance also depends upon the relative size of the two zones. However, the performance is not affected by P' , θ and ϵ' which is not so in the case of linear polarization masks. The results obtained in case of right circular polarizer combination also remain valid for left circular combination.

The polarizing optical system masked with circular polarizers having large value of α_1 and small values of α_2 and moderate values of ϵ , is favourable for increasing the contrast in the resolved details as compared to an ordinary optical system. On the other hand, the polarizing optical system having small values of α_1 , large values of α_2 and relatively large values of ϵ , is preferable for increasing the two-point resolution in the images as compared to an ordinary optical system.

References

- 1 Gupta S D, *Opt Acta (GB)*, 30 (1983) 607.
- 2 Azzam R M A & Bashara N M, *Ellipsometry and polarised light* (North Holland Publishing Co., Amsterdam, New York) 1977.
- 3 Goodman J W, *Introduction to Fourier optics* (McGraw-Hill Book Co., New York) 1968, Chap. 6.
- 4 Shurecliff W A, *Polarised light* (Harvard University, Cambridge, Massachusetts), 1962.
- 5 Bennett J M & Bennet H E, *Handbook of optics*, edited by W G Driscoll and W Vaughan (McGraw-Hill, New York) 1978, Chap. 10.

Microwave Absorption, Curie Temperature & Ultrasonic Attenuation in Ferroelectric Solids

G N BALUNI & U C NAITHANI

Department of Physics, Dr B G R Constituent College, Pauri, Pauri-Garhwal 246 001

Received 22 October 1985; revised received 27 May 1986

Expressions for the dielectric constant, microwave absorption, Curie temperature, ultrasonic attenuation constant and velocity change in ferroelectric solids having general formula ABO_3 are obtained by using Green's function technique and the model Hamiltonian which includes anharmonicity up to fourth order due to interactions of the soft mode coordinates. The linear frequency dependences of loss tangent and attenuation constant have also been discussed. The soft mode frequency is held responsible for the anomalous behaviour of the ferroelectrics at the stage when T approaches T_c .

Introduction

It is now revealed both experimentally and theoretically that the soft or ferroelectric mode plays an essential role in the perovskite compounds. Number of reviews are available in the literature¹⁻⁵ and references therein are quite numerous. Also details of work on ultrasonic propagation in displacive ferroelectrics are available in the literature⁶⁻¹⁴. We¹⁵ have previously obtained expressions for microwave absorption, Curie temperature, dielectric constant, ultrasonic attenuation constant and velocity change in displacive ferroelectrics using Silverman-Joseph Hamiltonian¹⁶ and the Green's function technique¹⁷.

Recently, a calculation based on a model Hamiltonian containing a small number of temperature-independent parameters was able to give a quantitative description of the structural transition in the perovskites¹⁸. This transition involves rotations of octahedral units. The soft mode damping at a displacive phase transition has also been calculated¹⁹ with the help of a model Hamiltonian constructed by expending the potential energy of the strained crystal in terms of the strain and the oxygen ion displacement field. The aim of the present paper is to obtain the expressions for the complex dielectric constant, microwave absorption, Curie temperature, ultrasonic attenuation constant and velocity change in ferroelectric solids having general formula ABO_3 , by using Green's function technique¹⁷ and the Dyson's equation treatment in presence of higher order anharmonic, resonant interaction and scattering terms in the model Hamiltonian, in the tetragonal phase.

Here Dyson's equation treatment has been found convenient to derive the shift and width of the frequency response function and hence to describe the properties of these ferroelectrics.

2 Hamiltonian and Green's Functions

The Hamiltonian which includes the fourth order anharmonicity due to interactions of the soft mode coordinates resonant interaction and the scattering terms can be written as:

$$\begin{aligned}
 H = & \sum_{\lambda} \frac{\omega_{\lambda}^0}{4} (A_{\lambda}^0 A_{\lambda}^0 + B_{\lambda}^0 B_{\lambda}^0) \\
 & + \sum_{\mu} \frac{\omega_{\mu}^a}{4} (A_{\mu}^a A_{\mu}^a + B_{\mu}^a B_{\mu}^a) \\
 & + (\Gamma'_1/4) \sum_{\lambda} A_{\lambda}^{0*}(l) + (\Gamma'_2/2) \sum_{\lambda \neq \lambda'} A_{\lambda}^{0*}(l) A_{\lambda'}^0(l) \\
 & + \frac{1}{2} \sum_{\lambda \lambda' l l'} \mathbf{V} A_{\lambda}^0(l) A_{\lambda'}^0(l') \\
 & + iA \sum_{\lambda \mu q} \mathbf{F} A_{\mu}^0(q) A_{\lambda}^0(q_R - q) \\
 & + \sum_{k q \lambda \lambda' \mu} \mathbf{H} A_{\mu}^a(q) A_{\lambda}^0(-k) A_{\lambda'}^0(k - q) \quad \dots (1)
 \end{aligned}$$

with

$$\Gamma'_1 = \Gamma_1 / (\omega_{\lambda}^0 \omega_{\lambda'}^0)^{\dagger}, \Gamma'_2 = \Gamma_2 / (\omega_{\lambda}^0 \omega_{\lambda'}^0)^{\dagger}$$

$$\mathbf{V} = v_{\lambda \lambda'} / (\omega_{\lambda}^0 \omega_{\lambda'}^0)^{\dagger}$$

$$\mathbf{F} = f_{\lambda}(\mu q) / (\omega_{\mu}^a \omega_{\mu}^0)^{\dagger}$$

and

$$\mathbf{H} = h_{\lambda \lambda'}(\mu k q) / (\omega_{\mu}^a \omega_{\lambda}^0 \omega_{\lambda'}^0)^{\dagger}$$

The notations used in Eq.(1) are the same as in Ref. 18, 19, except the normal coordinates Q and its conjugate momenta P are transformed to the form of Bose operators.

The real part of the dielectric constant and microwave loss tangent²⁰ ($\tan \delta$) are related to the soft phonon Green's function

$$G(\omega + i\epsilon) = \ll A_\lambda^0(t); A_\lambda^0(t') \gg_{\omega + i\epsilon} \\ = G'(\omega) - i G''(\omega) \quad \dots (2)$$

$$\text{as } \epsilon'(\omega) - 1 = -8\pi^2 M_s^2(0) G'(\omega) \quad \dots (3)$$

$$\text{and } \tan \delta = G''(\omega) / G'(\omega) \quad \dots (4)$$

Writing the equation of motion for the Green's function (2) with the help of this Hamiltonian (1), Fourier transforming and writing it in the Dyson's equation form, one obtains¹⁵,

$$G(\omega + i\epsilon) = \omega_\lambda^0 / \pi [\omega^2 - v^2(\omega) + i\Gamma^0(\omega)] \quad \dots (5a)$$

$$\text{where } v^2(\omega) = (\tilde{\omega}_\lambda^0)^2 + \Delta^0(\omega) \quad \dots (5b)$$

$$\text{with } (\tilde{\omega}_\lambda^0)^2 = -(\omega_\lambda^0)^2 - \omega_\lambda^0 V \quad \dots (5c)$$

and

$$\Delta^0(\omega) = \text{Re } \omega_\lambda^0 \left[\sum_{l,\lambda} 12 (\Gamma'_1)^2 [(1 + (3N_\lambda^0)^2) \right. \\ \times \frac{3\Omega}{\omega^2 - (3\Omega)^2} - [1 - (N_\lambda^0)^2] \frac{\Omega}{\omega^2 - \Omega^2}] \\ + \sum_{l,\lambda} \left[18 (\Gamma'_2)^2 N_\lambda^0 \frac{2\Omega}{\omega^2 - (2\Omega)^2} \right. \\ - 64 A^2 \sum_{\lambda,\mu,q} \omega_\mu^a |\mathbf{H}|^2 |\mathbf{F}|^2 N_\lambda^0 \frac{2\Omega}{\omega^2 - (2\Omega)^2} \\ + 32 \sum_{k,q,\lambda,\mu} |\mathbf{H}|^2 \left[\sum (N_\lambda^0 \pm N_\mu^a \right. \\ \left. \left. \frac{\tilde{\omega}_\mu^a \pm \Omega}{\omega^2 - (\tilde{\omega}_\mu^a \pm \Omega)^2} \right] \right] \quad \dots (6)$$

$$\Gamma^0(\omega) = \pi \omega_\lambda^0 \left[\sum_{l,\lambda} 6 (\Gamma'_1)^2 [(1 + (3N_\lambda^0)^2) [\delta(\omega - 3\Omega) \right. \\ - \delta(\omega + 3\Omega)] - (1 - (N_\lambda^0)^2) [\delta(\omega - \Omega) \\ - \delta(\omega + \Omega)] \left. \right] + \sum_{l,\lambda} 9 (\Gamma'_2)^2 N_\lambda^0 [\delta(\omega - 2\Omega) \\ - \delta(\omega + 2\Omega)] - 32 A^2 \sum_{\lambda,\mu,q} \omega_\mu^a |\mathbf{H}|^2 |\mathbf{F}|^2 \\ \times N_\lambda^0 [\delta(\omega - 2\Omega) - \delta(\omega + 2\Omega)] + 16 \sum_{k,q,\lambda,\mu} |\mathbf{H}|^2$$

$$\times \sum_{\pm} [N_\lambda^0 \pm N_\mu^a] [\delta(\omega - \omega_\mu^a \pm \Omega) \\ - \delta(\omega + \omega_\mu^a \pm \Omega)] \quad \dots (7)$$

We also introduce the following Green's function¹⁷ for the acoustic phonons,

$$\mathbf{D}(\omega) = \ll A_\mu^a(t); A_\mu^a(t') \gg \quad \dots (8)$$

writing the equation of motion for the Green's function (8) with the help of the Hamiltonian (1), Fourier transforming and writing it in the Dyson's equation from¹⁵, one obtains

$$\mathbf{D}(\omega + i\epsilon) = \omega_\mu^a / \pi [\omega^2 - (\tilde{\omega}_\mu^a)^2 + i\Gamma^a(\omega)] \quad \dots (9)$$

where

$$(\tilde{\omega}_\mu^a)^2 = (\omega_\mu^a)^2 + \Delta_{(\omega)}^0, \quad \dots (10)$$

with

$$(\tilde{\omega}_\mu^a)^2 = (\omega_\mu^a)^2 + 2iA\omega_\mu^a |\mathbf{F}| \quad \dots (11)$$

$$\Delta^0(\omega) = 32 \omega_\mu^a \sum_{\lambda,h,\mu,q} |\mathbf{H}|^2 N_\lambda^0 \frac{2\Omega}{\omega^2 - (2\Omega)^2} \quad \dots (12)$$

and

$$\Delta^0(\omega) = 16\pi \omega_\mu^a \sum_{\lambda,h,\mu,q} |\mathbf{H}|^2 N_\lambda^0 \\ \times [\delta(\omega - 2\Omega) - \delta(\omega + 2\Omega)] \quad \dots (13)$$

with

$$N_\lambda^0 = \coth(\hbar\Omega / 2k_B T) \text{ and}$$

$$N_\mu^a = \coth(\hbar\tilde{\omega}_\mu^a / 2k_B T).$$

3 Curie Temperature

The real part of the complex dielectric constant in Eq. (3) now takes the form

$$\epsilon'(\omega) = \frac{-8\pi M_s^2 \omega_\mu^0 [\omega^2 - v^2(\omega)]}{[\omega^2 - v^2(\omega)]^2 + [\Gamma^a(\omega)]^2} \quad \dots (14)$$

In the presence of anharmonicity, resonant interaction and scattering terms, the real part of the Green's function given by Eq. (5a) gives temperature-dependent frequency $\Omega(T)$ as the self-consistent solution of the equation:

$$\Omega^2 = -(\omega_\mu^0)^2 - \omega_\mu^0 V + \Delta^0(\Omega) \quad \dots (15)$$

where $\Delta^0(\omega)$ is given by Eq. (6). Hence by comparing Eqs (15) and (5b), one can approximate $v(\omega)$ as Ω . For a ferroelectric having cubic symmetry, the soft optical mode frequency Ω is very high compared to the mic-

rowave frequency ω , so that $v(\omega) \gg \omega$ and no relaxation effects are observed. In paraelectrics, the value of $\epsilon'(\omega)$ is very high compared to those in alkali halides, so that $\epsilon'(\omega) \gg 1$. Also the temperature dependence of $v^2(\omega)$ can be written as¹⁵

$$v^2(\omega) = -(\omega_\mu^0)^2 - \omega_\mu^0 V + \gamma_1 T + \gamma_2 T^2 + \gamma_3 T^3 \dots (16)$$

where γ_1, γ_2 are the coefficients of T and γ_3 is that of T^2 in Eq. (5b).

Here one can easily see that the soft optic mode frequency $[\Omega \sim (T - T_c)^{1/2}]$, which is imaginary ($i\omega_\mu^0$) in the harmonic approximation, is stabilized in the presence of anharmonicity, resonant interaction and scattering terms. The lowest order anharmonic interaction stabilizing Ω , is the fourth order interaction. Thus the presence of these terms plays a fundamental role in ferroelectric crystals because most of the physical properties of these crystals result from the temperature dependence of the soft mode. Thus from Eqs (14) and (16) we conclude that

$$\epsilon'(\omega) = C/[T - T_c + \xi T^2 - \omega_\mu^0 V/\gamma] \dots (17)$$

where

$$C = 8\pi M_s^2(0) \omega_\mu^0/\gamma \dots (17a)$$

$$T_c = (\omega_\mu^0)^2/\gamma \dots (17b)$$

and

$$\xi = \gamma_3/\gamma \text{ with } \gamma = \gamma_1 + \gamma_3 \dots (17c)$$

Eq. (17) can be rewritten as

$$\epsilon'(\omega) = C/[T - T_c + \xi T^2] \dots (18)$$

where

$$T_c = T_c + \Delta(T_c) \dots (19)$$

with

$$\Delta(T_c) = \omega_\mu^0 V/\gamma \dots (20)$$

Expression (20) shows that the change in the Curie temperature depends both on the resonant coupling coefficient and scattering coefficients via γ which depends upon anharmonic force constants, scattering terms and the interaction coefficients, as evident from Eqs (17c) and (16). Clearly this is a combined effect of the resonant interaction and scattering processes in presence of anharmonicity. The shift in the Curie temperature will depend on the relative magnitudes of the anharmonic, resonant interaction and scattering coupling coefficients and will have different signs for different crystals.

4 Microwave Absorption

For a crystal model considered here using Green's function given by Eq. (5a) for microwave photons

$[\omega \ll v(\omega)]$, we write the expression for loss tangent as

$$\tan\delta(\omega) = -\Gamma^0(\omega)/v^2(\omega) \dots (21)$$

$\Gamma^0(\omega)/2v(\omega)$ corresponds to half-width associated with the damping of the soft ferroelectric optic mode frequency. From Eq. (16) we can write

$$v^2(\omega) = \gamma(T - T_c + \xi T^2) \dots (22)$$

Hence

$$\gamma(T - T_c + \xi T^2) \tan\delta = -\Gamma^0(\omega)$$

or

$$\gamma(T - T_c + \xi T^2) \tan\delta = bT + dT^2 \dots (23)$$

where b and d are the coefficients of T and T^2 terms in Eq. (7). Eq. (23) can also be rewritten as

$$(T - T_c + \xi T^2) \tan\delta = A + BT + DT^2 \dots (24)$$

$$\text{where } A = 0, B = b/\gamma \text{ and } D = d/\gamma \dots (25)$$

It follows from Eq. (24) that the microwave loss tangent strictly depends upon anharmonic, resonant interaction and scattering terms. The presence of these terms increases the loss tangent. On calculation, it can be seen that the coefficients B and D and hence $\tan\delta$ vary linearly with frequency (ω), in agreement with the previous results^{15,16,18,20}.

In our subsequent paper, we will show that the coefficient A is not zero in the case of the doped crystal. The deviation from the Curie-Weiss law at high temperature is characterized by the parameter ξ [Eq. (17c)]. In the vicinity of T_c , $\tan\delta$ increases anomalously and the soft mode frequency (Ω) is responsible for this behaviour.

5 Attenuation Constant

The attenuation constant is given by⁶

$$\alpha(\omega) = \Gamma^0(\omega)/c \dots (26)$$

where the damping constant $\Gamma_{(\omega)}^a$ is given by Eq. (13) and c is the sound velocity. Now it is evident from Eqs (26) and (13), that the presence of scattering terms and anharmonic and resonant interaction terms [via N_λ^0 and hence Ω , in Eq. (13)] increases the attenuation constant. The calculations show that the frequency dependence of $\alpha(\omega)$ is linear. The dependence is in agreement with the previous results^{19,21,22}. From Eq. (13) it can be seen that in the high temperature limit, $\Gamma^a(\omega) \sim cT$, besides the temperature dependence through renormalized frequencies; c_1 being the coefficient of T in Eq. (13). In presence of the stabilizing factors, we approximate the strong temperature dependence of the soft optic mode frequency by $\Omega \propto (T - T_c)$, if the temperature is not very high. Thus taking this temperature variation of the soft mode fre-

quency for small values of wavenumbers, the temperature dependence of $\alpha(\omega)$ can also be expressed as

$$\alpha(\omega) = (A_1/c)[T/(T - T_c)^{1/2}] \quad \dots (27)$$

where A_1 denotes the temperature-independent term in Eq. (13).

The expression (27) does not give the explicit temperature dependence of $\alpha(\omega)$ because of the renormalized effects. The renormalized frequencies of each phonon mode appearing in real and imaginary parts of polarization operation may produce some change in the temperature dependence. In the vicinity of the Curie temperature T_c ($T \rightarrow T_c$, N_λ^0 becomes anomalously large and hence there are interactions of the low lying transverse optic modes with the longitudinal acoustic modes), the attenuation constant increases anomalously in agreement with the previous results^{6,9,21,22}. This anomalous increase can be attributed to the temperature dependence of the soft mode frequency. This is also shown experimentally by Heuter and Neuhaus⁷. The anharmonic, resonant interaction and scattering process giving rise to the sound attenuation can be seen by the δ factors appearing in Eq. (13).

6 Velocity Change

The expression for the velocity change of sound $\Delta c = (\tilde{\omega}_\mu^a - \omega_\mu^a)/\mu$ can be easily obtained with the help of Eqs (10)-(12) and can be discussed on the above grounds. In the vicinity of the Curie temperature, the sound velocity decreases anomalously because the ultrasonic frequencies ω will be smaller than the soft optic mode frequency Ω in cubic ferroelectrics ($\omega \ll \Omega$). The results are in agreement with previous results^{6,13,19}. Here the Dyson's equation treatment has been found convenient to derive the shift and width of the frequency response function and hence to describe the properties of these ferroelectrics. The treatment adopted here, leads one to see the comparative variation of dielectric and ultrasonic properties with the variation of the anharmonic, resonant interaction and scattering terms. The qualitative dependences discussed here agree with previous experimental and theoretical results. The anomalous specific heats of these crystals have been discussed else-

where²³. Recently we have experimentally measured²⁴, the dielectric constant, tangent loss, electrical conductivity and ultrasonic attenuation constant of BaTiO₃.

Acknowledgement

The authors are thankful to Dr B S Semwal for helpful discussions. They are grateful to Professors S K Joshi, E C Subba Rao, A Mansingh, G S Verma and K Mahesh for encouragement. Financial assistance from the Department of Science and Technology, New Delhi, is also thankfully acknowledged.

References

- 1 Pytte E, *Phys Rev B (USA)*, **5** (1971) 3758.
- 2 Muller K A, Berlinger W & Wallner W, *Phys Rev Lett (USA)*, **21** (1968) 814.
- 3 Shirane G & Yamada Y, *Phys Rev (USA)*, **117** (1969) 858.
- 4 Cochran W & Zia A, *Physica Status Solidi (Germany)*, **25** (1968) 273.
- 5 Axe J D, Shirane G & Muller K A, *Phys Rev (USA)*, **183** (1969) 820.
- 6 Tani K & Naoyuki Tsuda, *J Phys Soc Jpn (Japan)*, **26** (1969) 113.
- 7 Heuter N P & Neuhaus D P, *J Acoust Soc Am (USA)*, **27** (1955) 292.
- 8 Barrett H H, *Phys Lett (Netherlands)*, **26** (1968) 217.
- 9 Jones C K & Holm J K, *Phys Lett (Netherlands)*, **26** (1968) 182.
- 10 Kashida Shoji, Hatha Ichiro, Ikushima Akira & Yamada Yasusada, *J Phys Soc Jpn (Japan)*, **34** (1973) 997.
- 11 Luthi B & Moran T, *Phys Rev B (USA)*, **2** (1970) 1211.
- 12 Tani K, *J Phys Soc Jpn (Japan)*, **26** (1969) 93.
- 13 Naithani U C & Semwal B S, *Proc Natl Acad Sci Sec a (India)*, **52** (1982) 386.
- 14 Dvorak V & Zech C, *J Phys B (GB)*, **21** (1971) 836.
- 15 Naithani U C & Semwal B S, *Pramana (India)*, **14** (1980) 149; **15** (1980) 371; **14** (1980) 19; **11** (1978) 423.
- 16 Silverman B D & Joseph R I, *Phys Rev (USA)*, **129** (1963) 2062.
- 17 Zubarev D N, *Sov Phys Usp (USSR)*, **3** (1960) 320.
- 18 Pytte E & Feder J, *Phys Rev (USA)*, **187** (1969) 1077.
- 19 Pytte E, *Phys Rev B (USA)*, **1** (1970) 924.
- 20 Bahádur Rita & Sharma P K, *Phys Rev (USA)*, **12** (1975) 448.
- 21 Mavroyannis C & Pathak K N, *Phys Rev (USA)*, **182** (1969) 872.
- 22 Naithani U C & Semwal B S, *J Phys (France)*, **42** (1981) (Suppl) C 5-659.
- 23 Naithani U C & Baluni G N, *Indian J Pure & Appl Phys*, **23** (1985) 261.
- 24 Baluni G N & Naithani U C, *Solid St Ionics (Netherlands)*, (1986) in Press.

Temperature & Thickness Dependence of Electrical Conductivity of Polypropylene

H P SINGH

Department of Physics, A N College, Patna 800 001

and

D GUPTA

Department of Physics, B N College, Patna 800 005

Received 29 July 1985

The electrical conductivity (σ) of polypropylene has been studied as a function of temperature and thickness of the sample at different fixed voltages. From $\ln \sigma$ versus $1/T$ plots, it is found that the conductivity is proportional to the exponential of inverse of temperature. The plots have different slopes above and below the softening temperature (390 K). The observed high value of activation energy at temperatures above 390 K indicates that conduction is intrinsic in this region while the low value of activation energy in the low temperature region indicates impurity conduction. Low values of activation energies (≤ 1 eV) in both the regions indicate the predominance of electronic conduction. The conductivity of the polymer is found to increase with increasing sample thickness.

1. Introduction

The study of electrical conductivity of polymers sandwiched between metal electrodes has attracted many investigators particularly due to the discovery of memory phenomenon¹ in them and their possible use in thin film devices². Polymers are now being extensively used as insulating and heat resistant materials. Thus, the study of their electrical properties becomes imperative.

The conductivity of a dielectric may be either ionic or electronic or both. Experimentally, the ionic or electronic conduction are distinguished by measuring the activation energy. Low activation energy ≤ 1 eV corresponds to electronic current and high value to ionic current. The conductivity varies due to different external conditions such as changing pressure, humidity, temperature, thickness of the sample, etc.

The sample, polypropylene, is an organic polymer of industrial importance. We have studied the electrical conduction³ in the sample earlier. Observations on the hysteresis effect in the sample, the effects of pressure and electrode materials on conductivity have already been reported. The present paper gives the temperature and thickness dependence of the electrical conductivity of the sample at fixed voltages. An attempt has been made to explain the results on the basis of prevalent theories.

2 Experimental Details

A small amount of the sample was heated to melt and then pressed to uniform thickness. A piece of the sample thus prepared was placed on the lower electrode of the sample holder, the upper electrode having

been attached to the leg of a spherometer-type arrangement. The whole assembly was then heated in an electric oven to make the sample soft and free of air bubbles.

The stud of the spherometer was rotated to press the sample between the electrodes to required thickness. The electrodes were kept embedded in the bulk of the sample to avoid surface conduction. The sample between the electrodes was kept short-circuited for about 24 hr to make it ready for observations.

A high voltage dc unit and a resistance of $1 \text{ M}\Omega$ were connected in series with the electrodes. A Philips VTVM was connected across the $1 \text{ M}\Omega$ resistor and the currents were calculated from the voltage drop across this resistor, taking into consideration the input resistances of the VTVM in different ranges. The sample holder with the sample was placed in a thermostat U-10 for maintaining a constant temperature. The sample was heated for an hour to attain a particular temperature.

3 Results

Figs 1-3 depict the $\ln \sigma$ versus T^{-1} plots for different sample thicknesses at different fixed applied voltages. The plots are almost linear, showing a change in the slope near about the softening temperature of the sample (390 K). Thus, the curves may be divided into two regions: region I of high temperature (above 390 K) and region II of low temperature (below 390 K).

The linear-nature of the plots in the two regions clearly shows that the conductivity is proportional to the exponential of inverse of temperature which, in general, applies to all organic solids. The activation

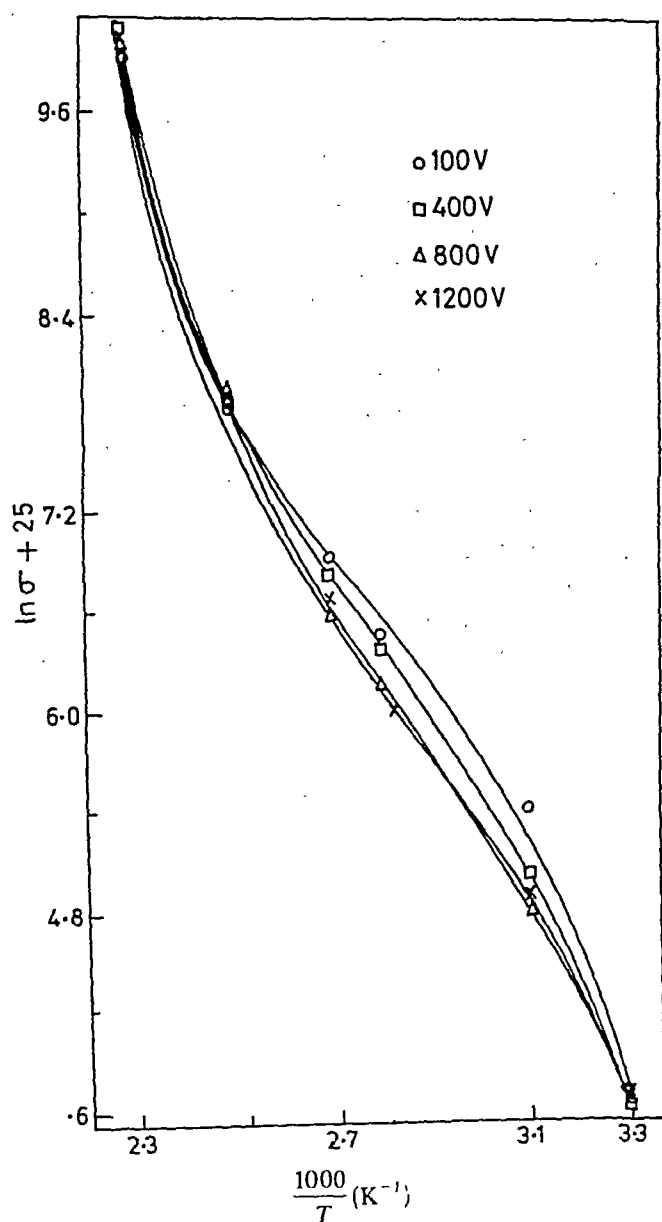


Fig. 1— $\ln \sigma$ versus $1/T$ plots for a sample of thickness 2 mm at different voltages

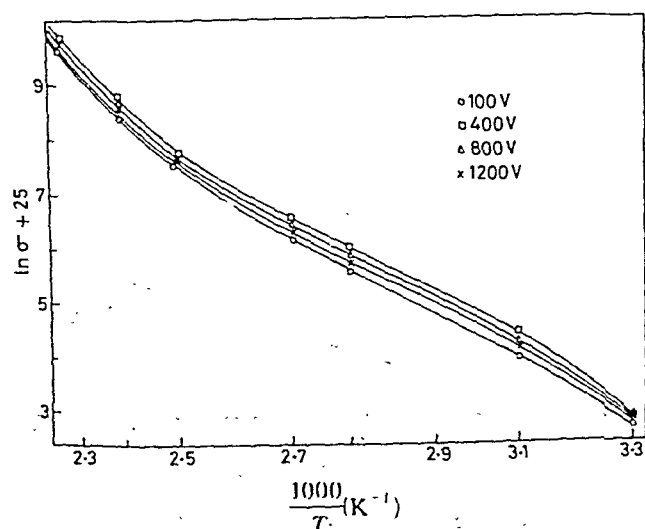


Fig. 2—Plot similar to Fig. 1 for a sample of thickness 1 mm

energies, calculated from slopes of the curves, are found to be greater in region I than in region II. However, the values of these activation energies are small in both the regions, as shown in Table 1.

4 Discussion

The observed variation of σ with T is due to the combined effect of change in conductivity with temperature and the nature of trap distribution in the sample⁴. O'Dwyer⁵ has suggested the existence of *numerous* isolated shallow traps covering an energy range ΔW below the continuum of free electron levels. Deep traps whose energy W is between the conduction and valence levels also exist. At 0 K, all the trapped electrons would be in deep traps, but at a finite temperature and in presence of an applied field, some of these electrons can be excited into shallow traps or conduc-

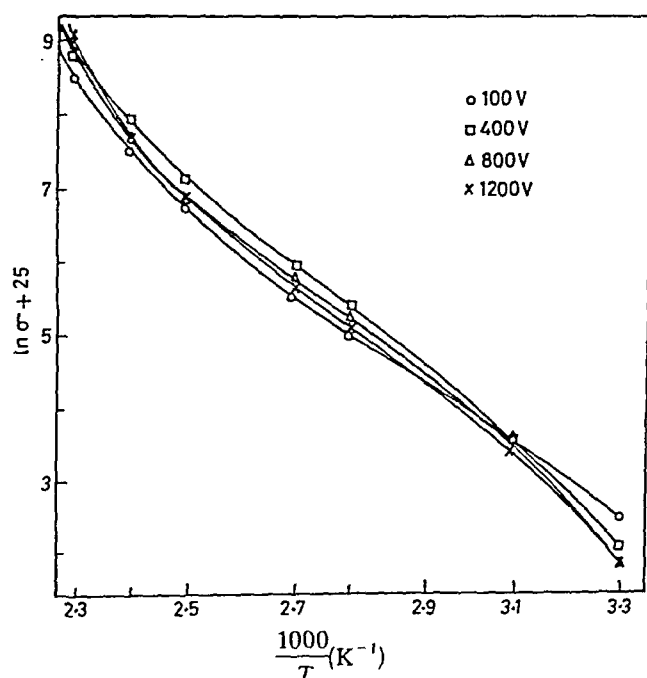


Fig. 3—Plots similar to Fig. 1 for a sample of thickness 0.5 mm

Table 1—Values of Activation Energies (W_E) for Regions I & II Calculated from Plots in Figs 1-3

Thickness	Applied voltage	W_E (eV)	
		Region I	Region II
2 mm	100	0.652	0.422
	400	0.708	0.429
	800	0.556	0.388
	1200	0.739	0.389
1 mm	100	0.549	0.439
	400	0.546	0.396
	800	0.598	0.417
	1200	0.525	0.416
0.5 mm	100	0.516	0.379
	400	0.552	0.312
	800	0.539	0.366
	1200	0.525	0.386

tion levels either thermally or due to action of applied field. These electrons then take part in conduction. The increase in temperature does not alter the total amount of space charge but increases the fraction of this space charge in the conduction band, which increases exponentially with the inverse of absolute temperature.

Thermal agitation gives rise to defects in the material of the sample. Generally, in semiconductors or dielectrics, the structure consists of a loose network with a large number of interstices that are only partly occupied by ions. Conduction can take place by movement of ions from an occupied site to an unoccupied site. The activation energy involved in this process exhibits exponential dependence of conductivity on temperature.

Thermodynamical calculations have shown that the defects increase with temperature at higher temperatures and are independent of temperature at lower temperatures, because at higher temperatures additional defects are created and at lower temperatures, they are frozen in. Hence, the conductivity variation with temperature may be divided into two regions: (I) pertaining to high temperature and (II) pertaining to lower temperature. The $\ln \sigma$ versus T^{-1} plots in the case of samples studied by us show a similar behaviour. The plots (Figs 1-3) can be best expressed by the equation:

$$\sigma = A \exp(-W_E/kT) \quad \dots (1)$$

where A and W_E are two constants having different values for the regions above and below the softening temperature of the sample.

At high temperatures, the conductivity is mainly determined by the intrinsic defects. Hence the high temperature region is often called the intrinsic conduction region. In the low temperature region, the curves slope more gently. This region is influenced by impurity conduction. The activation energies have been calculated from the curves using the relation:

$$W_E = k \times \text{slope} \quad \dots (2)$$

where W_E = activation energy and k = Boltzmann's constant. The low values of activation energies (≤ 1 eV) as shown in Table 1 indicate the predominance of electronic conduction^{6,7}.

The increase in the conductivity at higher temperatures may be due to the softening⁸ of the sample. Because of softening, the injected charge carriers can move more easily into the volume of the sample, giving rise to a large current and increase in conductivity at high temperature.

According to Brown and Aftergut⁹ as well as to Srivastava and Agrawala¹⁰, the presence of two slopes in $\ln \sigma$ versus T^{-1} plots is an indication of impurities. The

current in the impure semiconductor is due to two competing processes which act simultaneously.

In the first process, an electron occupying an isolated donor has a wavefunction located about the impurity and an energy slightly below the conduction band minimum. Because there is a small but finite overlap of the wavefunction of an electron of one donor with those of the neighbouring donors, a conduction process is possible in certain circumstances in which the electrons may move between centres by the tunneling effect without activation into the conduction band.

The second process is responsible for the current usually observed and which is carried by electrons in the conduction band in thermal equilibration with electrons on donor impurities. This is called the impurity conduction.

Several other methods and models have been suggested by different investigators for the explanation of the temperature dependence of electrical conductivity¹¹.

For the polypropylene sample, the defect conduction seems to be more appropriate. The sample, polypropylene, is a polymer and its conductivity depends upon the presence of free-ions not connected chemically with the macromolecules. The molecular chain proper does not participate in the transfer or electric charges. Thus, the conductivity of polymers largely depends upon the presence of low molecular impurities that can serve as the source of ions. A similar view has been expressed by Chutia and Barua¹² in the case of polystyrene.

The increase of electrical conductivity with increasing sample thickness may be explained as follows.

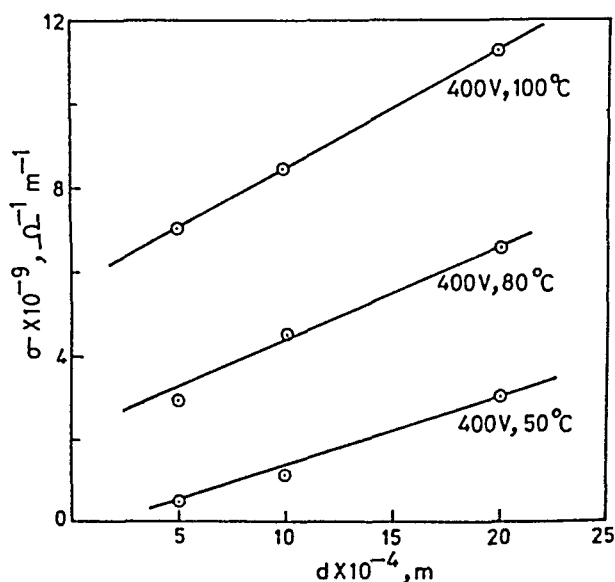


Fig. 4—Plot of conductivity (σ) versus thickness (d) of the sample at fixed temperatures and voltages

When the thickness grows, the number of charge carriers in the sample increases at a fixed electric field. Also, since the conductivity $\sigma = J/E$ where J = current density and E = electric field = V/d , V = voltage applied and d = thickness of the sample; we have

$$\sigma = J/E = J \div V/d = Jd/V \quad \dots (3)$$

Thus at constant temperature and applied voltage, σ should increase with d .

Again, as impurity conduction is supposed to dominate in the sample under study, the increase in the sample thickness is likely to enhance the impurity atom concentration in the material. Hence the conductivity will rise with increase in sample thickness, as is evident from Fig. 4.

Acknowledgement

The authors express their gratitude to Professor L S Singh and R S Prasad of the Department of Physics,

Patna University, Patna, for valuable suggestions and encouragement during the study.

References

- 1 Kryezewski M, *J Polym Sci Polym Symp (USA)*, **50** (1975) 359.
- 2 Mead C A, *J Appl Phys (USA)*, **32** (1961) 646.
- 3 Singh H P & Gupta D, *Indian J Pure & Appl Phys*, **23** (1985) 35.
- 4 Lampert M A, *Phys Rev (USA)*, **103** (1956) 1648.
- 5 O'Dwyer J J, *J Appl Phys (USA)*, **37** (1966) 2599.
- 6 Lamb D R, *Electrical conduction mechanism in thin insulating films* (Methuen, London), 1967.
- 7 Beam G P, Fisher J C & Vermilyce D A, *Phys Rev (USA)*, **101** (1956) 551.
- 8 Tripathy A K & Srivastava A P, *Indian J Pure & Appl Phys*, **20** (1982) 863.
- 9 Brown G P & Aftergut S, *J Chem Phys (USA)*, **38** (1963) 6, 1356.
- 10 Srivastava G P & Agrawala S R, *Phys Lett A (Netherlands)*, **46** (1974) 322.
- 11 Gupta D & Prasad R S, *Indian J Pure & Appl Phys*, **17** (1979) 505.
- 12 Chutia J & Barua K, *Indian J Pure & Appl Phys*, **19** (1981) 1210.

An Ultrasonic A-Scan Ophthalmoscope for Diagnosis of Eye Abnormalities

V N BINDAL, V R SINGH & REETA GUPTA

National Physical Laboratory, New Delhi 110 012

Received 7 February 1985; revised received 25 June 1986

The design, development and fabrication of an ultrasonic A-scan ophthalmoscope, using indigenous resources, are described. Characterization and calibration of such ophthalmic systems for the diagnosis of various eye abnormalities like tumours, haemorrhages, trauma and foreign objects are also discussed. Clinical results obtained on *in vitro* goat eyes and *in vivo* human eyes are given. The ophthalmoscope developed will save foreign exchange, be cheaper than imported ones and easily portable. Both ocular and orbital examinations of the eye are possible with the present system.

1 Introduction

Ultrasound was first introduced into ophthalmology by Mundt and Hughes¹ in 1956. A-mode display was mainly used in different forms, manually or automatically^{2,3}, but in 1958, time-intensity, two-dimensional ultrasonography and B-scan, were developed⁴ and used in ophthalmology for better localization of the shape of the lesions. Both the techniques were then recommended⁵ to be used together but, after sometime, emphasis was placed on the use of A-scan technique alone⁶ as the results for orbital diagnosis were as good as with B-scan technique. A-mode technique had an advantage of repeatable simple geometry to identify the anterior and posterior surface of the globe, the bony orbit and the retrobulbar fat. Deviation from the normal disposition of echoes, either in position or relative amplitudes, had correlations with various pathological conditions⁷. The A-scan technique permitted better tissue differentiation also. Agreeing well with the concepts, development of an indigenous ultrasonic A-scan ophthalmoscope was taken up in the laboratory in order to meet the needs of the country⁸. Design and fabrication of complete prototype models with their diagnostic results on *in vitro* goat eyes and *in vivo* human eyes are reported in the present paper.

2 Ophthalmoscope

An ultrasonic A-scan ophthalmoscope comprised an ophthalmic probe, a transmitter, a receiver and a display unit. Fig. 1 depicts the block diagram of an ultrasonic A-scan ophthalmoscope. A number of ophthalmic probes using NPL-made PZT ceramic discs⁹ of frequencies 8-12 MHz and diameter of 6-8 mm, were made with better resolution and diagnostic potentiality, by using proper backing materials. Electronic circuitry and associated parts^{8,10} were fabricated^{8,9} for better diagnostic potentiality of the instrument to operate at 10 MHz. The clock generator and

pulser used integrated circuits to generate pulses of 300 V with a pulse width of $0.02 \mu\text{s}$ and pulse repetition rate of 500-1000 Hz. The receiver consisted of a low-noise, cascade rf amplifier of 60 dB gain in the 5-15 MHz range. An active transmit-receive switch was employed to limit the signal to transmit and re-

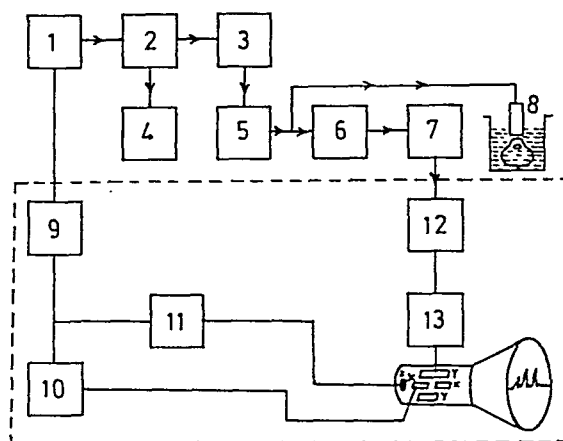


Fig. 1 - Block diagram of an ultrasonic A-scan ophthalmoscope [1 Timing generator, 2 pulse generator, 3 attenuator, 4 high voltage power supply, 5 transmitter, 6 receiver, 7 rf amplifier, 8 probe, 9 swept generator, 10 time base, 11 bright up generator, 12 demodulator detector, 13 video amplifier]

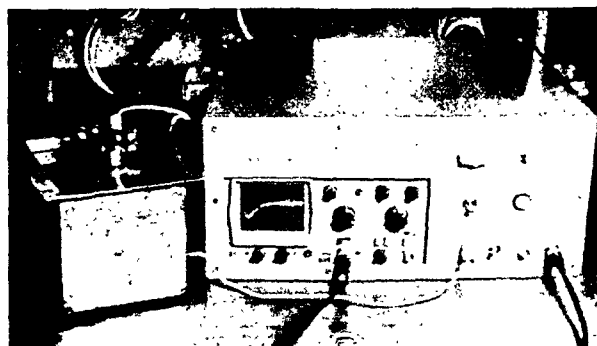


Fig. 2 - Photograph of an ultrasonic A-scan ophthalmoscope with *in vitro* goat eye immersed in a tank under examination

ceive alternately. A commercial portable oscilloscope of 15 MHz was used for the display of A-scan echo patterns.

The present ophthalmoscope (see Fig. 2) has a number of controls like power on/off switch, PRF, switch for a single/double probe, T/R switch, sensitivity control, and a damping control.

3 Characterization and Calibration

The ophthalmoscope developed was calibrated by using a standard perspex block as well as with other conventional techniques. The system was mainly characterized for its diagnostic potentiality, i.e. for its resolution, sensitivity and beam parameters like beam width, directivity and pattern, with the help of a 'two-wire method' developed in the laboratory¹⁻¹² and with various conventional techniques¹³⁻¹⁵. In the two-wire method, one wire was kept free to rotate around the other one kept fixed. The wires were then resolved for their minimum horizontal distance achieved by rotating the first wire around the second one. The respective echo patterns were observed on the CRO screen till both the echoes just merge. The apparatus made by Med Corp (USA) was also used

for measuring the axial and lateral resolution and the beam characteristics. Technical specifications of the ophthalmoscope are given in Table 1.

The eye has a homogeneous structure separated by large regular surfaces that reflect the ultrasonic waves. The difference in acoustic density among the different ocular structures is small. The ultrasonic velocity is about 1640 and 1530 m/s in the lens and vitreous respectively. Therefore only a small part (5%) of the energy is reflected to the receiver and the major part is transmitted after refraction. The absorption of ultrasound energy in the eye is minimal which is mostly due to the lens (10 dB). The eye has an advantage of its anterior and superficial situation, i.e. it is easily reached from various directions and the transducer may be put directly on the eye.

The echographic picture obtained from the same structure depends upon the technical characteristics of the equipment. Thus, the use of a standardized reference point became necessary. Different calibration devices like a plate of glass or steel placed in water or oil, were used. The maximum penetration distance in oil or the height of the repetition echo from the glass or steel was measured for different amplifications.

A biological method was used¹³ for calibration of the echogram. The sclera of the examined eye was used as the reference point. The system sensitivity necessary to obtain a maximal 1 mm echo from the sclera was read in decibels. The sclera had constant value of ± 2 dB; therefore, a quantitative echography was used. The difference in decibels between the amplification necessary to obtain a 1 mm echo from the sclera and from the examined structure was measured. This value gave the nature of reflecting surface.

The same sclera reference was used¹⁴ to measure the 'ultrasound absorption' when the beam directed through and bypassing the examined structure. The decibel difference between the two settings gave the absorption in the examined lesion (in dB/ μ s). Echo height, i.e. the maximal echo, was obtained from a given surface. The beam was, therefore, directed perpendicular to the surface. The echo type depended on the internal structures of the tissues, i.e. on the histological pattern and thus allowed a morphological diagnosis. Structures with internal distance of less than 0.03 mm were acoustically 'silent' because the wavelength of a transducer say of 8 MHz was 0.19 mm. Denser tumours showed less reflectivity, but more absorption¹⁵.

4 Diagnostic Results and Discussion

The ultrasonic A-scan ophthalmoscope was used to get scans on phantom, *in vitro* goat eyes, and *in vivo* human eyes. The phantom consisted of a perspex block with five parallel nylon threads 1 mm apart but

Table 1 - Technical Specifications of Ultrasonic Ophthalmoscope Developed at NPL

Dimensions	
Size	: 400 mm \times 350 mm \times 120 mm
Weight	: 8.5 kg (with CRO)
Electrical power switch	
Frequency	: 60 Hz
Voltage	: 220 V
Stabilization	: ± 10 of nominal value
Range	
Bulbus	: $> 0.5 \mu\text{s/mm} \pm 5$
Orbital	: $1 \mu\text{s/mm} \pm 5$
Pulse	: 500-1000 Hz
repetition rate	
Pulse	: $0.02 \mu\text{s}$
width	
Receiver	
Frequency	: 10 MHz (8-12 MHz with 3 dB)
range	: (10-20 MHz with low sensitivity)
Sensitivity	: 0-60 dB
control	
Mode of	: One or two probe heads
operation	
Electronic scale	
Scale	: Can be calibrated in μs or mm tissues
Adjustable	: For comparison of signal amplitude
time	
Display	
CRT	: 15 MHz, make Aplab Model 3030
Power supply for pulser	
Voltage	: 600 ± 2 V
Current	: 0.25 A
Resolution	: < 0.3 mm

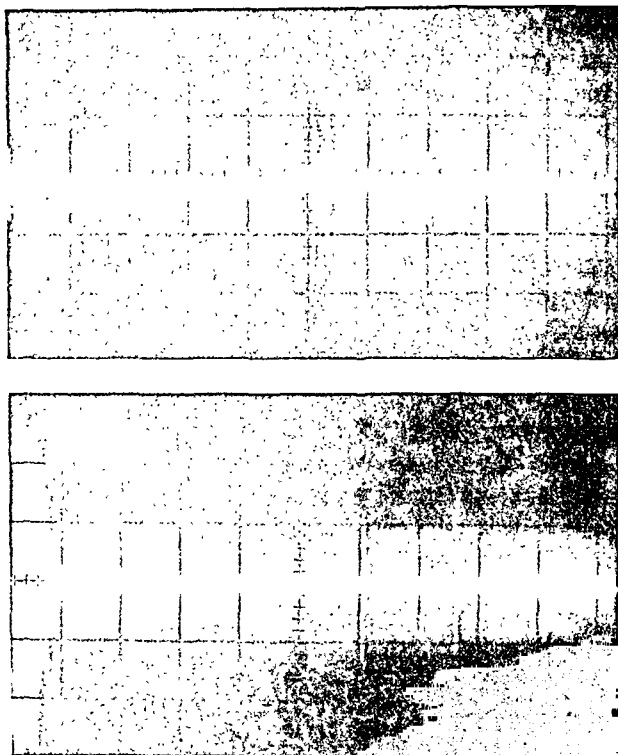


Fig. 3 – A-scan pattern in *in vitro* goat eye in axial and lateral modes

giving less spacing and depth by their rotation. Scans were also obtained on the *in vitro* goat eye and are shown in Fig. 3 in axial and lateral directions, by tying the eye on a perspex block with nylon threads and keeping the lens upwards facing the probe head, both (eye and probe) being immersed in the water (Fig. 2). Scans (Fig. 4) were obtained on the patients in the hospital by putting a cup on the eye filled with saline solution and keeping the ophthalmic probe in the solution facing the lens to get echoes from all parts of the eye. Total eye was also examined by taking scans at various parts of the eye by moving the probe head with the hand over the whole eye with proper acoustic contact by using saline solution or suitable liquid drops in the eye.

Thus with the present system, it was possible to get scans from various eye structures, viz. cornea, anterior of the lens, position between retina and sclera in the axial mode, and further details of the eye portion between retina, sclera and retrobulbar parts in the lateral mode. The vitreous-retinal interface echo was followed by a complex of echoes representing retina, choroid, sclera and retrobulbar fat. The echoes in the retrobulbar fat diminished gradually to the baseline. Scans from sclera were clearly visible with the present model. For the biometry of the eye, the echogram was calibrated by using one of the techniques described above. Distance between the scans from front and rear of the lens gave the lens size while the distance be-

tween the scans from posterior wall of the lens and retina gave the length of the vitreous, and so on. Total size of the eye could be measured by measuring the distance between the front wall and the rear wall of the eye, i.e. between cornea and retina. The eye could also be examined with the present system; for example, if there was abnormality of haemorrhage, blood clotting or foreign object present in the vitreous, additional spikes would be seen between the scans of posterior lens capsule and retina. This gave the actual diagnosis and location of the abnormality or disease. The innovative changes made in the design of conventional circuitry and transducer, with local supplies, were thus successful.

The results of the indigenous system have also been compared with those of the imported units, Kretz and Sonometrics used in the present investigation, and been found quite comparable¹⁶ for various eye abnormalities.

5 Conclusions

An indigenous ultrasonic A-scan ophthalmoscope has been developed and used successfully in the localization and diagnosis of eye abnormalities as well as in the measurement of the physical size of the structures in the eye. The instrument developed is simple, easy to operate, less expensive and has low weight. Availability of such an instrument would make the country self-sufficient and would help in saving of huge amount of foreign-exchange. India is thus able to pro-

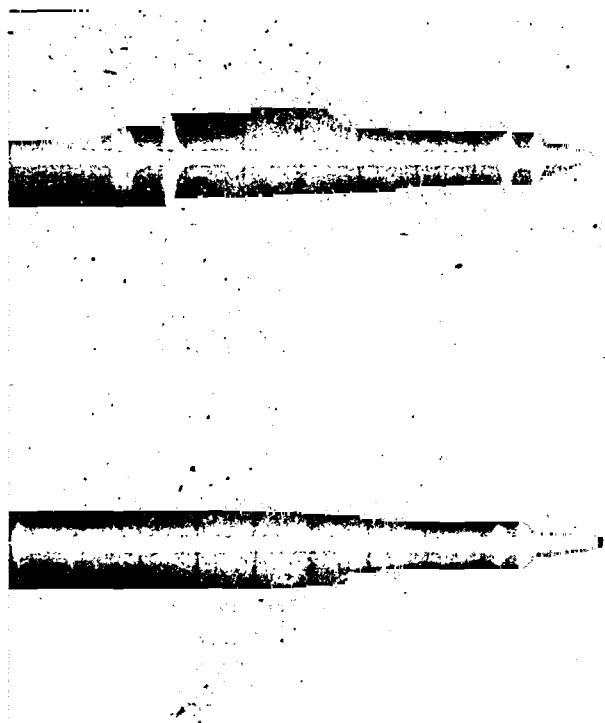


Fig. 4 – A-scan results in human eye in axial and lateral modes

duce with local supplies a machine comparable to imported ones at a lower cost and with innovative changes.

The detailed diagnosis of various eye abnormalities like detection of foreign objects, tumours, haemorrhages, retina detachment, cataract, etc., with the present system, is in progress.

Acknowledgement

The authors are thankful to Dr A P Mitra, Director, NPL and Prof. Madan Mohan, Chief of Dr R P Centre of Ophthalmological Sciences, All India Institute of Medical Sciences, New Delhi, for their constant encouragement in the present investigations. Dr I M Bhatia of R P Centre is also acknowledged for his help in the clinical trials. Technical assistance, from Electroceramics Section of NPL, is thankfully acknowledged for making available indigenously the PZT discs used in the present work. Mr Ram Dass of Ultrasonography Laboratory of R P Centre of Ophthalmological Sciences deserves special thanks for continuous help in clinical trials in the hospital.

References

- 1 Mundt G H & Hughes W E, *Am J Ophthalmol* (USA), **42** (1956) 488.
- 2 Bronson N R, *Arch Ophthalmology* (USA), **90** (1973) 237.
- 3 Dadd M J, Kossoff G & Hughes H, *Med J Aust* (Australia), **1** (1974) 580.
- 4 Baum G & Greenwood I, *Arch Ophthalmology* (USA), **60** (1958) 269.
- 5 Ossonig K in *Ultrasonics in ophthalmology*, edited by A Oksala & H Gemet (Karger S, Basel, Switzerland), 1967, 88-96 & 116-133.
- 6 Francois J & Goss F in *Present and future of diagnostic ultrasound*, edited by I Donald & S Levi (John Wiley & Sons, New York, USA), 1976, 109-127.
- 7 Robinson D E & Kossoff G in *Ultrasound: its applications in medicine, Part II*, edited by J F Fry, 1978, 624-626.
- 8 Agarwal L P, Chivers R C, Bhatia I M, Gogia V K, Singh V R *et al.*, *Int Conf & Exhb on ultrasonics: conf papers* (National Physical Laboratory, New Delhi), 1980, 399-404.
- 9 Jain G C, Bindal V N, Singh J, Singh V *et al.*, *Indian J Pure & Appl Phys*, **21** (1983) 373.
- 10 Bindal V N, Singh V R, Gupta Reeta & Bhatia I M, *Proc 3rd World instrumentation symp* (Wisitex Foundation, New Delhi), 1984, 12 CI-DI/2/1-6.
- 11 Bindal V N, Singh V R & Gupta Reeta, Resolution Studies in Diagnostic Ultrasonic Systems. Paper presented at 2nd National Symposium on Ultrasonics NPL, New Delhi, 23-24 Feb, 1982.
- 12 Bindal V N, Singh V R & Gupta Reeta, Characterisation of an ultrasonic ophthalmic probe, *J Pure & Appl Ultrasonics*, (India) (1986) in press.
- 13 Ossonig K, in *Ultrasonographia medica (SIDUO III)*, edited by J Bock & K Ossonig K (Verlag der Wiener Med Akad Vienna, Austria), 1971, 423-436.
- 14 Poujol J, Ref. 13, p. 275.
- 15 Poujol J, Iris I & Armand M J, in *Ultrasonography in ophthalmology*, edited by J Francois & F Goss (Bidi Ophthalm, Basel, Switzerland), **83** (1975) 172-177.
- 16 Bindal V N, Singh J M, Singh V R *et al.*, *Trends in transducers*, edited by V R Singh, B Kapur, S K Thapar, S Middelhock & R Prashad (TECA Publications, New Delhi), 1985, 114-118.

Compound-Nucleus Effects in Inelastic Deuteron Scattering from ^{24}Mg at $E_d = 10\text{-}15$ MeV

S R VERMA

Department of Physics, DBS(PG) College, Dehra Dun 248 001

&

R PRASAD

Physics Section, Z H Engineering College, Aligarh Muslim University, Aligarh

Received 10 January 1986; revised received 17 March 1986

Compound-nucleus contributions, calculated from Hauser-Feshbach theory, have been added to differential cross-sections calculated from distorted wave Born approximation for deuteron inelastic scattering to the 2^+ (1.37 MeV) state of ^{24}Mg , in the region of $E_d = 10\text{-}15$ MeV. It has been shown that the fits to the differential cross-sections at backward angles are improved by the addition of compound-nucleus contributions, and as expected, compound-nucleus contribution is less at $E_d = 14, 15$ MeV as compared to that at 10 MeV.

The examination of published data for the inelastic scattering of deuterons from ^{24}Mg at $E_d = 10, 14$ and 15 MeV shows that angular distributions cannot be reproduced completely by Distorted Wave Born Approximation (DWBA) calculations, particularly at backward angles. Only for elastic scattering, DWBA calculations agree with experimental data. This discrepancy between experimental results and theoretical calculations may be due to the presence of compound-nucleus contributions. In many cases, direct reaction and compound-nucleus reaction may simultaneously contribute to the reaction in a particular channel. The compound-nucleus contributions seem to be important for the deuteron inelastic scattering to the 2^+ (1.37 MeV) state of ^{24}Mg .

It is not possible to separate the experimental data into levels for which there is only a direct reaction mechanism and levels for which there are only compound-nucleus contributions. At intermediate energies, most of the levels are populated through an incoherent mixture of the two extreme forms of reaction mechanism. Since the lifetime of the compound-nucleus process is quite long compared to the time required for the direct process, these processes are expected to be incoherent. The expression for the total differential cross-section may be given as:

$$\frac{d\sigma}{d\Omega} = \left(\frac{d\sigma}{d\Omega}\right)_{\text{DR}} + R\left(\frac{d\sigma}{d\Omega}\right)_{\text{HF}}$$

where $(d\sigma/d\Omega)_{\text{DR}}$ is the cross-section calculated by direct reaction theory, $(d\sigma/d\Omega)_{\text{HF}}$ the cross-section calculated by Hauser-Feshbach theory and R the reduction factor. The fluctuations and interference effects are comparatively very small and do not invalidate the model in any substantial way.

The studies of Satchler¹ and others² show that calculations made with DWBA improve the fitting of theoretical angular distribution data with observed values at forward angles, but have little agreement at backward angles. In case of compound-nucleus theory, the phases of wavefunction describing the compound-nucleus states which contribute to the reaction are assumed to be essentially random. As a consequence of this assumption, angular distribution of reaction products is symmetrical about 90° .

Schmick and coworkers³ have performed Hauser-Feshbach (HF) calculations at $E_d = 14$ and 15 MeV for this level. They have predicted negligible compound-nucleus contribution on the basis of calculations where the important parameters of the expression have values: $\sigma = 2.65$ and $\rho = 3050$. In the expression for angular distribution of scattering, the inverse of $P[P = 2\pi(\Gamma/D)]$, multiplies the HF angular distributions and spin cut-off factors (σ). $\sigma^2 = I\iota/h^2$ where I is the nuclear moment of inertia taken as the rigid body moment of inertia, h the Planck's constant, and ι the nuclear temperature. The quantities Γ and D are the mean level width and mean level spacing of compound-nucleus states for the lowest J value to be formed⁴. The angular distribution and correlation depend on Γ/D and σ^2 . The choice of σ^2 essentially determines the shape of the curves. The angular distributions for the level 2^+ (1.37 MeV) reproduced by HF calculations with $\sigma = 3.16$ are better than those with $\sigma = 2.65$ as the value of $\sigma = 3.16$ gives a lower value of the reduction factor. If this value of $\sigma (= 3.16)$ is used for finding out compound-nucleus contributions, as was tried⁵ for the reaction $^{24}\text{Mg}(d,p)$ at $E_d = 10$ MeV, the compound-nucleus contributions may not be negligible at these energies. There is no other means for making a definite estimate of the reduction factor. In our present study, the reduction factor is part of the parameter ρ .

In the present study, HF calculations are made and the results analyzed to assess the importance of compound-nucleus contributions. The compound-nucleus contributions calculated from HF theory⁶ have been added to those obtained from DWBA calculations. The experimental data along with DWBA calculations for angular distribution for the level 2^+ (1.37 MeV) have been taken from literature^{3,7}.

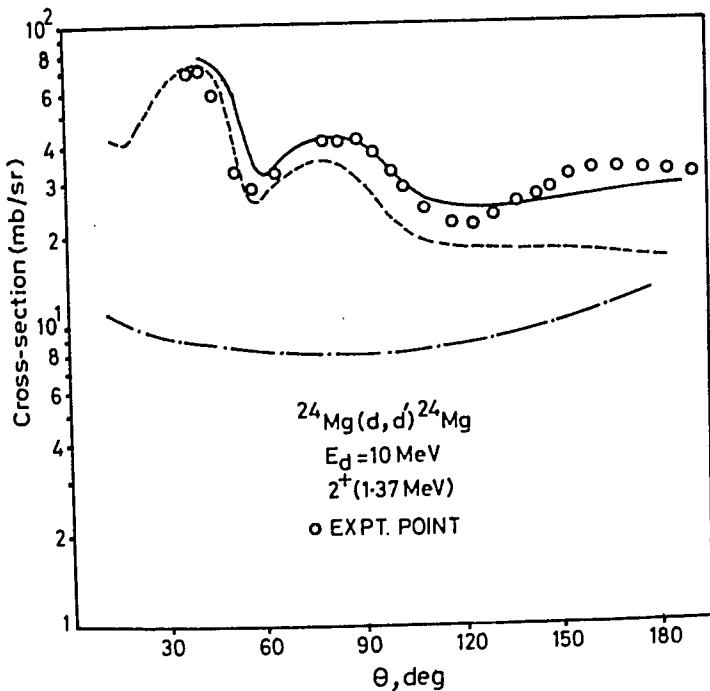


Fig. 1—Angular distribution of deuteron scattering cross-section for $^{24}\text{Mg}(d, d')^{24}\text{Mg}$ at $E_d = 10$ MeV [DWBA (---), HF analyses (— · —) and DWBA plus HF analyses (—). Circles represent experimental data for deuteron inelastic scattering.]

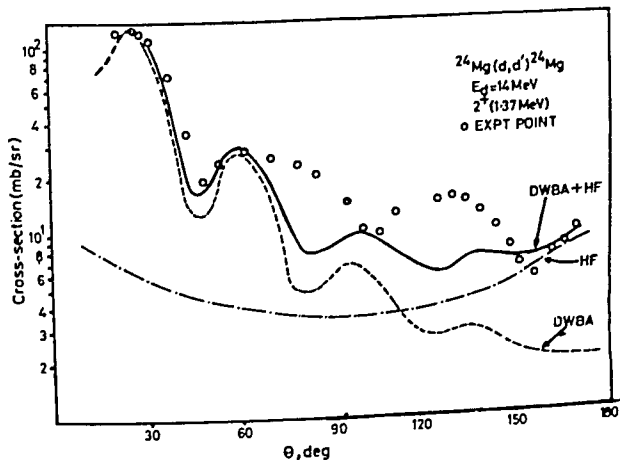


Fig. 2—Plot similar to Fig. 1 at $E_d = 14$ MeV

For HF calculations, the expressions for differential cross-sections given by Sheldon⁸ are used. The cross-sections have been calculated using the computer programme MANDYF developed by Sheldon and coworkers⁹. The programme was modified to include the expression for $\Sigma T_{ij}(E)$ and to increase the limit of restriction on the angular momenta^{10,11}. The transmission coefficients for entrance and exit channels were calculated using optical model parameters as used in DWBA analyses.

Theoretical cross-sections have been obtained by adding DWBA cross-sections to those obtained from

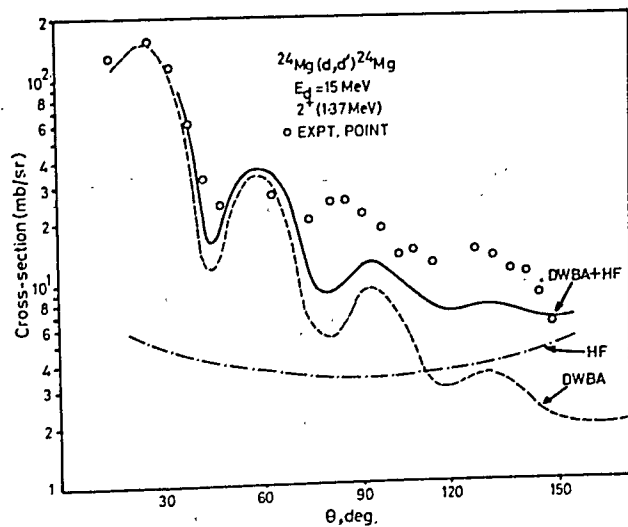


Fig. 3—Plot similar to Fig. 1 at $E_d = 15$ MeV

HF calculations. The experimental data together with calculated angular distributions are presented in Figs 1-3. It is seen that addition of compound-nucleus contributions improves the fits to the experimental data for the inelastic scattering of deuterons from ^{24}Mg at $E_d = 10, 14$ and 15 MeV. The present study demonstrates that the linear combination of direct and compound-nucleus parts leads to a good reproduction of data, particularly at backward angles. As expected, the contribution of compound-nucleus process is less at $E_d = 14$ and 15 MeV as compared to that at 10 MeV in the reaction $^{24}\text{Mg}(d, d')^{24}\text{Mg}$; but it cannot be neglected.

One of the authors (SRV) is thankful to the University Grants Commission, New Delhi, for financial help.

References

- 1 Satchler G R, *Nucl Phys (Netherlands)*, **55** (1964) 1.
- 2 Blatchley D E & Bent R D, *Nucl Phys (Netherlands)*, **61** (1965) 641.
- 3 Schmitt T A, Kemper, Bindal R K & Koshel R D, *Phys Rev C (USA)*, **10** (1974) 556.
- 4 Ebrahard K A & Trombik W, *Nucl Phys A (Netherlands)*, **193** (1972) 489.
- 5 Verma S R & Prasad R, *J Phys Soc Jpn (Japan)*, **47** (1979) 361.
- 6 Hauser W & Feshbach H, *Phys Rev (USA)*, **87** (1982) 366.
- 7 Machintosh R S, *Nucl Phys A (Netherlands)*, **203** (1973) 177.
- 8 Sheldon E, *Rev Mod Phys (USA)*, **35** (1963) 1975.
- 9 Sheldon E, Mathur S & Donati D, *Computer physics communications*, Vol. 2 (North-Holland Publishing Co, Amsterdam), 1971, 272.
- 10 Prasad R, Hofmann A & Vogler F, *Phys Rev C (USA)*, **10** (1974) 1577.
- 11 Prasad R, Hoffmann A & Vogler F, *Nucl Phys A (Netherlands)*, **255** (1975) 64.

Influence of Correlation Function on Evaluation of the Correlation Energy

M A KAMEL, A Y GHALY & M K ABDEL-HADY*

Faculty of Education, Ain Shams University, Cairo, Egypt

Received 26 December 1985; revised received 18 May 1986

The influence of various correlation functions is studied and applied to He atom and its isoelectronic series in ground states. Two-particle approximation is used for the evaluation of the correlation energies (E_c). In the ground states, values of E_c obtained using functions of the type $\chi = \alpha\phi(r_{12})$ and $\chi = \beta\phi(r_1 + r_2)$ agree with the exact values. But results approaching 95-98% of the exact values are obtained using function of the type:

$$\chi = \phi[\alpha r_{12} + \beta(r_1 + r_2) + \gamma r_1(r_1 + r_2)].$$

Nowadays in the theory of many-electron system, different methods are used taking the electronic correlation into account. One of these methods is the two-particle approximation. Two-particle approximation is a generalization of one-electron Hartree-Fock approximation, in which every two electrons move in the potential of the other ($N-2$)-electron system. This method was first discussed by Sinanoglu¹. In Sinanoglu's method, the solution of the two-electron problem is correct only within the limits of the second order perturbation theory. The two-electron correlation without using perturbation theory can be calculated using Brenig's method².

In this note Brenig's method is used for the calculation of the correlation energy of He atom and its isoelectronic series. The influence of various correlation functions on the correlation energy is studied.

Theoretical aspects and considerations — Brenig's expression for the correlation energy in the two-particle approximation can be divided exactly into different pair contributions³. This expression for He atom and its isoelectronic series can be written in the form:

$$E_c = [(\phi_{1st}(x_1)\phi_{1st}(x_2))\{h(x_1) + h(x_2)\} \\ \times \chi_{1st1st}(x_1x_2)] + \frac{1}{2}[\phi_{1st}(x_1)\phi_{1st}(x_2) \\ \times U(x_1x_2)\chi_{1st1st}(x_1x_2)] \quad \dots (1)$$

where

$$h(x_i) = -\frac{1}{2}\nabla_i^2 - \frac{Z}{r_i} \quad \text{and} \quad U(x_1x_2) = \frac{1}{r_{12}}$$

r_i is the distance of electron i from the nucleus, and r_{12} , the interelectronic distance. $\chi_{1st1st}(x_1x_2)$ is the correlation part of the two-particle wavefunction

$\Phi^{1st1st}(x_1x_2)$ which is taken in the form⁴:

$$\Phi^{1st1st}(x_1x_2) = \phi_{1st1st}(x_1x_2)[1 + \alpha r_{12} \\ + \beta(r_1 + r_2) + \gamma r_1 r_2(r_1 + r_2) + \delta(r_1 - r_2)^2 \\ + \epsilon(r_1 + r_2)^2 + \xi r_{12}^2] \dots (2)$$

where

$$\Phi^{1st1st}(x_1x_2) = \phi_{1st1st}(x_1x_2) + \chi_{1st1st}(x_1x_2) \dots (3)$$

and $\phi_{1st1st}(x_1x_2)$ is chosen in the ant-symmetric form.

$$\phi_{1st1st}(x_1x_2) = \frac{1}{\sqrt{2}} [\phi_{1st}(r_1)\phi_{1st}(r_2) \\ - [\phi_{1st}(r_2)\phi_{1st}(r_1)]] \quad \dots (4)$$

$\alpha, \beta, \gamma, \delta, \epsilon$ and ξ in Eq. (2) are variational parameters and can be determined using the variational procedure, which leads to the equation

$$|H_{KL} - EN_{KL}| = 0 \quad \dots (5)$$

where

$$N_{KL} = \int \psi_K^* \psi_L dx_1 dx_2$$

$$H_{KL} = \int \psi_K^* H \psi_L dx_1 dx_2$$

$$\psi_K = f_K(x_1x_2)\phi_{1st1st}(x_1x_2)$$

$$f_1(x_1x_2) = r_{12}, f_2(x_1x_2) = (r_1 + r_2)$$

$$f_3(x_1x_2) = r_{12}(r_1 + r_2), f_4(x_1x_2) = (r_1 - r_2)^2$$

$$f_5(x_1x_2) = (r_1 + r_2)^2, f_6(x_1x_2) = r_{12}^2$$

while $f_0(x_1x_2)$ is taken as unity.

In all the above calculations we have used the analytic one-electron function⁵.

Result and discussion — On the basis of the two-particle approximation method, the correlation energy of the He atom and its isoelectronic series in ground states were calculated. The variational parameters for various correlation functions used are given in Table 1. The corresponding values of the correlation energy (E_c) are given in Table 2. Comparison of our results and those obtained by Clementi⁶ indicates that the calculated values of E_c agree reasonably with exact values. It is pointed out that the method used in this study follows a simple procedure for calculating the correla-

*University College for Women, Ain Shams University, Cairo, Egypt

Table 1 — Calculated Values of the Variational Parameters

Function used	Parameter	Z : 2	3	4	5	6
f_0, f_1	α	0.0102	0.0075	0.0058	0.0047	0.0042
f_0, f_2	β	0.0089	0.0065	0.0050	0.0041	0.0034
f_0, f_3	γ	0.0047	0.0050	0.0057	0.0061	0.0064
f_0, f_5	ε	0.0033	0.0035	0.0038	0.0040	0.0042
f_0, f_6	ξ	0.0050	0.0054	0.0059	0.0064	0.0068
$f_0, f_1 f_2$	α	0.0069	0.0045	0.0033	0.0026	0.0023
	β	0.0059	0.0037	0.0028	0.0023	0.0018
f_0, f_1, f_3	α	0.0071	0.0055	0.0047	0.0040	0.0035
	γ	0.0062	0.0048	0.0041	0.0035	0.0031
$f_0, f_1 f_2, f_3$	α	0.0052	0.0037	0.0030	0.0024	0.0021
	β	0.0045	0.0031	0.0025	0.0021	0.0018
	γ	0.0040	0.0028	0.0021	0.0017	0.0016

Table 2 — Correlation Energies of the Ground State of He Atom and Its Isoelectronic Series

(Unit of E_c is in H with reversed sign.)

Parameter used	Z: 2	3	4	5	6
α	241	293	312	322	331
β	280	342	365	384	391
γ	201	233	272	305	320
ε	182	224	251	271	293
ξ	170	202	235	252	270
α, β	351	368	382	397	405
α, γ	381	392	410	419	423
α, β, γ	402	414	431	440	446
Ref. 6	421	435	443	448	451

tion energy and does not involve complicated calculations. Despite this, from Table 2 it is clear that reliable values of E_c are obtained using functions of the form:

$$\chi_{1s1s1s}(x_1 x_2) = \alpha \phi_{1s1s1s}(x_1 x_2) r_{12}$$

and

$$\chi_{1s1s1s}(x_1 x_2) = \beta \phi_{1s1s1s}(x_1 x_2) (r_1 + r_2)$$

The function $[\delta \phi_{1s1s1s}(x_1 x_2) (r_1 + r_2)]$ gives very small values of E_c and hence we do not report about it. Better results are obtained using the function of the form:

$$\chi_{1s1s1s}(x_1 x_2) = \phi_{1s1s1s}(x_1 x_2) [\alpha r_{12} + \beta (r_1 + r_2) + \gamma r_{12} (r_1 + r_2)]$$

This function leads to $\approx 95\text{--}98\%$ of the exact values of E_c .

References

- 1 Sinanoglu O, *Adv Chem & Phys (USA)*, **6** (1964) 315, **14** (1969) 237.
- 2 Brenig W, *Nucl Phys (Netherlands)*, **4** (1957) 363.
- 3 Kamel M A & Labzowsky L N, *Int J Quant Chem (USA)*, **9** (1975) 35.
- 4 Zaschekhen M N & Labzowsky L N, *Opt & Spektrosc (USSR)*, **29** (1970) 817.
- 5 Veselov M G, Antonova I M, Bratzev V F & Kerelove I V, *Opt & Spektrosc (USSR)*, **10** (1961) 693.
- 6 Clementi E, *J Chem Phys (USA)* **38** (1963) 2248.

Vibrational Spectrum of Isopropylammonium Dihydrogenoctamolybdate Dihydrate

V RAMAKRISHNAN, G ARULDHAS

Department of Physics, University of Kerala, Kariavattom,
Trivandrum 695 581

&

M KANAKAVEL

Analytical & Spectroscopic Division,
Vikram Sarabhai Space Centre, Trivandrum 695 022

Received 17 March 1986; revised received 8 July 1986

The IR and Raman spectra of $(C_3H_{10}N)_6H_2Mo_8O_{28} \cdot 2H_2O$ have been recorded and analyzed on the basis of vibrations due to $(C_3H_{10}N)^+$, MoO_6 and H_2O . Considerable changes in the frequencies of MoO_6 octahedra have been observed due to the distortions produced in the octamolybdate ion. The inactive ν_6 vibration of MoO_6 octahedra has appeared at 304 cm^{-1} in Raman.

A number of isopolymolybdates and tungstates have been identified and subjected to a series of investigations^{1,2}. X-ray studies of these compounds suggest the existence of shared (corner and edge) octahedral MoO_6 or WO_6 groups. Vibrational spectra of these compounds in the $400\text{--}4000\text{ cm}^{-1}$ region were studied and the characteristic vibrations of the octahedral MoO_6 or WO_6 groups identified^{3,4}. A vibrational analysis of dihydrogenoctamolybdate $(H_2Mo_8O_{28})^{6-}$ complex belonging to a new structural family of octamolybdate ion is reported in this note.

The powdered isopropyl ammonium dihydrogenoctamolybdate (6-) dihydrate (abbreviated as IAMD) was used for investigation. SPEX Ramalog 1401 double monochromator equipped with a spectra Physics model 165 Ar^+ laser was used to record the Raman spectrum in the Stokes region of the green line 5145 \AA . The IR spectrum of the sample in the $20\text{--}400$ and $400\text{--}4000\text{ cm}^{-1}$ regions was obtained using FIR 30 Polytec and PE 283 spectrophotometers.

IAMD crystallizes in the triclinic space group $P\bar{1}$ with one formula unit per unit cell². The unit cell contains $(H_2Mo_8O_{28})^{6-}$ complex anion, six $(C_3H_{10}N)^+$ cations and two water molecules. All the atoms occupy general positions. The $H_2Mo_8O_{28})^{6-}$ anion is composed of MoO_6 octahedra and built by means of shared corners and shared edges (no shared faces). The factor group analysis predicts $192 A_g$ and $189 A_u$ fundamentals at $K=0$.

From Raman and IR data of ordered Perovskite compounds of type A_2BMO_6 (MoO_6 retains its oc-

tahedral symmetry in these crystals), it has been inferred⁵ that the stretching and bending frequencies of MoO_6 octahedra occur in the regions $600\text{--}800\text{ cm}^{-1}$ and $300\text{--}450\text{ cm}^{-1}$ respectively. When the MoO_6 oc-

Table 1 – Spectral Data and Assignments

IR cm^{-1}	Raman cm^{-1}	Assignment
3420 br	3410 3385	O – H str. (water)
3140 br	3170	N – H str. (NH_3^+)
3040 br	3060	
2980 w	2970	asym. str. CH_3
2930 w	2920	sym. str. CH_3
2860 w	2858	sym. str. CH_2
1620 vs	1620	asym. bend. (NH_3^+)
1600 vs	1605	
1500 s	1509	– C – C – C – str.
1470 m	1465 1454	CH_3 bend
1395 s	1401	CH_2 bend
1380 s	1379	C – N str.
1350 m	1352	CH_2 wag
1210 m	1221	CH_3 – C – str.
1165 vs	1170	CH_3 rock
1015 m	1028 930	sym. bend (NH_3^+)
928 s	924	$\nu_1 MoO_6$
892 s	894	
860 s	857	$\nu_3 MoO_6$
800 w	804	
700 w	700	CH_2 rock
680 w	676	Water rock
640 vw	640	$\nu_2 MoO_6$
630 s	628	
565 m	576	$\nu_3 MoO_6$
538 w	546	
480 w	473	Water twist
460 w	469	C – CH_3 bend
443 m	449	Water wag
385 vw	397	$\nu_4 MoO_6$
368 m	372	
340 m	354 304	$\nu_6 MoO_6$
250 w	255	
220 w	220	
200 w		
175 m		
156 w		
	154	
134 w		
122 m	124	Lattice modes
114 w		
	104	
87 w	80	
78 w	76	
63 w	62	

tahedral ion loses its O_h symmetry by the sharing (edges and corners) of oxygen atoms, appreciable changes in the frequencies of its normal modes are expected to occur.

The very strong band at 924 cm^{-1} with a shoulder at 930 cm^{-1} is assigned to the totally symmetric stretching ν_1 mode of MoO_6 group. The splitting of this non-degenerate mode into two components is due to the vibrational interaction between MoO_6 groups. The corresponding IR absorption is observed as a strong band at 928 cm^{-1} . Such a high frequency for this mode is probably due to the distortions produced in the MoO_6 octahedra. The bands in the region $800\text{--}900\text{ cm}^{-1}$ are due to the anti-symmetric stretching frequencies of the shared octahedral MoO_6 groups. These bands are found to be less intense in IR. The observed splitting of about 90 cm^{-1} is generally expected for distorted MoO_6 octahedra.

The doubly degenerate ν_2 mode, the anti-symmetric (with respect to ternary C_3 axis of octahedron) stretching appeared as a doublet both in Raman (628 and 640 cm^{-1}) and in IR (630 and 640 cm^{-1}). The bands with medium intensity at 546 and 576 cm^{-1} (Raman) and 538 and 565 cm^{-1} (IR) are assigned to

the two split components of ν_5 mode. The anti-symmetric bending mode ν_4 which usually occurs in the $300\text{--}400\text{ cm}^{-1}$ region, is observed at 397 , 372 and 354 cm^{-1} in Raman and at 385 , 368 and 340 cm^{-1} in IR. Though ν_6 vibration is inactive under O_h symmetry, it is observed at 304 cm^{-1} in Raman.

The small shifting of OH stretching modes from the free state value indicates the existence of very weak hydrogen bonds in the crystal. The vibrations due to NH_3 , CH_3 , CH_2 , $-\text{C}-\text{C}-\text{C}-$, $\text{C}-\text{N}$, $\text{C}-\text{CH}_3$ groups and bending and librational motions of water are identified and the complete assignment is given in Table 1.

One of the authors (V R) is grateful to CSIR, New Delhi, for the award of a fellowship.

References

- 1 Lindqvist I, *Ark Kemi (Switzerland)*, **2** (1950) 325.
- 2 Isobe M, Marumo F, Yamase T & Ileawa T, *Acta Crystallogr Sect B (Denmark)*, **34** (1978) 2728.
- 3 Aveston J, Ancker E W & Johnson J S, *Inorg Chem (USA)*, **3** (1964) 735.
- 4 Ka Yunn Simon Ng & Erdogan Gulari, *Polyhedron (GB)*, **3** (1984) 1001.
- 5 Liegeois-Duyckaerts G & Tarte P, *Spectrochim Acta Sect A (GB)*, **30** (1984) 1771.

Rhombic Symmetry Crystalline Field & Ground State Wavefunctions of Vanadyl Ion Complexes

A YADAV, R S BANSAL & V P SETH

Department of Physics, M D University, Rohtak 124 001

Received 16 August 1985; revised received 21 July 1986

Using crystal field approach, a theoretical estimate of the ground state wavefunction of vanadyl ion doped in crystal has been made, using ESR data. Rhombic symmetry crystalline field was assumed for these ions.

Many attempts have been made by a number of workers to formulate a precise ground state wavefunction of vanadyl ion VO^{2+} . The chemistry of this ion has been reviewed by Selbin^{1,2}. The knowledge of ground state wavefunction of such a paramagnetic ion doped in a crystal is useful to study the ESR parameters g and A and to evaluate the dipolar hyperfine coupling constant P and the Fermi contact parameter K .

In an earlier work, Seth *et al.*³ have determined the ground state wavefunction of the vanadyl ion in crystalline field of ligands which is of octahedral symmetry with a tetragonal distortion. In the present work, the authors are interested to study the ground state wavefunction of vanadyl ion doped in crystals which give crystalline field of orthorhombic symmetry.

When the vanadyl ion is embedded in a crystal lattice, it is subjected to the crystalline field due to surrounding ligands. In general, one very short V—O bond preserves⁴ the identity of the VO^{2+} ion. In such vanadyl-doped crystals, the crystal field⁵ is of octahedral symmetry with tetragonal distortion and a small perturbation (orthorhombic field) lowering the symmetry for which the equivalent Hamiltonian operator can be written^{6,7} as:

$$H_{\text{CF}} = B_4(O_4^0 + 5O_4^4) + B_2^0O_2^0 + B_4^0O_4^0 + B_2^0O_2^0 \quad \dots (1)$$

where B_4 is the magnitude of the octahedral field, the second and third terms represent the tetragonal distortion of second and fourth degrees in the potential, respectively, and the last term is because of orthorhombic distortion. For d^1 configuration in octahedral symmetry, B_4 is a positive quantity⁶, B_2^0 and B_4^0 are negative^{3,8,9} for a compression along the z -axis which is applicable in the present case. When the site symmetry is tetragonal, the ground state is d_{xy} with slight admixture of the excited states $d_{x^2-y^2}$, d_{xz} and d_{yz} ; this mixing is due to spin-orbit coupling³; d_{xz} and d_{yz} states

are degenerate in the tetragonal crystal field. If the site symmetry is rhombic or lower, the degeneracy of d_{xz} and d_{yz} is removed and the ground state wavefunction can be written in the following form³:

$$|\pm\rangle = \pm C_1|\pm 2 \pm \frac{1}{2}\rangle \mp C_2|\mp 2, \pm \frac{1}{2}\rangle \pm C_3|\mp 1 \pm \frac{1}{2}\rangle \pm C_4|\pm 1 \mp \frac{1}{2}\rangle \quad \dots (2)$$

where the coefficients C_1 , C_2 , C_3 and C_4 give information about the admixture of these states. Here we have neglected the perturbation due to mixing of $d_{3z^2-r^2}$ state to the d_{xy} state. It is appropriate to relate C_1 , C_2 , C_3 and C_4 with the g factor. This is done by the method given in Ref. 3 and we obtain:

$$g_x = 4(C_1 + C_4)(C_2 - C_3) \quad \dots (3)$$

$$g_y = 4(C_1 - C_4)(C_2 - C_3) \quad \dots (4)$$

and

$$g_z = 2(3C_1^2 - C_2^2 - 2C_3^2) \quad \dots (5)$$

Further, the normalization of the eigenfunction $|\pm\rangle$ gives

$$C_1^2 + C_2^2 + C_3^2 + C_4^2 = 1 \quad \dots (6)$$

Using experimental value of g_x , g_y and g_z and solving Eqs (3) to (6) for C_1 , C_2 , C_3 and C_4 we get the ground state wavefunction of the system as given in Eq (2). The ground state wavefunctions thus obtained are used to get the hyperfine structure constant^{5,6} in the following form:

$$A_x = 2P[(\frac{2}{7} - K)C_1C_2 + (K + \frac{1}{7})C_3C_4 + \frac{3}{7}C_4^2 - \frac{11}{7}C_1C_3 + \frac{17}{7}C_2C_4] \quad \dots (7)$$

$$A_y = [(\frac{2}{7} - K)C_1C_2 - (K + \frac{1}{7})C_3C_4 + \frac{3}{7}C_4^2 - \frac{11}{7}C_1C_3 - \frac{17}{7}C_2C_4] \quad \dots (8)$$

and

$$A_z = 2P[-\frac{1}{2}K(C_1^2 + C_2^2 - C_3^2 - C_4^2) + \frac{7}{1}(12C_1^2 - 16C_2^2 - 8C_3^2 + 6C_4^2 - 6C_2C_3)] \quad \dots (9)$$

From Eqs (3) and (4) we find $g_x - g_y = 8C_4(C_2 - C_3)$ and if the ground state is mainly d_{xy} state as determined by Seth *et al.*³ for tetragonal site symmetry, then C_1 and C_2 should be of the order of 0.7 and $C_3 \ll C_1$ and $C_4 \ll C_1$. In that case $g_x - g_y \approx 8C_2C_4$. In-plane anisotropy for A value can also written from Eqs (7) and (8) in the following form:

Table 1 — Calculated Values of C_1, C_2, C_3, C_4, P, K & A_y , for Vanadyl-doped $K_2Mg(SO_4) \cdot 6H_2O$ Single Crystal

[Value of C_5 is used as an input.]

C_5	C_1	C_2	C_3	C_4	P 10^{-4} cm^{-1}	K	A_y
0.0000	0.7009	0.7138	0.0004	0.0014	118.70	0.85	68.15
0.1000	0.6973	0.7096	0.0006	0.0014	120.26	0.85	68.17
0.2000	0.6865	0.6996	0.0000	0.0014	123.22	0.84	68.20

$$A_x - A_y = 4P[(K + \frac{1}{7})C_3 C_4 + \frac{17}{7}C_2 C_4]$$

or

$$A_x - A_y \approx \frac{68}{7} PC_2 C_4 \quad \dots (10)$$

Using $P = 120 \times 10^{-4} \text{ cm}^{-1}$ we find $A_x - A_y \approx 1166 C_2 C_4 \times 10^{-4} \text{ cm}^{-1}$. This suggests that if the in-plane anisotropy in the value of g is Δ and if the in-plane anisotropy in the value of A is approximately $150\Delta \times 10^{-4} \text{ cm}^{-1}$, then the ground wavefunction of the system is d_{xy} with a slight admixture of $d_{x^2-y^2}$, d_{xz} and d_{yz} . As an example, we consider vanadyl ion in triglycine sulphate (TGS) for which the experimental values^{10,11} are $g_x = 1.9852$, $g_y = 1.9982$, $g_z = 1.9288$, $A_x = 73.33 \times 10^{-4} \text{ cm}^{-1}$, $A_y = 71.76 \times 10^{-4} \text{ cm}^{-1}$ and $A_z = 178.17 \times 10^{-4} \text{ cm}^{-1}$. Using these values of splitting parameter and solving Eqs (3)-(6), we find $C_1 = 0.7008$, $C_2 = 0.7134$, $C_3 = 0.0029$ and $C_4 = -0.0023$. These values of C 's in Eqs (7) and (9) give $|P| = 114.23 \times 10^{-4} \text{ cm}^{-1}$ and $K = 0.91$.

These values of C_1, C_2, C_3, C_4, P and K are substituted in Eq (8) to get $A_y = 71.52 \times 10^{-4} \text{ cm}^{-1}$, which is equal to the experimentally determined value within the limits of error. Thus it appears that in TGS crystal, the ground state wavefunction of vanadyl ion is d_{xy} with a slight admixture of $d_{x^2-y^2}$, d_{xz} and d_{yz} .

In systems where the in-plane anisotropy in the value of A is much larger than $150\Delta \times 10^{-4} \text{ cm}^{-1}$ we have tried to define the ground state as d_{xy} with small mixing of $d_{x^2-y^2}$, d_{xz} , d_{yz} and $d_{3z^2-r^2}$. In these systems, the ground state may be defined as:

$$|\pm\rangle = C_1|\pm 2 \pm \frac{1}{2}\rangle \mp C_2|\mp 2, \pm \frac{1}{2}\rangle \pm C_3|\mp 1 \mp \frac{1}{2}\rangle \pm C_4|\pm 1 \mp \frac{1}{2}\rangle + C_3|0 \pm \frac{1}{2}\rangle \quad \dots (11)$$

In this case, we have also found expressions for g_x, g_y, g_z, A_x, A_y , and A_z , which have been used to determine the ground state wavefunction of vanadyl ion doped in $K_2Mg(SO_4) \cdot 6H_2O$ (Ref. 12): $g_x = 2.005$, $g_y = 1.997$, $g_z = 1.930$, $A_x = 67 \times 10^{-4} \text{ cm}^{-1}$, $A_y = 77 \times 10^{-4} \text{ cm}^{-1}$ and $A_z = 178 \times 10^{-4} \text{ cm}^{-1}$. Because there are five unknown quantities in this case, we

have solved the equations for C_1, C_2, C_3 and C_4 after putting $C_5 = 0.0, 0.1$ and 0.2 . Values obtained for C_1, C_2, C_3 and C_4 along with experimental values A_x and A_z are used to evaluate P and K and then the theoretical value of A_y is calculated. The values of C_1, C_2, C_3, C_4, P, K and A_y as determined in the three cases are given in Table 1, which shows that small mixing of $d_{3z^2-r^2}$ state does not give large in-plane anisotropy in A .

We can conclude from the present study that if the in-plane anisotropy in g is Δ and the corresponding in-plane anisotropy in A is approximately $150\Delta \times 10^{-4} \text{ cm}^{-1}$, then in our coordinate system d_{xy} with a slight admixture of excited states $d_{x^2-y^2}$, d_{xz} and d_{yz} is the ground state of vanadyl ion in the orthorhombic crystalline field. In such systems, the in-plane anisotropy is caused primarily by mixing of d_{xz} and d_{yz} rather than $d_{3z^2-r^2}$.

The authors are thankful to Prof. N M Atherton, the University of Sheffield for carefully reading through the manuscript. This work was financially supported by the CSIR, New Delhi.

References

- Selbin J, *Chem Rev (USA)*, **65** (1965) 153.
- Selbin J, *Coord Chem Rev (USA)*, **1** (1966) 293.
- Seth V P, Yadav S K & Jain V K, *Pramana (India)*, **21** (1983) 65.
- Kohin R P, *Magn Reson Rev (USA)*, **5** (1979) 75.
- Mc Garvey B R, in *Transition metal chemistry*, Vol 3, edited by R L Carlin (Marcel Dekker, New York) 1966, 115, 150.
- Abraham A & Bleaney B, *Electron paramagnetic resonance of transition ions* (Clarendon Press, Oxford) 1970, p 372-74, 787.
- Roitsin A B, *Phys Status Solidi B (Germany)*, **104** (1981) 11.
- Wertz J E & Bolton J R, *Electron spin resonance: Elementary theory and practical applications* (McGraw Hill, New York) 1972, 357.
- Poole C P (Jr) & Farach H A, *The theory of magnetic resonance*, (Wiley Interscience, New York) 1972, p 357.
- Hartmann E & Windsch W, *Phys Status Solidi a (Germany)*, **13** (1972) 119.
- Fujimoto M & Dressel L A, *Ferroelectrics (GB)*, **8** (1974) 611.
- Kasthurirengan S & Soundararajan S, *J Magn Resonance (USA)*, **19** (1975) 357.

ESR Studies on Some Copper(II) Complexes of Pyrazole

B A SASTRY, B BALAIAH, K V G REDDY & B MADHU
Solid State & Molecular Physics Laboratory, Department of
Physics, Osmania University, Hyderabad 500 007 India
and

G PONTICELLI, M MASSACESSI & G PUGGIONI
Institute of General, Inorganic & Analytical Chemistry, Uni-
versity of Cagliari, 09100, Cagliari, Italy

Received 29 October 1985; revised received 25 April 1986

ESR studies have been carried out on $\text{Cu}(\text{pyrazole})_2\text{Cl}_2$, $\text{Cu}(\text{pyrazole})_4\text{Br}_2$ and $\text{Cu}(\text{pyrazole})_4(\text{ClO}_4)_2$ in polycrystalline and solution forms. Solvation is found to be more in DMF ($\text{N,N}'$ -dimethylformamide) solution of bis-adduct compared to tetrakis-adducts. Strong solute-solvent interaction is noticed in the pyridine solutions of all the complexes. The equatorial and axial bond strengths are also calculated.

Reedijk *et al.*¹ synthesized and characterized a number of pyrazole copper(II) complexes by IR and ESR techniques to elucidate the coordination behaviour of these complexes. Since these studies were confined to ESR observations at X-band microwave frequencies in polycrystalline samples they gave only limited information about the coordination behaviour of pyrazole. The present authors have extended the ESR studies on polycrystalline samples of $\text{Cu}(\text{pyrazole})_2\text{Cl}_2$ (complex-I), $\text{Cu}(\text{pyrazole})_4\text{Br}_2$ (complex-II) and $\text{Cu}(\text{pyrazole})_4(\text{ClO}_4)_2$ (complex-III) to Q-band and in solutions of DMF ($\text{N,N}'$ -dimethylformamide) and pyridine at X-band microwave frequencies. The coordination behaviour of pyrazole and solute-solvent interactions are studied. From the earlier studies¹ it is found that all the above complexes possess distorted octahedral symmetries. In the case of complex-I it is found that chlorine acts as a bridging ligand occupying the four coordinate positions of the equatorial plane, whereas in the other two complexes these are occupied by four nitrogens, one each contributed by one pyrazole molecule.

Experimental procedure—The compounds under consideration were prepared according to the procedure given elsewhere¹. The ESR spectra in polycrystalline and solution forms were recorded by Varian E-4 X-band and E-112 Q-band spectrometers whose details were given elsewhere^{2,3}. The maximum errors in g and A are about ± 0.002 and ± 2 G respectively.

Results and discussion—The Q-band ESR spectra of complexes I and II in polycrystalline form are shown in Fig. 1. Complex I has yielded three g values ($g_1 = 2.272$, $g_2 = 2.093$ and $g_3 = 2.038$) and complex II

indicated two g values ($g_{\parallel} = 2.296$, $A_{\parallel} = 167$ G and $g_{\perp} = 2.058$). The G values $[(g_1 - 2)/\{ \frac{1}{2}(g_2 + g_3) - 2 \}]$ or $(g_{\parallel} - 2)/(g_{\perp} - 2)$ for the above two complexes respectively come out to be 4.2 and 5.0 which indicate that the molecules in the unit cell of these complexes are magnetically equivalent and that these g values are near to the molecular g values⁴⁻⁶. They also indicate that in both the complexes the ground state is dominated by the $d_{x^2-y^2}$ orbital. In the case of complex I, the rhombic nature of g values indicates mixing of the d_{z^2} orbital with that of the ground state $d_{x^2-y^2}$. The g and A values of these complexes are comparable with the corresponding values of other pyrazole complexes¹.

ESR spectra of these complexes in DMF at 300 K are broad single lines and partially resolved hyperfine lines are observed in pyridine solutions. ESR spectra

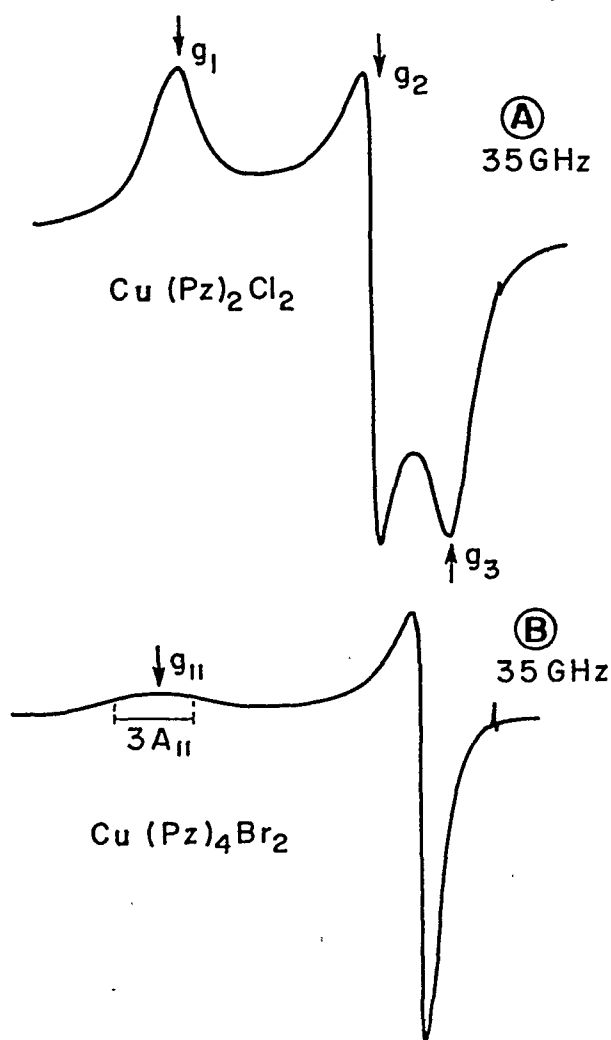


Fig. 1 - ESR spectra of polycrystalline samples of (A) $\text{Cu}(\text{Pz})_2\text{Cl}_2$; and (B) $\text{Cu}(\text{Pz})_4\text{Br}_2$ at 300 K.

of these complexes in frozen DMF and pyridine solutions are shown in Fig. 2. Spin-Hamiltonian constants obtained from these spectra by usual methods² are given in Table 1 along with the corresponding values obtained in some bis- and tetrakis-adducts of oxazole

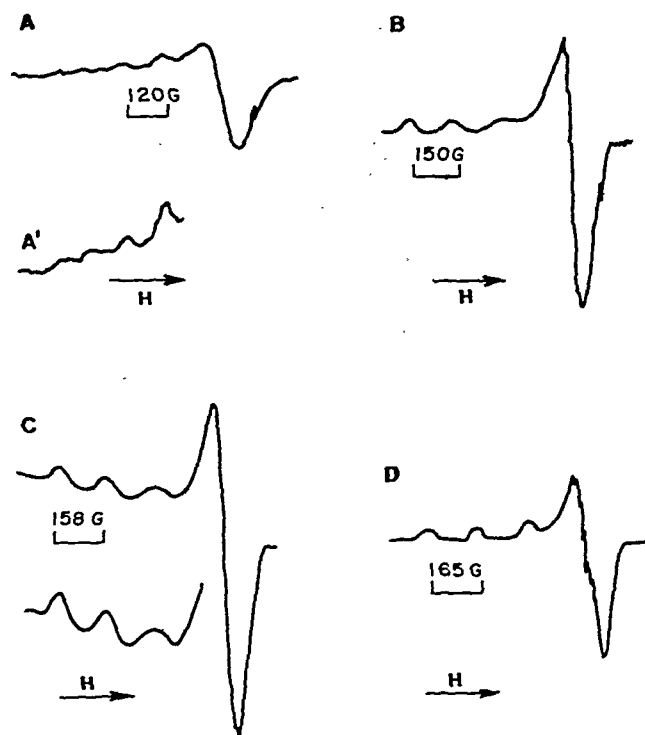


Fig. 2 — ESR spectra of pyrazole complexes in frozen solutions [(A) $\text{Cu}(\text{Pz})_2\text{Cl}_2$ in DMF; (A') parallel features of (A) are magnified; (B) $\text{Cu}(\text{Pz})_4\text{Br}_2$ in DMF; (C) $\text{Cu}(\text{Pz})_4(\text{ClO}_4)_2$ in DMF; and (D) $\text{Cu}(\text{Pz})_4(\text{ClO}_4)_2$ in pyridine]

and isoxazole derivatives for the purpose of comparison. The g values of complex I in DMF solution are very much different from the corresponding values in its polycrystalline form indicating that the solute-solvent interaction is strong in DMF solution. The high g_{\parallel} and low A_{\parallel} values in DMF solution also indicate oxygen coordination which is most probably arising from the attachment of DMF molecules to copper(II) ion in all its coordinate positions⁷. From the small deviation of g values of the species in frozen DMF solution of complex III from its values in polycrystalline form it is likely that all the coordinate positions may not be occupied by solvent molecules. In the case of complex II, the g and A values of polycrystalline sample are near to the corresponding values in DMF solution indicating weak solute-solvent interaction which is unusual for complexes formed with heterocyclic ligands^{3,9,10}. From these studies it appears that solute-solvent interaction of bis-adducts of pyrazole complexes is more than that of the tetrakis-adducts. The g and A values of all the three complexes in frozen pyridine solutions are almost equal indicating strong solute-solvent interaction in all the cases. The ligand hyperfine structure on the perpendicular features of these spectra and the low g and high A values (Table 1) indicate nitrogen coordination which is most probably brought out by the attachment of pyridine molecules to the copper(II) ions of these complexes.

In the frozen solutions of complexes II and III, an increase in line-width of the signals in the parallel features is observed (Fig. 2), as one moves from the line

Table 1 — Spin-Hamiltonian Constants Obtained in Some Copper(II) Complexes of Pyrazole & Derivatives of Oxazole & Isoxazole

Compound**	Solid/Solvent	g	A (G)	g	g _⊥	A	A _⊥	A ^N	Ref.
						(G)			
Cu(Pz) ₂ Cl ₂	DMF†	2.168	68	2.349	2.077	120	40	15	Present study
	Pridine	2.131	75	2.259	2.060	165	38		
Cu(Pz) ₄ Br ₂	DMF	2.138	57	2.295	2.069	150	33	15	Present study
	Pyridine	2.140	75	2.256	2.061	160	36		
Cu(Pz) ₄ (ClO ₄) ₂	Solid			2.250	2.050	175			1
	DMF	2.165	57	2.307	2.090	158	25	15	Present study
	Pyridine	2.123	70	2.251	2.060	165	38		
Cu(BO) ₂ Cl ₂	Solid*			2.243(g _r)	2.056(g _r)				
					2.0309(g _r)				
	DMF Species 1	2.133	50.	2.379	2.07	115	16		3
Cu(PPO) ₂ (ClO ₄) ₂ 4H ₂ O	Species 2			2.333		120			
	Solid*			2.336(g _r)	2.217(g _r)	137(A _r)	94(A _r)		8
					2.098(g _r)	60(A _r)			
	DMF	2.191	50	2.389	2.092	120	15		7
Cu(DMI) ₃ (ClO ₄) ₂	DMF	2.196	44	2.407	2.091	122	5		10
Cu(MPI) ₃ (ClO ₄) ₂	DMF	2.194	46	2.404	2.09	120	7		10

† Average spin-Hamiltonian constants

* Q-band spectrum at 300 K; ** BO = Benzoxazole, PPO = 2,5-diphenyloxazole, DMI = 3,5-dimethylisoxazole, MPI = 3-methyl,5-phenylisoxazole

$m_1 = -3/2$ to $+3/2$ due to the spread of g_{\parallel} and A_{\parallel} values arising from strains while freezing¹¹. In contrast to this observation, the line-widths in the case of complex I are found to decrease as one moves from $m_1 = -3/2$ to $+3/2$ (Fig. 1A) which is attributed to the superposition of the spectra coming from at least two types of copper(II) species. The g and A values (g_{\parallel} , g_{\perp} , A_{\parallel} , A_{\perp}) and the shape of the frozen solution spectra (perpendicular feature is more intense than parallel feature) in DMF and pyridine in all the complexes indicate that the ground state of copper(II) is $d_{x^2-y^2}$. Using the standard procedures described earlier², the in-plane σ -bond parameter (α^2) and the fraction of $3d$ orbital in $3d-4s$ ground state (f^2) which is a measure of axial bond strength, are calculated. These values of α^2 and f^2 in the case of frozen DMF solutions of complexes I, II and III come out to be (0.68, 1.00), (0.80, 0.973) and (0.86, 0.973) respectively. The corresponding values in pyridine solutions come out to be (0.76, 0.997), (0.72, 1.00) and (0.78, 0.961). From these values it is evident that species in DMF and pyridine solutions of $\text{Cu}(\text{Pz})_2\text{Cl}_2$ and pyridine solution of $\text{Cu}(\text{Pz})_4\text{Br}_2$ have strong equatorial bonds and weak axial bonds, whereas the species existing in the DMF

and pyridine solutions of $\text{Cu}(\text{Pz})_4(\text{ClO}_4)_2$ and DMF solution of $\text{Cu}(\text{Pz})_4\text{Br}_2$ have weak equatorial and strong axial bonds.

References

- 1 Reedijk J, Windhorst J C A, Van Ham N H M & Groeneveld W L, *Recueil (France)*, **111** (1971) 234.
- 2 Sastry B A, Asadullah S Md, Ponticelli G & Massaccesi M, *J Chem Phys, (USA)*, **70** (1979) 2834.
- 3 Chary K V R, Reddy K V G, Sastry B A, *et al.*, *Indian J Pure & Appl Phys*, **21** (1983) 698.
- 4 Porcter I M, Hathaway B J & Nichols P, *J Chem Soc A (GB)*, (1968) 1678.
- 5 Tomlinson A A G & Hathaway B J, *J Chem Soc A (GB)*, (1968) 1685.
- 6 Beu M J, Hathaway B J & Fereday R J, *J Chem Soc A (GB)*, (1972) 1229.
- 7 Sastry B A, Asadulla S Md, Ponticelli G & Pinna R, *Chem Phys Lett (Netherlands)*, **73** (1980) 118.
- 8 Sastry B A, Asadulla S Md, Balaiah *et al.*, *Indian J Pure & Appl Phys*, **20** (1982) 395.
- 9 Sastry B A, Asadullah S Md, Reddy K V G *et al.*, *J Mol Struct (Netherlands)*, **55** (1979) 143.
- 10 Ponticelli G, Pelizzi G, Sastry B A *et al.*, *Indian J Pure & Appl Phys*, **18** (1980) 212.
- 11 Francis W & Hyde J S, *J Chem Phys (USA)*, **73** (1980) 3123.

Towards a Thermal Conductivity Minimum—Thermoelectric Applications

C M BHANDARI

Department of Physics, University of Allahabad,
Allahabad 211002

and

D M ROWE

Department of Physics, Electronics & Electrical
Engineering, UWIST, Cardiff CF1 3XE, UK

Received 25 October 1985

The concept of a thermal conductivity minimum finds an important application in thermoelectric optimization programmes. The search for improved thermoelectric materials is in part directed towards decreasing lattice thermal conductivity without significantly degrading the electrical properties of materials. The case of lead telluride-based material is discussed in this context and a comparison is made between the calculated minimum thermal conductivity and its measured value at the melting point corrected to include the effect of grain-boundary scattering.

The concept of a thermal conductivity minimum was first discussed by Roufosse and Klemens¹. Slack² later on elaborated the theoretical framework and obtained compact expressions for the minimum thermal conductivity (λ_{\min}) and sought a comparison between the calculated minimum and the measured thermal conductivity (λ_m) at the melting point. A maximum scattering of phonons in terms of an optimized phonon-phonon scattering justifies this procedure as a first step in obtaining a meaningful comparison. A somewhat better approach would be to take into account the phonon scattering by alloy disorder and by grain boundaries, apart from the usual phonon-phonon scattering.

The usefulness of accomplishing lower values of thermal conductivity has significance in thermoelectric applications^{3,4}. Good thermoelectric materials possess a relatively high value of the electrical to-thermal conductivity ratio (σ/λ). The efforts to optimize the thermoelectric figure-of-merit ($Z = \alpha^2 \sigma/\lambda$, where α is the Seebeck coefficient) have in part been directed towards maximizing this ratio (σ/λ).

The present note reports an attempt to obtain a high value of Z for lead telluride and the materials based on it. These materials are amongst the best known thermoelectric materials for terrestrial applications in the temperature range 600-900 K.

Mixed Crystals and Sintered Materials

Use of mixed crystals is prompted by the consideration that alloy disorder considerably reduces the

thermal conductivity (λ) whereas the electrical conductivity (σ) changes only slightly^{4,5}. A large mass-difference between the constituent atoms such as in silicon-germanium alloys gives rise to an order of magnitude reduction in thermal conductivity.

Following the suggestion by Goldsmid and Penn⁶, the grain-boundary scattering was shown to have a significant effect on the thermal conductivity even at high temperatures. In fine-grained materials, low frequency phonons can be effectively scattered in the presence of an alloy disorder which scatters high frequency phonons (ω^4 dependence of the corresponding scattering rate). The electronic mean free-path is not appreciably affected and this leads to an increase of the ratio σ/λ . This concept leads to the possibility of obtaining higher values⁷⁻⁹ of Z . However, this will not be possible beyond a limiting value of the grain-size below which electrons are also effectively scattered. This limit can be set around a grain size of about $1 \mu\text{m}$; any further reduction in the grain-size would have an adverse effect on the ratio σ/λ .

Theoretical Framework

Minimum thermal conductivity—Slack² has described the calculation of thermal conductivity minima for various types of crystals. For crystals with more than one atom per unit cell, optic phonon modes are also included in the thermal conductivity calculation. The total minimum thermal conductivity at the melting point is written as

$$\lambda_{\min, \infty} = \lambda_{\min, \infty}^{\text{ac}} + \lambda_{\min, \infty}^{\text{op}} \quad \dots (1)$$

where

$$\lambda_{\min}^{\text{ac}} = 3 k_B V^2 / 2 \delta^3 \nu_A \quad \dots (2)$$

where ν is the acoustic phonon velocity, δ the cube root of atomic volume and ν_A the highest acoustic mode frequency.

Further, the optic phonon contribution is

$$\lambda_{\min, \infty}^{\text{op}} = \frac{k_B}{n \delta} \sum_{i=1}^{n-1} \nu_{\text{oi}} \quad \dots (3)$$

where ν_{oi} is the optic mode frequency and n is the number of atoms per primitive cell.

Reduction in thermal conductivity for thermoelectric applications—For a sintered semiconductor alloy, the thermal conductivity variation with alloying and sintering is given by^{8,9}

$$\frac{\lambda_l}{\lambda_0} = (1 + 5k_0/9)^{-1} \times \left[L_2(A_1 C) + \frac{k_0 L_d^2}{(1 + k_0) A L_8 + L_6 + (1 + k_0) V_s L_4} \right] \quad \dots (4)$$

where

$$L_n(A, C) = \int_0^1 \frac{x^n dx}{A x^4 + x^2 + C} \quad \dots (5)$$

parameters A and C describe the measure of alloy-disorder and doping, and are defined by

$$C = \frac{2\pi^* \lambda_0 v_s^2}{k_B \omega_D^3 L(1 + 5k_0/9)} \quad \dots (6)$$

and

$$A = \frac{\pi \lambda_0 \Gamma \Omega_0 \omega_D}{2 v_s^2 k_B (1 + 5k_0/9)} \quad \dots (7)$$

In Eq. (7), λ_0 is the thermal conductivity of the perfect (notional) large single crystal where only three-phonon scatterings are present, k_B the Boltzmann constant, ω_D the Debye frequency, V_s the average phonon velocity, L the average grain size, Ω_0 the volume per atom, Γ the disorder parameter and k_0 the ratio of phonon relaxation times corresponding to three-phonon umklapp and normal processes, assuming a similar frequency dependence for both the processes^{8,9}.

Lead Telluride-based Material

Hence it is possible to obtain a semiquantitative estimate of the minimum thermal conductivity relevant for thermoelectric applications. Following the procedure outlined earlier¹⁰, we have calculated¹¹ the reduction in the lattice thermal conductivity due to grain boundary scattering in the alloy systems PbSnTe and PbGeTe at 300 K. Table 1 gives the estimated reductions for undoped and optimally doped PbSnTe and PbGeTe respectively. Optimal doping refers to the doping level which corresponds to a maximum in Z versus Fermi energy curves.

According to Slack², the calculated minimum thermal conductivity of PbTe is $3.28 \times 10^{-3} \text{ Wcm}^{-1}\text{deg}^{-1}$ (see Table XVII of Ref. 2). The measured value¹² of λ at the melting point is $4.8 \times 10^{-3} \text{ Wcm}^{-1}\text{deg}^{-1}$. A further estimated reduction of about 30 percent for $0.1 \mu\text{m}$ grain-size material would bring the thermal conductivity down to $3.4 \times 10^{-3} \text{ Wcm}^{-1}\text{deg}^{-1}$. The calculated minimum value is quite close to the expected observed minimum for a heavily disordered material at the melting point.

No further reductions in thermal conductivity are therefore expected for temperatures approaching the

Table 1—The Ratio $\lambda/\lambda_{\text{single}}$ for PbSnTe and PbGeTe with Decrease in Grain Size

$L(\mu\text{m})$	$\lambda/\lambda_{\text{single}}$	
	Undoped	Optimally doped*
PbSnTe		
10	0.96	0.98
1.0	0.90	0.92
0.2	0.79	0.83
0.1	0.72	0.75
PbGeTe		
10	0.96	0.98
1.0	0.87	0.90
0.2	0.74	0.78
0.1	0.67	0.71

*Refers to the doping level which corresponds to maxima in Z versus Fermi-energy plots.

melting point. However, at room temperature where phonon-phonon scattering has not attained its maximum effectiveness, grain-boundary scattering of phonons supported by alloy-disorder scattering could lead to reduction in λ with a decrease in the grain-size. The fact that any further reduction in grain size is undesirable for thermoelectric applications, has been emphasized in Ref. 4.

These estimates are at best semiquantitative although the agreement between the calculated and the observed values can in some cases be excellent. In the present context, we have discussed the case of either undoped or moderately doped materials in calculating the effect of grain-size. However, at the optimum doping, the contribution of electrons to the total scattering cross-section of phonons is significant and should also be taken into account. This aspect of the problem is currently being investigated.

References

- 1 Roufosse M & Klemens P G, *J Geophys Res(USA)*, **79** (1974) 703.
- 2 Slack G A, *Solid State Phys(USA)*, **34** (1979) 1.
- 3 Rosi F D, *Solid State Electron(GB)*, **11** (1968) 833.
- 4 Rowe D M & Bhandari C M, *Modern thermoelectrics* (Holt-Saunders Ltd, London) 1983.
- 5 Drabble J R & Goldsmid H J, *Thermal conduction in semiconductors* (Pergamon Press, Oxford), 1961.
- 6 Goldsmid H J & Penn A W, *Phys Lett A (Netherlands)*, **27** (1968) 523.
- 7 Parrott J E, *J Phys(GB)*, **2** (1969) 147.
- 8 Bhandari C M & Rowe D M, *Contemp Phys(GB)*, **21** (1980) 219.
- 9 Meddins H R & Parrott J E, *J Phys C(GB)*, **9** (1976) 1263.
- 10 Bhandari C M & Rowe D M, *J Phys D(GB)*, **16** (1983) L75.
- 11 Rowe D M & Bhandari C M, *Appl Phys Lett B(USA)*, **47** (1985) 255.
- 12 Devyatkov E D & Smirnov I A, *Sov Phys - Solid State(USA)*, **3** (1962) 1666.

SCOPE

The journal welcomes, for publication, full papers and short notes, reporting significant new results of research, in all areas of physics except space physics. The applied fields covered are electronics, electrical engineering, instrumentation and applied mathematics. However, papers in applied mathematics with emphasis on only derivation and proofs and having no direct physical significance, will not be considered. Review articles are not published normally.

SUBMISSION OF MANUSCRIPT

Manuscripts for consideration should be submitted, *in duplicate*, to Editor, Indian Journal of Pure & Applied Physics, Publications & Information Directorate, Hillside Road, New Delhi 110012. They should neither have been already published nor be under consideration elsewhere.

Manuscripts should be in English and typewritten on only one side of good quality paper, in double space, with adequate margin on all four sides. One original and one carbon or photo-copy, each complete in all respects including abstract, illustrations, appendixes, etc. are to be submitted.

PREPARATION OF MANUSCRIPT

Authors may consult recent issues of the Journal to familiarize themselves with the general style and practices adopted in regard to the various elements of a paper.

General

Manuscript should be presented in as concise a form as possible. Good attention should be given to spelling and grammar. In giving names of chemical compounds and structures, abbreviations of units of measurements, symbols and notations, the style and practices recommended by the IUPAP and IUPAC, should be followed.

Frequently repeating combinations of words, e.g. electric field gradient (EFG), junction field effect transistor (JFET), stimulated Raman emission (SRE), should be abbreviated subsequently, indicating the abbreviated form in parenthesis, as shown, at the place of their first occurrence.

Pages should be numbered consecutively and arranged in the following order: Title, authors' names with their institutional affiliations and abstract, along with relevant footnotes whenever necessary (on a separate sheet); introduction; experimental details/theory/method/analysis; results; discussion; conclusion(s); acknowledgement; references and appendixes. Tables, captions for figures (with legends) and appendixes should be typed *on separate sheets* and attached at the end of the manuscript.

Title

The title should be neither too brief/general nor unnecessarily long. It should reflect the content of the paper so as to derive the maximum advantage in indexing. If a paper forms part of a general series, a specific subtitle, indicating the particular aspect of the work covered in the paper, should be provided.

A short running title for the paper, the broad PACS subject heading under which it should be classified in the contents page (authors may consult the January or July issue of the journal for this purpose), and the author's name and address for correspondence, should also be provided on the title page.

Abstract

The abstract, usually not exceeding 200 words, should indicate the scope and significant content of the paper,

highlighting the principal findings and conclusions. It should be in such a form that abstracting periodicals can use it without modification.

Introduction

Long and elaborate introduction should be avoided. It should be brief and state the exact scope of the study in relation to the present status of knowledge in the field. Literature review should be limited strictly to what is necessary to indicate the essential background and the justification for undertaking the study.

Materials, methods, apparatus, etc.

The sources of materials and their purity, methods of preparation, procedure for measurements and their accuracies, etc. should be clearly stated to enable any other worker to repeat the work if necessary. New methods, techniques, theories, etc. should be described in adequate detail; but if they are well known, a mere literature reference to them will do; differences from standard ones, improvements or innovations should, however, be clearly mentioned.

Results

Only such primary data as are essential for understanding the discussion and main conclusions emerging from the study should be included. All secondary data as are of interest to a specific category of readership *should not be included* in the paper. Such data should be retained by the authors for supply, on request, to any interested research worker. A footnote to this effect may be inserted at the relevant place in the paper.

The results must be presented in a coherent sequence in a unified logical structure, avoiding repetition or confusion. Limitations of the results should be clearly stated.

The same data should not be presented in both tabular and graphic forms. Only such tables and figures as are essential should be included. Simple linear plots that can easily be discussed in the text, should not be included. Infrared, ultraviolet, NMR and other spectra, DTA curves, etc. should be included only if they pertain to new compounds and/or are essential to the discussion; otherwise only significant numerical data should be given in the text or in a table.

Discussion

Long rambling discussion should be avoided. The discussion should deal with the interpretation of results without repeating information already presented under results. It should relate new findings to the known and include logical deductions. A separate section on 'conclusions' can be given only when they are well established and of outstanding significance. Mere observation of qualitative trends of results should be distinguished from firm conclusions. Also, limitations, if any, to the conclusions should be clearly pointed out.

Mathematical portions

Special attention should be given to the mathematical portions of the paper. Equations must be well separated from the text and written clearly with good separation between the successive lines. The usual norms of breaking long mathematical expressions should be adhered to. Equations should be numbered consecutively in Arabic numerals with the number in parenthesis near the right hand margin. Superscripts and subscripts should be clearly indicated in pencil by V and \wedge sign respectively. Capital and small letters,

particularly of the same letter when both occur, as well as letters or symbols likely to be confused one for the other, should be clearly distinguished. Special characters (e.g. Greek, script, vector, tensor, etc.) required must be indicated by marginal notes. Letters and symbols which should appear in bold face must be clearly indicated. To simplify typesetting: (i) long and complicated mathematical expressions which are frequently repeated should be replaced with single letter/symbol, without clashing with the others used in the paper; (ii) the "exp" form of complex exponential functions should be used; and (iii) to simplify fractions, the solidus (/) is to be used and fractional exponents are to be used instead of root signs, e.g.

write $\exp\{-i\omega_0(t_1 - t_2)/2\}$ and not $e^{-i\omega_0(t_1 - t_2)/2}$

write $(4\omega_{pf} K_{3\lambda}^2 / \tilde{\omega} K_D^2)^{1/2}$ and not $\sqrt{\frac{4\omega_{pf} K_{3\lambda}^2}{\tilde{\omega} K_D^2}}$

Tables

Tables should be numbered consecutively in Arabic numerals and should bear brief titles. Column headings should be brief. Units of measurement should be abbreviated and placed below the headings. Nil results should be indicated and distinguished clearly from absence of data. Inclusion of structural formulae inside the tables should be avoided as far as possible. Tables should be referred to in the text by numbers and not by terms like 'above', 'below', 'preceding' or 'following'. Results should not be presented to a greater accuracy than that of the method employed.

Illustrations

The number of illustrations should be kept to the minimum. Wherever possible, e.g. a number of individual analogous figures referring to different variables, substances, molecules, etc. may be combined into one composite figure. All illustrations should be numbered consecutively in Arabic numerals. Captions and legends to the figures should be self-explanatory. Line drawings should be made with Indian ink on white drawing paper/cellophane sheet/tracing cloth, and drawn to approximately twice the printed size.

The lettering should be uniform, preferably in stencil, so as to be not less than 1.5 mm after reduction widthwise to full page size (165 mm) or column size (80 mm). The size of geometrical shapes (used to distinguish different graphs), dots, lines, etc. should be sufficiently large to permit the necessary reduction without loss of detail. In the case of photographs, prints must be on glossy paper and contrasty. If an illustration is taken from another publication, reference to the source should be given and prior permission secured. Illustrations should be referred to in the text by numbers and not by terms like 'above', 'following' etc.

Acknowledgement

Acknowledgements should not be exuberant and must be made only to real assistance rendered in connection with the work reported in the paper.

References

References cited should be limited to the absolute minimum (particularly in the case of short notes) based on their essential relevance. In the text, references to literature should be numbered consecutively, in the order of their first occurrence, and should be indicated by superscript Arabic numbers at the relevant places; as far as possible the placement of references on numerals or other symbols should be avoided; in such cases the reference may be given in parenthesis in running text, e.g. "this yielded for n a value of 2.3 (Ref. 5)". Full bibliographic details for all the references mentioned in the text should be listed in serial order at the end of the paper.

In citing references to research papers, names and initials of authors should be followed, in order, by the title of the periodical in the abbreviated form (underlined), the volume number (two lines underneath), the year within circular brackets and the page number [e.g. Chandra B P & Shrivastava KK, *J Phys & Chem Solids (GB)*, 39 (1978) 939]. For names of periodicals, the abbreviations followed by the *Physics Abstracts* should be used. For periodicals not covered by *Physics Abstracts*, the title abbreviations should be according to the *Bibliographic Guide for Editors and Authors*, 1974, published by the American Chemical Society, Washington DC, USA; additionally the country from which the journal is published should be given in parenthesis immediately after the title abbreviation. If a paper has been accepted for publication, the names of the authors and the journal (with volume number and year, if known) should be given followed by the words "in press" [e.g. Wahi P K & Patel N D, *Can J Spectrosc (Canada)*, in press.].

In references containing up to four authors, the names of all the authors with their respective initials should be given. The abbreviations *et al.*, *idem* and *ibid* should be avoided. When there are more than four authors, only the names of the first three authors with their respective initials should be given, followed by the words '*et al.*'

Reference to a book should include details in the following order: name and initials of authors, the title of the book (underlined), name of publisher and place of publication within circular brackets and year and page (s) [e.g. Clayton G B, *Operational amplifiers* (Newnes-Butterworths, London), 4th Edn, 1977, 26]. If the reference is to the work of an author published in a book by a different person, the fact that it is cited from the source book should be clearly indicated [e.g. Turnhout Van J, 'Thermally stimulated discharge of electrets' in *Topics in applied physics: Vol. 33—Electrets*, edited by C M Sessler (Springer Verlag, Berlin), 1980, 130].

Proceedings of conferences and symposia should be treated in the same manner as books. Reference to a paper presented at a conference, the proceedings of which are not published, should include, in the following order, names and initials of authors, title of the paper (underlined), name of the conference, and where and when it was held (e.g. Herczeg P, *Symmetry-violating kaon decays*, paper presented to the International Conference on High Energy Physics and Nuclear Structure, Vancouver, Canada, 13-17 August 1979).

Reference to a thesis should include the name of the author, title of the thesis (underlined), university or institution to which it was submitted and year of submission (e.g. Mehrotra S N, *Many-body techniques and their applications to interacting bosons*, Ph D thesis, Ranchi University, 1976).

Reference to a patent should include names of patentees, country of origin (underlined) and patent number, the organization to which the patent has been assigned (within circular brackets), date of acceptance of the patent and reference to an abstracting periodical where available [e.g. Labes M M, *US Pat.* 4,066,567 (to Temple University), 3 January 1978; *Chem. Abstr.*, 88 (No. 20) (1978), 138350 n].

PROOFS & REPRINTS

The edited manuscript will be sent to the author for his final approval before giving it to the press. No galley proofs will be sent to the authors for corrections, since the proofs will be checked at the editorial office. Authors are given 25 free reprints for each paper. Extra reprints can be ordered by the author while returning the edited manuscript. If the reprints order is not received, it will be presumed that no extra reprints are needed.

CSIR SCIENTIFIC PERIODICALS

JOURNAL OF SCIENTIFIC & INDUSTRIAL RESEARCH (Monthly)

With a fine record of over 45 years' service to the scientific community, this journal has grown into India's leading general science periodical. Intended to fulfil the responsibility of helping the research workers to keep themselves abreast of current developments in various fields of science and technology, the journal carries editorial features highlighting important scientific events in India and abroad, articles on science policy and management of science review articles on topics of current research interest, technical reports on international and national conferences, reviews of scientific and technical publications, and notes on major advances in various fields.

Annual subscription	Rs 120.00	\$ 40.00	£ 23.00
Single copy	12.00	4.00	2.30

INDIAN JOURNAL OF CHEMISTRY (Monthly)

Section A: Started in the year 1963, the journal is devoted to papers in Inorganic, Physical, Theoretical and Analytical Chemistry.

Annual subscription	Rs 160.00	\$ 53.00	£ 30.00
Single copy	16.00	5.30	3.00

Section B: This journal is devoted to papers in Organic Chemistry including Medicinal Chemistry.

Annual subscription	Rs 160.00	\$ 53.00	£ 30.00
Single copy	16.00	5.30	3.00

INDIAN JOURNAL OF PURE & APPLIED PHYSICS (Monthly)

Started in the year 1963, this journal is devoted to original research communications (full papers and short communications) in all conventional branches of physics (except radio and space physics).

Annual subscription	Rs 180.00	\$ 60.00	£ 34.00
Single copy	18.00	6.00	3.40

INDIAN JOURNAL OF RADIO & SPACE PHYSICS (Bimonthly)

The journal, which is being published beginning from March 1972, is intended to serve as a medium for the publication of the growing research output in various areas of radio and space physics, such as ionospheric propagation, magnetosphere, radio and radar astronomy, physics and chemistry of the ionosphere; neutral atmosphere; airglow, winds and motion in the upper atmosphere; stratosphere-mesosphere coupling, ionosphere-magnetosphere coupling, solar-terrestrial relationship, etc.

Annual subscription	Rs 100.00	\$ 34.00	£ 19.00
Single copy	20.00	6.80	3.80

INDIAN JOURNAL OF TECHNOLOGY (INCLUDING ENGINEERING) (Monthly)

This journal publishes papers reporting results of original research of applied nature pertaining to unit operations, heat and mass transfer, products, processes, instruments and appliances, etc. The journal is of special interest to research workers in departments of applied sciences in universities, institutes of higher technology, commodity research laboratories, industrial cooperative research institutes, and industrial research laboratories.

Annual subscription	Rs 120.00	\$ 40.00	£ 23.00
Single copy	12.00	4.00	2.30

INDIAN JOURNAL OF EXPERIMENTAL BIOLOGY (Monthly)

This journal, devoted to the publication of research communications in the fields of experimental botany, zoology,

microbiology, pharmacology, endocrinology, nutrition, etc., is the only one in India with such a wide coverage and scope.

Annual subscription	Rs 180.00	\$ 68.00	£ 34.00
Single copy	18.00	6.80	3.40

INDIAN JOURNAL OF BIOCHEMISTRY & BIOPHYSICS (Bimonthly)

This journal, published in association with the Society of Biological Chemists (India), Bangalore, is the only research journal in India devoted exclusively to original research communications in biochemistry and biophysics.

Annual subscription	Rs 65.00	\$ 23.00	£ 12.00
Single copy	13.00	4.60	2.40

INDIAN JOURNAL OF MARINE SCIENCES (Quarterly)

Commencing publication from June 1972, this journal is devoted to research communications (full papers and short communications) pertaining to various facets of marine research, viz. biological, physical, geological and chemical oceanography.

Annual subscription	Rs 90.00	\$ 30.00	£ 17.00
Single copy	26.00	8.70	5.00

RESEARCH AND INDUSTRY (Quarterly)

Intended to serve as a link between science and industry, this journal is addressed primarily to technologists, engineers, executives and others in industry and trade. It publishes informative original articles containing practical details of processes and products devoted in India, which show promise of ready utilization, and technical digests on new processes, products, instruments and testing methods which are of interest to industry. Developments in Indian industry are regularly reported.

Annual subscription	Rs 70.00	\$ 23.00	£ 13.00
Single copy	22.00	7.00	4.00

INDIAN JOURNAL OF TEXTILE RESEARCH (Quarterly)

Commencing publication from March 1976, this journal is devoted to the publication of papers reporting results of fundamental and applied researches in the field of textiles.

Annual subscription	Rs 50.00	\$ 17.00	£ 10.00
Single copy	15.00	5.00	3.00

MEDICINAL & AROMATIC PLANTS ABSTRACTS (Bimonthly)

Carries informative abstracts of scientific papers published in important Indian and foreign journals relating to different aspects of medicinal and aromatic plants. Each issue contains about 350 abstracts with a subject index.

Annual subscription	Rs 120.00	\$ 40.00	£ 23.00
Single copy	24.00	8.00	4.60

CURRENT LITERATURE ON SCIENCE OF SCIENCE (Monthly)

Carries abstracts, digests, book reviews, news & notes and R&D statistics with emphasis on problems of S&T in developing countries. It also covers the areas of science policy, R&D planning and management, technology transfer, technology assessment and science and society.

Annual subscription	Rs 100.00	\$ 30.00	£ 12.00
---------------------	-----------	----------	---------

Please contact

SALES AND DISTRIBUTION OFFICER
PUBLICATIONS & INFORMATION
DIRECTORATE, CSIR
Hillside Road, New Delhi-110012

CSIR PUBLICATIONS

WEALTH OF INDIA

An encyclopaedia of the economic products and industrial resources of India issued in two series

RAW MATERIALS SERIES—contains articles on plant, animal and mineral resources

	Rs	\$	£
Vol. I (A-B)	80.00	30.00	13.00
Vol. II (C)	95.00	33.00	17.00
Vol. III (D-E)	105.00	32.00	20.00
Vol. IV (F-G)	65.00	27.00	12.00
Supplement (Fish & Fisheries)	55.00	16.00	10.50
Vol. V (H-K)	114.00	34.00	21.00
Vol. VI (L-M)	90.00	34.00	15.00
Supplement (Livestock)	102.00	34.00	19.50
Vol. VII (N-Pe)	100.00	30.00	19.00
Vol. VIII (Ph-Rc)	86.00	32.00	14.00
Vol. IX (Rh-So)	104.00	35.00	19.00
Vol. X (Sp-W)	225.00	75.00	42.50
Vol. XI (X-Z)	115.00	38.50	22.00

INDUSTRIAL PRODUCTS SERIES—

deals with major, small-scale and cottage industries

Part I (A-B)	58.00	20.00	11.00
Part II (C)	74.00	24.00	14.00
Part III (D-E)	100.00	33.50	19.50
Part IV (F-H)	126.00	42.00	24.00
Part V (I-L)	80.00	23.00	17.00
Part VI (M-P)	28.00	8.00	2.80
Part VII (Pi-Sh)	60.00	18.00	6.00
Part VIII (Si-Ti)	65.00	27.00	10.00
Part IX (To-Z)	80.00	34.00	12.00

BHARAT KI SAMPADA (Hindi Edition of Wealth of India. Raw Materials)

Vol. I (अ-क)	38.00	16.00	6.50
Vol. II (ख)	36.00	15.00	6.00
Vol. III (ग-घ)	36.00	15.00	6.00
Vol. IV (ङ)	83.00	34.00	16.00
Vol. V (च-छ)	60.00	22.00	10.00
Vol. VI (ज-झ)	80.00	27.00	13.00
Vol. VII (ञ-ट)	135.00	40.00	25.00
Livestock (Kuskrut Palan)	34.00	15.00	6.00
Fish & Fisheries (Matsya aur Matsyaki)	49.00	21.00	8.00
A Dictionary of Generic & Specific Names of Plants and Animals Useful to Man with their English and Latin pronunciation in Devanagari	30.00	11.00	5.00

OTHER PUBLICATIONS

Proceedings: seminar on primary communications in Science & Technology in India by Sh. R.N. Sharma & S. Seetharama	52.00	17.50	9.00
Flora of Delhi by J.K. Maheshwari	28.00	8.00	2.80
Indian Fossil Pteridophytes by K.R. Surange	66.00	22.00	12.50
Indian Thysanoptera by T.N. Ananthakrishnan	26.00	8.00	2.60
The Millipede Thyropygus by G. Krishnan	12.00	3.50	1.20
Drug Addiction with special reference to India by R.N. Chopra & I.C. Chopra	12.00	3.50	1.20
Glossary of Indian Medicinal Plants by R.N. Chopra & I.C. Chopra	35.00	13.00	6.00
Fluidization & Related Processes	12.00	4.00	1.20
Evolution of Life by M.S. Randhawa, A.K. Dey, Jagjit Singh & Vishnu Mitre	22.50	7.00	2.25
Collected Scientific Papers of Meghnad Saha	30.00	9.00	3.00
Proteaceae by C. Venkata Rao	72.00	24.00	13.50
Pinus by P. Maheshwari & R.N. Konar	30.00	11.00	5.00
Cellulose Research I	3.00	0.90	0.30
Cellulose Research II	6.00	1.75	0.60
Chemical Process Design	9.00	2.50	0.90
Low Temperature Carbonization of Non-coking Coals & Lignites & Briquetting Coal Fines: Vol. I & Vol. II (each volume)	17.50	5.50	1.75
Nucleic Acids	10.00	3.00	1.00
IGY Symposium: Vol. I	9.00	2.50	0.90
IGY Symposium: Vol. II	9.00	2.50	0.90
CNS Drugs	16.50	5.00	1.65
Kinetics of Electrode Processes & Null Points of Metals	2.50	0.75	0.25
Indian Sardines by R.V. Nair	22.00	7.00	2.20
Termite Problems in India	9.00	3.00	0.90
Loranthaceae by B.M. Johri & S.P. Bhatnagar	55.00	18.50	10.50
Abies and Picea by K.A. Chowdhury	14.00	6.00	2.10
Gnetum by P. Maheshwari and Vimla Vasil	20.00	6.00	2.00
Aquatic Angiosperms by K. Subramanyam	20.00	6.00	2.00
Supplement to Glossary of Indian Medicinal Plants by R.N. Chopra, I.C. Chopra & B.S. Varma	18.00	7.00	3.00
Herbaceous Flora of Dehra Dun by C.R. Babu	144.00	60.00	22.00
Diosgenin and Other Steroid Drug Precursors by Y.R. Chadha & Miss L.V. Asolkar	36.00	13.00	6.00
Research & Development Management by Inder Dev	25.00	10.00	—
Rural Development and Technology—A Status Report cum Bibliography by P.R. Bose & V.N. Vashist	100.00	38.00	17.00
Cholera Bacteriophages by Sachinmohan Mukherjee	30.00	10.00	6.00

Packing and Postage extra

Please contact:

SALES AND DISTRIBUTION OFFICER
PUBLICATIONS & INFORMATION DIRECTORATE, CSIR
Hillside Road, New Delhi 110012

Indian J Pure & Appl Phys, Vol 24 No 10 pp 465-514

OCTOBER 1986

CODEN : IJOPAU ISSN : 0019-5596

24(10) 465-514 (1986)

PR-109
G-1 *cost*

INDIAN JOURNAL OF PURE & APPLIED PHYSICS



Published by
PUBLICATIONS & INFORMATION DIRECTORATE, CSIR
NEW DELHI

in association with
THE INDIAN NATIONAL SCIENCE ACADEMY, NEW DELHI

Announcing

The Wealth of India

Raw Materials: Volume-I: A

(Revised Edition)

Contains 204 entries: 198 on plant genera and 6 on minerals

This volume is the first of the revised and enlarged edition of this encyclopaedic classic on Indian Raw Materials, brought out with updated information. It covers economically important raw materials of plants and minerals contained in the alphabet A. Each plant entry gives the correct nomenclature of the genus and species dealt with, their distribution in India, and a short description of the economically important parts.

The articles on crop plants, medicinal and timber yielding plants etc. give in considerable detail the methods of cultivation, silvicultural practices, agricultural inputs, harvesting and storage etc. besides mentioning diseases and pests and their control measures. Chemical composition and utilization of raw materials are covered in detail for important economic crops and products; statistical data concerning area, production, export, import etc. are given. In the case of minerals, their occurrence and distribution in the country, methods of mining, extraction, chemical composition and utilization are given.

Adequate references to the sources of information are provided at appropriate places. The articles are illustrated with half-tones, line drawings, charts and colour plates. The Index covers botanical and zoological names, and names of chemical compounds, besides common English, regional and trade names.

The revised edition provides useful updated information to research workers, students, industrialists, planners, and others interested in the raw material resources of India.

Pages: Text, 513 + Index, 54

Price: Rs. 200.00

\$ 47.00

£ 37.00

Kindly send your orders to:

The Sales & Distribution Officer

Publications & Information Directorate, CSIR

Hillside Road, New Delhi 110 012

RENEWAL NOTICE

Your subscription which expires with the despatch of December 1986 issue of the journal, stands for renewal. We request you to be so good as to return the enclosed order form duly filled, early, so as to ensure continuity in despatch.

Sales & Distribution Officer

DATED:

The Sales & Distribution Officer
PUBLICATIONS & INFORMATION DIRECTORATE
HILLSIDE ROAD, NEW DELHI-110012 (INDIA)

Dear Sir,

Please renew my subscription/enrol me as subscriber to:

		Rs.	\$	£
1 Journal of Scientific & Industrial Research	(Monthly)	140.00	46.00	26.00
2 Indian Journal of Chemistry, Section A	(Monthly)	200.00	65.00	38.00
3 Indian Journal of Chemistry, Section B	(Monthly)	200.00	65.00	38.00
4 Indian Journal of Experimental Biology	(Monthly)	180.00	68.00	34.00
5 Indian Journal of Technology	(Monthly)	120.00	40.00	23.00
6 Indian Journal of Pure & Applied Physics	(Monthly)	180.00	60.00	34.00
7 Indian Journal of Biochemistry & Biophysics	(Bimonthly)	80.00	27.00	15.00
8 Indian Journal of Radio & Space Physics	(Bimonthly)	100.00	34.00	19.00
9 Indian Journal of Marine Sciences	(Quarterly)	100.00	34.00	19.00
10 Indian Journal of Textile Research	(Quarterly)	70.00	23.00	13.00
11 Research & Industry	(Quarterly)	90.00	30.00	17.00
12 Current Literature on Science of Science	(Monthly)	100.00	30.00	12.00
13 Medicinal & Aromatic Plants Abstracts	(Bimonthly)	160.00	53.00	30.00

(Please tick off the periodicals you would like to subscribe).

for one year from January 1987 for which I/we have remitted to you
a sum of Rs£ \$ by Cheque/Demand

Draft No. dated in favour of

PUBLICATIONS & INFORMATION DIRECTORATE, NEW DELHI.

COMPLETE MAILING ADDRESS

Name

Address

Country/State

(Signature)

Note:

1. Subscribers at annual rates for all the periodicals are enlisted for the full volumes, i.e. for the period from January to December only.
2. The Cheque Demand Draft may please be drawn in favour of "PUBLICATIONS & INFORMATION DIRECTORATE, NEW DELHI". Banking charges shall be borne by the subscriber. For inland outstation cheques please add Rs. 3.50. For foreign cheques please add \$ 1.00 or £ 0.45.
3. The supply will commence on receipt of subscription in advance.

Indian Journal of Pure & Applied Physics

EDITORIAL BOARD

Prof. S. Chandrasekhar
Raman Research Institute
Bangalore

Prof. S P Pandya
Physical Research Laboratory
Ahmedabad

Prof. R V Gopala Rao
Jadavpur University
Calcutta

Dr K R Rao
Bhabha Atomic Research Centre
Bombay

Prof. S K Joshi
Indian National Science Academy
New Delhi/Roorkee University
Roorkee

Prof. D K Rai
Banaras Hindu University
Varanasi

Prof. P Krishna
Indian National Science Academy,
New Delhi/Banaras Hindu University
Varanasi

Prof. B V Sreekantan
Tata Institute of Fundamental Research
Bombay

Prof Kehar Singh
Indian Institute of Technology
New Delhi

Prof. R Srinivasan
University of Madras
Madras

Prof C L Mehta
Indian Institute of Technology
New Delhi

Prof. Suresh Chandra
Banaras Hindu University
Varanasi

Shri S P Ambasta, Editor-in-Chief (*Ex-officio*)

EDITORIAL STAFF

Editors

D S Sastry & K S Rangarajan

Assistant Editors

J B Dhawan, Tarun Banerjee & (Mrs) Poonam Bhatt

Published by the Publications & Information Directorate, CSIR, Hillside Road, New Delhi 110 012

Editor-in-Chief: S P Ambasta

The Indian Journal of Pure & Applied Physics is issued monthly. The Directorate assumes no responsibility for the statements and opinions advanced by contributors. The editorial staff in its work of examining papers received for publication is assisted, in an honorary capacity, by a large number of distinguished scientists, working in various parts of India.

Communications regarding contributions for publication in the journal should be addressed to the Editor, Indian Journal of Pure & Applied Physics, Publications & Information Directorate, Hillside Road, New Delhi 110 012.

Correspondence regarding subscriptions and advertisements should be addressed to the Sales Distribution Officer, Publications & Information Directorate, Hillside Road, New Delhi 110 012.

Annual Subscription

Rs. 180.00 £ 34.00 \$ 60.00

Single Copy

Rs. 18.00 £ 3.40 \$ 6.00

50% Discount is admissible to research workers and students and 25% discount to non-research individuals, on annual subscription. Payments in respect of subscriptions and advertisements may be sent by cheque, bank draft, money order or postal order marked payable *only* to Publications & Information Directorate, New Delhi 110 012. Claims for missing numbers of the journal will be allowed only if received within 3 months of the date of issue of the journal plus the time normally required for postal delivery of the journal and the claim.

Announcement
Physics & Technology of Particle Accelerators
and Their Applications
(Calcutta, 29 Jan-3 Feb 1987)

The above seminar, to be organized at the Variable Energy Cyclotron Centre, Bidhan Nagar, Calcutta, will cover all aspects of accelerators and their applications. Four copies of abstracts of papers intended for the seminar should be submitted before 8 December 1986 neatly typed on a rectangular space of 13 cm \times 19 cm. The title should be typed in all capitals followed by the names of the authors and their institutions with initial capitals. The registration fee is Rs. 100/- for sponsored and individual participants. Further information can be had from:

Dr Surya N Chintalapudi
Convener, IPS Seminar, PATPAA
Variable Energy Cyclotron Centre
1/A F Bidhan Nagar, Calcutta 700 064

CONTENTS

General Physics

- Interference-free Determination of Manganese in Water by Graphite Furnace Atomic Absorption Spectrophotometry 465
Animesh Kumar, M Z Hasan & B T Deshmukh*

Nuclear Physics

- High-Spin Properties in Deformed Nuclei Using Weak Coupling Model 469
A M Khalaf
- A Semi-Empirical Formula for the Total Gamma Ray Streaming through Pipes 499
F M Sayed ahmed

Classical Areas of Phenomenology (Including Applications)

- Probability of Phase Orientation & Thermal Conduction in Heterogeneous Multi-phase Systems 472
Ramvir Singh*, R S Beniwal, R N Pande & D R Chaudhary
- Measurement of Effective Thermal Conductivity of Food-grains at Interstitial Air Pressures 506
Ramvir Singh*, R S Beniwal & D R Chaudhary
- Design of a Pulsed Xenon Ion Laser. 477
R Chari* & G Chakrapani
- Temperature & Concentration Dependence of Ultrasonic Velocity & Allied Parameters of Monochloroacetic Acid in Aqueous Ethanol 502
P S Nikam* & Mehdi Hasan

Fluids, Plasmas & Electrical Discharges

- Plasma Density & Electron Temperature Enhancements in a Constricted Type Plasma Source 481
F F Elakshar* & A M Nossair

Condensed Matter: Structure, Mechanical & Thermal Properties

- Coherent States & Symmetry Breaking in Superfluid⁴ He 486
S K Tikoo, M Ahmad*, S B Ahmad & T K Raina
- Thermophysical Properties of Syndiotactic Polypropylene 493
M S Mostafa* & A Gaber
- Migrational Enthalpies for Alkali Halides Using Ballistic Model & Their Dependence on Structural Properties 508
Shanta Palchoudhuri & G K Bichile*

Condensed Matter: Electronic Structure, Electrical, Magnetic & Optical Properties

Electric Field Dependence of Specific Heat of a Displacive Ferroelectric Crystal with Impurities	496
U C Naithani* & G N Baluni	
Optical Losses of ZrO ₂ Films in UV Region	510
K V S R Apparao*, N K Sahoo & T C Bagchi	
Energy Transfer from Acriflavine to Rhodamine B in Cellulose Acetate	513
H C Joshi*, K K Pandey, K K Pant, G C Joshi & T C Pant	

The author for correspondence is indicated by () mark, in case of papers with more than one author

Interference-free Determination of Manganese in Water by Graphite Furnace Atomic Absorption Spectrophotometry

ANIMESH KUMAR & M Z HASAN

National Environmental Engineering Research Institute, Nagpur 440 020
and

B T DESHMUKH

Department of Physics, Nagpur University, Nagpur 440 010

Received 20 March 1986; revised received 10 June 1986

An interference-free graphite furnace atomic absorption spectrophotometric method for the determination of manganese in water has been developed. The method utilizes a matrix modification reagent consisting of a mixture of ascorbic acid and ammonium nitrate for the removal of matrix interferences. Optimum atomization conditions followed are: drying at 90°C for 50 s, charring at 1000°C for 30 s and atomization at 2700°C for 5 s. Use of pyrolytically coated graphite tube and normal mode of heating gave optimum results. The interferences caused by alkali metals, alkaline earth metals, their chlorides and sulphates and iron were successfully removed in the present method. The minimum detection limit and sensitivity of the method are 0.5 µg/l and 0.1 µg/l of manganese respectively.

1 Introduction

Manganese (Mn) occurs in water as hexavalent manganates and divalent metal ions. Monitoring of Mn in ground water and in water from municipal supply mains, in general, and in water found in mines, in particular, is essential both for aesthetic and health reasons¹. This programme requires accurate, precise and sensitive analytical methods for the determination of Mn. Atomic absorption (AA) spectrophotometric methods have been universally accepted for trace metal analyses in water². The detection limit for Mn by flame AA spectrophotometric method is, however, higher than its permissible limit in water³. The sample is required to be pre-concentrated to bring its concentration in the detection range^{4,5}. The application of flameless atomization techniques in AA spectrophotometry for trace metals determinations has increased manyfold during the last decade⁶ due to their higher sensitivity as compared to flame methods. However, the technique suffers from matrix interferences and requires their removal by chemical treatments^{7,8}.

Numerous studies have been made on the determination of Mn by flameless AA spectrophotometry using a graphite furnace (GF), a carbon rod and a tantalum boat. Mn was determined in natural water by direct comparison with aqueous standards⁹. During determination of Mn by using a tantalum heating element in a stream of argon in a pyrex enclosure, it was observed that manganese phosphate produces a higher absorption signal compared to manganese chloride and bromide. The atomization of Mn was also suppressed by the presence of Na, K, Al, CO, Ni, Ca and

Sr; however, Fe did not produce any suppression¹⁰. In another experiment, manganese chloride was found to interfere significantly and this was compensated by using a background corrector¹¹ or by introducing the sample on a tungsten wire after the GF has reached a constant pre-set temperature¹². Halide interferences were also removed by addition of ammonium salt of ethylene diamine tetra acetic acid (EDTA)¹³. This process prevented metal halide complexation and produced volatile ammonium halide which is removed during the charring stage. Perchloric acid was also found to suppress the Mn, AA signal considerably; however, this suppression effect was avoided by evaporation of the acid before atomization¹⁴. The macrocomponents present in the sample produce incongruent volatilization in the carbon rod atomizer; however, such a volatilization could be reduced by thermal pre-treatment of the sample¹⁵.

The present paper reports a new method for the determination of Mn in water developed at the National Environmental Engineering Research Institute (NEERI), Nagpur. The method utilizes a mixture of ammonium nitrate and ascorbic acid as a matrix modification reagent (MMR) for the suppression of anionic and cationic interferences. The effect of heating rate on peak atomization has also been studied.

2 Experimental Details

2.1 Instrumentation

A Perkin-Elmer Model-372 atomic absorption spectrophotometer equipped with a HGA-2200 gra-

phite furnace and deuterium background corrector lamp was used. Measurements were made with Intensitron hollow cathode lamp of Mn operated at 20 mA lamp current with the wavelength setting at 279.5 nm and a spectral slit width at 0.2 nm. Initial studies were conducted with both the standard graphite (SG) tube and pyrolytically coated graphite (PCG) tube but later on it was restricted to PCG tube only as it gave more precise results. Inert atmosphere in and around the graphite tube was maintained by continuously purging nitrogen at a flow rate of 50 ml/min. The Mn absorbance signals were recorded on 10 mV span Perkin-Elmer Model-56 recorder for the computation of the results. Eppendorf microlitre pipette with disposable tips was used to transfer the solutions into the GF.

2.2 Reagents

Stock solution of Mn (1000 $\mu\text{g/ml}$) was prepared by dissolving 0.3076 g $\text{MnSO}_4 \cdot \text{H}_2\text{O}$ (99% pure, BDH, AR) in 1 ml concentrated nitric acid (BDH, AR) and subsequently making up the volume to 100 ml with deionized distilled water. Standard Mn solutions of various concentrations were then prepared by two step dilutions of Mn stock solution with 1% nitric acid. MMR was prepared by dissolving 1 g of ammonium nitrate (99% pure, AR, BDH) and 1 g of ascorbic acid (99.9% pure, AR, BDH) in 100 ml of deionized distilled water.

2.3 Procedure

Water samples for determination of total Mn were prepared by acidifying the sample with nitric acid to bring the pH to 2-3, boiling vigorously for 5 min and filtering the cooled water samples through 0.45 micron filter paper. Blanks were prepared by taking deionized distilled water and processing them in the same way as the samples. The standards were also given similar treatments. A 20 μl of the sample and 20 μl of the MMR were transferred into the GF. The furnace was then programmed at the pre-determined optimum operating conditions (drying at 90°C for 5 s, charring at 1000°C for 30 s, atomizing at 2700°C for 5 s) using

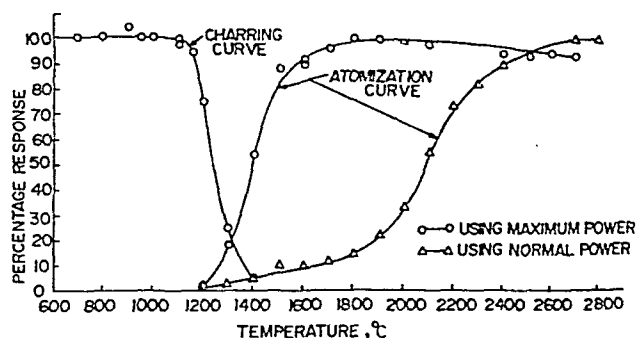


Fig. 2—Curves of Fig. 1 taken using pyrolytically coated graphite tube

normal mode of heating. Results were computed from the mean of several readings after compensating for reagent blanks.

3 Results and Discussion

3.1 Optimization of Atomization Parameters

Experimental charring and atomization curves were plotted using the AA signals obtained by atomizing 20 μl of synthetic water sample containing 4 $\mu\text{g/l}$ Mn and 20 μl of MMR in both SG and PCG tubes using both normal mode of heating and temperature-controlled maximum power (TCMP) mode of heating (Figs 1 and 2). It was observed that a loss of Mn occurred at 900°C when SG tube was used and insignificant loss of Mn was observed up to 1050°C when atomized in the PCG tube. Optimum atomization temperatures with (i) normal mode of heating and (ii) with TCMP mode of heating were 2700 and 2200°C respectively in case of SG tube; and they were 2700 and 1900°C respectively in case of PCG tube. The charring time of 40 s was found suitable and atomization time of 5 s was sufficient to bring the AA signal back to the base line. PCG tube has a high thermal conductivity which permits uniform heating of furnace and, therefore, provides a more uniform temperature of the atomic vapour and high resistance to oxidation. A high charring temperature is usually desired since it ensures complete decomposition of organic matters and volatilization of inorganic matrices at the charring stage. PCG tube was, therefore, used for the analyses of water samples. The atomization profiles recorded (Figs 3 and 4) by heating an aliquot of Mn standard solution with MMR, using different heating rates showed that the peak atomization of Mn occurred at a higher temperature when higher heating rates were used. Improvement in analytical sensitivity with faster heating rates was also observed and it was optimum when normal mode of heating was used. TCMP mode of heating showed no further improvement in analytical sensitivity. Optimum sensitivity was achieved at lower atomization temperature of 1900°C using TCMP mode of heating. However, relative scattering

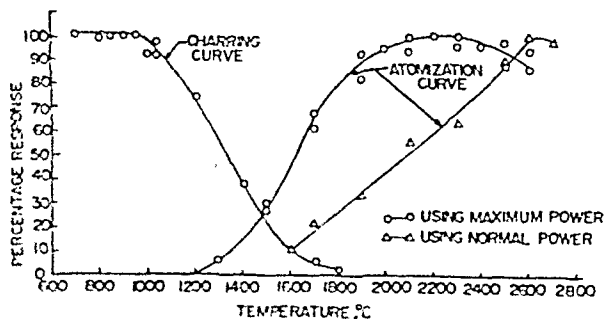
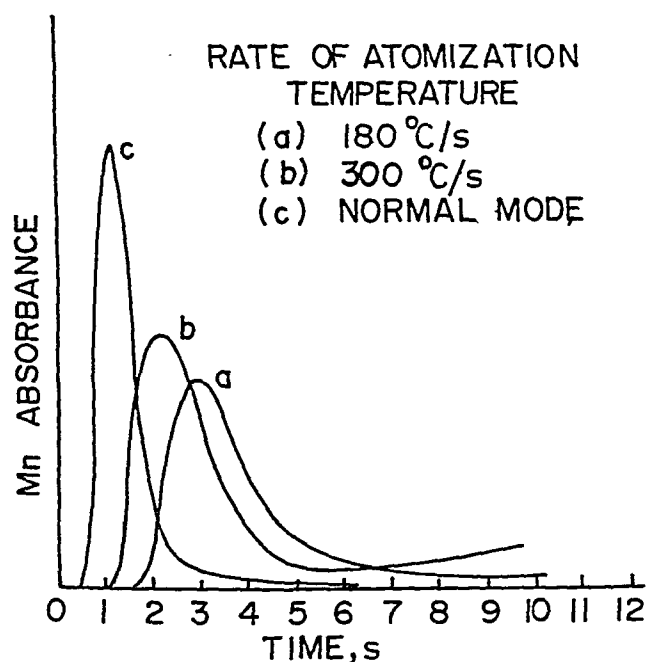
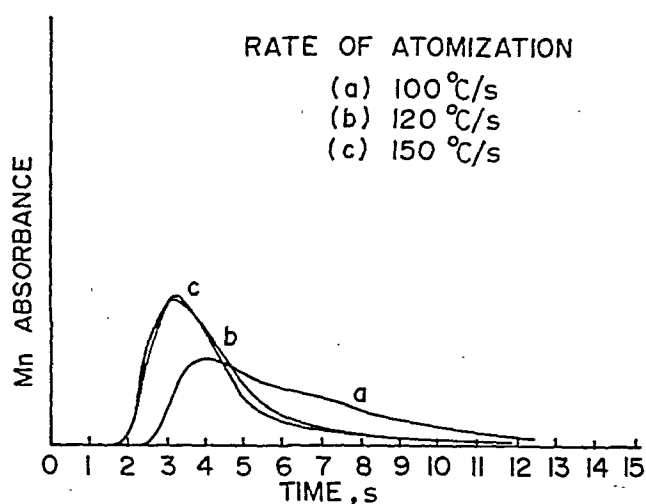


Fig. 1—Charring and atomization curves for Mn using standard graphite tube



of replicates was observed to be more in this case. In order to obtain precise results, analyses were carried out using an atomization temperature of 2700°C and normal mode of heating.

3.2 Effect of Diverse Ions and Their Suppression by Matrix Modification

Studies were conducted to find out the effect of anions and cations normally present in water, on manganese atomization. A solution containing 4 µg/l Mn was spiked with varying amount of diverse ions. Metals were added as their nitrates and anions as their respective acids. Mn AA signals were recorded for the solutions. It was observed that Na, Mg sulphate and chloride ions, when present at a concentration of 100 µg/ml significantly suppressed the Mn AA signal. Metals

Ca and K did not show any significant effect when present up to 500 µg/l. Iron suppressed Mn atomization at a level of 0.5 µg/ml. However, presence of Cd, Pb, Zn and Ni showed an insignificant effect. Presence of Mg in the solution reduced AA signal of Mn present in a matrix of magnesium oxide. Mn vaporization was also delayed until entire magnesium oxide was vaporized¹⁶. A study on the effect of nitrates of Mg and Ca, sulphate of Mg and chlorides of Mg, Ca and Na on pulse characterization time of Mn carbon furnace AA signal revealed that the atomization mechanisms were different for different interferences¹⁷. The suppression and enhancement of analyte atomization in GF, therefore, bear no simple relationship to the concentration of any individual matrix constituent¹⁸. These matrices, if not removed, may cause a depletion of the atomic vapour owing to the formation of molecular species and reduce the AA signal. Matrices may also cause a delay in the formation of atomic vapour, leading to both height reduction and broadening of absorption peak. Experiments were, therefore, conducted for reducing the effects of these matrices by chemical modification. A number of chemical reagents were used for this purpose. AA signals were recorded for the solution containing matrices in presence of these MMRs. Experiments showed that ascorbic acid removed the interferences due to Na, Mg and Fe; and ammonium nitrate removed the interference due to chloride, sulphate and Mg ions. The addition of ascorbic acid shifts the atomization peak of Mn to a higher temperature^{19,20} and the CO or CO₂ generated by its pyrolysis participates in the suppression of interferences¹⁹. Ammonium nitrate transforms easily to volatile ammonium chloride which volatilizes during the charring stage and, therefore, the interferences due to the presence of chloride are removed. A mixture of ascorbic acid and ammonium nitrate was found to be able to suppress the interferences considerably (Table 1). This was, therefore, used as MMR in the analysis of water samples. A study to optimize the concentration of ascorbic acid and ammonium nitrate for elimination of matrix interferences showed that 20 µl solution of a mixture of 1% of each by wt was suitable (Fig. 5).

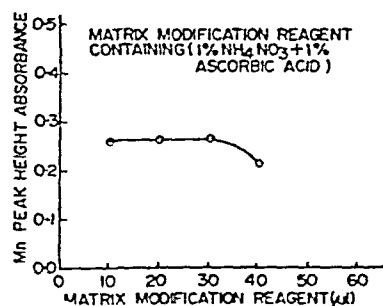


Table 1—Effect of MMR on Manganese Response

Ions added	Concentration µg/ml	[4 µg/l Mn response taken as 100%] % Response	
		Without MMR	With MMR
Ca ²⁺	500	90	98
Na ⁺	500	78	95
K ⁺	100	90	98
Mg ²⁺	200	83	105
Cl ²⁻	1000	70	100
SO ²⁻	1000	75	99
Fe ³⁺	1.0	77	96

Table 2—Accuracy and Precision of the Results for Manganese Determination

[Ground water containing 20 µg/l manganese and mine water containing 25 µg/l manganese were diluted 5 times for this study]

Manganese added µg/l	Ground water (Intrinsic content 20 µg/l)		Municipal supply water (Intrinsic content 1 µg/l)		Mine water (Intrinsic content 25 µg/l)	
	Rec. %	RSD %	Rec. %	RSD %	Rec. %	RSD %
1	95	6.2	97	3.7	93	4.3
2	98	7.4	91	4.2	98	3.8
3	99	5.4	101	3.8	102	3.7
4	103	4.3	98	3.6	99	5.0
5	97	3.8	99	3.9	100	4.2

3.3 Accuracy, Precision, Linearity Range and Minimum Detection Limit

The accuracy of the method was evaluated by determining the percentage recovery of Mn in spiked water samples of ground water, municipal supply water and mine water (Table 2). Percentage recovery at various concentration ranges was found between 91 and 107%. Percentage scatter of replicate analyses showed that relative standard deviation (RSD) varied between 3.7 and 7.4%. The calibration curve of absorbance versus concentration was drawn for aqueous solutions of Mn and MMR. The curve was found to be linear up to Mn conc. of 8 µg/l. the regression equation of concentration (C) versus absorbance (A) is given by: $C = 17.01 A - 0.38$. The minimum detection limit was calculated from $\bar{X}_{BI} + 3\sigma_{BI}$ where \bar{X}_{BI} is the mean of blank replicates and σ_{BI} is the standard deviation of blank replicates. Computation of \bar{X}_{BI} and σ_{BI} of blank gave a minimum detection limit of 0.5 µg/l of Mn. The sensitivity of the method expressed as concentration of Mn required to produce 1% absorption

Table 3—Results of Analysis of Some Water Samples

Sample	Manganese concentration (µg/l)			
	Ground water	Mine water	Municipal supply water	River water
A	11	18	3	9
B	14	25	1	12
C	32	29	0.5	13
D	33	14	1	13
E	13	16	2	7

(0.0044 absorbance) is 0.1 µg/l. The results of analysis of some water samples are shown in Table 3.

Acknowledgement

The authors are grateful to Mr K R Bulusu, Acting Director, NEERI, Nagpur, for his permission for publication of this paper. They are also thankful to Dr V R Bhawe and Dr K L Saxena for their encouragement during the study.

References

- 1 Bull R J & Crown G F, *J Am Water Works Assoc (USA)*, **69** (1977) 662.
- 2 Ediger R D, *At Absorpt Newslett (USA)*, **12** (1973) 151.
- 3 *Specifications for drinking water* (Indian Standard Institution, New Delhi), **IS 10500**, 1983.
- 4 Kinrade J D & Vanloon J C, *Anal Chem (USA)*, **46** (1974) 1966.
- 5 Hasan M Z, *J Indian Inst Sci Sec B (India)*, **63** (1981) 203.
- 6 Hageman L, Mubarak A & Woodriff R, *Appl Spectrosc (USA)*, **33** (1979) 226.
- 7 Reagan J G T & Warren J, *Analyst (GB)*, **101** (1976) 220.
- 8 Ediger R D, *At Absorpt Newslett (USA)*, **14** (1975) 127.
- 9 Bernard W M & Fishman M J, *At Absorpt Newslett (USA)*, **12** (1973) 118.
- 10 Maruta T & Takeuchi T, *Bunseki Kagaku (Japan)*, **23** (1974) 723.
- 11 Suzuki M, Ohta K & Yamakita T, *Anal Chem (USA)*, **53** (1981) 9.
- 12 Manning D C & Slavin W, *Anal Chim Acta (Netherlands)*, **118** (1980) 301.
- 13 Matsusaki K, *Anal Chim Acta (Netherlands)*, **141** (1982) 233.
- 14 Julshamn K, *At Absorpt Newslett (USA)*, **16** (1977) 149.
- 15 Belyaev Yu I, Shcherbakov V I & Karyalin A V, *Zh Anal Khim (USSR)*, **35** (1980) 2074.
- 16 Slavin W, Carnerick G R & Manning D C, *Anal Chem (USA)*, **54** (1982) 621.
- 17 Smeyers V J, Michotte Y & Massart D L, *Anal Chem (USA)*, **50** (1978) 10.
- 18 Reagan J G T & Warren J, *At Absorpt Newslett (USA)*, **17** (1978) 89.
- 19 Tominaga M & Umezaki Y, *Anal Chim Acta (Netherlands)*, **139** (1982) 279.
- 20 Tominaga M & Umezaki Y, *Anal Chim Acta (Netherlands)*, **148** (1983) 285.

High-Spin Properties in Deformed Nuclei Using Weak Coupling Model

A M KHALAF

Department of Physics, Faculty of Applied Sciences & Engineering, Umm Al-Qura University, Makkah Almukarramah, Saudi Arabia

Received 6 November 1985; revised received 21 March 1986

Weak coupling of a rigid rotor and a single neutron in $j = 13/2, 11/2$ and $9/2$ shells is used to explain the high-spin states of pure rotational bands, as weak as aligned-state bands in odd-mass nuclei. The nuclear Hamiltonian employed in the calculations is made up of three parts, which describe the core rotation, the single-particle motion in spherical field and their interaction which depends on the quadrupole operators of the core and the particle. The computed energy spectra are in good agreement with the corresponding experimental data.

1 Introduction

Experiments have been performed on odd-mass nuclei to test back-bending behaviour in adjacent nuclei^{1,2}. The results obtained on odd-neutron $^{155-159}\text{Er}$ nuclei³ and $^{155-159}\text{Dy}$ nuclei⁴ are in good agreement with the rotation-alignment model⁵ based on $i_{13/2}$ orbitals. The odd-proton $^{157-161}\text{Ho}$ nuclei⁶ also show rotation-aligned bands based on the $h_{11/2}$ proton orbital and these bands have been observed to back-bend at the same rotational frequency in the even cores. The rotation-aligned band in ^{165}Yb nuclei⁷ on the $h_{9/2}$ neutron orbital also exhibits back-bending at the same point as the core. Stephens⁸ explained the alignment by decoupling of the odd particle from the rotating core.

In the present study, a model of weak coupling between an even-even rotating core and the odd-particle is proposed in order to describe the aligned-state bands in some rotational odd-mass nuclei. We have started from states of decoupled core-particle system; then after switching on an interaction, the deviations from complete decoupling have been examined.

2 Formalism

The Hamiltonian for the system of a single nucleon coupled to an even-even rotating core with an angular momentum R and a moment of inertia θ is given by:

$$H = \frac{\hbar^2}{2\theta} R^2 + \{T + V(r)\} + H_{\text{int}} \quad \dots (1)$$

where the first term on the RHS represents the core rotation, the second term the single-particle motion in the spherical field and H_{int} is the Hamiltonian which describes the interaction between the core and the particle in the form:

$$H_{\text{int}} = -k \sum_v (-1)^v Q_{2v} q_{2v} \quad \dots (2)$$

The symbols Q_{2v} and $q_{2v} = 4(\pi/5)^{1/2} r^2 Y_{2v}$ are quadrupole operators of the core and particle respectively in the laboratory system. The parameter k describes the strength of the interaction and v is only even; r is the particle position operator and Y_{2v} are spherical harmonic functions.

The basic vectors of our model space are the eigenvectors obtained by vector coupling of core and particle wavefunctions as:

$$|(nlj, RM)JM_J\rangle = \left(\frac{2R+1}{8\pi^2}\right)^{1/2} \times \sum_{Mm} \langle RjMm | JM_J \rangle D_{MO}^R(\theta_i) \Phi_{nlj}^m(r) \quad \dots (3)$$

where n, l and j are the quantum numbers of the last odd nucleon, R the angular momentum of the core and $J = R + j$ the total angular momentum of the system with projection quantum number M .

The basic vectors are the eigenfunctions of the unperturbed Hamiltonian $H_{\text{core}} + H_{\text{particle}}$.

$$(H_C + H_P) |(nlj, RM)JM_J\rangle = \left[\frac{\hbar^2}{2\theta} R(R+1) + E_{nlj} \right] |(nlj, RM)JM_J\rangle \quad \dots (4)$$

where E_{nlj} is the energy of the single nucleon.

The eigenvector of the total Hamiltonian H can be written as a linear combination of the basic vectors:

$$|JM_J\rangle = \sum_{JRM} A_{JRM}^J |(nlj, RM)JM_J\rangle \quad \dots (5)$$

where the amplitudes A_{JRM}^J are found by diagonalizing the energy matrices for each possible total angular momentum J .

The off-diagonal matrix elements of the energy matrix are obtained by the use of some Racah algebra and are given by:

$$\begin{aligned}
 & \langle n l j, R M J M_J | H_{\text{int}} | n l j, R M J M_J \rangle \\
 & = -kQ_0 (-1)^{J-1/2} (2R+1)^{1/2} \\
 & \times \langle 2R00 | R0 \rangle \left\{ \begin{matrix} j & R & J \\ R & \bar{j} & 2 \end{matrix} \right\} M_J^2 \quad \dots (6)
 \end{aligned}$$

where Q_0 is the core quadrupole moment which is assumed to be a constant and M_J^2 the R - and J -independent part and is given by:

$$\begin{aligned}
 M_{ij}^2 & = \langle j || q_2 || j \rangle \\
 & = (-1)^{1/2-j} \langle j | r_p^2 | j \rangle \langle j^{1/2} j^{-1/2} | 20 \rangle \\
 & \times \left[\frac{(2j+1)(2j+1)}{4\pi} \right]^{1/2} \left[1 + (-1)^{j+l} \right] \quad \dots (7)
 \end{aligned}$$

and any spherical field wavefunction can be used to evaluate the radial integral $\langle j | r_p^2 | j \rangle$. As the strength

coupling parameter, the product kQ_0 is used and this is related to the usual quadrupole deformation δ by:

$$kQ_0 = (1/3\delta(\hbar\omega)^2 m/\hbar^2) \quad \dots (8)$$

3 Analysis of Calculations

First we computed the matrix elements $\langle H_{\text{int}} |$ using the single-particle wavefunction which is the solution of the usual Woods-Saxon potential and constructed the Hamiltonian matrices to be diagonalized for $J=1/2$ to $J=33/2$ for coupling the $j=13/2$, $11/2$ and $9/2$ neutron states to a pure rotational ground-state band. These matrices include the effective single-particle spacings ΔE_j which are regarded as adjustable parameters since these spacings cannot be extracted from experimental information. The strength parameter kQ_0 which is related to the usual quadrupole deformation is also regarded as an adjustable parameter. We diagonalized the corresponding matrices repeatedly by varying the free parameters so as to get an optimal fit for the measured level spacings.

For $kQ_0=0.5$ and 0.15 MeV fm^{-2} , the energy levels are given as points in energy-spin diagrams Fig. 1(a&b). States of the same multiplet which form a bent curve instead of horizontal line (when $kQ_0=0$) are connected with solid lines. On the other hand, states which in the extreme strong limit belong to the same band are connected with dashed lines. The high-spin states with $J=J_{\text{max}}$, $J=J_{\text{max}}-1$ in any multiplet (R and j ,

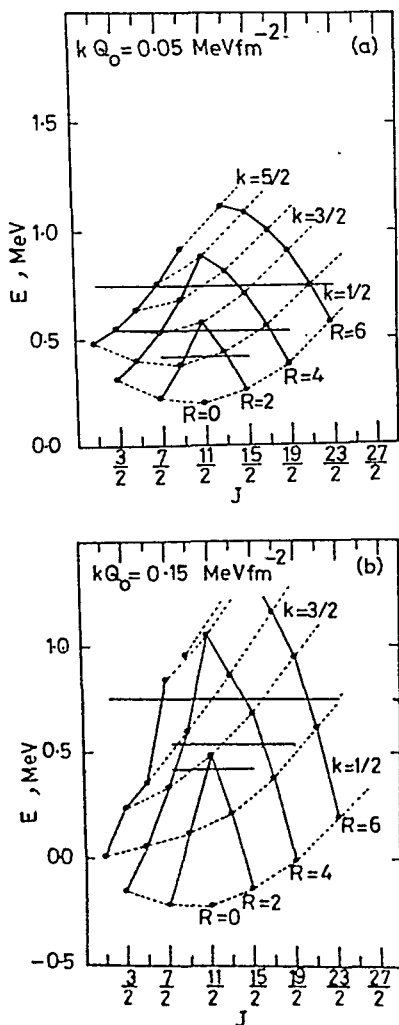


Fig. 1—Calculated energy levels for $kQ_0=0.05$ and 0.15 MeV fm^{-2} obtained by weak coupling of $l_1=h_{1,2}$ neutron to a prolate core for the multiplet $R=2, 4$ and 6 . The horizontal lines represent the limit of complete decoupling ($kQ_0=0$)

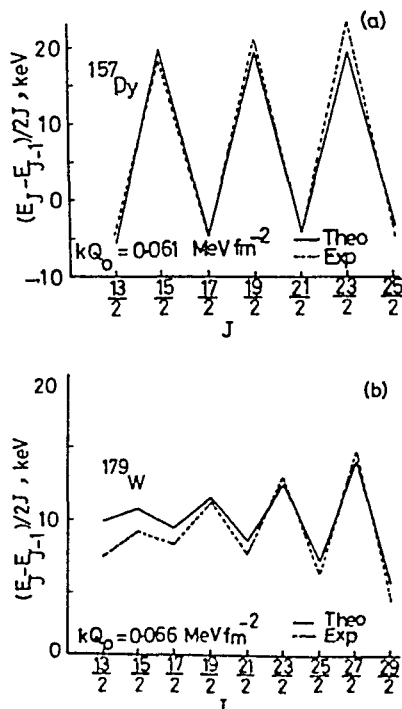


Fig. 2—Experimental transition energy $(E_J - E_{J-1})/2J$ plotted as a function of the spin J , compared with the present theoretical study for the nuclei ^{157}Dy and ^{179}W

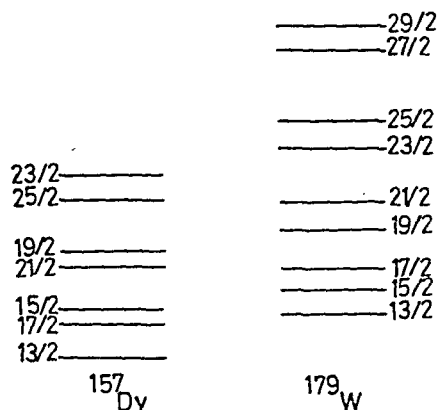


Fig. 3—Calculated energy levels in ^{157}Dy and ^{179}W nuclei

parallel aligned states) cannot interact with a state of lower-lying multiplet and are relatively pure. A similar situation appears for $J=J_{\min}$ and $J=J_{\min}+1$ (R and j , anti-parallel anti-aligned states) where an interaction with states of higher-lying multiplet is impossible ($R > j$). On the same plot, we present also results of the limit of complete decoupling $kQ_0=0$ (horizontal lines).

To compare our model calculations with the experimental data, the odd-mass nuclei are treated assuming a nuclear core of even number of protons and even number of neutrons and distributing the single neutron in the valence level $j=13/2$. We adjusted the parameters by means of a fit to the experimental levels. The decoupled bands have been explained in terms of the rotation-alignment scheme⁹ in which the odd particle is decoupled from the rotating core by a strong Coriolis force acting on the single-particle angular momentum j . As a result, this particle is aligned along the axis of rotation of the nucleus.

In Fig. 2(a & b), the weighted transition energy ($E_J - E_{J-1}$)/ $2J$ is plotted as a function of the spin J

beginning at $J=13/2$ for the $k=5/2$ -based bands for the odd-neutron nuclei ^{157}Dy and ^{179}W . As expected, the weighted transition energy deviates from linearity.

The comparison between the experimental data^{10,11} and our theoretical results reveals good agreement [Fig. 2 (A&b)]. The agreement for the nucleus ^{179}W is not as good as for ^{157}Dy . In ^{157}Dy , the regular $\Delta J=1$ energy spacing is lost in the extreme low k limit; so the J plus even number states are lower than the J plus odd number states forming the familiar decoupled band as can be seen from Fig. 3.

References

- 1 Gaardhoye J J, Andersen O, Garrett J D, et al., *International conference on nuclear behaviour at high angular momentum*, Strasbourg, 1980.
- 2 Hammoren E, Liukkonen E & Piiparinen M, *Nucl Phys A (Netherlands)*, **321** (1979) 71.
- 3 Grosse E, Stephens F S & Diamond R M, *Phys Rev Lett (USA)*, **31** (1973) 840.
- 4 Davidson W F, Lieder R M, Beuscher H, Neskakis A & Mayer-Borick C, *Proc international conference on nuclear physics, Munich*, Vol 1, edited by J de Boer & H J Mang (North Holland, Amsterdam) 1973, p 190.
- 5 Stephens F S & Simon R S, *Nucl Phys A (Netherlands)*, **183** (1972) 257.
- 6 Grosse E, Stephens F S & Diamond R M, *Phys Rev Lett (USA)*, **32** (1974) 74.
- 7 Riedinger L L, Stelson R H, Hagemann G B, et al., *Bull Phys Soc II (USA)*, **19** (1974) 524.
- 8 Stephens F S, *Rev Mod Phys (USA)*, **47** (1974) 43.
- 9 Stephens F S, Diamond R M & Nilsson S G, *Phys Lett B (Netherlands)*, **44** (1973) 429.
- 10 Klamra W, Hjorth S A, Boutet J, Andre S & Bourneand D, *Nucl Phys A (Netherlands)*, **199** (1973) 81.
- 11 Lindblad Th, Ryde H & Kleinheinz K, *Nucl Phys A (Netherlands)*, **201** (1973) 369.

Probability of Phase Orientation & Thermal Conduction in Heterogeneous Multi-phase Systems

RAMVIR SINGH, R S BENTWAL, R N PANDE & D R CHAUDHARY

Department of Physics, University of Rajasthan, Jaipur 302 004

Received 19 February 1986

An attempt is made to investigate the probability (n) of phase orientation by treating the phases as resistors aligned along and perpendicular to the direction of heat flow in heterogeneous multi-phase systems. The theory developed is used to estimate the effective thermal conductivity λ_e of two- and three-phase system. The values of λ_e estimated through the present method are in good agreement with available experimental data.

1 Introduction

The flow of heat energy through heterogeneous mixtures depends not only upon porosity, grain size and thermal conductivity values of constituent phases but also on the geometry of phase distribution. A complete description of the structure is possible in ordered systems only. Nevertheless, for a random mixture, it is a usual practice to consider the probability of association of any phase with the other one during the energy flow. To describe the phase distribution in a two-phase mixture, some workers have empirically defined a term formation factor¹⁻⁴. However, no serious attempt is made to find the material structure and orientation of phases during the flow of heat. A number of workers in the field have estimated the effective thermal conductivity (λ_e), of random two-phase mixtures⁵⁻⁹ avoiding details of the material structure. In addition, a section of researchers assumed a regular geometry¹⁰⁻¹³.

Several workers^{14,15} considered the probability of phase orientation (n) for estimation of λ_e of two-phase systems. Chaudhary *et al.*¹⁴ on considering phases as resistors, obtained an empirical relation for n for a two-phase mixture but apart from making certain qualitative predictions about n , they could not exploit it for estimation of λ_e . In the present study, an attempt is made to extend the approach of Chaudhary *et al.*¹⁴ to multi-phase systems, where we first find an expression for n and then determine λ_e of multi-phase systems.

2 Theory

In order to obtain a formula for the probability of orientation of phases (n), let us consider that the thermal conductivities of the constituent phases are $\lambda_1, \lambda_2, \lambda_3, \dots$ and λ_i , having volume fractions $\phi_1, \phi_2, \phi_3, \dots$ and ϕ_i , respectively. The mixture is supposed to be made up of layers oriented parallel and perpendicular to the direction of heat flow alternately. The effective thermal conductivity of parallel layers (λ_{\parallel}) is given by

the weighted arithmetic mean and that of perpendicular layers (λ_{\perp}) by weighted harmonic mean. The corresponding expressions are:

$$\lambda_{\parallel} = \sum_i \lambda_i \phi_i \quad \dots (1)$$

and

$$\lambda_{\perp} = \left\{ \frac{\sum_i \phi_i}{\sum_i \lambda_i} \right\}^{-1} \quad \dots (2)$$

where

$$\sum_i \phi_i = 1$$

The effective thermal conductivity (λ_e) of a multi-phase system will obviously lie between these two limits. An expression of λ_e proposed by Chaudhary *et al.*¹⁴ for a two-phase system is the weighted geometric mean of λ_{\parallel} and λ_{\perp} :

$$\lambda_e = \lambda_{\parallel}^n \lambda_{\perp}^{1-n} \quad \dots (3)$$

where n may be thought as the probability of phase orientation factor of the mixture.

Taking logarithmic differential of Eq. (3) and then substituting the values of $d\lambda_{\parallel}$ and $d\lambda_{\perp}$ obtained from Eqs (1) and (2) in this expression, we get

$$\frac{1}{\lambda_e} d\lambda_e = \frac{n}{\lambda_{\parallel}} \sum_i \lambda_i d\phi_i - (1-n) \lambda_{\perp} \sum_i \frac{d\phi_i}{\lambda_i} \quad \dots (4)$$

2.1 Two-Phase Systems

In case of a two-phase system, $i=1, 2$, $\phi_1 + \phi_2 = 1$ (because $\sum \phi_i = 1$), and let $\phi_1 = -d\phi_2 = d\phi$. Thus We find an expression for two-phase systems as:

$$\frac{1}{\lambda_c} \frac{d\lambda_c}{d\phi} = \frac{\partial n}{\partial \phi} \ln \left(\frac{\lambda_{\parallel}}{\lambda_{\perp}} \right) + (\lambda_1 - \lambda_2) \left\{ \frac{n}{\lambda_{\parallel}} + \frac{(1-n)}{\lambda_1 \lambda_2} \lambda_{\perp} \right\} \quad \dots (5)$$

Now, Eq. (5) must satisfy the phase boundary conditions, i.e. a two-phase system must tend to either solid or fluid phase as ϕ approaches zero or unity

i.e. As $\phi \rightarrow 0$, $\lambda_{\parallel} \rightarrow \lambda_1$ and λ_{\perp} also $\rightarrow \lambda_1$

Similarly

as $\phi \rightarrow 1$, $\lambda_{\perp} \rightarrow \lambda_2$ and λ_{\parallel} also $\rightarrow \lambda_2$

Effectively the above two boundary conditions are mathematically equivalent to

(i) $\phi \rightarrow 0$, $\lambda_{\parallel} \rightarrow \lambda_{\perp}$

and

(ii) $\phi \rightarrow 1$, $\lambda_{\perp} \rightarrow \lambda_{\parallel}$

Substituting these conditions in Eq. (5), we get the following two different relations for limiting porosity values ($\phi \rightarrow 0$ and 1)

$$\frac{1}{\lambda_c} \frac{d\lambda_c}{d\phi} = (\lambda_1 - \lambda_2) \left\{ \frac{n_1}{\lambda_{\parallel}} + \frac{(1-n_1)}{\lambda_1 \lambda_2} \lambda_{\parallel} \right\} \quad \dots (6)$$

and

$$\frac{1}{\lambda_c} \frac{d\lambda_c}{d\phi} = (\lambda_1 - \lambda_2) \left\{ \frac{n_1}{\lambda_{\perp}} + \frac{(1-n_1)}{\lambda_1 \lambda_2} \lambda_{\perp} \right\} \quad \dots (7)$$

Here we have used the notation n_1 instead of n , as the former depicts the orientation of the layers for fixed extremum porosity values. Eqs (6) and (7) become equivalent as $\lambda_{\parallel} \rightarrow \lambda_{\perp}$, which also means that the two slopes given by these expressions are equivalent for $\phi \rightarrow 0$ and 1. On equating Eqs (6) and (7) we find,

$$n_1 = \frac{\lambda_1 \lambda_{\perp}}{\lambda_1 \lambda_2 + \lambda_{\parallel} \lambda_1} \quad \dots (8)$$

For intermediate values of ϕ , n is found as follows. Let us consider two values of ϕ around the point $\phi \rightarrow 0.5$,

such that $\phi_1 + \phi_2 = 1$. At these values of ϕ , $\frac{\partial \lambda_c}{\partial \phi}$

should nearly be same, as $d\phi_1 = -d\phi_2$. Thus,

$$\frac{\partial \lambda_c}{\partial \phi} = \frac{\partial \lambda_c}{\partial \phi_1} = - \frac{\partial \lambda_c}{\partial \phi_2} \quad \dots (9)$$

Similarly, for the above mentioned values of ϕ we also find $\frac{\partial n}{\partial \phi}$, i.e. as $\phi \rightarrow 0.5$. Eq. (5) yields

$$\frac{1}{\lambda_c} \frac{\partial \lambda_c}{\partial \phi} = \frac{\partial n}{\partial \phi} \ln \left\{ \frac{(\lambda_1 + \lambda_2)^2}{4\lambda_1 \lambda_2} \right\} + 2 \frac{(\lambda_1 - \lambda_2)}{(\lambda_2 + \lambda_1)} \quad \dots (10)$$

because

$$\left\{ \frac{n}{\lambda_{\parallel}} + \frac{(1-n)}{\lambda_1} \right\} \rightarrow \frac{2}{(\lambda_2 + \lambda_1)}$$

One notes that $\frac{1}{\lambda} \frac{\partial \lambda_c}{\partial \phi}$ gives equal slopes at ϕ_1 and ϕ_2 through Eq. (9). The variation in ϕ for $\phi \rightarrow 0.5$ affects

$\left(\frac{\partial n}{\partial \phi} \right)$ only in Eq. (10). Thus one has

$$\frac{\partial n}{\partial \lambda_1} = - \frac{\partial n}{\partial \lambda_2} \quad \dots (11)$$

Substituting Eqs (9) and (11) in Eq. (5) and on simplifying we get

$$\begin{aligned} & \left\{ \frac{n}{(1-\phi_1)\lambda_1 + \phi_1\lambda_2} + \frac{(1-n)}{(1-\phi_1)\lambda_2 + \phi_1\lambda_1} \right\} \\ &= \left\{ \frac{n}{\phi_1\lambda_1 + (1-\phi_1)\lambda_2} + \frac{(1-n)}{\phi_1\lambda_2 + (1-\phi_1)\lambda_1} \right\} \end{aligned} \quad \dots (12)$$

Evaluating n from Eq. (12),

$$n = \frac{\left\{ \frac{1}{\phi_1\lambda_1 + (1-\phi_1)\lambda_2} - \frac{1}{(1-\phi_1)\lambda_1 + \phi_1\lambda_2} \right\}}{2 \left\{ \frac{1}{\phi_1\lambda_1 + (1-\phi_1)\lambda_2} - \frac{1}{(1-\phi_1)\lambda_1 + \phi_1\lambda_2} \right\}} = \frac{1}{2} \quad \dots (13)$$

This can be further tested. As $\phi \rightarrow 0.5$, $\lambda_{\parallel} \lambda_{\perp} \rightarrow \lambda_1 \lambda_2$ and Eq. (8) also yields

$$n_1 = \frac{1}{2} \quad \dots (14)$$

2.2 Three-Phase Systems

In a three-phase system, $i=1, 2, 3$, $\phi_1 + \phi_2 + \phi_3 = 1$ and $d\phi_3 = -(d\phi_1 + d\phi_2)$. For such a system, Eq. (4) reduces to:

$$\begin{aligned} \frac{1}{\lambda_c} d\lambda_c &= \frac{n}{\lambda_1} \left\{ (\lambda_1 - \lambda_2) d\phi_1 + (\lambda_2 - \lambda_3) d\phi_2 \right\} \\ &- (1-n)\lambda_{\perp} \left\{ \left(\frac{1}{\lambda_1} - \frac{1}{\lambda_3} \right) d\phi_1 + \left(\frac{1}{\lambda_2} - \frac{1}{\lambda_3} \right) d\phi_2 \right\} \end{aligned} \quad \dots (15)$$

Let us assume that there is a dilute dispersion of the phases λ_1 and λ_2 compared to the dominant phase λ_3 . Here, $d\phi_1 \approx d\phi_2 \approx d\phi$ and $\lambda_{||} \rightarrow \lambda_{\perp}$. Using these limiting conditions for a dilute dispersion of the phases λ_1 and λ_2 into λ_3 at fixed values of ϕ_1 and ϕ_2 , we obtain two limiting expressions as:

$$\frac{1}{\lambda_e} \frac{d\lambda_e}{d\phi} = \frac{n}{\lambda_{||}} \left\{ \lambda_1 + \lambda_2 - 2\lambda_3 \right\} - (1-n)\lambda_{||} \left\{ \frac{1}{\lambda_1} + \frac{1}{\lambda_2} - \frac{2}{\lambda_3} \right\} \quad \dots (16)$$

and

$$\frac{1}{\lambda_e} \frac{d\lambda_e}{d\phi} = \frac{n}{\lambda_{\perp}} \left\{ \lambda_1 + \lambda_2 - 2\lambda_3 \right\} - (1-n)\lambda_{\perp} \left\{ \frac{1}{\lambda_1} + \frac{1}{\lambda_2} - \frac{2}{\lambda_3} \right\} \quad \dots (17)$$

Comparing the above relations, one obtains n for the dilute dispersion of the phases λ_1 and λ_2 as:

$$n = \frac{\lambda_{||}\lambda_{\perp}}{\lambda_{||}\lambda_{\perp} + \left\{ \frac{(2\lambda_3 - \lambda_1 - \lambda_2)\lambda_1\lambda_2\lambda_3}{\lambda_2\lambda_3 + \lambda_1\lambda_3 - 2\lambda_1\lambda_2} \right\}} \quad \dots (18)$$

This expression estimates n for a three-phase system and then λ_e of the system may be obtained through Eq. (3). When $\lambda_1 = \lambda_2$ (i.e. system turns to a two-phase system), Eq. (18) reduces to Eq. (8).

3 Comparison with Experimental Results and Discussion

To test the validity of the values of n estimated by the different expressions, we chose different natural systems. Eq. (8) predicts relative orientations of the two phases to form parallel and perpendicular zones of resistors. This value of n substituted in Eq. (3) yields the value of λ_e . Dispersion of parallel and perpendicular zones of resistors for a three-phase system is predicted through Eq. (18). These values of n used in Eq. (3) estimate λ_e .

Values of λ_e estimated for the two-phase and three-phase systems are reported in Tables 1 and 2 and compared with experimental values. It is observed that by using Eqs (3) and (8), the percentage of deviation of the calculated value of λ_e from the experimental data is minimum compared to other methods. Further, the validity of the relations is tested over three categories of dispersions. It is found that the proposed equations are equally good over the whole range of dispersion.

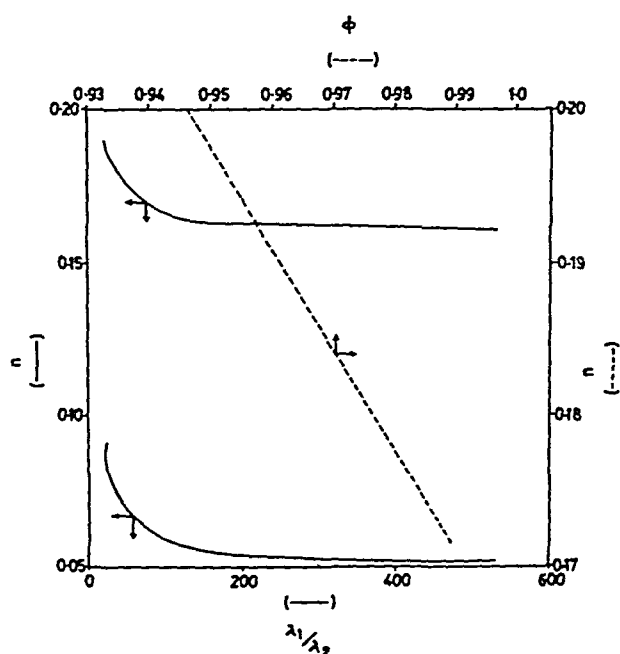
The validity of Eq. (18) is checked in Table 2, where values of λ_e obtained by different methods are com-

Table 1 — Comparison of Calculated Values of λ_e ($\text{W m}^{-1} \text{K}^{-1}$) with Reported Results for Two-Phase Systems

System		λ_1 / λ_2	ϕ	n	Value of λ_c						
					Exptl	Maxwell's relation ⁵	Deviation from exptl data (%)	Cheng's relation ¹⁵	Deviation from exptl data (%)	Present relation	Deviation from exptl data (%)
Category I											
Bismuth powder/ silicone rubber ¹⁶	(i)	21.64	0.05	0.0898	0.4331	0.4355	+0.8	0.4814	+11.2	0.4273	-1.3
	(ii)	21.64	0.16	0.1900	0.5897	0.5708	-3.2	0.6438	+9.1	0.5803	-1.6
Lead power/ silicone rubber ¹⁶	(i)	90.18	0.05	0.0599	0.4626	0.4426	-4.1	0.5108	+10.5	0.4461	-3.6
	(ii)	90.18	0.16	0.1675	0.6626	0.5956	-10.2	0.7132	+7.6	0.6991	+5.5
Aluminium powder/ silicone rubber ¹⁶	(i)	532.08	0.05	0.0517	0.4743	0.4449	-6.2	0.5238	+10.5	0.4782	+0.8
	(ii)	532.08	0.16	0.1613	0.7651	0.6026	-21.3	0.7439	-2.7	0.9107	+9.0
Nickel powder/ silicone rubber ¹⁶	(i)	234.48	0.05	0.0538	0.4590	0.4449	-3.0	0.5214	+13.5	0.4620	+0.7
	(ii)	234.48	0.16	0.1629	0.6556	0.6003	-8.5	0.7333	+11.8	0.8037	+22.6
Category II											
Cellosize/flexol plasticizer ¹⁷		3.03	0.9	0.2286	0.209	0.194	-7.2	0.261	+24.9	0.206	-1.4
Copper/solder ¹⁸	(i)	5.09	0.9876	0.1724	78.8	81.0	+2.8	81.0	+2.8	79.4	+0.8
	(ii)	5.09	0.9864	0.1732	78.8	81.3	+3.2	82.2	+3.0	79.6	+1.0
	(iii)	5.09	0.9737	0.1817	81.1	81.7	+0.7	83.6	+3.0	81.0	+0.1
	(iv)	5.09	0.9714	0.1832	81.7	84.9	+3.9	84.0	+2.8	81.2	-0.6
	(v)	5.09	0.9413	0.2035	83.7	86.3	+3.1	89.2	+6.6	84.8	+1.3
Rajasthan desert sand ¹⁹	(i)	126.98	0.4052	0.5	0.336	1.67	+397.0	1.507	+348.5	0.357	+6.3
	(ii)	126.98	0.4394	0.5	0.312	1.56	+400.0	1.325	+324.7	0.333	+6.7
Blood (37°C) ²⁰	(i)	0.819	0.59	0.5	0.546	0.546	0.0	0.546	0.0	0.546	0.0
	(ii)	0.819	0.56	0.5	0.542	0.543	+0.2	0.543	+0.2	0.539	-0.6
Water/mineral oil ²¹		4.114	0.6	0.5	0.293	0.346	+18.1	0.276	-5.8	0.267	-8.9
Glass/hydrogen ²²		7.88	0.6	0.5	0.459	0.298	-35.1	0.293	-36.2	0.419	-8.7
Uranium oxide/sodium ²³		0.1	0.5	0.5	29.00	25.199	-13.1	37.8	+29.7	28.46	-1.9

Table 2 — Comparison of Calculated and Reported Values of λ_c ($\text{W m}^{-1} \text{K}^{-1}$) for Three-Phase Systems

ϕ_1	ϕ_2	n	Values of λ_c						
			Exptl.	Litchnecker's relation ⁶	Deviation from exptl data (%)	Cheng's relation ¹⁵	Deviation from exptl data (%)	Present relation	Deviation from exptl data (%)
System I: Lead and bismuth powder in silicone rubber ¹⁶ ($\lambda_1 = 34.62, \lambda_2 = 8.309, \lambda_3 = 0.384$)									
0.08	0.10	0.1794	0.692	0.749	+8.2	0.814	+17.5	8.175	+3.3
0.08	0.04	0.1522	0.592	0.623	+5.2	0.656	+10.8	0.596	+0.7
System II: Aluminium and nickel powder in silicone rubber ¹⁶ ($\lambda_1 = 204.258, \lambda_2 = 90.012, \lambda_3 = 0.384$)									
0.06	0.04	0.1089	0.559	0.696	+24.5	0.626	+12.1	0.634	+13.4
System III: Aluminium and bismuth powder in silicone rubber ¹⁶ ($\lambda_1 = 204.258, \lambda_2 = 8.309, \lambda_3 = 0.384$)									
0.04	0.08	0.0873	0.637	0.631	-0.9	0.694	+8.9	0.567	-10.9
System IV: Water and air in calcareous sandstone ²⁴ ($\lambda_1 = 0.6322, \lambda_2 = 0.0275, \lambda_3 = 1.856$)									
0.100	0.045	0.8984	1.415	1.379	-2.6	1.569	+10.9	1.445	+2.1
0.075	0.070	0.8635	1.380	1.275	-7.6	1.581	+14.6	1.310	-5.1
0.134	0.048	0.8898	1.322	1.313	-0.7	1.499	+13.4	1.383	+4.5
0.100	0.082	0.8423	1.2045	1.180	-2.0	1.488	+23.5	1.291	+6.7

Fig. 1 — Variation of n with λ_1 / λ_2 and ϕ .

pared for three-phase systems. It is observed that the present model predicts the λ_c values with a reasonable accuracy, when the phases λ_1 and λ_2 are dilutely dispersed.

The variations of n with λ_1 / λ_2 and ϕ are presented in Fig. 1. At constant dispersion, n decreases exponentially as the ratio λ_1 / λ_2 increases. This indicates that the probability of orientation of the dispersed phase in parallel orientation decreases compared to that of the continuous phase, as the conductivity of dispersed phase increases. Further, Fig. 1 indicates that as $\lambda_1 / \lambda_2 \rightarrow \infty$, $n \rightarrow 0$. The dependence of n on ϕ at a constant

λ_1 / λ_2 ratio is also indicated in Fig. 1. One finds that n has a linear dependence on ϕ . The phase resistors oriented in parallel gradually change to a series orientation as dispersion increases.

Acknowledgement

The authors express their thanks to Prof R C Bhandari, Dr P V Bakore, Mr V Kumar and Dr N S Saxena for suggestions. Financial assistance from CSIR, New Delhi, is gratefully acknowledged.

References

- 1 Archie G E, *Trans Am Inst Min Metall Engrs (USA)*, **146** (1942) 54.
- 2 Wyllie MRJ & Southwick P F, *J Petrol Technol (USA)*, **6** (1954) 44.
- 3 Sauer M C, Southwick P F, Speigler K S & Wyllie M R J, *Ind Engng Chem (USA)*, **47** (1955) 2187.
- 4 Woodside W & Messmer J H, *J Appl Phys (USA)*, **32** (1961) 1688.
- 5 Maxwell J C, *A treatise on electricity and magnetism*, Vol 1 (Clarendon Press, Oxford) 3rd Edn 1904, 440.
- 6 Litchnecker K, *Phys Z (Germany)*, **27** (1926) 115.
- 7 Fricke H, *Phys Rev (USA)*, **24** (1924) 575.
- 8 Brailsford A D & Major K G, *J Phys D (GB)*, **15** (1964) 313.
- 9 Johansen S, *Frost I & Jord N R (Norway)*, **16** (1975) 13.
- 10 Rayleigh L, *Philos Mag (GB)*, **34** (1892) 481.
- 11 Weiner O, *Phys Z (Germany)*, **5** (1904) 332.
- 12 Meredith R E & Tobias C W, *J Appl Phys (USA)*, **31** (1960) 1270.
- 13 Mc Phedran R C & Mc Kenzie D R, *Proc R Soc London Ser A (GB)*, **359** (1978) 45-63.
- 14 Chaudhary D R & Bhandari R C, *J Phys D (GB)*, **1** (1968) 815.
- 15 Cheng S C & Vachon R I, *Int J Heat & Mass Transfer (USA)*, **12** (1969) 249.

- 16 Cheng S C, Law Y S & Kwan C C Y, *Int J Heat & Mass Transfer (USA)*, **15** (1972) 355.
- 17 Nahas N C & Couper J R, *Res Rep Ser No 7* (University of Arkansas, Arkansas, USA) 1966.
- 18 Lee H J & Taylor R E, *J Appl Phys (USA)*, **47** (1976) 143.
- 19 Kumar V & Chaudhary D R, *Indian J Pure & Appl Phys*, **18** (1980) 984.
- 20 Ahuja A S, *J Appl Phys (USA)*, **37** (1974) 765.
- 21 Kaudsen J G & Wand R H, *Ind Engng Chem (USA)*, **50** (1958) 1667.
- 22 Prins J A, Schenk J & S Charm A J G L, *Physica (Germany)*, **16** (1950) 379.
- 23 Huetz J, *Progress Heat & Mass Transfer (GB)*, **5** (1972) 285.
- 24 Sugawara A, *Jpn J Appl Phys (Japan)*, **30** (1961) 899.

Design of a Pulsed Xenon Ion Laser

R CHARI & G CHAKRAPANI*

Department of Physics, Indian Institute of Technology, Kanpur 208 016

Received 8 April 1986

The fabrication details and main operating characteristics of a pulsed xenon ion laser are reported. The lasing transitions studied belong to XeIV and exhibit very high gains in the pulsed regime. Thus, the high peak power output coupled with the fairly long pulse widths obtainable ($< 1 \mu\text{s}$ to $50 \mu\text{s}$) makes this laser a useful tool for many experiments in nonlinear optics.

1 Introduction

Ion lasers are suitable as sources of coherent radiation for many scientific and industrial applications¹. Noble gas ion lasers form an important class of ion lasers capable of both pulsed and CW operation in the visible and near UV and near ir regions of the spectrum.

Most of the transitions observed in noble gas ion lasers arise from singly-ionized species such as the well known blue, green lines of Ar^+ . Transitions from multiply ionized species are more easily excited in the pulsed mode due to the higher currents required. Among these transitions, is a set of lines belonging to xenon laser most powerful in the pulsed mode. The highest power output reported so far in these lines is 80 kW (Ref. 2).

*Present address: Department of Physics, Alabama A&M University, Normal, Alabama 35762, USA.

In this paper, we present the constructional details and characteristics of a pulsed xenon ion laser which can be easily fabricated in the laboratory to give up to 1 kW of peak output power in the visible region.

2 Plasma Tube Construction and Processing

The average input power in pulsed lasers is very much lower as compared to CW lasers so that elaborate cooling arrangements for the plasma tube are not required. In the present work, pyrex glass tubes have been used to construct plasma tubes according to the design shown in Fig. 1.

To a tube of required length (we used 1 m) and diameter, two tungsten pins are attached through small side tubes (cups). A small pellet of pure indium metal is dropped in each cup and melted in place around the pins to form the electrodes. This type of cold cathode has been found to be more advantageous compared

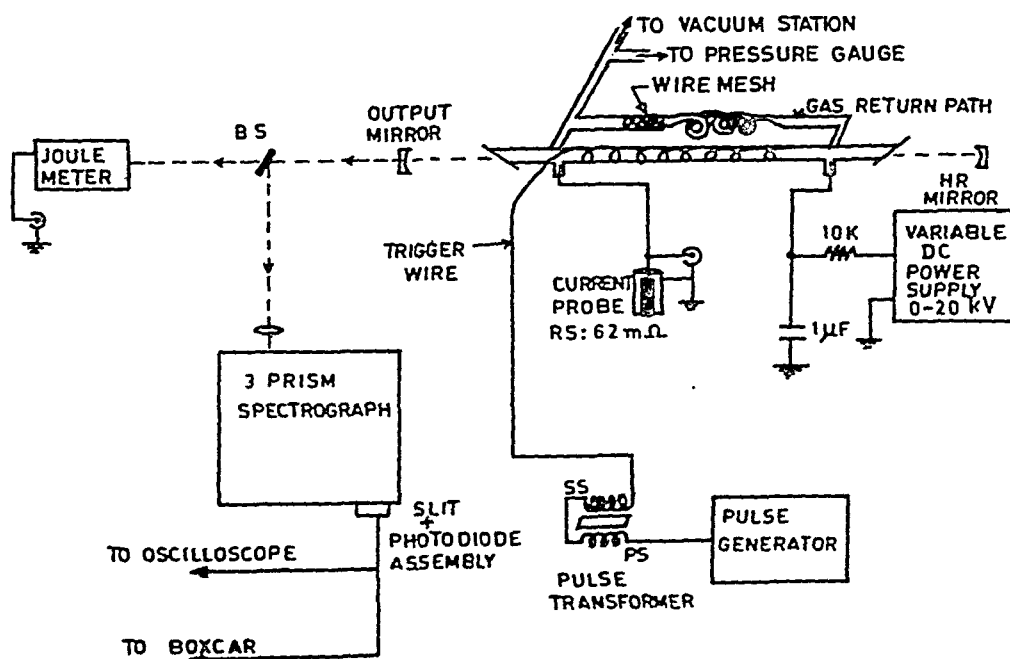


Fig. 1 – Block diagram of the experimental set-up

to large, current-limited thermionic cathodes in the domain of high peak currents (≥ 500 A)³.

A large diameter tube is attached in parallel to the plasma tube to serve as the ballast and gas return path. To ensure that the discharge does not run through the return path, its length can be made longer by giving it a helical form and inserting a length of wire mesh as shown in Fig. 1.

Brewster terminations of slightly larger diameter are attached to the plasma tube ends. The processing of the plasma tubes involved the following steps. Before attaching a tube to the vacuum station, it is cleaned with sodium hydroxide and chromic acid. Then it is thoroughly washed with distilled water and finally rinsed with GR grade acetone. Then it is connected to the vacuum station and quartz windows are attached at the ends by an epoxy resin (Torr seal). The tube is evacuated and degassed by baking it at 150 °C. The vacuum system consists of an oil diffusion pump with an LN trap attached.

After this initial processing, the plasma tube is filled with spectroscopic grade xenon gas (99.995% pure) and the discharge is run at a repetition rate of several (15-20) pulses per second. This process releases the contaminating gases adsorbed by the glass walls of the plasma tube as well as the electrodes. After running the discharge for a few hours, the tube is flushed out and refilled. This process is repeated several times to reduce the level of contamination. To further ensure that during the experiment the contamination due to discharge-produced impurities is low, the tube is flushed out and refilled after several hours of continuous operation.

Plasma tubes used in this work had an active length of 100 cm and total length of about 125 cm. The bore diameters tried in this work were 10, 8, 6.3, 4, 2.7, and 1.5 mm. Xenon gas pressures used were in the range 3–20 mT.

3 Optical Cavity

The optical cavity has been formed using mirrors of equal radii of curvature of 2 m, separated by 145 cm. Two sets of mirrors have been used in our experiments. One set consists of a pair of Spectra Physics mirrors normally used with their model 165 argon ion laser. These mirrors are referred to as Ar^+ mirrors in the rest of the paper. The second set is a pair of He-Ne mirrors.

4 Power Supply

The excitation energy for the discharge has been supplied by discharging 1.0 μF capacitor which is charged from a variable dc power supply. The voltage to which the capacitor is charged has been measured with an HP VTVM (model No. 4108). With 1.0 μF capacitor, the highest voltages used were 6-7 kV, the current pulse width was 10 μs . Reducing the capacitance to 0.1 μF , allowed us to reach 12-13 kV where discharge instability sets in and lasing stopped. The laser pulse widths were 5 μs and 1 μs with 1 μF and 0.1 μF capacitors respectively.

To initiate the discharge, a high voltage (15 kV) pulse is applied to the plasma tube wall through a copper wire wound round it for nearly three quarters of its length, commencing from the cathode end. This pulse comes from an EG & G pulse transformer (model No. TS 185), the primary of which is fed with a 300 V pulse generated in a variable prf pulse generator. The circuit is given in Fig. 2. The pulse repetition could be varied from 1 pulse in 5 s to 50 pps. However, during the experiment the laser was operated at 1-2 pps so that thermal and gas pumping effects are negligible.

5 Detection System

The laser output was monitored using a spectrograph, exit slit and PIN photodiode combination so that power output at each lasing wavelength could be

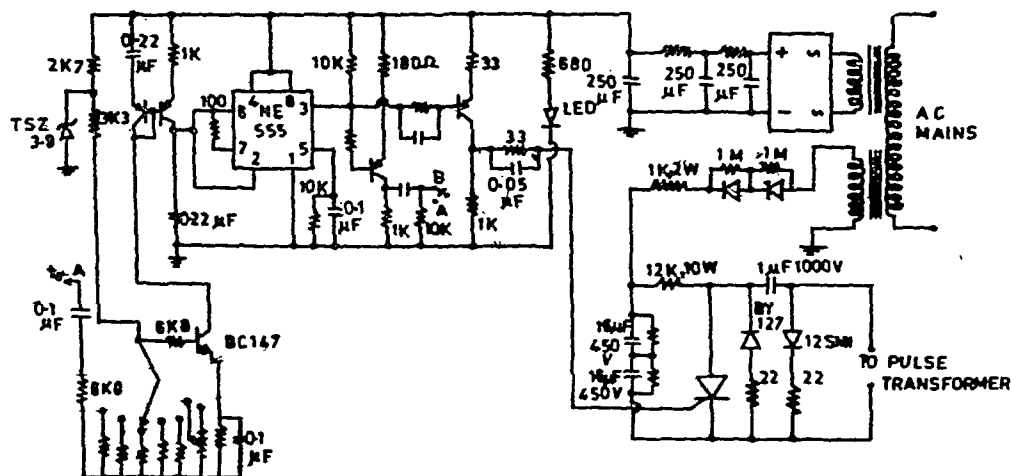


Fig. 2 – Pulse generator circuit

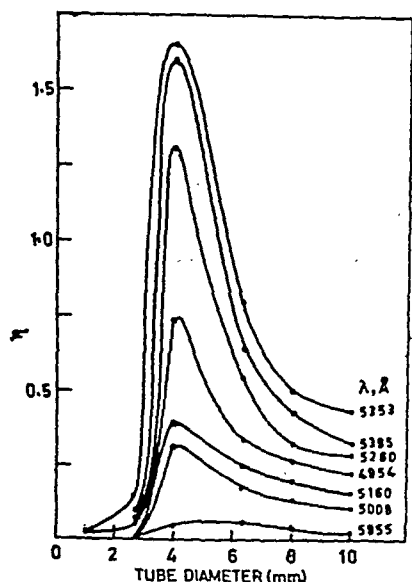


Fig. 3 - η vs tube diameter. Values of η multiplied by appropriate scale constant

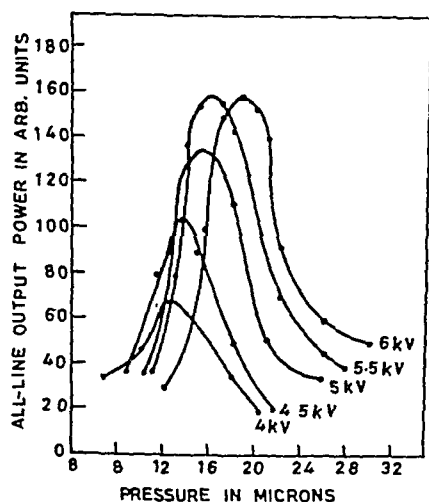


Fig. 4 - All-line power output vs pressure for different excitation voltages. Tube diameter: 6.3 mm

measured. The output of the photodiode was fed to a boxcar integrator to measure the total pulse energy⁴.

6 Results

We observed lasing at the following wavelengths: 4954.13, 5007.8, 5159.08, 5260.19, 5352.92, 5394.62 and 5955.67 Å. With Ar⁺ mirrors, the orange line (5955.69 Å) lased only occasionally while the other six lased strongly. To study the behaviour of this line, He-Ne mirrors were used.

As mentioned in Sec. 2, we tried several plasma tubes of different bore diameters. Defining an efficiency factor (η), as the ratio of output power at each wavelength to total input energy (under optimum operating conditions), the variation of η versus tube bore diameters showed a peak around 4 mm (Fig. 3).

The optimization of laser output has to be done with respect to both pressure and the excitation vol-

Table 1 - Distribution of Total Output Power at All-Line Optimum Pressure

[Tube diam, 6.3 mm; excitation voltage, 4.5 kV; energy storage capacitor, 1 μ F]

Wavelength Å	Peak output power W
5394.62	131
5352.92	213
5260.19	147
5159.08	4
5007.8	36
4954.13	69

Table 2 - Maximum Small Signal Gains (in dB/m) observed at Different Wavelengths

[Tube diameter = 4 mm]

Wavelength Å	Capacitance, μ F	
	1.0	0.1
4954.13	5.5	11.2
5007.8	3.8	4.0
5159.08	3.8	4.2
5260.19	3.7	6.9
5352.92	8.3	12.5
5394.62	6.9	5.5
5955.67	2.7	1.0

tage. A typical curve showing the change in output power with these parameters is shown in Fig. 4. It is further observed that lasing at each wavelength is optimized at different pressures. At the pressure where the total all-line output power is maximum, the distribution of power among various lines is given in Table 1. At higher pressures, the relative output at the following wavelengths becomes higher: 5394.62, 5260.19, 5007.8 and 5955.67 Å. At very low pressures, the output at wavelengths 4954.13 and 5159.08 Å becomes stronger⁴.

We also measured the small signal gain at each wavelength by introducing measurable losses in the cavity till lasing is quenched. The values observed in our work are the highest reported so far⁵. The highest values of gain coefficients observed at each wavelength are given in Table 2.

7 Conclusion

In laboratory experiments (especially in spectroscopic applications) this laser can serve as an attractive alternative to the pulsed argon ion laser due to the wider range of wavelengths and higher peak power available. It can also be used to pump dye lasers efficiently⁶⁻⁸.

Acknowledgement

The authors wish to acknowledge the technical help provided by Mr Bhaskaran and Mr Sadagopan.

References

- 1 Davis C C & King T A, *Gaseous Ion Lasers*, in *Advances in quantum electronics*, Vol. 3, edited by B W Goodwin (Academic Press, New York) 1975, 418.
- 2 Harper C D & Gunderson M, *Rev Sci Instrum* (USA), **45** (1974) 400.
- 3 Simmons W W & Witte R S, *IEEE J Quantum Electron* (USA), **6** (1970) 648.
- 4 Chari R & Chakrapani G, *Physica C* (Netherlands), **138** (1986) 344.
- 5 Chari R, *Studies on some visible lasing transitions in pulsed XeIV laser*, Ph D thesis, Indian Institute of Technology, Kanpur, 1984.
- 6 Chari R & Chakrapani G, *Appl Opt* (USA), July (1986), in press.
- 7 Gallardo M, Duchowicz R, Tocho J O, *et al.*, *IEEE J Quantum Electron* (USA), **15** (1979) 541.
- 8 Hansch T W, Schawlow A L & Toschek P, *IEEE J Quantum Electron* (USA), **9** (1973) 553.

Plasma Density & Electron Temperature Enhancements in a Constricted Type Plasma Source

F F ELAKSHAR*

Physics Department, Faculty of Science, Mansoura University, Egypt

&

A M NOSSAIR†

Physics Department, Faculty of Science, Azhar University, Egypt

Received 16 September 1985; revised received 13 June 1986

An experimental study of plasma density and electron temperature enhancements in the arc of a constricted type of plasma source has been performed at different gas pressures. At low pressures (less than 0.2 Torr), the plasma was fully ionized, the density maximum ($\approx 10^{14} \text{ cm}^{-3}$) and the electron temperature high (20 eV). Only weakly ionized plasma was formed in the high pressure range (0.2-1 Torr), and the density and temperature decreased by about an order of magnitude. The experimental data are explained on the basis of established theories of electrical discharges through gases.

1 Introduction

Initiation of a high density plasma is always possible when a low pressure arc is formed between a hot cathode and a hollow anode. Moreover, if the discharge is strongly concentrated by using an additional hollow intermediate electrode and by applying a strong axial magnetic field, an enhanced plasma density and a high degree of ionization are formed¹. Also the large electric field formed between the electrodes may accelerate the electrons and high energy electrons are ejected out². Description and investigation of this type of plasma sources (such as the duoplasmatron) have been extensively discussed in the literature³⁻⁵. However, the physical processes governing the behaviour of the discharge inside the source and the theoretical explanation received less attention. Since the geometry of the plasma source as well as a large number of parameters influence the density, magnetic field distribution and the diffusion of ions in the plasma, it is extremely difficult to predict the optimum conditions for adopting a plasma source to a particular application. Hence each set-up is considered separately regarding the variation of its characteristics with design parameters.

Previous measurements⁶ proved that a plasma of the duoplasmatron type is fully ionized at certain pressures. The various factors and processes influencing the density of such plasmas are: (i) discharge current, (ii) radial and longitudinal electric field, (iii) ionization processes, (iv) shape of plasma

boundaries and (v) diffusion processes toward the discharge tube wall. Considering these factors, Von Engle and Steenbeck⁷, and more recently Lejeune⁸, derived expressions for estimating the plasma density. The study of ion losses either by diffusion⁹ or under the influence of the radial electric field¹⁰ leads to expressions for electron temperature. These expressions for density and temperature are used to explain the experimental data of the arc discharge.

2 Experimental Procedure

A schematic illustration of the plasma source is given in Fig. 1. It consists mainly of a gas inlet valve, a high energy electron source (filament) working also as a cathode, a hollow intermediate electrode (1 mm dia) used for mechanical confinement of the plasma and a hollow anode (2 mm dia). The filament and the

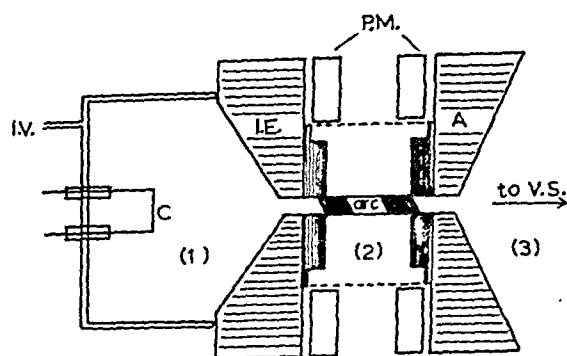


Fig. 1—Plasma source layout [I.V: gas inlet valve, C: cathode (filament), I.E: hollow intermediate electrode, P.M: permanent magnets, A: hollow anode, V.S: vacuum system. Dotted lines represent edge of the tuflon tube. Parts: (1) cathode region, (2) arc region and (3) region of output plasma]

Present addresses:

* Al-Ahsa TT College, Post Box No. 2313, Hufuf, Saudi Arabia

† Faculty of Science, Saraa University, Yemen

other electrodes are water cooled because of the high temperature (2000-3000 °C) inside the source. An arc is formed between the hollow intermediate and anode electrodes. An insulating PTFE tube is fixed between the two electrodes. This tube contains a glass window which allows observation of the arc discharge. A magnetic confinement is obtained using two permanent magnets surrounding the insulating tube. The magnetic field is inhomogeneous (Fig. 2) and its maximum is about 3000 G. Vacuum is obtained by connecting the anode to a vacuum system which produces residual air pressure less than 10^{-6} Torr. Operating gas pressure is about 10^{-5} - 10^{-4} Torr in the vacuum system, as measured by an ionization gauge. This corresponds to a pressure of about 0.1-1 Torr in the arc region and 1-4 Torr in the cathode region, as measured by a Macleod gauge. The discharge is initiated by 3000 V and the arc is then self-sustained.

Because of the high power density in the arc which causes excessive heating and damage to probes, determinations of the arc parameters are made using spectroscopic techniques. Arc emission spectra are observed using a monochromator-cum-photomultiplier and the output is plotted on a chart recorder. The hydrogen continuum intensity is used to estimate¹¹ the values of plasma density. The electron temperatures (T_e) are measured using the technique described by Griem¹². Ratios of line-to-line or line-to-continuum intensities are determined using the above set-up for calculating T_e . The output plasma (injected into the vacuum system) is detected by a single probe fixed at 15 cm from the anode hole.

3 Results and Discussion

Following the experimental procedure outlined above, the variation of plasma density N_p as a function of the gas pressure was measured. In Fig. 3, the

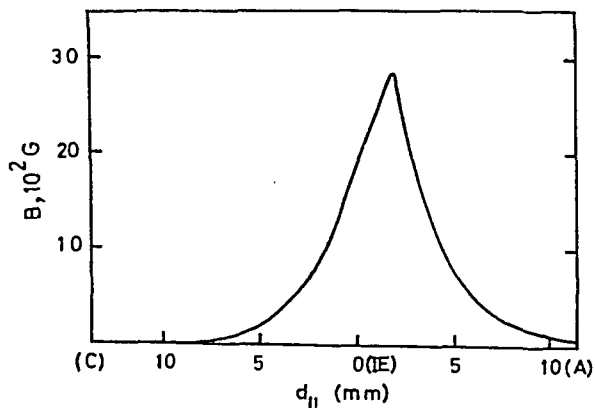


Fig. 2—Magnetic field distribution as measured by a fine Hall-probe. ($d_{||}$ represents the distance along the plasma device axis. The zero distance refers to the I.E. surface, A is the anode and C the cathode.)

experimental data are compared with the theoretical prediction based on expressions due to Von Engle and Steenbeck⁷ and Lejeune⁸. According to Von Engle and Steenbeck⁷, the plasma density N_p is related to the electron drift velocity (v_d), the discharge current ($I_{dis.}$) and tube radius (R) by:

$$N_p = \frac{I_{dis}}{1.36 e v_d R^2} \text{ cm}^{-3} \quad \dots (1)$$

Eq. (1) was used to find N_p at different values of p for a fully ionized arc (low pressure) taking into consideration the following assumptions: (i) The drift velocity v_d in the direction parallel to the magnetic field is nearly equal to the ion sound speed⁴. (ii) Since R is the electrode radius at a particular distance, the arc radius R_{arc} is used instead of the tube radius. (iii) I_{arc} is set equal to I_{dis} . The expression due to Lejeune⁸ is similar to Eq. (1) except for a new factor γ which represents the reduction of the total current between the cathode and the anode as a result of current losses caused by the intermediate electrode. In other words, γ is the coefficient of ion losses in the intermediate electrode canal and it is taken to be 1/20 for the present calculations where v_d is replaced by the electron thermal velocity v_e . It is seen that the theoretical predictions (curves a and c) agree within 20% of the experimental data (curve b).

High pressure arc is not fully ionized⁷. Collisions between ions and neutral particles dominate and the electron drift velocity is nearly equal to its thermal velocity in this case. Applying these conditions and

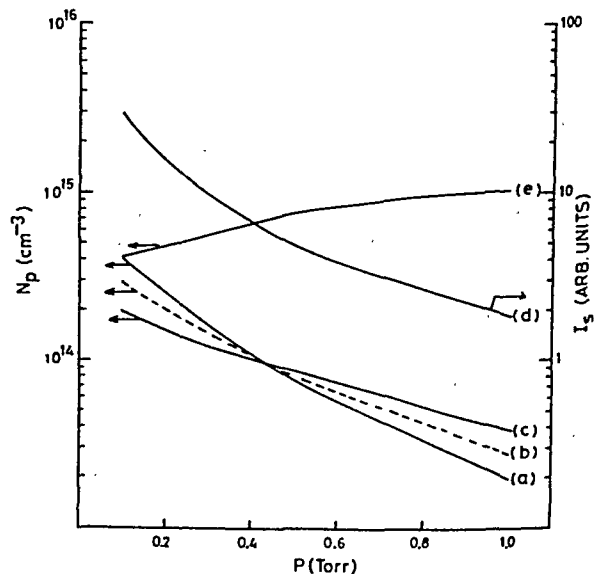


Fig. 3—Comparison of the measured values of the plasma density N_p as a function of gas pressure p (curve b) with theoretical variations based on Eq. (1) of Von England Steenbeck's theory (curve a), Lejeune's theory (curve c) and Eq. (1) modified by changing value of v_d (curve e). Variation of plasma density with pressure measured using single probe at 15 cm from source is also shown (curve d)

modifying Eq. (1), it is seen that the theoretical predictions agree with the experimental data over the high pressure ranges. However, if the value of v_d is taken as the same for low pressures, a discrepancy between theoretical (curve e) and experimental values of N_p is observed. The modified formula of Lejeune agrees only when γ is about 1/2.

Observation of the plasma injected into the vacuum system yields data confirming the density enhancement at low pressure. The measurements were made using a single cylindrical probe which collects plasma at 15 cm away from the source. The ion saturation current of the probe (I_s) was used to represent the plasma density N_p in curve (d), Fig. 3. The probe indicates also that the ion saturation current (I_s), and consequently the plasma density N_p , increases as the arc current is raised up to 14 A (Fig. 4). This is expected from Eq. (1) since N_p is proportional to the discharge current; however, the slight deviation from linearity is attributed to the difference between I_{dis} and I_{arc} as a result of a fraction of current flowing between cathode and the intermediate electrode.

Rates of diffusion across the magnetic field in the arc are investigated at various pressures. At low pressures, Coulomb collisions dominate, since the plasma is fully ionized. Like-particle collisions give rise to a negligible diffusion rate, but in this case, high rates of diffusion are expected because of unlike-particle collisions. The collisions of unlike particles have high frequencies ($\approx 10^6$ - 10^7 s $^{-1}$) at a pressure of 0.1-0.2 Torr. Because of the large disparity between the masses of electron and ion, the diffusion processes are different; electrons diffuse by random-walk process while ions shift slightly in each collision and are moved by frequent bombardments. However, the same rate of diffusion

should be expected for both according to the law of conservation of momentum in collisions. Therefore, ambipolar diffusion takes place in the arc; consequently the rate of diffusion can be calculated using either the semiempirical formula of Bohm *et al.*¹³:

$$D_B = kT_e / 16 e B \quad \dots (2)$$

or the classical diffusion equation¹⁴:

$$D_c = N_p (kT_e + kT_i) / B^2 \quad \dots (3)$$

where D_B and D_c are respectively Bohm and classical diffusion rates. The specific resistivity of the plasma is given by¹⁵:

$$\eta = 3.3 e^2 m_e^{1/2} Z \ln \Lambda / (kT_e)^{3/2} \quad \dots (4)$$

where $\ln \Lambda$ is a factor reported by Spitzer¹⁵. Values of rate of diffusion calculated from different procedures are compared in Table 1. The difference between values of D_B and D_c is attributed to the fact that D_c is used for a quiet plasma and D_B for an unstable plasma. At low pressures, the arc becomes unstable and a starvation mode takes place⁶; therefore, Bohm diffusion is believed to be the dominant process.

At high pressures, the charged particles diffuse as a result of collisions with neutral particles. The mean free-path of ions ($L_i = 0.02$ cm) is about an order of magnitude less than the arc length $L (= 0.2$ cm) and the rate of diffusion D_w in a weakly ionized plasma is given by Simon¹⁶:

$$D_w = \frac{0.41 m_i^2 v_i^2 c^2}{L_i e^2 B^2} \quad \dots (5)$$

where v_i is the ion velocity and c the velocity of light. Value of D_w reported in Table 1 is at least one order of magnitude higher than D_c . Nevertheless, ambipolar diffusion may not take place at high pressures since ions and electrons could not diffuse at the same rate as explained in the following. If ions collide with neutral particles, they will diffuse by a random-walk process in a direction opposite to ∇n (density gradient). This occurs in steps of a length nearly equal to the ion gyro-radius (Larmor radius) r_{Li} . Random-walk process

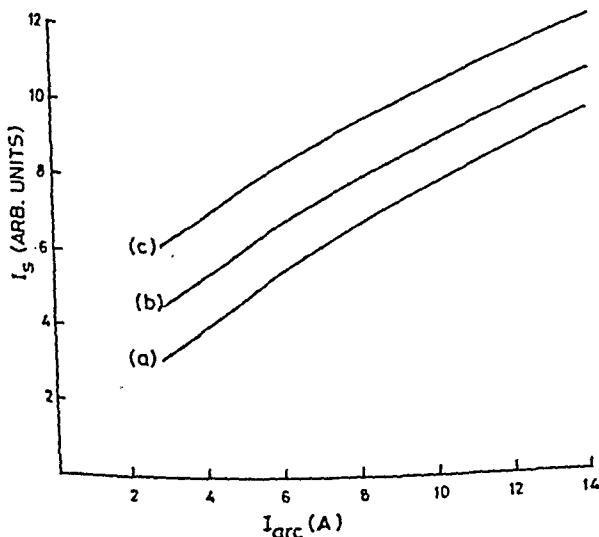


Fig. 4—Variation of ion saturation current of the probe (I_s) with the arc current (I_{arc}) at different pressures [(a) at 1 Torr, (b) at 0.8 Torr and (c) at 0.6 Torr]

Table 1—Values of Diffusion Rates of Particles through Plasma Calculated by Different Procedures

Diffusion formula used	$\eta \times 10^{-15}$ (esu)	Gas pressure (Torr)	Region	Value (cm ² s ⁻¹)
D_B [Eq. (2)]	2.1	0.1	arc	6.3×10^4
D_c [Eq. (3)]	2.1	0.1	arc	1.0×10^4
D_w [Eq. (5)]	6.0	1.0	arc	0.32×10^6
D_s [Eq. (6)]	—	1.0	cathode	30×10^6
D_a [Eq. (6)]	—	4.0	cathode	10×10^6

happens also for the electrons but with slow rates according to the small electron Larmor radius (r_{Le}). A transverse electric field (E_{\perp}) would then be set up. A short-circuit of this (E_{\perp}) is not possible since the field lines are terminated by two conducting electrodes. Unfortunately, there is no simple solution concerning the problem of diffusion through a very short plasma in the literature. The produced field (E_{\perp}) may cause the arc to rotate and develop instability of the plasma. It also must affect ion motion in a direction perpendicular to the magnetic field, i.e. toward the tube wall as discussed later in this paper. Lower rates of diffusion may cause the density enhancement, depicted in Fig. 3. The lower rate of plasma decaying to the wall results in retaining more particles in the plasma of the arc; hence one expects higher N_p at low pressure.

Investigation of diffusion is extended to the cathode region (region 1 in Fig. 1). Apart from the inhomogeneous plasma at the neck of the hollow intermediate electrode, weakly ionized plasma is formed near the cathode where the magnetic field is almost zero and α -T ownsend ionization takes place. Previous observations by Demirkhanov *et al.*¹ have shown that the density is at least one order of magnitude less and the electron temperature four times less than those in the arc region. Consequently, we should expect a density about 10^{13} - 10^{12} cm⁻³ and temperature about 5-0.5 eV in the cathode discharge region. Because of this low electron temperature, the rate coefficient of electron-molecule dissociation (for hydrogen) is negligible. Therefore, the neutral collision cross-section and hence the collision frequency ν_{i-n} are low by less than two orders of magnitude. The ambipolar diffusion rate (D_a) is calculated using the known formula of Chen¹⁴:

$$D_a = \frac{kT_i}{m_i} \gamma_{i-n} \frac{T_e}{T_i} \quad \dots (6)$$

Table 1 shows that D_a is higher than D_w by three orders of magnitude even if the measurements are made at low pressures. This high value of D_a may be attributed to the small cross-section of collisions in the cathode region.

Measurements of the electron temperature (T_e) in the arc region confirm the enhancement of temperature also at low pressures (Fig. 5). By increasing the gas pressure p (or the product Rp , where R is the tube radius), the temperature can be decreased ten-fold. T_e is determined by using the relative line-to-line intensity ratio or that of line-to-continuum. The experimental data are compared with theoretical calculations based on Schottky's⁹ and Tonks and Langmuir's¹⁰ theories. Both the theories assumed that a balance must occur between ions production and losses. In Schottky's analysis, losses of ions were

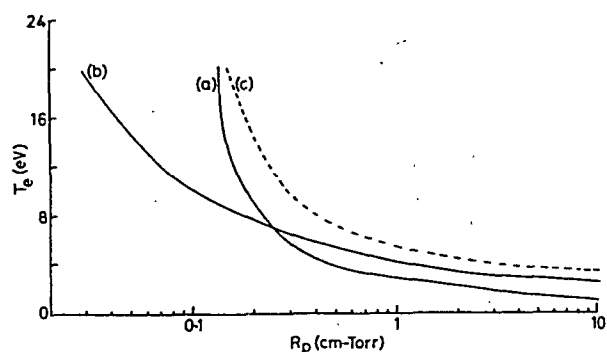


Fig. 5—Comparison of the measured values of the electron temperature (T_e) as a function of Rp (curve c) with calculated variations based on Schottky's theory (curve a) and Tonks and Langmuir's theory (curve b)

attributed to diffusion processes. If the ion mean free-path L_i is small compared to the tube radius (R), by applying Von Engle's expression¹⁷, analysis based on Schottky's theory yields:

$$(1/Rp)^2 = 13.8 \times 10^{19} a V_i (v_e/v_s) Q_{i-n} (T_i/T_{gas}) \\ (1/T_e)(1 + 2kT_e/eV_i) \exp(-eV_i/kT_e) \quad \dots (7)$$

where a is a constant which depends on the gas used, V_i the ionization potential and Q_{i-n} the collision cross-section. Tonks and Langmuir¹⁰ related the ion losses to the influence of the radial electric field and the following expression is derived also using Von Engle's equation:

$$(1/Rp) = 1.49 a V_i (v_e/v_s) (1 + 2kT_e/eV_i) e \\ \times \exp(-eV_i/kT_e) \quad \dots (8)$$

where v_e , v_i , v_s are respectively the velocities of electrons, ions and ion sound. The last parameter is given by:

$$v_s = (kT_e/m_i)^{1/2}$$

Fig. 5 shows that the experimental data approximate closely to those derived on the basis of Schottky's theory (curve a) at low pressures (low Rp) and to those derived on the basis of Tonks and Langmuir's theory (curve b) at high pressures. These conflicting results are explained as follows. At high pressures, a large radial electric field is developed because of the separation of ions and electrons by diffusion. This field imparts to the ions a high drift velocity towards the tube wall. Therefore, ion drift velocity is not a small fraction of the random velocity and the Boltzmann distribution, assumed in the Schottky theory, is no longer valid. As a result of this rapid transport of the ions to the wall, the electron temperature required is higher than that derived on the basis of Schottky's theory. Consequently, diffusion of

ions, under the influence of the radial electric field, approximates more closely to the data.

At low pressures, ambipolar diffusion takes place and Schottky's theory is thus applicable. Hence calculated data agree more closely with the measurements. The magnetic field reduces the diffusion rates and hence the radial electric field required to maintain ambipolar flow, is decreased. Therefore, ions diffuse to the wall with a drift velocity small compared to the random velocity and the assumption of Boltzmann's distribution remains valid. Increase of pressure (or Rp) leads to increase of the effect of the radial electric field on the ion motion. At conditions corresponding to the point of intersection of curves (a) and (b) in Fig. 5, the effects due to the diffusion process and the electric field equalize. At pressures beyond this level, the influence of the radial electric field dominates and hence one could explain the agreement between curves (b) and (c) at high values of Rp .

4 Conclusion

The physical processes governing the behaviour of the constricted type plasma source depend mainly on the gas pressure. Two modes for the operation are found: the first occurs at low pressures and the other at high pressures. In the low pressure mode, fully ionized plasma is formed in the arc region and plasma density and electron temperature enhancements are possible. Diffusion is ambipolar and has a slow rate. At high pressures, gas is weakly ionized and has low density and temperature. Diffusion is no longer ambipolar since random-walk process takes place with different rates for ions and electrons. Short-circuit mechanism does not occur because of the very short length plasma formed in the arc.

Application of the discharge theories due to Von Engle and Steenbeck. Schottky and Tonks and Langmuir has been done successfully. It is concluded that, within the limits of the present experiment, the theories can be used to explain the processes which affect the parameters of the constricted type plasma sources. The theory due to Schottky is valid only for

the low pressure mode, while Tonks and Langmuir's theory describes the high pressure mode more closely. Moreover, Lejeune analysis fits the data if the coefficient of ion losses at the hollow intermediate electrode canal is set equal to $1/20$ and $1/2$ for the two modes respectively.

Acknowledgement

The authors gratefully acknowledge their indebtedness to Prof M G Rusbridge and Dr K Phillips for their encouragement and helpful discussions. Thanks are also due to the Plasma Group, Institute of Science and Technology of the Manchester University, for providing experimental facilities.

References

- 1 Demirkhanov R A, Frohlich H, Kursanov V V & Gutkin T T, Ion source with plasma contraction by inhomogeneous field, *B N L Report*, 767 1962, 218.
- 2 Elakshar F F & Nossair A M, *Egyptian J Phys, Part 2*, 15 (1984) 221.
- 3 Burton B S (Jr), The duoplasmatron: Theoretical studies & experimental observations, *ARS Conf on Electrostatic Propulsion*, November 1960.
- 4 Jacobsen R A & Eubank H P, *Plasma Phys (GB)*, 15, (1973) 243.
- 5 Watanabe M & Suita T, *Jpn J Appl Phys (Japan)*, 6 (1967) 758.
- 6 Elakshar F F & Phillips K, *J Phys D (GB)*, 13 (1980) 57.
- 7 Von Engle A & Steenbeck M, *Elektrische Gaseitladungen*, (Springer Berlin), Vol 1, 1932; Vol 2, 1934.
- 8 Lejeune C, *Nucl Instrum & Meth Netherlands*, 116 (1974) 417.
- 9 Schottky W, *Phys Z (Germany)*, 25 (1924) 635.
- 10 Tonks L & Langmuir I, *Phys Rev (USA)*, 34 (1929) 876.
- 11 McWhirter R W P, *Plasma diagnostic techniques*, Eds H Huddleston & S L Leonard (Academic Press, New York) 1965.
- 12 Griem H R, *Plasma spectroscopy* (McGraw-Hill New York), 1964.
- 13 Bohm D, Burhop E H S & Massey H S W, *The characteristics of electrical discharge in magnetic fields*, Eds A Guthrie & R K Wakerling (McGraw-Hill, New York), 1949, Ch. 2.
- 14 Chen F F, *Introduction to plasma physics* (Plenum Press, New York), 1974.
- 15 Spitzer I, *Physics of fully ionized gases* (Interscience Publishers, New York), 1956.
- 6 Simon A, *Proc 2nd UN Int Conf on Peaceful Uses of Atomic Energy, Geneva* (International Atomic Energy Agency, Vienna), 32 (1958) 343.
- 17 Von Engle A, *Ionized gases* (Clarendon Press, Oxford), 1955.

Coherent States & Symmetry Breaking in Superfluid ^4He

S K TIKOO, M AHMAD, S B AHMAD & T K RAINA

Department of Physics, University of Kashmir, Srinagar 190 006

Received 30 September 1985; revised received 8 May 1986

Symmetry breaking by the phenomenological disappearance of phase invariance in superfluidity is exploited to study the formation of coherent states in phonon region of superfluid ^4He . The creation of higher excitation visualized from phonons in the system is discussed.

1 Introduction

Coherent states have been discovered by Schrödinger¹ and used in quantum mechanical systems nearly a decade ago². These in the harmonic oscillator problem correspond to the minimum uncertainty positions of momentum states, and are made use of when an oscillator is coupled linearly to a prescribed classical force². These states find a fruitful application in the systematic quantum mechanical description of intense radiation fields for which the classical electrodynamics provides a valid, but incomplete description³. Coherent states have also been investigated in quantum fluids and ordered phenomena^{4,5}.

The coherent states become useful for dealing with superfluid ^4He , for the reason that this system behaves in some sense classically, because the boson modes which exist in this system are highly occupied. This way the function $\psi(r)$ describing the bose field becomes a classical Schrödinger field which describes completely many-boson systems in just the same way as Maxwell field describes the classical limit of quantum electrodynamics.

Heisenberg⁶ and then Nambu and Jona-Lasinio⁷ propounded that the vacuum state of a field theory might be less symmetrical than the basic symmetrical laws, i.e. the field equations. The discussions on the subject of breaking symmetry in field theories had led to the remarkable theorem of Goldstone⁸, according to which there is always a zero mass particle associated with a broken symmetry of a continuous group. This theorem has been exploited to explain the creation of phonons in liquid ^4He , giving rise to the superfluid behaviour at very low temperatures⁹.

Here we exploit the phenomenological phase variance as the broken symmetry condition in superfluidity resulting in the creation of phonons and forming coherent superposition of states. The phase symmetry of the free Hamiltonian can be broken by the interaction terms of the total Hamiltonian. So this approach of broken symmetry leads us to the

production of phonons and the translation of Boson field operator. The creation of phonons is thus a dynamical effect taking place between two particles or sub-systems. In this way, we have gapless excitations in the limit of vanishing momentum. Mathematically it means that by imposing some asymmetric condition on the vacuum state phonons are created and the vacuum state changes into a different possible ground state. This asymmetric condition violates the law of conservation of Hamiltonian.

The study of phonons in the superfluid ^4He is of great interest, because helium is isotropic, has no impurities except a very small amount of ^3He and there are no structural defects apart from vortices which can be usually ignored.

2 Coherent States and Superfluidity

The order parameter $\psi(r)$ for superfluid ^4He is conventionally defined as the thermodynamic expectation value of boson field operator. This order parameter has been chosen to be the coherent state representation of pure quantum states^{4,5}.

The free Bose operator for the superfluid system obeys the following commutation relations:

$$[\Psi(r), \Psi^\dagger(r')] = \delta(r - r') \quad \dots (1)$$

In the Fourier representation:

$$\Psi(r) = \frac{1}{\sqrt{\Omega}} \sum a_k e^{ik \cdot r} \quad \dots (2)$$

where

$$[a_k, a_{k'}^\dagger] = \delta_{kk'} \quad \dots (3)$$

and Ω is the quantisation volume.

When the interactions in the system of bosons are switched on via the interaction Hamiltonian, a translation of the operators occurs as:

$$\Psi(r) = \Psi(r) + \alpha \quad \dots (4)$$

or $a_k = a_k + \alpha$

where α is a c -number. The theory based on Eq. (1) is invariant under this transformation. Translation or displacement term was used by Glauber¹⁰, because Eq. (4) can be induced by a unitary operator of the form:

$$D(\alpha) = \exp\{\alpha_k a_k^\dagger - \alpha_k^* a_k\} \quad \dots (5)$$

In these terms, the vacuum state can be converted to the eigenstate of the operator a_k :

$$|\alpha_k\rangle = D(\alpha)|j, 0\rangle$$

where

$$a_k|\alpha_k\rangle = \alpha_k|\alpha_k\rangle \quad \dots (6)$$

such states are called the coherent states^{2,3,11} and are defined by:

$$|\alpha_k\rangle = \exp\left\{-\frac{1}{2}|\alpha|^2\right\} \times \sum_{n=0}^{\infty} \frac{\alpha_k^n}{\sqrt{n_k!}} |j, n_k\rangle \quad \dots (7)$$

They are normalized, but not orthogonal. However, they do form a complete set^{2,3}. Accordingly the set of all the states of the form:

$$\prod_k |\alpha_k\rangle \equiv |\{\alpha_k\}\rangle \equiv |\{\psi\}\rangle$$

$$\Psi(r)|\{\psi\}\rangle = \psi(r)|\{\psi\}\rangle \quad \dots (8)$$

form a complete set for the many boson system. In Eq. (8), $|\{\psi\}\rangle$ are the eigen states of $\Psi(r)$ with eigen value $\psi(r)$ which is also the order parameter. In this formalism, the order parameter turns out as:

$$\psi(r) = \frac{1}{\sqrt{\Omega}} \sum \alpha_k e^{ik \cdot r} \quad \dots (9)$$

The coherent states are most useful for dealing with many-body systems in which boson modes are highly occupied, i.e. those systems which behave in some sense classically³¹. Such a validity of classical description for the many-particle-Bose system implies superfluidity. Accordingly superfluidity is a phenomenon best suited for an analysis of the properties of coherent states in the classical limit. Such an analysis is slightly tedious for the reason that the states $|\alpha_k\rangle$ are the eigenstates of non-hermitian annihilation operator a_k . Therefore to facilitate our analysis, it is proper to pursue the classical limit by introducing a coordinate q and its conjugate momentum p , i.e. we take

$$q_k = \frac{1}{\sqrt{2}}(a_k^\dagger + a_k); p_k = \frac{2}{\sqrt{2}}(a_k^\dagger - a_k) \quad \dots (10)$$

This leads us to³

$$\langle q'|\alpha\rangle = \pi^{-1/4} \exp\left\{-\frac{1}{2}(q'-q)^2 + ip(q'-q) + \frac{1}{2}p^2\right\} \dots (11)$$

where

$$\alpha = \frac{1}{\sqrt{2}}(q + ip) \quad \dots (11a)$$

and $|q'\rangle$ are eigenstates of the operator q_k . In this formalism, the coherent state is a Gaussian wave packet centred at q in the coordinate representation and at p in the momentum representation. This wave packet in either representation becomes very narrow in the classical limit, i.e.

$$\langle n \rangle = \langle \alpha_k | a_k^\dagger a_k | \alpha \rangle = |\alpha_k|^2 \gg 1 \quad \dots (12)$$

This means that $\hbar|\alpha_k|^2$ remains finite as $\hbar \rightarrow 0$. In this way, Eq. (11) becomes a Dirac δ -function. Thus coherent states provide a representation for the quantum mechanical or semi-classical systems.

When the Boson mode k with occupation $|\alpha_k|^2$ is large enough so that the classical approximation is valid, then the Hamiltonian equations of motion for this system are:

$$dp_k/dt = -\partial H/\partial q_k, dq_k/dt = \partial H/\partial p_k \quad \dots (13)$$

These with the help of Eq. (11a) and (9) give:

$$\frac{d\psi(r)}{dt} = -i \frac{\partial H}{\partial \Psi^*(r)}; \frac{d\Psi^*(r)}{dt} = \frac{i\partial H}{\partial \Psi(r)} \quad \dots (14)$$

If

$$\psi(r) = f(r) \exp(i\varphi(r)) \quad \dots (15)$$

with f and φ being the real functions of r , then in a pure coherent state or in the classical limit $f^2(r)$ is the local density given by:

$$n(r) = \langle \Psi^*(r), \Psi(r) \rangle = |\psi(r)|^2 = f^2(r) \quad \dots (16)$$

In terms of n and φ (action and angle variables), we have Eq. (14) as:

$$\frac{dn(r)}{dt} = \frac{\delta(H)}{\delta\varphi(r)}, \frac{d\varphi(r)}{dt} = -\frac{\delta H}{\delta n(r)} \quad \dots (17)$$

These are equations of motion for superfluidity as derived by Anderson¹². This evidently shows that coherent state representation suits well the phenomenon of superfluidity.

3 Breaking Symmetry and Coherent States

The Hamiltonian of the system of N bosons is given by:

$$H = H_0 + H_1 \quad \dots (18)$$

where

$$H_0 = \sum_k E_k a_k^\dagger a_k; E_k = \frac{k^2}{2m} \quad \dots (19)$$

$$H_1 = \frac{1}{2} \sum_{k,k',q} V_k(q) a_{k+k'}^\dagger a_{k-k'}^\dagger a_k a_q \quad \dots (20)$$

$V_k(q)$ is the Fourier transform of the two-body interaction potential. If $a_k = e^{i\theta} a_k$ (where θ is some phase), then we find that H_0 remains invariant, while H_1 can possess a lower symmetry so that the total Hamiltonian of the system also possesses the lower symmetry. Thus, the phase change makes the Hamiltonian of the system asymmetric so that the conservation law of Hamiltonian is violated. This way, the ground state of the system changes into a different possible ground state. Since in the non-relativistic many-body theory, every local change of state can be described as a production of quasi-particles, the change of ground state into a different possible ground state is intimately connected with the production of phonons. The change in the phase can be brought about by subjecting the system to some external potential. In that case, the magnitude of the phase change equals $T \times t$, where T is the potential and t the time duration for which the system was acted upon the potential¹³. Now the purpose of subjecting the system to some external potential, is to cause dynamic interactions between two particles or two sub-systems in the ground state. This results in (i) the formation of phonons, (ii) translation of the boson field operator and (iii) the production of coherent superposition of states. This is analogous to the production of higher excited states from the oscillating condensed boson states, wherein, when the frequencies of the oscillating condensed bosons become different, we visualize a broken symmetry or an extended non-compact symmetry leading naturally to the excited states¹⁴. The transition probability from the states of oscillating condensed boson to the phonon states is given by¹⁵:

$$\begin{aligned} \tau_{m,0} &= m!(-1)^m \left(\frac{\tanh \theta}{2} \right)^m \\ &\times \left| \sum \frac{(4/\sinh^2 \theta)^\lambda}{2\lambda!(m/2 - \lambda)! \lambda!} \right|^2 \text{ for even } m. \\ &= \frac{m!(-1)^{m-1} \left(\frac{\tanh \theta}{2} \right)^{m-1}}{\cosh^2 \theta} \\ &\times \left| \sum \frac{(4/\sinh^2 \theta)^\lambda}{(2\lambda+1)! \{1/2(m-1) - \lambda\}! (\lambda+1/2)!} \right|^2 \quad \dots (21) \end{aligned}$$

The displacement of boson field operator and a scaling transformation gives¹⁶ the excitation spectrum of superfluid ^4He , which tallies well with that obtained by Landau and Khalitnikov¹⁷.

In physical terms, we can bring about a phase change by rotating the entire vessel of He-II system about its vertical axis of rotation. Such a rotation of the entire vessel called an active transformation has no physical significance in the volume limit $\Omega \rightarrow \infty$.

Again the entire phonon spectrum in superfluid ^4He is to be understood in the limit $\Omega \rightarrow \infty$ and if we go out of the volume limit, we are going out of the Fock space, in which the original boson field operators are defined⁹. Thus we consider a passive transformation, i.e. bringing about of a coordinate transformation in the opposite sense. This transformation can be performed in any Fock representation in which Ψ is defined.

In order to simplify the Hamiltonian of Eq. (18), we consider the Foldy model¹⁸ wherein we limit ourselves to the case where there are only three states in the system, so that k', q, k take values $-1, 0, +1$ only, such that $E_{\pm 1} = E$; $V_{\pm 1} = V$; $E_0 = 0$ and $V_0 = 0$. For $V=0$, the ground state would consist of all the N particles in the zero momentum state. As the zero momentum state is macroscopically occupied, we may take the operators a_0 and a_0^\dagger as equal to a c -number viz. $\sqrt{N_0}$ where $N_0 = \langle a_0^\dagger a_0 \rangle$. This is the physical assumption which gives rise to the superfluid character of the model¹⁸. Accordingly the reduced Hamiltonian becomes:

$$\begin{aligned} H_{\text{red}} &= \frac{1}{2} N_0^2 V_0 + \sum (E_k + N_0 V_k + N_0 V_0) a_k^\dagger a_k \\ &+ \frac{1}{2} N_0 \sum V_k (a_k^\dagger a_{-k}^\dagger + a_k a_{-k}) \quad \dots (22) \end{aligned}$$

This Hamiltonian is further simplified by the use of the generators of a non-compact group $SU(1,1)$ which describes the excited states up to the phonon level¹⁴. The set of linear canonical transformation used for diagonalizing the Hamiltonian to solve the problem of superfluidity forms also a direct product of the group $SU(1,1)$. The generators of this group $SU(1,1)$ obey the following commutation relations:

$$\begin{aligned} [j_1, j_2] &= -ij_3; [j_2, j_3] = ij_1 \\ [j_3, j_1] &= ij_2; [J^+, J^-] = j_3 \\ [j_3, J^\pm] &= \pm J^\pm \end{aligned}$$

$$\text{where } J^\pm = \frac{1}{\sqrt{2}} [ij_2 \pm j_1] \quad \dots (23)$$

So the eigenvalues are obtained by solving the Schrödinger equation:

$$H|\Psi_k\rangle = E_k|\Psi_k\rangle \quad \dots (24)$$

Its solution is simplified by rotating away one of the generators j_1 or j_3 by a certain angle θ about j_2 axis, i.e. bringing about a coordinate transformation to have a phase change as mentioned earlier. This is equivalent to having a Bogoliubov's canonical transformation¹⁹ of the form:

$$\begin{aligned} R(\theta)j_1R^{-1}(\theta) &= \cosh \theta j_1 + \sinh \theta j_3 \\ R(\theta)j_3R^{-1}(\theta) &= \cosh \theta j_3 + \sinh \theta j_1 \quad \dots (25) \end{aligned}$$

The value of θ , however, depends upon whether we rotate away from j_1 or j_3 . This also depends upon whether the potential is attractive or repulsive, as for the attractive potential, $\theta = \tanh^{-1} \mu$ and for the repulsive potential^{14,20} $\theta = \coth^{-1} \mu$ where $\mu = (1 + E/N_0 V_k)$. With attractive potential, we obtain a continuous spectrum as that of the spectrum of non-compact generator j_1 and with the repulsive potential, the spectrum we obtain is discrete and integer spaced as that of the spectrum of the compact generator j_3 which is also discrete and integer spaced.

For the unitary representation, the spectrum is bounded from below and is obtained by solving the eigenvalue equation²¹

$$j_3 |j, n\rangle = (n + \sigma) |j, n\rangle \quad \dots (26)$$

where $\sigma = -j_k$

Accordingly we get:

$$E_1 = (2n + 1 + |\Delta_k|) E'_k - N_0 V - E_k \quad \dots (27)$$

where

$$E'_k = (E_k^2 + 2E_k N_0 V_k)^{1/2} \quad \dots (28)$$

and $n = 0, 1, 2, \dots$

Eq. (28) represents the Bogoliubov spectrum.

Thus the coherent superposition of states in the phonon region of the superfluid ⁴He are obtained by applying a 'Block rotation' to an extremal (vacuum) state in a semi-bounded²² unitary irreducible representation of the non-compact group SU (1, 1).

i.e.

$$\begin{aligned} |\alpha'_n\rangle &= R^{-1}(\theta) |J, 0\rangle = e^{-iJ_2 \theta} |J, 0\rangle \\ &= \sum (-1)^{S_n/2} \left(\frac{\theta}{\sqrt{2}} \right)^n \left\{ \frac{\Gamma(J+n+1)^{1/2}}{\Gamma(J-n+1)^{1/2} \Gamma(n+1)} \right\} J^{\dagger n} |J, 0\rangle \end{aligned} \quad \dots (29)$$

with the ground state defined by:

$$J |J, 0\rangle = 0; e^{-J^-} |J, 0\rangle = |J, 0\rangle$$

The norm of the state is given by:

$$\langle \alpha_n | \alpha_n \rangle = \sum (-1)^{3n} \left(\frac{\theta}{\sqrt{2}} \right)^{2n} \times \left\{ \frac{\tau(j+n+1)}{\tau(j-n+1)} \right\} \left\{ \frac{1}{\tau(n+1)} \right\}^2 \quad \dots (30)$$

From the finite nature of the norm, we conclude that the coherent states $|\alpha_n\rangle$ for all values of n do span the Hilbert space, as in the case with $|N_k\rangle$ forming the basis of the number operator N and entailing the complete orthonormal set¹⁴.

Now after the formation of the coherent superposition of state, we have the boson field operator as:

$$\Psi(r) = \frac{1}{\sqrt{\Omega}} \left\{ \sum a_k \exp(ik \cdot r) + \sum \alpha_k \exp(ik \cdot r) \right\} \quad \dots (31)$$

Accordingly the density matrix becomes:

$$\begin{aligned} \rho(r', r) &= \langle \Psi^\dagger(r') \Psi(r) \rangle \\ &= \frac{1}{\Omega} \sum \langle a^\dagger_k a_k \rangle \exp\{ik(r-r')\} \\ &\quad + \left[\frac{1}{\sqrt{\Omega}} \sum \alpha_k^* e^{-ik \cdot r'} \right] \left[\frac{1}{\sqrt{\Omega}} \sum \alpha_k e^{ik \cdot r} \right] \end{aligned}$$

From Eq. (9) we have

$$\rho(r', r) = \frac{1}{\Omega} \sum \langle n_k \rangle \exp\{ik(r-r')\} + \Psi^\dagger(r') \psi(r) \quad \dots (32)$$

and $\langle n_k \rangle$ is the average number of phonons with momentum k . The first term of the expression Eq. (32) describes the normal (uncondensed) phonons in the system. This term on account of the oscillatory nature of the exponential vanishes when $|r-r'| \rightarrow \infty$ (particle correlations have a finite range). Therefore, it does not exhibit the long-range order. The second term depicts the phenomenon of off-diagonal long range order (ODLRO²³). $\psi^\dagger(r) = \langle \Psi^\dagger(r) \rangle$ is an off-diagonal matrix element between two states which differ only by the addition of one phonon to the condensate. $\psi(r)$ is the condensate wave function and to the extent we ignore fluctuations in the condensate population, $\psi(r)$ is regarded as the expectation value of the operator $\Psi(r)$. The concept of off-diagonal long range order has been introduced by Penrose and Onsager²³ to generalize the criterion of the momentum space condensation for the superfluid helium. The condensation into a given momentum mode was speculated by London²⁴, who assumed that the mechanism responsible for superfluidity should be analogous to the condensation in ideal Bose gas. This phenomenon of the condensation has a deeper relation with the phenomenon of coherence^{4,5}. Again it has been postulated that the condition for the complete coherence of a radiation field is that all correlation functions:

$$\begin{aligned} G^n(x, x') &= T_r \{ \rho \psi^\dagger(x_1), \psi^\dagger(x_2) \dots \psi^\dagger(x_n) \\ &\quad \times \psi^\dagger(x'_n) \dots \psi(x'_1) \} \end{aligned} \quad \dots (33)$$

factor completely³. Yang postulated that if fundamental definition of ODLRO is taken to be the existence of some finite degrees of factorization of an n th order reduced density matrix in the coordinate repre-

sentation, then the definitions of ODLRO and the coherence become identical²⁵. Thus we can say that the second term also depicts the coherence phenomenon in the phonon region of the superfluid helium-4.

4 Study of Phonon Excitation in the System

Phonon in the helium are the excitations of momenta less than 1 \AA^{-1} and the most important of them are those of fairly small momenta in the form of dispersion curve. Phonons produced can interact and decay simultaneously and their coherence character is determined by their uniform frequencies throughout a state. Even if only a single phonon is produced, it has its coherence character because of its uniform frequency throughout a state. This phonon can decay because of the zero-point motion which is always present. The most probable type of interaction is, in general, that which involves the smallest number of excitations. The behaviour of the liquid in phonon region can be accounted for by considering the interactions and decay processes of the excitations as detailed below.

4.1 Phonon-Phonon Interactions

The differential coefficient $dc/d\rho$ giving the dependence of velocity on density of the liquid is an important parameter in the study of magnitude of interaction between phonons and phonons and even between phonons and rotons. From the measurements of Abraham *et al.*²⁶

$$dc/d\rho = 2.84c/\rho_0 \quad \dots (33a)$$

The measurements of structure factor in ^4He as a function of density show²⁷ that the liquid structure factor seems to be shaper and increases in amplitude with the increase in pressure at the temperatures 1.67, 2.20 and 4.24 K. The X-ray scattering measurements used to determine changes in spatial order as a function of temperature at several fixed values of the density show²⁸ that the structure of ^4He is insensitive to the density. Accordingly a suitable experiment, may lead to c independent of ρ . However, so long as this is not well established, the dependence of velocity on density may be taken as valid.

The phonons under consideration in liquid helium can be taken as sound waves with same frequencies (because of coherent nature) and different amplitudes. Considering two such waves with wave-vectors k_1 and k_2 and amplitudes $\Delta\rho_1$ and $\Delta\rho_2$ each of frequency ω which interact such that the wave with wave-vector k_1 produces a local density variation resulting in the local variation of velocity of sound (phonons of different velocities). This change in velocity is equivalent to the change in refractive index which may be considered to produce a diffraction grating having spacing and orientation fixed by k_1 and moving with some phase

velocity c_1 of the wave. The wave with wave-vector k_2 will be scattered by this moving grating and the most intense scattered waves will be those with wave-vectors given by $k_2 \pm k_1$. Accordingly we can say that the two phonons get absorbed into one and produce a new phonon with energy and momentum given by:

$$E_3 = E_1 + E_2 \text{ and } P_3 = P_1 + P_2 \quad \dots (34)$$

or a single phonon may decay into two with energies and momenta given by:

$$E_3 = E_2 - E_1 \text{ and } P_3 = P_2 - P_1 \quad \dots (35)$$

However, the angle between a pair of momenta is very small. Classically the difference between the two processes is that, in the first case the moving grating does work on the second wave, whereas in the second case, the grating absorbs energy from the second wave. So from the physical argument, we find the matrix elements for the phonon-phonon scattering are proportional to $dc/d\rho$. This factor also depends on: (i) the energy of the phonons involved and (ii) the relative directions of their wave-vectors. But the three-phonon process in liquid helium mentioned above seems to be unlikely, because of the fact that the phonons are the longitudinal waves with the same dispersion relation $E = cp$ and c decreases²⁹ with the increasing value of p . Accordingly it is impossible to satisfy both the above conditions for thermal phonons. This is because, the slight curvature in the phonon spectrum results in an energy deficit for the three-phonon process which makes it impossible to satisfy simultaneously the above conservation laws. However, because of the finite life-time of the thermal phonons, their energies are not sharp, therefore, the energy certainties may be sufficient to permit both conditions to be satisfied by a three-phonon process. In particular, when one of the phonon is a low energy quantum of sound, the deficit may be quite small³⁰. Under this situation the three-phonon process may be possible. If the curvature of the spectrum in the phonon region is expressed in terms of the constant γ , then the energy deficit for the three-phonon process with one of the phonons being a low energy quantum of sound is³⁰:

$$\Delta E = 3\gamma p^2 \hbar \omega \quad \dots (36)$$

where p is the momentum of thermal phonon and ω the angular frequency of the sound wave. Hence the simplest permitted reaction would appear to be a four-phonon process. Landau and Khalatnikov¹⁷ obtained by considering the four-phonon process, the dispersion curve for the superfluid ^4He for a small value of p (momentum) as:

$$E = cp(1 - \gamma p^2) \quad \dots (37)$$

4.2. Spontaneous Decay of Phonons

As mentioned earlier, a single phonon if present and having no scattering process therein, can decay into two phonons according to the conditions:

$$E_1 = E_2 + E_3; P_1 = P_2 + P_3 \quad \dots (38)$$

These conditions for $E = cp$ for all p exactly linear reduce to

$$p_1 = p_2 + p_3; P_1 = P_2 + P_3 \quad \dots (39)$$

This can only be possible if the velocities of phonons 2 and 3 are smaller than those of the first phonon and the angle between them negligibly small, otherwise the phonon is stable against decay into two phonons for the reason that the above relation does not hold good. This result can be generalized and we can say that the decay into any number of phonons is impossible only if all the phonons have velocities greater than the velocity of the original phonon. Thus, for a general dispersion law, when a phonon decays, at least one of the phonons produced must have a lower velocity than the original phonon.

For low energy phonons, the velocity increases with the increasing energy. These phonons with increasing energy therefore, always have velocities greater than the velocities of all phonons of low energy. Hence the decay process is possible, however, the difference in their velocities is very small. For phonons of higher energy, the velocity starts to decrease during decay process and some of the lower energy phonons have a higher velocity. The decay possibility then becomes restricted and above some critical energy E_0 , phonons become totally stable against decay. At this stage, there is only the interaction of phonons and this interaction of attractive nature can lead to the bunching of phonon excitations. This bunching of phonons results in the creation of the roton like excitation. So we can say that the roton excitations are the outcome of the bunching of phonons. Accordingly the critical energy at which the phonons become stable against any decay can correspond to the minimum energy required for the creation of rotons. This is vivid from the fact that the value of the critical energy at which the phonons become stable against any decay into a large number of phonons as found by Dyne and Narayanmurti³² at zero pressure is 9.5 K, and as found by Maris³³ is 9.86 K, while the minimum energy required for the creation of roton as calculated from the thermodynamic data is given by:

$$\frac{\Delta}{k_B} = 9.6 \text{ K}$$

and this as calculated from neutron scattering data is²⁹:

$$\frac{\Delta}{k_B} = 8.6 \text{ K}$$

The theory of roton excitation is still far less developed compared to the theory of phonon excitations in superfluid ^4He . According to Anderson³⁶ vortex nucleation in superfluid ^4He is the biggest puzzle in its theory and hence the dynamical formulation of the energy gap needed for the roton excitation is still to be understood by a refined microscopic theory. Much trouble in this regard crops up whenever one wants to describe the overall spectrum of the system. Landau³⁷ tried to obtain some justification for the spectrum from the study of quantum hydrodynamics. However, this is not a complete detailed atomic approach. Encouraged by the idea of the existence of a complete analogy between the production of hadrons and the creation of excitations in condensed matter physics³⁹, one of us⁹ has formulated a theory of roton-like excitations in He-II exploiting the three-dimensional rotation group and by introduction of roton operators, to incorporate roton-like excitations including many states in the roton region of Landau spectrum of superfluid ^4He . Recently two of us³⁴ used the second quantized technique to study the thermodynamic behaviour of roton-like excitation in liquid ^4He . The temperature dependence and density dependence of the energy gap needed for roton-like excitations are obtained from this model and it is found that the temperature dependence of the energy gap is more or less in consonance with the results obtained experimentally²⁹.

5 Conclusion

The phenomenological phase variance is the broken symmetry condition for superfluid ^4He . This phase variance causes a translation of the boson field operator and produces the coherent superposition of the states. The phase symmetry of the free Hamiltonian is broken by the interaction terms of the Hamiltonian. Setting in of the interaction within the system can be treated as the dynamical effect taking place between the particles or the sub-systems, resulting in the creation of phonons and violating thereby the law of conservation of the Hamiltonian thus breaking the symmetry of the ground state. The phonons produced can decay into a number of low energy phonons or interact among themselves. At the stage when the phonons become stable against any decay, there are the possibilities of the bunching of phonons leading to the formation of roton-like excitations.

The coherent states obtained in the phonon region bear a deep interrelation with those in the other sectors of the liquid helium system³⁵. The excitation spectrum obtained by the use of displacement of the boson field

operator and a scaling transformation¹⁶ tallying well with that obtained by Landau and Khalatnikov¹⁷, lends support to this idea of symmetry breaking and production of coherent superposition of states in the phonon region of superfluid helium-4.

References

- 1 Schrodinger E, *Naturwissenschaften* (Germany), **14** (1926) 664.
- 2 Carruthers P & Nieto M M, *Am J Phys* (USA), **33** (1965) 537.
- 3 Glauber R J, *Phys Rev* (USA), **131** (1963) 2766.
- 4 Cumming F W & Johnson J R, *Phys Rev* (USA), **151** (1966) 105.
- 5 Langer J S, *Phys Rev* (USA), **167** (1968) 183.
- 6 Heisenberg W, *Rev Mod Phys* (USA), **29** (1967) 269.
- 7 Nambu Y & Lasino-Jona, *Phys Rev* (USA), **122** (1961) 345.
- 8 Goldstone J A, *Nuovo Cimento* (Italy), **19** (1961) 154.
- 9 Ahmad M, *Czech J Phys B*, (Czechoslovakia), **25** (1975) 1127.
- 10 Glauber R J, *Phys Rev* (USA), **130** (1963) 2529.
- 11 Carruthers P & Dye K S, *Phys Rev* (USA), **147** (1966) 214.
- 12 Anderson P W, *Rev Mod Phys* (USA), **38** (1966) 298.
- 13 Mirman R, *Phys Rev* (USA), **186** (1969) 1380.
- 14 Ahmad M, *Phys Rev B* (USA), **25** (1982) 6673.
- 15 Ahmad M & Tikoo S K, *Transition probabilities in superfluid ⁴He* (International Centre for Theoretical Physics, Trieste) 1985, IC/85/22.
- 16 Ahmad M, Tikoo S K, Bashir S & Raina T K, *Proc Indian Natl Sci Acad A*, **51** (1985) 529.
- 17 Landon L D & Khalatnikov I M, *Zn Eksp Teor Fiz* (USSR), **19** (1949) 709, 637.
- 18 Bassichis W H & Foldy L L, *Phys Rev* (USA), **133** (1964) 935.
- 19 Bogoliubov N N, *J Phys* (USSR), **11** (1947) 23.
- 20 Solomon A I, *J Math Phys* (USA), **12** (1971) 390.
- 21 Ahmad M, *J low Temp Phys* (USA), **23** 5/6 (1976) 673.
- 22 Miller W, *On Lie algebra and some special functions of mathematical physics*, Memoirs of the American Mathematical Soc 50 (Am Math Soc Providence RI) (1964); Miller W, *Lie theory & special function* (Academic Press, New York) 1964.
- 23 Penrose O & Onsager L, *Phys Rev* (USA), **104** (1978) 576.
- 24 London F, *Superfluids* (John Wiley & Sons, New York) 1954.
- 25 Yang C N, *Rev Mod Phys* (USA), **34** (1962) 694.
- 26 Abraham B M, Eckstein Y, Ketterson J B, Kuchnir M & Roach P R, *Phys Rev A* (USA), **1** (1970) 250; **2** (1970) 550.
- 27 Robkoff H N & Hallock R B, *Phys Rev B* (USA), **25** (1982) 1572.
- 28 Wirth F W, Even D A & Hallock R B, *Phys Rev* (USA), **27** (1983) 5530.
- 29 Hensaw D G & Woods A D B, *Phys Rev* (USA), **121** (1961) 1266.
- 30 Wilks J, *The properties of liquid and solid helium* (Clarendon Press, Oxford) 1967, 150.
- 31 Kobe D H, *Phys Rev A* (USA), **5** (1972) 854.
- 32 Dyne R C & Naraynmurti V, *Phys Rev B* (USA), **12** (1975) 1720.
- 33 Maris H C, *Phys Rev A* (USA), **9** (1974) 1412.
- 34 Ahmad M & Tikoo S K, *Proc Indian Natl Sci Acad A*, **52** (1986) in press.
- 35 Ahmad M, Tikoo S K, Ahmad S B & Raina T K, *Symmetric structures of coherent states* (unpublished, communicated).
- 36 Anderson P W, *Macroscopic coherence and superfluidity*, (International Centre for Theoretical Physics, Trieste) 1968 SMR 5/4.
- 37 Landau L D, *J Phys* (USSR), **11** (1947) 9.
- 38 Heisenberg H, *Prog Theor phys* (Suppl) (Japan) Extra No. (1965) 298.

Thermophysical Properties of Syndiotactic Polypropylene

M S MOSTAFA & A GABER

Physics Department, Faculty of Science, Assiut University, Assiut, Egypt

Received 11 April 1986

The temperature dependence of the thermal properties (specific heat, thermal diffusivity and thermal conductivity) of the syndiotactic polypropylene (SSP) studied by means of the plane temperature wave techniques shows that they depend effectively on the temperature and the degree of crystallinity of the material. The recovery temperature of SPP from deformations, as well as the recrystallization temperature have been determined. The thermal conductivity of SPP is found to vary from 1.7×10^{-4} to 3.8×10^{-4} cal cm⁻¹ s⁻¹ K⁻¹ over the range of temperatures investigated (300-410 K). It is deduced that SPP is a good thermal insulator in this range of temperature. The deduction is substantiated by a study using a DTA analyser.

1 Introduction

The use of thermal insulation materials and systems for industrial and commercial insulating fields is very important from the point of view of energy conservation. For this reason, a study of the thermophysical properties of SPP is desirable especially under conditions corresponding to industrial applications, for minimizing the energy loss during the translational processes.

The study of the heat capacity of different types of polypropylene by calorimetric methods has been made by several workers in the last two decades¹⁻⁹. The differential scanning calorimetry (DSC) techniques were used for tracing the recovery of the deformed polymers⁴. In addition, the temperature dependence of the recrystallization kinetics for isotactic polypropylene (PP) has been reported^{4,5}. Further, X-ray techniques and differential thermal analysis (DTA) were used for studying the PP transformations from one form to another as well as the effect of the pressure on the recrystallization temperature³.

In the present investigation, the method of the plane temperature wave is used. Compared to the calorimetric methods known earlier, this method yields more accurate results. Since the temperature dependence of the thermophysical properties of SPP is very important particularly in following its crystallization processes and for judging its suitability for thermal insulation in industry, the results of the study will have a wide appeal.

2 Experimental Procedure

The specimens used in this investigation are syndiotactic polypropylene (SSP) of density 0.821 g/cm³ which are supplied from Naga Hammady Sugar Factory, Egypt. For thermal measurements, disc-shaped specimens (thickness 0.4 cm

and diameter 2 cm) were machined from a sheet stock material. The novelty of the present study rests on the fact, that our measurements are carried out using the plane temperature wave technique with some experimental modifications¹⁰. One surface of the disc-shaped specimen is periodically heated by an appropriate heat source with a small heat capacity. The temperature oscillations of the rear surface are monitored by a copper-constantan thermocouple and recorded by a sensitive x-t recorder. The details of the experimental technique have been described elsewhere¹¹.

The phase shift (ϕ) between the modulated input heat power on one surface and the temperature oscillations on the opposite surface is used to calculate the thermal diffusivity (α) according to the formula¹².

$$\alpha = \frac{\omega L^2}{\phi^2} f(\phi, B) \quad \dots (1)$$

where ω is the angular frequency of the applied heat source, L the thickness of the specimen and $f(\phi, B)$ is a correction function, where B is the Biot number.

The specific heat (C_p) is determined from a knowledge of the absorbed heat power (Q) and the measured amplitude of the temperature oscillations (θ) from the relation¹²:

$$C_p = \frac{Q}{m\omega\theta} f(\phi, B) \quad \dots (2)$$

where m is the mass of the specimen. The maximum error in the determination of the thermal diffusivity and the specific heat is 3.5%.

The thermal conductivity (K) is determined according to the relation:

$$K = \rho \cdot \alpha \cdot C_p \quad \dots (3)$$

where ρ is the density of the sample material. The maximum error in calculating the thermal conductivity is consequently about 7%.

For differential thermal analysis (DTA), very tiny granules of the SPP material under investigation were prepared. These samples and an equal number of glass beads of nearly same weight were mixed and placed in a separate pan in the sample holder chamber of the Du Pont 1090 thermal analyser (instruments division, USA). The glass beads as reference material were chosen in such a way that it matches the SPP sample as closely as possible in thermal properties (thermal diffusivity, specific heat and thermal conductivity) and does not possess any chemical, phase or structural changes over the whole temperature range of the experiment. The DTA runs were carried out at a heating rate of 20 K/min over the temperature range from room temperature to about 420 K. A new sample was used for each DTA run to avoid structural transformations that may have occurred in the preceding cycle.

3 Results and Discussion

The specific heat of SPP (C_p) is plotted against the temperature (T , K) in Fig. 1. It is seen that C_p varies non-uniformly with temperature. C_p increases slowly with temperature up to about 350 K (point b). This increase may be due to the thermal agitation of the structure molecules.

Above 350 K, a slight decrease in C_p takes place with increasing temperature up to about 390 K (point c). This decrease of C_p in this range of temperature (350-390 K) could be interpreted as due to the molecules rearranging themselves to a perfect order. In other words, at about 350 K, the material begins to recover from the deformations that existed in the SPP specimen before the experiment started. This behaviour is in good accordance with the observation that the recovery temperature of PP is⁴ 353 K. This recovery process continues up to 390 K when the SPP material is expected to be completely recovered from deformations.

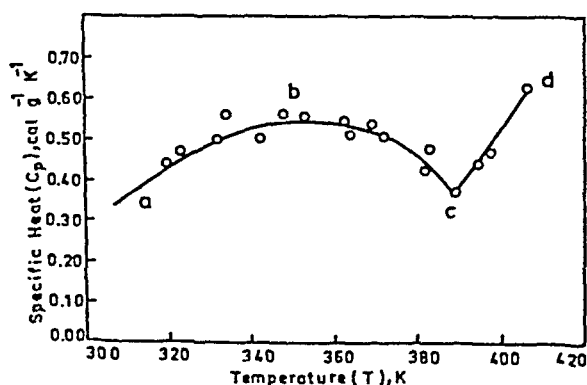


Fig. 1—Temperature dependence of the specific heat (C_p) of SPP

On raising the temperature above 390 K, a sharp increase in the specific heat is found. This behaviour is similar to that of semicrystalline samples. The rate of increase becomes smaller as the crystallinity becomes higher. Consequently, one can deduce that the recrystallization process begins about 390 K. The recrystallization process continues with further increase in temperature up to about 410 K (point d). Above 410 K, the specimen gets softened and no further measurements could be performed by the method chosen.

The Du Pont DTA analyser is allowed to scan the SPP specimen over the range of temperature 300-420 K. A typical thermogram of the DTA results (ΔT against T) as well as the variation rate of the specimen temperature (dT/dt vs T) are shown in Fig. 2. It is observed that the DTA curve flattens around 350 K and the curve of dT/dt vs T shows a peak in that region. Further, the DTA curve indicates a phase change above 390 K. This phase transition can be attributed to the recrystallization of the specimen material. This is substantiated by the steep rise shown by the dT/dt vs T curve above this temperature. These results are in good agreement with the results reported by Kardos *et al.*³ The DTA studies also support the deduction made on the basis of the variation of C_p with T reported in this paper.

However, it is still uncertain in the case of PP, whether the differences between syndiotactic (sample studied in the present study) and other types of atactic and isotactic polypropylene measured by some investigators²⁻⁷ are due exclusively to a difference in tacticity or whether they are ascribed to a difference in the molecular structure of the polymer chain.

The thermal diffusivity (α) of SPP is measured in

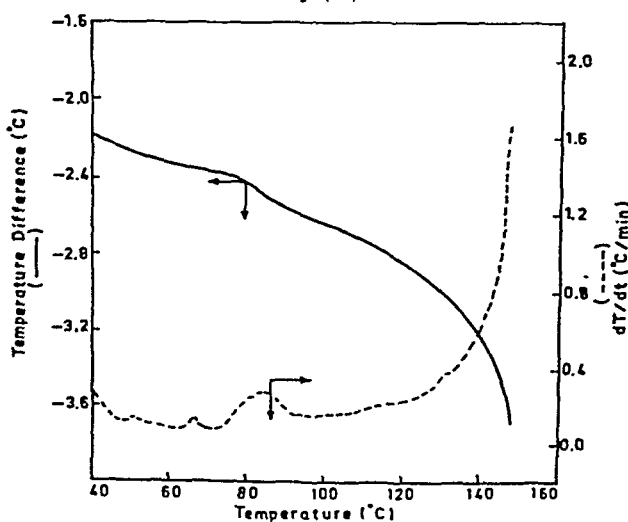


Fig. 2—DTA thermogram of SPP together with the variation rate of the specimens temperature (dT/dt) as a function of temperature.

the temperature range from 320 to 410 K. The variation of α with temperature is shown in Fig. 3. The variation of α with T is in accordance with the variation of C_p with T . This lends support to the deduction regarding a phase transition at about 350 K and the process of recrystallization around 390 K.

It is unfortunate that we are unable to cite any published work which could corroborate our findings about the variation of thermal conductivity with temperature. While our studies have used the latest and accurate plane temperature wave technique, earlier studies have followed techniques which cannot be fully relied upon to yield accurate results. The thermal conductivity (K) variation with T is shown in Fig. 4. The values of K were calculated from measurements of the density, the specific heat and the thermal diffusivity using Eq. (3). The behaviour of K with increas-

ing the temperature is nearly similar to that of C_p in Fig. 1. The values of K were found in the range from 1.7×10^{-4} to $3.8 \times 10^{-4} \text{ cal cm}^{-1} \text{ s}^{-1} \text{ K}^{-1}$ for the temperature range studied. The abrupt change in K at 390 K is, again, attributable to the initiation of crystallization kinetics.

The recrystallization temperature (T_{cr}) for SPP as observed in this study is about 390 K. Unfortunately, published data do not exist for a comparison. However, Kardos *et al.*³ report that recrystallization kinetics starts for PP at about 395 K. This observation is consistent with our observation within limits of experimental error. On the other hand, the recrystallization temperature for isotactic PP was found by Carfagna *et al.*⁵ to be 430 K. This difference in the recrystallization temperature could be attributed to the difference in the degree of crystallinity between IPP and our specimen. Therefore, one can conclude that the thermophysical properties of PP depend effectively on the degree of the specimen crystallinity.

We conclude on the basis of our observations that the SPP material is a good thermal insulator and that its structure indicates that the polymer chain alternates regularly. The recovery temperature (T_r) and the recrystallization temperature (T_{cr}) are at about 350 K (lower than that for PP⁴) and 390 K (lower than that for IPP⁵) respectively for this substance. Both these temperatures depend on the degree of crystallinity of the polymer under investigation.

Acknowledgement

The authors thank Prof. M. S. Kamel, Chemistry Department, Faculty of Science, Assiut University, Assiut, Egypt, for useful discussions and careful reading of the manuscript.

References

1. Majurey M J, *Plastic & Rubber Inter (USA)*, 2 (1977) 111.
2. Bares V & Wunderlich B, *J Polym Sci (USA)*, 11 (1973) 1301.
3. Kardos J L, Christiansen A W & Eric Baer, *J Polym Sci Part A (USA)*, 4 (1966) 777.
4. Park J B & Uhlmann D R, *J Appl Phys (USA)*, 44 (1973) 210.
5. Carfagna C, De Rosa C, Guerra G & Petraccone V, *Polymer (USA)*, 25 (1984) 1962.
6. Per Anndersson & Sundqvist B, *J Polym Sci Phys (USA)*, 13 (1975) 243.
7. Bares V & Wunderlich B, *J Polym Sci Polym Phys (USA)*, 11 (1973) 861.
8. Hendra P J, Vile J, Willis H A & Zichy V, *Polymer (USA)*, 25 (1984) 785.
9. Methot V B, *Polymer (USA)*, 25 (1984) 579.
10. Mostafa M S, *Energy transfer and physical properties of some complex compounds*, PhD thesis, Assiut University, Assiut, Egypt, 1983.
11. Wakkad M M, *Measurements of thermophysical properties of dielectric materials at high temperatures*, M.Sc. thesis, Assiut University, Assiut, Egypt, 1979.
12. Fillipov L P, *Measurements of the thermal properties of solid and liquid metals at high temperatures*, Report, Moscow State University, Moscow, 1967.

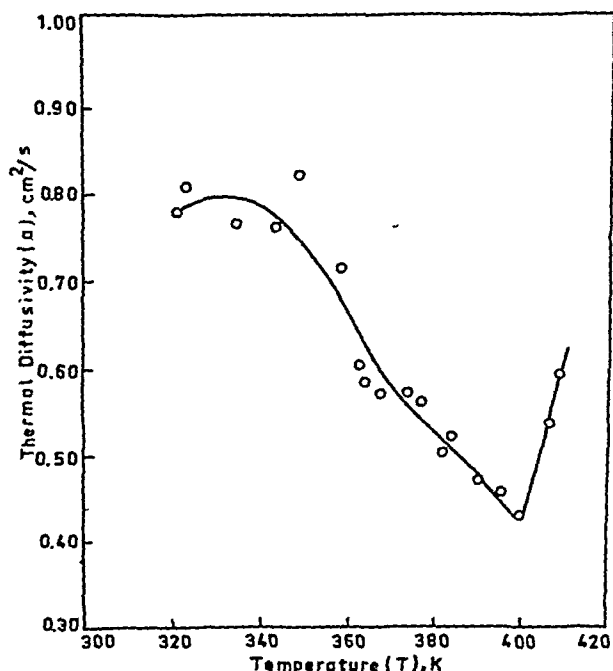


Fig. 3—Variation of thermal diffusivity (α) of SPP with increasing temperature

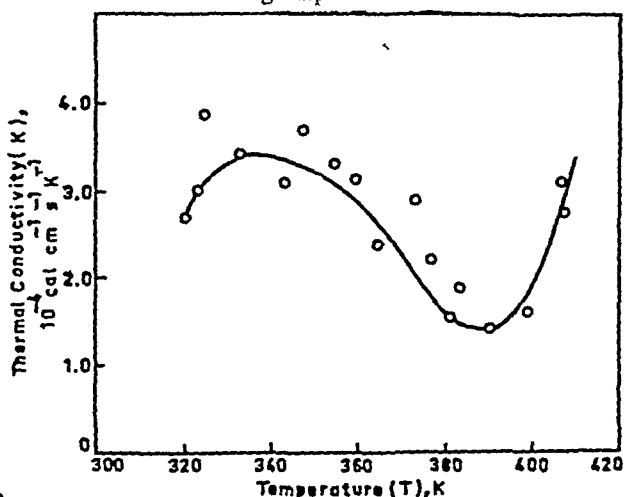


Fig. 4—Variation of the thermal conductivity (K) of SPP with temperature

Electric Field Dependence of Specific Heat of a Displacive Ferroelectric Crystal with Impurities

U C NAIETHANI & G N BALUNI

Theoretical Physics Division, Department of Physics, Dr. B G R Constituent College, Pauri (Garhwal) 246001

Received 9 January 1986

The electric field dependence of the specific heat of an anharmonic doped ferroelectric crystal is calculated in its paraelectric phase using the author's earlier approach [*Indian J Pure & Appl Phys*, 23 (1985) 261]. A cross term of defect parameters with electric field and anharmonic parameters is obtained. The combined effect of the defect and field dependence upon specific heat can be observed in presence of anharmonicity. In the vicinity of the Curie temperature, the Cochran soft mode is held responsible for the anomalous behaviour of the specific heat.

1 Introduction

In a previous paper¹, hereafter referred to as I, we discussed the electric field dependence of the specific heat of displacive ferroelectric materials such as BaTiO₃, SrTiO₃ etc. in the paraelectric phase in presence of an external electric field, using Kubo formalism and Green's function technique², taking into account only the contribution of soft modes towards specific heats. The present study differs from I in that now the crystal is also isotopically disordered. The impurities introduced are characterized³ by a different mass than the host atoms and with modified nearest neighbour harmonic force constant around their sites. The effect of mass change and force constant change between impurity and host lattice atoms due to the introduction of defects is taken into account. Their influence on the anharmonic coefficients in the Hamiltonian is neglected. The combined effect of the field and impurity dependence upon the soft mode frequency and hence upon the specific heat is observed in presence of anharmonicity. The results are in agreement with those from the experiments⁴⁻⁷.

2 Hamiltonian and Green's Functions

The modified Silverman Hamiltonian of displacive ferroelectrics in the paraelectric phase which includes defects, dominant third- and fourth-order anharmonicity and higher order electric moment in an external electric field \mathbf{E} can be written as

$$H' = H + H_D \quad \dots (1)$$

where H denotes the Hamiltonian for a pure anharmonic ferroelectric crystal in presence of an external electric field and is exactly given by Eq.(3.1) in I. H_D is the defect Hamiltonian and it involves the effect of mass change and harmonic force constant change

between the impurity and host lattice atoms due to substitutional defects and is given by³

$$H_D = -\hbar(0,0)B_0^0B_0^0 + \hbar D(0,0)A_0^0A_0^0 - \hbar B_0^0X + \hbar A_0^0Y + \hbar Z \quad \dots (2)$$

with

$$X = \sum_{k,\lambda} C(k^\lambda, 0)B_k^\lambda \quad \dots (2.1)$$

$$Y = \sum_{k,\lambda} D(k^\lambda, 0)A_k^\lambda \quad \dots (2.2)$$

and

$$Z = \sum_{k_1, k_2, \lambda} [D(k_1^\lambda, k_2^\lambda)A_{k_1}^\lambda A_{k_2}^\lambda - C(k_1^\lambda, k_2^\lambda)B_{k_1}^\lambda B_{k_2}^\lambda] + \sum_{k_1, k_2} [D(k_1^a, k_2^0)A_{k_1}^a A_{k_2}^0 - C(k_1^a, k_2^0)B_{k_1}^a B_{k_2}^0] \quad \dots (2.3)$$

Here $\lambda = a, 0$; for acoustic and optic modes respectively.

The defect parameters $C(k_1, k_2)$ and $D(k_1, k_2)$ depend upon the changes in the mass and force constants due to the substitutional defects respectively and are given by

$$C(k_1, k_2) = \frac{1}{2\mu} (M_0/2N)(\omega_{k_1}\omega_{k_2})^{1/2} \mathbf{e}(k_1)\mathbf{e}(k_2) \times \left\{ \sum_i^N f \times \exp. [i(\mathbf{k}_1 + \mathbf{k}_2) \cdot \mathbf{R}(i)] - \sum_i^n \exp. [i(\mathbf{k}_1 + \mathbf{k}_2) \cdot \mathbf{R}(i)] \right\} \quad \dots (2.4)$$

and

$$D(k_1, k_2) = \frac{1}{4N} (\omega_{k_1} \omega_{k_2})^{-1/2} \times \sum_{l, l', \beta} [\Delta \Phi_{\alpha\beta}(l, l') / M_0] \times e(k_1) e(k_2) \times \exp. [i\{k_1 \cdot R(l) + k_2 \cdot R(l')\}] \quad \dots (2.5)$$

where $e(k)$ is the polarization vector, $R(l)$ the equilibrium position vector of the l th atom, $C(k_1, k_2)$ vanishes when n is either zero or N . $\Delta \Phi_{\alpha\beta}$ denotes the force constant change, l and l' refer to the impurity and its nearest neighbours and $\mu = [MM' / (M' - M)]$. M_0 is the weighted harmonic mean of the masses of all atoms and is defined by the relation

$$1/M_0 = f/M' + (1 - f)/M \quad \dots (2.6)$$

with $f = n/N$. Here N is the total number of atoms in the crystal whose $(N - n)$ lattice sites are occupied by atoms of mass M while n sites are occupied by randomly distributed substitutional impurities each of mass M' .

In order to get the effect of electric field on the soft mode frequency and hence on specific heat, we transform H' using the approach of I. The necessity of transformation has been well discussed in I. The modified transformed Hamiltonian (H_T) is thus obtained as

$$H_T = H_T + H_D + 2\hbar Y g E - 4\hbar g E A_0^0 D(0, 0) \quad \dots (3)$$

Here H_T is exactly given by Eq. (3.15) in I and H_D is given by Eq. (2).

We now evaluate the Green's function $G^0(t - t')$ [Eq. (3) in I] with the help of H_T in the presence of defects and electric field, using the approach of I. The expression for the defect, electric field and temperature-dependent soft mode frequency ($\Omega(T, E)_D$) is thus obtained as

$$\Omega^2(T, E)_D = \Omega^2(T, E) + \Omega_D^2 + \Omega_{D,E}^2 \quad \dots (4)$$

where $\Omega^2(T, E)$ is the field- and temperature-dependent part of the square of the effective soft mode frequency $\Omega(T, E)_D$ and is essentially the same as given by Eq. (4) in I. Ω_D^2 is the contribution towards $\Omega^2(T, E)_D$ due to defect term $C(k_1, k_2)$ and $D(k_1, k_2)$ and its value is obtained as

$$\Omega_D^2 = 4\omega_0^0 D(0, 0) + (4/\omega_0^0) \times \text{Re} \sum_{k, \lambda} \frac{1}{(\omega^2 - \omega_k^2)} \{ (\omega_0^0)^2 \omega_k^2 D^2(k^\lambda, 0) + \omega^2 \omega_k^2 C^2(k^\lambda, 0) + \omega^2 \omega_0^0 [C(k^\lambda, 0) D^*(k^\lambda, 0) + C^*(k^\lambda, 0) D(k^\lambda, 0)] \} \quad \dots (4.1)$$

Also, the value of the third term $\Omega_{D,E}^2$ in Eq. (4) is obtained as

$$\Omega_{D,E}^2 = 48E^2 \left[\frac{\bar{\omega}_{k_1}^0}{\omega^2 - \bar{\omega}_{k_1}^0 \bar{\omega}_{k_2}^0} \right] \times \left[\sum_k D(k^0, 0) \sum_k (B^0(k) - 4g\beta^0(k)) \times \sum_{k_1, k_2} \{ D(k_1, k_2, -k) - 2g\psi(k_1, k_2, -k) \} \times \sum_{k_1, k_2} (N_{k_1}^0 \pm N_{k_2}^0) \frac{\omega_{k_1}^0 \pm \omega_{k_2}^0}{\omega^2 - (\omega_{k_1}^0 \pm \omega_{k_2}^0)^2} \right] \quad \dots (4.2)$$

where

$$\bar{\omega}_{k_1}^0 = \omega_k^0 + 4 \sum_k C(k_1^0, -k) \quad \dots (4.3)$$

and

$$\bar{\omega}_{k_2}^0 = \omega_k^0 + 4 \sum_k D(k_1^0, -k) + 8E^2 \times [2g^2 \sum_k \beta^0(k) - g \sum_k B^0(k)] \quad \dots (4.4)$$

3 Impurity and Electric Field Dependence of Specific Heat

It is evident from Eq. (1) in I that the impurity and field dependence of specific heat is a clear consequence of the impurity and field dependence of soft mode frequency. The square of the defect, temperature and field-dependent soft mode frequency [Eq. (4)] varies with the defect and electric field parameters in presence of anharmonicity. The presence⁸ of these effects stabilizes the soft mode frequency. The temperature independent part of the effective soft mode frequency is due to defect [second term in Eq. (4)]. The relationship between this mode and the properties of the ferroelectric and paraelectric state has been discussed by Cochran⁹, Anderson¹⁰ and many others. The influence of defect and electric field on this mode also affects the interaction¹¹ of soft mode with other modes, thus giving rise to defect and field dependence of various dynamic properties. The first term in Eq. (4) is due to the presence of an external electric field in presence of anharmonicity and has been well described by Eq. (4) in I. The third term in Eq. (4) [$\Omega_{D,E}^2$] gives the combined effect of defect and field dependence upon effective soft mode frequency. It is interesting to note that this term is missing if either defect is zero or field is not applied.

In the absence of defects, it is clear from Eq. (4) of the present paper and Eqs (1) and (2) in I that the pres-

ence of an applied electric field will increase the soft mode frequency and hence will decrease the specific heat, in conformity with the experimental results of Lawless⁴. These results have been fully discussed in I.

In a defect ferroelectric crystal unaided by any external electric field ($E = 0$) the second- and third-term in Eq. (4) will be missing. Thus, in the first approximation for the crystal model considered here, it follows from Eq. (4.1) that the effect of impurity upon effective soft mode frequency (and hence upon the specific heat) depends only on the changes in the harmonic force constants between the impurity and host lattice ions and can be either positive or negative, depending on the sign of force-constant change resulting from the doping of the crystal. In this approximation, the mass change of the impurity atom has no effect on the specific heat. However, when the concentration of impurities is high, the contribution of the effect of change in mass of impurity appears in the specific heat. The square of the magnitudes of the coefficients responsible for the force-constant change and mass change, $|D|^2$ and $|C|^2$ respectively may give cancellation or reinforcement effects according as they are of opposite or equal signs. Hence, their effect seems to mutually compensate each other's effect to some extent. The magnitudes of the parameters C and D are responsible for the change in specific heat. The results are similar to those obtained in Refs 5-7.

In presence of both the effects (the field and impurity), the combined effect of the defect and field de-

pendence upon specific heat can be observed, in presence of anharmonicity. In the vicinity of the Curie temperature T_c , the soft mode frequency ($\Omega^2 \sim T - T_c$) tends to zero thus rendering the value of specific heat anomalously large, in agreement with the results of Lawless¹².

Acknowledgement

The authors are thankful to Profs S K Joshi, G S Verma and K Mahesh for helpful discussions. They are grateful to Dr B S Semwal and Dr R C S Rawat for the encouragement given.

References

- 1 Naithani U C & Baluni G N, *Indian J Pure & Appl Phys*, **23** (1985) 261.
- 2 Zubarev D N, *Sov Phys Usp (USSR)*, **3** (1960) 320.
- 3a Bahadur Rita & Sharma P K, *Phys Rev B (USA)*, **12** (1975) 448.
- 3b Naithani U C & Semwal B S, *Pramana (India)*, **11** (1978) 423.
- 4 Lawless W N, *Phys Rev B (USA)*, **18** (1978) 2394.
- 5 Todd S S & Lorenson R E, *J Am Chem Soc (USA)*, **74** (1952) 2043.
- 6 Shirane G & Takeda A, *J Phys Soc Jpn (Japan)*, **6** (1951) 329.
- 7 Salamon M B & Garnier P R, *J Phys & Chem Solids (GB)*, **35** (1974) 851.
- 8 Naithani U C & Semwal B S, *Pramana (India)*, **14** (1980) 149; **15** (1980) 371.
- 9 Cochran W, *Adv Phys (GB)*, **18** (1969) 157.
- 10 Anderson P W, *Izv Akad Nauk SSSR (USSR)*, **290** (1960).
- 11 Tani K, *J Phys Soc Jpn (Japan)*, **36** (1974) 406.
- 12 Lawless W N, *Ferroelectrics (GB)*, **17** (1977) 341.

NOTES

A Semi-Empirical Formula for the Total Gamma Ray Streaming through Pipes

F M SAYEDAHMED

Reactor & Neutron Physics Department, Nuclear Research Centre
Atomic Energy Authority, Cairo, Egypt

Received 14 October 1985; revised received 2 June 1986

The variation of total dose of gamma rays along air-filled ducted ilmenite concrete blocks ($\rho = 4.6 \text{ g/cm}^3$) has been measured for different duct diameters ($2r$) and lengths (L) using one of the horizontal channels of Egyptian Research Reactor-1 (ETRR-1) and ^7LiF (TLD) detector embedded in teflon. An empirical formula connecting the gamma ray streaming through air-filled ducted ilmenite concrete with L and r has been deduced to fit the experimental data.

The most troublesome aspects of radiation shield design are those dealing with geometric irregularities in the shield. It is well known that slots, gaps, voids and streaming paths are often introduced inside the reactor shield after the conceptual design is completed. It is well known that in some reactor types, the radiations are circulated through bare pipe systems. As previously reported by Rockwell¹ that once this streaming is known, the average exposure rate behind a shield with a number of penetrations can be calculated. Moreover, Rockwell¹ showed that gamma fluxes escaping from an air void in a shield depend on the geometry of the void and the angular distribution of radiations emerging from the source. He reported the following formulae for the angular distribution of radiations passing through an air-filled duct of radius r and length L :

- (a) $\phi_L/\phi_0 = \frac{1}{2}r^2/L^2$ (Spherical distribution)
- (b) $\phi_L/\phi_0 = r^2/L^2$ (Cosine distribution)
- (c) $\phi_L/\phi_0 = 1.268 r^2/L^2$ (Fermi distribution)

where ϕ_L is the flux at any distance L and ϕ_0 represents the incident flux.

However, data calculated on the basis of the above formulae showed a remarkable discrepancy with the measured data. The present study was undertaken with a view to deriving an empirical expression for the total gamma dose passing through air-filled ducted ilmenite concrete.

The gamma dose streaming through ducted ilmenite concrete shield of density 4.6 g/cm^3 was measured using a relatively large concrete medium. The concrete media used for such studies were shaped in the form of rectangular blocks each of $120 \times 120 \times 40 \text{ cm}^3$ dimension. During the preparation of concrete blocks,

particular attention was paid to homogeneity and identity of concrete. For this purpose, the quantities of each concrete ingredient were carefully measured and mixed in each particular case. The ilmenite concrete composition and relative constituents of ilmenite concrete are already reported in an earlier publication by Megahed *et al.*²

Three concrete blocks each with a central hole of 10 cm diameter, when placed in a row, provided an air-filled duct of 120 cm length. To construct ducts with different diameters, cylindrical, removal plugs were used. These plugs were made of two concentric aluminium cylinders each of 40 cm length and with the space in between filled with identical concrete. These fabricated materials were good enough to construct air-filled ducts of diameters 2.9, 5.8 or 10 cm and of length 120 cm. A perspex sample holder with special openings was used to fix the detectors at the desired position along the duct axis. A simple mechanical device was used to press the concrete blocks as close as possible and thus avoid the presence of air gaps in between.

The ducted ilmenite concrete shield blocks were arranged in front of one of the horizontal channels of the ETRR-1. It was reported by Megahed *et al.*² that the total gamma exposure emerging from the reactor channel used for this study was 3.25 R/s and that the fast neutron flux ($E > 1.8 \text{ MeV}$) was $8.54 \times 10^8 \text{ n.cm}^{-2}\text{s}^{-1}$. The experimental set-up was the same as in our earlier studies³.

The gamma doses were measured using ^7LiF teflon thermoluminescence (TL) detectors, each 12.7 mm in diameter and 0.4 mm thickness. The isotopic abundance of ^7Li was 99.99% and that of ^6Li was 0.01% in these detectors. The ^7LiF -type phosphor had a very low response to thermal neutrons; hence it served as a detector suited for gamma-ray intensity measurement in mixed fields of radiations as those from a nuclear reactor. In addition, it had the advantage of accumulating the incident doses for any irradiation time and, therefore, could be used for measurements of very low intensity gamma doses^{4,5}. The ^7LiF teflon dosimeters were annealed before measurements by placing them in a pre-heated oven at 300°C for 4 hr and then transferred to a pre-heated oven at 80°C for 24 hr and finally left to cool gradually.

The annealing procedure was repeated for each dosimeter. The ^7LiF dosimeters were first calibrated against gamma doses using ^{137}Cs as the standard gamma source. The calibration coefficients obtained were used to convert the dosimeter responses in terms

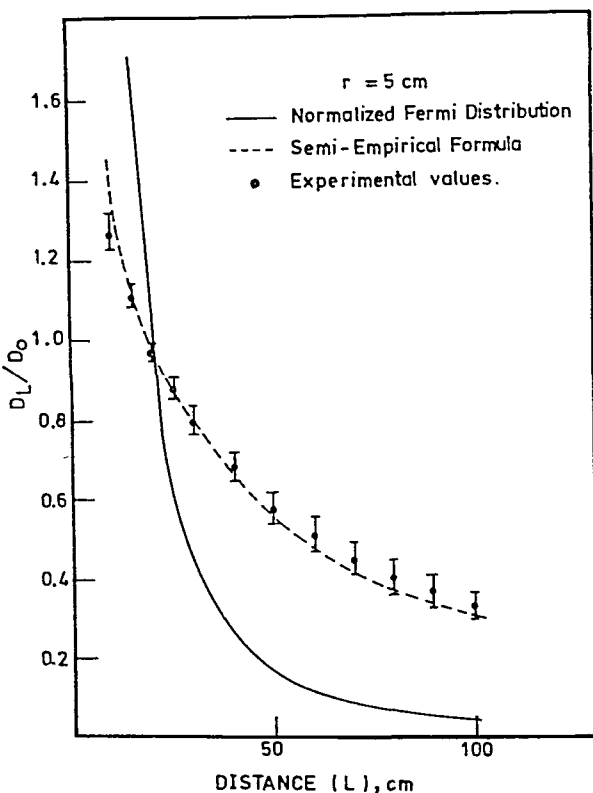


Fig. 1—Variation of D_L/D_0 with duct length for duct radius (r)=5 cm

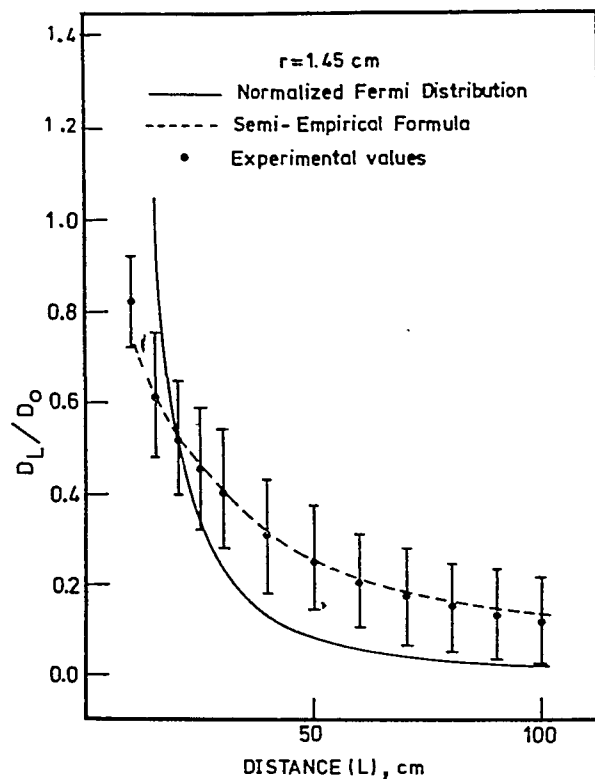


Fig. 3—Plot similar to Fig. 1 for $r=1.45$ cm

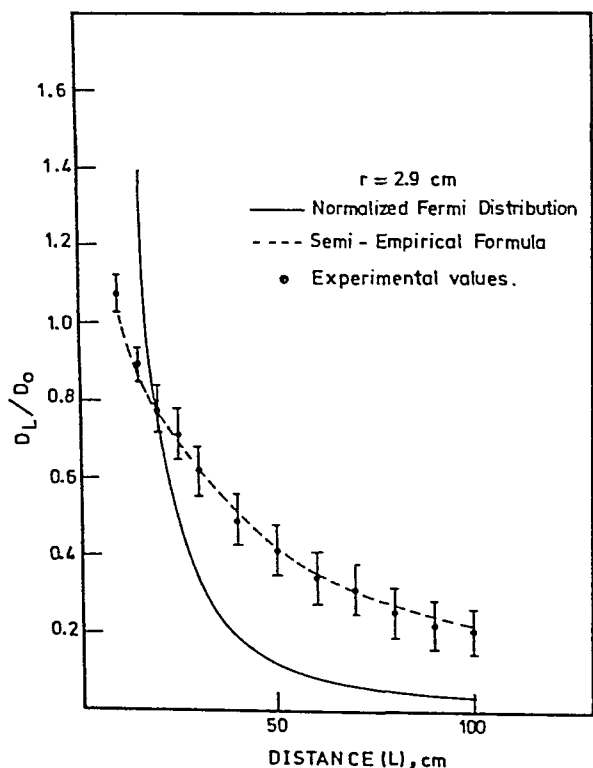


Fig. 2—Plot similar to Fig. 1 for $r=2.9$ cm

measurements were checked using a standard ^{14}C source. This source was fixed at a specific position in the experimental set-up. Each measurement was repeated at least twice to get consistent data, with a view to reducing the possibility of uncertainties in reactor power and time of irradiation which vitiate the observations.

Results and discussion—Figs 1-3 show the variation of D_L/D_0 as a function of distance L along the duct axis for 3 different values of r . The normalized Fermi distribution is also shown in the figures. It is evident that the actual rate of decrease of D_L/D_0 with L is not as steep as expected according to the normalized Fermi calculations. The normalization was done assuming the length of the duct to be 120 cm for all ducts studied. It is also seen that calculations of D_L/D_0 based on the formulae for spherical, cosine or Fermi distributions differ considerably from experimental data. The wide deviations between theoretical and experimental data may be due to the scattered components of the albedo and leakage doses, scattered and reflected radiations from the duct walls and the shield. The difference in physical properties of the shield and the surrounding medium and the geometrical factors of the design of reactor might also have caused the wide difference between theoretical and experimental data.

The observed data could, however, be fitted into an empirical formula of the form corresponding to Fermi distribution but with the addition of a term G to take

of absolute gamma doses. The response of the TL dosimeter was measured using a TL detector readout instrument (model Teledyne Isotopes-7300). The stability and standardization factor during each set of

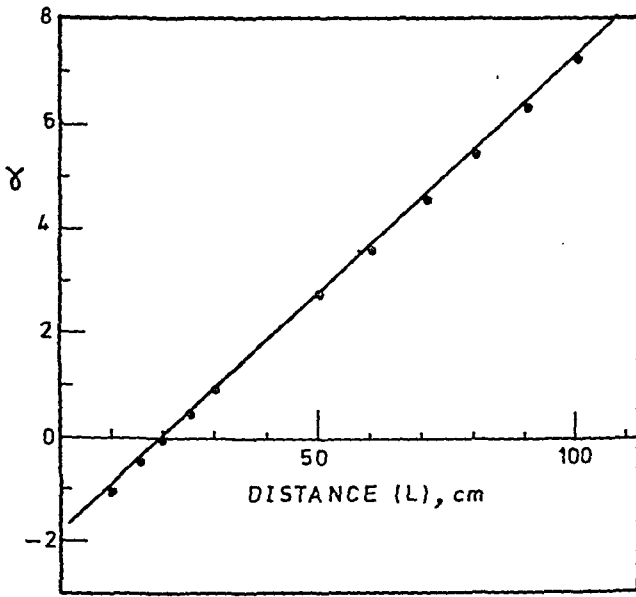


Fig. 4—Linear plot of γ versus L estimating value of γ for use in the empirical formula

into account the scattering due to geometrical factors of the reactor and duct and by multiplying the term r^2/L^2 by a complex term which depends on various factors. The modified empirical formula is given by:

$$D_d/D_0 = 1.268 G r^2/L^2 [1 + \gamma(r/r_0)^{1/4} e^{-r/L}]$$

where $G = 1.433 \times 10^4 e^{-6.20(r/r_0)^{1/4}}$, γ = value taken from the linear plot of γ vs L (Fig. 4), r = duct radius and r_0 = chemical radius (≈ 5 cm).

The dashed lines in Figs 1-3 represent the variation of D_d/D_0 calculated using the semi-empirical formula. One can see the good agreement between the experimental results and the calculated ones.

The author is grateful to Prof. M Adib for his cooperation and useful discussions and to Dr A S Makarious for his assistance during the experimental work.

References

- 1 Rockwell T, *Reactor shielding design manual* (McGraw-Hill, New York) Vol. III, 1956.
- 2 Megahed R M, Makarious A & El-Kolaly M A, *Egyptian J Phys*, 12 (1981) 1.
- 3 Sayedahmed F M & Abboud A, *Indian J Pure & Appl Phys*, 24 (1986).
- 4 Eid A M & Gomaa M A & Morsy S M, *Nucl Instrum & Methods (Netherlands)*, 160 (1979) 371.
- 5 Eid A M & Delafield H J, *The neutron response of a ^7LiF thermoluminescent dosimeter incorporated in OKAMA criticality dosimeters* (Atomic Energy Research Establishments, Harwell) M-2803, 1976.

Temperature & Concentration Dependence of Ultrasonic Velocity & Allied Parameters of Monochloroacetic Acid in Aqueous Ethanol

P S NIKAM & MEHDI HASAN

P G Department of Physical Chemistry, M S G College, Malegaon
Camp 423 105

Received 4 April 1986; revised received 2 June 1986

Ultrasonic velocities in aqueous ethanol solutions of monochloroacetic acid have been measured in the concentration range 0.05-0.4 mol/l at 25, 30, 35 and 40°C. Specific acoustic impedance, molar sound velocity, molar compressibility, relative association and solvation number have been evaluated and discussed in the light of solute-solvent interaction.

From the ultrasonic velocity (u)^{1,2}, values of adiabatic compressibility (β_{ad}), intermolecular free-length (L_f), specific acoustic impedance (Z), apparent molar compressibility (ϕ_K), molar sound velocity (R), molar compressibility (W), relative association (R_A) and solvation number (S_n) are calculable.

We have already reported^{3,4} data on densities, viscosities and some of the ultrasonic parameters like β_{ad} , ϕ_K and L_f of this system. In the present note, values of parameters like Z , R , W , R_A and S_n of this system are reported. The trends of variation of these parameters with concentration of added electrolyte and temperature of measurement are presented graphically.

Monochloroacetic acid was recrystallized from hot benzene and dried in vacuum. Melting point determination revealed the alpha form of the acid. The purified form of the acid was stored in a desiccator under vacuum. The desiccator was fully covered with black paper to prevent even the slightest amount of photolysis of the acid. Water and ethanol purified by standard methods were mixed by weight to give mixtures of different dielectric constants⁵. Solutions of different molarities were prepared by dissolving accurately known weights of the acid in a solvent mixture and kept for some time. The densities were measured pycnometrically with an accuracy of 1 in 10⁻⁴.

The velocities of ultrasonic waves of frequency 1.5 MHz in these solutions were measured following the interferometric method at different temperatures in the range 25-40°C using Mittal's M-82 instrument. The error in velocity measurements is $\pm 0.03\%$.

In the present system, variation of density with the concentration of the added electrolyte ($d\rho/dc$) is always positive. However, the variation of adiabatic

compressibility with respect to concentration of the added electrolyte ($d\beta_{ad}/dc$) is negative for solutions with 0.8 and 16.4 wt% ethanol and positive for solutions with 25.3, 34.4 and 54.1 wt% ethanol. The variation of ultrasonic velocity (u) with solute concentration (mol/l) is expressed by the equation:

$$\frac{du}{dc} = -\frac{u}{2} \left[\frac{1}{\rho} \cdot \frac{d\rho}{dc} + \frac{1}{\beta_{ad}} \cdot \frac{d\beta_{ad}}{dc} \right] \quad \dots(1)$$

For solutions with 0.8 and 16.4 wt% ethanol, the second term $(1/\beta_{ad}) \cdot (d\beta_{ad}/dc)$ is more negative than $(1/\rho) \cdot (d\rho/dc)$ making the term (du/dc) positive. In other words, u increases with increase in concentration (Fig. 1). However, for solutions with 25.3, 34.4 and 54.1 wt% ethanol, $(1/\beta_{ad}) \cdot (d\beta_{ad}/dc)$ is positive, thereby making (du/dc) negative, i.e. the ultrasonic velocity decreases with increase in concentration (Fig. 1) for these solutions.

It is found that u increases with increase of temperature for solutions with 0.8 and 16.4 wt% ethanol. This can be attributed to the weakening in the already strong solute-solvent interaction with rise in temperature. For solutions with 25.3, 34.4 and 54.1

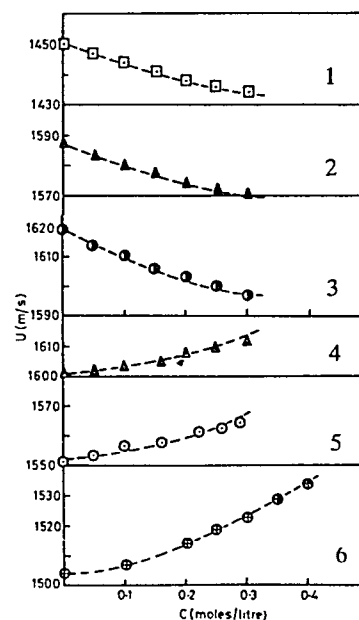


Fig. 1—Plots of ultrasonic velocity (u) vs concentration (c) for various solvent mixtures at 30°C.

Curve No.	Wt% of ethanol
1	Nil
2	8
3	16.4
4	25.3
5	34.4
6	54.1

wt% ethanol, u decreases with increase in temperature. This is probably due to the solute-solvent interaction being stronger compared to ion-ion interactions. In all these systems, the variation of u with temperature is always nonlinear (Fig. 2).

The parameter Z shows a linear variation when plotted against c (Fig. 3). The slopes of the lines are found to be positive in solutions with 0.8 and 16.4 wt% ethanol and negative in solutions with 25.3, 34.4 and 54.1 wt% ethanol. This trend is retained at all temperatures. The negative gradient of Z vs c plot can be explained from the fact that the rate at which ρ increases with c is lesser compared to the rate at which u decreases with c . The empirical relation, $10^{-5}(dZ/dc) \approx (-A/\beta_{0,ad})$ is valid for all the solutions and at all temperatures. In the above relation, A is the constant used in Bachem's equation and $\beta_{0,ad}$ is the adiabatic compressibility of the solvent mixture.

At any given concentration, Z increases linearly with temperature for solutions with 0 and 8 wt% ethanol (Fig. 4). For solutions with 16.4 wt% ethanol, Z first increases reaches a maximum value at 30°C and then decreases with further rise in temperature. The increase in Z with increase in temperature may be explained in the light of Eucken's theory⁶ which states that there is a decrease in the number of aggregates of solvent molecules as the temperature rises. Consequently, water and alcohol start behaving like unassociated liquids as the temperature increases. Further, the addition of a salt to a solvent mixture accelerates the process of breaking of aggregates of

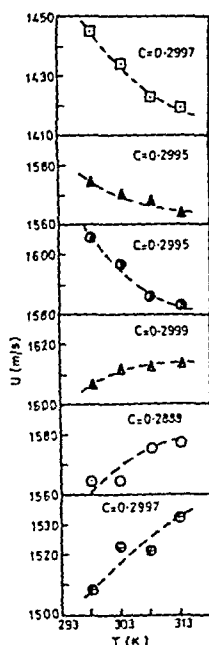


Fig. 2—Plots of ultrasonic velocity (u) vs temperature (T) for various solvent mixtures. Legend same as in Fig. 1

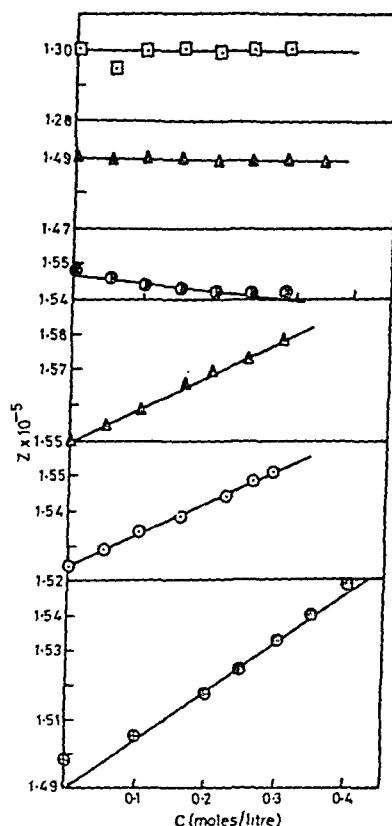


Fig. 3—Plots of specific acoustic impedance (Z) vs concentration (c) for various solvent mixtures at 30°C. Legend same as in Fig. 1.

solvent molecules. This process leads to the inhibition of propagation of sound waves due to large sized electrolyte molecules acting as structure promoters.

In solvents with 25.3, 34.4 and 54.1 wt% ethanol, value of Z of the system decreases with increase in temperature for all concentrations of solute with the result that a high value of Z occurs only at the lowest temperature possible (Fig. 4).

The molar sound velocity also known as Rao's constant R for monochloroacetic acid is a linear function of concentration of the solute, expressed in mole fractions (c_m), except in solutions with 8 and 16.4 wt% ethanol (Fig. 5). The mole fraction values beyond which the nonlinearity occurs, are dependent on temperature. These values (c_m) shift to lower ones at higher temperatures. This nonlinearity between R and c_m indicates the solute-solvent interaction. It is also seen that R increases with increase in temperature at any concentration of solute in all solvent mixtures. The variation is more or less linear (Fig. 6).

For all the systems studied, the relative association (R_A) increases linearly with increase in concentration (Fig. 7). This could be explained from the fact that R_A increases due to association of solvent molecules on addition of an electrolyte or due to increased solvation of ion of solute. In the present investigation, association of solvent molecules is found to predominate over the solvation of ions of the solute.

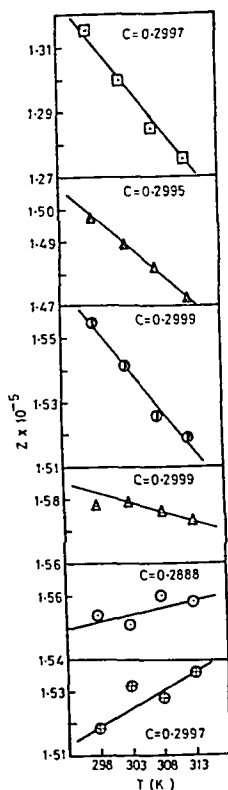


Fig. 4—Plots of specific acoustic impedance (Z) vs temperature (T) for various solvent mixtures. Legend same as in Fig. 1.

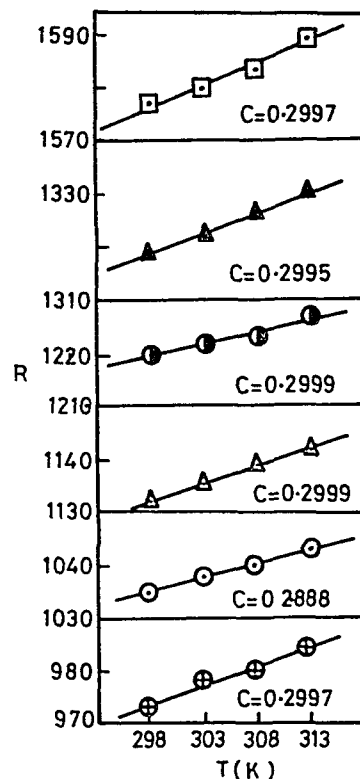


Fig. 6—Plots of molar sound velocity (R) vs temperature (T) for various solvent mixtures. Legend same as in Fig. 1.

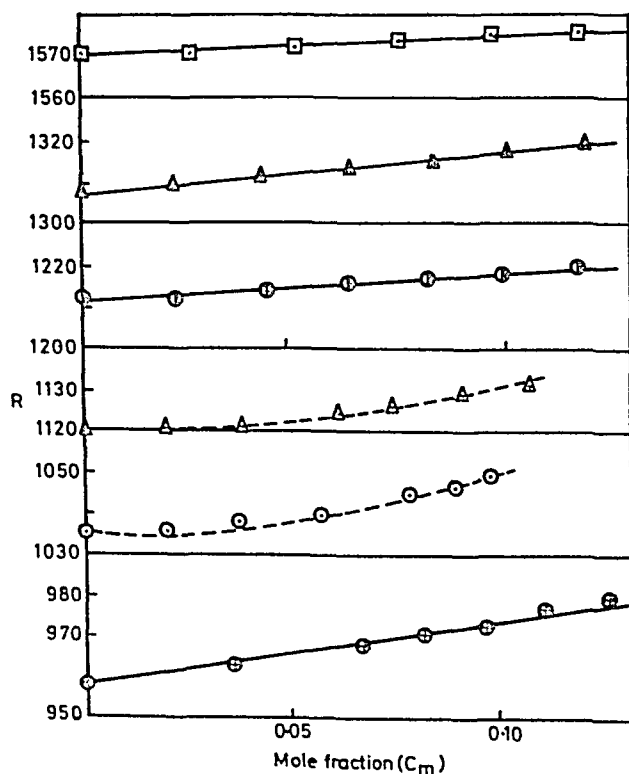


Fig. 5—Plots of molar sound velocity (R) vs concentration for various solvent mixtures at 25°C. Legend same as in Fig. 1.

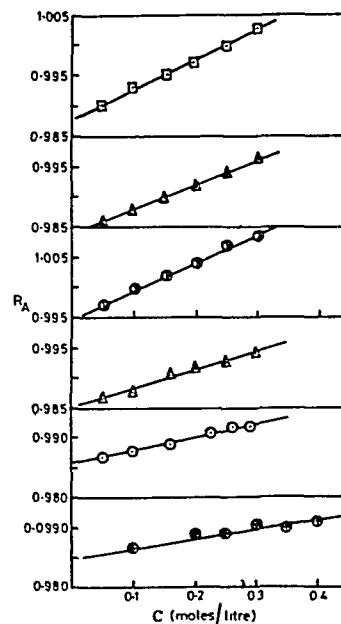


Fig. 7—Plots of relative association (R_A) vs concentration (c) for various solvent mixtures at 25°C. Legend same as in Fig. 1.

For all the solutions, value of R_A decreases with increase of temperature (Fig. 8). This indicates the increase in the degree of dissociation of aggregates of solvent molecules with increase in temperatures.

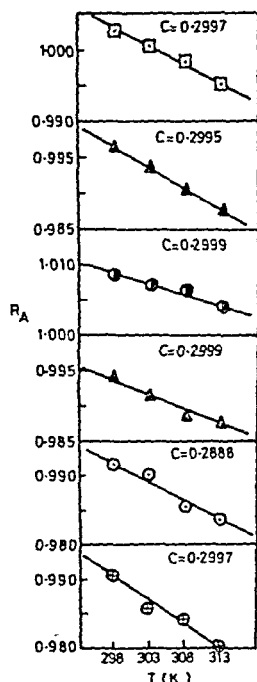


Fig. 8—Plots of relative association (R_A) vs temperature (T) for various solvent mixtures. Legend same as in Fig. 1.

The solvation number (S_n) is calculated using the equation

$$S_n = \frac{n_1}{n_2} \left(1 - \frac{\beta_{ad}}{\beta_{0,ad}} \right) \quad \dots (2)$$

where n_1 and n_2 are the moles of solvent and solute respectively. β_{ad} and $\beta_{0,ad}$ are the adiabatic compressibilities of the solution and solvent respectively. Values of S_n in solutions with 0.8 and 16.4 wt% ethanol, though very small, are positive; however, those for solutions with 25.3, 34.4 and 54.1 wt%

Table 1—Variation of Solvation Number (S_n) with Dielectric Constant of Solvent

Wt% ethanol	Dielectric constant	Concentration mole	Solvation number S_n	
			a	b
0	78.74	0.2997	0.30	2.64
8	74.07	0.2888	0.27	2.09
16.4	70.42	0.2999	0.20	0.90
25.3	65.36	0.2999	-0.01	-5.37
34.4	58.48	0.2995	-0.06	-3.83
54.1	46.73	0.2997	-0.07	-3.39

a: By using Eq. (2); b: By using Eq. (3)

ethanol are negative. This indicates the decrease in the tendency of solvation of ions with decrease in dielectric constant of the solvent mixtures. Values of S_n are also calculated using the equation:

$$S_n = -\phi_K / \beta_{0,ad} (M_0 / \rho_0) \quad \dots (3)$$

as suggested by Wada *et al.*⁷ (Table 1) and these agree with the values calculated by using Eq. (2).

The authors express their sincere gratitude to Shri R V K Khairnar, Principal of the College, for the facilities provided.

References

- 1 Prakash O & Prakash S, *J Acoust Soc India*, 6 (1978) 11, 39.
- 2 Mark G W J, *J Acoust Soc Am (USA)*, 31 (1959) 936.
- 3 Nikam P S & Mehdi Hasan, *Curr Sci (India)*, 53 (1984) 26.
- 4 Nikam P S & Mehdi Hasan, *J Chem Eng Data (USA)*, 1986, in press.
- 5 Mandal A K & Lahiri S C, *Indian J Chem Sect A*, 15 (1977) 728.
- 6 Eucken A, *Z Electrochem (Germany)*, 51 (1948) 6.
- 7 Wada Y, Shimbo S & Oda M, *J Acoust Soc Am (USA)*, 22 (1950) 880.

Measurement of Effective Thermal Conductivity of Food-grains at Interstitial Air Pressures

RAMVIR SINGH, R S BENIWAL & D R CHAUDHARY
Department of Physics, University of Rajasthan, Jaipur 302 004
Received 24 March 1986; revised received 10 June 1986

Using a laboratory-made thermal conductivity probe, effective thermal conductivity of some food-grains has been measured at normal and different interstitial air pressures (normal-0.5 mm mercury). It is observed that at low pressures, heat-transfer through food-grains is poor, whereas at atmospheric pressure there is a marked increase in their conducting character.

In the literature, one finds values of thermal conductivity and diffusivity of some furits and juices^{1,2}. The thermal conductivity of fruits as a function of moisture content has also been measured^{3,4}. In the present note, we are reporting the effective thermal conductivity of wheat of different varieties, rice, bajra, makka, rajma, soyabean, moong and masoor at different interstitial air pressures. Details about these grains are listed in Table 1. This knowledge has its usefulness from the storage point of view in that partial evacuation of the bulk may lead to better storage.

Effective thermal conductivity of food-grains at normal as well as at interstitial air pressures has been

measured with a laboratory-made thermal conductivity probe⁵. A stainless steel needle of length 15.2 cm having length-to-diameter ratio 92.12 was taken as the probe. A constantan wire having resistance of 56.2 Ω

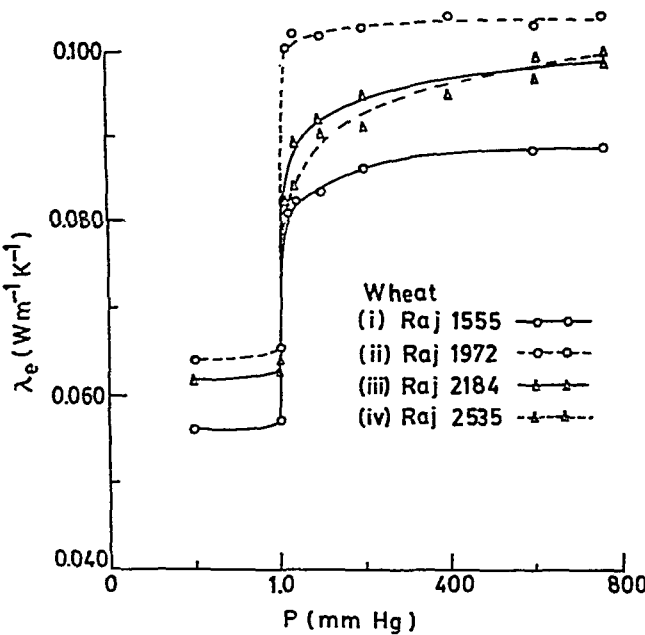


Fig. 1—Variation of effective thermal conductivity (λ_e) with interstitial air pressure of various wheat samples

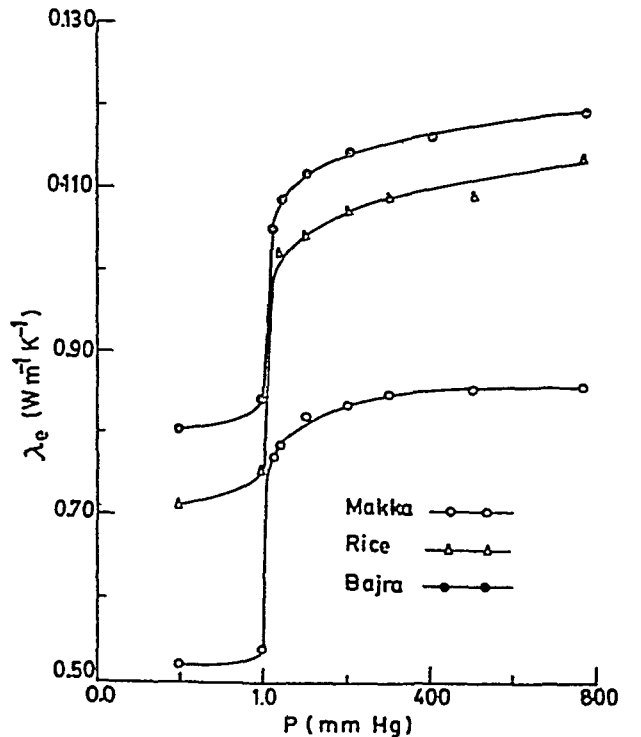


Fig. 2—Plots similar to Fig. 1 for makka, rice and bajra samples

Table 1—Specifications of Food-Grains Used in the Experiment

Local name	Botanical name	Bulk porosity	Bulk density g/cc
1. Wheat	<i>Triticum aestivum</i> Luin		
(i) Raj 1955		0.37	0.77
(ii) Raj 1972		0.34	0.84
(iii) Raj 2184		0.35	0.78
(iv) Raj 2535		0.35	0.80
2. Rice	<i>Oryze sativa</i> Luin	0.39	0.85
3. Makka	<i>Zea mays</i> Luin	0.35	0.78
4. Bajra	<i>Pennisetum typhoides</i> (Burm f) stapf and C.E. Hubb	0.325	0.82
5. Rajma	<i>Vigna unguiculata</i> (L.) Walp sub. sp. Cylindrical (L) Eseltine	0.375	0.79
6. Soyabean	<i>Glycine wightii</i> (Grah. ex. W and A.) Verdcourt	0.375	0.74
7. Moong	<i>Vigna angularis</i> (willed) Ohwe	0.35	0.86
8. Masoor	<i>Lens cultivaris</i> Medik	0.36	0.83

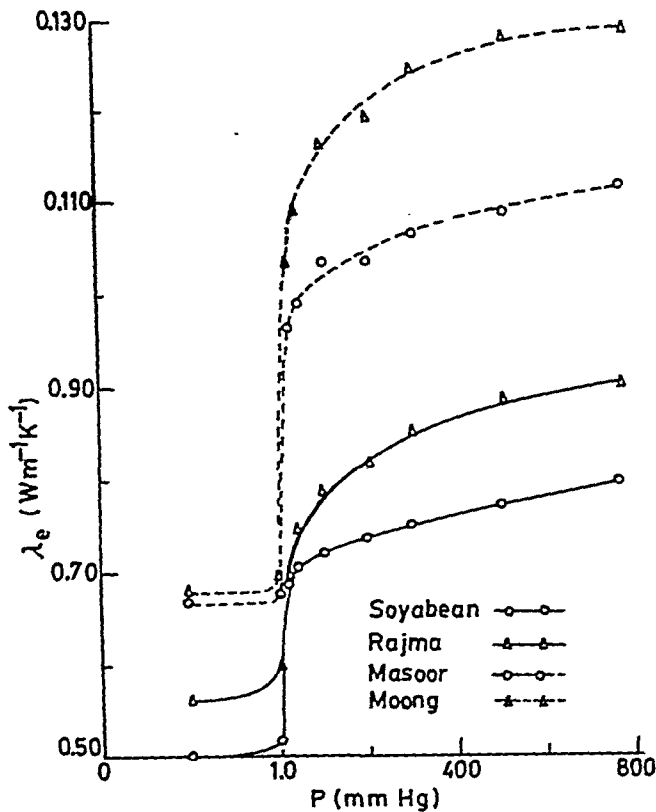


Fig. 3—Plots similar to Fig. 1 for soyabean, rajma, masoor and moong samples

stretched centrally along the needle and having a copper-constantan thermocouple at its middle point served as the heater. The void space if any within the hollow needle was filled with zirconia powder. An ebonite handle was provided at one end of the needle through which leads of heater and thermocouple were taken out. The other end was closed with a solid metal cone, facilitating an easy insertion of the needle in the test material. The pressure chamber and circuit used for the measurement of effective thermal conductivity are already described by Pande *et al.*⁵

The effective thermal conductivity of the material

in which the thermal probe is placed is given by the relation⁶

$$\lambda_e = \frac{Q}{4\pi(\theta_2 - \theta_1)} \ln(t_{2/n}) \quad \dots (1)$$

where θ_2 and θ_1 are temperatures of the probe surface at time t_2 and t_1 . Q is the power per unit length supplied to the probe.

The thermal probe was initially tested by measuring the thermal conductivity of pure glycerine to be $0.282 \text{ W m}^{-1} \text{ K}^{-1}$ at 18°C . Since the value reported in literature is $0.288 \text{ W m}^{-1} \text{ K}^{-1}$ at 20°C , the error is not more than 3%.

The food-grains were used after drying. Variations of λ_e of the selected food-grains with interstitial air pressures are exhibited in Figs 1-3. We observe that as the pressure is reduced from normal towards 1.00 mm of Hg, value of λ_e decreases. But below 1.0 mm of Hg pressure, there is only a slight variation in λ_e . The rate of variation of λ_e with pressure is large in the range 1-200 mm of Hg and small in the range 200 mm Hg to normal pressure. An explanation to this behaviour is already reported by Pande *et al.*⁵

The authors are thankful to the Agriculture Research Centre, Durga Pura, Jaipur, for providing samples of food-grains. One of them (RSB) is grateful to CSIR, New Delhi, for the award of a senior research fellowship.

References

- 1 Rha C K, Thermal properties of food materials in *Theory, determination and control of physical properties of food materials* (D Reidel Publications Co, Dordrecht, Holland), 1975.
- 2 Qashou S, Vachon R J & Touloukian Y S, *ASHRAE Semi Annual Meeting, New Orleans, LA (USA)* 23-27 Jan, 1972.
- 3 Sweat V E, *J Food Sci (GB)*, **39** (1974) 1080.
- 4 Jorge E, Martin J U & Enrique R, *J Food Sci (GB)*, **44** (1979) 198.
- 5 Pande R N, Saxena N S & Chaudhary D R, *Indian J Technol*, **22** (1984) 66.
- 6 Carslaw H S & Jaeger, *Conduction of heat in solids* (Oxford University Press, Oxford), 2nd Edn, 1959, 261.

Migrational Enthalpies for Alkali Halides Using Ballistic Model & Their Dependence on Structural Properties

SHANTA PALCHOUDHURI & G K BICHILE

Department of Physics, Marathwada University, Aurangabad

Received 9 December 1985; revised received 29 May 1986

The migrational enthalpies ΔH_m of alkali halides are evaluated by using the ballistic model developed in terms of 'absolute-rate' theory of diffusion. The enthalpy of migration is expressed in terms of macroscopic parameters of the normal crystal. The calculated values of enthalpies of migration agree favourably well with experimental values.

There has been a great deal of renewed interest in the study of ionic charge transport (or conductivity) in solids. This interest derives from the need to find new materials with high ionic conductivity which are useful to develop advanced electrochemical systems.

The conductivity σ in the intrinsic regime where one mobile species dominates can be written as¹

$$\sigma T = \left(\frac{A N q^2 v r^2}{k} \right) \exp \left(\frac{\Delta S_f}{2k} + \frac{\Delta S_m}{k} \right) \times \left(\frac{-\Delta H_f}{2kT} - \frac{\Delta H_m}{kT} \right) \dots (1)$$

where A is the dimensionless geometrical factor (of order unity), N the number of ions per unit volume, q the charge of the mobile ion, v the vibrational (or attempt) frequency of the effect, r the jump distance, k the Boltzmann's constant; ΔS and ΔH are the entropy and enthalpy, respectively associated with the defects,

and the subscripts f and m are associated with formation and migration of defects respectively.

In dealing with the experimental data, Eq. (1) is more commonly written as:

$$\sigma T = \sigma_0 \exp (-E/kT) \dots (2)$$

The objective of the present work was to test the validity of the ballistic model² to find the enthalpy of vacancy migration ΔH_m for alkali halide type crystals. The presently used ballistic model (BM) is developed in terms of 'absolute-rate' theory of diffusion³. The details of the ballistic-migrational process and the theory involved is explained by Van Vechten². According to the ballistic model for vacancy motion, the enthalpy of vacancy migration is given by

$$\Delta H_m (V) = \frac{1}{2} M r^2 + \frac{h}{\tau_m} \dots (3)$$

where h is Planck's constant, M the mass of mobile atom and τ_m the vibrational period of the butting atoms in the appropriate migration mode. The second term represents the phonon energy of the butting atoms in the migration mode and is negligibly small compared with the first term, because the amplitude of their vibration is not large.

Thus, we approximate

$$\Delta H_m (V) = \frac{1}{2} M r^2 \dots (4)$$

where r is the velocity of the mobile atom and is given by

$$\dot{r} = d/\tau_m \dots (5)$$

Table 1 — Calculated and Measured Enthalpies of Single Vacancy Migration

	F		Cl		Br		I	
	$\theta_D (K)$	$\Delta H_m (eV)$	$\theta_D (K)$	$\Delta H_m (eV)$	$\theta_D (K)$	$\Delta H_m (eV)$	$\theta_D (K)$	$\Delta H_m (eV)$
Li	733.8	2.5	429.1	2.2	274.2	2.2	—	—
Na	492.3	2.4	321.4	2.1	224.8	2.0	167.8	1.95
				(1.56-1.86)		(1.98)		
K	334.3	2.0	238.8	1.8	174.3	1.7	133.7	1.65
				(1.75)		(1.62) ^a		
Rb	212.3	1.6	171.2	1.7	138.9	1.6	110.6	1.56
Cs	—	—	159.6	1.2	149.5	1.4	126.2	1.50
				(0.96)				

Values in parentheses are taken from Ref. 7.

where d is the distance that the mobile atom jumps (here taken to be the interatomic spacing in the perfect crystal). In the Debye approximation,

$$\tau_m = h/k\theta_D \quad \dots (6)$$

where k is the Boltzmann's constant, and θ_D the Debye temperature. Using Eqs (5) and (6)

$$\Delta H_m(V) = \frac{1}{2} M(Fdk\theta_D/h)^2 \quad \dots (7)$$

where the factor $F \approx 1.0$ is structure-dependent parameter which is to be adjusted empirically to account for the approximation made in the model. $F(\text{bcc}) = 0.8$ and $F(\text{fcc}) = F(\text{hcp}) = 0.9$. The Debye temperature θ_D has been calculated by averaging the elastic coefficients. The details of this method are given in our earlier papers^{4,5}. The values of d are taken from Wyckoff⁶.

The values of $\Delta H_m(V)$ calculated in the present work are given in Table 1; for the sake of comparison, the experimentally obtained values of Samara⁷ also are given in parenthesis. It should be noted that the calculated values are in fair agreement with the values obtained using the ballistic model.

The values of $\Delta H_m(V)$ obtained in the present work were against the structural microscopic properties like ionic radii (r), the polarizability (α), mass (M), Debye temperature (θ_D) and melting point (T_m), and a regular behaviour was observed. The values obtained by the ballistic model are also in good agreement with those obtained from semi-empirical model of Varotsos and Alexopoulos^{8,9}.

The authors wish to thank the University Grants Commission, New Delhi, for financial assistance.

References

- 1 Crawford J H (Jr) & Skliskin L M, *Point defects in solids* (Plenum Press, New York) 1972.
- 2 Van Vechten J A, *Phys Rev B (USA)*, **12** (1975) 1247.
- 3 Vineyard G H, *J Phys & Chem Solids (GB)*, **3** (1957) 121.
- 4 Bichile G K, *Indian J Pure & Appl Phys*, **22** (1984) 468.
- 5 Bichile G K, *Indian J Pure & Appl Phys*, **24** (1986) 150.
- 6 Wyckoff R W G, *Crystal structure*, Vol 1 (Interscience, New York) 1960.
- 7 Samara G A, *Solid State Physics*, (Academic Press, New York) Vol 18, 1984, 1.
- 8 Varotsos P & Alexopoulos K, *Phys Status Solidi a (Germany)*, **47** (1978) K 133; **55** (1979) K 63.
- 9 Varotsos P & Alexopoulos K, *Phys Rev B (USA)*, **15** (1977) 2348.

Optical Losses of ZrO_2 Films in UV Region

K V S R APPARAO, N K SAHOO* & T C BAGCHI

Spectroscopy Division, Bhabha Atomic Research Centre, Trombay,
Bombay 400 085

Received 10 June 1985; revised received 18 November 1985

The dependence of optical losses on different evaporation parameters has been studied in the UV region (from 240 nm to 400 nm) for thin ZrO_2 films prepared by the method of reactive evaporation. Low loss ZrO_2 films have been achieved for UV laser applications above 300 nm by optimizing different process parameters. The optical losses of ZrO_2 films at different UV laser wavelengths have also been evaluated.

A knowledge of optical losses of thin films is essential for the development of efficient dielectric high reflecting mirrors for different laser applications in the UV region from 240 nm to 400 nm. Such applications require suitable low loss ($L \leq 0.5\%$) high index ($n \geq 2.0$) optical films. Thin films of HfO_2 , Sc_2O_3 , Al_2O_3 , $2\text{Y}_2\text{O}_3$, Al_2O_3 , Sb_2O_3 , $\text{MgO} \cdot \text{Al}_2\text{O}_3$, ZrO_2 prepared by different evaporation processes were investigated¹⁻⁵ for similar applications. Very few high index films suitable for UV region are known and even for these materials data of optical losses in the UV region are not available for films prepared by vacuum evaporation. Thin films data, as is well known, are different from data obtained on bulk samples and greatly depend on the various process parameters used during the preparation of the films⁵⁻⁸.

Our aim is to study and establish the dependence of the optical losses in the UV region on the various process parameters for different high index films using the method of vacuum evaporation which is the most convenient method of fabricating thin film devices. In this note, we report our results concerning the optical losses in the UV region of thin ZrO_2 films prepared by the method of reactive evaporation. The dependence of the optical losses on rate of evaporation, substrate temperature, ambient oxygen pressure, film thickness and chopping the vapour before reaching the substrate, have been studied and the results are presented.

Experimental details— ZrO_2 films were deposited on 25 mm diameter fused silica substrates by evaporating optical grade ZrO_2 using the electron beam gun in Balzer's Model BA 510 vacuum coating plant. The chamber was evacuated to better than 2×10^{-6} mbar

before evaporating the material. For reactive evaporation IOLAR grade pure oxygen from a high pressure cylinder was admitted into the chamber and maintained at the required value ranging from 3×10^{-4} to 5×10^{-6} mbar by controlling the needle valve and other pressure-regulating valves. Substrates were heated to the assigned temperature ranging from 50°C to 400°C using the built-in resistance heater provided in the chamber. Rate of evaporation which ranged from 1 to 100 \AA/s was measured and controlled with the quartz crystal monitor. Chopped films were prepared by introducing a suitable rotating mask in between the substrate and the source. A total of 35 samples of ZrO_2 films were prepared for the present studies, each with different evaporating parameters. For all the samples prepared, uniformity of film thickness over the whole surface was found to be within $\pm 2\%$ of the average thickness. The transmittance spectrum of each sample substrate was recorded before and after depositing the film using Hitachi Model 330 double beam spectrophotometer (photometric accuracy $\pm 0.2\%$). The spectra were used to compute the optical losses of the films deposited under different evaporation conditions. The results of some of the important and relevant spectra are reported.

Optical losses of each sample film were determined using the transmission spectrum. A typical spectrum of 300 nm thick ZrO_2 film of refractive index n deposited on a substrate of index s is shown in Fig. 1. The transmission spectrum of the substrate before coating the film is also shown in Fig. 1. The percentage losses L of the film at wavelength λ_0 were determined from the spectrum using the relation

$$L = (T_s - T_{PM})$$

where T_s is the transmission of the substrate at the maximum peak wavelength λ_0 and T_{PM} is the peak maximum transmission. T_{PM} should be equal to the substrate transmission T_s if there were no losses in the film. The percentage losses were determined at all fringe maxima wavelength points where the optical film thickness was an even multiple of $\lambda/2$ and acted as an absentee layer. The refractive index n , and physical thickness t of the film were determined by the method of Swanepoel⁹ using its transmission spectrum. The derived constants are expected to be accurate to within $\pm 1\%$ of the true values⁹.

Results and discussion—The measured percentage losses were plotted against wavelength on a logarithmic scale, for all the samples of ZrO_2 films

* Multi-Disciplinary Research Scheme, Bhabha Atomic Research Centre, Bombay 400 085

prepared. It was found that all the results except those of chopped films were reproducible within experimental errors. The reasons for the discrepancies for the dependence of losses on chopping are being investigated and hence these results are not presented. The results are grouped into four sets. Each set of films were coated under identical conditions but with one variable parameter. Figs 2-5 show the results of such sets wherein the dependence of losses of ZrO_2 films on rate of evaporation R , substrate temperature T , ambient oxygen pressure and film thickness t respectively are shown.

The optical losses and refractive index at 250 nm ($L=8\%$ and $n=2.35$) for our best films of 275 nm thickness were found to be comparable with those

prepared by the method of sputtering³ ($L=9\%$ and $n=2.47$). The optical losses at different UV laser wavelength points for our best 275 nm thick ZrO_2 films are given in Table 1. The losses of those films in the visible region above 440 nm were found to be less than 0.01%. The refractive indices of these films at 248, 355 and 515 nm were found to be 2.35, 2.10 and 2.01 respectively which indicates that the films have appreciable dispersion in the UV region.

It was found in the present investigations that, in general, the losses in ZrO_2 films decrease as the rate of evaporation decreases (Fig. 2). This decrease is more prominent as we go to shorter wavelengths. As expected, the optical losses are reduced at higher substrate temperatures (Fig. 3). For a given rate of evaporation and substrate temperature, the optical losses are reduced still further if the films were deposited at a particular oxygen ambient pressure, namely 2×10^{-4} mbar (Fig. 4).

The optical losses of thin films, in general, include losses due to absorption, scattering and fluorescence.

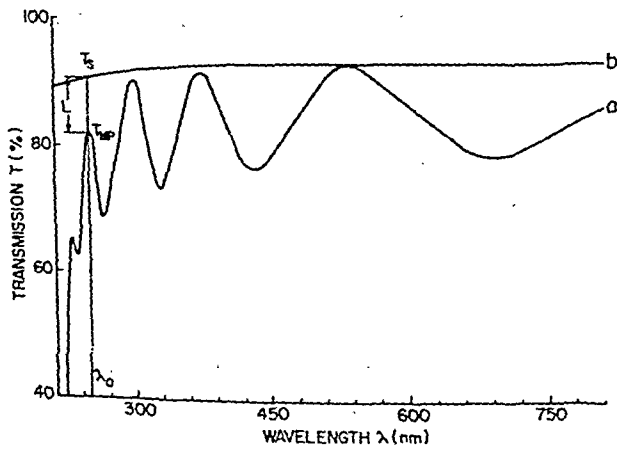


Fig. 1—Transmission spectrum of: (a) ZrO_2 film of about 300 nm thickness and (b) the substrate before coating the film

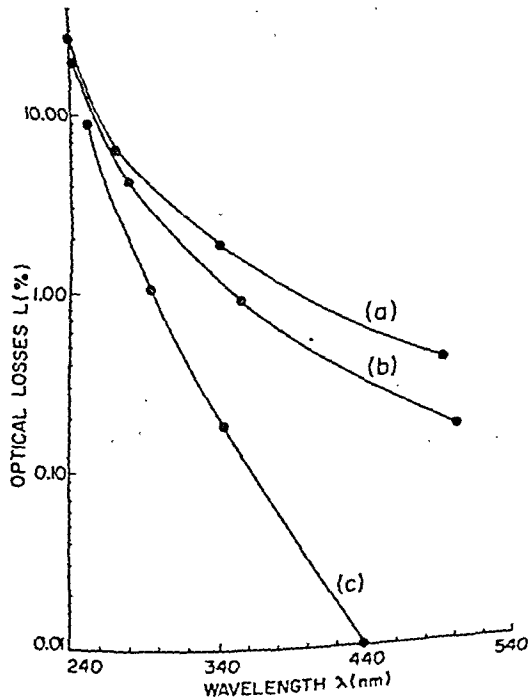


Fig. 2—Dependence of optical losses of ZrO_2 films on rate of evaporation [(a), 20 Å/s; (b) 10 Å/s; and (c) 5 Å/s; ($t \approx 275$ nm, $T = 260^\circ\text{C}$, pressure of ambient $\text{O}_2 = 2 \times 10^{-4}$ mbar)]

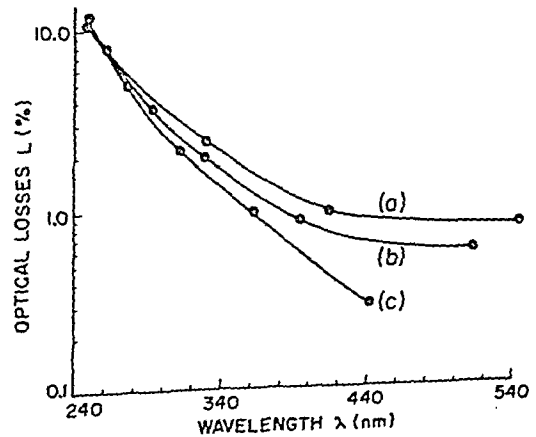


Fig. 3—Dependence of optical losses of ZrO_2 films on substrate temperature [(a), 100°C ; (b), 260°C ; and (c) 400°C ($t \approx 400$ nm, $R = 5$ Å/s, pressure of ambient $\text{O}_2 = 1 \times 10^{-4}$ mbar)]

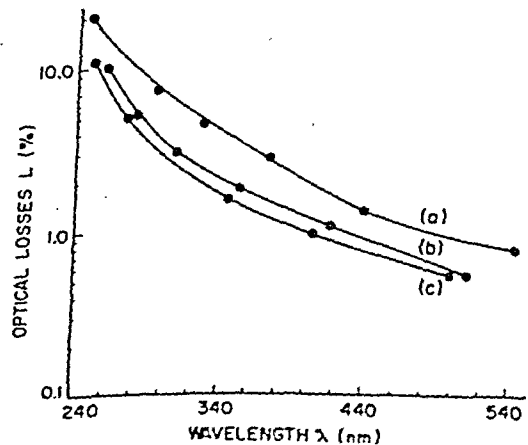


Fig. 4—Dependence of optical losses of ZrO_2 films on oxygen ambient pressure [(a), 5×10^{-4} mbar; (b), 1×10^{-4} mbar; and (c) 2×10^{-4} mbar; ($t \approx 550$ nm, $R = 5$ Å/s, $T = 300^\circ\text{C}$)]

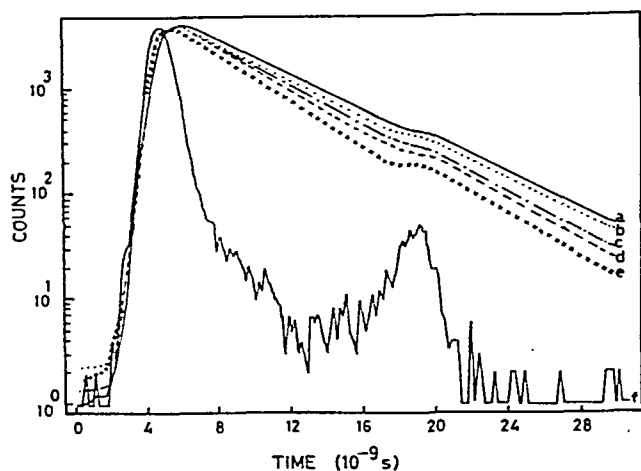


Fig. 1—Fitted decay curves for acriflavine (conc. $5 \times 10^{-4} M$) in presence of acceptor rhodamine B in cellulose acetate [Rhodamine B conc. are: (a) 0 M (b) $7.5 \times 10^{-5} M$ (c) $1 \times 10^{-4} M$ (d) $4 \times 10^{-5} M$ (e) $1 \times 10^{-3} M$ and (f) lamp profile]

where t is the donor decay time in the absence of the acceptor, $\gamma = C_A/C_A^0$ in which C_A^0 is the critical transfer. The various fitted parameters are given in Table 1. The χ^2 values suggest that the fitting is good and the critical transfer distances R_0 corresponding to C_A^0 are consistent for all the acceptor concentrations.

The critical transfer distance for Forster mechanism of transfer was also calculated from spectroscopic data using the following expression:

$$R_0^6 = 9.0 \times 10^{-25} \beta^2 \phi_D \Omega n^{-4}$$

where β^2 is the orientation factor which is 2/3 for random orientation, Ω the overlap integral, ϕ_D the quantum yield of the donor in the absence of acceptor and n the refractive index of the matrix.

The value of R_0 from this expression comes out to be 55 Å, which is in perfect agreement with the result of the above analysis of donor decay time. Thus, the non-radiative energy transfer is found to occur through Forster mechanism (dipole-dipole interaction).

In Fig. 2, the various curves show the combined spectra of acriflavine-rhodamine B system in cellulose acetate for a fixed concentration of acriflavine and varying concentrations of rhodamine B under the same geometrical conditions. The exciting wavelength 3480 Å is practically not absorbed by rhodamine B. Therefore, the acceptor emission is largely via the energy transfer from acriflavine. The energy transfer appears to be radiative also, because the acriflavine band shifts to shorter wavelength with increasing acceptor concentration.

The authors are thankful to the Department of Science & Technology, Government of India, New Delhi, for financial assistance.

References

- 1 Weber W H & Lambe J, *Appl Opt (USA)*, 15 (1976) 2299.

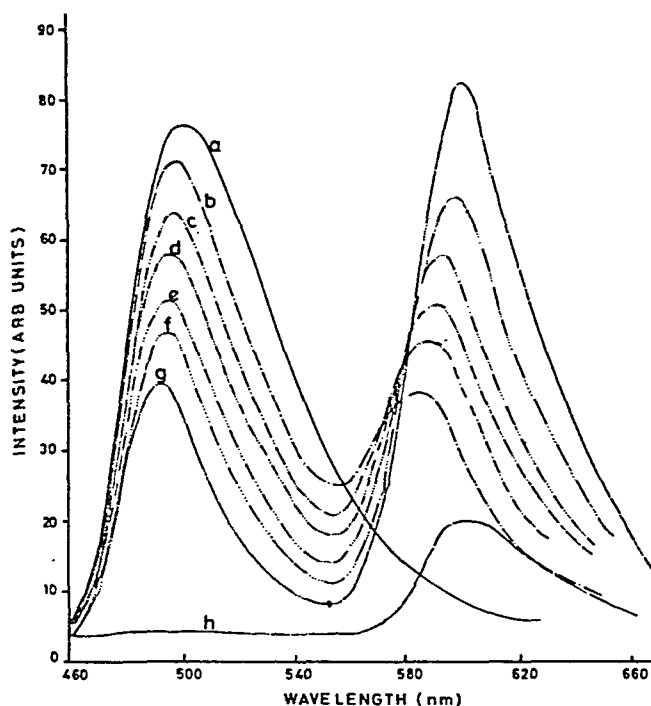


Fig. 2—Variation of fluorescence intensities of acriflavine (donor)-rhodamine B (acceptor) system in cellulose acetate at different rhodamine B concentrations [Rhodamine Conc.: (a) 0 M (b) $5 \times 10^{-5} M$ (c) $1 \times 10^{-4} M$ (d) $2 \times 10^{-4} M$ (e) $3 \times 10^{-4} M$ (f) $5 \times 10^{-4} M$ (g) $2 \times 10^{-3} M$ and (h) pure rhodamine B ($2 \times 10^{-3} M$)]

Table 1—Values of Parameters Used to Fit the Fluorescence Response According to Forster Mechanism

$\gamma = C_A/C_A^0$	Acceptor concentration $C_A (M)$	Critical concentration $C_A^0 (M)$	$R_0 (\text{Å})$	χ^2
—	Donor conc. $C_D = 5 \times 10^{-4} M$			—
0.034	7.5×10^{-5}	2.2×10^{-3}	56	1.104
0.054	10^{-4}	1.96×10^{-3}	59	1.054
0.177	4×10^{-4}	2.3×10^{-3}	55.6	0.946
0.230	5×10^{-4}	2.2×10^{-3}	56	1.411
0.338	10^{-3}	2.7×10^{-3}	51	1.120

- 2 Geotzberger A & Wittwer V, *Adv Solid St Phys (Netherlands)*, 19 (1979) 427.
- 3 Geotzberger A & Greubel B, *Appl Phys (Germany)*, 14 (1977) 123.
- 4 Wienreb A, *J Chem Phys (USA)*, 35 (1961) 91.
- 5 Durgapal A B, Agarwal A K, Pant K C & Pant T C, *Indian J Pure & Appl Phys*, 22 (1984) 58.
- 6 Mataga N, Kobashi H & Okada T, *Chem Phys Lett (Netherlands)*, 1 (1967) 133.
- 7 Pant T C, Bhatt B C & Pant D D, *J Luminescence (Netherlands)*, 27 (1982) 425.
- 8 Lu P Y, Alfano R R U Z X & Gersten G I, *Phys Rev A (USA)*, 27 (1983) 2100.
- 9 Swartz B A, Cole T & Zewail A H, *Opt Lett (USA)*, 1 (1977) 73.
- 10 Kellog R E, *J Chem Phys (USA)*, 41 (1964) 3046.
- 11 Bozarski C, *Acta Phys Pol (Poland)*, 33 (1968) 573.
- 12 Durgapal A B, Agarwal A K, Pant T C & Pant K C, *Indian J Phys Part B*, 58 (1984) 522.
- 13 Connor D V O & Philips D, *Time correlated single photon counting* (Academic Press, New York) 1984.
- 14 Forster T H, *Disc Faraday Soc (GB)*, 27 (1959).

Indian Journal of Pure & Applied Physics

INSTRUCTIONS TO AUTHORS

SCOPE

The journal welcomes, for publication, full papers and short notes, reporting significant new results of research, in all areas of physics except space physics. The applied fields covered are electronics, electrical engineering, instrumentation and applied mathematics. However, papers in applied mathematics with emphasis on only derivation and proofs and having no direct physical significance, will not be considered. Review articles are not published normally.

SUBMISSION OF MANUSCRIPT

Manuscripts for consideration should be submitted, *in duplicate*, to Editor, Indian Journal of Pure & Applied Physics, Publications & Information Directorate, Hillside Road, New Delhi 110012. They should neither have been already published nor be under consideration elsewhere.

Manuscripts should be in English and typewritten on only one side of good quality paper, in double space, with adequate margin on all four sides. One original and one carbon or photo-copy, each complete in all respects including abstract, illustrations, appendixes, etc. are to be submitted.

PREPARATION OF MANUSCRIPT

Authors may consult recent issues of the Journal to familiarize themselves with the general style and practices adopted in regard to the various elements of a paper.

General

Manuscript should be presented in as concise a form as possible. Good attention should be given to spelling and grammar. In giving names of chemical compounds and structures, abbreviations of units of measurements, symbols and notations, the style and practices recommended by the IUPAP and IUPAC, should be followed.

Frequently repeating combinations of words, e.g. electric field gradient (EFG), junction field effect transistor (JFET), stimulated Raman emission (SRE), should be abbreviated subsequently, indicating the abbreviated form in parenthesis, as shown, at the place of their first occurrence.

Pages should be numbered consecutively and arranged in the following order: Title, authors' names with their institutional affiliations and abstract, along with relevant footnotes whenever necessary (on a separate sheet); introduction; experimental details/theory/method/analysis; results; discussion; conclusion(s); acknowledgement; references and appendixes. Tables, captions for figures (with legends) and appendixes should be typed *on separate sheets* and attached at the end of the manuscript.

Title

The title should be neither too brief/general nor unnecessarily long. It should reflect the content of the paper so as to derive the maximum advantage in indexing. If a paper forms part of a general series, a specific subtitle, indicating the particular aspect of the work covered in the paper, should be provided.

A short running title for the paper, the broad PACS subject heading under which it should be classified in the contents page (authors may consult the January or July issue of the journal for this purpose), and the author's name and address for correspondence, should also be provided on the title page.

Abstract

The abstract, usually not exceeding 200 words, should indicate the scope and significant content of the paper,

highlighting the principal findings and conclusions. It should be in such a form that abstracting periodicals can use it without modification.

Introduction

Long and elaborate introduction should be avoided. It should be brief and state the exact scope of the study in relation to the present status of knowledge in the field. Literature review should be limited strictly to what is necessary to indicate the essential background and the justification for undertaking the study.

Materials, methods, apparatus, etc.

The sources of materials and their purity, methods of preparation, procedure for measurements and their accuracies, etc. should be clearly stated to enable any other worker to repeat the work if necessary. New methods, techniques, theories, etc. should be described in adequate detail; but if they are well known, a mere literature reference to them will do; differences from standard ones, improvements or innovations should, however, be clearly mentioned.

Results

Only such primary data as are essential for understanding the discussion and main conclusions emerging from the study should be included. All secondary data as are of interest to a specific category of readership *should not be included* in the paper. Such data should be retained by the authors for supply, on request, to any interested research worker. A footnote to this effect may be inserted at the relevant place in the paper.

The results must be presented in a coherent sequence in a unified logical structure, avoiding repetition or confusion. Limitations of the results should be clearly stated.

The same data should not be presented in both tabular and graphic forms. Only such tables and figures as are essential should be included. Simple linear plots that can easily be discussed in the text, should not be included. Infrared, ultraviolet, NMR and other spectra, DTA curves, etc. should be included only if they pertain to new compounds and/or are essential to the discussion; otherwise only significant numerical data should be given in the text or in a table.

Discussion

Long rambling discussion should be avoided. The discussion should deal with the interpretation of results without repeating information already presented under results. It should relate new findings to the known and include logical deductions. A separate section on 'conclusions' can be given only when they are well established and of outstanding significance. Mere observation of qualitative trends of results should be distinguished from firm conclusions. Also, limitations, if any, to the conclusions should be clearly pointed out.

Mathematical portions

Special attention should be given to the mathematical portions of the paper. Equations must be well separated from the text and written clearly with good separation between the successive lines. The usual norms of breaking long mathematical expressions should be adhered to. Equations should be numbered consecutively in Arabic numerals with the number in parenthesis near the right hand margin. Superscripts and subscripts should be clearly indicated in pencil by V and \wedge sign respectively. Capital and small letters,

particularly of the same letter when both occur, as well as letters or symbols likely to be confused one for the other, should be clearly distinguished. Special characters (e.g. Greek, script, vector, tensor, etc.) required must be indicated by marginal notes. Letters and symbols which should appear in bold face must be clearly indicated. To simplify typesetting: (i) long and complicated mathematical expressions which are frequently repeated should be replaced with single letter/symbol, without clashing with the others used in the paper; (ii) the "exp" form of complex exponential functions should be used; and (iii) to simplify fractions, the solidus (/) is to be used and fractional exponents are to be used instead of root signs, e.g.

write $\exp\{-i\omega_0(t_1 - t_2)/2\}$ and not $e^{-i\omega_0(t_1 - t_2)/2}$

write $(4\omega_{pl} K_{3\lambda}^2 / \bar{\omega} K_D^2)^{1/2}$ and not $\sqrt{\frac{4\omega_{pl} K_{3\lambda}^2}{\bar{\omega} K_D^2}}$

Tables

Tables should be numbered consecutively in Arabic numerals and should bear brief titles. Column headings should be brief. Units of measurement should be abbreviated and placed below the headings. Nil results should be indicated and distinguished clearly from absence of data. Inclusion of structural formulae inside the tables should be avoided as far as possible. Tables should be referred to in the text by numbers and not by terms like 'above', 'below', 'preceding' or 'following'. Results should not be presented to a greater accuracy than that of the method employed.

Illustrations

The number of illustrations should be kept to the minimum. Wherever possible, e.g. a number of individual analogous figures referring to different variables, substances, molecules, etc. may be combined into one composite figure. All illustrations should be numbered consecutively in Arabic numerals. Captions and legends to the figures should be self-explanatory. Line drawings should be made with Indian ink on white drawing paper/cellophane sheet/tracing cloth, and drawn to approximately twice the printed size.

The lettering should be uniform, preferably in stencil, so as to be not less than 1.5 mm after reduction widthwise to full page size (165 mm) or column size (80 mm). The size of geometrical shapes (used to distinguish different graphs), dots, lines, etc. should be sufficiently large to permit the necessary reduction without loss of detail. In the case of photographs, prints must be on glossy paper and contrasty. If an illustration is taken from another publication, reference to the source should be given and prior permission secured. Illustrations should be referred to in the text by numbers and not by terms like 'above', 'following' etc.

Acknowledgement

Acknowledgements should not be exuberant and must be made only to real assistance rendered in connection with the work reported in the paper.

References

References cited should be limited to the absolute minimum (particularly in the case of short notes) based on their essential relevance. In the text, references to literature should be numbered consecutively, in the order of their first occurrence, and should be indicated by superscript Arabic numbers at the relevant places; as far as possible the placement of references on numerals or other symbols should be avoided; in such cases the reference may be given in parenthesis in running text, e.g. "this yielded for n a value of 2.3 (Ref. 5)". Full bibliographic details for all the references mentioned in the text should be listed in serial order at the end of the paper.

In citing references to research papers, names and initials of authors should be followed, in order, by the title of the periodical in the abbreviated form (underlined), the volume number (two lines underneath), the year within circular brackets and the page number [e.g. Chandra B P & Shrivastava KK, *J Phys & Chem Solids* (GB), 39 (1978) 939]. For names of periodicals, the abbreviations followed by the *Physics Abstracts* should be used. For periodicals not covered by *Physics Abstracts*, the title abbreviations should be according to the *Bibliographic Guide for Editors and Authors*, 1974, published by the American Chemical Society, Washington DC, USA; additionally the country from which the journal is published should be given in parenthesis immediately after the title abbreviation. If a paper has been accepted for publication, the names of the authors and the journal (with volume number and year, if known) should be given followed by the words "in press" [e.g. Wahi P K & Patel N D, *Can J Spectrosc* (Canada), in press.].

In references containing up to four authors, the names of all the authors with their respective initials should be given. The abbreviations *et al.*, *idem* and *ibid* should be avoided. When there are more than four authors, only the names of the first three authors with their respective initials should be given, followed by the words 'et al.'

Reference to a book should include details in the following order: name and initials of authors, the title of the book (underlined), name of publisher and place of publication within circular brackets and year and page (s) [e.g. Clayton G B, *Operational amplifiers* (Newnes-Butterworths, London), 4th Edn, 1977, 26]. If the reference is to the work of an author published in a book by a different person, the fact that it is cited from the source book should be clearly indicated [e.g. Turnhout Van J, 'Thermally stimulated discharge of electrets' in *Topics in applied physics*: Vol. 33—*Electrets*, edited by C M Sessler (Springer Verlag, Berlin), 1980, 130].

Proceedings of conferences and symposia should be treated in the same manner as books. Reference to a paper presented at a conference, the proceedings of which are not published, should include, in the following order, names and initials of authors, title of the paper (underlined), name of the conference, and where and when it was held (e.g. Herczeg P, *Symmetry-violating kaon decays*, paper presented to the International Conference on High Energy Physics and Nuclear Structure, Vancouver, Canada, 13-17 August 1979).

Reference to a thesis should include the name of the author, title of the thesis (underlined), university or institution to which it was submitted and year of submission (e.g. Mehrotra S N, *Many-body techniques and their applications to interacting bosons*, Ph D thesis, Ranchi University, 1976).

Reference to a patent should include names of patentees, country of origin (underlined) and patent number, the organization to which the patent has been assigned (within circular brackets), date of acceptance of the patent and reference to an abstracting periodical where available [e.g. Labes M M, *US Pat.* 4,066,567 (to Temple University), 3 January 1978; *Chem. Abstr.*, 88 (No. 20) (1978), 138350 n].

PROOFS & REPRINTS

The edited manuscript will be sent to the author for his final approval before giving it to the press. No galley proofs will be sent to the authors for corrections, since the proofs will be checked at the editorial office. Authors are given 25 free reprints for each paper. Extra reprints can be ordered by the author while returning the edited manuscript. If the reprints order is not received, it will be presumed that no extra reprints are needed.

CSIR SCIENTIFIC PERIODICALS

JOURNAL OF SCIENTIFIC & INDUSTRIAL RESEARCH (Monthly)

With a fine record of over 45 years' service to the scientific community, this journal has grown into India's leading general science periodical. Intended to fulfil the responsibility of helping the research workers to keep themselves abreast of current developments in various fields of science and technology, the journal carries editorial features highlighting important scientific events in India and abroad, articles on science policy and management of science review articles on topics of current research interest, technical reports on international and national conferences, reviews of scientific and technical publications, and notes on major advances in various fields.

Annual subscription	Rs 120.00	\$ 40.00	£ 23.00
Single copy	12.00	4.00	2.30

INDIAN JOURNAL OF CHEMISTRY (Monthly)

Section A: Started in the year 1963, the journal is devoted to papers in Inorganic, Physical, Theoretical and Analytical Chemistry.

Annual subscription	Rs 160.00	\$ 53.00	£ 30.00
Single copy	16.00	5.30	3.00

Section B: This journal is devoted to papers in Organic Chemistry, including Medicinal Chemistry.

Annual subscription	Rs 160.00	\$ 53.00	£ 30.00
Single copy	16.00	5.30	3.00

INDIAN JOURNAL OF PURE & APPLIED PHYSICS (Monthly)

Started in the year 1963, this journal is devoted to original research communications (full papers and short communications) in all conventional branches of physics (except radio and space physics).

Annual subscription	Rs 180.00	\$ 60.00	£ 34.00
Single copy	18.00	6.00	3.40

INDIAN JOURNAL OF RADIO & SPACE PHYSICS (Bimonthly)

The journal, which is being published beginning from March 1972, is intended to serve as a medium for the publication of the growing research output in various areas of radio and space physics, such as ionospheric propagation, magnetosphere, radio and radar astronomy, physics and chemistry of the ionosphere, neutral atmosphere; airglow, winds and motion in the upper atmosphere; stratosphere-mesosphere coupling, ionosphere-magnetosphere coupling; solar-terrestrial relationship, etc.

Annual subscription	Rs 100.00	\$ 34.00	£ 19.00
Single copy	20.00	6.80	3.80

INDIAN JOURNAL OF TECHNOLOGY (INCLUDING ENGINEERING) (Monthly)

This journal publishes papers reporting results of original research of applied nature pertaining to unit operations, heat and mass transfer, products, processes, instruments and appliances, etc. The journal is of special interest to research workers in departments of applied sciences in universities, institutes of higher technology, commodity research laboratories, industrial cooperative research institutes, and industrial research laboratories.

Annual subscription	Rs 120.00	\$ 40.00	£ 23.00
Single copy	12.00	4.00	2.30

INDIAN JOURNAL OF EXPERIMENTAL BIOLOGY (Monthly)

This journal, devoted to the publication of research communications in the fields of experimental botany, zoology,

microbiology, pharmacology, endocrinology, nutrition, etc., is the only one in India with such a wide coverage and scope.

Annual subscription	Rs 180.00	\$ 68.00	£ 34.00
Single copy	18.00	6.80	3.40

INDIAN JOURNAL OF BIOCHEMISTRY & BIOPHYSICS (Bimonthly)

This journal, published in association with the Society of Biological Chemists (India), Bangalore, is the only research journal in India devoted exclusively to original research communications in biochemistry and biophysics.

Annual subscription	Rs 65.00	\$ 23.00	£ 12.00
Single copy	13.00	4.60	2.40

INDIAN JOURNAL OF MARINE SCIENCES (Quarterly)

Commencing publication from June 1972, this journal is devoted to research communications (full papers and short communications) pertaining to various facets of marine research, viz. biological, physical, geological and chemical oceanography.

Annual subscription	Rs 90.00	\$ 30.00	£ 17.00
Single copy	26.00	8.70	5.00

RESEARCH AND INDUSTRY (Quarterly)

Intended to serve as a link between science and industry, this journal is addressed primarily to technologists, engineers, executives and others in industry and trade. It publishes informative original articles containing practical details of processes and products devoted in India, which show promise of ready utilization, and technical digests on new processes, products, instruments and testing methods which are of interest to industry. Developments in Indian industry are regularly reported.

Annual subscription	Rs 70.00	\$ 23.00	£ 13.00
Single copy	22.00	7.00	4.00

INDIAN JOURNAL OF TEXTILE RESEARCH (Quarterly)

Commencing publication from March 1976, this journal is devoted to the publication of papers reporting results of fundamental and applied researches in the field of textiles.

Annual subscription	Rs 50.00	\$ 17.00	£ 10.00
Single copy	15.00	5.00	3.00

MEDICINAL & AROMATIC PLANTS ABSTRACTS (Bimonthly)

Carries informative abstracts of scientific papers published in important Indian and foreign journals relating to different aspects of medicinal and aromatic plants. Each issue contains about 350 abstracts with a subject index.

Annual subscription	Rs 120.00	\$ 40.00	£ 23.00
Single copy	24.00	8.00	4.60

CURRENT LITERATURE ON SCIENCE OF SCIENCE (Monthly)

Carries abstracts, digests, book reviews, news & notes and R&D statistics with emphasis on problems of S&T in developing countries, it also covers the areas of science policy, R&D planning and management, technology transfer, technology assessment and science and society.

Annual subscription	Rs 100.00	\$ 30.00	£ 12.00
---------------------	-----------	----------	---------

Please contact

SALES AND DISTRIBUTION OFFICER
PUBLICATIONS & INFORMATION
DIRECTORATE, CSIR
Hillside Road, New Delhi-110012

CSIR PUBLICATIONS

WEALTH OF INDIA

An encyclopaedia of the economic products and industrial resources of India issued in two series

RAW MATERIALS SERIES—contains articles on plant, animal and mineral resources

	Rs	\$	£
Vol. I (A-B)	80.00	30.00	13.00
Vol. II (C)	95.00	33.00	17.00
Vol. III (D-E)	105.00	32.00	20.00
Vol. IV (F-G)	65.00	27.00	12.00
Supplement (Fish & Fisheries)	56.00	16.00	10.50
Vol. V (H-K)	114.00	34.00	21.00
Vol. VI (L-M)	90.00	34.00	15.00
Supplement (Livestock)	102.00	34.00	19.50
Vol. VII (N-Pe)	100.00	30.00	19.00
Vol. VIII (Ph-Re)	86.00	32.00	14.00
Vol. IX (Rh-So)	104.00	35.00	19.00
Vol. X (Sp-W)	225.00	75.00	42.50
Vol. XI (X-Z)	115.00	38.50	22.00

INDUSTRIAL PRODUCTS SERIES—deals with major, small-scale and cottage industries

Part I (A-B)	58.00	20.00	11.00
Part II (C)	74.00	24.00	14.00
Part III (D-E)	100.00	33.50	19.50
Part IV (F-H)	126.00	42.00	24.00
Part V (I-L)	90.00	23.00	17.00
Part VI (M-Pi)	28.00	8.00	2.80
Part VII (Pi-Sh)	60.00	18.00	6.00
Part VIII (Si-Ti)	66.00	27.00	10.00
Part IX (To-Z)	80.00	34.00	12.00

BHARAT KI SAMPADHA (Hindi Edition of Wealth of India, Raw Materials)

Vol. I (अ-क)	38.00	16.00	6.50
Vol. II (क)	36.00	15.00	6.00
Vol. III (ख-न)	36.00	15.00	6.00
Vol. IV (प)	83.00	34.00	16.00
Vol. V (फ-ये)	60.00	22.00	10.00
Vol. VI (य-र)	80.00	27.00	13.00
Vol. VII (रे-दा)	135.00	40.00	25.00
Livestock (Kukkut Palan)	34.00	15.00	6.00
Fish & Fisheries (Matsya aur Matsyaki)	49.00	21.00	8.00
A Dictionary of Generic & Specific Names of Plants and Animals Useful to Man with their English and Latin pronunciation in Devanagari.	30.00	11.00	5.00

OTHER PUBLICATIONS

Proceedings: seminar on primary communications in Science & Technology in India by Sh. R.N. Sharma & S. Seetharama	52.00	17.50	9.00
Flora of Delhi by J.K. Maheshwari	28.00	8.00	2.80
Indian Fossil Pteridophytes by K.R. Surange	66.00	22.00	12.50
Indian Thysanoptera by T.N. Ananthakrishnan	26.00	8.00	2.60
The Millipede Thyropygus by G. Krishnan	12.00	3.50	1.20
Drug Addiction with special reference to India by R.N. Chopra & I.C. Chopra	12.00	3.50	1.20
Glossary of Indian Medicinal Plants by R.N. Chopra & I.C. Chopra	35.00	13.00	6.00
Fluidization & Related Processes	12.00	4.00	1.20
Evolution of Life by M.S. Randhawa, A.K. Dey, Jagjit Singh & Vishnu-Mitre	22.50	7.00	2.25
Collected Scientific Papers of Meghnad Saha	30.00	9.00	3.00
Proteaceae by C. Venkata Rao	72.00	24.00	13.50
Pinus by P. Maheshwari & R.N. Konar	30.00	11.00	5.00
Cellulose Research I	3.00	0.90	0.30
Cellulose Research II	6.00	1.75	0.60
Chemical Process Design	9.00	2.50	0.90
Low Temperature Carbonization of Non-coking Coals & Lignites & Briquetting Coal Fines: Vol. I & Vol. II (each volume)	17.50	5.50	1.75
Nucleic Acids	10.00	3.00	1.00
IGY Symposium: Vol. I	9.00	2.50	0.90
IGY Symposium: Vol. II	9.00	2.50	0.90
CNS Drugs	16.50	5.00	1.65
Kinetics of Electrode Processes & Null Points of Metals	2.50	0.75	0.25
Indian Sardines by R.V. Nair	22.00	7.00	2.20
Termite Problems in India	9.00	3.00	0.90
Loranthaceae by B.M. Johri & S.P. Bhatnagar	55.00	18.50	10.50
Abies and Picea by K.A. Chowdhury	14.00	6.00	2.10
Gnetum by P. Maheshwari and Vimla Vasil	20.00	6.00	2.00
Aquatic Angiosperms by K. Subramanyam	20.00	6.00	2.00
Supplement to Glossary of Indian Medicinal Plants by R.N. Chopra, I.C. Chopra & B.S. Varma	18.00	7.00	3.00
Herbaceous Flora of Dehra Dun by C.R. Babu	144.00	60.00	22.00
Diosgenin and Other Steroid Drug Precursors by Y.R. Chadha & Miss L.V. Asolkar	36.00	13.00	6.00
Research & Development Management by Inder Dev	25.00	10.00	—
Rural Development and Technology—A Status Report-cum-Bibliography by P.R. Bose & V.N. Vashist	100.00	38.00	17.00
Cholera Bacteriophages by Sachinmohan Mukherjee	30.00	10.00	6.00

Packing and Postage extra

Please contact:

SALES AND DISTRIBUTION OFFICER
PUBLICATIONS & INFORMATION DIRECTORATE, CSIR
Hillside Road, New Delhi 110012

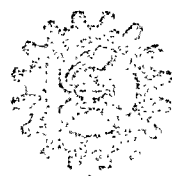
Printed & Published by D.S. Sastry, Editor, Publications & Information Directorate (PID)
 Hillside Road, New Delhi 110012, at PID Photocomposition Unit

Indian J Pure & Appl Phys, Vol 24 No 12 pp 565-614

DECEMBER 1986

CODEN : IJOPAU ISSN : 0019-5596
24(12) 565-614 (1986)

INDIAN JOURNAL OF PURE & APPLIED PHYSICS



Published by
PUBLICATIONS & INFORMATION DIRECTORATE, CSIR
NEW DELHI

in association with
THE INDIAN NATIONAL SCIENCE ACADEMY, NEW DELHI

Announcing

The Wealth of India

Raw Materials: Volume-I: A

(Revised Edition)

Contains 204 entries: 198 on plant genera and 6 on minerals

This volume is the first of the revised and enlarged edition of this encyclopaedic classic on Indian Raw Materials, brought out with updated information. It covers economically important raw materials of plants and minerals contained in the alphabet A. Each plant entry gives the correct nomenclature of the genus and species dealt with, their distribution in India, and a short description of the economically important parts.

The articles on crop plants, medicinal and timber yielding plants etc. give in considerable detail the methods of cultivation, silvicultural practices, agricultural inputs, harvesting and storage etc. besides mentioning diseases and pests and their control measures. Chemical composition and utilization of raw materials are covered in detail for important economic crops and products; statistical data concerning area, production, export, import etc. are given. In the case of minerals, their occurrence and distribution in the country, methods of mining, extraction, chemical composition and utilization are given.

Adequate references to the sources of information are provided at appropriate places. The articles are illustrated with half-tones, line drawings, charts and colour plates. The Index covers botanical and zoological names, and names of chemical compounds, besides common English, regional and trade names.

The revised edition provides useful updated information to research workers, students, industrialists, planners, and others interested in the raw material resources of India.

Pages: *Text*, 513 + *Index*, 54

Price: Rs. 200.00

\$ 47.00

£ 37.00

Kindly send your orders to:

The Sales & Distribution Officer

Publications & Information Directorate, CSIR

Hillside Road, New Delhi 110 012

RENEWAL NOTICE

Your subscription which expires with the despatch of December 1986 issue of the journal, stands for renewal. We request you to be so good as to return the enclosed order form duly filled, early, so as to ensure continuity in despatch.

Sales & Distribution Officer

DATED:

The Sales & Distribution Officer
PUBLICATIONS & INFORMATION DIRECTORATE
HILLSIDE ROAD, NEW DELHI-110012 (INDIA)

Dear Sir,

Please renew my subscription/enrol me as subscriber to:

		Rs.	\$	£
1 Journal of Scientific & Industrial Research	(Monthly)	140.00	46.00	26.00
2 Indian Journal of Chemistry, Section A	(Monthly)	200.00	65.00	38.00
3 Indian Journal of Chemistry, Section B	(Monthly)	200.00	65.00	38.00
4 Indian Journal of Experimental Biology	(Monthly)	180.00	68.00	34.00
5 Indian Journal of Technology	(Monthly)	120.00	40.00	23.00
6 Indian Journal of Pure & Applied Physics	(Monthly)	180.00	60.00	34.00
7 Indian Journal of Biochemistry & Biophysics	(Bimonthly)	80.00	27.00	15.00
8 Indian Journal of Radio & Space Physics	(Bimonthly)	100.00	34.00	19.00
9 Indian Journal of Marine Sciences	(Quarterly)	100.00	34.00	19.00
10 Indian Journal of Textile Research	(Quarterly)	70.00	23.00	13.00
11 Research & Industry	(Quarterly)	90.00	30.00	17.00
12 Current Literature on Science of Science	(Monthly)	100.00	30.00	12.00
13 Medicinal & Aromatic Plants Abstracts	(Bimonthly)	160.00	53.00	30.00

(Please tick off the periodicals you would like to subscribe).

for one year from January 1987 for which I/we have remitted to you
a sum of Rs£ \$ by Cheque/Demand
Draft No. dated in favour of
PUBLICATIONS & INFORMATION DIRECTORATE, NEW DELHI.

COMPLETE MAILING ADDRESS

Name

Address

Country/State

(Signature)

Note:

1. Subscribers at annual rates for all the periodicals are enlisted for the full volumes, i.e. for the period from January to December only.
2. The Cheque Demand Draft may please be drawn in favour of "PUBLICATIONS & INFORMATION DIRECTORATE, NEW DELHI". Banking charges shall be borne by the subscriber. For inland outstation cheques please add Rs. 3.50. For foreign cheques please add \$ 1.00 or £ 0.45.
3. The supply will commence on receipt of subscription in advance

Indian Journal of Pure & Applied Physics

EDITORIAL BOARD

Prof. S. Chandrasekhar
Raman Research Institute
Bangalore

Prof. R V Gopala Rao
Jadavpur University
Calcutta

Prof. S K Joshi
Indian National Science Academy
New Delhi/Roorkee University
Roorkee

Prof. P Krishna
Indian National Science Academy,
New Delhi/Banaras Hindu University
Varanasi

Prof Kehar Singh
Indian Institute of Technology
New Delhi

Prof C L Mehta
Indian Institute of Technology
New Delhi

Prof. S P Pandya
Physical Research Laboratory
Ahmedabad

Dr K R Rao
Bhabha Atomic Research Centre
Bombay

Prof. D K Rai
Banaras Hindu University
Varanasi

Prof. B V Sreekantan
Tata Institute of Fundamental Research
Bombay

Prof. R Srinivasan
University of Madras
Madras

Prof. Suresh Chandra
Banaras Hindu University
Varanasi

Shri S P Ambasta, Editor-in-Chief (*Ex-officio*)

EDITORIAL STAFF

Editors

D S Sastry & K S Rangarajan

Assistant Editors

J B Dhawan, Tarun Banerjee & (Mrs) Poonam Bhatt

Published by the Publications & Information Directorate, CSIR, Hillside Road, New Delhi 110012

Editor-in-Chief: S P Ambasta

The Indian Journal of Pure & Applied Physics is issued monthly. The Directorate assumes no responsibility for the statements and opinions advanced by contributors. The editorial staff in its work of examining papers received for publication is assisted, in an honorary capacity, by a large number of distinguished scientists, working in various parts of India.

Communications regarding contributions for publication in the journal should be addressed to the Editor, Indian Journal of Pure & Applied Physics, Publications & Information Directorate, Hillside Road, New Delhi 110012.

Correspondence regarding subscriptions and advertisements should be addressed to the Sales Distribution Officer, Publications & Information Directorate, Hillside Road, New Delhi 110012.

Annual Subscription

Rs. 180.00 £ 34.00 \$ 60.00

Single Copy

Rs. 18.00 £ 3.40 \$ 6.00

50% Discount is admissible to research workers and students and 25% discount to non-research individuals, on annual subscription. Payments in respect of subscriptions and advertisements may be sent by cheque, bank draft, money order or postal order marked payable *only* to Publications & Information Directorate, New Delhi 110012. Claims for missing numbers of the journal will be allowed only if received within 3 months of the date of issue of the journal plus the time normally required for postal delivery of the journal and the claim.

Announcement

Diamond Jubilee of the Discovery of 'Raman Effect'

The 'Raman Effect' made known to the world in 1928, is still an active field of research. As part of the celebrations of the 'Diamond Jubilee' of this discovery, the Indian Journal of Pure & Applied Physics is bringing out a special issue in March 1988 devoted to 'Raman Effect' studies.

Short articles not exceeding 4 pages of the journal and reporting new findings in this field are invited for this issue. All papers will be refereed and those recommended for publication will be included in this issue. Authors intending to contribute to this issue should send advance information to the editor about the title of the paper, authors and institutions, by 1 April 1987.

Manuscripts in triplicate (with one set of Indian ink drawings and two xerox copies) should reach the editor before end of July 1987.

Indian Journal of Pure & Applied Physics

VOLUME 24

NUMBER 12

DECEMBER 1986

CONTENTS

General Physics

- Interference-Free Determination of Nickel in Water by Graphite Furnace Atomic Absorption Spectrophotometry 594
Animesh Kumar, M Z Hasan & B T Deshmukh*

Physics of Elementary Particles & Fields

- Charmed Mesons in a Simple Two-Step Potential Model 596
Purnima Khare & L K Sharma*

Nuclear Physics

- Method for Estimation of Uranium, Thorium & Potassium in Rocks using Gamma Ray Spectrometry. 565
N P Singh, Manwinder Singh, Surinder Singh & H S Virk*

Atomic & Molecular Physics

- Laser Raman Spectra of 2 Fluoro-5-Chlorotoluene & 3 Fluoro-6-Chlorotoluene 570
S Mohan* & Feridoun Payami

- Vibrational Spectrum & Normal Coordinate Treatment of Potassium Phosphorodifluoride 574
S Mohan*, S Gunasekaran & M Parasuraman

- Electronic Absorption Spectrum of Ni^{2+} Ions Doped in Lithium Caesium Sulphate Single Crystal 577
B C Venkata Reddy* & B Munibhadraiah

- Green's Function Analysis of Vibrations of Thioformaldehyde 598
R Namasivayam & K Kannan*

- Infrared Absorption & Electronic Spectra of 2-Methylmercapto-3-methylpyrazine . . . 600
S L Srivastava*, M Prasad & Ranjeet Singh

Classical Areas of Phenomenology (Including Applications)

- Thermal Conduction & Probability of Phase Orientation in Porous & Dispersed Two-Phase Systems 580
Ramvir Singh*, R S Beniwal, R N Pande & V Kumar

- A Laser Interferometer for Vibration Amplitude Measurement of Power Ultrasonic Sources V.N Bindal*, S K Jain & Yudhisther Kumar 584

- Mirror Galvanometer X-Y Scanning System for Laser Beam Processes 588
S G Lokhre*, S Chandrasekhar & S K Roy

- Ultrasonic Investigation of Molecular Interactions in Binary Liquid Mixtures 602
S N Gour, J S Tomar & R P Varma*

Continued overleaf

CONTENTS

Condensed Matter: Structure, Mechanical & Thermal Properties

A Study on Thallium Sulphide Films	605
G D Talele* & A Goswami	

Condensed Matter: Electronic Structure, Electrical, Magnetic & Optical Properties

Dielectric Relaxation of Streptomycin at High Frequencies	592
V K Farkya* & Dinesh Kumar	

Correlation of Dielectric Relaxation Time & NMR Spin-lattice Relaxation Time of Some Substituted Glycol Methylethers	607
N K Mehrotra	

Effect of dc Field & X-ray Irradiation on the Optical Absorption and Thermoluminescence of LiF Single Crystals	609
N Veeraiah	

Wide-line PMR Study of Intramolecular Motion in Solid <i>p</i> -Hydroxybenzoic Acid	612
A Singh & R C Gupta*	

The author for correspondence is indicated by () mark in case of papers with more than one author

Method for Estimation of Uranium, Thorium & Potassium in Rocks using Gamma Ray Spectrometry

N P SINGH, MANWINDER SINGH, SURINDER SINGH & H S VIRK

Department of Physics, Guru Nanak Dev University, Amritsar 143 005

Received 22 August 1985; revised received 17 November 1986

Gamma ray spectrometric method for rapid determination of uranium, thorium and potassium in rocks using well-type NaI (Tl) crystal coupled to multichannel analyzer, is described. Critical sample weight requirement is found to be 16 g for 4π detector geometry. Combination of gamma ray peaks at 1.46, 1.76 and 2.62 MeV is found to be most suitable for K, U and Th analysis. The experimental set-up provides a good reproducibility of results.

1 Introduction

The method of estimating concentration of three radioactive elements, viz. U, Th and K by gamma ray spectrometry is well known¹⁻³. In the U spectrum, the prominent gamma ray peaks at 0.61, 1.12 and 1.76 MeV are often employed for the analysis of uranium. In the Th spectrum, prominent peaks at 0.24, 0.94 and 2.62 MeV are used for analysis of thorium, while the prominent 1.46 MeV peak of ⁴⁰K is used for potassium². Based on these gamma energy peaks of U, Th and K spectra, the combinations of gamma ray peaks used for analysis in various energy regions are as follows:

High (MeV)	Medium (MeV)	Low (MeV)
1.46	1.46	1.46
1.76	1.12	0.61
2.62	0.94	0.24

Using 10.16×5.08 cm NaI(Tl) detector coupled to a single channel analyzer, Rao¹ has described relative errors in analysis with 400 g samples in 2π geometry using high energy peaks centred at 1.46, 1.76 and 2.62 MeV. In the present work, we have employed well-type 7.62 (dia) $\times 7.62$ cm NaI(Tl) detector coupled to highly stabilized multichannel analyzer set-up. Using 4π detector geometry, the following studies have been undertaken:

- (a) The requirements for set-up (viz. the critical mass and background),
- (b) The comparison of errors using gamma peaks in various energy regions, and
- (c) The errors, reproducibility and comparison of gamma peaks in high energy region.

2 Experimental Details

Description of spectrometric set-up—The detector is an integral assembly consisting of a well-type 7.62

(dia) $\times 7.62$ cm NaI (Tl) crystal coupled to a photo-multiplier tube obtained from Bicron Ltd, USA. The detector offers provision for sample analysis in 4π geometry using a well-type crystal (Fig. 1). Resolution of the detector is 7.5% for ¹³⁷Cs. This detector is coupled to a multichannel analyzer (MCA) through preamplifier, amplifier and analog-to-digital converter (ADC). The spectrometer is calibrated using different gamma sources of known energy.

Background reduction—A basic requirement in low level counting is the reduction of background ra-

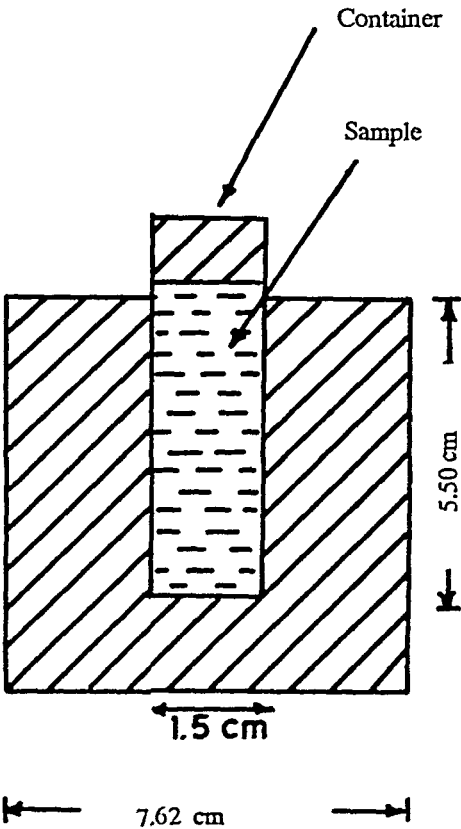


Fig. 1—Sample in 4π detector geometry

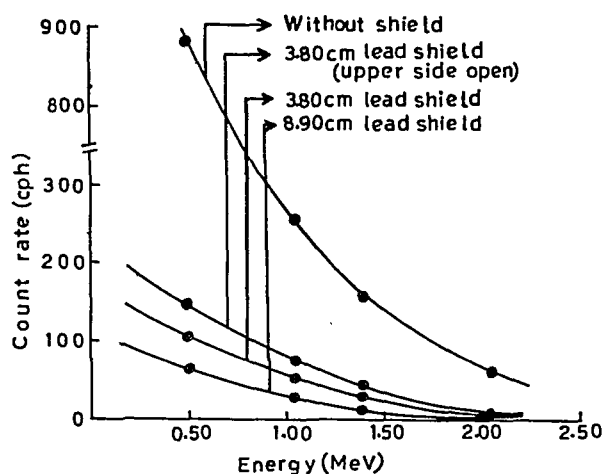


Fig. 2—Variation of count rate per hour (cph) with energy using different lead shields

Table 1—Results of Total/Background Ratio for Gamma Peaks of Different Energies in 4π Detector Geometry

Source	Around gamma peak (MeV)	Total/background
Uranium (312 ppm)	0.61	1.17
	1.12	1.75
	1.76	4.83
Thorium (166 ppm)	0.24	4.07
	0.94	1.91
	2.62	3.25
Potassium (26.6%)	1.46	2.22

dations and the enhancement of total background (T/B) ratio. Lead shield is employed for background reduction. Background count rate variation in 0 to 2.5 MeV energy region is studied using lead shielding of different geometrical thicknesses (Fig. 2).

Values of T/B ratio achieved for different gamma peaks with U (312 ppm), Th (166 ppm) and K (26.6%) sources in 4π detector geometry for a counting time of 1 hr, are reported in Table 1.

Critical mass studies—To find out the minimum limit for sample weight required for the analysis, experiments with varying sample weights are performed. The plot of count rate versus sample weight (Fig. 3) shows that the count rate becomes independent of weight beyond 16 g in 4π detector geometry.

Preparation of standard and the sample—Uranium and thorium standards are prepared from samples obtained from the National Geophysical Research Institute, Hyderabad. These samples, 350 g each, are U and Th ores diluted in dunite. U standard contains 312 ppm and 53 ppm Th. Th standard contains 166

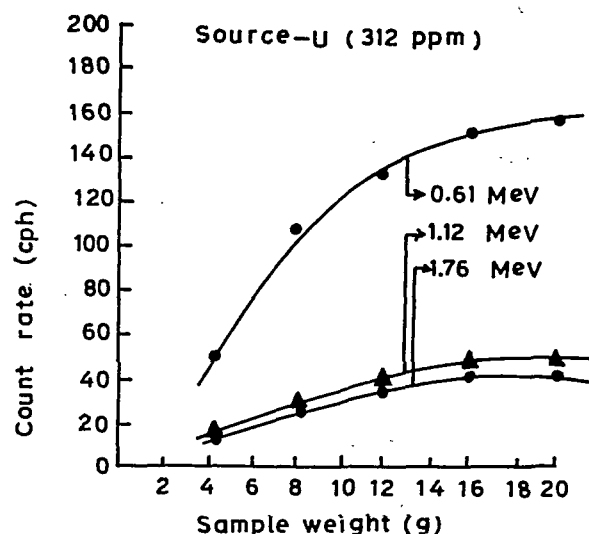


Fig. 3—Plot of count rate versus sample weight in 4π detector geometry

ppm Th and 5 ppm U. Potassium dichromate salt (26.6% K) is used as K standard. The sample to be analyzed is ground to 100 mesh and is sealed in a container. The containers are ranon-tight cylindrical plastic jars.

Counting procedure—Sample is placed in the well and the spectrum is taken for sufficient time, depending on the activity of the sample. Spectra of U, Th and K standards (Fig 4a, b, c) of comparable activity are recorded along with background spectrum for the same period using a teleprinter (Decwriter IV) coupled to MCA.

Method of data analysis—Matrix method developed by Stromswold and Kosanke⁴ is used for data analysis as follows:

The observed count rate R due to a concentration C of gamma-emitting elements can be written as:

$$R = AC \quad \dots (1)$$

where A is proportionality constant.

The right side of Eq. (1) can be expanded as follows to include contributions to the counts R , from all gamma rays

$$R = AC + \sum A' C' \quad \dots (2)$$

where the summation (\sum) is over all gamma emitters that contribute to R by energy shifts into the R window. For K, U and Th analyses, there are three terms on the right side of Eq. (2):

$$R = A_1 C_1 + A_2 C_2 + A_3 C_3 \quad \dots (3)$$

where C_1 , C_2 , and C_3 represent the concentrations of potassium, uranium, and thorium, respectively.

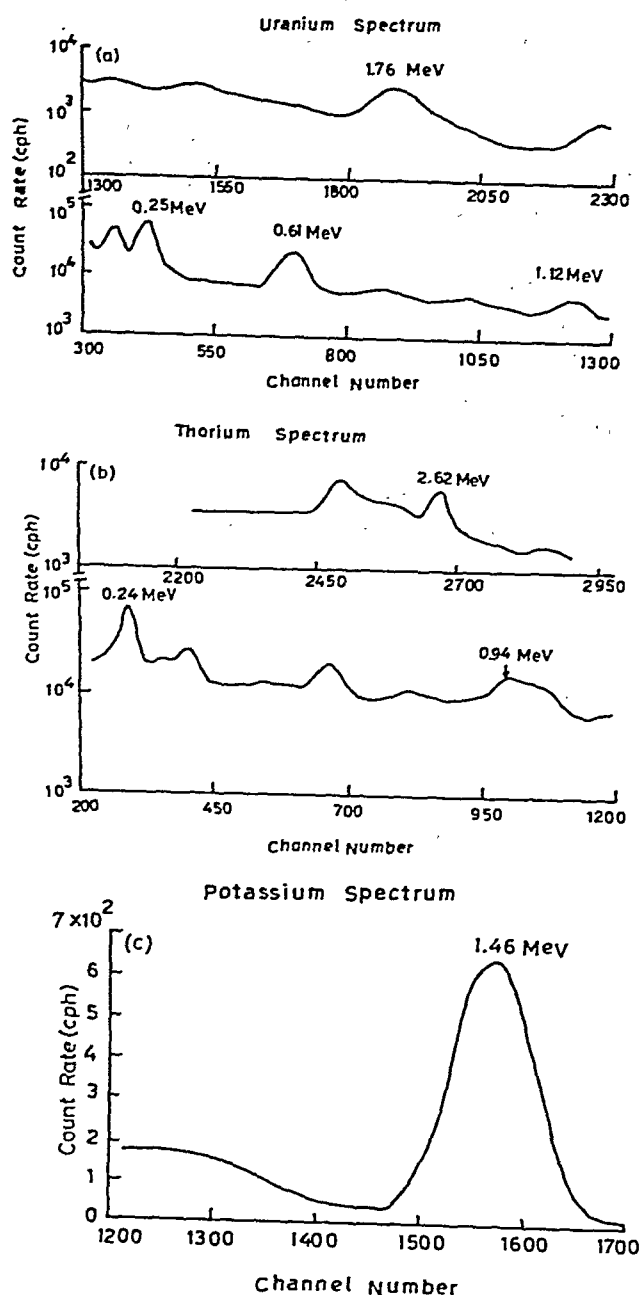


Fig. 4—Spectra of (a) uranium (b) thorium, and (c) potassium samples taken with 7.62×7.62 cm well-type NaI(Tl) detector

Because R can represent the count rate in any energy window, it is convenient to adopt the following index notation:

$$R_i = \sum_{l=1}^3 A_{il} C_l \quad \dots (4)$$

where R_i is the count rate in the i th window, C_l , concentration of l th radioactive element, and A_{il} is the constant relating count rate in i th window to the concentration of l th element.

Eq. (4) can be written in a matrix notation as:

$$R = AC \quad \dots (5)$$

where R and C are 3×1 matrices and A is a 3×3 . In this approach, Eq. (4) specifies one element, R_i , of the matrix R .

Eq. (5) can be inverted to give:

$$C = A^{-1} R \quad \dots (6)$$

where A^{-1} is the matrix inverse of A .

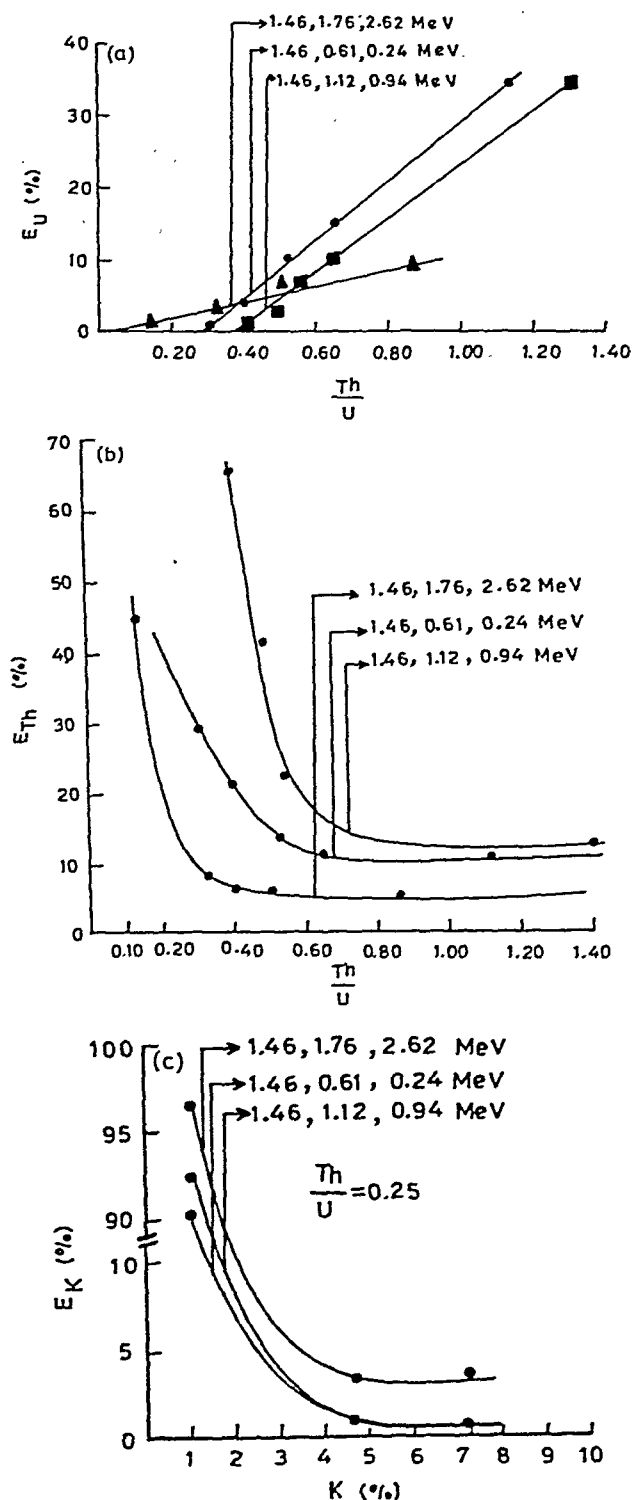


Fig. 5—Relative error of (a) uranium (b) thorium as a function of Th/U, and (c) potassium as a function of K

The matrices A and A^{-1} are determined by detector system calibration using sources of known concentration.

3 Results and Discussion

Set-up requirement of studies—The set-up requirements as ascertained by initial studies, are summarized as follows:

(a) From the variation of count rate in 0-2.5 MeV energy range, using different lead shields, it is observed that 8.90 cm thickness of lead reduces the background sufficiently (Fig. 2). With our set-up, the background reduction is better as compared to the set-up reported by Rao¹ (using 15.24 cm thick mild steel + 7.62 cm thick lead shield).

(b) The variation of count rate with sample weight in 4π detector geometry is shown in Fig. 3, and it is found to be independent of sample weight greater than 16 g. Thus the sample requirement for 4π geometry is fixed at 20g to avoid sample weight correction.

Selection of gamma ray peaks—Combinations of gamma ray peaks in low, medium and high energy regions are tried in sample analysis. T/B and relative errors (error in estimation of one element due to relative abundance of other elements) are studied for selec-

tion of gamma ray peaks (Table 1). From comparison it is evident that peaks under high energy region show better T/B ratio compared to peaks under low and medium energy regions. Using three combinations of gamma peaks, relative errors in analysis are also evaluated [Figs 5(a, b and c)]. Figs 5(a and b) show that high energy combination results in low relative error both in U and Th analysis. But relative error in K analysis is slightly more for high energy combination compared to low and medium energy combinations (Fig. 5c). This may be due to the fact that 1.46 MeV energy region lies in the back-scattered Compton contributions of high energy gamma rays⁵ (viz. 1.76 and 2.62 MeV).

Overall, the high energy combination is found to be the most suitable due to (i) high T/B under gamma peaks (ii) low relative error and (iii) the ease in computation work².

Sample analysis—Samples are analyzed using high energy combination of gamma peaks (1.46, 1.76, 2.62 MeV) and 4π detector geometry. Using standard samples, relative errors encountered in the analysis are studied [Figs 5(a, b and c) and 6(a, b, c and d)]. Fig. 5(a and b) shows the variation of relative errors with Th/U. Errors depending upon the relative abundance of K are reported in Fig 6(a, b, c and d). These

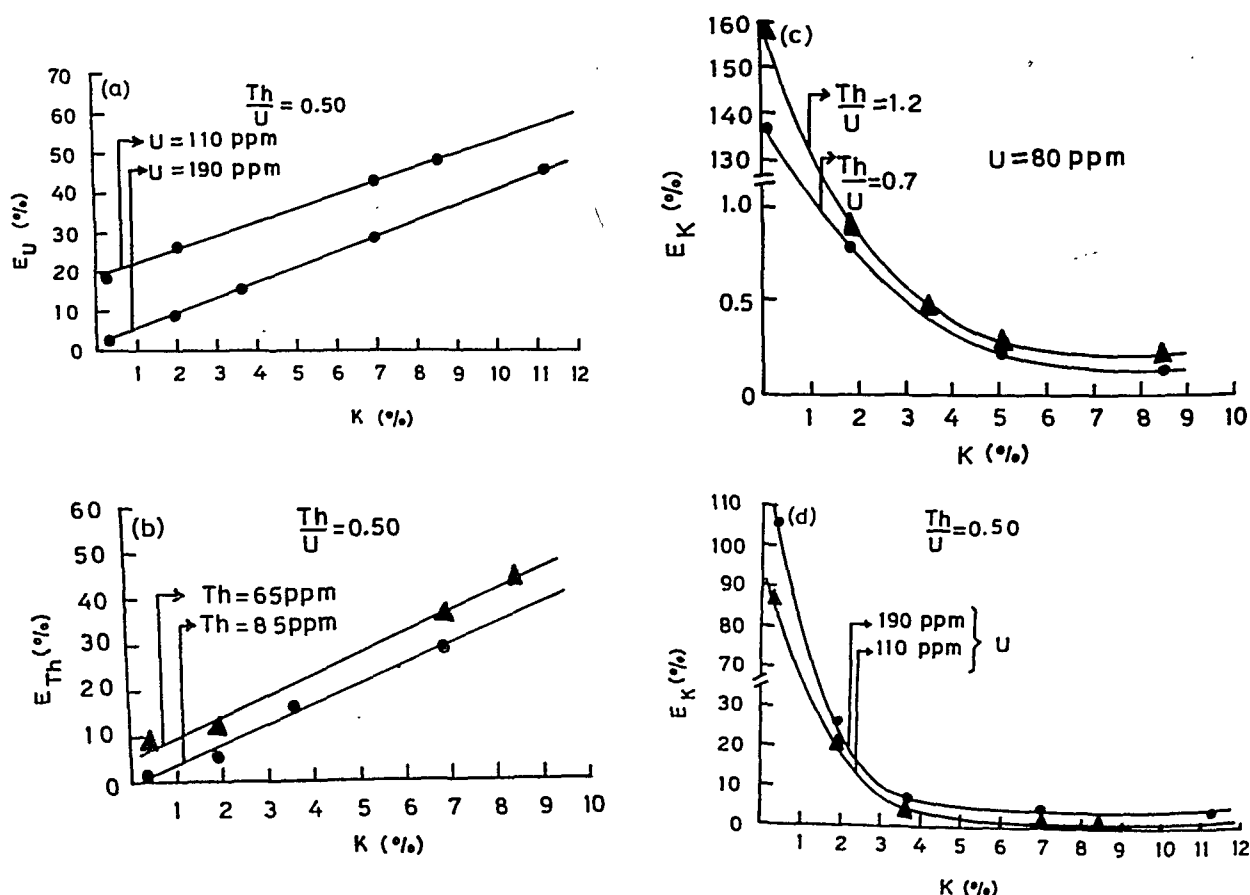


Fig. 6—Relative error of (a) uranium (b) thorium (c) potassium and (d) potassium as a function of K

Table 2—Comparison of Gamma Ray Spectrometric Results with Fission Track Analysis

Sample No	Gamma ray spectrometry			Fission track analysis
	U (ppm)	Th (ppm)	K (%)	U (ppm)
Quartzite from Jari in Himachal Pradesh				
Q1	671.00 ± 5.00	100.90 ± 0.70	3.14 ± 0.20	667.00 ± 5.00
Q2	367.00 ± 4.00	149.10 ± 0.80	24.20 ± 0.60	348.00 ± 3.00
Q3	168.00 ± 2.60	35.90 ± 0.40	5.30 ± 0.26	178.60 ± 1.30
Phosphorite from Maldeota in Uttar Pradesh				
P1	49.50 ± 1.40	7.95 ± 0.19	1.01 ± 0.11	44.10 ± 0.50

errors are incorporated to get the final results. Reproducibility of results is also checked by repeating the analysis of the same sample at three different times. The quartzite samples collected from Jari (Kulu) HP and phosphorite sample from Maldeota (Mussoorie Syncline) UP are analyzed using this set-up. The concentrations of U, Th and K in quartzite samples are found to vary from 168.00 ± 2.60 to 671.00 ± 5.00 ppm, 35.90 ± 0.40 to 149.10 ± 0.80 ppm and 3.14 ± 0.20 to $24.20 \pm 0.60\%$ respectively (Table 2). The concentrations of U, Th and K in phosphorite sample are found to be 49.50 ± 1.40 ppm, 7.95 ± 0.19 ppm and $1.01 \pm 0.11\%$, respectively. The concentration of U in these samples is pronouncedly higher than that reported by Menon *et al.*³ This is due to the presence of uranium mineralization in these areas^{6,7}. A comparison of the results for U content in these samples with fission track method^{8,9} is also reported (Table 2). The results obtained by the two techniques are in good agreement.

4 Conclusion

The gamma ray spectrometric technique using well-type detector provides the facility for analyzing samples where large amounts are not available. The technique is quite efficient for U, Th and K analyses and the results show a good reproducibility.

Acknowledgement

The authors acknowledge the financial assistance by CSIR, New Delhi. The authors are also grateful to Dr Kulwant Singh for his help in data analysis.

References

- 1 Rao R U, *Geophys Res Bull (India)*, **12** (1974) 19.
- 2 Woolenberg H A, *Nuclear methods in mineral exploration*, edited by J G Morse (Elsevier Scientific Publishing Co, New York) 1977.
- 3 Menon M R, Mishra U C, Lalit B Y, Shukla V K & Ramachandran T V, *Proc Indian Acad Sci Sect B*, **91** (1982) 127.
- 4 Stromswold D C, Kosanke K L, *IEEE Trans Nucl Sci (USA)*, **25** (1978) 782.
- 5 Rangarajan C, Mishra U C, Gopalakrishnan S & Sadasivan S, *Analysis of complex NaI (Th) gamma-spectra from mixtures of nuclides*, Rep BARC-686 (Bhabha Atomic Research Centre, Bombay), (1973) 1.
- 6 Narayan Dass G R, Parthasarathy T N & Taneja P C, *J Geol Soc (India)*, **20** (1979) 95.
- 7 Saraswat A C, Sankaran A V, Vardaraju H N, Taneja P C & Bargaje V B, *Unesco-Ecafe session on geochemical prospecting, Colombo, Ceylon* (ECAFE, Paris) 1970.
- 8 Fisher D E, *Anal Chem (USA)*, **38** (1977) 477.
- 9 Fleischer R L, Price P B & Walker R M, *Nuclear tracks in solids: principles and applications* (University of California Press, Berkeley, USA) 1975.

Laser Raman Spectra of 2-Fluoro-5-Chlorotoluene & 3-Fluoro-6-Chlorotoluene

S MOHAN & FERIDOUN PAYAMI

Division of Applied Sciences, Anna University, Madras Institute of Technology, Madras 600 044

Received 24 July 1986; revised received 21 November 1986

The laser Raman spectra of 2-fluoro-5-chloro- and 3-fluoro-6-chlorotoluenes have been recorded on a Cary model 82 grating spectrophotometer with an argon laser source. The observed frequencies have been assigned to the various modes of vibrations in terms of the fundamentals, overtones and combinations assuming C_s point group symmetry.

1 Introduction

The vibrational spectra of some halogenated toluenes, xylene and toluenes have been extensively studied by a number of workers¹⁻⁶. Green *et al.*⁷ and Dwivedi and Sharma⁸ have studied the vibrational spectra of a few dihalogenotoluenes of the TXY type toluene halogens. However, the vibrational analysis of 2-fluoro-5-chloro- and 3-fluoro-6-chlorotoluenes using either infrared or Raman data has not been reported so far. In the present paper, we present the results and analysis of the laser Raman spectra (Figs 1 and 2) of these uninvestigated compounds.

2 Experimental Details

Spectroscopically pure chemicals (liquid at room temperature) were obtained from M/s Koch-Light Laboratories, England, and were used as such. The polarized laser Raman spectra of 2-fluoro-5-chloro- and 3-fluoro-6-chlorotoluenes have been recorded using 488 nm line of Ar^+ for excitation in the region 100-4000 cm^{-1} at the Indian Institute of Technology, Madras, on a Cary model 82 grating spectrophotometer and using a 4 W argon laser. The frequencies for all the sharp bands are accurate to ± 1 cm^{-1} .

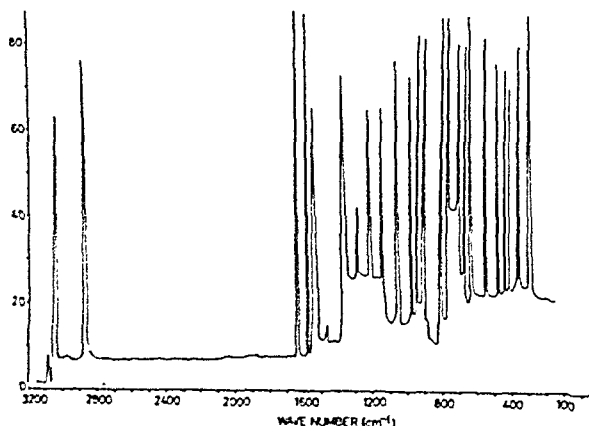


Fig. 1— Raman spectrum of 3-fluoro-6-chlorotoluene

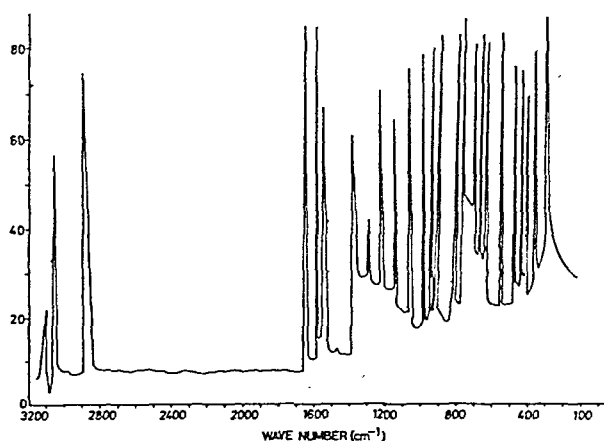


Fig. 2— Raman spectrum of 2-fluoro-5-chlorotoluene

3 Results and Discussion

The observed frequencies of 2-fluoro-5-chlorotoluene and 3-fluoro-6-chlorotoluene along with their relative intensities and probable assignments are presented in Table 1. The observed spectra are explained on the basis of C_s point group symmetry for the molecules under consideration by assuming the CH_3 group as a point mass. C_s symmetry leads to two types of vibrations distributed as:

$$\Gamma = 21a' \text{ (planar)} + 9a'' \text{ (non-planar)}$$

All vibrations are active both in Raman and infrared. The species a' gives rise to polarized lines with a'' species gives depolarized lines in Raman spectrum. In addition to these vibrations, 9 group vibrations due to CH_3 group also appear. Assignments have been made on the basis of relative intensities, magnitudes of the frequencies and the depolarization of the Raman lines. Assignments are also made on the basis of similar assignments in spectra of molecules of similar structure. The vibrations of the molecules are clearly divided into two groups: (i) phenyl ring vibrations and (ii) methyl group vibrations.

Table 1—Assignments of Fundamental Vibrational Frequencies (in cm^{-1}) of Fluorochlorotoluenes

2-Fluoro-5-chlorotoluene	3-Fluoro-6-chlorotoluene	Assignment
282 VS	261 M	C—CH ₃ non-planar bending
344 VS	344 VS	β (C—Cl) in-plane bending
350 M	352 M	ϕ (C—F) out-of-plane bending
382 M	375 M	β (C—CH ₃) planar bending
396 VW	—	
415 S(dp)	411 M(dp)	ϕ (C—C—C) out-of-plane bending
446 VS	448 VS	β (C—F) in-plane bending
460 VS	478 VS	α (C—C—C) out-of-plane bending
562 VS	563 VS	β (C—C—C) in-plane bending
—	591 W	
638 S	634 S	β (C—C—C) in-plane bending
690 S	693 S	ϕ (C—C—C) out-of-plane bending
762 VS	755 VS	ν (C—Cl) stretching
770 MS(p)	772 MS(p)	ν (C—C) ring breathing
810 VS	809 VS	ϕ (C—H) out-of-plane bending
—	821 S	ϕ (C—H) out-of-plane bending
867 VS	867 S	ϕ (C—H) out-of-plane bending
890 S	—	ϕ (C—H) out-of-plane bending
950 VS	961 VS	ϕ (C—H) out-of-plane bending
970 M	—	
996 VS	1005 VS	β (C—C—C) trigonal bending
1040 VS	1038 VS	(CH ₃ rocking)
1089 VS(dp)	1071 S(dp)	(CH ₃ rocking)
1099 S	—	β (C—H) in-plane bending
1115 VS	1116 VS	β (C—H) in-plane bending
1186 VS	1178 VS	β (C—H) in-plane bending
1235 S(p)	1238 S(p)	ν (C—CH ₃) stretching
1265 S	1268 S	β (C—H) in-plane bending
1289 VS(p)	1290 VS(p)	ν (C—F) stretching
1310 M(p)	1301 M(p)	ν (C—C) stretching
1376 M	1371 M	(C—H) symmetric deformation in methyl group
1408 S(p)	1411 S(p)	ν (C—C) stretching
1439 M	1436 M	(C—H) asymmetric deformation in methyl group
1479 VW	1480 VW	(C—H) asymmetric deformation in methyl group
1536 S(p)	1536 S(p)	ν (C—C) stretching
1589 VS(p)	1592 VS(p)	ν (C—C) stretching
1621 VS	1628 VS	ν (C—C) stretching
2910 M	2921 M	ν (C—H) symmetric stretching in methyl group
2941 VS	2961 VS	ν (C—H) asymmetric stretching in methyl group
2978 S	2985 S	ν (C—H) asymmetric stretching in methyl group
3055 M	3044 M	ν (C—H) stretching aromatic
3098 S	3095 S	ν (C—H) stretching aromatic
3112 VW	3116 VW	ν (C—H) stretching aromatic

VS: very strong; S: strong; MS: medium strong; M: medium; W: weak; VW: very weak; (p): polarized; (dp): depolarized

3.1 Phenyl Ring Vibrations

Carbon vibrations— Benzene has two doubly degenerate modes e_{2g} (1596 cm^{-1}) and e_{1u} (1485 cm^{-1}) and two non-degenerate modes b_{2u} (1310 cm^{-1}) and a_{1g} (995 cm^{-1}) due to skeleton stretching of C—C bonds. Bonds between 1400 cm^{-1} and 1650 cm^{-1} in benzene derivatives are assigned to these modes. The actual positions are determined not so much by the nature of the substituents but by the form of the substitution around the ring⁹. All the frequencies except that of the ring breathing mode (995 cm^{-1}) remain practically unaffected by substitution. The two doubly degenerate frequencies split into four totally symmetric

components under C_s symmetry. Four bands observed at 1621 , 1589 , 1536 and 1408 cm^{-1} in 2-fluoro-5-chlorotoluene and 1628 , 1592 , 1536 and 1411 cm^{-1} in 3-fluoro-6-chlorotoluene respectively have been assigned to these two degenerate vibrations of benzene.

The in-plane carbon bending vibrations are derived from non-degenerate b_{1u} (1010 cm^{-1}) and degenerate e_{2g} (606 cm^{-1}) modes of benzene. The e_{2g} (606 cm^{-1}) degenerate frequency splits into two totally symmetric vibrations under C_s symmetry and has been observed at 638 and 562 cm^{-1} in 2-fluoro-5-chlorotoluene and at 634 and 596 cm^{-1} in 3-fluoro-6-chlorotoluene.

The carbon out-of-plane bending vibrations are derived from the non-degenerate b_{2g} (703 cm^{-1}) and degenerate e_{2u} (404 cm^{-1}) modes of benzene. The former is found to be constant in substituted benzenes¹⁰ and in the present case it is observed at 690 cm^{-1} in 2-fluoro-5-chlorotoluene and 693 cm^{-1} in 3-fluoro-6-chlorotoluene. The degenerate e_{2u} (404 cm^{-1}) vibration splits into two non-totally symmetric components and the bands observed at $415, 460\text{ cm}^{-1}$ in 2-fluoro-5-chlorotoluene and at $411, 478\text{ cm}^{-1}$ in 3-fluoro-6-chlorotoluene are assigned to this vibration.

The C—C ring breathing a_{1g} (995 cm^{-1}) and C—C—C trigonal bending non-degenerate b_{1u} (1010 cm^{-1}) vibrations of benzene under C_s symmetry give rise to combined modified modes. In trisubstituted benzenes, one mode is observed at about 800 cm^{-1} while the other appears at about 1000 cm^{-1} . The C—C—C trigonal bending and C—C ring breathing vibrations are assigned to 996 and 770 cm^{-1} in 2-fluoro-5-chlorotoluene and to 1005 and 772 cm^{-1} in 3-fluoro-6-chlorotoluene in the present case. The present conclusion is in agreement with the assignments made for fluorobromotoluenes⁸ and fluoroaminotoluenes¹¹.

C—H Vibrations— The trisubstituted benzenes which form the subject of the present investigation give rise to three C—H stretchings, three C—H out-of-plane deformations and three C—H in-plane bendings. The aromatic structure shows the presence of C—H stretching vibrations in the region $3000\text{--}3100\text{ cm}^{-1}$, which permits a ready identification for this structure. In this region, the bands are not appreciably affected by the nature of the substituents. The frequencies $3055, 3098$ and 3112 cm^{-1} in 2-fluoro-5-chlorotoluene and $3044, 3095$ and 3116 cm^{-1} in 3-fluoro-6-chlorotoluene respectively have been assigned to C—H stretching modes. The rest of the vibrations, viz. three C—H in-plane bendings and three C—H out-of-plane bendings of 2-fluoro, 5-chlorotoluene and 3-fluoro-6-chlorotoluene molecules are given in Table 1. They are in good agreement with literature values^{8,11}.

C—CH₃ Vibrations— It is noted from the literature that a strong band around 1200 cm^{-1} appears due to valence oscillations in toluenes and substituted toluenes. Hence the strong bands at 1235 cm^{-1} in 2-fluoro-5-chlorotoluene and at 1238 cm^{-1} in 3-fluoro-6-chlorotoluene have been assigned to C—CH₃ stretching modes. The bands at 282 cm^{-1} in 2-fluoro-5-chlorotoluene and 261 cm^{-1} in 3-fluoro-6-chlorotoluene are assigned to C—CH₃ non-planar bending while the bands at 382 cm^{-1} in 2-fluoro-5-chlorotoluene and at 375 cm^{-1} in 3-fluoro-6-chlorotoluene are assigned to C—CH₃ planar bending

modes. This conclusion agrees well with the literature values¹¹.

C—Cl Stretching mode— The C—Cl stretching frequency is usually obtained¹² in the region $550\text{--}750\text{ cm}^{-1}$. In accordance with the above conclusion, very strong bands at 762 and 755 cm^{-1} in 2-fluoro-5-chlorotoluene and 3-fluoro-6-chlorotoluene molecules respectively, have been assigned to C—Cl stretching modes.

C—F Stretching mode— Dwivedi and Sharma⁷ and Smith *et al.*¹³ have assigned the C—F stretching mode for fluorobromotoluenes and trifluorobenzenes respectively. In accordance with their assignment, we have assigned the strong bands at 1289 and 1290 cm^{-1} in 2-fluoro-5-chloro- and 3-fluoro-6-chlorotoluenes respectively to the C—F stretching vibration.

3.2 Methyl Group Vibrations

Group frequencies are determined in terms of the motions that the nuclei in a structural group in the molecule undergo during the vibration and they appear in fairly constant regions in the spectrum.

For one methyl group attached to the benzene ring, two rocking modes are expected. In *o*-chlorotoluene, Mooney¹⁴ assigned the frequencies at 1041 and 1090 cm^{-1} to methyl rocking modes. Similarly, the frequencies at 1071 and 1038 cm^{-1} in *o*-bromotoluene have also been assigned to methyl rocking mode by Mooney¹⁴. In accordance with his observation, the strong bands at 1089 and 1040 cm^{-1} in 2-fluoro-5-chlorotoluene and the strong bands at 1071 and 1038 cm^{-1} in 3-fluoro-6-chlorotoluene have been assigned to two CH₃ rocking modes.

In methyl group, there exist three stretching vibrations distributed as one symmetric and two asymmetric vibrations. The symmetric and asymmetric vibrations in methyl group in 2-fluoro-5-chlorotoluene and 3-fluoro-6-chlorotoluene are assigned to $2910, 2941, 2978\text{ cm}^{-1}$ and $2921, 2961$ and 2985 cm^{-1} respectively. These assignments are in agreement with the literature values¹⁴.

References

- 1 Wilmschurst J K & Bernstein H J, *Can J Chem (Canada)*, **35** (1957) 911.
- 2 Padhya M R & Varadarajan T S, *Proc Indian Acad Sci*, **50** (1959) 51.
- 3 Randle R R & Whiffen D H, *J Chem Soc (GB)*, (1955) 3497.
- 4 Joshi G & Singer N L, *Spectrochim Acta (GB)*, **22** (1966) 1501.
- 5 Mehrotra V K, *Indian J Pure & Appl Phys*, **6** (1968) 691.
- 6 Thakur G, Singh V B & Singh N L, *Indian J Pure & Appl Phys*, **7** (1969) 107.

- 7 Green J H S, Harrison D J & Kynaston W, *Spectrochim Acta(GB)*, **27** (1971) 739.
- 8 Dwivedi C P D & Sharma S N, *Indian J Pure & Appl Phys*, **11** (1973) 447.
- 9 Bellamy L J, *The infrared spectra of complex molecules* (John Wiley, New York) 1959, 70.
- 10 Green J H S, *Spectrochim Acta(GB)*, **18** (1962) 39.
- 11 Singh S J & Pandey S J, *Indian J Pure & Appl Phys*, **12** (1974) 300.
- 12 Rao C N R, *Chemical applications of infrared spectroscopy* (Academic Press, New York) 1963, 309.
- 13 Smith D C, Ferguson E E, Hudson R L & Nielsen J R, *J Chem Phys(USA)*, **21** (1953) 1457, 1727.
- 14 Mooney E F, *Spectrochim Acta(GB)*, **20** (1964) 1343.

Vibrational Spectrum & Normal Coordinate Treatment of Potassium Phosphorodifluoride

S MOHAN

Division of Applied Sciences, Anna University, Madras Institute of Technology,
Chromepet, Madras 600 044

and

S GUNASEKARAN & M PARASURAMAN

Department of Physics, Pachaiyappa's College, Madras 600 030

Received 11 February 1985; revised received 6 October 1986

The infrared spectrum in the region $200\text{--}4000\text{ cm}^{-1}$ for potassium phosphorodifluoride compound is presented. The vibrational analysis is made on the basis of C_{2v} symmetry for this ion for the first time and the results are briefly discussed.

The molecular geometry of XY_2Z_2 -type molecules, belonging to C_{2v} point group, is of great interest to molecular spectroscopists and chemists. Several investigations¹⁻⁷ have been carried out for this type of molecules in recent years. But most of the work is based on the symmetry coordinates given by Devis *et al.*¹ According to them, the R_1 and R_2 symmetry coordinates of A_1 species correspond to symmetric $X-Y$ and $Z-Z$ stretching combination of the whole system. But the frequencies assigned for these molecules in the A_1 species, in the earlier work⁸ correspond to individual $X-Y[\nu_s(XY)]$ and $X-Z[\nu_s(XZ)]$ stretchings. During our study on this type of molecules, we have come across a very interesting compound, viz. KPO_2F_2 . Hence, the present investigation is aimed at recording the infrared spectrum of this compound and to study its vibrational analysis.

The spectrum has been recorded in Perkin-Elmer IR-983 double beam grating spectrometer and presented in Fig. 1. The observed frequencies along with their assignments are given in Table 1. The frequencies for all the sharp bands are accurate to $\pm 1\text{ cm}^{-1}$.

Frequency assignment—The appearance of four frequency bands at 1315, 1155, 855 and 533 cm^{-1} suggests the C_{2v} molecular symmetry for this ion. The high frequency fundamentals (stretching modes) can be assigned on the basis of their relative intensity. Comparing the present spectrum with POF_3 spectrum⁹, four frequencies have been assigned easily. For non-planar molecules, one expects $\nu_6(B_1)$ mode to be much more intense than $\nu_1(A_1)$. On this basis P-O stretching frequency 1315 cm^{-1} is assigned to $\nu_6(B_1)$ while 1155 cm^{-1} is assigned to $\nu_1(A_1)$. In line with this observation, P-F stretching frequencies 855 and 840 cm^{-1} are assigned to $\nu_8(B_2)$ and $\nu_2(A_1)$ modes re-

Table 1—Assignment of Fundamental Infrared Frequencies of Phosphorodifluoride Ion

Frequency cm^{-1}	Relative intensity	Assignment
218	VW	$\nu_7 - \nu_4$
279	W	$\nu_4(A_1)$ Syn. FPF bent
295	VW	$\nu_1 - \nu_8$
360	M	$\nu_8 - \nu_7$
390	M	$2\nu_9 - \nu_3$
463	S	$\nu_9(B_2)$ $\delta(\text{OPF})$
500	S	$\nu_7(B_1)$ $\delta(\text{OPF})$
533	M	$\nu_3(A_1)$ sym. OPO bent
560	VW	$2\nu_8 - \nu_1$
610	VW	$2\nu_1 - 2\nu_8$
680	VW	$2\nu_2 - 2\nu_7$
720	Sh	$2\nu_8 - 2\nu_7$
840	S	$\nu_2(A_1)$ Sym. P.F. stretching
855	S	$\nu_8(B_2)$ asym. P.F. stretching
1000	M	$2\nu_7$
1110	Sh	$\nu_2 + \nu_4$
1155	S	$\nu_1(A_1)$ sym P.O. stretching
1315	S	$\nu_6(B_1)$ asym P-O stretching

S, strong; M, medium; W, weak; VW, very weak; Sh, shoulder

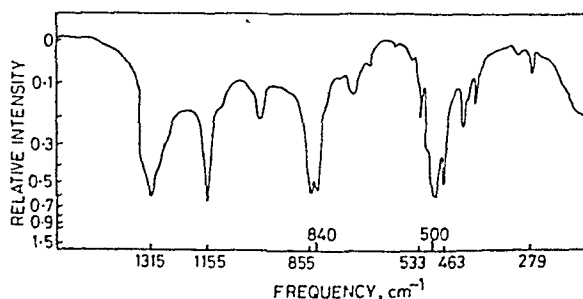


Fig. 1—Infrared spectrum of KPO_2F_2

Table 2—Force Constants (f 's in 10^2 N/m), Mean Amplitudes (l 's in 10^{-2} \AA) at 298.16 K, Coriolis Coupling Constants and Centrifugal Distortion Constants (D , R and δ in kHz)

f_d f_D	f_{dd} f_{DD} f_{Dd}	f_a f_β f_γ	f_{da} $f_{d\beta}$ $f_{d\gamma}$	f_{dy} $f_{D\gamma}$	$f_{a\beta}$ $f_{D\beta}$ $f_{D\gamma}$	$f_{a\gamma}$ $f_{\beta\gamma}$	$f_{\gamma\gamma}$ $f_{\gamma\gamma}$ $f_{\gamma\gamma}$
13.7026	-3.2639	0.4545	0.2154	-1.4677	0.6415	-0.3211	0.1266
5.9240	-1.5357	0.4784	-0.220	-0.1749	0.6488	-0.0332	-0.3618
	0.4172	1.0904	1.4712		0.1708	-0.395	-0.7824

$l_{d(X-Y)}$	$l_{D(X-Z)}$	$l_{P(Y...Y)}$	$l_{Q(Z...Z)}$	$l_{H(Y...Z)}$
3.6036	4.1991	6.6293	8.4807	5.9999

ξ_{15}^Z	ξ_{16}^Y	ξ_{17}^Y	ξ_{18}^X	ξ_{19}^X	ξ_{56}^X	ξ_{68}^Z
ξ_{25}^Z	ξ_{26}^Y	ξ_{27}^Y	ξ_{28}^X	ξ_{29}^X	ξ_{57}^X	ξ_{69}^Z
ξ_{35}^Z	ξ_{36}^Y	ξ_{37}^Y	ξ_{38}^X	ξ_{39}^X	ξ_{58}^X	ξ_{78}^Z
ξ_{45}^Z	ξ_{46}^Y	ξ_{47}^Y	ξ_{48}^X	ξ_{49}^X	ξ_{59}^X	ξ_{79}^Z
-0.5441	0.7983	0.3083	0.3451	0.3138	-0.3276	0.4283
0.6628	0.3758	-0.8447	-0.3348	0.7642	0.9827	-0.7018
0.5118	-0.4631	-0.3765	0.8442	-0.5087	0.2893	0.3565
-0.0504	-0.1083	0.2615	-0.1735	0.2480	-0.3525	-0.9599

$D_J = 1.4405$	$D_{JK} = -3.7409$	$D_K = 3.3014$
$R_5 = -0.1085$	$R_6 = -0.0834$	$\delta_J = -0.2171$

spectively. These assignments agree quite well with the assignments for POCl_3 and POBr_3 (Refs 10, 11). The OPO bending mode is assigned to 533 cm^{-1} while FPF bending mode is assigned to 279 cm^{-1} . These assignments agree very well with bending assignments for PO_3F^{2-} , POF_3 and PF_6 cases¹². The remaining two sharp bands, viz. 500 and 463 cm^{-1} are assigned to $\nu_7 \delta(\text{OPF})$ and $\nu_9 \delta(\text{OPF})$ modes respectively. Further, the rest of the observed frequencies in Table 1 may be accounted for as resulting from allowed combinations or overtones of the selected eight fundamentals which give additional support for their choice.

Normal coordinate analysis—A normal coordinate analysis of KPO_2F_2 has been carried out following Wilson's F - G matrix method on the basis of C_{2v} point group, using a modified set of symmetry coordinates⁸, and molecular kinetic constants and a set of potential constants have been reported. The potential constants, vibrational mean amplitudes at 298.16 K, Coriolis coupling constants and centrifugal distortion constants are given in Table 2.

The fact that the force constant f_d is higher than f_D suggests that P—O bond is much stronger than P—F bond. These values agree quite well with the values reported in Ref. 13. The vibrational mean amplitudes for the bonded and the non-bonded distances obtained in the present work are in the expected range and they are found to exhibit characteristic values. The high values of Coriolis coupling constants ξ_{25}^Z ,

Table 3—Potential Energy Distribution

Frequencies cm^{-1}	PED %	
ν_1 1155	100	S_1
ν_2 840	100	S_2
ν_3 533	98	S_3
ν_4 279	95	S_4
ν_6 1315	100	S_6
ν_7 500	94	S_7
ν_8 855	100	S_8
ν_9 463	92	S_9

ξ_{16}^Y , ξ_{27}^Y , ξ_{38}^X , ξ_{29}^X , ξ_{57}^Y , ξ_{69}^Z and ξ_{79}^Z indicate that the coupling between the vibrations concerned is significant. Further, the zeta values are found to obey the following quadratic sum rules

$$\sum_{ij} (\xi^X)^2 = 1 \quad (i = 1 \text{ to } 4, j = 8, 9)$$

$$\sum_{ij} (\xi^Y)^2 = 1 \quad (i = 1 \text{ to } 4, j = 6, 7)$$

$$\sum_{ij} (\xi^Z)^2 = 1 \quad (i = 1 \text{ to } 4, j = 5)$$

As expected, the centrifugal distortion constant D_{JK} is negative for this molecule.

Thus, the evaluated molecular constants which are in the expected range confirm the correctness of assignments for this ion.

To check whether the chosen set of assignments contributes maximum to the potential energy associated with normal coordinates of the molecule, the potential energy distribution (PED) has been calculated using the relation

$$PE = \frac{F_{ii} L_{ia}^2}{\lambda_a}$$

The potential energy distribution is given in Table 3.

Further, from the study of potential constants, the frequency for normal vibration ν_5 (twist) is predicted to be 388 cm^{-1} for this ion in the present work.

References

- 1 Davis A, Cleveland F F & Meister A G, *J Chem Phys (USA)*, **20** (1952) 454.
- 2 Decker C E, Meister A G & Cleveland F F, *J Chem Phys (USA)*, **21** (1953) 1781.
- 3 Venkateswarlu K & Joseph P A, *Indian J Pure & Appl Phys*, **9** (1971) 235.
- 4 Ziomole J S, Ferraro J R & Peppard D F, *J Mol Spectrosc (USA)*, **8** (1962) 212.
- 5 Shimanouchi T & Iso Suzuki, *J Mol Spectrosc (USA)*, **8** (1962) 221.
- 6 Venkateswarlu K & Malathi Devi V, *Indian J Pure & Appl Phys*, **3** (1965) 195.
- 7 Namasivayam R & Viswanathan S, *Proc Indian Acad Sci Sect A*, **89** (1980) 469.
- 8 Mohan S & Gunasekaran S, *Proc II Natl Conf on Vib Spectrosc* (1985) 53.
- 9 Selig H & Classen H H, *J Chem Phys (USA)*, **44** (1966) 1404.
- 10 Dung J R & Clark J W, *J Chem Phys (USA)*, **46** (1967) 3057.
- 11 Maiants L S, Popov E M & Kabachink M I, *Opt & Spectrosc (USA)*, **6** (1959) 384.
- 12 Buhler K & Bues W, *Z Anorg Allegem Chem (Germany)*, **308** (1961) 62.
- 13 Jacob E J, Danielson D D & Sandal S, *J Mol Struct (Netherlands)*, **62** (1980) 143.

Electronic Absorption Spectrum of Ni^{2+} Ions Doped in Lithium Caesium Sulphate Single Crystal

B C VENKATA REDDY & B MUNIBHADRAIAH

Department of Physics, College of Engineering, Sri Venkateswara University,
Tirupati 517 502

Received 9 December 1985; revised received 22 September 1986

The electronic absorption spectrum of Ni^{2+} ions doped in lithium caesium sulphate has been studied at room and liquid nitrogen temperatures. From the nature and position of the bands, a successful interpretation of all the observed bands could be made assuming octahedral symmetry. The splittings observed for ${}^3T_{1g}(\text{F})$ band at liquid nitrogen temperature have been explained as due to spin-orbit interaction. The extra bands observed at about $19,000\text{ cm}^{-1}$ at low temperature have been interpreted to be the superposition of vibrational mode of SO_4^{2-} radical on ${}^3T_{1g}(\text{F})$ band. The observed band positions have been fitted with four parameters B , C , Dq and ζ .

1 Introduction

The electronic absorption spectrum of Ni^{2+} ions in several hydrated bromates, sulphates, selenates and fluosilicates has extensively been studied by several research workers¹⁻⁴. In these hydrated Ni^{2+} salts a number of small peaks are observed at liquid nitrogen temperature on the higher energy side of the ${}^3T_{1g}(\text{F})$ band. Piper and Koentge¹ and Datta & Debabala⁴ attributed these bands to an asymmetric H-O vibration mode. The separation of about 500 cm^{-1} between the individual peaks were ascribed to Ni-O vibrations. On the other hand, Pryce *et al.*², who observed these peaks at liquid helium temperature in $\text{NiSiF}_6 \cdot 6\text{H}_2\text{O}$, attributed them to H-O vibration modes superposed on different electronic states of Ni^{2+} .

The present study reports the electronic absorption spectrum of Ni^{2+} ions doped in lithium caesium sulphate (LiCsSO_4). At room temperature, LiCsSO_4 is orthorhombic (phase I) with space group⁵ $Pcmn$. At low temperatures, it is monoclinic (phase III) with space group⁵ $P2_1/n$ (Ref. 5).

2 Experimental Details

Single crystals of LiCsSO_4 doped with Ni^{2+} were grown by slow evaporation at room temperature from an aqueous solution containing equimolar weights of lithium sulphate and caesium sulphate to which 0.5 mol % by weight of NiSO_4 was added as an impurity. The electronic absorption spectra were recorded both at room and liquid nitrogen temperatures on Cary-2300 spectrophotometer. The oscillator strengths were calculated by computing the area under the absorption curves.

3 Theory

Ni^{2+} has eight $3d$ electrons. Among the electronic

states arising from the ground and excited electronic configurations of Ni^{2+} , ${}^3A_{2g}(\text{F})$ state lies at the lowest and forms the ground state of the ion. The energy expressions for all the states of Ni^{2+} in the absence of spin-orbit interaction have been given in the form of matrices by Tanabe and Sugano⁶. These matrices are kept in the form of linear expression by Boxall *et al.*⁷ In the presence of spin-orbit interaction, the energy levels are designated as Γ_1 , Γ_2 , Γ_3 , Γ_4 and Γ_5 . The energy matrices for these spin-orbit levels were presented by Liehr and Ballhausen⁸ in terms of F_2 , F_4 , Dq and λ and in terms of B , C , Dq and ζ by Lakshman and Rao⁹.

4 Results and Analysis

The electronic absorption spectra of Ni^{2+} doped in LiCsSO_4 recorded at room and liquid nitrogen temperatures are shown in Figs 1 and 2 respectively. In all, six bands have been observed at room temperature, one in the near infrared at 8772 cm^{-1} , four in the visible at 13986, 14925, 15267 and 22222 cm^{-1} and one in the near ultraviolet at 25477 cm^{-1} . On cooling the crystal to liquid nitrogen temperature, the bands at 14925 and 15267 cm^{-1} have been found to split into four components with maxima at 14981, 15674, 16129 and 16529 cm^{-1} while the remaining bands at 8772, 13986, 22222 and 25477 cm^{-1} have been shifted to 8969, 14184, 22722 and 25974 cm^{-1} respectively.

From the nature and position of the observed bands, they have been attributed to Ni^{2+} ion in octahedral symmetry. For Ni^{2+} ion in O_h symmetry, three spin allowed transitions, viz. ${}^3A_{2g}(\text{F}) \rightarrow {}^3T_{2g}(\text{F})$, ${}^3A_{2g}(\text{F}) \rightarrow {}^3T_{1g}(\text{F})$ and ${}^3A_{2g}(\text{F}) \rightarrow {}^3T_{1g}(\text{P})$, in the order of increasing energy, are expected. Often, most of the $\text{Ni}(\text{H}_2\text{O})_6^{2+}$ complexes show a double peaked band³ at 300 K. Indeed in the present study also, we ob-

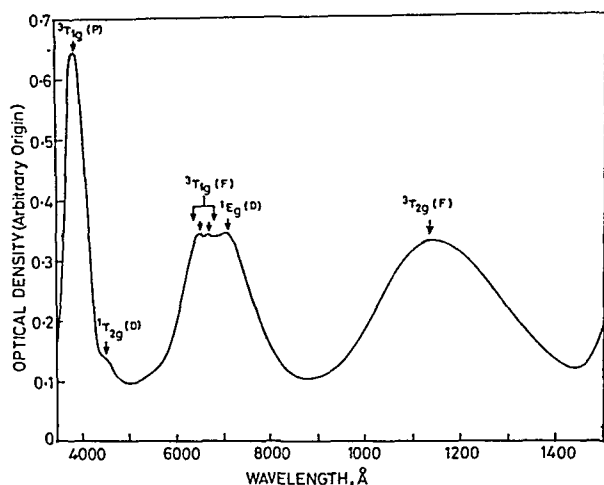


Fig. 1—Absorption spectrum of Ni^{2+} in lithium caesium sulphate at room temperature (300 K)

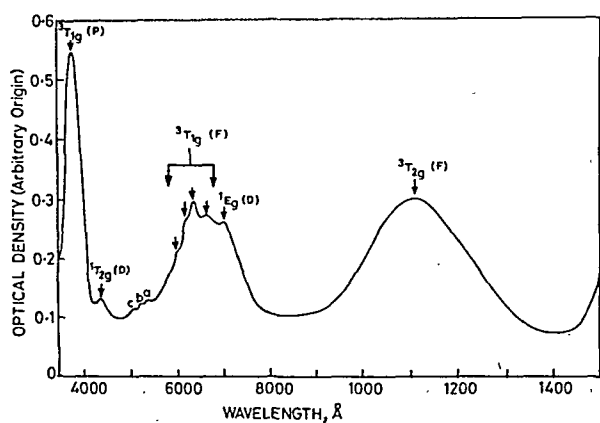


Fig. 2—Absorption spectrum of Ni^{2+} in lithium caesium sulphate at liquid nitrogen temperature (77 K)

served a double peaked band separated by 342 cm^{-1} located at 14925 and 15267 cm^{-1} . The intense bands observed at 8772 and 25479 cm^{-1} at room temperature correspond to the transitions to the levels ${}^3T_{2g}(\text{F})$ and ${}^3T_{1g}(\text{P})$ respectively and the double peaked band is ascribed to ${}^3T_{1g}(\text{F})$ level.

According to the theory, some spin-forbidden triplet-to-singlet bands could also appear but the intensity of such bands would be lower. In the present investigation, the intense band at 13986 cm^{-1} on the lower energy side of the double peaked ${}^3T_{1g}(\text{F})$ band is assigned to ${}^1E_g(\text{D})$ level. The high intensity of this spin-forbidden band is due to configurational interaction with ${}^3T_{1g}(\text{F})$, through which it gains intensity and similar instances have been reported by several workers^{10,11}. The weak shoulder band observed at 22222 cm^{-1} at 300 K is assigned to the ${}^1T_{2g}(\text{D})$ level. On cooling the crystal to 77 K , in addition to the room temperature bands, a series of three weak bands appeared at 18692 , 19084 and 19608 cm^{-1} . These bands are marked as a, b and c in Fig. 2.

The linear energy expressions of Boxall *et al.*⁷ have been solved for different values of Dq , B and C . It has been found that the best fit for the observed room temperature bands could be obtained for $Dq = 900\text{ cm}^{-1}$, $B = 890\text{ cm}^{-1}$ and $C = 3600\text{ cm}^{-1}$. The band maximum positions, calculated with these parameters along with the observed band positions and oscillator strengths, are presented in Table 1.

5 Discussion

From the nature of the splitting observed for ${}^3T_{1g}(\text{F})$ band at liquid nitrogen temperature, it appears that the splitting is due to spin-orbit interaction. The energy matrices inclusive of spin-orbit interaction⁹ have been diagonalized on DCM spectrum 31 mini-computer for different values of ζ and Dq with $B = 890\text{ cm}^{-1}$ and $C = 3600\text{ cm}^{-1}$. The best fit of the observed bands could be obtained with $Dq = 950\text{ cm}^{-1}$ and $\zeta = 600\text{ cm}^{-1}$ as shown in Fig. 3. The observed and calculated band maxima positions along

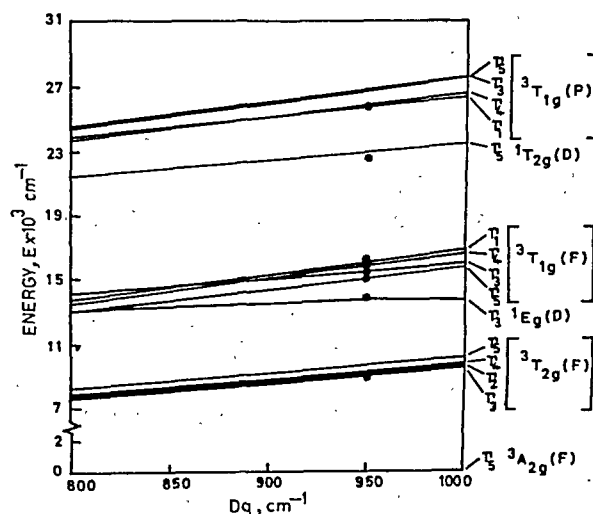


Fig. 3—Energy level diagram of Ni^{2+} in lithium caesium sulphate in cubic environment plotted as a function of crystal field parameter Dq with $B = 890\text{ cm}^{-1}$, $C = 3600\text{ cm}^{-1}$ and $\zeta = 600\text{ cm}^{-1}$. The solid circles show the experimental values at 77 K

Table 1—Observed and Calculated Energies, Assignments and the Oscillator Strengths for the Bands of Ni^{2+} in LiCsSO_4 at 300 K

$B = 890\text{ cm}^{-1}$; $C = 3600\text{ cm}^{-1}$ and $Dq = 900\text{ cm}^{-1}$

Transition from	Obs band positions		Calc $\nu(\text{cm}^{-1})$	Oscillator strengths (f)
${}^3A_{2g}(\text{F})$	$\lambda(\text{\AA})$	$\nu(\text{cm}^{-1})$		
${}^3T_{2g}(\text{F})$	11400	8772	9000	22.96×10^{-5}
${}^1E_g(\text{D})$	7150	13986	13947	13.57×10^{-7}
${}^3T_{1g}(\text{F})$	6700	14925	14944	5.13×10^{-7}
${}^1T_{2g}(\text{D})$	6550	15267		10.72×10^{-7}
${}^3T_{1g}(\text{P})$	3925	25477	25406	47.13×10^{-5}

Table 2—Observed and Calculated Energies, Oscillator Strengths and the Assignments for the Bands of Ni^{2+} in LiCsSO_4 at 77 K

$B = 890 \text{ cm}^{-1}$; $C = 3600 \text{ cm}^{-1}$; $Dq = 950 \text{ cm}^{-1}$ and $\zeta = 600 \text{ cm}^{-1}$

Transition from ${}^3A_{2g}(\text{F})$	Γ_5	Band positions (cm^{-1})		Oscillator strengths (f)
		Obs	Calc	
${}^3T_{2g}(\text{F})$	Γ_3	8969	9261	15.91×10^{-5}
	Γ_2		9289	
	Γ_4		9408	
	Γ_5		9769	
${}^1E_g(\text{D})$	Γ_3	14184	13896	10.49×10^{-7}
	Γ_5	14981	15296	
${}^3T_{1g}(\text{F})$	Γ_3	15674	15513	42.44×10^{-7}
	Γ_4	16129	15875	
	Γ_1	16529	16062	
${}^1T_{2g}(\text{D})$	Γ_5	22722	23095	25.28×10^{-6}
	Γ_1		25770	
	Γ_4	25974	25900	
${}^3T_{1g}(\text{P})$	Γ_3		26768	32.48×10^{-5}
	Γ_5		26852	

with their oscillator strengths are presented in Table 2.

It is easily seen from Tanabe-Sugano diagram⁶, given for d^8 configuration that the positive slope of ${}^3T_{2g}(\text{F})$ is smaller than that of ${}^3T_{1g}(\text{P})$ band and hence at 77 K, the former band should show a smaller blue shift than the latter band. It has indeed been found to be so in the present investigation with blue shifts of 197 cm^{-1} and 497 cm^{-1} for the ${}^3T_{2g}(\text{F})$ and ${}^3T_{1g}(\text{P})$ bands respectively thus confirming the assignments. No such observation could however be made for the ${}^3T_{1g}(\text{F})$ band as it is split into four components at 77 K. The blue shifts of 198 and 500 cm^{-1} in the case of ${}^1E_g(\text{D})$ and ${}^1T_{2g}(\text{D})$ respectively are also in accordance with the positive slopes of their respective levels in the Tanabe-Sugano diagram⁶.

The optical absorption spectra in the visible region in the case of first group transition metal ions arise due to electric dipole transitions and they generally contain vibronic side bands in addition to pure electronic bands. The vibronic side-bands result from the superposition of the vibrational modes of the ligand nuclei on the electronic energy levels of the transition metal ion.

In the present study, three bands are observed at 18692 , 19084 and 19608 cm^{-1} . These bands are associated with the ${}^3T_{1g}(\text{F})$ band. Taking the energy difference between the unassigned bands (marked as a, b, c in Fig. 2) and the last split component of the ${}^3T_{1g}(\text{F})$ in the present work, we have

Table 3—Observed Non-ligand Field Bands, Energy Separation from the ${}^3T_{1g}(\text{F})$ Band at 77 K, Calculated Energies and Their Assignments in $\text{Ni}^{2+} : \text{LiCsSO}_4$ Calculated from Fundamental Vibrational Frequencies of SO_4^{2-} Radical¹²

Vibronic Band Position (E) at 77 K cm^{-1}	$E - 16529 \text{ cm}^{-1}$	Assignment	Calculated Energy (in cm^{-1}) on the Basis of the Assignment
18692	2163	$\nu_2 + \nu_3 + \nu_4$	2168
19084	2555	$2\nu_1 + \nu_4$	2575
19608	3079	$2\nu_1 + \nu_3$	3066

$$18692 - 16529 = 2163 \text{ cm}^{-1}$$

$$19084 - 16529 = 2555 \text{ cm}^{-1}$$

$$19608 - 16529 = 3079 \text{ cm}^{-1}$$

A comparison of the vibrational frequencies of SO_4^{2-} radical with the values shown in Table 3 suggests that these bands arise due to the vibrational modes of SO_4^{2-} radical, superposing on the ${}^3T_{1g}(\text{F})$ electronic state.

Acknowledgement

The authors are thankful to Prof K Sreerama Murthy, for his encouragement. Thanks are also due to Prof P T Manoharan, Regional Sophisticated Instrumentation Centre, Indian Institute of Technology, Madras, for providing spectrometer and low temperature facilities and to Prof S V J Lakshman for giving permission to use their minicomputer. One of the authors (BM) is thankful the University Grants Commission, New Delhi, for providing financial assistance.

References

- Piper T S & Koentge N, *J Chem Phys (USA)*, **32** (1960) 559.
- Pryce M H L, Agnetta G, Garofano T, Palmavito Relli M B & Palma M V, *Philos Mag (GB)*, **10** (1964) 477.
- Solomon E I & Ballhausen C J, *Mol Phys (GB)*, **29** (1975) 279.
- Datta S K & De Debabala, *Indian J Cryogenics*, **1** (1) (1976) 45.
- Kurglik A I, Simonov M A, Zhelezin E P & Belov N V, *Sov Phys Dokl (USA)*, **24** (8) (1979) 596.
- Tanabe Y & Sugano S, *J Phys Soc Jpn (Japan)*, **9** (1954) 753.
- Boxall L G, Fung K W & Johnson K E, *J Inorg Nucl Chem (GB)*, **35** (1972) 3523.
- Liehr A D & Ballhausen C J, *Ann Phys (USA)*, **6** (1959) 134.
- Lakshman S V J & Lakshman Rao J, *Spectrochim Acta Vol A (GB)*, **35** (1979) 703.
- Jorgensen C K, *Acta Chem Scand (Denmark)*, **9** (1955) 1362.
- Holmes O G & McClure D S, *J Chem Phys (USA)*, **26** (1957) 1686.
- Herzberg G, *Molecular spectra and molecular structure: 2—Infrared and Raman spectra of polyatomic molecules* (Van Nostrand, London), 1962, 281.

Thermal Conduction & Probability of Phase Orientation in Porous & Dispersed Two-Phase Systems

RAMVIR SINGH, R S BENIWAL, R N PANDE & V KUMAR

Thermal Physics Laboratory, Department of Physics, University of Rajasthan, Jaipur-4

Received 3 June 1985

An expression for orientation of phases in natural two-phase systems has been derived. This relation has been used to predict the effective thermal conductivity of two-phase systems. The calculated values of effective thermal conductivity are in good agreement with the reported experimental results.

1 Introduction

Complete information on effective thermal conductivity (K) of dispersed two-phase systems is often needed by persons working in heat transport through soils, engineering and insulating materials. Many attempts have been made to predict the value of K of such materials. The expressions are mainly classified as exact formulations¹⁻⁵ and semi-empirical relations⁶⁻⁹. But so far no attempt has been made to study the orientation of phases in a random two-phases mixture to obtain an expression for K .

In an earlier work¹⁰, an expression for K based on the probability of orientation of phases has been proposed. However, the value of K has not been obtained from a knowledge of the actual value of orientation of phases. The present study is an extension of the previous one. Here we first find an expression for the probability (n) of orientation along the direction of heat flow of a particular phase and then use this value of n to determine K of natural samples.

2 Theoretical Formulation

Let us consider a two-phase mixture consisting of a solid of thermal conductivity K_s and a gas of thermal conductivity K_r . Let the volume fraction of gas (porosity) be φ ; obviously the volume fraction of solid will be $(1 - \varphi)$. Further, we assume that solid and gas phases are arranged in alternate layers in which some part of the layers is oriented parallel to the direction of the heat flow and the remaining part perpendicular to the direction of heat flow. The value of K of such a mixture will be given by the relation¹⁰:

$$K = K_{\parallel}^n K_{\perp}^{1-n} \quad \dots (1)$$

where

$$K_{\parallel} = \varphi K_r + (1 - \varphi) K_s, \quad \dots (1a)$$

and

$$K_{\perp} = \left\{ \frac{\varphi}{K_r} + \frac{(1 - \varphi)}{K_s} \right\}^{-1} \quad \dots (1b)$$

In Eq. (1) n is the probability of orientation of the sample along the direction of heat flow.

Taking the logarithmic differential of Eq. (1) and substituting the values of $(\partial K_{\parallel} / \partial \varphi)$ and $(\partial K_{\perp} / \partial \varphi)$ from Eqs (1a) and (1b),

$$\frac{1}{K} \frac{\partial K}{\partial \varphi} = \frac{\partial n}{\partial \varphi} \ln \left(\frac{K_{\parallel}}{K_{\perp}} \right) + (K_r - K_s) \left\{ \frac{n}{K_{\parallel}} + \frac{(1 - n)}{K_s K_r} K_{\perp} \right\} \quad \dots (2)$$

Eq (2) must satisfy the phase boundary conditions, i.e. the two-phase system must tend to solid or fluid phase respectively as φ approaches zero or unity. Under these limiting conditions, we find that

as $\varphi \rightarrow 0$, $K_{\parallel} \rightarrow K_s$

and K_{\perp} also $\rightarrow K_s$

Similarly

as $\varphi \rightarrow 1$, $K_{\perp} \rightarrow K_r$

and K_{\parallel} also $\rightarrow K_r$

Effectively the above two boundary conditions are mathematically equivalent to the following relations. These are:

(i) $\varphi \rightarrow 0$, $K_{\parallel} \rightarrow K_1$

and (ii) $\varphi \rightarrow 1$, $K_{\perp} \rightarrow K_{\parallel}$

Substituting these conditions in Eq. (2), we get the following two different relations for limiting porosity values ($\varphi \rightarrow 0$ and 1):

$$\frac{1}{K} \frac{\partial K}{\partial \phi} = (K_f - K_s) \left\{ \frac{n_1}{K_{\parallel}} + \frac{(1-n_1)K_{\parallel}}{K_s K_f} \right\} \quad \dots (3)$$

and

$$\frac{1}{K} \frac{\partial K}{\partial \phi} = (K_f - K_s) \left\{ \frac{n_1}{K_{\perp}} + \frac{(1-n_1)}{K_s K_f} K_{\perp} \right\} \quad \dots (4)$$

Here we have used n_1 instead of n as this depicts the orientation of the layers for fixed extremum porosity values. Eqs (3) and (4) become equivalent expressions as $K_{\parallel} \rightarrow K_{\perp}$. This implies that the two slopes given by Eqs (3) and (4) are equivalent for $\phi \rightarrow 0$ and unity. Equating these two and solving for n_1 , we find

$$n_1 = \frac{K_{\parallel} K_{\perp}}{K_s K_f + K_{\parallel} K_{\perp}} \quad \dots (5)$$

For intermediate values of ϕ , n may be found as follows. Let us consider two values of ϕ around the point $\phi \rightarrow 0.5$ in K - ϕ curve as shown in Fig. 1. Here $\phi_1 + \phi_2 = 1$. At these values of ϕ , $(\partial K / \partial \phi)$ should be nearly same, as $d\phi_1 = -d\phi_2$.

Thus for ϕ_1 and $\phi_2 \rightarrow 0.5$

$$\frac{\partial K}{\partial \phi} = \frac{\partial K}{\partial \phi_1} = -\frac{\partial K}{\partial \phi_2} \quad \dots (6)$$

Similarly, for these values of ϕ , we also find the value of $(\partial n / \partial \phi)$.

For $\phi \rightarrow 0.5$ Eq. (2) yields

$$\frac{1}{K} \frac{\partial K}{\partial \phi} = \frac{\partial n}{\partial \phi} \ln \frac{(K_s + K_f)^2}{4K_s K_f} + 2 \frac{(K_f - K_s)}{(K_f + K_s)} \quad \dots (7)$$

because

$$\left\{ \frac{n}{K_{\parallel}} + \frac{(1-n)}{K_{\parallel}} \right\} \rightarrow \frac{2}{(K_f + K_s)}$$

As $[(1/K)(\partial K / \partial \phi)]$ yields equal slopes at ϕ_1 and ϕ_2 through Eq. (6) and the variation in ϕ for $\phi \rightarrow 0.5$ affects $(\partial n / \partial \phi)$ only in Eq. (7), one notes that for

$$\left(\frac{1}{K} \frac{\partial K}{\partial \phi_1} \right) = - \left(\frac{1}{K} \frac{\partial K}{\partial \phi_2} \right)$$

$$\frac{\partial n}{\partial \phi_1} = - \left(\frac{\partial n}{\partial \phi_2} \right) \quad \dots (8)$$

Substituting Eqs (6) and (8) in Eq. (2) and on simplifying we get:

$$\begin{aligned} & \left\{ \frac{n}{K_s(1-\phi_1) + K_f \phi_1} + \frac{(1-n)}{K_f(1-\phi_1) + K_s \phi_1} \right\} \\ &= \left\{ \frac{n}{K_s \phi_1 + (1-\phi_1)K_f} + \frac{(1-n)}{K_f \phi_1 + (1-\phi_1)K_s} \right\} \quad \dots (9) \end{aligned}$$

Evaluating n from Eq. (9), yields

$$\begin{aligned} n &= \frac{\left\{ \frac{1}{K_s \phi_1 + (1-\phi_1)K_f} - \frac{1}{K_s(1-\phi_1) + K_f \phi_1} \right\}}{2 \left\{ \frac{1}{K_s \phi_1 + (1-\phi_1)K_f} - \frac{1}{K_s(1-\phi_1) + K_f \phi_1} \right\}} \\ &= \frac{1 \left\{ (K_{\perp} / K_s K_f) - 1 / K_{\parallel} \right\}}{2 \left\{ (K_{\perp} / K_s K_f) - 1 / K_{\parallel} \right\}} \end{aligned}$$

$$\text{or } n = \frac{1}{2} \quad \dots (10)$$

This can be further tested through Eq. (5). We find that at $\phi \rightarrow 0.5$, $K_{\parallel} K_{\perp} \rightarrow K_s K_f$. Therefore, Eq. (5) yields

$$n_1 = \frac{1}{2} \quad \dots (11)$$

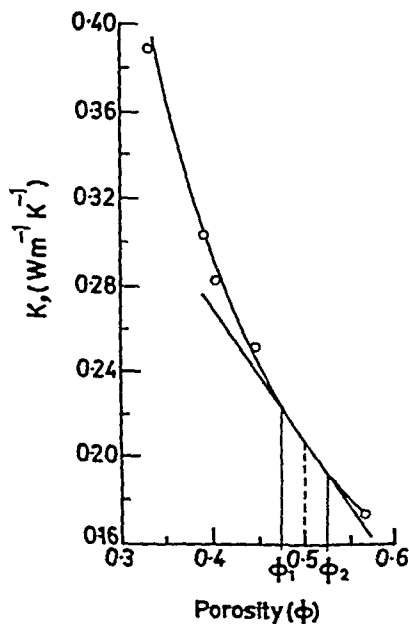


Fig. 1—Effective thermal conductivity (K) of Miami silt loam plotted against fractional porosity (ϕ)

3 Comparison with Experimental Results and Discussion

The value of K , can be estimated using Eq. (1) from a knowledge of n . Using Eq. (5), we evaluate values of n for porosity values $\phi \rightarrow 0$ and 1. For $\phi \rightarrow 0.5$, however, n is evaluated using Eq. (10). The calculated values of n and K are reported in Tables 1-3 where experimental values of K are also given for comparison. It is observed that calculated values are in good agreement with the experimental results.

The scheme presented here for the calculation of K is simple and provides useful information regarding the orientation of different layers of the phases in a two-phase porous system. It is found that when porosity values are near 0 and 1, a reasonable prediction of K is obtained. When porosity is nearly 0.5, the recommended value of n is 0.5. This agrees with the results of the previous investigation made by

Table 1—Calculated Values of n and K for Porosity Value of $\phi \rightarrow 1$

System	K_s/K_f	ϕ	n Using Eq. (5)	K_{calc} $W m^{-1}K^{-1}$	K_{exptl} $W m^{-1}K^{-1}$	Error (%)
Cellosize/flexol plasticizer ¹¹	3.03	0.7	0.3994	0.257	0.257	0.00
Cellosize/polypropylene glycol ¹¹	3.73	0.7	0.385	0.234	0.234	0.00
Copper/solder ¹²	(i) 5.09	0.9876	0.1724	79.42	78.8	0.79
	(ii) 5.09	0.9864	0.1732	79.56	78.8	0.97
	(iii) 5.09	0.9714	0.1832	81.23	81.7	-0.58
Forsterite/magnesia ¹³	0.16	0.868	0.7649	2.445	2.479	-1.37
Blood ¹⁴ (24°C)	(i) 0.819	0.97	0.5464	0.561	0.567	-1.05
	(ii) 0.819	0.92	0.5415	0.556	0.563	-1.24
	(iii) 0.819	0.89	0.5383	0.552	0.559	-1.25
	(iv) 0.819	0.82	0.5316	0.545	0.546	-0.18
	(v) 0.819	0.74	0.5237	0.536	0.538	-0.37
Silicone rubber/glass beads ¹⁵	5.35	0.911	0.2184	0.226	0.235	-3.83
Lead powder/silicone rubber ¹⁶	90.20	0.84	0.1675	0.701	0.665	5.41

Table 2—Calculated Values of n and K for Porosity Value of $\phi \rightarrow 0$

System	K_s/K_f	ϕ	n Using Eq. (5)	K_{calc} $W m^{-1}K^{-1}$	K_{exptl} $W m^{-1}K^{-1}$	Error (%)
Cellosize/flexol plasticizer ¹¹	0.33	0.1	0.2286	0.206	0.210	-1.9
Cellosize/flexol plasticizer ¹¹	0.286	0.1	0.313	0.182	0.182	0.00
Copper/solder	(i) 0.196	0.0507	0.198	83.82	83.7	0.14
	(ii) 0.196	0.0125	0.177	80.20	79.00	1.57
	(iii) 0.196	0.0263	0.182	80.97	81.10	-0.16
	(iv) 0.196	0.0286	0.183	81.23	82.6	-1.65
Blood ¹⁴ (37°C)	(i) 1.212	0.03	0.545	0.587	0.596	-1.52
	(ii) 1.212	0.07	0.541	0.582	0.592	-1.68
	(iii) 1.212	0.12	0.537	0.577	0.588	-1.87
Lead powder/silicone rubber ¹⁶	0.011	0.04	0.050	0.432	0.463	-6.69

Table 3—Calculated Values of n and K for Porosity Values of $\phi \rightarrow 0.5$

System	K_s/K_f	ϕ	$n=0.5$ Using Eq. (10)	K_{calc} $W m^{-1}K^{-1}$	K_{exptl} $W m^{-1}K^{-1}$	Error (%)
Rajasthan desert sand ¹⁰	(i) 126.98	0.3850	0.5	0.424	0.387	9.56
	(ii) 126.98	0.4052	0.5	0.357	0.336	6.25
	(iii) 126.98	0.4394	0.5	0.333	0.312	6.73
Blood ¹⁴ (37°C)	(i) 1.2124	0.59	0.5	0.546	0.546	0.00
	(ii) 1.2124	0.56	0.5	0.539	0.542	-0.38
Water/mineral oil ¹⁷	4.14	0.6	0.5	0.267	0.293	-8.87
Uranium oxide/sodium ¹⁸	0.1	0.5	0.5	28.46	29	-1.86
Miami silt loam ¹⁹	123.013	0.332	0.5	0.374	0.386	-3.1

Bruggeman⁷, who estimated that for $\phi \rightarrow 0.5$, K is given as:

$$K = (K_f K_1)^{1/2} = (K_s K_f)^{1/2}$$

The probability of orientation n is found to depend upon ϕ and K_s/K_f ratio.

Acknowledgement

Thanks are due to Prof. R.C. Bhandari, Dr P V Bakore, Dr D R Chaudhary and Dr N S Saxena for valuable discussions and suggestions. Financial assistance from Department of Science and Technology, Government of India, New Delhi, is gratefully acknowledged.

References

- Wiener O, *Phys Z (Germany)*, 5 (1904) 332.
- Woodside W & Messmer J N, *J Appl Phys (USA)*, 32 (1961) 1688.
- Powers A E, *Conductivity in aggregates* (Knolls Atomic Power Laboratory New York) KAPL-2145, 1961.
- Maxwell J C, *A treatise on electricity and magnetism* 3rd Edn, Vol 1 (Clarendon Press, Oxford) 1904 p. 440.
- Chaudhary D R & Bhandari R C, *Indian J Pure & Appl Phys*, 6 (1968) 274.
- Lichtenecker K, *Phys Z (Germany)*, 27 (1926) 115.
- Bruggeman D A G, *Ann Phys (Germany)*, 24 (1935) 636.
- Sugawara A & Yoshizawa Y, *Aust J Phys (Australia)*, 14 (1961) 469.
- De Veries D A, *Madedelingen Van de Landbouwhogeschool te Wageningen (Netherlands)*, 52(1) (1952) 1-73.

- 10 Chaudhary D R & Bhandari R C, *J Phys D Ser 2 (GB)*, **1** (1968) 815.
- 11 Nahas N C & Couper J R, *Res Rep Ser No 7* (University of Arkansas, Arkansas, USA) 1966.
- 12 Lee H J & Taylor R E, *J Appl Phys (USA)*, **47** (1976) 143.
- 13 Kingrey W D, *J Am Ceram Soc (USA)*, **42** (1959) 617.
- 14 Ahuja A, *J Appl Physiol (USA)*, **37** (1974) 765.
- 15 Hayashi K, Saijo Y & Uei J, *Yokai-Shi (Japan)*, **82** (1976) 318.
- 16 Cheng S C, Law Y S & Kwan C C Y, *Int J Heat & Mass Transfer (GB)*, **15** (1972) 355.
- 17 Knudsen J G & Wand R H, *Ind Eng Chem C (USA)*, **5** (1958) 1667.
- 18 Huetz J, *Progress Heat & Mass Transfer (GB)*, **5** (1972) 285.
- 19 Smith W O, *Soil Sci (USA)*, **3** (1942) 435.

A Laser Interferometer for Vibration Amplitude Measurement of Power Ultrasonic Sources

V N BINDAL, S K JAIN & YUDHISTHER KUMAR
National Physical Laboratory, New Delhi 110 012

Received 4 February 1986; revised received 30 July 1986

A laser interferometer for the absolute vibration amplitude measurement of power ultrasonic sources is reported. The instrument can provide direct and real time measurement of vibration amplitude having surface velocity of the order of 100 cm/s, i.e. about 8 μ m at 20 kHz. The measurement accuracy is about 5%. Results of measurement on a high power ultrasonic horn of an emulsifier and a sandwich transducer are given, which demonstrate the usefulness of the interferometer in the characterization of high power ultrasonic devices.

1 Introduction

Vibrational amplitude is one of the important parameters for the evaluation and characterization of high power ultrasonic devices¹, such as plastic welders, sonifiers, disintegrators, etc. A number of optical instruments have been used for the absolute measurement of vibration amplitude of power ultrasonic devices which is usually above a few microns. Some of these are based on capacitive transducer², opto-electronic sensors³ and laser interferometers⁴⁻⁷. Most of these, however, require elaborate optical arrangements or complex electronic circuitry. Further, the measurement of vibrational amplitude by these methods is by indirect evaluation. The optical microscope can be used to measure amplitudes, which are significantly larger than the wavelength of the optical radiation used in the microscope. This method has also been recommended by the International Electrotechnical Commission (IEC)¹. But this method also suffers from the drawback that point-to-point scanning of the vibrating surface cannot be done. A laser interferometer has been reported by Bruce and Fitzpatrick⁸ for the vibration amplitude measurement of remote rough surfaces. This interferometer suffers from the limitation that its use is restricted to low frequencies (~ 1 kHz).

The present work reports on a laser interferometer, which can be used to measure vibration amplitude of power ultrasonic transducers. The interferometer is similar in principle to that of Bruce and Fitzpatrick, but incorporates modifications which make it particularly suited for measurements on ultrasonic transducers.

2 Principle of Operation

The laser interferometer used is basically the Michelson interferometer, in which the optical paths of the two split up beams are made approximately identical

by use of a self-compensating beam splitter. The schematic of the optical arrangement is shown in Fig. 1. Since the optical paths of the reference (d_1) and the object beams (d_2) are almost equal, a complete interference between the two beams is obtained in the direction of the detector. Under this condition, intensity of the interfering laser light can be expressed as⁹

$$I = I_0 \cos^2 \left[\frac{\pi}{\lambda_L} (d_1 - d_2) \right] = \frac{I_0}{2} \times \left[1 + \cos \frac{2\pi}{\lambda_L} (d_1 - d_2) \right] \quad \dots (1)$$

where I_0 is the intensity at the interference maxima and λ_L is the wavelength of the laser light. If the object mirror is substituted with a vibrating surface, the optical path difference varies as a function of time t according to the relation

$$d_1 - d_2 = \xi_a \sin (\omega_a t + \phi_a) \quad \dots (2)$$

where ξ_a is the amplitude of the acoustically vibrating surface, ω_a is the angular frequency and ϕ_a is the initial phase at time $t=0$. Intensity I in Eq. (1), therefore, shows a time variation which after neglecting the constant term, looks like a phase-modulated waveform as shown in Fig. 2. Each full cycle in Fig. 2 corresponds

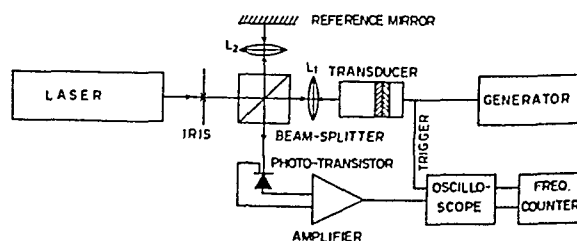


Fig. 1—Block diagram of the laser interferometer set-up

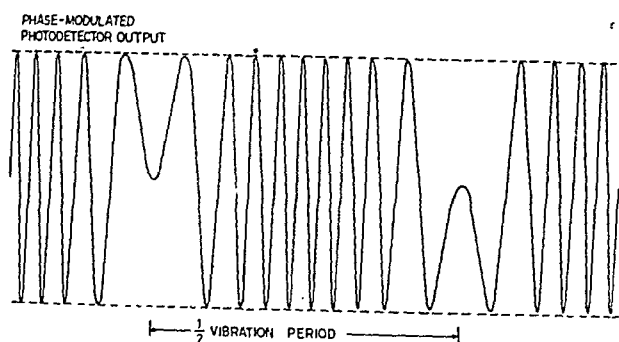


Fig. 2—Time-response of the interference signal

to an optical path difference of λ_L except for the ones near the turning points of the vibration, where it corresponds to a fraction thereof.

If γ be the number of cycles per vibration period, the amplitude of vibration would be given to a good approximation by $\gamma\lambda_L/8$. The approximation is due to the fact that the fractional contribution near the turning points gets rounded off to either nil or one full cycle. The higher the value of γ , the better would be the approximation. Therefore, higher amplitude can be measured more accurately.

Value of γ can be measured by taking the ratio between the pulse frequency of the interference signal and that of the acoustic signal.

3 Description of Interferometer

A 2 mW helium-neon laser of wavelength 0.6328μ has been used as the coherent source of light. A beam-splitting prism together with collimating lenses L_1 and L_2 placed equi-distant from the prism at 90° to each other, ensure self-compensation of the optical path difference introduced in the two beams by prism and lenses (Fig. 1). The lenses L_1 and L_2 are identical. The reference mirror and the transducer front surface are placed at the foci of the lenses. This makes the interferometer tilt compensated and the output signal is then unaffected by any tilt in the transducer front surface. The surface of the vibrating object is pasted with a thin aluminium foil to act as the object mirror. Any effects due to surface roughness of the vibrating object (even after the aluminium foil has been pasted), are reduced, because the light is focussed by the lens L_1 on a point on the surface.

The optical components and the laser have been mounted in a micro-bench in such a way that the whole of the interferometer becomes one single compact unit. This arrangement has the advantage that once the interferometer has been aligned properly, it cannot be easily disturbed from its setting. A heavy marble plate, resting on a cushion of foam rubber, has been used as a base for the interferometer, in order to reduce the effect of ambient vibration.

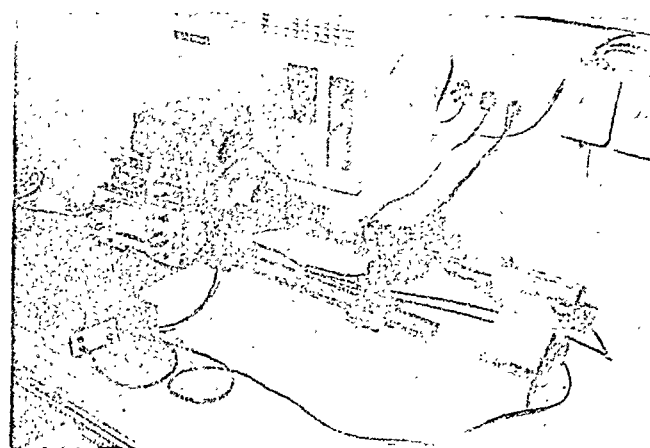


Fig. 3—Photograph of the laser interferometer set-up

The interference signal has been converted into an electrical signal using a silicon photo-transistor, which is followed by a wideband amplifier stage. The amplifier has a lower cut-off frequency, so that the contribution to the interference signal due to ambient vibration gets eliminated. A sensitive frequency counter has been used to record the pulse-frequency in the interference signal. Fig. 3 is the photograph of the complete set-up used for measurements.

It would be worthwhile to mention that the laser interferometer is similar to the one described by Bruce and Fitzpatrick⁸, but incorporates some modifications. Intensity of the interference beams going into the photodetector is high enough, so that amplifier gain required is not very high. This enables to obtain a large bandwidth of the photodiode amplifier. Further, alignment of the interferometer is simpler, since self-compensation of the optical paths has been used.

4 Measurements

Measurements of vibration amplitude have been carried out on a 20 kHz high-power ultrasonic horn of an emulsifier (DAWE Instrument Ltd) and on a commercial sandwich transducer. ENI power generator has been used to drive the ultrasonic transducer, to ensure the stability of the applied frequency.

The frequency counter has been operated on its averaging mode, which gives average of pulse frequency count every 10 s, so that fluctuation in frequency counter reading due to ambient vibrations and instability of the applied frequency gets suppressed.

5 Results

In order to verify the validity of the amplitude measurement by the laser interferometer, its variation with the rf voltage applied to the transducer has been studied. Fig. 4 shows the variation of vibration amplitude (calculated from frequency ratio) of the emulsifier horn with the applied rf voltage. The variation is fairly linear, which indicates the validity of the meth-

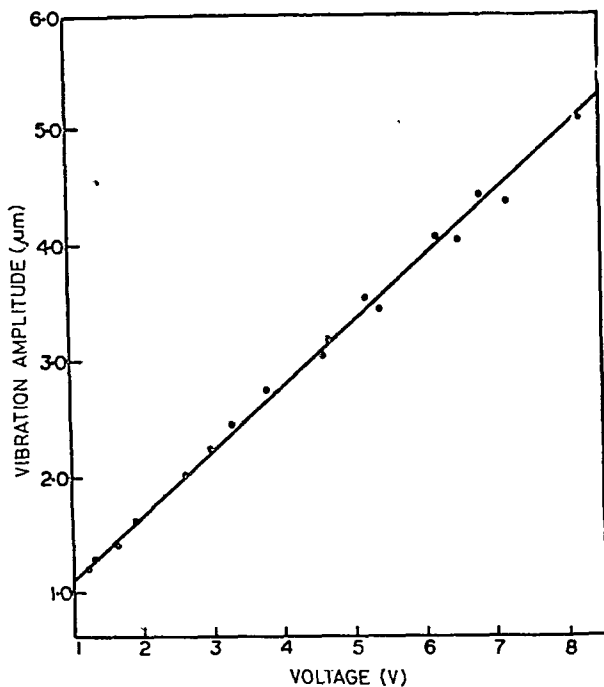


Fig. 4—Variation of vibration amplitude of the emulsifier horn with the applied rf voltage

od. The statistical scatter of the points is estimated to be about 5% or $0.25 \mu\text{m}$, which seems to be the accuracy of measurement by this instrument. It is to be noted that the main contribution to this error is due to the fractional fringes, which cannot be registered in the frequency counter. Maximum error introduced this way would be $\lambda_L/4$ or about $0.16 \mu\text{m}$.

It has been observed that at high amplitude, interference signal becomes very weak and its pulse frequency cannot be measured in the frequency counter, which has a finite sensitivity. At amplitudes of about $8 \mu\text{m}$, pulse frequency of the interference signal becomes very high ($\sim 1.5 \text{ MHz}$). At these frequencies, gain-factor of the photo-transistor used becomes so low that the output signal cannot be measured in the frequency counter. The limit of the amplitude that can be measured, using the present set-up at 20 kHz , seems to be about $8 \mu\text{m}$. This corresponds to a particle velocity amplitude of about 100 cm/s .

Amplitude resonance curves of a few transducers have been measured using the laser interferometer to show its usefulness in the characterization of power transducers. Figs 5 and 6 show the variation of amplitudes as a function of frequency of the emulsifier horn and the sandwich transducer at different power levels. The emulsifier horn shows the familiar resonance curve, which has a Q -factor of about 670. The sandwich transducer shows a small split in its resonance curve, which indicates existence of two closely placed resonance frequencies. At higher operational power levels, the half-power point bandwidth is seen

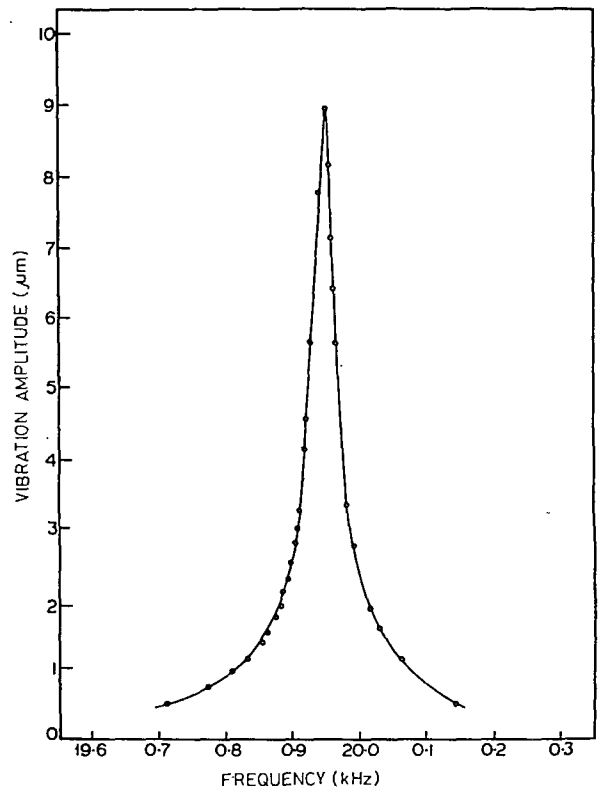


Fig. 5—Amplitude resonance curve of the emulsifier horn as measured by laser interferometer

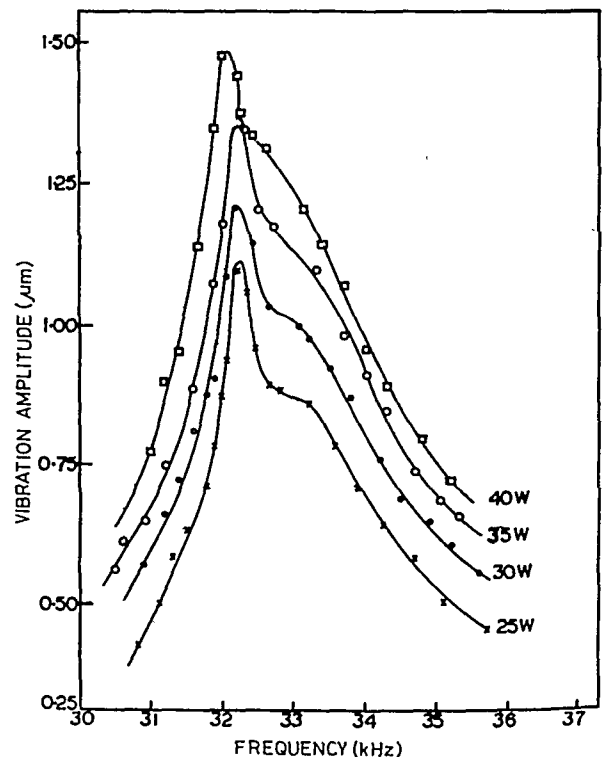


Fig. 6—Amplitude resonance curves of sandwich transducer at different power levels

to increase and the resonance frequency is seen to shift downwards. Fig. 7 shows the corresponding decrease in Q -factor as a function of increasing power level.

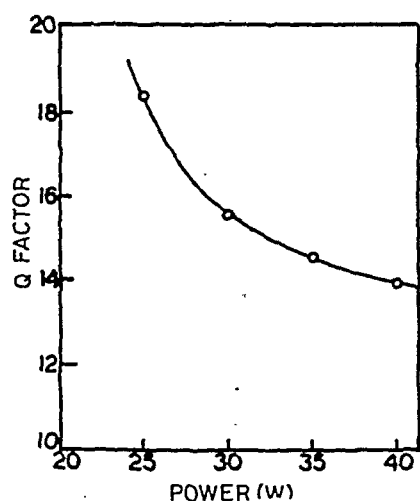


Fig. 7—Variation of Q of the sandwich transducer with power level

vels. The significance of this result is that, at higher power drives, there would be higher losses in the transducer, resulting in decrease in the efficiency of the transducer, and the transducer would get heated up. Further, this study also indicates that due consideration has to be given to the design of the driving circuit to accommodate the shift in the resonance frequency.

6 Concluding Remarks

A laser interferometer is reported which makes possible absolute measurement of vibration ampli-

tude in the range $1-8 \mu\text{m}$ at 20 kHz, with an accuracy of 5%. The range of measurement can be extended to higher values by using a fast rise-time photodetector. It is further expected that the measurement accuracy would improve at higher amplitudes, because the measurement error due to the fractional fringes remains the same.

The instrument would also be useful to study resonances and behaviour at higher power levels of power ultrasonic devices.

References

- 1 Measurement of ultrasonic magnetostrictive transducers (IEC Report, Publication), 782 (1984).
- 2 Bindal V N, Saksena T K & Jain S K, *Indian J Technol*, **22** (1984) 397.
- 3 Labs J & Bleich K H, *Feingeratetechnik (Germany)*, **26** (1977), 536.
- 4 Reibold & Molkenstruck W, *Acustica (Germany)*, **49** (1981) 205.
- 5 Speake J H, *Proc Evaluation and Calibration of Ultrasonic Transducers* (IPC Science & Technology Press, Guildford, UK), 1978, 106.
- 6 Lauer G, *Fortschr Akust DAGA-80. München* (VDE-Verlag, Berlin), 1980, 811.
- 7 Herbertz J & Jain S K, *Fortschr Akust DAGA-85, Stuttgart* (VDE-Verlag, Berlin), 1985, 803.
- 8 Bruce R A & Fitzpatrick G L, *Appl Opt (USA)*, **14** (1975) 1621.
- 9 Born M & Wolf E, *Principles of optics* (Pergamon Press, Oxford, UK), 1975, 302.

Mirror Galvanometer X-Y Scanning System for Laser Beam Processes

S G LOKHRE, S CHANDRASEKHAR & S K ROY

Solid State Electronics Group, Tata Institute of Fundamental Research, Bombay 400 005

Received 24 June 1986

Design and functioning of a X-Y scanning system equipped with mirror galvanometers for laser beam processes, are described. The focused laser beam can make linear and area scan over a heated or non-heated sample at speeds up to 50 cm/s. The uniform aberration free, scan area is of the order of $2 \times 1 \text{ cm}^2$, when lenses of suitable focal lengths are used. The appropriate electronic set-up used is described and the areas of applications are highlighted.

1 Introduction

High power laser beams are now being increasingly used in semiconductor research and development for a number of processes; for example, to anneal ion implantation damage¹, to recrystallize amorphous/polycrystalline material², to deposit, dope, alloy and etch by laser-assisted techniques like laser chemical vapour deposition (LCVD) and to trim resistors or fuse links in integrated circuits³. In all these applications, certain areas of semiconductor substrates are exposed to a finely focused laser beam, and the laser could be in continuous wave or pulsed mode. The important aspect of such a process is to scan the area in linear mode with the laser beam, either by keeping the substrate stationary and moving the beam or by keeping the beam stationary and moving the substrate. The present paper reports the design and functioning of a scanning system where the sample is stationary. The basic method is shown schematically in Fig. 1. With the sample stationary, the beam is deflected by two mirrors mounted orthogonally on two galvanometers which are driven by appropriate electronic circuits. The system can achieve a scanning speed of 1 to 50 cm/s, in the X-direction and small incremental movements in the Y-direction (minimum $10 \mu\text{m}$) in synchronous fashion. In the system corresponding to Fig. 1(a), the focusing lens is placed between the laser and the mirrors. The disadvantage of the configuration is that the sample is not in the focal plane at large scanning angles. This limits the size of the region that can be uniformly scanned. In the system corresponding to Fig. 1(b), the focusing lens is placed after the mirrors. This configuration has the advantage that with a flat field optical system, the focal surface on the sample can be anything other than a spherical surface and the area of uniform scan need not be narrowly limited. In addition, keeping the substrate stationary has an added advantage in that the sample can be mounted on a heated and fixed chuck for any thermal process requirements.

2 Design Requirement

In most experiments with focused laser beam scanning, the beam is required to be moved over the substrate with a typical pattern shown in Fig. 2. The beam has to be moved from initial position A to B by an amount of X-scan at a constant speed, and then deflect at right angle in the Y-direction from B to C by an amount Y-height and again move back from right to left from C to D at the same X-scan speed. The movement of the beam from B to C is at the fastest possible speed depending on the galvanometer response. The movement from A to B and then to C is called one scan. The Y-scan equals Y-height multiplied by the number of times X-scans are repeated (Y-steps). Thus, the four parameters, X-scan, X-speed, Y-height and the number of Y-steps are required to be manipulated for area scanning with laser beam. These parameters are to be realised by specific movements of two orthogonally mounted mirrors on two galvanometers driven by appropriate electronics. Since the laser beam is deflected, the linear displacement Z on the substrate is related to the angular displacement θ and focal length of the lens R by $Z = R\theta$. For a particular focal

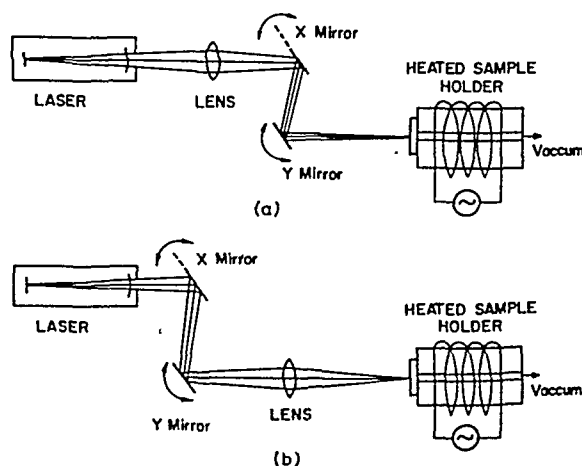


Fig 1(a)—Scanning with two galvanometers [(a): system with lens before mirrors and (b) system with lens after mirrors]

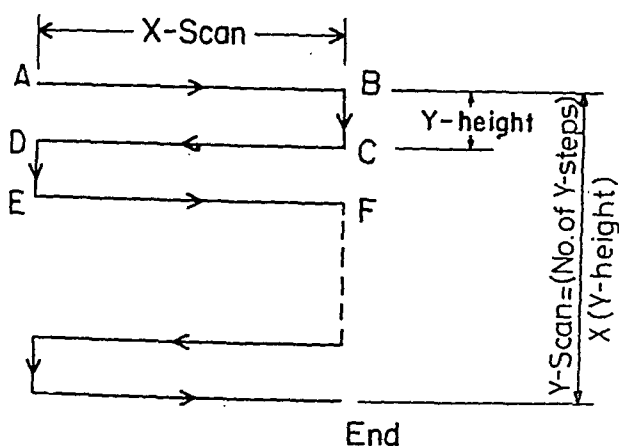


Fig. 2—Required scan pattern on substrate

length of lens, the scan speed is given by galvanometer's angular speed multiplied by focal length.

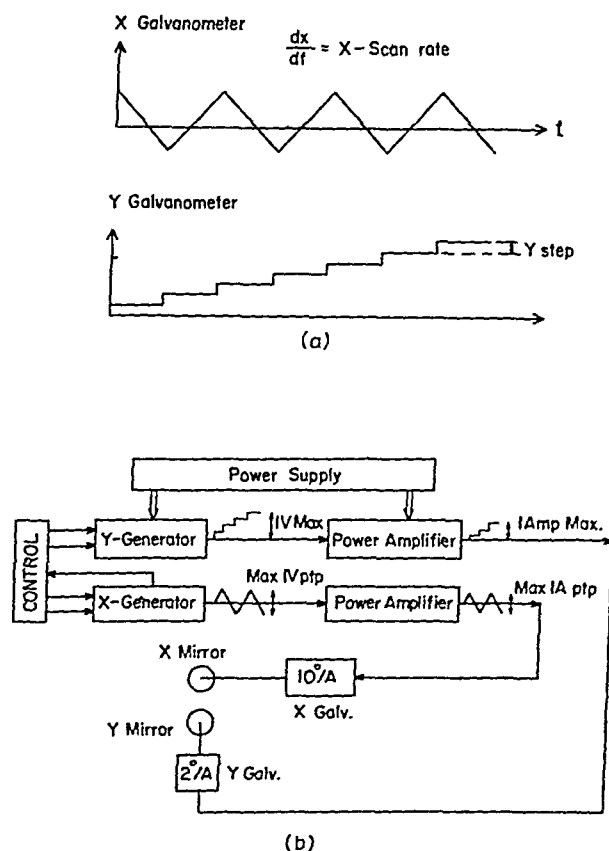
Two different types of galvanometers were chosen for X and Y -deflections (Model G310 for X -galvanometer with sensitivity 100 mA/deg, maximum peak-to-peak rotation 10° and Model G302 for Y -galvanometer with sensitivity of 550 mA/deg with maximum peak-to-peak rotation 2° . Both models are manufactured by M/s General Scanning Inc, USA and are provided with two lenses of focal lengths 10 and 25 cm. Basically the voltage waveform has to be generated and the converted into a current signal to drive the galvanometer. It was decided to use a gain of unity for voltage-to-current conversion. Therefore, the current limit of 1 A for each galvanometer became the voltage limit of 1 V peak-to-peak. With the requirement of X -speed between 1 to 50 cm/s, voltage ramp slopes from 0.25 V/s to 30 V/s were calculated, which when expressed as frequency for 1 V peak-to-peak corresponded to 15 Hz to 0.1 Hz respectively. Hence the design requirement of X -scan generator is a triangular ramp wave with frequency variable from 0.1 to 15 Hz and amplitude variable from 0 to 1 V peak-to-peak. Similarly, for a minimum Y -deflection of $10\mu\text{m}$, with a lens of focal length 10 cm, the Y -galvanometer deflection corresponds to 3 mV which is almost in the noise region. Taking a practical lower limit of 10 mV, the Y -waveform generator should produce staircase-type pulses with the height of the stairs being selectable in multiples of 10 mV with a maximum multiplier of 10. The total number of Y -steps is also selectable from 1 to 999 but limited to a maximum voltage signal of 1 V. Both X and Y waveforms have to have a dc bias for fine positioning the galvanometer before scanning.

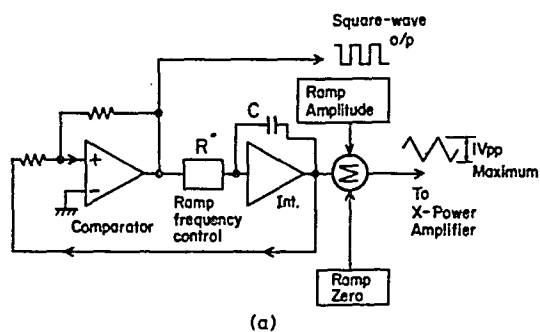
3 System Implementation

The purpose of the scanning electronics is to drive the two galvanometers synchronously with the

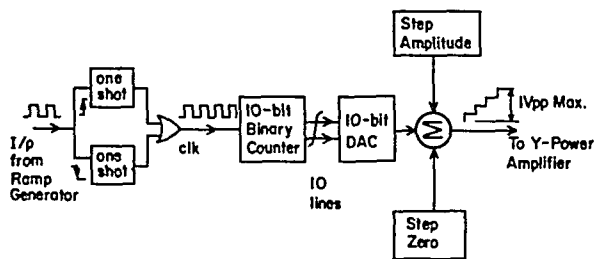
waveforms shown in Fig. 3(a). The X -galvanometer is driven by pulses of triangular waveform whose slope (which is the scan rate) and amplitude can be changed independently from scan to scan. The Y -galvanometer tilt angle is increased synchronously to account for the desired Y -height whenever the X -scan changes direction. When the Y -scan reaches a pre-set value (i.e. number of Y -steps), the X -waveform generator is stopped and the scan is halted. These voltage signals are fed to a unity-gain power amplifier that drives the mirrors mounted on the galvanometers. A general block diagram of the electronic set-up is given in Fig. 3(b).

The detailed block diagrams for the triangular ramp generator for X -movement and step generator for Y -movement are given in Figs 4(a) and 4(b) respectively. The triangular waveform is generated using two op-amps in a feedback system such that one op-amp acts as comparator producing square wave output and the other acts as an integrator, integrating the square wave across the capacitor C . This capacitor is charged through a resistor R which can be used to adjust the charging rate and hence the ramp frequency. As the capacitor C charges to a preset voltage, the comparator switches its output in the other direction and this reversed voltage charges the capacitor in the opposite direction. This pro-

Fig 3—(a) Driving waveforms of X - and Y - galvanometers and block diagram of the driving electronic set-up



(a)



(b)

Fig. 4—(a) Triangular ramp generator for X-axis and (b) step generator for Y-axis

duces a chain of triangular waves synchronised with the square waves. This square wave is also used to generate steps in the staircase generator and to make scanning *programmable*. The square wave output is also used to generate a clock of double the frequency by using two monostable multivibrators connected in tandem and applying it to a 10 bit binary counter. This doubling is necessary, because the scanning should be reversed at both the extreme ends of X-scan. Everytime the ramp changes its direction, the Y-galvanometer should advance one step. The output of the counter is applied to a digital-to-analog convertor (DAC-03, Precision Monolithic Inc, USA). The step waveform produced by the DAC is fed to a power amplifier through an op-amp and the off-set and gain of the op-amp can be adjusted. By adjusting the gain, the Y-height can be varied from 10 mV to 99 mV in steps of 10 mV. The output from the mono shot is also given to pre-settable binary coded decimal (BCD) counters. When the number of scans are entered, the BCD counters allow scanning until the number is reached. A new scan can be started by resetting the counters and reloading new values. Thus, control on the scanning parameter is achieved. A photograph of the scanner system along with the mirror-galvanometers is shown in Fig. 5.

4 Performance and Conclusion

In any processing, optical conditions are not known in advance. The electronic system has to be

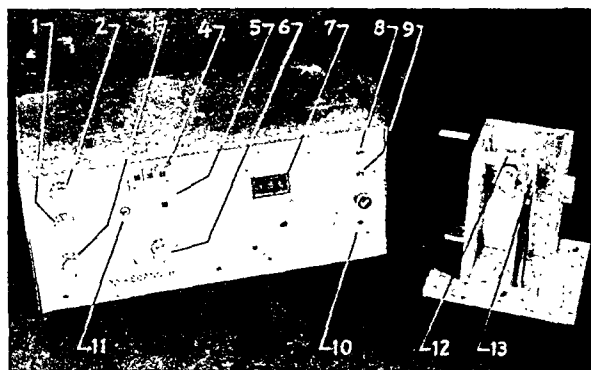


Fig. 5—Photograph of the scanner system with mirror galvanometers

- 1 Ramp amplitude control
- 2 Ramp frequency control
- 3 Ramp zero control
- 4 No. of Y-steps
- 5 Step height selector
- 6 Step zero control
- 7 Remaining steps
- 8 Switch S_2 (freeze/run)
- 9 Switch S_3 (programme/run)
- 10 Mains switch (on/off)
- 11 Switch S_1 (scan on/off)
- 12 X- and Y-galvanometers with mirrors
- 13 Plano-convex lens

versatile enough to suit the situation for any scanning used in terms of the required parameters. The X-Y scanning system designed and described above has the capability to meet varied scanning requirements. The system has been used consistently in some recent experiments⁴ for recrystallisation of polycrystalline silicon by laser annealing. Focused beam from high power (up to 18 W) argon ion laser (Spectra-Physics model 171-19) operating in CW-mode was made to scan areas of a heated substrate (temperature 350°C). The substrate was a multilayered structure having a polycrystalline silicon layer of thickness 0.5 μm grown on silicon dioxide of thickness 1 μm on a silicon slice. For optimum anti-reflection effect for laser heating, the substrate was capped with a thin layer (600 Å) of silicon nitride. By controlled scanning by the focused laser beam using the X-Y scanner, areas of the order of 2 cm by 1 cm could be recrystallised extending through the thickness of the polycrystalline silicon. Starting from a small grain (~ 500 Å) polycrystalline silicon, long crystallites (50 to 100 $\mu\text{m} \times 25$ to 50 μm) could be produced in chevron shape. Typical scanning parameters were: $X_{\text{speed}} = 10$ cm/s, $Y_{\text{height}} = 20$ μm and the gaussian beam, focused by a plano-convex lens of focal length 25 cm, d a diameter of 40-50 μm .

The recrystallized layer was found to be semiconductor-device worthy. It was possible to fabricate N-channel MOSFET with these materials.

The mirror galvanometer scanning system designed has been found to be versatile enough for laser beam recrystallization of polycrystalline silicon to give device-worthy crystalline material.

Acknowledgement

The authors would like to thank Prof K V Ramanathan, for his keen interest and useful suggestions during the implementation of the system. Discussions with Dr D K Sharma on some aspects of the design were helpful. The financial support from

the Department of Science and Technology (Grant DST No. 12/24)/(80-SERC), is gratefully acknowledged.

References

- 1 *Narayan J, Young R T & White C W, *J Appl Phys (USA)*, **49** (1978) 3912.
- 2 Gut A, Gerzberg L, Gibbon J F, Magee T J, Peng J & Hong J D, *Appl Phys Lett (USA)*, **33** (1978) 775.
- 3 Ehrlich D J & Tsao J Y *VLSI Electronics microstructure science*, edited by N G Einspruch (Academic Press Inc, New York), Vol 7, 1983, ch 3, 129.
- 4 Chandrasekhar S, Pai S P & Roy S K, *Proc 4th national seminar on physics of semiconductors and devices*, edited by J C Garg & P C Mathur (J C Garg, Jaipur), 1985, 116.

Dielectric Relaxation of Streptomycin at High Frequencies

V K FARKYA & DINESH KUMAR

Department of Postgraduate Studies & Research in Physics, Rani Durgawati Vishwavidyalaya, Jabalpur 482 001

Received 13 October, 1986

The dielectric relaxation times obtained from the maxima of the imaginary components of the complex permittivity for this antibiotic compound, varies from 9.36 to 10.62 ns for pressure values lying between 5 to 8 tons, corresponding to frequencies 17, 16.5, 15.5 and 15 MHz.

1 Introduction

Streptomycin is an important antibiotic compound and it is used in treatments of tuberculosis, meningitis and pneumonia. It is a laevorotatory solid¹ and is composed of three units: streptose, N-methyl-L-glucosamine and streptidine (Fig. 1). Hence dielectric relaxation studies of this complex compound are important as they will elucidate the behaviour of the compound, specially when it is subjected to high frequency perturbations^{2,3}.

2 Experimental Details

From one gram streptomycin powder (Sarabhai Chemicals) four wafers of 250 mg each were prepared by subjecting the powders to 5, 6, 7 and 8 ton of pressures using a compression machine fitted with a die of area of cross-section = 1.76 sq cm. A *Q*-meter EE-13 was set for resonance and the corresponding capacitance and *Q*-factor were measured using a high frequency cable connected to the external terminals and following the resonance technique. The streptomycin wafer sandwiched between two electrodes was connected across the capacitance terminals of the *Q*-meter. The circuit was resonated and the capacitance and the *Q*-value were determined again for a fixed frequency. The experiment was repeated at specific frequencies in the range 10-30 MHz. The observations were taken for each of

the four streptomycin wafer samples. The real (ϵ') and imaginary (ϵ'') components of the complex permittivity (ϵ^*) were computed using the relations^{4,5}:

$$\epsilon' = \frac{1}{C_0} \frac{C_{\text{obs}}}{1 + (\tan \delta)^2} - C_{\text{cable}} \quad \dots (1)$$

$$\epsilon'' = \frac{1}{C_0} \frac{C_{\text{obs}} \tan \delta}{1 + (\tan \delta)^2} \quad \dots (2)$$

$$\tan \delta = \tan \delta' - \tan \delta'' \quad \dots (3)$$

$$\tan \delta' = \frac{C_1}{C_1 - C_2} \left[\frac{1}{Q_1} - \frac{1}{Q_2} \right] \quad \dots (4)$$

$$\tan \delta'' = \frac{C_3}{C_3 - C_4} \left[\frac{1}{Q_3} - \frac{1}{Q_4} \right] \quad \dots (5)$$

where, C_{obs} is the capacitance between electrodes with streptomycin wafer; C_{cable} the capacitance of high frequency cable; C_0 the capacitance between electrodes without dielectric; $\tan \delta$ the loss factor of streptomycin; $\tan \delta'$ the loss factor of capacitor with streptomycin wafer + high frequency cable; $\tan \delta''$ the loss factor of high frequency cable; Q_1 , C_1 and Q_2 , C_2 are the *Q*-factors and capacitances observed respectively with and without the streptomycin sample and Q_3 , C_3 and Q_4 , C_4 are the *Q*-factors and capacitances observed respectively with and without the high frequency cable.

3 Results and Discussion

The computed values of both $C_0 \epsilon'$ and $C_0 \epsilon''$ are plotted against the frequencies in Fig. 2 for samples prepared at different pressures. It is observed that these curves follow the Debye's dispersion relations^{6,7}:

$$\epsilon' = \epsilon_{\infty} + \frac{\epsilon_0 - \epsilon_{\infty}}{1 + (\omega \tau)^2} \quad \dots (6)$$

$$\epsilon'' = \frac{(\epsilon_0 - \epsilon_{\infty}) \omega \tau}{1 + (\omega \tau)^2} \quad \dots (7)$$

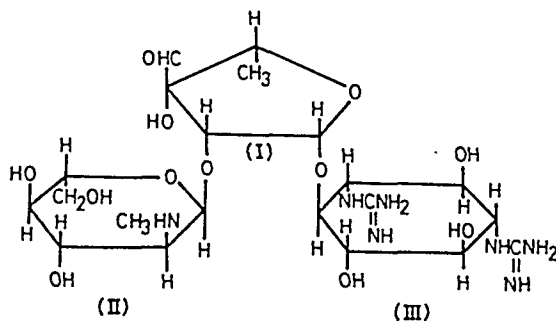


Fig. 1—Structure of streptomycin (I, streptose; II, N-Methyl-L-glucosamine, III, streptidine)

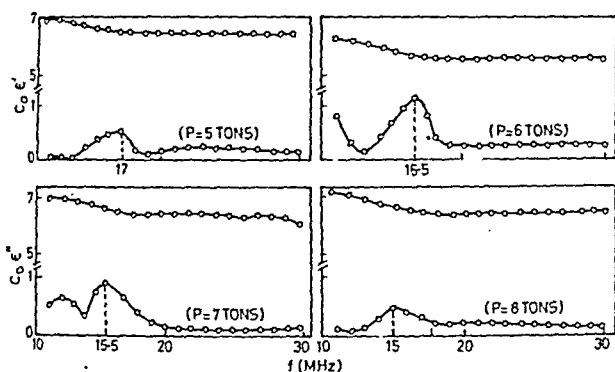


Fig. 2—Variation of $C_0 \epsilon'$ and $C_0 \epsilon''$ with frequency for streptomycin wafer sample fabricated at different pressures

where, ϵ_0 is the static dielectric constant, ϵ_∞ the instantaneous value of the dielectric constant, ω the angular frequency and τ the dielectric relaxation time. The value of τ can be evaluated from ϵ_{\max} value when

$$\tau = \frac{1}{\omega} \quad \dots (8)$$

Values of τ for the streptomycin wafer samples fabricated at different pressures are given in Table 1.

The values of τ vary between 9.36 to 10.62 ns. The graph of the pressure of formation versus τ shown in Fig. 3 shows nonlinearity. As streptomycin is composed of three different complex molecules, detailed studies by different methods are essential to determine the contribution by the individual structures to the observed dielectric relaxation time and the effect of pressures⁸. The value of τ reported in Table 1 are in agreement with the theoretical values computed⁹.

Acknowledgement

The authors are thankful to Prof. Gopalakrishna, Head of the Department of Applied Physics, Government Engineering College, Jabalpur, for providing the necessary facilities for carrying out these investigations. Further, thanks are also due to Shri S L Rakesh for assistance in the preparation of the an-

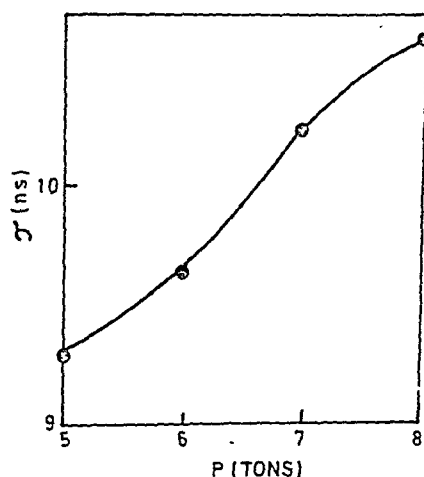


Fig. 3—Variation of τ with applied pressure

Table 1—Values of τ Calculated for Different Streptomycin Wafer Samples

Pressure (tons)	Thickness of sample (cm)	Frequency for maximum value of ϵ'' (MHz)	τ (ns)
5	0.149	17.0	9.36
6	0.146	16.5	9.65
7	0.144	15.5	10.27
8	0.143	15.0	10.62

tibiotic wafers by the application of different pressures at the Mechanical Engineering Laboratory.

References

- 1 Finar I L, *Organic chemistry* (English Language Book Society, London) 1977, 877.
- 2 Farkya V K, *Stud Biophys Berlin (Germany)*, 52 (1974) 274.
- 3 Farkya V K, *Stud Biophys Berlin (Germany)*, 88 (1982) 139.
- 4 Bandopadhyaya T K & Farkya V K, *Int J Electron (GB)*, 34 (1973) 253.
- 5 Farkya V K, Bandopadhyaya T K & Dasgupta S M, *Indian J Pure & Appl Phys*, 12 (1974) 465.
- 6 Dekker A J, *Solid state physics*, (MacMillan & Co, London) 1970, 151.
- 7 Wyard S J, *Solid state biophysics* (McGraw-Hill, New York) 1969, 296.
- 8 Farkya V K & Dinesh Kumar, *Stud Biophys Berlin (Germany)*, 93 (1987) in press.
- 9 Farkya V K & Dinesh Kumar, *Proc Natl Acad Sci (India)*, 55 (1985) 38.

Interference-Free Determination of Nickel in Water by Graphite Furnace Atomic Absorption Spectrophotometry

ANIMESH KUMAR & M Z HASAN

National Environmental Engineering Research Institute,
Nagpur 440 020

and

B T DESHMUKH

Department of Physics, Nagpur University, Nagpur 440 010

Received 1 July 1986; revised received 6 October 1986

An interference-free method for the determination of nickel in water by graphite furnace atomic absorption spectrophotometry is reported. The method utilizes fast heating rate and high atomization temperature to eliminate interferences from iron and magnesium.

The present note reports a new method for interference-free determination of Ni in water using graphite furnace atomic absorption (GFAA) spectrophotometry. The method utilizes a fast heating rate and a high atomization temperature to eliminate interferences.

Experimental details—Stock solution of Ni (1000 mg/l) was prepared by dissolving 0.4953 g Ni (NO_3)₂·6H₂O (98% pure, BDH, AR) in 1 ml nitric acid (BDH, AR) and subsequently diluting to 100 ml with deionized distilled water. Standard Ni solutions of various concentrations were then prepared by two step dilutions of Ni stock solution with 1% nitric acid.

A Perkin-Elmer model, 372 atomic absorption spectrophotometer equipped with HGA-22000 graphite furnace (GF) and deuterium background corrector lamp was used. Measurements were made with intensitron hollow cathode lamp of Ni operated at 25 mA lamp current with wavelength setting at 232.0 nm and spectral slit width at 0.2 nm. Pyrolytically coated graphite (PCG) tube gave better analytical sensitivity and precision. An inert atmosphere in and around the graphite tube was maintained by continuously purging nitrogen at a flow rate of 50 ml/m. The Ni absorbance signals were recorded of 10 mV span recorder (Perkin-Elmer Model-56) for the computation of the results. Eppendorf microlitre pipette with disposable tips was used to transfer the solutions into the GF.

Water sample for determination of total Ni were prepared by acidifying the sample with nitric acid to bring the pH to 2-3, boiling vigorously for 5 min

and filtering the cooled water samples through 0.45 μm filter paper. Blanks were prepared by taking deionized distilled water and processing them in the same way as the samples. The standards were also given similar treatments. A sample of 20 μl was transferred into the GF which was programmed at optimized operating conditions of (i) drying at 100°C for 20 s (ii) charring at 900°C for 30 s (iii) atomizing at 2600°C for 5 s using 'temperature controlled maximum power' (TCMP) mode of heating. One blank cycle was given after every sample atomization. Results were computed from the mean of several readings after compensating for reagent blanks.

Results and discussion—Experimental charring and atomization curves plotted for Ni showed no loss of Ni at the charring stage up to a temperature of 800°C with a standard graphite (SG) tube and up to 900°C with a PCG tube. This compares favourably against the limits of 700°C (ref. 1) and 600°C (ref. 2) of earlier studies. The loss of Ni above the optimum charring temperature occurs due to reduction of nickel oxide by the carbon in the tube followed by evaporation of Ni in purge gas stream. The optimum atomization temperature was found to be greater than 2700°C in case of normal mode of heating with both types of tubes. However, while using TCMP mode of heating it was 2200 and 2500°C with PCG tube and SG tube respectively. In another experiment, the atomization profiles recorded by atomizing the sample at different heating rates showed with the faster heating rates a shift in the initial and the peak pulse to higher temperature. It was also observed that the peak height absorbance increased linearly with the increase in heating rate. The change in heating rate changes the rate of reduction of the analyte oxide and the average residence time of the analyte atoms in the atomizer tube, thereby, produces a shift in appearance temperature and an increase in the peak height absorbance^{3,4}.

In order to assess the effect of anions and cations on the Ni absorbance signal, a solution containing 50 μg Ni/l was spiked with varying amounts of anions and cations and then absorbance signals were recorded for Ni. It was found that significant suppression of the Ni absorbance signal occurred in the presence of Fe and Mg (Table 1). Magnesium imbeds the analyte in a matrix of magnesium oxide, thereby delays the vaporization of the analyte until entire magnesium oxide is vaporized⁵. It is obvious

Table 1—Effect of Mg & Fe on Ni Absorbance Signal

(50 µg/l Ni signal is taken as 100)

Effect of Fe

Effect of Mg

Fe added µg/l	Response %	Mg added µg/ml	Response %
10	66	10	83
20	74	20	75
50	72	50	70
100	70	100	67
200	70	200	70
500	72	500	70

Table 2—Accuracy & Precision of Results for Ni Determination

Ni added µg/l	Ground water		Municipal supply water		Mine water	
	Intrinsic content 4.2 µg/l		Intrinsic content 5.0 µg/l		Intrinsic content 20.0 µg/l	
	Recovery %	RSD %	Recovery %	RSD %	Recovery %	RSD %
5	102	8.2	108	4.2	91	3.3
10	107	7.1	104	6.6	108	3.0
20	99	4.1	99	5.3	101	4.6

that the Ni atomization temperature is suppressed in presence of magnesium.

An examination of the graphite tube, while using a Fe hollow cathode lamp during the atomization cycle showed that Fe was retained in the graphite tube and gave a peak height signal of 0.761 absorbance units. However, subsequent heating of the tube, four times, at 2600°C for 5 s each, brought down the peak height to 0.1 absorbance. Later, it was observed that using atomization temperature of 2600°C and the TCMP mode of heating, Mg interference was eliminated. It was also observed that giving one blank cycle after every sample atomization, helps in removing Fe interference and yields reproducible results. However, the tube loses sensitivity, after 40 to 50 runs, due to fragility of the pyrocoating at the high temperature, and needs replacement. The use of a fast heating rate and high atomization temperature increases the degree of analyte atomization and eliminates matrix interferences.

Determination of Ni in water—The accuracy of the method was determined by spiking Ni at various levels in ground water, mine water and municipal supply water samples. The accuracy which is determined as the percentage recovery was found to vary between 91 and 108% for various spiking concentrations (Table 2). Percentage scatter of replicate analyses showed that the highest relative standard deviation (RSD) for mine water, ground water and municipal supply water was 4.6, 8.2 and 6.6% respectively. The calibration curve of absorbance (*A*) versus Ni concentration (*C*) was linear up to 60 µg/l and the regression equation was ($C = 250.43A - 6.96$). The minimum detection limit was calculated from $\bar{X}_{BI} + 3\sigma_{BI}$, where \bar{X}_{BI} is the mean of blank replicates and σ_{BI} is the standard deviation of blank replicates. Computation of \bar{X}_{BI} and σ_{BI} gave a minimum detection limit of 2 µg Ni/l. The sensitiv-

Table 3—Results of Analysis of Some Water Samples

Sample	Ni concentration µg/l			
	Ground water	Mine water	Municipal supply water	Synthetic water
A	2.0	5	2.0	2.1
B	2.5	20	3.0	3.2
C	1.0	30	2.5	4.2
D	0.9	55	2.4	5.2
E	2.0	60	3.0	10.2
F	1.2	65	0.9	7.6
G	0.5	70	6.4	25.9
H	0.4	20	4.5	16.0
I	0.9	10	4.6	12.3
J	1.5	35	6.4	21.1

ity of the method expressed in concentration of Ni giving absorbance of 0.0044 was 1.1 µg/l (or 0.193 absorbance per nanogram of Ni).

The method was used for the determination of Ni in different water samples and the results of analyses are shown in Table 3. Results of the synthetic samples match with the actual values.

The authors are grateful to Shri K R Bulusu, Acting Director, National Environmental Engineering Research Institute (NEERI), Nagpur, for his permission to publish this paper. They are also thankful to Drs V R Bhawe and K L Saxena, scientists, NEERI, for their encouragement during the study.

References

- 1 Kobayashi T, Yokota P & Ohya K, *Aichi-Ken Kogyo Shidosho Hokoku (Japan)*, **14** (1978) 76; *Chem Abstr (USA)*, **90** (1979) 636.
- 2 Fuller CW, *Anal Chim Acta (Netherlands)*, **62** (1972) 442.
- 3 Salmon S G & Holcombe J A, *Anal Chem (USA)*, **54** (1982) 630.
- 4 Sturgeon R E, Chakrabarti C L & Bertels P C, *Anal Chem (USA)*, **47** (1975) 1250.
- 5 Slavin W, Cameric G R & Manning D C, *Anal Chem (USA)*, **54** (1982) 621.

Charmed Mesons in a Simple Two-Step Potential Model

PURNIMA KHARE & L K SHARMA

Department of Applied Physics, Government Engineering
College, Jabalpur 482 011

Received 24 July 1986; revised received 24 October 1986

The mass spectra and decay widths of Ψ resonances in a simple quark-confining, analytically solvable, two-step potential model to study the charmonium system, have been studied. Results are found to be in good agreement with experiments and also with the values predicted by others.

A number of inter-quark potential models have been suggested and investigated in the spectroscopy of Ψ families¹⁻⁵. Apart from structural details, all these potentials have two broad features in common, which include a coulomb-like singular part and a long range confining part. Many authors such as Eichten *et al.*⁶ and Lichtenberg and Wills⁷ added a coulombian term to their confining potential to account for the short range behaviour. As the superposition of two potentials dilutes the role of the individual potential, the idea of a two-step potential has been proposed for the $q\bar{q}$ interaction. Kaushal⁸ used the two-step potential in which coulombian form is used for short range and a linear form for the long range part.

In this note we have investigated a two-step potential in which the short range form is the same, but for the long range, instead of a linear, an oscillator potential has been considered. In our calculations, Ψ mesons are assumed to be states of a charmed τ quark and its anti-quark, bounded by a phenomenologic potential of the form

$$V_1(r) = \frac{G}{r} + J, \quad r \leq Z \quad \dots (1a)$$

$$V_1(r) = Ar^2 + B, \quad r > Z \quad \dots (1b)$$

where G and A are constants and J and B are matching parameters.

Here Z is the distance at which the forces caused by the coulomb and the oscillator potentials are the same. Physically, Z will be realized as first Bohr radius for the light quark system. At a distance $r = Z$, the formation of an additional $q\bar{q}$ pair takes place out of the original field between q and \bar{q} . This new pair of q and \bar{q} after interaction with the original light quark pair forms the charmed mesons (heavy quarks, Q and \bar{Q}).

In order to calculate the mesonic energy levels we obtain the appropriate wavefunctions and energy eigenvalues

by solving the Schrödinger equation separately for the potentials V_1 and V_2 . Since the charmed quarks are massive particles, they have been treated nonrelativistically. As is well known, the energy eigenvalue expression for the potential V_1 is given by⁹

$$E_{nc} = -\frac{\mu G^2}{2n^2} - J \quad \dots (2)$$

where, μ is the reduced mass.

We argue that the low-lying states of the Ψ system may depend on the coulomb potential (1a), while the higher excitations should depend on the oscillator potential (1b), since the radial separation between the quark-antiquark pair will be larger in this case ($r > Z$). So the binding energies for short ranges $n=1$ and $n=2$ are calculated by Eq. (2).

We have assumed that the two potentials join smoothly at $r = Z$. By equating the potentials (1a) and (1b), and also their first derivatives at $r = Z$, we get the following two relations:

$$\begin{aligned} \frac{G}{Z} + J &= AZ^2 + B \\ Z &= \left(\frac{G}{2A} \right)^{1/3} \end{aligned} \quad \dots (3)$$

Eq. (3) shows the transition from first to the second potential.

Now we consider the potential V_2 and write its well known energy eigenvalue expression⁹

$$E_{nH} = (n + 3/2)\omega + B \quad \dots (4)$$

where, $\omega = (2A/\mu)^{1/2}$. The binding energies corresponding to $n > 2$ are calculated by this expression.

The masses of the charmonium bound states are obtained by $M_n = 2m_c + E_n$ (where m_c is the mass of charmed quark). These masses have been shown in Table 1.

Further, we have calculated the leptonic decay widths of charmed mesons using the standard result

$$\Gamma(\psi \rightarrow e^+ e^-) = \frac{16\pi e_q^2 \alpha^2}{M_n^2} |\psi_n(0)|^2 \quad \dots (5)$$

Here $\alpha = 1/137$ is a fine structure constant, $e_q (\approx 2/3)$ is charge of charmed quark, $|\psi_n(0)|^2$ is the square of the wavefunction at the origin and M_n is the mass of the meson. The values of $\psi_n(0)$ for the coulomb part is ob-

Table 1—Mass(in GeV) of the $c\bar{c}$ Bound States

State	A	B	C
1s	3.096	3.095	3.096
2s	3.686	3.684	3.686
3s	4.160	4.040	4.16
4s	4.415	4.414	4.415

A Present calculations

B Prediction of Kulshreshtha and Kaushal¹²C Available experimental data¹¹

List of constants

$Q=1.303$	$J=0.1785 \text{ GeV}$
$A=0.03 \text{ GeV}^3$	$B=0.436 \text{ GeV}$
$A=2.7 \text{ GeV}^{-1}$	$m_c=1.852 \text{ GeV}$

tained from the standard solution of the Schrödinger equation

$$\psi_{1s}(r) = 2 \left(\frac{G}{a_0} \right)^{3/2} e^{-Gr/a_0}$$

$$\psi_{2s}(r) = \left(\frac{G}{2a_0} \right)^{3/2} \left(2 - \frac{Gr}{a_0} \right) e^{-Gr/a_0}$$

In Eq. (6) G and a_0 are constants.

In the oscillator part, the expression for ψ contains the Laguerre polynomial, the value of which cannot be determined for alternate values of n . Thus we use here the following semi-classical formula derived by Quigg and Rosner¹⁰ for the values of the s -wavefunction at the origin for deriving an explicit expression for the leptonic decay widths:

$$|\psi_n(0)|^2 = \frac{(2\mu)^{3/2}}{4\pi^2} E_n^{1/2} \frac{dE_n}{dn} \quad \dots (7)$$

where E_n is the binding energy of the n th state and dE_n/dn is the derivative of the eigenvalue expression with respect to n .

The decay widths calculated have been listed in Table 2; for comparison, the corresponding experimental results have also been included.

In the present work, the mass spectra and leptonic decay widths of the various $c\bar{c}$ bound states in a two-step potential have been obtained. The results ob-

Table 2—Leptonic Decay Widths $\Gamma(\psi \rightarrow e^+ e^-)$ for the $c\bar{c}$ Bound States (keV)

States	A	B	C
$\psi(3.096)$	25.0	26.1	4.8 ± 0.6
$\psi(3.686)$	2.2	2.3	2.1 ± 0.3
$\psi(4.16)$	0.73	0.57	0.75 ± 0.10
$\psi(4.415)$	0.40	0.20	0.44 ± 0.14

The symbols A, B and C are the same as in Table 1.

tained by us (see Table 1) clearly show that the two-step potential consisting of a combination of the coulomb and oscillator potentials provides a better agreement with the experimental data¹¹ on the masses of the Ψ resonances than the two-step potential used by Kulshreshtha and Kaushal¹². Further, our results for the leptonic decay widths also show better agreement with the experimental values than those obtained by Kulshreshtha and Kaushal¹². Though the results of Eichten *et al.*⁶ are somewhat better than our results for the lower states, for higher states our results are in better agreement with the available experimental data.

The authors are grateful to Prof. Kamal Kumar, Principal, Government Engineering College, Jabalpur, for encouragement.

References

- Greenberg O W, *Phys Rev Lett (USA)*, **13** (1964) 598.
- Joshi G C & Mitra A N, *Hadronic J (USA)*, **1** (1978) 1591.
- Choubey J & Sharma L K, *Indian J Pure & Appl Phys*, **18** (1980) 878.
- Sharma L K & Sharma G S, *Pramāna (India)*, **22** (1984) 539.
- Bhargava A & Sharma L K, *Indian J Pure & Appl Phys*, **22** (1984) 627.
- Eichten E, Gottfried K & Kinoshita T, *et al*, *Phys Rev Lett (USA)*, **34** (1975) 369.
- Lichtenberg D B & Wills J G, *Nuovo Cimento A (Italy)*, **47** (1978) 483.
- Kaushal R S, *Phys Lett B (Netherlands)*, (1975) 354.
- Schiff L I, *Quantum mechanics* (McGraw-Hill, New York) ,1968.
- Quigg C & Rosner J L, *Semiclassical Sum Rules*, Fermilab preprint 77/106 THY (1977) (USA).
- Particle Data Group: Review of Particles Properties, *Rev Mod Phys (USA)*, **56** (No. 2) (Part II) (1984) S10 (by M Aguilar-Benitez, R N Cahn *et al.*)
- Kulshreshtha D S & Kaushal R S, *Phys Rev, D (USA)*, **26** (1982) 2331.

Green's Function Analysis of Vibrations
of Thioformaldehyde

R NAMASIVAYAM

Department of Physics, Annamalai University,
Annamalainagar 608 002

and

K KANNAN

Department of Physics, C N College, Erode 638 004

Received 24 April 1986; revised received 4 August 1986

The Green's function analysis of substituted and perturbed molecules is applied to the study of vibrations of thioformaldehyde. Elegant isotopic rules are formulated for both in-plane and out-of-plane vibrations. The potential energy constants and mean vibrational amplitudes are evaluated. The force constants of the present study display a very good agreement with the literature values.

The availability of isotopic data for thioformaldehyde makes it ideal for the application of the Green's function procedure¹⁻⁴ in fixing its force field. Thioformaldehyde belongs to the C_{2v} point group with six vibrations which are distributed as: $3A_1 + 1B_1 + 2B_2$.

Method of computation—The isotopic rules for different vibrational species for the perturbation $H_2CS \rightarrow D_2CS$ are derived by solving the secular equation:

$$|\varepsilon \omega^2 G(\omega^2) + I| = 0 \quad \dots (1)$$

The normal coordinates giving the reliable solution for the A_1 species are chosen as follows:

$$\begin{aligned} Q_1 &= S_1 \\ Q_2 &= (S_2 + aS_3)/(1 + a^2)^{1/2} \\ Q_3 &= (S_3 - aS_2)/(1 + a^2)^{1/2} \end{aligned} \quad \dots (2)$$

where a is the mixing parameter. The normal coordinates for the B_2 species are:

$$\begin{aligned} Q_5 &= (S_5 + bS_6)/(1 + b^2)^{1/2} \\ Q_6 &= (S_6 - bS_5)/(1 + b^2)^{1/2} \end{aligned} \quad \dots (3)$$

where b is the mixing parameter. There is only one vibrational motion in B_1 species.

$$\text{Hence } Q_4 = S_4 \quad \dots (4)$$

The determinantal Eq. (1) takes the form:

$$\begin{aligned} & \{[\varepsilon \omega^2 G_{22}(\omega^2) + \varepsilon \omega^2 G_{25}(\omega^2) + 1] \\ & \times \{\varepsilon \omega^2 G_{33}(\omega^2) + \varepsilon \omega^2 G_{36}(\omega^2) + 1\} \\ & - \{\varepsilon \omega^2 G_{23}(\omega^2) - \varepsilon \omega^2 G_{26}(\omega^2) + 1\}^2\} = 0 \end{aligned}$$

$$\begin{aligned} & \times \{[\varepsilon \omega^2 G_{22}(\omega^2) + \varepsilon \omega^2 G_{25}(\omega^2) + 1] \\ & \times \{\varepsilon \omega^2 G_{33}(\omega^2) + \varepsilon \omega^2 G_{36}(\omega^2) + 1\} \\ & - \{\varepsilon \omega^2 G_{23}(\omega^2) - \varepsilon \omega^2 G_{26}(\omega^2) \\ & + 1\}^2\} = 0 \end{aligned} \quad \dots (5)$$

for the in-plane vibrations and

$$\{[\varepsilon \omega^2 G_{11}(\omega^2) + 1]^2 - \{\varepsilon \omega^2 G_{14}(\omega^2)\}^2\} = 0 \quad \dots (6)$$

for the out-of-plane vibration. These relations give the frequencies of the isotopically substituted molecule. The mixing parameter matrix A is constructed from the isotopic rules and the force constants are obtained using the procedure outlined in Ref. 3. The mean amplitudes of vibration are calculated following the standard procedure^{5,6}.

Results and discussion—The molecular parameters, the internal symmetry coordinates and the vibrational frequencies are taken from Ref. 7. The elements of the inverse kinetic energy matrix are obtained by the method of Wilson *et al.*⁸

Thioformaldehyde has been the subject of several interesting spectroscopic studies since the first observation of the microwave spectrum by Johnson and Powell⁹. Infrared spectra of H_2CS and D_2CS have been observed in the gas phase by Turner *et al.*⁷

The force field study of H_2CS has been attempted elsewhere^{7,10}. Following Wilson's FG matrix method, the force constants of H_2CS have been computed by Natarajan and Rajalakshmi¹⁰. A general harmonic force field for this molecule has been determined to fit the vibrational wavenumbers, Coriolis constants and centrifugal distortion constants by Turner *et al.*⁷ In the present work, the force constants in symmetry coordinate system are computed directly from the isotopic rules which are derived without employing any force

Table 1—Force Constants of H_2CS (mdyn/Å) in Internal Coordinate System

Force constants	Present work
f_r	4.9279*
f_R	6.7572
f_a	0.3735
f_ϕ	0.3192
f_π	0.1098
f_{rR}	0.2743
$(f_{ra} - f_{r\phi})$	0.0445
$(f_{Ra} - f_{R\phi})$	-0.0922

*The number of significant figures is retained to secure internal consistency in calculations.

Table 2—Mean Amplitudes of Vibration in Å at 298 K

	Present work	Literature
σ_{C-H}	* 0.0778*	0.0760 (Ref. 18) 0.0778 (Ref. 10)
σ_{C-S}	0.0411	0.0389 (Ref. 19) 0.0417 (Ref. 10)
$\sigma_{H...H}$	0.1227	
$\sigma_{H...S}$	0.1008	

*Same as in Table 1

field model. The force constants of H_2CS in internal coordinate system are reported in Table 1. The C—H force constant of the present study ($f_{C-H} = 4.9279$ mdyn/Å) is close to the value reported in literature^{7,10} ($f_{C-H} = 4.961$ mdyn/Å in Ref. 7 and 4.9484 mdyn/Å in Ref. 10). The value of f_{C-S} calculated here is also in agreement with the previously reported values. The values of f_α and f_β are also comparable with the literature values¹⁰. Some of the observations pointed out by the earlier workers in respect of symmetrized force constants F_{13} , F_{23} and F_{12} are also followed here. On the basis of hybrid orbital model, Mills¹¹ pointed out negative value for F_{23} and positive value for F_{13} in order to fit the vibrational frequencies (in the present work $F_{23} = -0.1212$ mdyn and $F_{13} = 0.0410$ mdyn). Further, the positive value of $F_{12} = 0.3879$ mdyn/Å indicates the tendency of the CH_2 group to contract as the CS bond is stretched. It is also interesting to compare the force field of thioformaldehyde with that of formaldehyde obtained elsewhere¹²⁻¹⁷. It is clear that the C—H bond length is shorter and the HCH bond angle larger for H_2CS than for H_2CO . This is accordance with a trend which matches the change in the C—H stretching force constants of these two molecules.

Also the antisymmetric C—D stretching frequency is estimated to be 2248 cm^{-1} with the use of isotopic product rules pertaining to B_2 species. The out-of-plane force constant F_{44} is calculated to be 0.3635 mdyn/Å.

The L matrix constructed through the Green's function formalism is used along with the vibrational frequencies to compute the mean amplitudes of vibration. The mean vibrational amplitudes for both bonded and non-bonded distances at 298 K are given in Table 2. The force constant of C—H bond is smaller than that of C—S bond and hence we find that the mean square amplitude for C—H bond ($\sum_{C-H} = 60.4893 \times 10^{-4} \text{ Å}^2$) is found to be larger

than that ($\sum_{C-S} = 16.8665 \times 10^{-4} \text{ Å}^2$) for C—S bond. The values of mean amplitudes of vibration calculated here ($\sigma_{C-H} = 0.0778 \text{ Å}$ and $\sigma_{C-S} = 0.0411 \text{ Å}$) are in agreement with the experimental values^{18,19} ($\sigma_{C-H} = 0.0760 \text{ Å}$ in Ref. 18 and $\sigma_{C-S} = 0.0389 \text{ Å}$ in Ref. 19). The present values of σ_{C-H} and σ_{C-S} are also close to the calculated values given in literature¹⁰.

It is clear that the Green's function method is well suited for interpretation of force field of polyatomic molecules for which the parent frequencies and the isotopic frequencies are available. The mixing parameter is determined from these observed frequencies. Another advantage of this method lies in the fact that no assumptions are made regarding the force fields and all calculations are solely based on experimental values. The force constants thus obtained give a better physical picture. The most important point here is that the force constants can be generated directly from the frequencies without employing a force constant model.

References

- DeWames R E & Wolfram T, *J Chem Phys (USA)*, **40** (1964) 853.
- DeWames R E, Wolfram T, Bass C D & Lynds L, *J Chem Phys (USA)*, **40** (1964) 3611.
- DeWames R E, Wolfram T, Bass C D & Lynds L, *Bull Chem Soc Jpn (Japan)*, **39** (1966) 201.
- DeWames R E & Wolfram T, *Bull Chem Soc Jpn (Japan)*, **39** (1966) 207.
- Cyvin S J, *Spectrochim Acta (GB)*, **15** (1959) 828.
- Ramaswamy K, Sathianandan K & Cleveland F F, *J Mol Spectrosc (USA)*, **2** (1962) 107.
- Turner P H, Halonen L & Mills I M, *J Mol Spectrosc (USA)*, **88** (1981) 402.
- Wilson E B (Jr), Decius J C & Cross P C, *Molecular vibrations* (McGraw-Hill, New York) 1955.
- Johnson D R & Powell F X, *Science (USA)*, **169** (1970) 679.
- Natarajan A & Rajalakshmi R, *Indian J Phys Part B*, **58** (1984) 439.
- Mills I M, *Spectrochim Acta (GB)*, **19** (1963) 1585.
- Duncan J L & Mallinson P D, *Chem Phys Lett (Netherlands)*, **23** (1973) 597.
- Tanaka Y & Machida K, *J Mol Spectrosc (USA)*, **64** (1977) 429.
- Palaniappan P L R M & Karunanidhi S, *Bull Soc Chim Belg (Belgium)*, **88** (1979) 647.
- Shimanouchi T & Suzuki I, *J Chem Phys (USA)*, **42** (1965) 296.
- Becher H J & Adrian A, *J Mol Struct (Netherlands)*, **7** (1971) 323.
- Ramaswamy K & Chandrasekaran V, *Acta Phys PolA (Poland)*, **51** (1977) 51.
- Bartell L S & Higginbotham H K, *J Chem Phys (USA)*, **42** (1965) 851.
- Cyvin S J, *Molecular vibrations & mean square amplitudes*, (Elsevier, Amsterdam and Oslo) 1968.

Infrared Absorption & Electronic Spectra of 2-Methylmercapto-3-methylpyrazine

S L SRIVASTAVA, M PRASAD* & RANJEET SINGH†

Department of Physics, University of Gorakhpur,
Gorakhpur 273 009

Received 23 January 1986; accepted 30 October 1986

The electronic spectra of 2-methylmercapto-3-methylpyrazine in vapour and liquid states in the region $50000\text{--}28000\text{ cm}^{-1}$, and the infrared absorption spectrum in liquid state in the region $4000\text{--}400\text{ cm}^{-1}$ have been investigated. Various electronic transitions are classified. The infrared bands are interpreted in terms of fundamentals, their combinations and overtones. Modal assignments of the fundamentals are also made.

In pyrazine, usually an $n\text{--}\pi$ and two $\pi\text{--}\pi$ band systems are observed. The $n\text{--}\pi$ band system shows a regular vibrational structure and is of spectroscopic interest due to the involvement of the forbidden vibronic band. Investigations have been made by several research workers on the spectra of pyrazine and substituted pyrazines¹⁻⁸. In the present note, we have studied the spectra of 2-methylmercapto-3-methylpyrazine and concentrated on classifying the various elec-

tronic transitions and to make a vibrational assignment of the infrared bands. In the absence of vapour phase infrared absorption spectra together with Raman shifts, our assignment of infrared bands is tentative and is based on group frequency approach together with the data available for substituted pyrazines.

The electronic spectra have been recorded in vapour phase with a cell of path-length 5 cm and in liquid state with a cell of 1 cm path-length on a CZ UV-VIS double beam spectrophotometer in the region $50000\text{--}28000\text{ cm}^{-1}$. The concentration of the sample in the liquid state has been varied from 10^{-3} to 10^{-6} M. The analysis of bands together with their correlation with those of pyrazine and a few methylsubstituted pyrazines, is presented in Table 1. The accuracy of our measurement for these bands is $\pm 40\text{ cm}^{-1}$. The infrared spectrum in the liquid state in the region $4000\text{--}400\text{ cm}^{-1}$ has been recorded on a CZ specord 75 IR spectrophotometer. The bands are analyzed in terms of various normal modes of the ring and of the functional groups and are presented in Table 2. The accuracy of measurement of these bands is $\pm 7\text{ cm}^{-1}$.

The substitution of the methyl group at position 3 and the methylmercapto group at position 2 in the conventional structure of pyrazine does not provide any plane other than the plane containing all the atoms and hence C_s point group has been ascribed to this molecule. Four band systems are observed but ex-

*Department of Physics, St Andrew's College, Gorakhpur

†Department of Physics, Shivapati Degree College, Shohratgarh, Basti

Table 1—Analysis of the UV Absorption Spectrum of 2-Methylmercapto-3-methylpyrazine in Liquid and Vapour State and its Correlation with Those of Pyrazine and a Few Methyl Substituted Pyrazines

All values are in cm^{-1} .

Molecule	Solvent	$n\text{--}\pi$ system due to non-bonded electron of the nitrogen atom	First $\pi\text{--}\pi$ system	Second $\pi\text{--}\pi$ system	Third $\pi\text{--}\pi$ system	Ref.
Pyrazine	Vapour	30876	37839	50880	60700	7
Pyrazine	Hexane	30500	38400	51500	—	
	Ethyl alcohol	32400	38200	—	—	
	Water	33200	38400	—	—	8
2,5-Dimethylpyrazine	Cyclohexane	31900	36600	—	—	
2-Methylpyrazine	Cyclohexane	31241(320 $m\mu$)	37583	—	—	9
			(266 $m\mu$)			
2-Methylmercapto-3-methylpyrazine	Vapour	36240	33440	41360	43760	Present work
	Dioxane	34000	31600	40320	—	
	Water	34400	31440	40400	44640	
	N/10 Sulphuric acid	—	28720	38160	41760	
	N/10 Sodiumhydroxide	34640	31360	40320	45360	
	Methyl alcohol	34320	31600	40400	44400	
	Chloroform	34240	31520	40080	—	
	Carbon tetrachloride	34080	31760	38880	—	

Table 2—Infrared Absorption Bands of 2-Methylmercapto-3-methylpyrazine in Liquid State and Assignments

(All values are in cm^{-1})

Position of the bands	Assignment	Position of the bands	Assignment
433 (sh) [†]	—	1360 (vs)	CH_3 sym bending
440 (vs)	ν_{16b}	1373 (vs)	CH_2 bending
520 (w)	ν_{6b}	1426 (ms)	ν_{19b}
573 (w)	ν_{6a}	1446 (ms)	CH_3 asym bending
600 (w)	1500-900	1500 (sh)	ν_{19a}
673 (m)	ν_4	1513 (vs)	ν_{8b}
727 (w)	1247-520	1600 (w)	ν_{8a}
747 (w)	$\gamma(\text{C}-\text{H})$	1633 (w)	1073 + 573
866 (vs)	ν_1	1780 (ms)	1100 + 673
900 (w)	1426-520	1900 (ms)	747 + 1147
980 (vs)	$\gamma(\text{C}-\text{H})$	2020 (m)	866 + 1147
1027 (w)	1600-573	2327 (ms)	1147 + 1187
1040 (w)	—	2420 (w)	1073 + 1353
1053 (w)	1500-440	2440 (w)	1073 + 1360
1073 (vs)	ν_{14}	2540 (w)	1187 + 1360
1100 (vvs)	ν_{12}	2620 (w)	1247 + 1373
1147 (ms)	$\beta(\text{C}-\text{H})$	2713 (m)	2 × 1353
1187 (vvs)	$\beta(\text{C}-\text{H})$	2846 (w)	—
1213 (w)	—	2920 (vs)	
1247 (w)	$\nu(\text{C}-\text{CH}_3)$	2940 (vs)	$\nu(\text{C}-\text{H})$ aliph
1313 (m)	$\beta(\text{CH}_2\text{SH})$	2980 (ms)	
1353 (vs)	CH_2 bending	3040 (s)	$\nu(\text{C}-\text{H})$
3100 (w)	$\nu(\text{C}-\text{H})$		
3440 (s)*	$\nu(\text{N}-\text{H})?$		

[†]The relative intensity is shown in parentheses as follows: sh, shoulder; s, strong; vs, very strong; m, medium; w, weak; v, stretching; β , in-plane bending; γ , out-of-plane bending

*Obtained at higher concentration

cept for a broad envelope none of them shows any structure. All the three π - π transitions show a red shift whereas the n - π system shows a blue shift with respect to the spectra of pyrazine (Table 1). This result is in accordance with the general observation for similar molecules. Also, the n - π transition is absent in *N*/

10 sulphuric acid solvent, as is expected. In the light of the blue shift of n - π system, it has been deciphered that the substituents are acting as electron donors and are stabilizing the ground state more than the excited state.

Nearly all the vibrations as obtained in the infrared spectrum have been assigned and presented in Table 2. Some observations on the ring vibrations are noteworthy. The ν_1 and ν_6 modes, which are the ring stretching and bending modes respectively, have been found to be mass dependent by Simmons *et al.*³ On the basis of the observations available for similar molecules, the ν_1 mode has been assigned at 866 cm^{-1} and 520 and 573 cm^{-1} have been taken as the components of the ν_6 mode. The other ring vibrations which are not very sensitive to mass are ν_4 , ν_{12} , ν_{14} , ν_8 and ν_{19} . These are assigned on the basis of the data available for pyrazine and substituted pyrazines and are included in Table 2.

References

- 1 Thakur S N & Innes K K, *J Mol Spectrosc (USA)*, **52** (1974) 130.
- 2 Upadhyaya P C, Rai D K, Upadhyaya K N & Mishra P C, *Indian J Phys*, **46** (1972) 306.
- 3 Simmons J D, Innes K K & Begun G M, *J Mol Spectrosc (USA)*, **14** (1964) 490.
- 4 Sanyal N K, Srivastava S L, Devi A & Nath T, *J Mol Spectrosc (USA)*, **78** (1979) 335.
- 5 Srivastava S L, Rohitashava & Pande A N, *Indian J Pure & Appl Phys*, **21** (1983) 258.
- 6 Prasad M, *On studies of some heterocyclic molecules using spectroscopic methods*, Ph D Thesis, Gorakhpur University, Gorakhpur, 1984.
- 7 Innes K K, Byrne J P & Ross I G, *J Mol Spectrosc (USA)*, **22** (1967) 137.
- 8 *Electronic absorption spectroscopy in organic chemistry*, 3rd edition, edited by E S Stern and C J Timmons (Edward Arnold, London), 1970, 152.
- 9 *Theory and applications of ultraviolet spectroscopy*, edited by H H Jaffe and M Orchin (John Wiley & Sons, New York), 1965, 379.

Ultrasonic Investigation of Molecular Interactions in Binary Liquid Mixtures

S N GOUR*, J S TOMAR* & R P VARMA†

D A V College, Muzaffarnagar 251 001

Received 1 January 1986; accepted 7 October 1986

Molecular interactions in binary liquid mixtures: 1-butanol + benzene, 1-butanol + tetrachloromethane, and 1-butanol + acetone, have been studied at different temperatures (35–50°C) by ultrasonic velocity measurements. Adiabatic compressibility, intermolecular free-length and available volume for these systems show positive deviation at all temperatures. This indicates weak interaction between molecules of the components in the mixtures. The nature of variation of the acoustical parameters and their excess values give information about the type of interaction taking place in these binary systems.

Ultrasonic investigations find extensive application in characterizing aspects of the physico-chemical behaviour of liquid mixtures. Considerable work¹⁻⁵ has been reported on the measurement of ultrasonic velocity in binary liquid mixtures to investigate the molecular interaction. In our previous communication⁶, the molecular interactions in binary liquid mixtures have been studied by viscosity measurements. In order to confirm our findings and evaluate several acoustic parameters, the ultrasonic studies have been carried out. The present note deals with the study of adiabatic compressibility, intermolecular free-length and available volume for three binary systems: 1-butanol + benzene, 1-butanol + tetrachloromethane and 1-butanol + acetone at different temperatures (35–50°C).

Experimental details—Merck or B.D.H. reagent grade liquids were purified by standard methods⁷ and their boiling points were found: 1-butanol, 116–117°C, benzene, 80°C, tetrachloromethane, 76.5°C and acetone, 56°C. Mixtures of known composition were prepared by volume taking precautions as far as possible to keep the solutions out of contact with atmosphere.

The densities were measured at constant temperature ($\pm 0.005^\circ\text{C}$) with a dilatometer constructed of pyrex glass having a reservoir volume of 15 ml. The measuring section was constructed of precisely bored graduated capillary. The uncertainty in density measurement is $\pm 10^{-4} \text{ g ml}^{-1}$.

Ultrasonic velocity in samples was measured with the help of a single-crystal ultrasonic interferometer

(Mittal Enterprises, New Delhi) working at a fixed frequency of 2 MHz. Water maintained at the desired temperature and controlled up to $\pm 0.05^\circ\text{C}$ by a thermostat was passed through the jacket of the cell before the measurement was actually made. The measured velocities have an uncertainty of $\pm 0.5 \text{ m s}^{-1}$.

Theoretical aspects—From the measured velocity the adiabatic compressibility (β_{ad}) of a solution is determined by using the relation

$$\beta_{\text{ad}} = \frac{1}{U^2 \rho} \quad \dots (1)$$

where U is the ultrasonic velocity in the medium of density ρ .

Intermolecular free-length (L_t) has been calculated by using semi-empirical relation given by Jacobson⁸:

$$L_t = \left(\frac{\beta_{\text{ad}}}{K} \right)^{1/2} \quad \dots (2)$$

where K is a temperature-dependent constant.

Molar volume (V) has been calculated from the equation:

$$V = M/\rho \quad \dots (3)$$

where $M = X_1 M_1 + (1 - X_1) M_2$; X being the mole fraction, M the molecular weight and suffixes 1 and 2 stand for the first and second components respectively.

Available volume (V_a) has been obtained by the following equation⁹:

$$V_a = V \left(1 - \frac{U_t}{U_0} \right) \quad \dots (4)$$

where V is the molar volume and U_t and U_0 are the sound velocities at temperature t and 0°C respectively.

Molar sound velocity (R) has been calculated as:

$$R = \frac{M}{\rho} U^{1/3} \quad \dots (5)$$

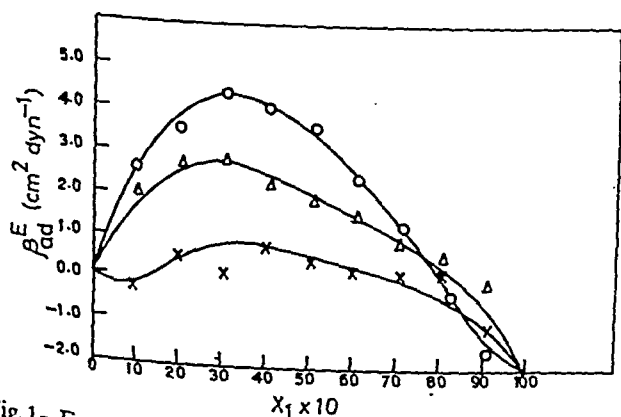
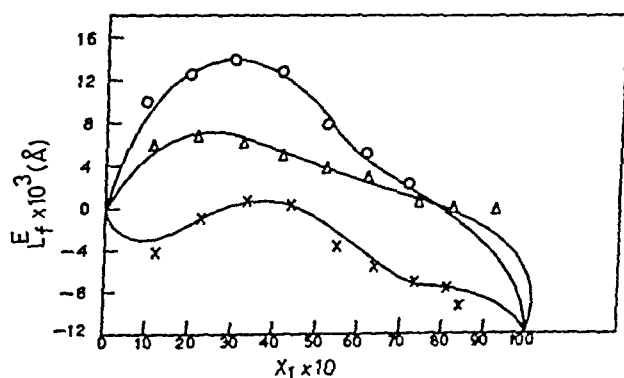
Results and discussion—Values of U and allied parameters for the systems: 1-butanol + tetrachloromethane, 1-butanol + benzene and 1-butanol + acetone have been given in Table 1. U increases with increase in mole fraction of benzene whereas it decreases with the increase in mole fraction of tetrachloromethane and acetone. This indicates that the interaction is not similar in all the cases. The ultrasonic velocity varies nonlinearly with concentration in each system at different temperatures. In each system the velocity at any con-

*Department of Physics

†Department of Chemistry

Table 1—Ultrasonic Velocity and Allied Parameters in Binary Liquid Systems at 35°C

Mole fraction of 1-butanol	ρ (g ml ⁻¹)	U (m s ⁻¹)	$\beta_{ad} \times 10^{12}$ (cm ² dyn ⁻¹)	L_f (Å)	V (ml mol ⁻¹)	V_a (ml mol ⁻¹)	R cm ³ mol ⁻¹ (cm s ⁻¹) ^{1/3}
1-Butanol + tetrachloromethane							
0.000	1.5680	881	80.33	0.4192	90.0	32.0	4365
0.1042	1.48058	891	86.64	0.4337	98.3	32.7	4390
0.2075	1.4058	907	86.51	0.4343	97.8	31.2	4392
0.3098	1.3327	932	86.38	0.4350	96.9	29.3	4393
0.4111	1.2565	958	86.64	0.4347	96.3	27.2	4408
0.5111	1.1844	990	86.21	0.4343	95.4	24.7	4413
0.6110	1.1143	1024	85.65	0.4329	94.3	22.0	4414
0.7096	1.0439	1060	85.26	0.4319	93.2	19.2	4417
0.8073	0.9669	1106	84.54	0.4301	92.5	15.9	4442
0.9049	0.8951	1156	83.60	0.4276	91.2	12.2	4443
1.0000	0.8970	1206	86.00	0.4337	92.8	9.0	4584
1-Butanol + benzene							
0.000	0.8635	1247	74.44	0.4036	90.5	6.0	4519
0.0969	0.8552	1228	77.54	0.4124	90.9	7.3	4517
0.1945	0.8472	1221	79.20	0.4165	91.3	8.8	4528
0.2927	0.8413	1218	80.12	0.4186	91.4	8.0	4533
0.3916	0.8344	1214	81.24	0.4216	91.7	8.3	4542
0.4923	0.8286	1211	82.29	0.4243	91.9	8.5	4546
0.5916	0.8229	1208	83.27	0.4268	92.0	8.8	4550
0.6926	0.8159	1205	84.43	0.4298	92.3	9.0	4561
0.7944	0.8093	1201	85.58	0.4327	92.6	9.3	4568
0.8977	0.8055	1187	88.32	0.4395	92.7	10.3	4515
1.0000	0.8970	1206	86.00	0.4337	92.8	9.0	4584
1-Butanol + acetone							
0.000	0.7736	1112	104.61	0.4784	75.1	12.6	3611
0.0817	0.7752	1118	103.39	0.4756	76.6	12.4	3690
0.1668	0.7791	1130	100.95	0.4699	78.0	12.0	3771
0.2556	0.7799	1136	99.77	0.4672	79.7	11.9	3860
0.3481	0.7823	1141	98.71	0.4647	81.4	11.8	3948
0.4451	0.7867	1153	96.24	0.4588	82.9	11.3	4035
0.5458	0.7882	1162	94.72	0.4552	84.8	11.0	4138
0.6515	0.7913	1174	92.76	0.4505	86.6	10.4	4240
0.7622	0.7922	1185	90.74	0.4455	88.7	10.0	4359
0.8793	0.7945	1194	89.21	0.4418	90.8	9.6	4474
1.0000	0.8970	1206	86.00	0.4337	92.8	9.0	4584

Fig. 1—Excess adiabatic compressibility (β_{ad}^E) vs mole fraction of 1-butanol (X_1) in system: 1-butanol + tetrachloromethane (O—O), 1-butanol + benzene (Δ — Δ), 1-butanol + acetone (x—x) at 35°CFig. 2—Excess intermolecular free-length (L_f^E) vs mole fraction of 1-butanol (X_1) in system: 1-butanol + tetrachloromethane (O—O), 1-butanol + benzene (Δ — Δ), 1-butanol + acetone (x—x) at 35°C

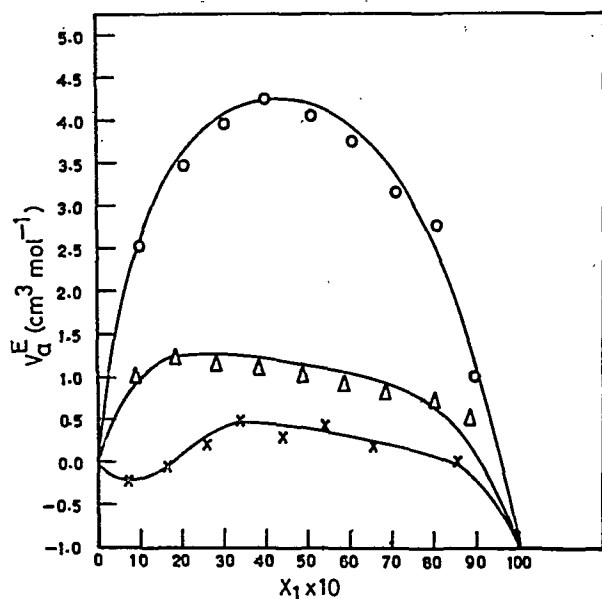


Fig. 3—Excess molar volume (V_a^E) vs mole fraction of 1-butanol (X_1) in system: 1-butanol + tetrachloromethane (O—O), 1-butanol + benzene (Δ — Δ), 1-butanol + acetone (x—x) at 35°C

centration is found to decrease with increasing temperature.

Values of β_{ad} are also shown in Table 1. At any particular concentration, the values of β_{ad} are found to increase with increasing temperature. The plots of β_{ad} vs X_1 show a change in slope at mole fractions 0.404, 0.40 and 0.70, in tetrachloromethane, acetone and benzene respectively.

The decreasing V_a values (Table 1) point to a closer packing of the molecules brought about by association interaction between them or due to inert molecules filling up interstitial position when the polar molecules associate to form a large molecule¹⁰. Therefore L_f decreases with increase in 1-butanol in the mixture and R increases. However, in case of 1-butanol + benzene mixtures the behaviour is otherwise (Table 1).

The excess properties such as β^E , L_f^E and V_a^E have been calculated and are plotted against mole fraction of 1-butanol in Figs 1-3. In each system the excess properties show a maximum at an intermediate concentration and the excess properties are found to decrease with increasing temperature.

Positive values in excess properties correspond mainly to the existence of dispersion forces¹¹, and a positive value tending towards a negative one shows that the strength of interaction increases. In case of 1-butanol + tetrachloromethane, the positive values tend to a negative value showing the strong interaction between the unlike molecules. The interaction strength in the system of 1-butanol + tetrachloromethane is greater than that in 1-butanol + acetone and 1-butanol + benzene. In conclusion, the present study corroborates the inferences of our earlier work⁶.

The authors are thankful to the College authorities for providing laboratory facilities. One of the authors (J.S.T.) is grateful to the University Grants Commission, New Delhi, for financial assistance.

References

- 1 Pandey P, Prakash O & Prakash S, *J Pure & Appl Ultrasonics (India)*, **4** (1982) 12.
- 2 Kiyohara O & Benson G C, *J Chem Thermodyn (GB)*, **11** (1979) 861.
- 3 Pandey J D & Mishra R L, *Acustica (Germany)*, **40** (1978) 335.
- 4 Kaulgud M V, Pandya G H & Rao K S H, *Indian J Pure & Appl Phys*, **16** (1978) 95.
- 5 Choudhary N V, Rama Murthy M, Shastry G S & Naidu P R, *Indian J Pure & Appl Phys*, **16** (1978) 459.
- 6 Varma R P, Gour S N & Tomar J S, *Z Phys Chem (Germany) (Leipzig)*, **263** (1982) 628.
- 7 Vogel A I, *A text book of practical organic chemistry* (ELBS and Longmans Group Ltd, London) 3rd Edn, 1968, 170-176.
- 8 Jacobson B, *Acta Chem Scand*, **6** (1952) 1485.
- 9 Schaffs W, *Z Phys (Germany)*, **114** (1939) 110; **115** (1940) 59.
- 10 Subba Rao & Gopal Krishnan R, *J Acoust Soc India*, **7** (1979) 5.
- 11 Forte R J & Moore W R, *Trans Faraday Soc (GB)*, **61** (1965) 2102.

A Study on Thallium Sulphide Films

G D TALELE

Department of Physics, South Gujarat University, Surat
395 007

&

A GOSWAMI

National Chemical Laboratory, Pune 411 008

Received 3 January 1986; revised received 8 July 1986

Vacuum deposited Ti_2S films when formed on different faces of rocksalt crystals grew epitaxially developing $2-d\{00.1\}$ orientation without any phase change and retaining the bulk structure (rhombohedral, hexagonal; $a = 12.20 \text{ \AA}$, $c = 18.20 \text{ \AA}$). It is concluded that Ti_2S is a stable compound and does not undergo any dissociation during vacuum deposition.

Tallium sulphide films have attracted considerable attention because of their interesting semiconducting, photoconducting^{1,2}, photovoltaic³, lasing and other properties. A literature survey showed that no study has yet been made on the nature of vacuum-deposited thallium sulphide films. Since many sulphide films such as tin sulphide⁴, nickel sulphide and indium sulphide films⁵ showed phase changes during vacuum deposition, an investigation has been made on thallium sulphide films formed on single crystal substrates at different substrate temperatures (t_s), to find out if any such change occurs on thallium sulphide films also.

Experimental procedure—Bulk thallium sulphide was prepared by passing H_2S gas through a solution of thallos nitrate (BDH) acidified with acetic acid. Blackish precipitates thus formed were then washed several times with distilled water, dried in vacuum and then pressed to form pellets which were evaporated in vacuum (10^{-5} mm of Hg) from tungsten basket type of filaments (pre-flashed) at different temperatures. The substrates used were (100), (110) and (111) faces of rocksalt, cleavage faces of mica and also polycrystalline sodium chloride tablets as well as amorphous glass pieces. The deposited films were then examined by electron diffraction method by reflection and transmission, as the case may be.

Results—Vacuum-deposited films formed on polycrystalline sodium chloride tablet at room temperature led to the formation of highly oriented sulphide films as can be judged from the diffraction patterns. The patterns shown in Figs 1 and 2, were obtained re-

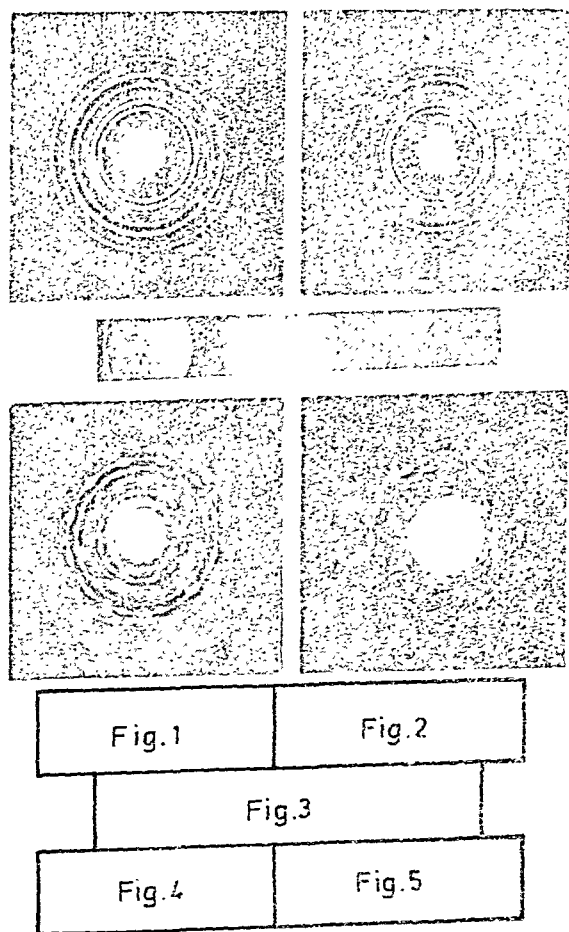


Fig. 1—Electron diffraction pattern of highly oriented polycrystalline deposits of Ti_2S (normal incident beam)

Fig. 2—Diffraction pattern similar to Fig. 1 for an oblique beam ($\approx 30^\circ$)

Fig. 3—X-ray diffraction pattern of Ti_2S powder

Fig. 4—Diffraction patterns revealing $2-d\{00.1\}$ orientations of Ti_2S (the crystallites rotated by 30°) formed on NaCl (100) face at 200°C

Fig. 5—Diffraction patterns revealing $2-d\{00.1\}$ orientation of Ti_2S , formed on NaCl (110) and (111) faces

spectively by normal and oblique (by 30°) incidences of an electron beam. The d -values (Table 1) correspond exactly with those of Ti_2S films obtained from X-ray data (ASTM card No. 6-0378). The bulk powder examined by X-ray diffraction powder method (Fig. 3) also revealed that it has a rhombohedral structure (hexagonal $a = 12.20 \text{ \AA}$, $c = 18.20 \text{ \AA}$) corresponding to thallium sulphide (Ti_2S) compound. A slight variation of intensity of reflections in the X-ray and electron diffraction patterns was noticed which was no doubt due to the formation of highly oriented Ti_2S films.

Deposits formed on the cleavage faces of rocksalt

*Present address: Post Graduate Department of Physics, M.J. College, Jalgaon 425 002

Table 1—Analysis of Electron Diffraction Pattern (Fig. 1)

I/I_0	$d(\text{\AA})$	$(hk.l)$
w	6.04	11.0
s	3.52	30.0
s	3.05	22.0,00.6,30.3
w	2.75	22.3
vw	2.60	40.0
vw	2.39	32.1,21.6
m	2.28	30.6
vw	2.16	10.8
vs	2.02	33.0
vw	1.76	60.0
m	1.68	33.6
vw	1.61	33.8
vw	1.52	44.0,60.6
w	1.47	44.3

Hexagonal; $a = 12.20 \text{\AA}$; $c = 18.21 \text{\AA}$; $c/a = 1.49$

w weak, m medium, s strong, and v very

became epitaxial at temperatures as low as about 100°C and a better crystallinity was obtained at higher t_s from films formed at $t_s = 200^\circ\text{C}$, suggesting that the deposits developed $2\text{-}d\{00.1\}$ orientations of the Ti_2S films, with the crystallites being rotated by 30° (Fig. 4). Films formed both on (110) and (111) faces of rocksalt also developed $2\text{-}d\{00.1\}$ orientations (Fig. 5), but the crystallites did not show any azimuthal rotation, unlike those formed on (100) faces. On mica, as well as on glass substrate, the deposits mostly developed a preferred $1\text{-}d\{00.1\}$ orientation, often mixed with other $1\text{-}d$ oriented crystallites, such as $\{10.0\}$, $\{10.1\}$ and $\{10.2\}$.

Discussion— Ti-S system forms two well-known compounds, viz. Ti_2S (rhombohedral, hexagonal; $a = 12.20 \text{\AA}$, $c = 18.20 \text{\AA}$ and $c/a = 1.49$) and TiS (tetragonal; $a = 7.79 \text{\AA}$, $c = 6.80 \text{\AA}$ and $c/a = 0.88$), though the formations of other sulphides such as Ti_4S_3 , Ti_3S_2 , Ti_8S_7 , Ti_7S_{13} and TiS_2 have also been reported⁶. It is interesting to note that the deposits formed at various substrate temperatures retained the bulk structures without undergoing any phase change unlike those of In-S , Ni-S ⁵ and S_xS films⁴. Earlier, Barua and Goswami⁷ have observed that thallos selenide and thallos telluride also retain the bulk structures. The present study thus shows that Ti_2S is a stable compound and does not undergo any dissociation during vacuum deposition. Further, these deposits also become crystalline, even when formed at room temperature, and have a low epitaxial temperature, presumably due to the low melting point of Ti_2S compound (m.p. 443°C).

References

- 1 Hippel A V, Chesley F C, Denmark H S, Ulin P B & Rittnar E S, *J Chem Phys (USA)*, **14** (1946) 355.
- 2 Ostrowaki J W & Sosnowaki L, *Bull Acad Polon Sci Classe (Poland)*, **3** (No 2) (1954) 382.
- 3 Nix F C & Treptow A W, *J Opt Soc Am (USA)*, **29** (1939) 457.
- 4 Badachhappe S B & Goswami A, *Indian J Pure & Appl Phys*, **2** (1964) 250.
- 5 Goswami A & Talele G D, *Indian J Pure & Appl Phys*, **14** (1976) 262, 716.
- 6 Hansen P M, *Constitution of binary alloys* (McGraw-Hill Book Co, New York) 1958, 1168.
- 7 Barua K C & Goswami A, *Surface Sci (USA)*, **14** (1969) 415.

Correlation of Dielectric Relaxation Time & NMR Spin-lattice Relaxation Time of Some Substituted Glycol Methylethers

N K MEHROTRA

Physics Department, University of Lucknow,
Lucknow 226 007

Received 4 April 1986; revised received 27 October 1986

Experimental measurements of dielectric relaxation time (τ) of some substituted glycol methylethers are reported. The experimental values of nuclear spin-lattice relaxation time (T_1) found in the literature have been correlated with the calculated values of NMR spin-lattice relaxation time obtained using various equations for calculating the dielectric relaxation time. The calculated values of τ and T_1 obtained by Murty's equation are in better agreement with the experimental values. Therefore, it has been concluded that the Murty's equation is a better representation of the dielectric relaxation phenomenon.

Structural studies of the organic compounds using dielectric relaxation mechanism and nuclear magnetic resonance have long been a subject of interest. Bloembergen, and Purcell and Pound¹ (hereafter abbreviated as BPP) have derived an expression for the nuclear magnetic relaxation which is closely related to Doby's² theory of dielectric dispersion in polar liquids. Many workers have calculated nuclear spin-lattice relaxation time from BPP theory and found that the calculated values T_1 were ranging from 1/2 to 1/10 of the experimental values. In the present note the author has modified BPP equation using Murty equation for dielectric relaxation instead of Debye equation as used by BPP.

The spin-lattice relaxation of a single nuclear spin in a liquid is induced by the fluctuating local magnetic

field of neighbouring spins. If the spin which induces the relaxation is attached to the same molecule as the relaxing spin, the fluctuating field is produced by molecular reorientational motion. The contribution of this mechanism to the overall (T_1) is denoted by (T_1)_{rot}. If the relaxation which occurs when the relaxing spin and spin which induced relaxation are attached to different molecules is denoted by (T_1)_{trans}. Bloembergen *et al.*¹ have calculated the probability of transition induced as discussed in our earlier work³. Later Kubo and Tomita⁴ modified the Debye equation.

The author has calculated correlation time τ_c using Debye equation, Perrin⁵ modification in Debye equation, Writz and Spornol⁶ coworkers equation and Murty⁷ equations. The experimental values of dielectric relaxation time have been determined using the Higasi method⁸ as discussed in the earlier work⁹.

It is observed from Table 1 that the relaxation times of these polymers increase from monomethylene glycol methylether to tetraethylene glycol methylether which is in accordance with the increase in their molecular sizes. Further this may also be interpreted in terms of intramolecular rotation of methoxy group.

Table 1—Dielectric Relaxation Time of the Compounds at 293 K

Compound	τ (in ps) from				
	Exptl	Debye Eq	Perrin Eq	Writz Eq	Murty Eq
Monoethylene glycol methylether	44.6	145.2	52.3	25.4	52.8
Diethylene glycol methylether	69.4	188.6	67.9	33.6	67.2
Triethylene glycol methylether	86.7	242.8	87.4	46.4	88.4
Tetraethylene glycol methylether	105.6	297.7	107.2	61.3	110.9

Table 2—Spin-Lattice Relaxation Time from Various Equations at 293 K

Compound	T_1 (in s) from				
	Exptl (Ref. 11)	Debye Eq	Perrin Eq	Writz Eq	Murty Eq
Monoethylene glycol methylether	6.5	3.8	7.8	11.18	6.9
Diethylene glycol methylether	4.3	2.9	6.6	9.8	4.8
Triethylene glycol methylether	3.8	2.6	5.9	8.6	3.6
Tetraethylene glycol methylether	3.2	2.2	4.8	7.1	8.5

The addition of ethylene glycol groups in the higher polymers hinders the intramolecular rotations suggesting that the freedom of rotation of the methoxy group decreases from mono to tetra polymers, resulting in the observed increase in the relaxation time.

It is apparent from Table 2 that values of spinlattice relaxation time calculated using BPP equation are smaller than the experimental values. Moniz *et al.*¹⁰, also agreed with this view that BPP treatment gives much smaller value of T_1 , but according to them the discrepancy in results is due to the time dependence of rotational angular auto-correlation functions of these molecules; they suggested that this time dependence is dominated by dynamical coherence rather than by frictional forces as used in BPP theory.

When Writz and Perrin modifications are used in calculation for T_1 a better correlation has been obtained. The values of T_1 calculated using Murty equation are in quantitative agreement with the experimental values. Therefore it is concluded that the Murty equation is a better substitute for the correlation time.

However, any discrepancy which still remains between the calculated and experimental values of T_1 can be explained as due to the fact that dielectric re-

laxation equations are valid for dilute solutions whereas the spin-lattice relaxation time has been determined in pure liquid state of these compounds.

The authors are deeply indebted to Prof. V D Gupta, Head of the Physics Department, Lucknow University for his keen interest and kind encouragement throughout the progress of this work.

References

- 1 Bloembergen N, Purcell E M & Pound R V, *Phys Rev(USA)*, **73** (1948) 673.
- 2 Debye P, *Polar molecules* (Blackie & Sons Ltd, London & Catalogue) 1929, p 90.
- 3 Mehrotra N K, Somevansi S K S & Misra S C, *Indian J Phys Part B*, **52** (1978) 1.
- 4 Kubo R & Tomita K, *J Phys Soc Jpn (Japan)*, **9** (1954) 888.
- 5 Perrin F, *J Phys Radium (France)*, **5** (1934) 497.
- 6 Writz K & Spornol A, *Z Naturforsch a (Germany)*, **8** (1953) 522.
- 7 Murty C R K, *Indian J Phys*, **32** (1958) 580.
- 8 Higasi K, *Bull Chem Soc Jpn (Japan)*, **39** (1966) 2156.
- 9 Mehrotra N K, Misra S B L & Somevansi S K S, *Proc Indian Acad Sci*, **89** (1980) 43.
- 10 Moniz W B, Steele W A & Dixon J A, *J Chem Phys(USA)*, **38** (1963) 2418.
- 11 Nagrady T & Bergin A S V, *J Am Chem Soc(USA)*, **111** (1969) 389.

Effect of dc Field & X-ray Irradiation on the Optical Absorption and Thermoluminescence of LiF Single Crystals*

N VEERAAIAH†

Physics Department, Indian Institute of Technology,
Kharagpur 721 302

Received 8 July 1986; revised received 16 October 1986

The optical absorption in the region 200 to 800 nm and thermoluminescence (TL) of LiF single crystals subjected to different dc fields and simultaneously irradiated with X-rays, have been studied. The F-band absorption at 250 nm increases with dc field up to 10.4 kV/cm, beyond which it decreases. The bands at 310 and 380 nm — apparently due to F-aggregate centres — intensify with dc field. TL of X-ray irradiated LiF exhibits three glow peaks at 195, 325 and 352°C. The TL light output in the first peak increases with dc field up to 10.4 kV/cm, beyond which it decreases; however, the TL light output in the last two peaks increases uniformly with dc field. These results are explained on the basis of changes in ion vacancies and F-centre concentrations.

A study of the colour centre phenomena in KCl and some other alkali halide crystals subjected to large ac fields and later irradiated with X-rays—carried out in our laboratory—has yielded considerable insight into the electronic processes in these solids. For example, the ac field-treated samples, on X-ray irradiation, exhibited appreciable increase in the colour centre concentration, particularly in the F-band (compared to the virgin sample) though there was no shift in the F-band peak wavelength. Also the thermoluminescence (TL) light output from the crystal increased considerably, the pattern and the glow peak temperatures remaining unaffected¹⁻³. The dielectric properties of these ac field-treated samples showed an interesting behaviour^{3,4}. However, when these crystals were subjected to dc fields of corresponding values and later irradiated with X-rays, the increase in F-centre concentration and TL light output were much less⁴⁻⁶. Recently, it has been shown that, if the X-ray irradiation is carried out simultaneously while the dc field is being applied to the sample, the F-centre concentration as well as TL light output appreciably increases⁵⁻⁷.

The dielectric properties of LiF crystals as a function of frequency and temperature over moderately wide ranges were studied and reported from this la-

boratory⁸. LiF was earlier considered as a good material for TL dosimetry^{9,10}; its optical absorption and TL were well studied¹¹⁻¹⁶. In this note, we report data of our investigations on the effect of X-ray irradiations on LiF single crystals while they are being subjected to a dc field, and their optical absorption and TL characteristics.

Experimental details—The LiF crystals used in the present study were cleaved from the same chunk and had approximate dimensions $1 \times 1 \times 0.1$ cm³. Aluminium foils were attached to the large area faces for dc field application. The dc source is a stabilized power supply variable between 0 and 2.5 kV. The crystal was subjected to a dc field for 1 hr while the X-ray irradiation was done for $\frac{1}{2}$ hr on either side of the sample. It was ensured that the same face of the crystal carried the same polarity of the dc field.

X-ray irradiation (35 kV, 10 mA) of the sample was done at room temperature ($\approx 30^\circ\text{C}$) keeping the samples 2 cm from the window of Norelco X-ray unit. Optical absorption measurements were carried out with a Beckman spectrophotometer model 26 and the TL light output was recorded on an Esterline-Angus recorder using a conventional thermoluminescence set-up¹⁷. The flow peak temperatures could be measured with an accuracy of 4°C .

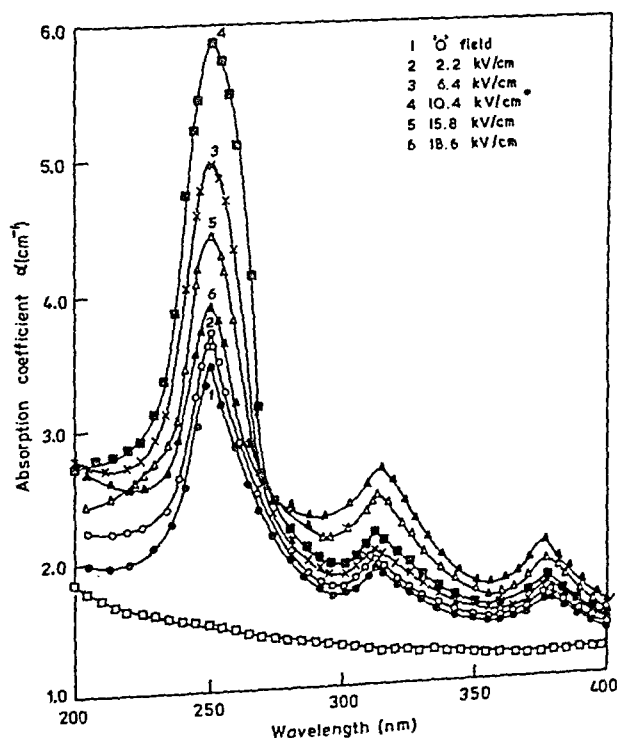


Fig. 1—Optical absorption coefficient (α) as a function of wavelength for LiF single crystals X-ray irradiated for 1 hr (at room temperature) under different dc fields

†Present address: Physics Department, A.P. Residential Degree College, Nagarjunasagar 522 439.

*Forms a part of the Ph D thesis submitted by the author to the Indian Institute of Technology, Kharagpur.

Results and discussion—Fig. 1 presents the optical absorption of LiF in the wavelength region 200–400 nm with X-ray irradiation under different dc fields along with the absorption of the crystals before irradiation. (It may be mentioned here that no absorption bands were observed in these samples beyond 400 nm; hence data were presented up to this wavelength only.) We observed three absorption bands with peaks at 250, 310 and 380 nm. It is seen from Fig. 1 that the absorption at the 250 nm increases with dc field up to a value of 10.4 kV/cm beyond which it decreases; the absorption at 310 and 380 nm goes on increasing with dc field.

The TL curves for samples X-ray irradiated under different fields are shown in Fig. 2. The virgin crystal exhibits glow peaks at 195, 325 and 352°C. The TL light output in the glow peak at 195°C increases with field up to 10.4 kV/cm and decreases beyond it. However, in the other two glow peaks at 325 and 352°C, the TL light output increases with dc field.

The absorption band at 250 nm in X-ray irradiated LiF is identified as the F-band. Earlier, the colour centres responsible for bands at 310 and 380 nm were reported^{11,12} to be the R_1 (an F-centre with a negative ion vacancy) and R_2 (an F-centre coupled with a pair of vacancies—positive and negative vacancy pair) centres respectively. However, recent work shows that the centres responsible for such absorption bands as these may be aggregate F-centres like F_3 centres which are composed of three nearest neighbour F-centres aligned along $\langle 100 \rangle$.^{18,19} Yet, other

reports^{20–22} show that these bands are due to the centres associated with Mg ions. But it must be admitted here that it is not possible to know, from the present measurements, the models of the colour centres responsible for the 310 and 380 nm absorption bands.

LiF crystals, in spite of their good quality, contain dislocations. When subjected to the dc field, it is possible that vacancies are generated at the defect regions due to the interaction between the field and the dislocations. Earlier measurements on KCl and NaCl crystals^{5–7} show that this interaction leads to generation of both negative and positive ion vacancies. X-ray irradiation converts these vacancies, along with the initially present vacancies in the crystal, into corresponding colour centres. The absorption bands due to V-centres generally lie below 200 nm⁹; so they could not be studied. The present measurements indicate that the increase in F-centre concentration up to a dc field of 10.4 kV/cm is apparently connected with the negative ion vacancies produced by the field. The present results also seem to indicate that when the F-centre concentration reaches a certain value corresponding to this dc field ($n_F = 7 \times 10^{16}$, calculated using Smakula's equation²³), the formation of F-aggregate centres is preferred more, thus decreasing the F-centre concentration beyond that for 10.4 kV/cm field.

The X-ray irradiated LiF crystals exhibited TL peaks at 195, 325 and 352°C; it was shown¹¹ from partial thermal bleaching experiments that, in these crystals, it was the F-band which was destroyed when the X-ray irradiated LiF crystals were heated to about 200°C. Also we notice that larger the concentration of F-centres destroyed, more is the TL light output. Thus the TL peak at 195°C seems to be connected mainly with the destruction of F-centres. It is interesting to correlate the two observations: (i) that the F-centre concentration decreases in X-ray irradiated LiF crystals under fields larger than 10.4 kV/cm and (ii) that the TL light output in the 195°C TL peak also decreases at these fields. The correlation supports the above mentioned conclusion. The destruction of F-aggregate centres seems to be responsible for the TL peaks at 325 and 352°C.

The study reported in this note has been carried out on LiF crystals from different sources (laboratory grown as well as commercially available), and the behaviour is found to be reproducible.

Further study is in progress now, on different aspects of colour centre phenomena, and dielectric measurements on these crystals are being carried out. It is expected that data collected will throw more light on the nature of defects, the mechanisms of their formation, etc. in these crystals when subjected to different treatments.

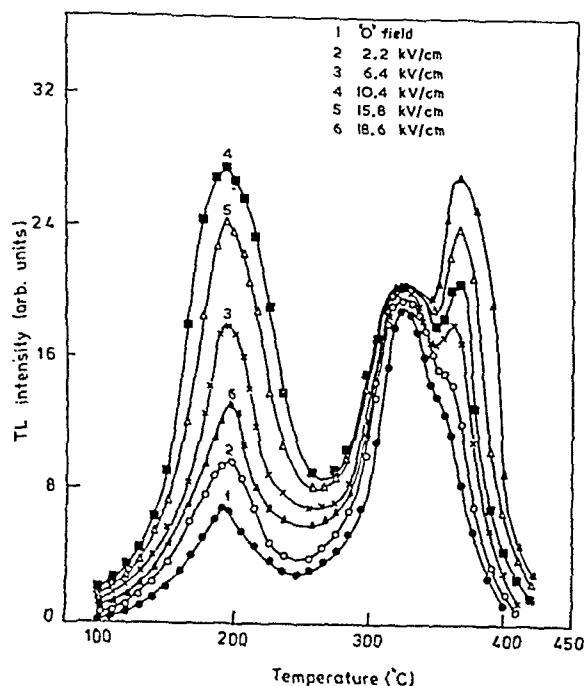


Fig. 2—Thermoluminescence curves for LiF crystals X-ray irradiated for 1 hr (at room temperature) under different dc fields

The author is deeply indebted to Prof K V Rao and Dr H B Gon for kindly suggesting the problem and for their guidance. He also wishes to thank Sri Y V Reddy, Principal, A P Residential Degree College, Nagarjunasagar, for his encouragement and interest in this study.

References

- 1 Govinda S & Rao K V, *Solid St Commun (USA)*, **16** (1975), 297.
- 2 Govinda S, *J Phys C (GB)*, **7** (1974), 1374.
- 3 Govinda S, *Effect of ac field and later X-ray irradiation on optical and dielectric properties of NaCl, KCl and TGS single crystals*, Ph D Dissertation, Indian Institute of Technology, Kharagpur, 1975.
- 4 Govinda S, *Physica (Netherlands)*, **192** (1975), 79B.
- 5 Subrahmanyam A & Rao K V, *Phys Status Solidi a (Germany)*, **52** (1979), K147.
- 6 Subrahmanyam A, *Effect of dc field and X-ray irradiation on optical absorption, thermoluminescence and dielectric properties of NaCl and KCl single crystals*, Ph D Dissertation, Indian Institute of Technology, Kharagpur, 1979.
- 7 Subrahmanyam A & Rao K V, *Indian J Pure & Appl Phys*, **17** (1979), 469.
- 8 Gon H B & Veeraiah N, *J Mater Sci (GB)*, **16** (1981), 2574.
- 9 Daniels F, *Science (GB)*, **343** (1953) 117.
- 10 Schulman J H & Compton W D, *Colour centres in solids* (Pergamon Press, London), 1963.
- 11 Rao K V & Sharma J, *Physica (Netherlands)*, **28** (1962) 653.
- 12 Kadelin K M, *Inorg Mater (USA)*, **10** (1974), 1261.
- 13 Cameron J R, *Proc Lum Conf (Tennessee)*, 1961.
- 14 Cameron J R, *Science (GB)*, **134** (1961), 333.
- 15 Cameron J R, *Luminescence dosimetry* (University of Wisconsin Press, Wisconsin, USA), 1968.
- 16 Grant R M & Cameron J R, *J Appl Phys (USA)*, **37** (1966), 3791.
- 17 Bose H N, *Proc Phys Soc B (GB)*, **68** (1955), 249.
- 18 Beamont J H, Harner A L & Hayes W, *J Phys C (GB)*, **5** (1972), 257, 266, 275, 475.
- 19 Gittus J, *Irradiation effects in crystallizing solids* (Applied Science Publishers, London), 1978, 47.
- 20 Christy R W, *J Appl Phys (USA)*, **38** (1967), 2099.
- 21 Radyabov E A & Nepomnyachikh A I, *Phys Status Solidi a (Germany)*, **77** (1981), 68.
- 22 Taylor G C & Lilley E, *J Phys D (GB)*, **15** (1982), 1253.
- 23 Smakula A, *Z Phys (Germany)*, **59** (1930), 603.

Wide-line PMR Study of Intramolecular Motion in Solid *p*-Hydroxybenzoic Acid

A SINGH & R C GUPTA

Department of Physics, University of Lucknow, Lucknow

Received 20 January 1986; revised received 10 June 1986

Wide-line PMR investigation of solid *p*-hydroxybenzoic acid has been made in the temperature range 77-390K at 7.5 MHz. Analysis of the second moment values suggests a rigid and non-rotating state of crystal lattice at 77K. Some protonic oscillations exist up to 265K. Abrupt change of proton second moment at 310K is considered to be suggestive of hindered reorientation of OH and COOH groups.

The present PMR study of *p*-hydroxybenzoic acid, a compound of biological importance^{1,2}, has been carried out in an effort to probe the nature of the crystal lattice at different temperatures, search for the existence of group mobility in solid phase and finally to ascertain the molecular structure.

In the absence of any precise data regarding the position of the hydrogen atom coordinates of *p*-hydroxybenzoic acid, a model of the molecule was made assuming the standard values of the bond distances and angles. The assumed structure is shown in Fig. 1.

The ring group was assumed asymmetrical with bond distance C-C = 1.361 Å and 1.440 Å alternatively, and C-H equal to 1.09 Å. The C-C bond connecting the COOH group was assumed to be 1.502 Å with C=O = 1.20 Å, C-O = 1.379 Å, O-H = 0.944 Å. The C-O bond connecting the -OH group was assumed to be 1.379 Å and $\angle\text{COH} = 105.04^\circ$.

The spectra were recorded at the Tata Institute of Fundamental Research, Bombay, using Varian variable frequency spectrometer³. Flow of heated or cooled nitrogen gas over the sample was regulated for

effecting temperature variations and a V-4340 variable temperature probe was used for controlling temperature. Thermocouples were used for temperature monitoring.

Second moment calculations—The PMR derivative tracings were recorded at the resonance frequency of 7.5 MHz. The values of experimental second moments (S_2) were calculated using the trapezium rule and applying a correction for finite modulation broadening⁴. The experimental value of S_2 of *p*-hydroxybenzoic acid at 77 K was found to be $18.40 \pm 1.0 \text{ G}^2$.

Calculated rigid lattice value of S_2 of the polycrystalline sample consists of two parts: (i) the intramolecular contribution and (ii) the intermolecular contribution. The intramolecular contribution (S_1) to the value of S_2 due to the interaction of the protons of the same molecule was calculated applying Van Vleck's⁵ formula and using Bearden and Watt's⁶ values of physical constants. The formula is of the form:

$$S_1 = \frac{715.9}{N} \sum_{j>k} r_{jk}^{-6} G^2 \quad \dots (1)$$

where N is the number of magnetic nuclei over which the sum is taken and r_{jk} the distance between the j th and k th nuclei. Value of S_1 calculated in the present case using the values of atomic coordinates is 13.51 G^2 , while the intermolecular contribution has been calculated to be 6.1 G^2 employing Andrew and Eades⁷ method. The value seems to be reasonable as compared to 6.8 G^2 , the corresponding value for substituted benzoic acids calculated by Agarwal and Gupta⁸. Thus the calculated value of proton second moment (S_2) comes out to be $13.51 \text{ G}^2 + 6.1 \text{ G}^2 = 19.61 \text{ G}^2$.

Results and Discussion—The variation of S_2 for this compound with temperature is shown in Fig. 2. A fair agreement between the mean experimental value ($18.40 \pm 1.0 \text{ G}^2$) at 77 K and the theoretical rigid lattice second moment (19.61 G^2) exists. This suggests that the lattice is rigid and non-rotating at 77K. The S_2 data are thus consistent with our assumed model of *p*-hydroxybenzoic acid. Since there is no molecular motion at low temperature, the applied steady magnetic field is greatly modified by the local magnetic field of surrounding nuclei; consequently, resonance line is broad and the line width is maximum. This broadening remains roughly constant up to 155K showing that there is no appreciable motion up to this temperature (Fig. 2).

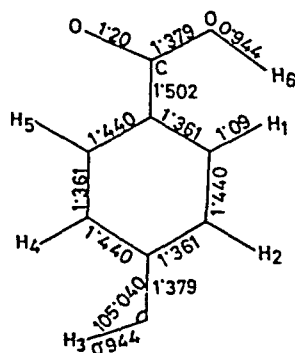


Fig. 1—Molecular model of *p*-hydroxybenzoic acid

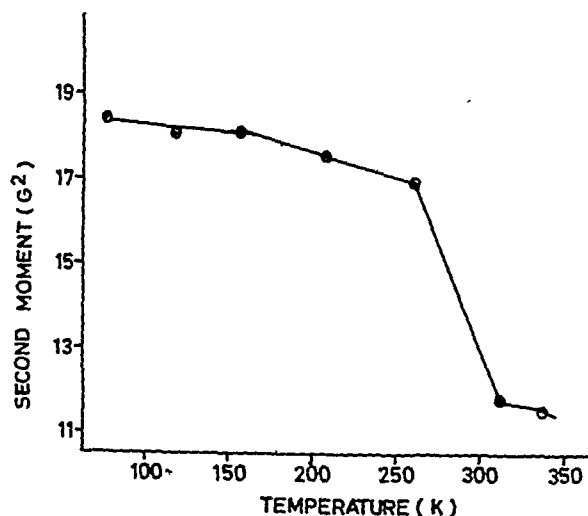


Fig. 2—Variation of second moment with temperature

The value of S_2 gradually decreases up to 265K, which may be due to the torsional oscillations of the hydroxy and carboxylic proton.

The abrupt fall in S_2 value above 265K suggests the onset of intramolecular motion. The possibility of molecular rotation as a whole may safely be ruled out considering the large size, the nature of the substituent, symmetry and intramolecular hydrogen bonding⁹⁻¹¹ of the molecule. The possibilities that present themselves for further investigation are the rotation of the OH and the COOH groups and their influence on each other. The two substituent groups OH and COOH being in *para* position with respect to each other, do not interact as strongly as they do in *ortho* or *meta* compounds, but still the hindrance is being offered by inter- and intragroup bonding.

The reduction in the value of S_1 brought about by group rotation can be calculated according to the theory of Gutowsky and Pake¹². The reduction in S_1 due to reorientation of the OH group about the C—O axis was calculated to be 5.01 G² while that due to the rotation of COOH group about C—C bond was 5.37 G². Therefore, the rotation of both OH and COOH groups reduces the value of S_1 by 10.38 G². Thus the value of S_2 becomes 3.13 G².

The estimation of the intermolecular contribution can be made by making use of reduction factors. Smith¹³ has given a range of reduction factors (0.65-0.50) for stationary-rotating interactions and another (0.42-0.25) for rotating-rotating interactions. If we consider both the OH and COOH to be freely rotating, then using the reduction factors, the intermolecular contribution is found to be in the range 2.56-1.52 G². Thus, the total reduced value of S_2 lies in the range 5.69-4.65 G², which is too low (even lower than the minimum observed S_2) and, as such, rules out the possibility of free and simultaneous rotation of the groups. If the OH group is taken to be stationary and

the COOH group to be rotating, the changed value of S_1 is 8.14 G². The intermolecular contribution is found using the reduction factor for stationary-rotating interactions. The contribution is found to be in the range 3.97-3.05 G². The reduced S_2 is thus found to be in the range 12.11-11.19 G². Similarly value of S_2 assuming the OH group to be rotating and the COOH group to be stationary, is found to be 12.47-11.5 G². Both these values of S_2 (with OH group rotating and COOH group stationary or vice-versa) compare favourably, within the limits of experimental error, with the observed value 11.86 G² at 310K and hence we conclude that both the groups are rotating simultaneously but their rotations are hindered due to the hydrogen bonding between the two groups¹⁴. The deduction regarding hindered reorientation of OH and COOH groups is also supported by the studies of Lehman *et al.*¹⁵ and Saxena *et al.*¹⁶.

The activation energy for the observed transition region was calculated using modified BPP equation (Ref. 17) and its value comes out to be 13.03 kcal/mol. The energy barrier to hindered motion in solids has been calculated by an approximate method given by Waugh and Fedin¹⁸ according to which:

$$E = 37 T_c \text{ (cal/mol)} \quad \dots (2)$$

where T_c is the transition temperature. Value of E calculated to be 11.47 kcal/mol at $T_c = 310\text{K}$ using Eq (2) is in reasonable agreement with the value calculated according to the BPP theory.

The authors express their gratitude to Prof. R Vijayaraghavan (Tata Institute of Fundamental Research, Bombay) for the experimental facilities provided. Thanks are also extended to Prof. K C Lal for encouragement and interest. The authors are thankful to the Univeristy Grants Commission, New Delhi, for financial assistance.

References

- 1 Power F W & Sheruein C P, *Arch Intern Med (USA)*, **39** (1927) 60.
- 2 Mussil J & Smeikal O, *Z Fleisch Milchhyg (Germany)*, **6** (1931) 117.
- 3 Agarwal V D, *Some NMR contributions in molecular solids*, PhD thesis, Lucknow University, Lucknow, 1970.
- 4 Andrew E R, *Phys Rev (USA)*, **91** (1953) 425.
- 5 Van Vleck J M, *Phys Rev (USA)*, **74** (1948) 1168.
- 6 Bearden J A & Walts N M, *Phys Rev B (USA)*, **1** (1951) 73.
- 7 Andrew E R & Eades R G, *Proc Phys Soc London Ser A (GB)*, **66** (1953) 415.
- 8 Agarwal S C & Gupta R C, *Indian J Pure & Appl Phys*, **10** (1972) 602.
- 9 Lutskii A E, Gorclienko V G & Beitis Yu I, *Zh Obshch Khim (USSR)*, **46** (1980) 2235.
- 10 Stephen G & Schulnian, *J Phys Chem (USA)*, **72** (1968) 3297.
- 11 Daeis M & Griffiths D M L, *J Chem Soc (GB)*, **23** (1955) 136.

- 12 Gutowsky H S Pake G E, *J Chem Phys(USA)*, **18** (1950) 162.
- 13 Smith G W, *J Chem Phys(USA)*, **42** (1965) 4229.
- 14 Forbes W F & Knight A R, *Can J Chem(Canada)*, **37** (1959) 335.
- 15 Lehman F, Pedro A & Shiz P E, *Rev Soc Quim Mex(Mexico)*, **13** (1969) 215.
- 16 Saxena M C, Mehrotra M K & Shukla J P, *Curr Sci(India)*, **35** (1966) 120.
- 17 Bloembergen N, Purcell E M & Pound R V, *Phys Rev(USA)* **73** (1948) 679.
- 18 Waugh J S & Fedin F J, *Sov Phys-Solid State(USA)*, **4** (1963) 1633.

SCOPE

The journal welcomes, for publication, full papers and short notes, reporting significant new results of research, in all areas of physics except space physics. The applied fields covered are electronics, electrical engineering, instrumentation and applied mathematics. However, papers in applied mathematics with emphasis on only derivation and proofs and having no direct physical significance, will not be considered. Review articles are not published normally.

SUBMISSION OF MANUSCRIPT

Manuscripts for consideration should be submitted, *in duplicate*, to Editor, Indian Journal of Pure & Applied Physics, Publications & Information Directorate, Hillside Road, New Delhi 110012. They should neither have been already published nor be under consideration elsewhere.

Manuscripts should be in English and typewritten on only one side of good quality paper, in double space, with adequate margin on all four sides. One original and one carbon or photo-copy, each complete in all respects including abstract, illustrations, appendixes, etc. are to be submitted.

PREPARATION OF MANUSCRIPT

Authors may consult recent issues of the Journal to familiarize themselves with the general style and practices adopted in regard to the various elements of a paper.

General

Manuscript should be presented in as concise a form as possible. Good attention should be given to spelling and grammar. In giving names of chemical compounds and structures, abbreviations of units of measurements, symbols and notations, the style and practices recommended by the IUPAP and IUPAC, should be followed.

Frequently repeating combinations of words, e.g. electric field gradient (EFG), junction field effect transistor (JFET), stimulated Raman emission (SRE), should be abbreviated subsequently, indicating the abbreviated form in parenthesis, as shown, at the place of their first occurrence.

Pages should be numbered consecutively and arranged in the following order: Title, authors' names with their institutional affiliations and abstract, along with relevant footnotes whenever necessary (on a separate sheet); introduction; experimental details/theory/method/analysis; results; discussion; conclusion(s); acknowledgement; references and appendixes. Tables, captions for figures (with legends) and appendixes should be typed *on separate sheets* and attached at the end of the manuscript.

Title

The title should be neither too brief/general nor unnecessarily long. It should reflect the content of the paper so as to derive the maximum advantage in indexing. If a paper forms part of a general series, a specific subtitle, indicating the particular aspect of the work covered in the paper, should be provided.

A short running title for the paper, the broad PACS subject heading under which it should be classified in the contents page (authors may consult the January or July issue of the journal for this purpose), and the author's name and address for correspondence, should also be provided on the title page.

Abstract

The abstract, usually not exceeding 200 words, should indicate the scope and significant content of the paper,

highlighting the principal findings and conclusions. It should be in such a form that abstracting periodicals can use it without modification.

Introduction

Long and elaborate introduction should be avoided. It should be brief and state the exact scope of the study in relation to the present status of knowledge in the field. Literature review should be limited strictly to what is necessary to indicate the essential background and the justification for undertaking the study.

Materials, methods, apparatus, etc.

The sources of materials and their purity, methods of preparation, procedure for measurements and their accuracies, etc. should be clearly stated to enable any other worker to repeat the work if necessary. New methods, techniques, theories, etc. should be described in adequate detail; but if they are well known, a mere literature reference to them will do; differences from standard ones, improvements or innovations should, however, be clearly mentioned.

Results

Only such primary data as are essential for understanding the discussion and main conclusions emerging from the study should be included. All secondary data as are of interest to a specific category of readership *should not be included* in the paper. Such data should be retained by the authors for supply, on request, to any interested research worker. A footnote to this effect may be inserted at the relevant place in the paper.

The results must be presented in a coherent sequence in a unified logical structure, avoiding repetition or confusion. Limitations of the results should be clearly stated.

The same data should not be presented in both tabular and graphic forms. Only such tables and figures as are essential should be included. Simple linear plots that can easily be discussed in the text, should not be included. Infrared, ultraviolet, NMR and other spectra, DTA curves, etc. should be included only if they pertain to new compounds and/or are essential to the discussion; otherwise only significant numerical data should be given in the text or in a table.

Discussion

Long rambling discussion should be avoided. The discussion should deal with the interpretation of results without repeating information already presented under results. It should relate new findings to the known and include logical deductions. A separate section on 'conclusions' can be given only when they are well established and of outstanding significance. Mere observation of qualitative trends of results should be distinguished from firm conclusions. Also, limitations, if any, to the conclusions should be clearly pointed out.

Mathematical portions

Special attention should be given to the mathematical portions of the paper. Equations must be well separated from the text and written clearly with good separation between the successive lines. The usual norms of breaking long mathematical expressions should be adhered to. Equations should be numbered consecutively in Arabic numerals with the number in parenthesis near the right hand margin. Superscripts and subscripts should be clearly indicated in pencil by V and A sign respectively. Capital and small letters,

particularly of the same letter when both occur, as well as letters or symbols likely to be confused one for the other, should be clearly distinguished. Special characters (e.g. Greek, script, vector, tensor, etc.) required must be indicated by marginal notes. Letters and symbols which should appear in bold face must be clearly indicated. To simplify typesetting: (i) long and complicated mathematical expressions which are frequently repeated should be replaced with single letter/symbol, without clashing with the others used in the paper; (ii) the "exp" form of complex exponential functions should be used; and (iii) to simplify fractions, the solidus (/) is to be used and fractional exponents are to be used instead of root signs, e.g.

write $\exp\{-i\omega_0(t_1 - t_2)/2\}$ and not $e^{-i\omega_0(t_1 - t_2)/2}$

write $(4\omega_{pl} K_{3\lambda}^2 / \tilde{\omega} K_D^2)^{1/2}$ and not $\sqrt{\frac{4\omega_{pl} K_{3\lambda}^2}{\tilde{\omega} K_D^2}}$

Tables

Tables should be numbered consecutively in Arabic numerals and should bear brief titles. Column headings should be brief. Units of measurement should be abbreviated and placed below the headings. Nil results should be indicated and distinguished clearly from absence of data. Inclusion of structural formulae inside the tables should be avoided as far as possible. Tables should be referred to in the text by numbers and not by terms like 'above', 'below', 'preceding' or 'following'. Results should not be presented to a greater accuracy than that of the method employed.

Illustrations

The number of illustrations should be kept to the minimum. Wherever possible, e.g. a number of individual analogous figures referring to different variables, substances, molecules, etc. may be combined into one composite figure. All illustrations should be numbered consecutively in Arabic numerals. Captions and legends to the figures should be self-explanatory. Line drawings should be made with Indian ink on white drawing paper/cellophane sheet/tracing cloth, and drawn to approximately twice the printed size.

The lettering should be uniform, preferably in stencil, so as to be not less than 1.5 mm after reduction widthwise to full page size (165 mm) or column size (80 mm). The size of geometrical shapes (used to distinguish different graphs), dots, lines, etc. should be sufficiently large to permit the necessary reduction without loss of detail. In the case of photographs, prints must be on glossy paper and contrasty. If an illustration is taken from another publication, reference to the source should be given and prior permission secured. Illustrations should be referred to in the text by numbers and not by terms like 'above', 'following' etc.

Acknowledgement

Acknowledgements should not be exuberant and must be made only to real assistance rendered in connection with the work reported in the paper.

References

References cited should be limited to the absolute minimum (particularly in the case of short notes) based on their essential relevance. In the text, references to literature should be numbered consecutively, in the order of their first occurrence, and should be indicated by superscript Arabic numbers at the relevant places; as far as possible the placement of references on numerals or other symbols should be avoided; in such cases the reference may be given in parenthesis in running text, e.g. "this yielded for n a value of 2.3 (Ref. 5)". Full bibliographic details for all the references mentioned in the text should be listed in serial order at the end of the paper.

In citing references to research papers, names and initials of authors should be followed, in order, by the title of the periodical in the abbreviated form (underlined), the volume number (two lines underneath), the year within circular brackets and the page number [e.g. Chandra B P & Shrivastava KK, *J Phys & Chem Solids (GB)*, 39 (1978) 939]. For names of periodicals, the abbreviations followed by the *Physics Abstracts* should be used. For periodicals not covered by *Physics Abstracts*, the title abbreviations should be according to the *Bibliographic Guide for Editors and Authors*, 1974, published by the American Chemical Society, Washington DC, USA; additionally the country from which the journal is published should be given in parenthesis immediately after the title abbreviation. If a paper has been accepted for publication, the names of the authors and the journal (with volume number and year, if known) should be given followed by the words "in press" [e.g. Wahi P K & Patel N D, *Can J Spectrosc (Canada)*, in press.].

In references containing up to four authors, the names of all the authors with their respective initials should be given. The abbreviations *et al.*, *idem* and *ibid* should be avoided. When there are more than four authors, only the names of the first three authors with their respective initials should be given, followed by the words '*et al.*'

Reference to a book should include details in the following order: name and initials of authors, the title of the book (underlined), name of publisher and place of publication within circular brackets and year and page (s) [e.g. Clayton G B, *Operational amplifiers* (Newnes-Butterworths, London), 4th Edn, 1977, 26]. If the reference is to the work of an author published in a book by a different person, the fact that it is cited from the source book should be clearly indicated [e.g. Turnhout Van J, 'Thermally stimulated discharge of electrets' in *Topics in applied physics*: Vol. 33—*Electrets*, edited by C M Sessler (Springer Verlag, Berlin), 1980, 130].

Proceedings of conferences and symposia should be treated in the same manner as books. Reference to a paper presented at a conference, the proceedings of which are not published, should include, in the following order, names and initials of authors, title of the paper (underlined), name of the conference, and where and when it was held (e.g. Herczeg P, *Symmetry-violating kaon decays*, paper presented to the International Conference on High Energy Physics and Nuclear Structure, Vancouver, Canada, 13-17 August 1979).

Reference to a thesis should include the name of the author, title of the thesis (underlined), university or institution to which it was submitted and year of submission (e.g. Mehrotra S N, *Many-body techniques and their applications to interacting bosons*, Ph D thesis, Ranchi University, 1976).

Reference to a patent should include names of patentees, country of origin (underlined) and patent number, the organization to which the patent has been assigned (within circular brackets), date of acceptance of the patent and reference to an abstracting periodical where available [e.g. Labes M M, *US Pat.* 4,066,567 (to Temple University), 3 January 1978; *Chem. Abstr.*, 88 (No. 20) (1978), 138350 n].

PROOFS & REPRINTS

The edited manuscript will be sent to the author for his final approval before giving it to the press. No galley proofs will be sent to the authors for corrections, since the proofs will be checked at the editorial office. Authors are given 25 free reprints for each paper. Extra reprints can be ordered by the author while returning the edited manuscript. If the reprints order is not received, it will be presumed that no extra reprints are needed.

CSIR SCIENTIFIC PERIODICALS

JOURNAL OF SCIENTIFIC & INDUSTRIAL RESEARCH (Monthly)

With a fine record of over 45 years' service to the scientific community, this journal has grown into India's leading general science periodical. Intended to fulfil the responsibility of helping the research workers to keep themselves abreast of current developments in various fields of science and technology, the journal carries editorial features highlighting important scientific events in India and abroad, articles on science policy and management of science review articles on topics of current research interest, technical reports on international and national conferences, reviews of scientific and technical publications, and notes on major advances in various fields.

Annual subscription	Rs 120.00	\$ 40.00	£ 23.00
Single copy	12.00	4.00	2.30

INDIAN JOURNAL OF CHEMISTRY (Monthly)

Section A: Started in the year 1963, the journal is devoted to papers in Inorganic, Physical, Theoretical and Analytical Chemistry.

Annual subscription	Rs 160.00	\$ 53.00	£ 30.00
Single copy	16.00	5.30	3.00

Section B: This journal is devoted to papers in Organic Chemistry, including Medicinal Chemistry.

Annual subscription	Rs 160.00	\$ 53.00	£ 30.00
Single copy	16.00	5.30	3.00

INDIAN JOURNAL OF PURE & APPLIED PHYSICS (Monthly)

Started in the year 1963, this journal is devoted to original research communications (full papers and short communications) in all conventional branches of physics (except radio and space physics).

Annual subscription	Rs 180.00	\$ 60.00	£ 34.00
Single copy	18.00	6.00	3.40

INDIAN JOURNAL OF RADIO & SPACE PHYSICS (Bimonthly)

The journal, which is being published beginning from March 1972, is intended to serve as a medium for the publication of the growing research output in various areas of radio and space physics, such as ionospheric propagation, magnetosphere, radio and radar astronomy, physics and chemistry of the ionosphere: neutral atmosphere, airglow, winds and motion in the upper atmosphere: stratosphere-mesosphere coupling, ionosphere-magnetosphere coupling, solar-terrestrial relationship, etc.

Annual subscription	Rs 100.00	\$ 34.00	£ 19.00
Single copy	20.00	6.80	3.80

INDIAN JOURNAL OF TECHNOLOGY (INCLUDING ENGINEERING) (Monthly)

This journal publishes papers reporting results of original research of applied nature pertaining to unit operations, heat and mass transfer, products, processes, instruments and appliances, etc. The journal is of special interest to research workers in departments of applied sciences in universities, institutes of higher technology, commodity research laboratories, industrial cooperative research institutes, and industrial research laboratories.

Annual subscription	Rs 120.00	\$ 40.00	£ 23.00
Single copy	12.00	4.00	2.30

INDIAN JOURNAL OF EXPERIMENTAL BIOLOGY (Monthly)

This journal, devoted to the publication of research communications in the fields of experimental botany, zoology,

microbiology, pharmacology, endocrinology, nutrition, etc., is the only one in India with such a wide coverage and scope.

Annual subscription	Rs 180.00	\$ 68.00	£ 34.00
Single copy	18.00	6.80	3.40

INDIAN JOURNAL OF BIOCHEMISTRY & BIOPHYSICS (Bimonthly)

This journal, published in association with the Society of Biological Chemists (India), Bangalore, is the only research journal in India devoted exclusively to original research communications in biochemistry and biophysics.

Annual subscription	Rs 65.00	\$ 23.00	£ 12.00
Single copy	13.00	4.60	2.40

INDIAN JOURNAL OF MARINE SCIENCES (Quarterly)

Commencing publication from June 1972, this journal is devoted to research communications (full papers and short communications) pertaining to various facets of marine research, viz. biological, physical, geological and chemical oceanography.

Annual subscription	Rs 90.00	\$ 30.00	£ 17.00
Single copy	26.00	8.70	5.00

RESEARCH AND INDUSTRY (Quarterly)

Intended to serve as a link between science and industry, this journal is addressed primarily to technologists, engineers, executives and others in industry and trade. It publishes informative original articles containing practical details of processes and products devoted in India, which show promise of ready utilization, and technical digests on new processes, products, instruments and testing methods which are of interest to industry. Developments in Indian industry are regularly reported.

Annual subscription	Rs 70.00	\$ 23.00	£ 13.00
Single copy	22.00	7.00	4.00

INDIAN JOURNAL OF TEXTILE RESEARCH (Quarterly)

Commencing publication from March 1976, this journal is devoted to the publication of papers reporting results of fundamental and applied researches in the field of textiles.

Annual subscription	Rs 50.00	\$ 17.00	£ 10.00
Single copy	15.00	5.00	3.00

MEDICINAL & AROMATIC PLANTS ABSTRACTS (Bimonthly)

Carries informative abstracts of scientific papers published in important Indian and foreign journals relating to different aspects of medicinal and aromatic plants. Each issue contains about 350 abstracts with a subject index.

Annual subscription	Rs 120.00	\$ 40.00	£ 23.00
Single copy	24.00	8.00	4.60

CURRENT LITERATURE ON SCIENCE OF SCIENCE (Monthly)

Carries abstracts, digests, book reviews, news & notes and R&D statistics with emphasis on problems of S&T in developing countries, it also covers the areas of science policy, R&D planning and management, technology transfer, technology assessment and science and society.

Annual subscription	Rs 100.00	\$ 30.00	£ 12.00
---------------------	-----------	----------	---------

Please contact

SALES AND DISTRIBUTION OFFICER
PUBLICATIONS & INFORMATION
DIRECTORATE, CSIR
Hillside Road, New Delhi-110012

CSIR PUBLICATIONS

WEALTH OF INDIA

An encyclopaedia of the economic products and industrial resources of India issued in two series

RAW MATERIALS SERIES—contains articles on plant, animal and mineral resources

	Rs	₹	£
Vol. I (A-B)	80.00	30.00	13.00
Vol. II (C)	95.00	33.00	17.00
Vol. III (D-E)	105.00	32.00	20.00
Vol. IV (F-G)	65.00	27.00	12.00
Supplement (Fish & Fisheries)	56.00	16.00	10.50
Vol. V (H-K)	114.00	34.00	21.00
Vol. VI (L-M)	90.00	34.00	15.00
Supplement (Livestock)	102.00	34.00	19.50
Vol. VII (N-Pe)	100.00	30.00	19.00
Vol. VIII (Ph-Re)	86.00	32.00	14.00
Vol. IX (Rh-So)	104.00	35.00	19.00
Vol. X (Sp-W)	225.00	75.00	42.50
Vol. XI (X-Z)	115.00	38.50	22.00

INDUSTRIAL PRODUCTS SERIES—

deals with major, small-scale and cottage industries

Part I (A-B)	58.00	20.00	11.00
Part II (C)	74.00	24.00	14.00
Part III (D-E)	100.00	33.50	19.50
Part IV (F-H)	126.00	42.00	24.00
Part V (I-L)	90.00	23.00	17.00
Part VI (M-Pi)	28.00	8.00	2.80
Part VII (Pl-Sh)	60.00	18.00	6.00
Part VIII (Si-Ti)	66.00	27.00	10.00
Part IX (To-Z)	80.00	34.00	12.00

BHARAT KI SAMPADA (Hindi Edition of Wealth of India. Raw Materials).

Vol. I (अ-इ)	38.00	16.00	6.50
Vol. II (ए)	36.00	15.00	6.00
Vol. III (उ-न)	36.00	15.00	6.00
Vol. IV (प)	83.00	34.00	16.00
Vol. V (फ-ये)	60.00	22.00	10.00
Vol. VI (झ-झ)	80.00	27.00	13.00
Vol. VII (जे-जा)	135.00	40.00	25.00
Livestock (Kukkut Palan)	34.00	15.00	6.00
Fish & Fisheries (Matsya aur Matsvaki)	49.00	21.00	8.00
A Dictionary of Generic & Specific Names of Plants and Animals Useful to Man with their English and Latin pronunciation in Devanagari	30.00	11.00	5.00

OTHER PUBLICATIONS

Proceedings: seminar on primary communications in Science & Technology in India by Sh. R.N. Sharma & S. Seetharama	52.00	17.50	9.00
Flora of Delhi by J.K. Maheshwari	28.00	8.00	2.80
Indian Fossil Pteridophytes by K.R. Surange	66.00	22.00	12.50
Indian Thysanoptera by T.N. Ananthakrishnan	26.00	8.00	2.60
The Millipede Thyropygus by G. Krishnan	12.00	3.50	1.20
Drug Addiction with special reference to India by R.N. Chopra & I.C. Chopra	12.00	3.50	1.20
Glossary of Indian Medicinal Plants by R.N. Chopra & I.C. Chopra	35.00	13.00	6.00
Fluidization & Related Processes	12.00	4.00	1.20
Evolution of Life by M.S. Randhawa, A.K. Dey, Jagjit Singh & Vishnu Mitre	22.50	7.00	2.25
Collected Scientific Papers of Meghnad Saha	30.00	9.00	3.00
Proteaceae by C. Venkata Rao	72.00	24.00	13.50
Pinus by P. Maheshwari & R.N. Konar	30.00	11.00	5.00
Cellulose Research I	3.00	0.90	0.30
Cellulose Research II	6.00	1.75	0.6
Chemical Process Design	9.00	2.50	0.90
Low Temperature Carbonization of Non-coking Coals & Lignites & Briquetting Coal Fines: Vol. I & Vol. II (each volume)	17.50	5.50	1.75
Nucleic Acids	10.00	3.00	1.00
IGY Symposium: Vol. I	9.00	2.50	0.90
IGY Symposium: Vol. II	9.00	2.50	0.90
CNS Drugs	16.50	5.00	1.65
Kinetics of Electrode Processes & Null Points of Metals	2.50	0.75	0.25
Indian Sardines by R.V. Nair	22.00	7.00	2.20
Termite Problems in India	9.00	3.00	0.90
Loranthaceae by B.M. Johri & S.P. Bhatnagar	55.00	18.50	10.50
Abies and Picea by K.A. Chowdhury	14.00	6.00	2.10
Gnetum by P. Maheshwari and Vimla Vasil	20.00	6.00	2.00
Aquatic Angiosperms by K. Subramanyam	20.00	6.00	2.00
Supplement to Glossary of Indian Medicinal Plants by R.N. Chopra, I.C. Chopra & B.S. Varma	18.00	7.00	3.00
Herbaceous Flora of Dehra Dun by C.R. Babu	144.00	60.00	22.00
Diosgenin and Other Steroid Drug Precursors by Y.R. Chaudha & Miss L.V. Asolkar	36.00	13.00	6.00
Research & Development Management by Inder Dev	25.00	10.00	—
Rural Development and Technology—A Status Report-cum-Bibliography by P.R. Bose & V.N. Vashist	100.00	38.00	17.0
Cholera Bacteriophages by Sachinmohan Mukherjee	30.00	10.00	6.0

Packing and Postage extra

Please contact:

SALES AND DISTRIBUTION OFFICER
PUBLICATIONS & INFORMATION DIRECTORATE, CSIR
Hillside Road, New Delhi 110012

Printed & Published by D.S. Sastry, Editor, Publications & Information Directorate (PID)
Hillside Road, New Delhi 110012, at PID Photocomposition Unit